





## VALUES OF MATERIAL AND PHYSICAL CONSTANTS

Name	Symbol	Value	Units
Room temperature	$T$	300 (= 27°C)	K
Boltzman constant	$k$	$1.38 \times 10^{-23}$	J/K
Electron charge	$q$	$1.6 \times 10^{-19}$	C
Thermal voltage	$\phi_T = kT/q$	26	mV (at 300 K)
Intrinsic Carrier Concentration (Silicon)	$n_i$	$1.5 \times 10^{10}$	$\text{cm}^{-3}$ (at 300 K)
Permittivity of Si	$\epsilon_{si}$	$1.05 \times 10^{-12}$	F/cm
Permittivity of SiO <sub>2</sub>	$\epsilon_{ox}$	$3.5 \times 10^{-13}$	F/cm
Resistivity of Al	$\rho_{Al}$	$2.7 \times 10^{-8}$	$\Omega\text{-m}$
Resistivity of Cu	$\rho_{Cu}$	$1.7 \times 10^{-8}$	$\Omega\text{-m}$
Magnetic permeability of vacuum (similar for SiO <sub>2</sub> )	$\mu_0$	$12.6 \times 10^{-7}$	Wb/Am
Speed of light (in vacuum)	$c_0$	30	cm/nsec
Speed of light (in SiO <sub>2</sub> )	$c_{ox}$	15	cm/nsec

UNIVERSITY OF MICHIGAN LIBRARIES

# FORMULAS AND EQUATIONS

## Diode

$$I_D = I_S(e^{V_D/\phi_T} - 1) = Q_D/\tau_T$$

$$C_j = \frac{C_{j0}}{(1 - V_D/\phi_0)^m}$$

$$K_{eq} = \frac{-\phi_0^m}{(V_{high} - V_{low})(1 - m)} \times [(\phi_0 - V_{high})^{1-m} - (\phi_0 - V_{low})^{1-m}]$$

## MOS Transistor

$$V_T = V_{T0} + \gamma(\sqrt{-2\phi_F + V_{SB}} - \sqrt{-2\phi_F})$$

$$I_D = \frac{k'_n W}{2L} (V_{GS} - V_T)^2 (1 + \lambda V_{DS}) \text{ (sat)}$$

$$I_D = v_{sat} C_{ox} W \left( V_{GS} - V_T - \frac{V_{DSAT}}{2} \right) (1 + \lambda V_{DS}) \text{ (velocity sat)}$$

$$I_D = k'_n \frac{W}{L} \left( (V_{GS} - V_T) V_{DS} - \frac{V_{DS}^2}{2} \right) \text{ (triode)}$$

$$I_D = I_S e^{\frac{V_{GS}}{nkT/q}} \left( 1 - e^{-\frac{V_{DS}}{kT/q}} \right) \text{ (subthreshold)}$$

## Deep Submicron MOS Unified Model

$$I_D = 0 \text{ for } V_{GT} \leq 0$$

$$I_D = k' \frac{W}{L} \left( V_{GT} V_{min} - \frac{V_{min}^2}{2} \right) (1 + \lambda V_{DS}) \text{ for } V_{GT} \geq 0$$

$$\text{with } V_{min} = \min(V_{GT}, V_{DS}, V_{DSAT})$$

$$\text{and } V_{GT} = V_{GS} - V_T$$

## MOS Switch Model

$$R_{eq} = \frac{1}{2} \left( \frac{V_{DD}}{I_{DSAT}(1 + \lambda V_{DD})} + \frac{V_{DD}/2}{I_{DSAT}(1 + \lambda V_{DD}/2)} \right) \approx \frac{3}{4} \frac{V_{DD}}{I_{DSAT}} \left( 1 - \frac{5}{6} \lambda V_{DD} \right)$$

## Inverter

$$V_{OH} = f(V_{OL})$$

$$V_{OL} = f(V_{OH})$$

$$V_M = f(V_M)$$

$$t_p = 0.69 R_{eq} C_L = \frac{C_L (V_{swing}/2)}{I_{avg}}$$

$$P_{dyn} = C_L V_{DD} V_{swing} f$$

$$P_{stat} = V_{DD} I_{DD}$$

## Static CMOS Inverter

$$V_{OH} = V_{DD}$$

$$V_{OL} = GND$$

$$V_M \approx \frac{r V_{DD}}{1 + r} \text{ with } r = \frac{k_p V_{DSATp}}{k_n V_{DSATn}}$$

$$V_{IH} = V_M - \frac{V_M}{g} \quad V_{IL} = V_M + \frac{V_{DD} - V_M}{g}$$

$$\text{with } g \approx \frac{1 + r}{(V_M - V_{Tn} - V_{DSATn}/2)(\lambda_n - \lambda_p)}$$

$$t_p = \frac{t_{pHL} + t_{pLH}}{2} = 0.69 C_L \left( \frac{R_{eqn} + R_{eqp}}{2} \right)$$

$$P_{av} = C_L V_{DD}^2 f$$

## Interconnect

$$\text{Lumped RC: } t_p = 0.69 RC$$

$$\text{Distributed RC: } t_p = 0.38 RC$$

RC-chain:

$$\tau_N = \sum_{i=1}^N R_i \sum_{j=i}^N C_j = \sum_{i=1}^N C_i \sum_{j=1}^i R_j$$

Transmission line reflection:

$$\rho = \frac{V_{refl}}{V_{inc}} = \frac{I_{refl}}{I_{inc}} = \frac{R - Z_0}{R + Z_0}$$

# **DIGITAL INTEGRATED CIRCUITS**

---

A DESIGN PERSPECTIVE



**Prentice Hall Electronics and VLSI Series**

Charles S. Sodini, Series Editor

LEE, SHUR, FIELDLY, YTTERDAL *Semiconductor Devices Modeling for VLSI*

LEUNG *VLSI for Wireless Communications*

PLUMMER, DEAL, GRIFFIN *Silicon VLSI Technology: Fundamentals, Practice, and Modeling*

RABAEY, CHANDRAKASAN, NIKOLIĆ *Digital Integrated Circuits: A Design Perspective, Second Edition*

# **DIGITAL INTEGRATED CIRCUITS**

---

**A DESIGN PERSPECTIVE  
SECOND EDITION**

**JAN M. RABAEY  
ANANTHA CHANDRAKASAN  
BORIVOJE NIKOLIĆ**

**PRENTICE HALL ELECTRONICS AND VLSI SERIES  
CHARLES G. SODINI, SERIES EDITOR**



**Pearson Education, Inc.  
Upper Saddle River, New Jersey 07458**

**Library of Congress Cataloging-in-Publication Data on file.**

Vice President and Editorial Director, ECS: *Marcia J. Horton*  
Publisher: *Tom Robbins*  
Editorial Assistant: *Eric Van Ostenbridge*  
Vice President and Director of Production and Manufacturing, ESM: *David W. Riccardi*  
Executive Managing Editor: *Vince O'Brien*  
Managing Editor: *David A. George*  
Production Editor: *Daniel Sandin*  
Director of Creative Services: *Paul Belfanti*  
Creative Director: *Carole Anson*  
Art and Cover Director: *Jayne Conte*  
Art Editor: *Greg Dulles*  
Manufacturing Manager: *Trudy Pisciotto*  
Manufacturing Buyer: *Lisa McDowell*  
Marketing Manager: *Holly Stark*

*About the Cover:* Detail of "Wet Orange," by Joan Mitchell (American, 1925–1992). Oil on canvas, 112 × 245 in. (284.5 × 622.3 cm). Carnegie Museum of Art, Pittsburgh, PA. Gift of Kaufmann's Department Store and the National Endowment for the Arts, 74.11. Photograph by Peter Harholdt, 1995.



© 2003, 1996 by Pearson Education, Inc.  
Pearson Education, Inc.  
Upper Saddle River, NJ 07458

The author and publisher of this book have used their best efforts in preparing this book. These efforts include the development, research, and testing of the theories and programs to determine their effectiveness. The author and publisher shall not be liable in any event for incidental and consequential damages in connection with, or arising out of, the furnishing, performance, or use of these programs.

All rights reserved. No part of this book may be reproduced, in any form or by any means, without permission in writing from the publisher.

Printed in the United States of America

10 9 8 7 6 5 4 3 2 1

ISBN 0-13-597444-5

Pearson Education Ltd., *London*  
Pearson Education Australia Pty, Ltd., *Sydney*  
Pearson Education Singapore, Pte. Ltd.  
Pearson Education North Asia Ltd., *Hong Kong*  
Pearson Education Canada Inc., *Toronto*  
Pearson Educación de Mexico, S.A. de C.V.  
Pearson Education—Japan, *Tokyo*  
Pearson Education Malaysia, Pte. Ltd.  
Pearson Education Inc., *Upper Saddle River, New Jersey*



*To Kathelijn, Karthiyayani, Krithivasan,  
and our Parents*

*“Qu’est-ce que l’homme dans la nature?  
Un néant a l’égard de l’infini,  
un tout al l’égard du néant,  
un milieu entre rien et tout.”*

*“What is man in nature?  
Nothing in relation to the infinite,  
everything in relation to nothing,  
a mean between nothing and everything.”*

Blaise Pascal, *Pensées*, n. 4, 1670.

# Preface

## What is New?

Welcome to second edition of “*Digital Integrated Circuits: A Design Perspective.*” In the six years since the publication of the first, the field of digital integrated circuits has gone through some dramatic evolutions and changes. IC manufacturing technology has continued to scale to ever-smaller dimensions. Minimum feature sizes have scaled by a factor of almost ten since the writing of the first edition, and now are approaching the 100 nm realm. This scaling has a double impact on the design of digital integrated circuit. First of all, the complexity of the designs that can be put on a single die has increased dramatically. Dealing with the challenges this poses has led to new design methodologies and implementation strategies. At the same time, the plunge into the deep-submicron space causes devices to behave differently, and brings to the forefront a number of new issues that impact the reliability, cost, performance, and power dissipation of the digital IC. Addressing these issues in-depth is what differentiates this edition from the first.

A glance through the table of contents reveals extended coverage of issues such as deep-sub micron devices, circuit optimization, interconnect modeling and optimization, signal integrity, clocking and timing, and power dissipation. All these topics are illustrated with state-of-the-art design examples. Also, since MOS now represents more than 99% of the digital IC market, older technologies such as silicon bipolar and GaAs have been deleted (however, the interested reader can find the old chapters on these technologies on the web site of the book). Given the importance of methodology in today’s design process, we have included *Design Methodology Inserts* throughout the text, each of which highlights one particular aspect of the design process. This new edition represents a major reworking of the book. The biggest change is the addition of two co-authors, Anantha and Bora, who have brought a broader insight into digital IC design and its latest trends and challenges.

## Maintaining the Spirit of the First Edition

While introducing these changes, our intent has been to preserve the spirit and goals of the first edition—that is, to bridge the gap between the **circuit and system visions** on digital design. While starting from a solid understanding of the operation of electronic devices and an in-depth analysis of the nucleus of digital design—the inverter—we gradually channel this knowledge into the design of more complex modules such as gates, registers, controllers, adders, multipliers, and memories. We identify the compelling questions facing the designers of today’s

complex circuits: What are the dominant design parameters, what section of the design should he focus on and what details could she ignore? Simplification is clearly the only approach to address the increasing complexity of the digital systems. However, oversimplification can lead to circuit failure since global circuit effects such as timing, interconnect, and power consumption are ignored. To avoid this pitfall it is important to design digital circuits with both a circuits and a systems perspective in mind. This is the approach taken in this book, which brings the reader the knowledge and expertise needed to deal with complexity, using both analytical and experimental techniques.

### How to Use This Book

The core of the text is intended for use in a *senior-level digital circuit design class*. Around this kernel, we have included chapters and sections covering the more advanced topics. In the course of developing this book, it quickly became obvious that it is difficult to define a subset of the digital circuit design domain that covers everyone's needs. On the one hand, a newcomer to the field needs detailed coverage of the basic concepts. On the other hand, feedback from early readers and reviewers indicated that an in-depth and extensive coverage of advanced topics and current issues is desirable and necessary. Providing this complete vision resulted in a text that exceeds the scope of a single-semester class. The more advanced material can be used as the basis for a *graduate class*. The wide coverage and the inclusion of state-of-the-art topics also makes the text useful as a reference work for professional engineers. It is assumed that students taking this course are familiar with the basics of logic design.

The organization of the material is such that the chapters can be taught or read in many ways, as long as a number of precedence relations are adhered to. The core of the text consists of Chapters 5, 6, 7, and 8. Chapters 1 to 4 can be considered as introductory. In response to popular demand, we have introduced a short treatise on semiconductor manufacturing in Chapter 2. Students with a prior introduction to semiconductor devices can traverse quickly through Chapter 3. We urge everyone to do at least that, as a number of important notations and foundations are introduced in that chapter. In addition, an original approach to the modeling of deep-submicron transistors enabling manual analysis, is introduced. To emphasize the importance of interconnect in today's digital design, we have moved the modeling of interconnect forward in the text to Chapter 4.

Chapters 9 to 12 are of a more advanced nature and can be used to provide a certain focus to the course. A course with a focus on the circuit aspects, for example, can supplement the core material with Chapters 9 and 12. A course focused on the digital system design should consider adding (parts of) Chapters 9, 10, and 11. All of these advanced chapters can be used to form the core of a graduate or a follow-on course. Sections considered *advanced* are marked with an *asterisk* in the text.

A number of possible paths through the material for a senior-level class are enumerated below. In the *instructor documentation*, provided on the book's web site, we have included a number of complete syllabi based on courses run at some academic institutions.



*Basic circuit class (with minor prior device knowledge):*

1, 2.1–3, 3, 4, 5, 6, 7, 8, (9.1–9.3, 12).

*Somewhat more advanced circuit coverage:*

1, (2, 3), 4, 5, 6, 7, 8, 9, 10.1–10.3, 10.5–10.6, 12.

*Course with systems focus:*

1, (2, 3), 4, 5, 6, 7, 8, 9, 10.1–10.4, 11, 12.1–12.2.

The *design methodology inserts* are, by preference, covered in concurrence with the chapter to which they are attached.

In order to maintain a consistent flow through each of the chapters, the topics are *introduced* first, followed by a detailed and in-depth discussion of the ideas. A *Perspective* section discusses how the introduced concepts relate to real world designs and how they might be impacted by future evolutions. Each chapter finishes with a *Summary*, which briefly enumerates the topics covered in the text, followed by *To Probe Further* and *Reference* sections. These provide ample references and pointers for a reader interested in further details on some of the material.

As the title of the book implies, one of the goals of this book is to stress the design aspect of digital circuits. To achieve this more practical viewpoint and to provide a real perspective, we have interspersed actual *design examples* and layouts throughout the text. These case studies help to answer questions, such as “How much area or speed or power is really saved by applying this technique?” To mimic the real design process, we are making extensive use of design tools such as circuit- and switch-level simulation as well as layout editing and extraction. Computer analysis is used throughout to verify manual results, to illustrate new concepts, or to examine complex behavior beyond the reach of manual analysis.

Finally, to facilitate the learning process, there are numerous examples included in the text. Each chapter contains a number of *problems or brain-teasers* (answers for which can be found in the back of the book), that provoke thinking and understanding while reading.

## The Worldwide Web Companion

A worldwide web companion (<http://bwrc.eecs.berkeley.edu/IcBook/index.htm>) provides fully worked-out design problems and a complete set of overhead transparencies, extracting the most important figures and graphs from the text.

In contrast to the first edition, we have chosen **NOT to include problems sets and design problems** in the text. Instead we decided to make them available **on the book’s web site**. This gives us the opportunity to dynamically upgrade and extend the problems, providing a more effective tool for the instructor. More than 300 challenging *exercises* are currently provided. The goal is to provide the individual reader an independent gauge for his understanding of the material and to provide practice in the use of some of the design tools. Each problem is keyed to the text sections it refers to (e.g., <1.3>), the design tools that must be used when solving the problem (e.g., SPICE) and a rating, ranking the problems on difficulty: (E) easy, (M) moderate, and

(C) challenging. Problems marked with a (D) include a design or research elements. Solutions to the problem sets are available only to instructors of academic institutions that have chosen to adopt our book for classroom use. They are available through the publisher on a password-protected web site.

Open-ended *design problems* help to gain the all-important insight into design optimization and trade-off. The use of design editing, verification and analysis tools is recommended when attempting these design problems. Fully worked out versions of these problems can be found on the web site.

In addition, the book's web site also offers samples of hardware and software laboratories, extra background information, and useful links.

### Compelling Features of the Book

- Brings both circuit and systems views on design together. It offers a profound understanding of the design of complex digital circuits, while preparing the designer for new challenges that might be waiting around the corner.
- Design-oriented perspectives are advocated throughout. Design challenges and guidelines are highlighted. Techniques introduced in the text are illustrated with real designs and complete SPICE analysis.
- Is the first circuit design book that *focuses solely on deep-submicron devices*. To facilitate this, a simple transistor model for manual analysis, called the *unified MOS model*, has been developed.
- Unique in showing how to use the latest techniques to design complex high-performance or low-power circuits. Speed and power treated as equal citizens throughout the text.
- Covers crucial real-world system design issues such as signal integrity, power dissipation, interconnect, packaging, timing, and synchronization.
- Provides unique coverage of the latest design methodologies and tools, with a discussion of how to use them from a designers' perspective.
- Offers perspectives on how digital circuit technology might evolve in the future.
- Outstanding illustrations and a usable design-oriented four-color insert.
- To Probe Further and Reference sections provide ample references and pointers for a reader interested in further details on some of the material.
- Extensive instructional package is available over the internet from the author's web site. Includes design software, transparency masters, problem sets, design problems, actual layouts, and hardware and software laboratories.

### The Contents at a Glance

A quick scan of the table of contents shows how the ordering of chapters and the material covered are consistent with the advocated design methodology. Starting from a model of the semiconductor devices, we will gradually progress upwards, covering the inverter, the complex logic gate (NAND, NOR, XOR), the functional (adder, multiplier, shifter, register) and the system

module (datapath, controller, memory) levels of abstraction. For each of these layers, the dominant design parameters are identified and simplified models are constructed, abstracting away the nonessential details. While this layered modeling approach is the designer's best handle on complexity, it has some pitfalls. This is illustrated in Chapters 9 and 10, where topics with a global impact, such as interconnect parasitics and chip timing, are discussed. To further express the dichotomy between circuit and system design visions, we have divided the book contents into two major parts: Part II (Chapters 4–7) addresses mostly the circuit perspective of digital circuit design, while Part III (Chapters 8–12) presents a more system oriented vision. Part I (Chapters 1–4) provides the necessary foundation (design metrics, the manufacturing process, device and interconnect models).

**Chapter 1** serves as a global *introduction*. After a historical overview of digital circuit design, the concepts of hierarchical design and the different abstraction layers are introduced. A number of fundamental metrics, which help to quantify cost, reliability, and performance of a design, are introduced.

**Chapter 2** provides a short and compact introduction to the *MOS manufacturing process*. Understanding the basic steps in the process helps to create the three-dimensional understanding of the MOS transistor, which is crucial when identifying the sources of the device parasitics. Many of the variations in device parameters can also be attributed to the manufacturing process as well. The chapter further introduces the concept of design rules, which form the interface between the designer and the manufacturer. The chapter concludes with an overview of the chip packaging process, an often-overlooked but crucial element of the digital IC design cycle.

**Chapter 3** contains a summary of the primary design building blocks, *the semiconductor devices*. The main goal of this chapter is to provide an intuitive understanding of the operation of the MOS as well as to introduce the device models, which are used extensively in the later chapters. Major attention is paid to the artifacts of modern submicron devices, and the modeling thereof. Readers with prior device knowledge can traverse this material rather quickly.

**Chapter 4** contains a careful analysis of the *wire*, with interconnect and its accompanying parasitics playing a major role. We visit each of the parasitics that come with a wire (capacitance, resistance, and inductance) in turn. Models for both manual and computer analysis are introduced.

**Chapter 5** deals with the nucleus of digital design, the *inverter*. First, a number of fundamental properties of digital gates are introduced. These parameters, which help to quantify the performance and reliability of a gate, are derived in detail for two representative inverter structures: the static complementary CMOS. The techniques and approaches introduced in this chapter are of crucial importance, as they are repeated over and over again in the analysis of other gate structures and more complex gate structures.

In **Chapter 6** this fundamental knowledge is extended to address the design of *simple and complex digital CMOS gates*, such as NOR and NAND structures. It is demonstrated that, depending upon the dominant design constraint (reliability, area, performance, or power), other



CMOS gate structures besides the complementary static gate can be attractive. The properties of a number of contemporary gate-logic families are analyzed and compared. Techniques to optimize the performance and power consumption of complex gates are introduced.

**Chapter 7** discusses how memory function can be accomplished using either positive feedback or charge storage. Besides analyzing the traditional bistable flip-flops, other sequential circuits such as the mono- and astable multivibrators are also introduced. All chapters prior to Chapter 7 deal exclusively with combinational circuits, that is circuits without a sense of the past history of the system. *Sequential logic circuits*, in contrast, can remember and store the past state.

All chapters preceding **Chapter 8** present a circuit-oriented approach towards digital design. The analysis and optimization process has been constrained to the individual gate. In this chapter, we take our approach one step further and analyze how gates can be connected together to form the building blocks of a system. The system-level part of the book starts, appropriately, with a discussion of *design methodologies*. Design automation is the only way to cope with the ever-increasing complexity of digital designs. In Chapter 8, the prominent ways of producing large designs in a limited time are discussed. The chapter spends considerable time on the different implementation methodologies available to today's designer. Custom versus semi-custom, hardwired versus fixed, regular array versus ad-hoc are some of the issues put forward.

**Chapter 9** revisits the impact of *interconnect wiring* on the functionality and performance of a digital gate. A wire introduces parasitic capacitive, resistive, and inductive effects, which are becoming ever more important with the scaling of the technology. Approaches to minimize the impact of these interconnect parasitics on performance, power dissipation and circuit reliability are introduced. The chapter also addresses some important issues such as supply-voltage distribution, and input/output circuitry.

In **Chapter 10** details how that in order to operate sequential circuits correctly, a strict ordering of the switching events has to be imposed. Without these *timing* constraints, wrong data might be written into the memory cells. Most digital circuits use a synchronous, clocked approach to impose this ordering. In Chapter 10, the different approaches to digital circuit timing and clocking are discussed. The impact of important effects such as clock skew on the behavior of digital synchronous circuits is analyzed. The synchronous approach is contrasted with alternative techniques, such as self-timed circuits. The chapter concludes with a short introduction to synchronization and clock-generation circuits.

In **Chapter 11**, the design of a variety of complex *arithmetic building blocks* such as adders, multipliers, and shifters, is discussed. This chapter is crucial because it demonstrates how the design techniques introduced in chapters 5 and 6 are extended to the next abstraction layer. The concept of the critical path is introduced and used extensively in the performance analysis and optimization. Higher-level performance models are derived. These help the designer to get a fundamental insight into the operation and quality of a design module, without having to resort to an in-depth and detailed analysis of the underlying circuitry.

**Chapter 12** discusses in depth the different memory classes and their implementation. Whenever large amounts of data storage are needed, the digital designer resorts to special circuit modules, called *memories*. Semiconductor memories achieve very high storage density by compromising on some of the fundamental properties of digital gates. Instrumental in the design of reliable and fast memories is the implementation of the peripheral circuitry, such as the decoders, sense amplifiers, drivers, and control circuitry, which are extensively covered. Finally, as the primary issue in memory design is to ensure that the device works consistently under all operating circumstances, the chapter concludes with a detailed discussion of memory reliability. This chapter as well as the previous one are optional for undergraduate courses.

## Acknowledgments

The authors would like to thank all those who contributed to the emergence, creation and correction of this manuscript. First of all, thanks to all the graduate students that helped over the years to bring the text to where it is today. Thanks also to the students of the eecs141 and eecs241 courses at Berkeley and the 6.374 course at MIT, who suffered through many of the experimental class offerings based on this book. The feedback from instructors, engineers, and students from all over the world has helped tremendously in focusing the directions of this new edition, and in fine-tuning the final text. The continuous stream of e-mails indicate to us that we are on the right track.

In particular, we would like to acknowledge the contributions of Mary-Jane Irwin, Vijay Narayanan, Eby Friedman, Fred Rosenberger, Wayne Burleson, Sekhar Borkar, Ivo Bolsens, Duane Boning, Olivier Franza, Lionel Kimerling, Josie Ammer, Mike Sheets, Tufan Karalar, Huifang Qin, Rhett Davis, Nathan Chan, Jeb Durant, Andrei Vladimirescu, Radu Zlatanovici, Yasuhisa Shimazaki, Fujio Ishihara, Dejan Markovic, Vladimir Stojanovic, SeongHwan Cho, James Kao, Travis Simpkins, Siva Narendra, James Goodman, Vadim Gutnik, Theodoros Konstantakopoulos, Rex Min, Vikas Mehrotra, and Paul-Peter Sotiriadis. Their help, input, and feedback are greatly appreciated. Obviously, we remain thankful to those who helped create and develop the first edition.

I am extremely grateful to the staff at Prentice Hall, who have been instrumental in turning a rough manuscript into an enjoyable book. First of all, I would like to acknowledge the help and constructive feedback of Tom Robbins, Publisher, Daniel Sandin, Production Editor, and David George, Managing Editor. A special word of thanks to Brenda Vanoni at Berkeley, for her invaluable help in the copy editing and the website creation process. The web expertise of Carol Sitea came in very handy as well.

I would like to highlight to role of computer aids in developing this manuscript. All drafts were completely developed on the FrameMaker publishing system (Adobe Systems). Graphs were mostly created using MATLAB. Microsoft Frontpage is the tool of choice for the web-page creation. For circuit simulations, we used HSPICE (Avant!). All layouts were generated using the Cadence physical design suite.

Finally, some words of gratitude to the people that had to endure the creation process of this book, Kathelijn, Karthiyayani, Krithivasan, and Rebecca. While the generation of a new edition brings substantially less pain than a first edition, we consistently underestimate what it takes, especially in light of the rest of our daily loads. They been a constant support, help and encouragement during the writing of this manuscript.

JAN M. RABAEY  
ANANTHA CHANDRAKASAN  
BORIVOJE NIKOLIĆ  
*Berkeley, Calistoga, Cambridge*

# Contents

<b>Preface</b>	<b>vii</b>
----------------	------------

---

<b>Part 1</b>	<b>The Fabrics</b>	<b>1</b>
---------------	--------------------	----------

---

<b>Chapter 1</b>	<b>Introduction</b>	<b>3</b>
------------------	---------------------	----------

1.1	A Historical Perspective	4
1.2	Issues in Digital Integrated Circuit Design	6
1.3	Quality Metrics of a Digital Design	15
1.3.1	Cost of an Integrated Circuit	16
1.3.2	Functionality and Robustness	18
1.3.3	Performance	27
1.3.4	Power and Energy Consumption	30
1.4	Summary	31
1.5	To Probe Further	31
	Reference Books	32
	References	33

<b>Chapter 2</b>	<b>The Manufacturing Process</b>	<b>35</b>
------------------	----------------------------------	-----------

2.1	Introduction	36
2.2	Manufacturing CMOS Integrated Circuits	36
2.2.1	The Silicon Wafer	37
2.2.2	Photolithography	37
2.2.3	Some Recurring Process Steps	41
2.2.4	Simplified CMOS Process Flow	42
2.3	Design Rules—The Contract between Designer and Process Engineer	47
2.4	Packaging Integrated Circuits	51
2.4.1	Package Materials	52
2.4.2	Interconnect Levels	53
2.4.3	Thermal Considerations in Packaging	59
2.5	Perspective—Trends in Process Technology	61
2.5.1	Short-Term Developments	61
2.5.2	In the Longer Term	63
2.6	Summary	64

2.7	To Probe Further	64
	References	64
<b><i>Design Methodology Insert A IC LAYOUT</i></b>		<b>67</b>
A.1	To Probe Further	71
	References	71
<b><i>Chapter 3 The Devices</i></b>		<b>73</b>
3.1	Introduction	74
3.2	The Diode	74
3.2.1	A First Glance at the Diode—The Depletion Region	75
3.2.2	Static Behavior	77
3.2.3	Dynamic, or Transient, Behavior	80
3.2.4	The Actual Diode—Secondary Effects	84
3.2.5	The SPICE Diode Model	85
3.3	The MOS(FET) Transistor	87
3.3.1	A First Glance at the Device	87
3.3.2	The MOS Transistor under Static Conditions	88
3.3.3	The Actual MOS Transistor—Some Secondary Effects	114
3.3.4	SPICE Models for the MOS Transistor	117
3.4	A Word on Process Variations	120
3.5	Perspective—Technology Scaling	122
3.6	Summary	128
3.7	To Probe Further	129
	References	130
<b><i>Design Methodology Insert B Circuit Simulation</i></b>		<b>131</b>
	References	134
<b><i>Chapter 4 The Wire</i></b>		<b>135</b>
4.1	Introduction	136
4.2	A First Glance	136
4.3	Interconnect Parameters—Capacitance, Resistance, and Inductance	138
4.3.1	Capacitance	138
4.3.2	Resistance	144
4.3.3	Inductance	148
4.4	Electrical Wire Models	150
4.4.1	The Ideal Wire	151
4.4.2	The Lumped Model	151
4.4.3	The Lumped RC Model	152
4.4.4	The Distributed $rc$ Line	156
4.4.5	The Transmission Line	159

4.5	SPICE Wire Models	170
4.5.1	Distributed $rc$ Lines in SPICE	170
4.5.2	Transmission Line Models in SPICE	170
4.5.3	Perspective: A Look into the Future	171
4.6	Summary	174
4.7	To Probe Further	174
	References	174

---

**Part 2    A Circuit Perspective    177**

---

**Chapter 5    The CMOS Inverter    179**

5.1	Introduction	180
5.2	The Static CMOS Inverter—An Intuitive Perspective	180
5.3	Evaluating the Robustness of the CMOS Inverter: The Static Behavior	184
5.3.1	Switching Threshold	185
5.3.2	Noise Margins	188
5.3.3	Robustness Revisited	191
5.4	Performance of CMOS Inverter: The Dynamic Behavior	193
5.4.1	Computing the Capacitances	194
5.4.2	Propagation Delay: First-Order Analysis	199
5.4.3	Propagation Delay from a Design Perspective	203
5.5	Power, Energy, and Energy Delay	213
5.5.1	Dynamic Power Consumption	214
5.5.2	Static Consumption	223
5.5.3	Putting It All Together	225
5.5.4	Analyzing Power Consumption Using SPICE	227
5.6	Perspective: Technology Scaling and its Impact on the Inverter Metrics	229
5.7	Summary	232
5.8	To Probe Further	233
	References	233

**Chapter 6    Designing Combinational Logic Gates in CMOS    235**

6.1	Introduction	236
6.2	Static CMOS Design	236
6.2.1	Complementary CMOS	237
6.2.2	Ratioed Logic	263
6.2.3	Pass-Transistor Logic	269
6.3	Dynamic CMOS Design	284
6.3.1	Dynamic Logic: Basic Principles	284
6.3.2	Speed and Power Dissipation of Dynamic Logic	287

6.3.3	Signal Integrity Issues in Dynamic Design	290
6.3.4	Cascading Dynamic Gates	295
6.4	Perspectives	303
6.4.1	How to Choose a Logic Style?	303
6.4.2	Designing Logic for Reduced Supply Voltages	303
6.5	Summary	306
6.6	To Probe Further	307
	References	308
<b><i>Design Methodology Insert C How to Simulate Complex Logic Circuits</i></b>		<b>309</b>
C.1	Representing Digital Data as a Continuous Entity	310
C.2	Representing Data as a Discrete Entity	310
C.3	Using Higher-Level Data Models	315
	References	317
<b><i>Design Methodology Insert D Layout Techniques for Complex Gates</i></b>		<b>319</b>
<b>Chapter 7</b>	<b>Designing Sequential Logic Circuits</b>	<b>325</b>
7.1	Introduction	326
7.1.1	Timing Metrics for Sequential Circuits	327
7.1.2	Classification of Memory Elements	328
7.2	Static Latches and Registers	330
7.2.1	The Bistability Principle	330
7.2.2	Multiplexer-Based Latches	332
7.2.3	Master-Slave Edge-Triggered Register	333
7.2.4	Low-Voltage Static Latches	339
7.2.5	Static SR Flip-Flops—Writing Data by Pure Force	341
7.3	Dynamic Latches and Registers	344
7.3.1	Dynamic Transmission-Gate Edge-triggered Registers	344
7.3.2	C <sup>2</sup> MOS—A Clock-Skew Insensitive Approach	346
7.3.3	True Single-Phase Clocked Register (TSPCR)	350
7.4	Alternative Register Styles*	354
7.4.1	Pulse Registers	354
7.4.2	Sense-Amplifier-Based Registers	356
7.5	Pipelining: An Approach to Optimize Sequential Circuits	358
7.5.1	Latch- versus Register-Based Pipelines	360
7.5.2	NORA-CMOS—A Logic Style for Pipelined Structures	361
7.6	Nonbistable Sequential Circuits	364
7.6.1	The Schmitt Trigger	364
7.6.2	Monostable Sequential Circuits	367
7.6.3	Astable Circuits	368
7.7	Perspective: Choosing a Clocking Strategy	370
7.8	Summary	371



















<b>Contents</b>		<b>xix</b>
7.9	To Probe Further	372
	References	372
<hr/>		
<b>Part 3</b>	<b>A System Perspective</b>	<b>375</b>
<hr/>		
<b>Chapter 8</b>	<b>Implementation Strategies for Digital ICS</b>	<b>377</b>
8.1	Introduction	378
8.2	From Custom to Semicustom and Structured-Array Design Approaches	382
8.3	Custom Circuit Design	383
8.4	Cell-Based Design Methodology	384
	8.4.1 Standard Cell	385
	8.4.2 Compiled Cells	390
	8.4.3 Macrocells, Megacells and Intellectual Property	392
	8.4.4 Semicustom Design Flow	396
8.5	Array-Based Implementation Approaches	399
	8.5.1 Prediffused (or Mask-Programmable) Arrays	399
	8.5.2 Prewired Arrays	404
8.6	Perspective—The Implementation Platform of the Future	420
8.7	Summary	423
8.8	To Probe Further	423
	References	424
 <b>Design Methodology Insert E Characterizing Logic and Sequential Cells</b>		<b>427</b>
	References	434
 <b>Design Methodology Insert F Design Synthesis</b>		<b>435</b>
	References	443
 <b>Chapter 9 Coping with Interconnect</b>		<b>445</b>
9.1	Introduction	446
9.2	Capacitive Parasitics	446
	9.2.1 Capacitance and Reliability—Cross Talk	446
	9.2.2 Capacitance and Performance in CMOS	449
9.3	Resistive Parasitics	460
	9.3.1 Resistance and Reliability—Ohmic Voltage Drop	460
	9.3.2 Electromigration	462
	9.3.3 Resistance and Performance—RC Delay	464
9.4	Inductive Parasitics*	469
	9.4.1 Inductance and Reliability— Voltage Drop	469
	9.4.2 Inductance and Performance—Transmission-line Effects	475
9.5	Advanced Interconnect Techniques	480

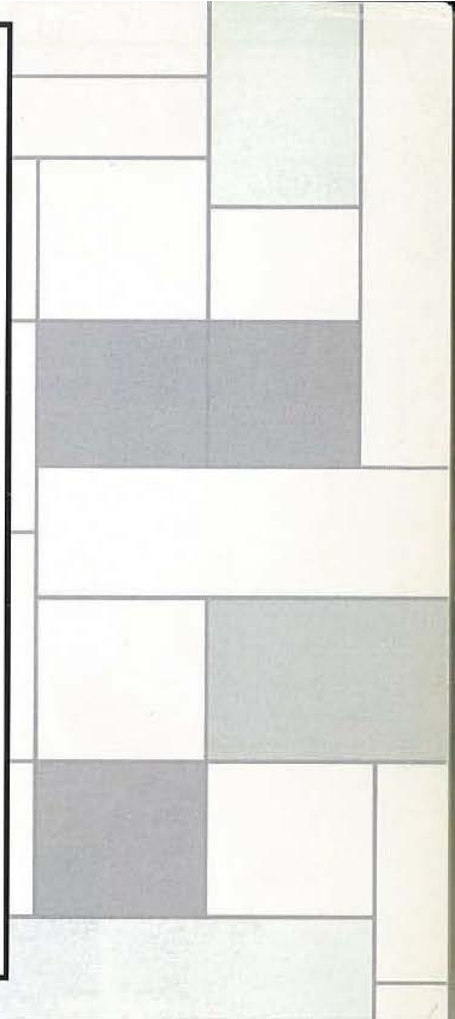


9.5.1	Reduced-Swing Circuits	480
9.5.2	Current-Mode Transmission Techniques	486
9.6	Perspective: Networks-on-a-Chip	487
9.7	Summary	488
9.8	To Probe Further	489
	References	489
<b>Chapter 10</b>	<b>Timing Issues in Digital Circuits</b>	<b>491</b>
10.1	Introduction	492
10.2	Timing Classification of Digital Systems	492
10.2.1	Synchronous Interconnect	492
10.2.2	Mesochronous interconnect	493
10.2.3	Plesiochronous Interconnect	493
10.2.4	Asynchronous Interconnect	494
10.3	Synchronous Design—An In-depth Perspective	495
10.3.1	Synchronous Timing Basics	495
10.3.2	Sources of Skew and Jitter	502
10.3.3	Clock-Distribution Techniques	508
10.3.4	Latch-Based Clocking*	516
10.4	Self-Timed Circuit Design*	519
10.4.1	Self-Timed Logic—An Asynchronous Technique	519
10.4.2	Completion-Signal Generation	522
10.4.3	Self-Timed Signaling	526
10.4.4	Practical Examples of Self-Timed Logic	531
10.5	Synchronizers and Arbiters*	534
10.5.1	Synchronizers—Concept and Implementation	534
10.5.2	Arbiters	538
10.6	Clock Synthesis and Synchronization Using a Phase-Locked Loop*	539
10.6.1	Basic Concept	540
10.6.2	Building Blocks of a PLL	542
10.7	Future Directions and Perspectives	546
10.7.1	Distributed Clocking Using DLLs	546
10.7.2	Optical Clock Distribution	548
10.7.3	Synchronous versus Asynchronous Design	549
10.8	Summary	550
10.9	To Probe Further	551
	References	551
<b>Design Methodology Insert G</b>	<b>Design Verification</b>	<b>553</b>
	References	557

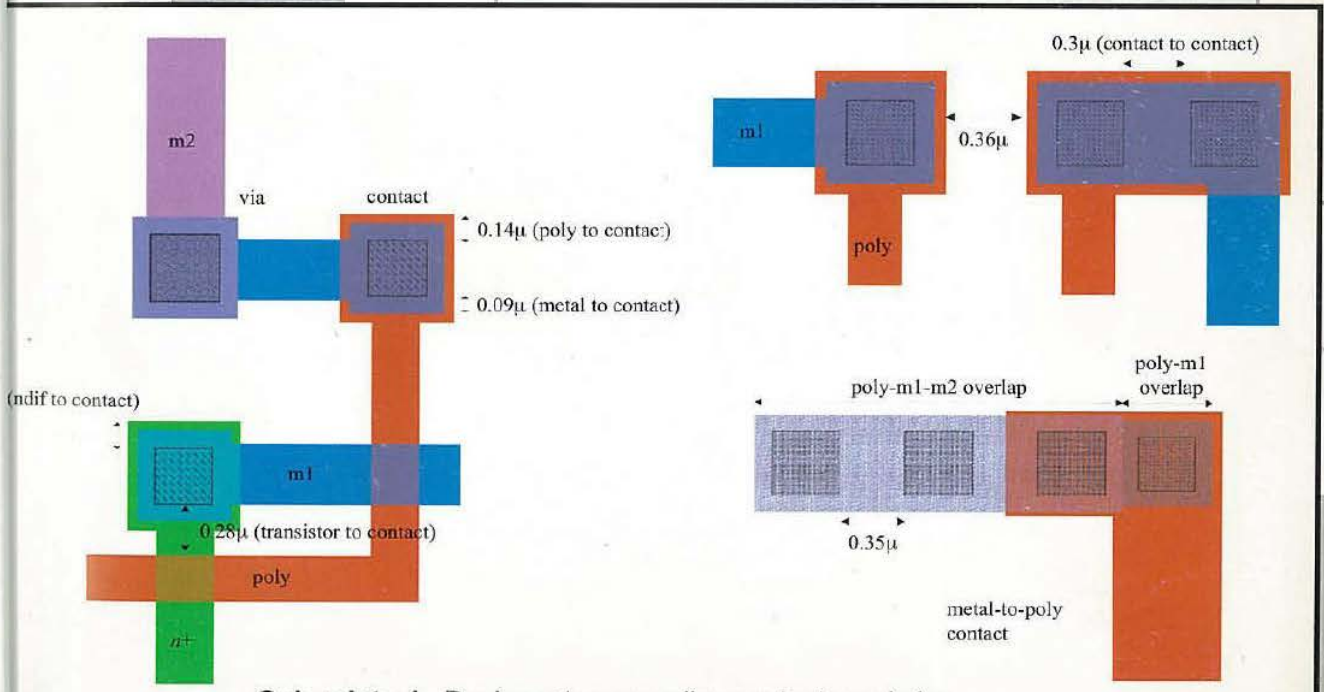
<b>Chapter 11</b>	<b>Designing Arithmetic Building Blocks</b>	<b>559</b>
11.1	Introduction	560
11.2	Datapaths in Digital Processor Architectures	560
11.3	The Adder	561
	11.3.1 The Binary Adder: Definitions	561
	11.3.2 The Full Adder: Circuit Design Considerations	564
	11.3.3 The Binary Adder: Logic Design Considerations	571
11.4	The Multiplier	586
	11.4.1 The Multiplier: Definitions	586
	11.4.2 Partial-Product Generation	587
	11.4.3 Partial-Product Accumulation	589
	11.4.4 Final Addition	593
	11.4.5 Multiplier Summary	594
11.5	The Shifter	594
	11.5.1 Barrel Shifter	595
	11.5.2 Logarithmic Shifter	596
11.6	Other Arithmetic Operators	596
11.7	Power and Speed Trade-offs in Datapath Structures*	600
	11.7.1 Design Time Power-Reduction Techniques	601
	11.7.2 Run-Time Power Management	611
	11.7.3 Reducing the Power in Standby (or Sleep) Mode	617
11.8	Perspective: Design as a Trade-off	618
11.9	Summary	619
11.10	To Probe Further	620
	References	621
<b>Chapter 12</b>	<b>Designing Memory and Array Structures</b>	<b>623</b>
12.1	Introduction	624
	12.1.1 Memory Classification	625
	12.1.2 Memory Architectures and Building Blocks	627
12.2	The Memory Core	634
	12.2.1 Read-Only Memories	634
	12.2.2 Nonvolatile Read-Write Memories	647
	12.2.3 Read-Write Memories (RAM)	657
	12.2.4 Contents-Addressable or Associative Memory (CAM)	670
12.3	Memory Peripheral Circuitry*	672
	12.3.1 The Address Decoders	672
	12.3.2 Sense Amplifiers	679
	12.3.3 Voltage References	686
	12.3.4 Drivers/Buffers	689
	12.3.5 Timing and Control	689

12.4	Memory Reliability and Yield*	693
12.4.1	Signal-to-Noise Ratio	693
12.4.2	Memory Yield	698
12.5	Power Dissipation in Memories*	701
12.5.1	Sources of Power Dissipation in Memories	701
12.5.2	Partitioning of the Memory	702
12.5.3	Addressing the Active Power Dissipation	702
12.5.4	Data-Retention Dissipation	704
12.5.5	Summary	707
12.6	Case Studies in Memory Design	707
12.6.1	The Programmable Logic Array (PLA)	707
12.6.2	A 4-Mbit SRAM	710
12.6.3	A 1-Gbit NAND Flash Memory	712
12.7	Perspective: Semiconductor Memory Trends and Evolutions	714
12.8	Summary	716
12.9	To Probe Further	717
	References	718
<b><i>Design Methodology Insert H Validation and Test</i></b>		
<b>of Manufactured Circuits</b>		<b>721</b>
H.1	Introduction	721
H.2	Test Procedure	722
H.3	Design for Testability	723
H.3.1	Issues in Design for Testability	723
H.3.2	Ad Hoc Testing	725
H.3.3	Scan-Based Test	726
H.3.4	Boundary-Scan Design	729
H.3.5	Built-in Self-Test (BIST)	730
H.4	Test-Pattern Generation	734
H.4.1	Fault Models	734
H.4.2	Automatic Test-Pattern Generation (ATPG)	736
H.4.3	Fault Simulation	737
H.5	To Probe Further	737
	References	737
<b>Problem Solutions</b>		<b>739</b>
<b>Index</b>		<b>745</b>

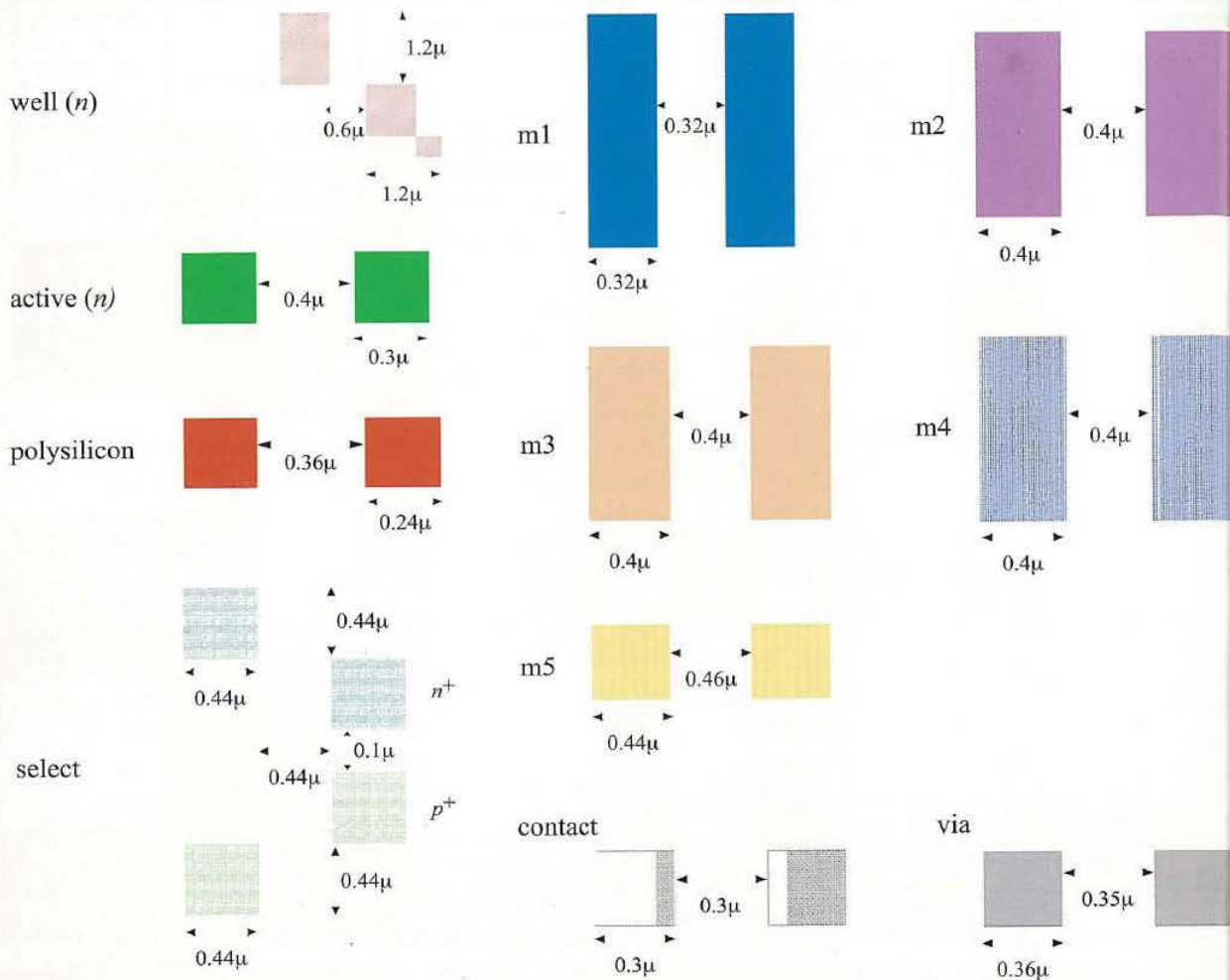
Layer Description	Representation				
metal	 m1	 m2	 m3	 m4	 m5
well	 nw				
polysilicon	 poly				
contacts & vias	 ct	 v12,v23,v34,v45	 nwc	 pwc	
active area and FETs	 ndif	 pdif	 nfet	 pfet	
select	 nplus	 pplus	 prb		



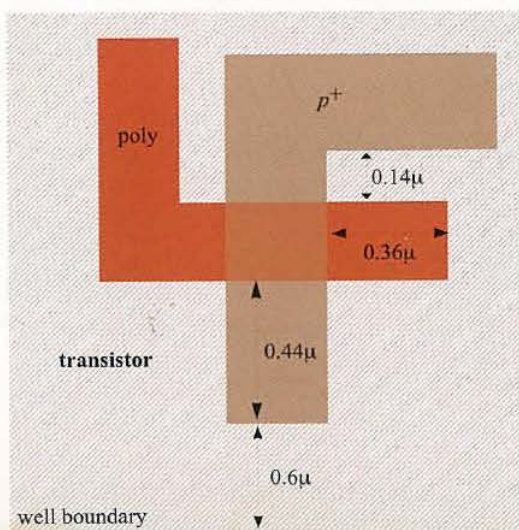
**Colorplate 1.** CMOS layers and representations (for vanilla 0.25  $\mu\text{m}$  CMOS process)



**Colorplate 4.** Design rules regarding contacts and vias. Overlapping layers are marked by merged colors.

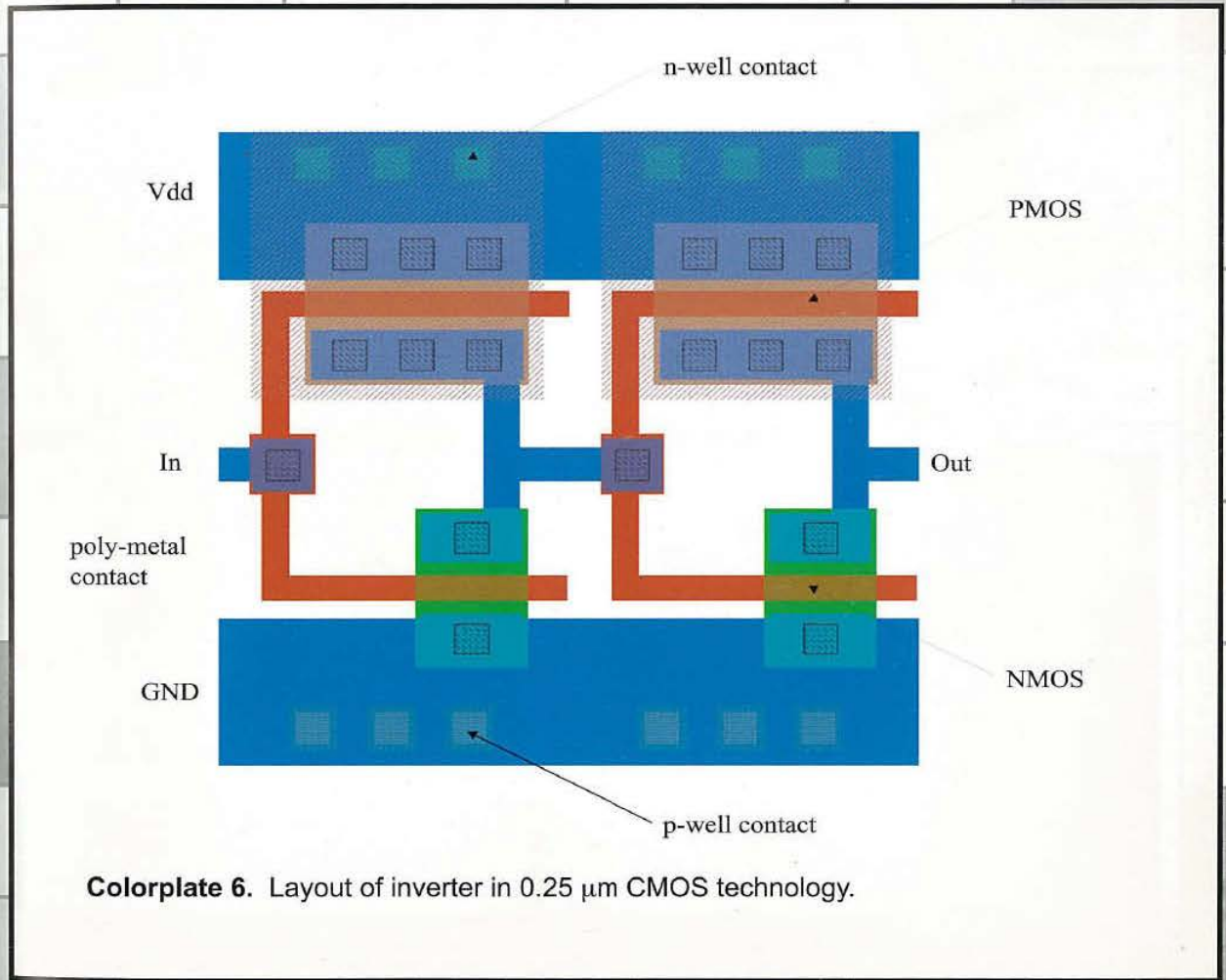
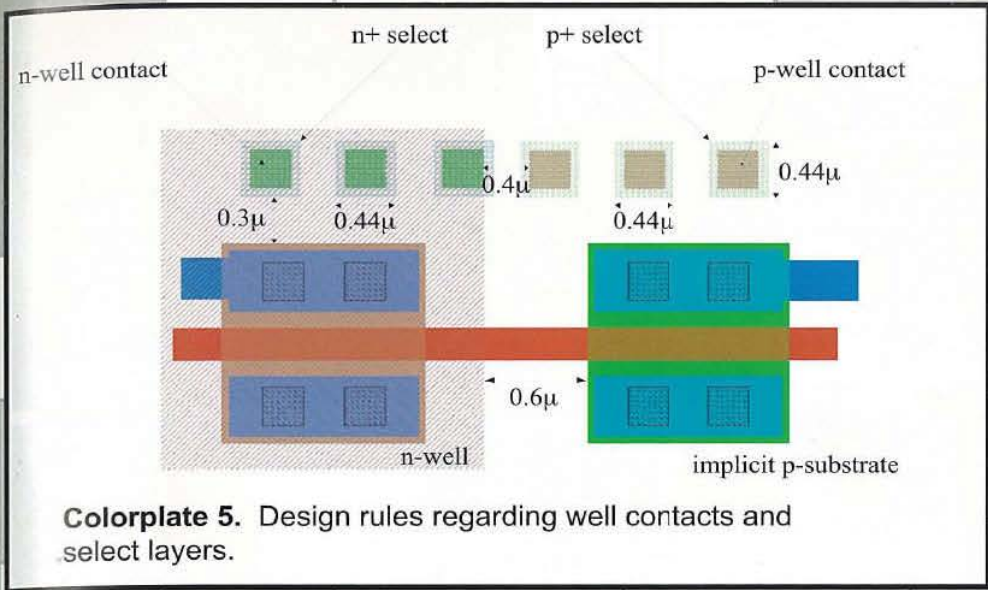


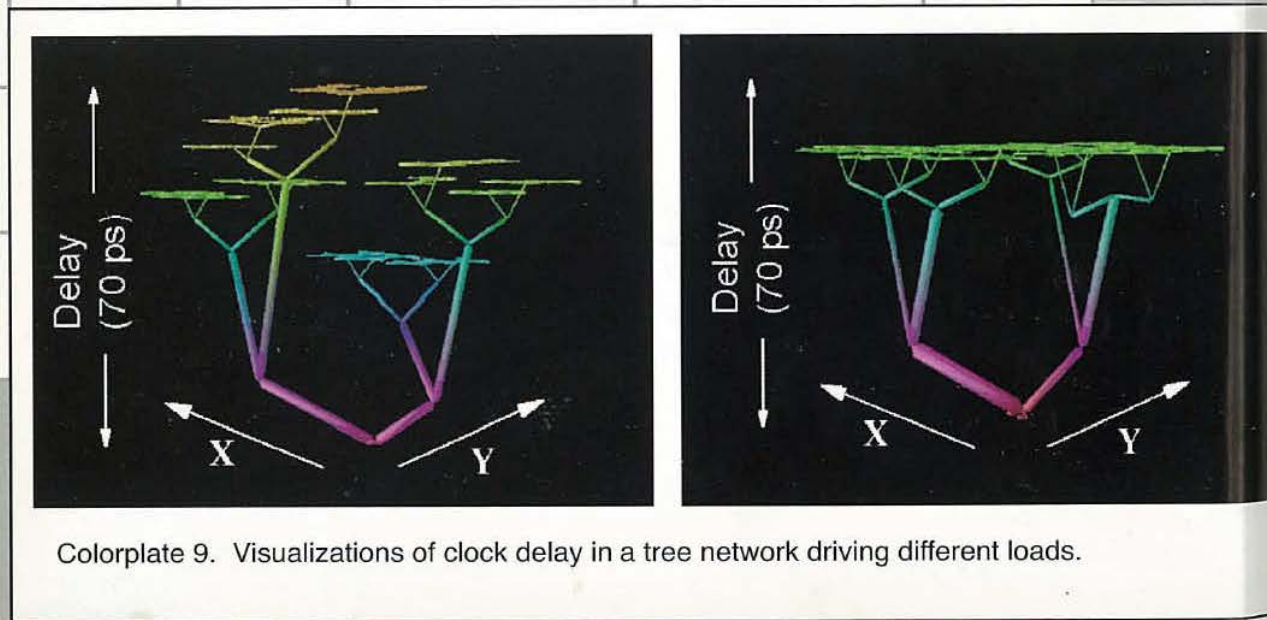
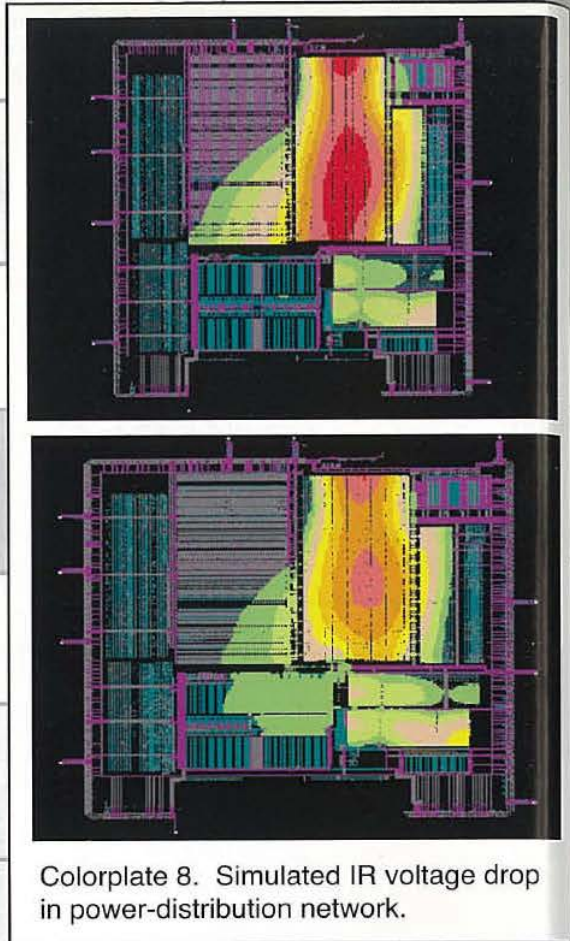
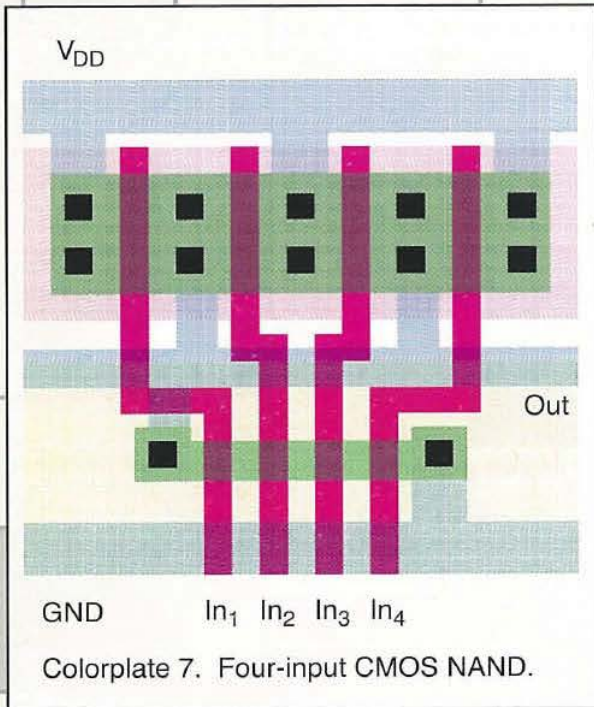
**Colorplate 2.** Intra-layer layout design rules, expressed as minimum dimensions and spacings.



**Colorplate 3.** Design rules concerning transistor layout. The device shown is a PMOS transistor.







## CHAPTER

# 2

# The Manufacturing Process

*Overview of manufacturing process*

*Design rules*

*IC packaging*

*Future Trends in Integrated Circuit Technology*

- 2.1 Introduction
- 2.2 Manufacturing CMOS Integrated Circuits
  - 2.2.1 The Silicon Wafer
  - 2.2.2 Photolithography
  - 2.2.3 Some Recurring Process Steps
  - 2.2.4 Simplified CMOS Process Flow
- 2.3 Design Rules—Between the Designer and the Process Engineer
- 2.4 Packaging Integrated Circuits
  - 2.4.1 Package Materials
  - 2.4.2 Interconnect Levels
  - 2.4.3 Thermal Considerations in Packaging
- 2.5 Perspective—Trends in Process Technology
  - 2.5.1 Short-Term Developments
  - 2.5.2 In the Longer Term
- 2.6 Summary
- 2.7 To Probe Further



## 2.1 Introduction

Most digital designers will never be confronted with the details of the manufacturing process that lay at the core of the semiconductor revolution. Still, some insight into the steps that lead to an operational silicon chip comes in quite handy in understanding the physical constraints imposed on a designer of an integrated circuit, as well as the impact of the fabrication process on issues such as cost.

In this chapter, we briefly describe the steps and techniques used in a modern integrated circuit manufacturing process. It is not our aim to present a detailed description of the fabrication technology, which easily deserves a complete course [Plummer00]. Rather, we aim at presenting the general outline of the flow and the interaction between the various steps. We learn that a set of *optical masks* forms the central interface between the intrinsics of the manufacturing process and the design that the user wants to see transferred to the silicon fabric. The masks define the patterns that, when transcribed onto the different layers of the semiconductor material, form the elements of the electronic devices and the interconnecting wires. As such, these patterns have to adhere to some constraints, in terms of minimum width and separation, if the resulting circuit is to be fully functional. This collection of constraints is called the *design rule set*, and acts as the contract between the circuit designer and the process engineer. If the designer adheres to these rules, he gets a guarantee that his circuit will be manufacturable. An overview of the common design rules encountered in modern CMOS processes is given, as well as a perspective on the *IC packaging* options. The package forms the interface between the circuit implemented on the silicon die and the outside world, and as such has a major impact on the performance, reliability, longevity, and cost of the integrated circuit.

## 2.2 Manufacturing CMOS Integrated Circuits

A simplified cross section of a typical CMOS inverter is shown in Figure 2-1. The CMOS process requires that both *n*-channel (NMOS) and *p*-channel (PMOS) transistors be built in the same silicon material. To accommodate both types of devices, special regions called *wells* must be created in which the semiconductor material is opposite to the type of the channel. A PMOS transistor has to be created in either an *n*-type substrate or an *n*-well, while an NMOS device resides in either a *p*-type substrate or a *p*-well. The cross section shown in Figure 2-1 features an

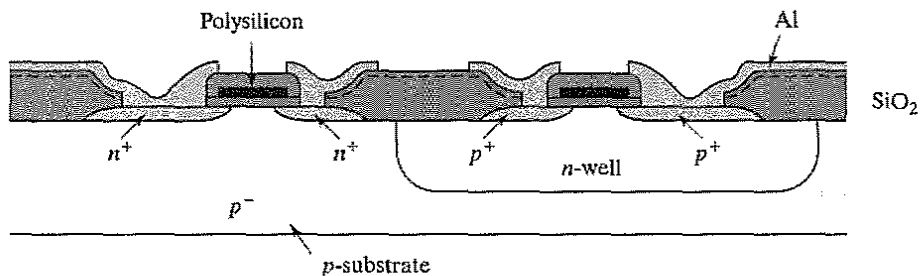


Figure 2-1 Cross section of an *n*-well CMOS process.

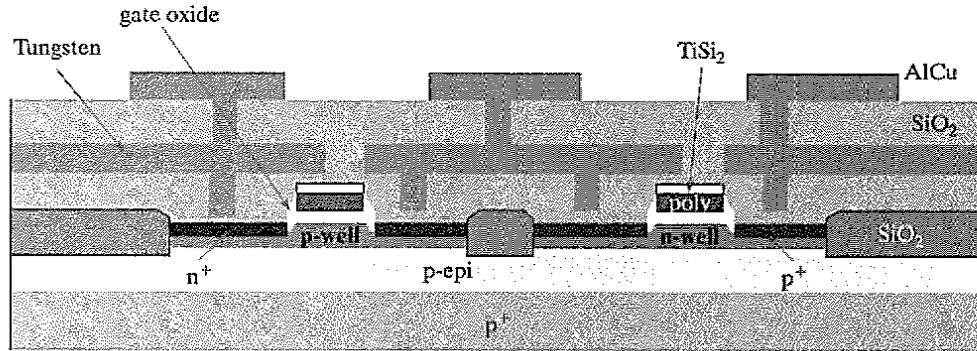


Figure 2-2 Cross section of modern dual-well CMOS process.

*n*-well CMOS process, where the NMOS transistors are implemented in the *p*-doped substrate, and the PMOS devices are located in the *n*-well. Modern processes are increasingly using a *dual-well* approach that uses both *n*- and *p*-wells, grown on top of an epitaxial layer, as shown in Figure 2-2.

The CMOS process requires a large number of steps, each of which consists of a sequence of basic operations. A number of these steps and/or operations are executed very repetitively in the course of the manufacturing process. Rather than immediately delving into a description of the overall process flow, we first discuss the starting material followed by a detailed perspective on some of the most frequently recurring operations.

### 2.2.1 The Silicon Wafer

The base material for the manufacturing process comes in the form of a single-crystalline, lightly doped *wafer*. These wafers have typical diameters between 4 and 12 inches (10 and 30 cm, respectively) and a thickness of, at most 1 mm. They are obtained by cutting a single-crystal ingot into thin slices (see Figure 2-3). A starting wafer of the *p*<sup>-</sup>-type might be doped around the levels of  $2 \times 10^{21}$  impurities/m<sup>3</sup>. Often, the surface of the wafer is doped more heavily, and a single crystal *epitaxial layer* of the opposite type is grown over the surface before the wafers are handed to the processing company. One important metric is the defect density of the base material. High defect densities lead to a larger fraction of nonfunctional circuits, and consequently an increase in cost of the final product.

### 2.2.2 Photolithography

In each processing step, a certain area on the chip is masked out using the appropriate optical mask so that a desired processing step can be selectively applied to the remaining regions. The processing step can be any of a wide range of tasks, including oxidation, etching, metal and polysilicon deposition, and ion implantation. The technique to accomplish this selective masking, called *photolithography*, is applied throughout the manufacturing process. Figure 2-4 gives

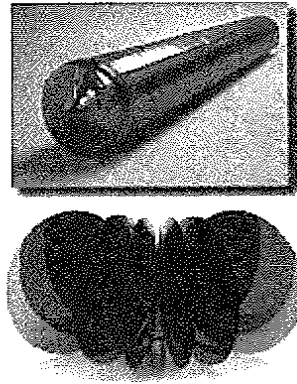


Figure 2-3 Single-crystal ingot and sliced wafers (from [Fullman99]).

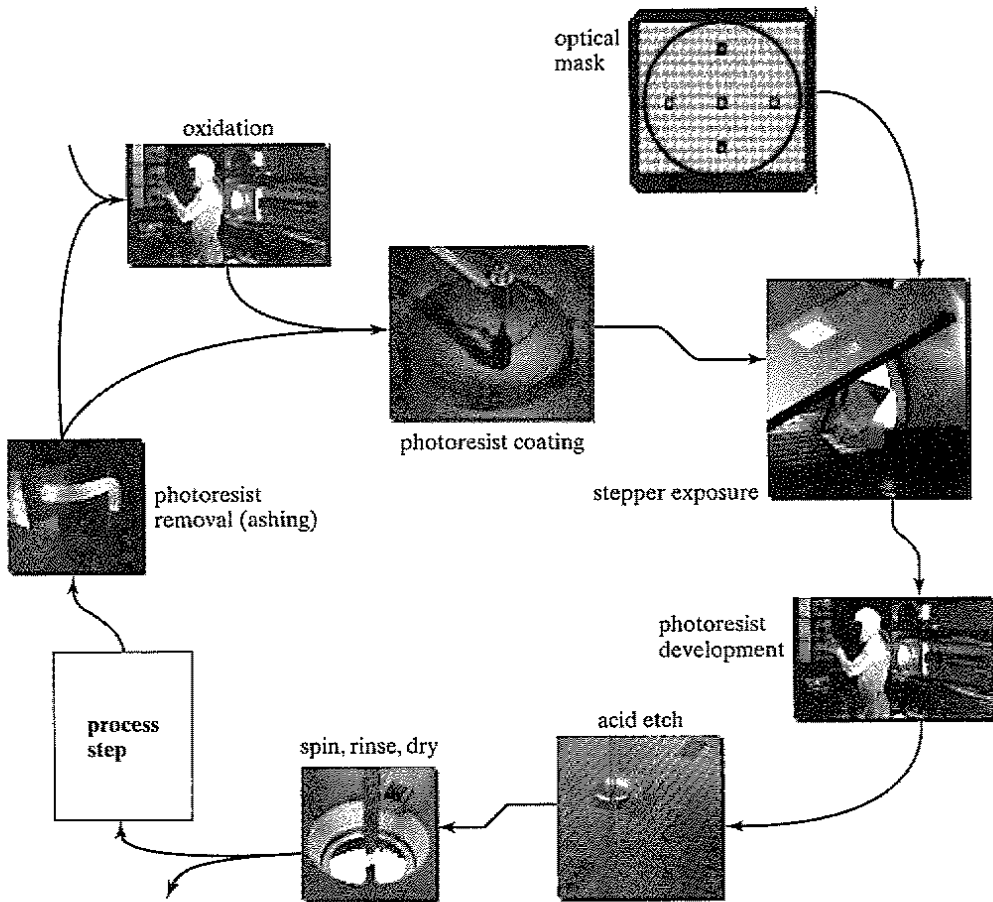


Figure 2-4 Typical operations in a single photolithographic cycle (from [Fullman99]).

a graphical overview of the different operations involved in a typical photolithographic process. The following steps can be identified:

1. *Oxidation layering*—this optional step deposits a thin layer of  $\text{SiO}_2$  over the complete wafer by exposing it to a mixture of high-purity oxygen and hydrogen at approximately  $1000^\circ\text{C}$ . The oxide is used as an insulation layer and also forms transistor gates.
2. *Photoresist coating*—a light-sensitive polymer (similar to latex) is evenly applied to a thickness of approximately  $1\ \mu\text{m}$  by spinning the wafer. This material is originally soluble in an organic solvent, but has the property that the polymers cross-link when exposed to light, making the affected regions insoluble. A photoresist of this type is called *negative*. A positive photoresist has the opposite properties; originally insoluble, but soluble after exposure. By using both positive and negative resists, a single mask can sometimes be used for two steps, making complementary regions available for processing. Since the cost of a mask is increasing quite rapidly with the scaling of technology, reducing the number of masks surely is a high priority.
3. *Stepper exposure*—a glass mask (or reticle) containing the patterns that we want to transfer to the silicon is brought in close proximity to the wafer. The mask is opaque in the regions that we want to process, and transparent in the others (assuming a negative photoresist). The glass mask can be thought of as the negative of one layer of the microcircuit. The combination of mask and wafer is now exposed to ultraviolet light. Where the mask is transparent, the photoresist becomes insoluble.
4. *Photoresist development and bake*—the wafers are developed in either an acid or base solution to remove the nonexposed areas of photoresist. Once the exposed photoresist is removed, the wafer is “soft baked” at a low temperature to harden the remaining photoresist.
5. *Acid etching*—material is selectively removed from areas of the wafer that are not covered by photoresist. This is accomplished through the use of many different types of acid, base and caustic solutions as a function of the material that is to be removed. Much of the work with chemicals takes place at large wet benches where special solutions are prepared for specific tasks. Because of the dangerous nature of some of these solvents, safety and environmental impact is a primary concern.
6. *Spin, rinse, and dry*—a special tool (called SRD) cleans the wafer with deionized water and dries it with nitrogen. The microscopic scale of modern semiconductor devices means that even the smallest particle of dust or dirt can destroy the circuitry. To prevent this from happening, the processing steps are performed in ultraclean rooms where the number of dust particles per cubic foot of air ranges between 1 and 10. Automatic wafer handling and robotics are used whenever possible. This explains why the cost of a state-of-the-art fabrication facility easily reaches multiple billions of dollars. Even then, the wafers must be constantly cleaned to avoid contamination and to remove the leftover of the previous process steps.

7. *Various process steps*—the exposed area can now be subjected to a wide range of process steps, such as ion implantation, plasma etching, or metal deposition. These are the subjects of the subsequent section.
8. *Photoresist removal (or ashing)*—a high-temperature plasma is used to selectively remove the remaining photoresist without damaging device layers.

In Figure 2-5, we illustrate the use of the photolithographic process for one specific example, the patterning of a layer of  $\text{SiO}_2$ . The sequence of process steps shown in the figure patterns exactly one layer of the semiconductor material and may seem very complex. Yet, the reader has to bear in mind that the same sequence patterns the layer of **the complete surface of the wafer**. Hence, it is a very parallel process, transferring hundreds of millions of patterns to the semiconductor surface simultaneously. The concurrent and scalable nature of the photolithographical process is what makes the cheap manufacturing of complex semiconductor circuits possible, and lies at the core of the economic success of the semiconductor industry.

The continued scaling of the minimum feature sizes in integrated circuits puts an enormous burden on the developer of semiconductor manufacturing equipment. This is especially true for the photolithographical process. The dimensions of the features to be transcribed surpass the wavelengths of the optical light sources, so that achieving the necessary resolution and accuracy

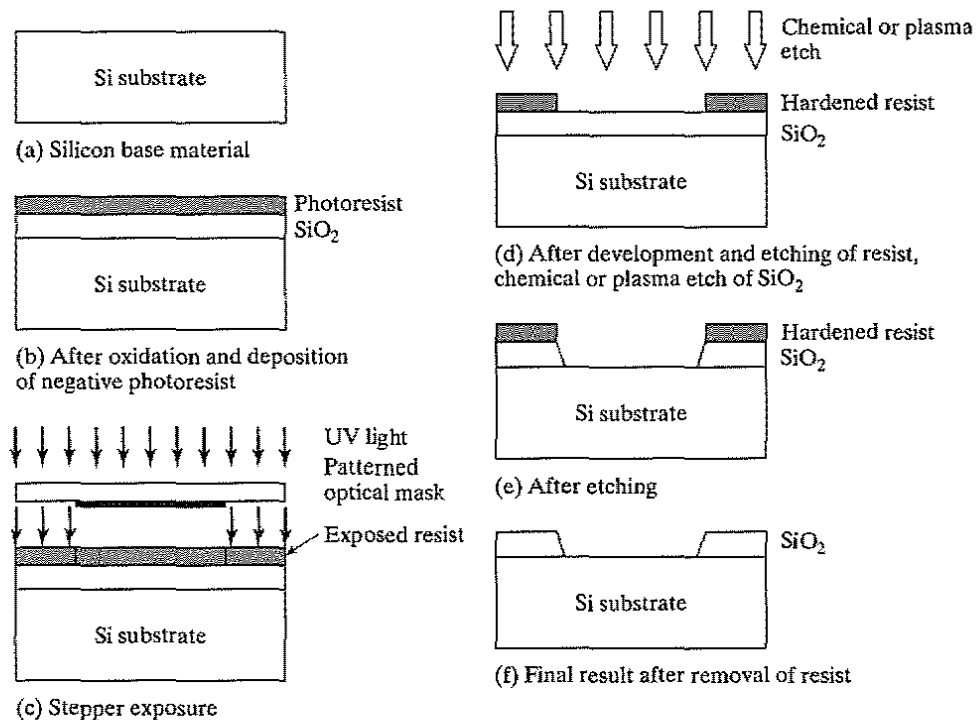


Figure 2-5 Process steps for patterning of  $\text{SiO}_2$ .

becomes more and more difficult. So far, electrical engineering has extended the lifetime of this process at least until the 100 nm (or 0.1  $\mu\text{m}$ ) process generation. Techniques such as *optical mask correction* (OPC) prewarp the drawn patterns to account for the diffraction phenomena, encountered when printing close to the wavelength of the available optical source. This adds substantially to the cost of mask making. In the foreseeable future, other solutions that offer a finer resolution, such as extreme ultraviolet (EUV), X ray, or electron beam, may be needed. These techniques, while fully functional, are currently less attractive from an economic viewpoint.

### 2.2.3 Some Recurring Process Steps

#### Diffusion and Ion Implantation

Many steps of the integrated circuit manufacturing process require a change in the dopant concentration of some parts of the material. Examples include the creation of the source and drain regions, well and substrate contacts, the doping of the polysilicon, and the adjustments of the device threshold. Two approaches exist for introducing these dopants—diffusion and ion implantation. In both techniques, the area to be doped is exposed, while the rest of the wafer is coated with a layer of buffer material, typically  $\text{SiO}_2$ .

In *diffusion implantation*, the wafers are placed in a quartz tube embedded in a heated furnace. A gas containing the dopant is introduced in the tube. The high temperatures of the furnace, typically 900 to 1100  $^{\circ}\text{C}$ , cause the dopants to diffuse into the exposed surface both vertically and horizontally. The final dopant concentration is the greatest at the surface and decreases in a gaussian profile deeper in the material.

In *ion implantation*, dopants are introduced as ions into the material. The ion implantation system directs and sweeps a beam of purified ions over the semiconductor surface. The acceleration of the ions determines how deep they will penetrate the material, while the beam current and the exposure time determine the dosage. The ion implantation method allows for an independent control of depth and dosage. This is the reason that ion implantation has largely displaced diffusion in modern semiconductor manufacturing.

Ion implantation has some unfortunate side effects, however, the most important one being lattice damage. Nuclear collisions during the high energy implantation cause the displacement of substrate atoms, leading to material defects. This problem is largely resolved by applying a subsequent *annealing* step, in which the wafer is heated to around 1000 $^{\circ}\text{C}$  for 15 to 30 minutes, and then allowed to cool slowly. The heating step thermally vibrates the atoms, which allows the bonds to reform.

#### Deposition

Any CMOS process requires the repetitive deposition of layers of a material over the complete wafer, to either act as buffers for a processing step, or as insulating or conducting layers. We have already discussed the oxidation process, which allows a layer of  $\text{SiO}_2$  to be grown. Other materials require different techniques. For instance, silicon nitride ( $\text{Si}_3\text{N}_4$ ) is used as a sacrificial buffer material during the formation of the field oxide and the introduction of the stopper

implants. This silicon nitride is deposited everywhere using a process called *chemical vapor deposition* or CVD. This process is based on a gas-phase reaction, with energy supplied by heat at around 850°C.

Polysilicon, on the other hand, is deposited using a chemical deposition process, which flows silane gas over the heated wafer coated with SiO<sub>2</sub> at a temperature of approximately 650°C. The resulting reaction produces a noncrystalline or amorphous material called *polysilicon*. To increase the conductivity of the material, the deposition has to be followed by an implantation step.

The Aluminum interconnect layers typically are deployed using a process known as *sputtering*. The aluminum is evaporated in a vacuum, with the heat for the evaporation delivered by electron-beam or ion-beam bombarding. Other metallic interconnect materials such as Copper require different deposition techniques.

### Etching

Once a material has been deposited, etching is used selectively to form patterns such as wires and contact holes. We already discussed the *wet etching* process, which makes use of acid or basic solutions. Hydrofluoric acid buffered with ammonium fluoride typically is used to etch SiO<sub>2</sub>, for example.

In recent years, *dry* or *plasma etching* has advanced substantially. A wafer is placed into the etch tool's processing chamber and given a negative electrical charge. The chamber is heated to 100°C and brought to a vacuum level of 7.5 Pa, then filled with a positively charged plasma (usually a mix of nitrogen, chlorine, and boron trichloride). The opposing electrical charges cause the rapidly moving plasma molecules to align themselves in a vertical direction, forming a microscopic chemical and physical "sandblasting" action which removes the exposed material. Plasma etching has the advantage of offering a well-defined directionality to the etching action, creating patterns with sharp vertical contours.

### Planarization

To reliably deposit a layer of material onto the semiconductor surface, it is essential that the surface be approximately flat. If special steps were not taken, this would definitely present problems in modern CMOS processes, where multiple patterned metal interconnect layers are superimposed onto each other. Therefore, a *chemical-mechanical planarization* (CMP) step is included before the deposition of an extra metal layer on top of the insulating SiO<sub>2</sub> layer. This process uses a slurry compound—a liquid carrier with a suspended abrasive component such as aluminum oxide or silica—to microscopically plane a device layer and to reduce the step heights.

#### 2.2.4 Simplified CMOS Process Flow

The gross outline of a potential CMOS process flow is given in Figure 2-6. The process starts with the definition of the *active regions*—these are the regions where transistors will be constructed. All other areas of the die will be covered with a thick layer of silicon dioxide (SiO<sub>2</sub>)

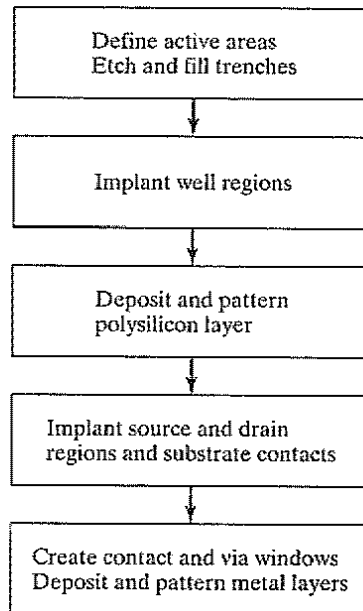


**Figure 2-6** Simplified process sequence for the manufacturing of a n-dual-well CMOS circuit.

called the *field oxide*. This oxide acts as the insulator between neighboring devices, and it is either grown (as in the process of Figure 2-1) or deposited in etched trenches (Figure 2-2)—hence, the name *trench insulation*. Further insulation is provided by the addition of a reverse-biased *np*-diode, formed by adding an extra  $p^+$  region called the *channel-stop implant* (or *field implant*) underneath the field oxide. Next, lightly doped *p*- and *n*-wells are formed through ion implantation. To construct an NMOS transistor in a *p*-well, heavily doped *n*-type *source* and *drain* regions are implanted (or diffused) into the lightly doped *p*-type substrate. A thin layer of  $\text{SiO}_2$  called the *gate oxide* separates the region between the source and drain, and is itself covered by conductive polycrystalline silicon (or *polysilicon*, for short). The conductive material forms the *gate* of the transistor. PMOS transistors are constructed in an *n*-well in a similar fashion (just reverse *n*'s and *p*'s). Multiple insulated layers of metallic (most often Aluminum) wires are deposited on top of these devices to provide for the necessary interconnections between the transistors.

A more detailed breakdown of the flow into individual process steps and their impact on the semiconductor material is shown graphically in Figure 2-7. While most of the operations should be self-explanatory in light of the previous descriptions, some comments on individual operations are worthwhile. The process starts with a *p*-substrate surfaced with a lightly doped *p*-epitaxial layer (a). A thin layer of  $\text{SiO}_2$  is then deposited, which will serve as the gate oxide for the transistors, followed by a deposition of a thicker sacrificial silicon nitride layer (b). A plasma etching step using the complementary of the active area mask creates the trenches used for insulating the devices (c). After providing the channel stop implant, the trenches are filled



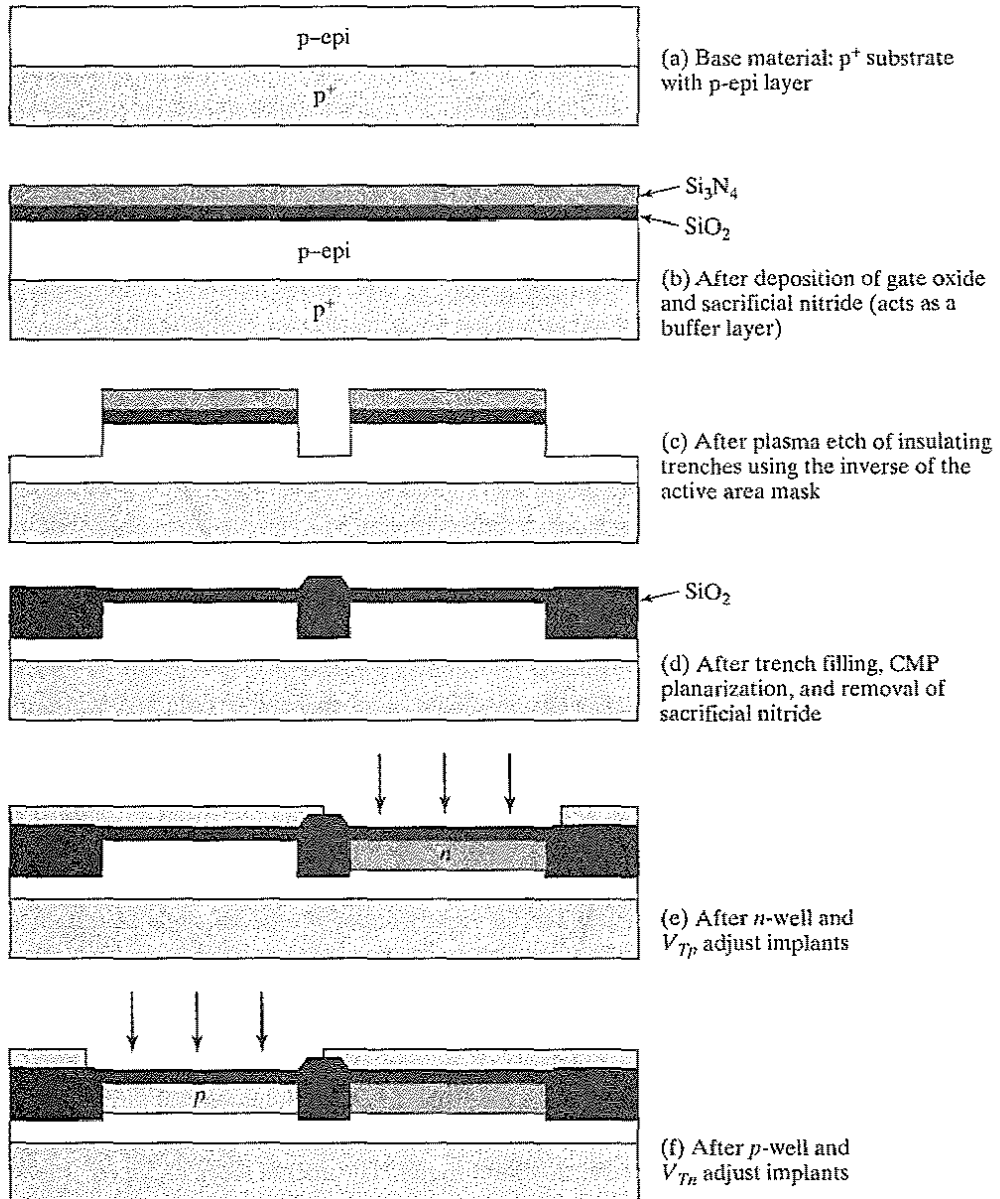


**Figure 2-7** Process flow for the fabrication of an NMOS and a PMOS transistor in a dual-well CMOS process. Be aware that the drawings are stylized for understanding and that the aspect ratios are not proportioned to reality.

with  $\text{SiO}_2$  followed by a number of steps to provide a flat surface (including inverse active pattern oxide etching, and chemical-mechanical planarization). At that point, the sacrificial nitride is removed (d). The  $n$ -well mask is used to expose only the  $n$ -well areas (the rest of the wafer is covered by a thick buffer material), after which an implant-annealing sequence is applied to

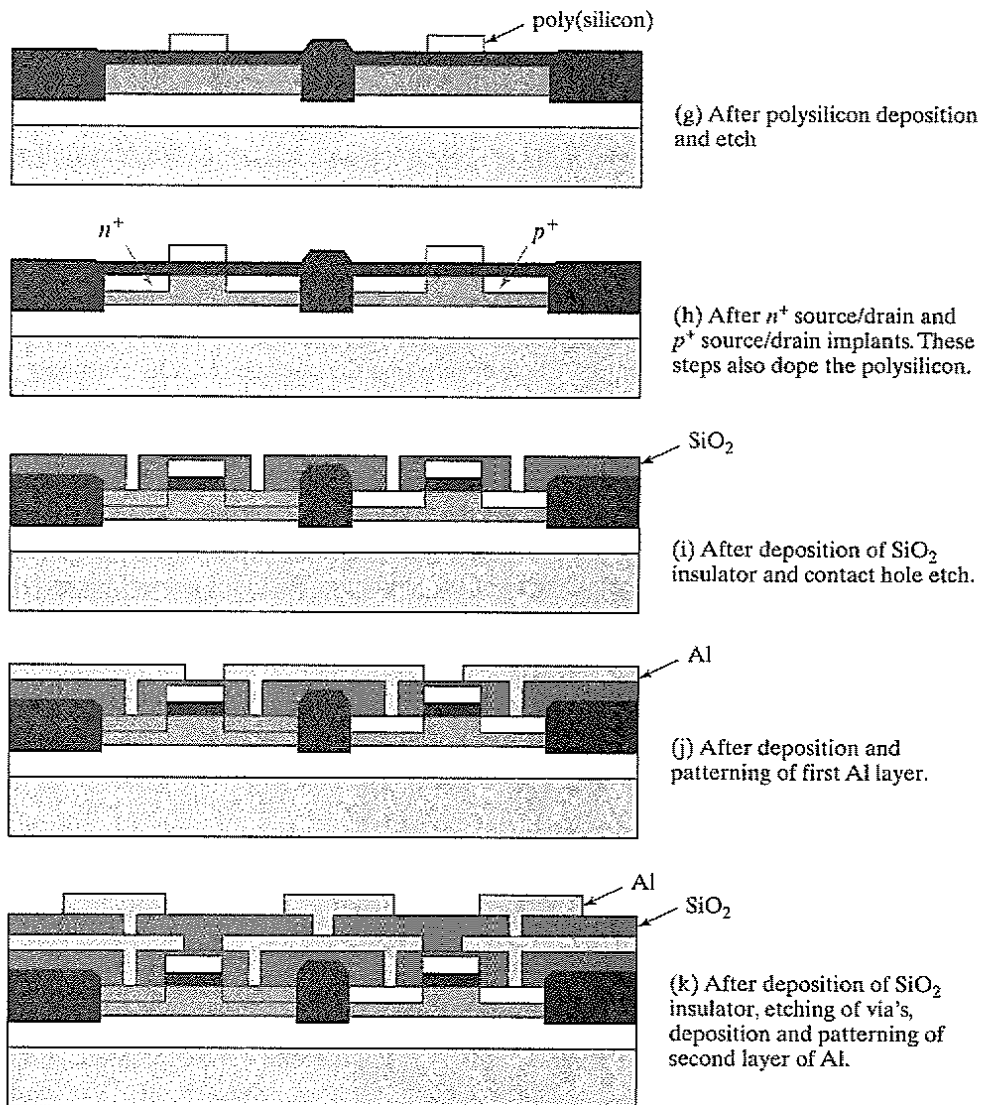


Figure 2-7 (cont.)

adjust the well-doping. This is followed by a second implant step to adjust the threshold voltages of the PMOS transistors. This implant only impacts the doping in the area just below the gate oxide (e). Similar operations (using other dopants) are performed to create the  $p$ -wells, and to adjust the thresholds of the NMOS transistors (f). A thin layer of polysilicon is chemically deposited and patterned with the aid of the polysilicon mask. Polysilicon is used both as gate electrode material for the transistors and as an interconnect medium (g). Consecutive ion implantations are used to dope the source and drain regions of the PMOS ( $p^+$ ) and NMOS ( $n^+$ ) transistors, respectively (h), after which the thin gate oxide not covered by the polysilicon is

etched away.<sup>1</sup> The same implants also are used to dope the polysilicon on the surface, reducing its resistivity. Undoped polysilicon has a very high resistivity. Note that the polysilicon gate, which is patterned before the doping, actually defines the precise location of the channel region, and thus the location of the source and drain regions. This procedure, called the *self-aligned process*, allows for a very precise positioning of the two regions relative to the gate. Self-alignment is instrumental in reducing parasitic capacitances in the transistor. The process continues with the deposition of the metallic interconnect layers. These consist of a repetition of the following steps (i–k): deposition of the insulating material (most often  $\text{SiO}_2$ ), etching of the contact or via holes, deposition of the metal (most often aluminum and copper, although tungsten often is used for the lower layers), and patterning of the metal. Intermediate planarization steps, using *chemical–mechanical polishing* or *CMP*, ensure that the surface remains reasonably flat, even in the presence of multiple interconnect layers. After the last level of metal is deposited, a final passivation or *overglass* is deposited for protection. This layer would be CVD  $\text{SiO}_2$ , although often an additional layer of nitride is deposited because it is more impervious to moisture. The final processing step etches openings to the pads used for bonding.

A cross section of the final artifact is shown in Figure 2-8. Observe how the transistors occupy only a small fraction of the total height of the structure. The interconnect layers take up the majority of the vertical dimension.

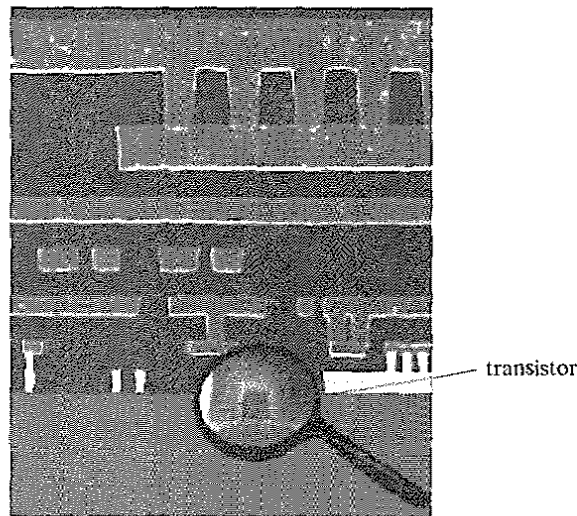


Figure 2-8 Cross section of state-of-the-art CMOS process.

<sup>1</sup>Most modern processes also include extra implants for the creation of the lightly doped drain regions (LDD), and the creation of gate spacers at this point. We have omitted these for the sake of simplicity.

### 2.3 Design Rules—Between the Designer and the Process Engineer

As processes become more complex, requiring the designer to understand the intricacies of the fabrication process and interpret the relations between the different masks is a sure road to trouble. The goal of defining a set of design rules is to allow for a ready translation of a circuit concept into an actual geometry in silicon. The design rules act as the interface or even the contract between the circuit designer and the process engineer.

Circuit designers generally want tighter, smaller designs, which lead to higher performance and higher circuit density. The process engineer, on the other hand, wants a reproducible and high-yield process. Consequently, design rules are a compromise that attempts to satisfy both sides.

The design rules provide a set of guidelines for constructing the various masks needed in the patterning process. They consist of minimum-width and minimum-spacing constraints and requirements between objects on the same or different layers.

The fundamental unity in the definition of a set of design rules is the *minimum line width*. It stands for the minimum mask dimension that can be safely transferred to the semiconductor material. In general, the minimum line width is set by the resolution of the patterning process, which is most commonly based on optical lithography. More advanced approaches use electron-beam EUV, or X-ray sources, all of which offer a finer resolution, but currently they are less attractive from an economical standpoint.

Even for the same minimum dimension, design rules tend to differ from company to company, and from process to process. This makes porting an existing design between different processes a time-consuming task. One approach to address this issue is to use advanced CAD techniques, which allow for migration between compatible processes. Another approach is to use *scalable design rules*. The latter approach, made popular by Mead and Conway [Mead80], defines all rules as a function of a single parameter, most often called  $\lambda$ . The rules are chosen so that a design is easily ported over a cross section of industrial processes. Scaling of the minimum dimension is accomplished by simply changing the value of  $\lambda$ . This results in a *linear scaling* of all dimensions. For a given process,  $\lambda$  is set to a specific value, and all design dimensions are consequently translated into absolute numbers. Typically, the minimum line width of a process is set to  $2\lambda$ . For instance, for a  $0.25\ \mu\text{m}$  process (i.e., a process with a minimum line width of  $0.25\ \mu\text{m}$ ),  $\lambda$  equals  $0.125\ \mu\text{m}$ .

This approach, while attractive, suffers from two disadvantages:

1. Linear scaling is possible only over a limited range of dimensions (for instance, between  $0.25\ \mu\text{m}$  and  $0.18\ \mu\text{m}$ ). When scaling over larger ranges, the relations between the different layers tend to vary in a nonlinear way that cannot be adequately covered by the linear scaling rules.
2. Scalable design rules are conservative: They represent a cross section over different technologies, and they must represent the worst case rules for the whole set. This results in overdimensioned and less dense designs.

For these and other reasons, scalable design rules normally are avoided by industry.<sup>2</sup> As circuit density is a prime goal in industrial designs, most semiconductor companies tend to use *micron rules*, which express the design rules in absolute dimensions and therefore can exploit the features of a given process to a maximum degree. Scaling and porting designs between technologies under these rules is more demanding and has to be performed either manually or using advanced CAD tools.

For this book, we have selected a “vanilla” 0.25  $\mu\text{m}$  CMOS process as our preferred implementation medium. The rest of this section is devoted to a short introduction and overview of the design rules of this process, which fall in the micron-rules class. A complete design-rule set consists of the following entities: a set of layers, relations between objects on the same layer, and relations between objects on different layers. We discuss each of them in sequence.

### Layer Representation

The layer concept translates the intractable set of masks currently used in CMOS into a simple set of conceptual layout levels that are easier to visualize by the circuit designer. From a designer’s viewpoint, all CMOS designs are based on the following entities:

- *Substrates and/or wells*, which are *p*-type (for NMOS devices) and *n*-type (for PMOS)
- *Diffusion regions* ( $n^+$  and  $p^+$ ), which define the areas where transistors can be formed. These regions are often called the *active areas*. Diffusions of an inverse type are needed to implement contacts to the wells or to the substrate. These are called *select regions*.
- One or more *polysilicon* layers, which are used to form the gate electrodes of the transistors (but serve as interconnect layers as well).
- A number of *metal interconnect* layers.
- *Contact and via* layers, which provide interlayer connections.

A layout consists of a combination of polygons, each of which is attached to a certain layer. The functionality of the circuit is determined by the choice of the layers, as well as the interplay between objects on different layers. For example, an MOS transistor is formed by the cross section of the diffusion layer and the polysilicon layer. An interconnection between two metal layers is formed by a cross section between the two metal layers and an additional contact layer. To visualize these relations, each layer is assigned a standard color (or stipple pattern for a black-and-white representation). The different layers used in our CMOS process are represented in Colorplate 1 (color insert).

### Intralayer Constraints

A first set of rules defines the minimum dimensions of objects on each layer, as well as the minimum spacings between objects on the same layer. All distances are expressed in  $\mu\text{m}$ . These constraints are presented in pictorial fashion in Colorplate 2.

---

<sup>2</sup>While not entirely accurate, lambda rules are still useful to estimate the impact of a technology scale on the area of a design.

### Interlayer Constraints

Interlayer rules tend to be more complex. Because multiple layers are involved, it is harder to visualize their meaning or functionality. Understanding layout requires the capability of translating the two-dimensional picture of the layout drawing into the three-dimensional reality of the actual device. This takes some practice.

We present these rules in a set of separate groupings:

1. *Transistor Rules* (Colorplate 3). A transistor is formed by the overlap of the active and the polysilicon layers. From the intralayer design rules, it is already clear that the minimum length of a transistor equals  $0.24\ \mu\text{m}$  (the minimum width of polysilicon), while its width is at least  $0.3\ \mu\text{m}$  (the minimum width of diffusion). Extra rules include the spacing between the active area and the well boundary, the gate overlap of the active area, and the active overlap of the gate.
2. *Contact and Via Rules* (Colorplates 2 and 4). A contact (which forms an interconnection between metal and active or polysilicon) or a via (which connects two metal layers) is formed by overlapping the two interconnecting layers and providing a contact hole, filled with metal, between the two. In our process, the minimum size of the contact hole is  $0.3\ \mu\text{m}$ , while the polysilicon and diffusion layers have to extend at least  $0.14\ \mu\text{m}$  beyond the area of the contact hole. This sets the minimum area of a contact to  $0.44\ \mu\text{m} \times 0.44\ \mu\text{m}$ . This is larger than the dimensions of a minimum-size transistor! Excessive changes between interconnect layers in routing should therefore be avoided. The figure, furthermore, points out the minimum spacings between contact and via holes, as well as their relationship with the surrounding layers.
3. *Well and Substrate Contacts* (Colorplate 5). For robust digital circuit design, it is important for the well and substrate regions to be adequately connected to the supply voltages. Failing to do so results in a resistive path between the substrate contact of the transistors and the supply rails, and can lead to possibly devastating parasitic effects, such as latchup. It is therefore advisable to provide numerous substrate (well) contacts spread over the complete region. To establish an ohmic contact between a supply rail, implemented in metal, and a  $p$ -type material, a  $p^+$  diffusion region must be provided. This is enabled by the *select* layer, which reverses the type of diffusion. A number of rules regarding the use of the *select* layer are illustrated in Colorplate 5.

Consider an  $n$ -well process, which implements the PMOS transistors into an  $n$ -type well diffused in a  $p$ -type material. The nominal diffusion is  $p^+$ . To invert the polarity of the diffusion, an  $n$ -select layer is provided that helps to establish the  $n^+$  diffusions for the well contacts in the  $n$ -region, as well as the  $n^+$  source and drain regions for the NMOS transistors in the substrate.

### Verifying the Layout

Ensuring that none of the design rules are violated is a fundamental requirement of the design process. Failing to do so will almost surely lead to a nonfunctional design. Doing so for a complex design that can contain millions of transistors is no simple task either, especially given the complexity of some design-rule sets. While design teams in the past used to spend numerous

hours staring at room-size layout plots, most of this work is now done by computers. Computer-aided *Design-Rule Checking* (called *DRC*) is an integral part of the design cycle for virtually every chip produced today. A number of layout tools even perform *on-line DRC* and check the design in the background during the time of conception.

### Example 2.1 Layout Example

An example of a complete layout containing an inverter is shown in Figure 2-9. To help the visualization process, a vertical cross section of the process along the design center is included, as well as a circuit schematic.

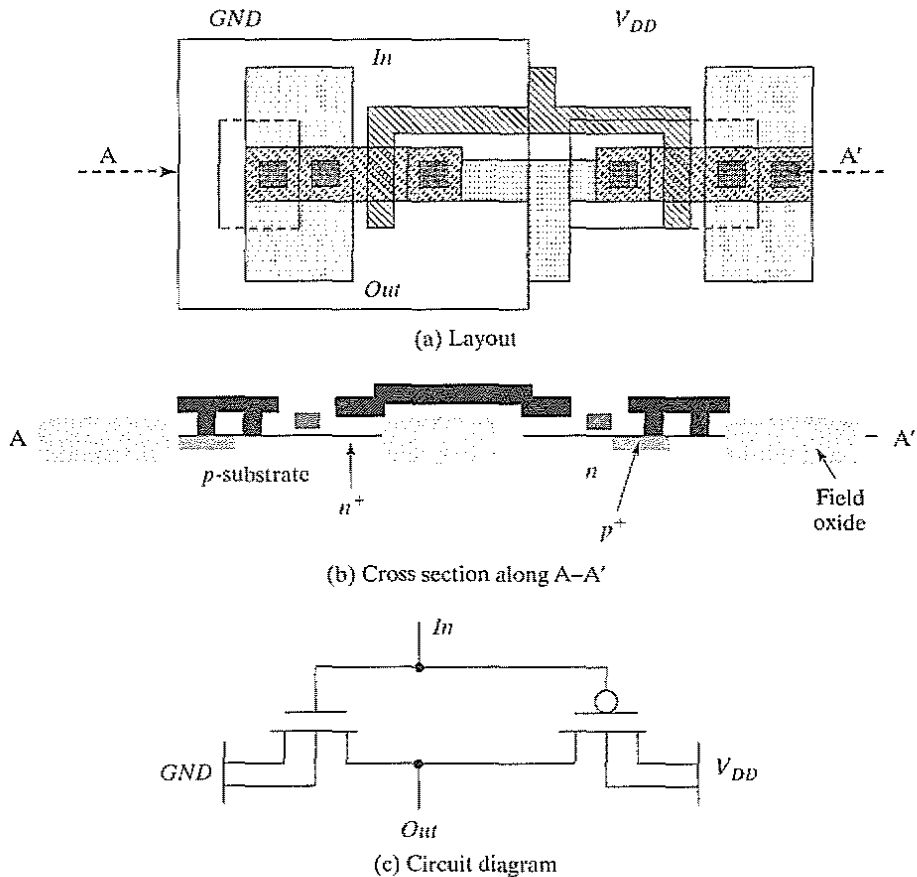


**Figure 2-9** A detailed layout example, including vertical process cross section and circuit diagram.

It is left as an exercise for the reader to determine the sizes of both the NMOS and the PMOS transistors.

## 2.4 Packaging Integrated Circuits

The IC package plays a fundamental role in the operation and performance of a component. Besides providing a means of bringing signal and supply wires in and out of the silicon die, it also removes the heat generated by the circuit and provides mechanical support. Finally, it also protects the die against environmental conditions such as humidity.

In addition, the packaging technology has a major impact on the performance and power dissipation of a microprocessor or signal processor. This influence is getting more pronounced as time progresses due to the reduction in internal signal delays and on-chip capacitance resulting from technology scaling. Currently, up to 50% of the delay of a high-performance computer is due to packaging delays, and this number is expected to rise. The search for higher performance packages with fewer inductive or capacitive parasitics has accelerated in recent years. The increasing complexity of what can be integrated on a single die also translates into a need for ever more input/output pins, as the number of connections going off-chip tends to be roughly proportional to the complexity of the circuitry on the chip. This relationship was first observed by E. Rent of IBM (published in [Landman71]), who translated it into an empirical formula that, appropriately, is called *Rent's rule*. This formula relates the number of input/output pins to the complexity of the circuit, as measured by the number of gates. It is written as

$$P = K \times G^\beta \quad (2.1)$$

where  $K$  is the average number of I/Os per gate,  $G$  the number of gates,  $\beta$  the Rent exponent, and  $P$  the number of I/O pins to the chip.  $\beta$  varies between 0.1 and 0.7. Its value depends strongly upon the application area, architecture, and organization of the circuit, as demonstrated in Table 2-1. Clearly, microprocessors display a very different input/output behavior compared to memories.

The observed rate of pin-count increase for integrated circuits varies from 8% to 11% per year, and it has been projected that packages with more than 2000 pins will be required by 2010. For all these reasons, traditional dual-in-line, through-hole mounted packages have been replaced by other approaches, such as surface-mount, ball-grid array, and multichip module

**Table 2-1** Rent's constant for various classes of systems ([Bakoglu90])

Application	$\beta$	$K$
Static memory	0.12	6
Microprocessor	0.45	0.82
Gate array	0.5	1.9
High-speed computer (chip)	0.63	1.4
High-speed computer (board)	0.25	82



techniques. It is useful for the circuit designer to be aware of the available options and their pros and cons.

Due to its multifunctionality, a good package must comply with a large variety of requirements:

- **Electrical requirements**—Pins should exhibit low capacitance (both interwire and to the substrate), resistance, and inductance. A large characteristic impedance should be tuned to optimize transmission line behavior. Observe that intrinsic integrated-circuit impedances are high.
- **Mechanical and thermal properties**—The heat removal rate should be as high as possible. Mechanical reliability requires a good matching between the thermal properties of the die and the chip carrier. Long-term reliability requires a strong connection from die to package, as well as from package to board.
- **Low Cost**—Cost is one of the more important properties to consider in any project. For example, while ceramics have a superior performance over plastic packages, they are also substantially more expensive. Increasing the heat removal capacity of a package also tends to raise the package cost. The least expensive plastic packaging can dissipate up to 1 W. Slightly more expensive, but still of somewhat low quality, plastic packages can dissipate up to 2 W. Higher dissipation requires more expensive ceramic packaging. Chips dissipating over 20 W require special heat sink attachments. Even more extreme techniques such as fans and blowers, liquid cooling hardware, or heat pipes are needed for higher dissipation levels.

Packing density is a major factor in reducing board cost. The increasing pin count either requires an increase in the package size or a reduction in the pitch between the pins. Both have a profound effect on the packaging economics.

Packages can be classified in many different ways: by their main material, the number of interconnection levels, and the means used to remove heat. In this brief section, we provide only sketches of each of those issues.

### 2.4.1 Package Materials

The most common materials used for the package body are ceramic and polymers (plastics). The latter have the advantage of being substantially cheaper, but they suffer from inferior thermal properties. For example, the ceramic  $\text{Al}_2\text{O}_3$  (alumina) conducts heat better than  $\text{SiO}_2$  and the polyimide plastic by factors of 30 and 100, respectively. Furthermore, its thermal expansion coefficient is substantially closer to the typical interconnect metals. The disadvantage of alumina and other ceramics is their high dielectric constant, which results in large interconnect capacitances.

### 2.4.2 Interconnect Levels

The traditional packaging approach uses a two-level interconnection strategy. The die is first attached to an individual chip carrier or substrate. The package body contains an internal cavity where the chip is mounted. These cavities provide ample room for many connections to the chip leads (or pins). The leads compose the second interconnect level and connect the chip to the global interconnect medium, which normally is a PC board. Complex systems contain even more interconnect levels, since boards are connected together using backplanes or ribbon cables. The first two layers of the interconnect hierarchy are illustrated in the drawing of Figure 2-10. The sections that follow provide a brief overview of the interconnect techniques used at levels one and two of the interconnect hierarchy, and a brief discussion of some more advanced packaging approaches.

#### Interconnect Level 1—Die-to-Package Substrate

For a long time, *wire bonding* was the technique of choice to provide an electrical connection between die and package. In this approach, the backside of the die is attached to the substrate using glue with a good thermal conductance. Next, the chip pads are individually connected to the lead frame with aluminum or gold wires. The wire-bonding machine used for this purpose operates much like a sewing machine. An example of wire bonding is shown in Figure 2-11. Although the wire-bonding process is automated to a large degree, it has some major disadvantages:

1. Wires must be attached serially, one after the other. This leads to longer manufacturing times with increasing pin counts.
2. Larger pin counts make it substantially more challenging to find bonding patterns that avoid shorts between the wires.
3. The exact value of the parasitics is hard to predict because of the manufacturing approach and irregular outlay.

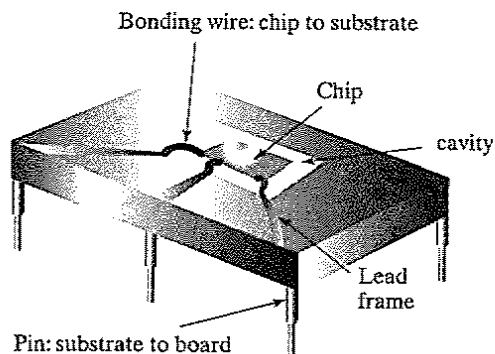
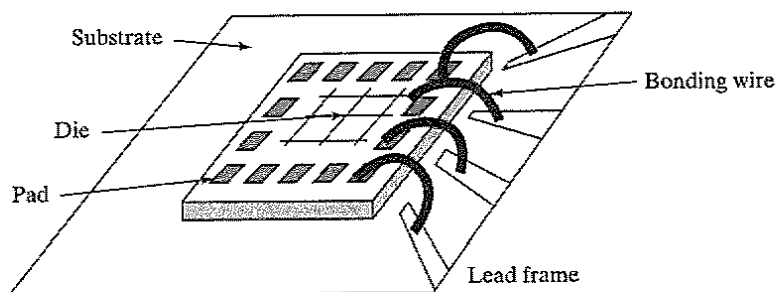


Figure 2-10 Interconnect hierarchy in traditional IC packaging.



**Figure 2-11** Wire bonding.

Bonding wires have inferior electrical properties, such as a high individual inductance (5 nH or more) and mutual inductance with neighboring signals. The inductance of a bonding wire is typically about 1 nH/mm, while the inductance per package pin ranges between 7 and 40 nH per pin, depending on the type of package as well as the positioning of the pin on the package boundary [Steidel83]. Typical values of the parasitic inductances and capacitances for a number of commonly used packages are summarized in Table 2-2.

New attachment techniques are being explored as a result of these deficiencies. In one approach, called *Tape Automated Bonding* (or TAB), the die is attached to a metal lead frame that is printed on a polymer film, typically polyimide (see Figure 2-12a). The connection between chip pads and polymer film wires is made using solder bumps (Figure 2-12b). The tape can then be connected to the package body using a number of techniques. One possible approach is to use pressure connectors.

The advantage of the TAB process is that it is highly automated. The sprockets in the film are used for automatic transport. All connections are made simultaneously. The printed approach helps to reduce the wiring pitch, which results in higher lead counts. Elimination of the long bonding wires improves the electrical performance. For instance, for a two-conductor layer, 48 mm

**Table 2-2** Typical capacitance and inductance values of package and bonding styles (from [Steidel83], [Franzon93], and [Harper00]).

Package Type	Capacitance (pF)	Inductance (nH)
68-pin plastic DIP	4	35
68-pin ceramic DIP	7	20
300 pin Ball Grid Array	1–5	2–15
Wire bond	0.5–1	1–2
Solder bump	0.1–0.5	0.01–0.1

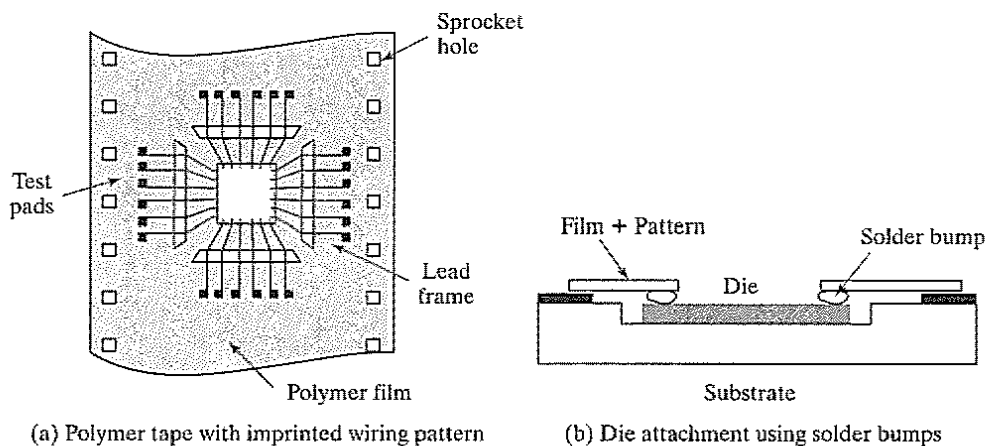


Figure 2-12 Tape-automated bonding (TAB).

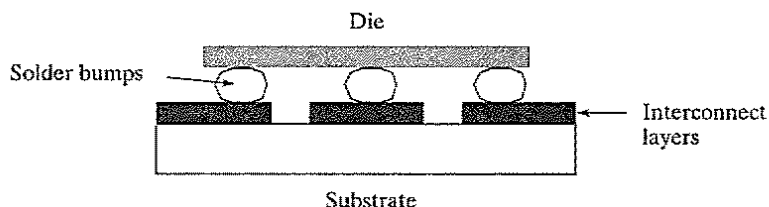


Figure 2-13 Flip-chip bonding.

TAB Circuit, the following electrical parameters hold:  $L \approx 0.3\text{--}0.5$  nH,  $C \approx 0.2\text{--}0.3$  pF, and  $R \approx 50\text{--}200$   $\Omega$  [Doane93, p. 420].

Another approach is to flip the die upside down and attach it directly to the substrate using solder bumps. This technique, called *flip-chip* mounting, has the advantage of a superior electrical performance (see Figure 2-13.) Instead of making all the I/O connections on the die boundary, pads can be placed at any position on the chip. This can help address the power- and clock-distribution problems, since the interconnect materials on the substrate (e.g., Cu or Au) typically are of better quality than the Al on the chip.

### Interconnect Level 2—Package Substrate to Board

When connecting the package to the PC board, *through-hole mounting* has been the packaging style of choice. A PC board is manufactured by stacking layers of copper and insulating epoxy glass. In the through-hole mounting approach, holes are drilled through the board and plated with copper. The package pins are inserted and electrical connection is made with solder (see Figure 2-14a). The favored package in this class was the *dual-in-line* package or DIP, as in Figure 2-15-2. The packaging density of the DIP degrades rapidly when the number of pins exceeds 64. This problem can be alleviated by using the *pin-grid-array* (PGA) package that has

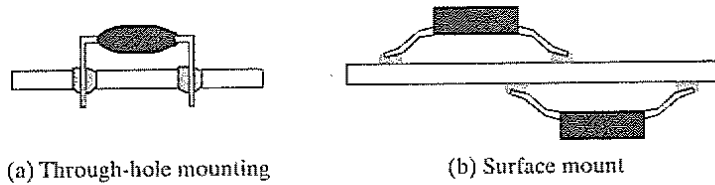


Figure 2-14 Board-mounting approaches.

leads on the entire bottom surface instead of only on the periphery (Figure 2-15-3). PGAs can extend to large pin counts (over 400 pins are possible).

The through-hole mounting approach offers a mechanically reliable and sturdy connection. However, this comes at the expense of packaging density. For mechanical reasons, a minimum pitch of 2.54 mm between the through holes is required. Even under those circumstances, PGAs with large numbers of pins tend to substantially weaken the board. In addition, through holes limit the board packing density by blocking lines that might otherwise have been routed below them, which results in longer interconnections. PGAs with large pin counts therefore require extra routing layers to connect to the multitudes of pins. Finally, while the parasitic capacitance and inductance of the PGA are slightly lower than that of the DIP, their values are still substantial.

Many of the shortcomings of the through-hole mounting approach are solved by using the *surface-mount* technique. A chip is attached to the surface of the board with a solder connection without requiring any through holes (Figure 2-14b). Packing density is increased for the following reasons: (1) through holes are eliminated, which provides more wiring space; (2) the lead pitch is reduced; and (3) chips can be mounted on both sides of the board. In addition, the elimination of the through holes improves the mechanical strength of the board. On the negative side, the on-the-surface connection makes the chip-board connection weaker. Not only is it cumbersome to mount a component on a board, but also more expensive equipment is needed, since a simple soldering iron will no longer suffice. Finally, testing of the board is more complex, because the package pins are no longer accessible at the backside of the board. Signal probing becomes difficult or almost impossible.

A variety of surface-mount packages are currently in use with different pitch and pin-count parameters. Three of these packages are shown in Figure 2-15: the *small-outline package* with gull wings, the *plastic leaded package* (PLCC) with J-shaped leads, and the *leadless chip carrier*. An overview of the most important parameters for a number of packages is given in Table 2-3.

Even surface-mount packaging is unable to satisfy the quest for ever higher pin counts. This is worsened by the demand for power connections: today's high performance chips, operating at low supply voltages, require as many power and ground pins as signal I/Os! When more than 300 I/O connections are needed, solder balls replace pins as the preferred interconnect medium between package and board. An example of such a packaging approach, called ceramic

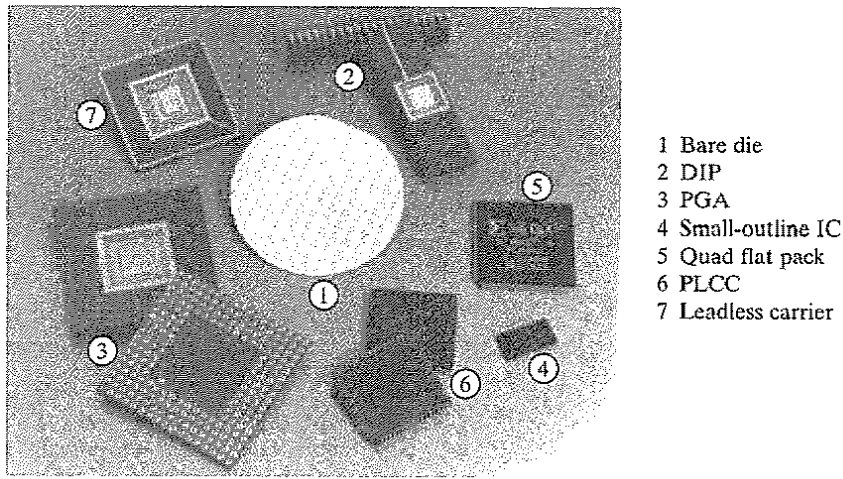


Figure 2-15 An overview of commonly used package types.

Table 2-3 Parameters of various types of chip carriers.

Package Type	Lead Spacing (Typical)	Lead Count (Maximum)
Dual in line	2.54 mm	64
Pin grid array	2.54 mm	> 300
Small-outline IC	1.27 mm	28
Leaded chip carrier (PLCC)	1.27 mm	124
Leadless chip carrier	0.75 mm	124

*ball grid array* (BGA), is shown in Figure 2-16. Solder bumps are used to connect both the die to the package substrate, and the package to the board. The area array interconnect of the BGA provides constant input/output density regardless of the number of total package I/O pins. A minimum pitch between solder balls of as low as 0.8 mm can be obtained, and packages with multiple thousands of I/O signals are feasible.

#### Multichip Modules—Die-to-Board

The deep hierarchy of interconnect levels in the package is becoming unacceptable in today's complex designs due to their higher levels of integration, large signal counts, and increased performance requirements. The trend, therefore, is toward reducing the number of levels. For the time being, attention is focused on the elimination of the first level in the packaging hierarchy. Removing one layer in the packaging hierarchy by mounting the die directly on the

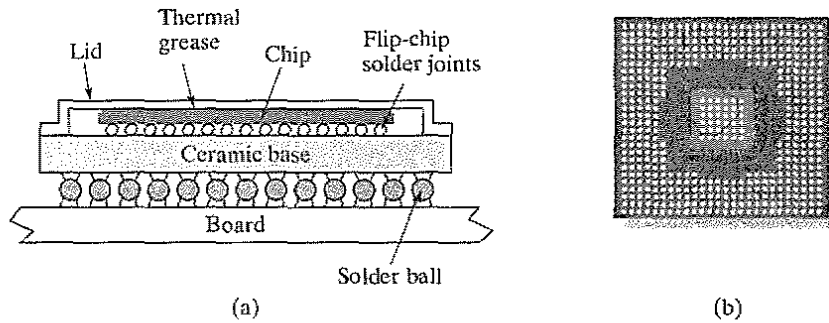


**Figure 2-16** Ball grid array packaging; (a) cross section, (b) photo of package bottom.

wiring backplanes—board or substrate—offers a substantial benefit when performance or density is a major issue. This packaging approach is called the multichip module technique (or MCM), and results in a substantial increase in packing density, as well as improved performance overall.

A number of the previously mentioned die-mounting techniques can be adapted to mount dies directly on the substrate, including wire bonding, TAB, and flip-chip, although the latter two are preferable. The substrate itself can vary over a wide range of materials, depending upon the required mechanical, electrical, thermal, and economical requirements. Materials of choice are epoxy substrates (similar to PC boards), metal, ceramics, and silicon. Silicon has the advantage of presenting a perfect match in mechanical and thermal properties with respect to the die material.

The main advantages of the MCM approach are the increased packaging density and performance. An example of an MCM module implemented using a silicon substrate (commonly dubbed *silicon on silicon*) is shown in Figure 2-17. The module, which implements an avionics processor module and is fabricated by Rockwell International, contains 53 ICs and 40 discrete devices on a  $2.2'' \times 2.2''$  substrate with aluminum polyimide interconnect. The interconnect wires are only an order of magnitude wider than what is typical for on-chip wires, since similar patterning approaches are used. The module itself has 180 I/O pins. Performance is improved by the elimination of the chip-carrier layer with its assorted parasitics, and through a reduction of the global wiring lengths on the die, a result of the increased packaging density. For instance, a solder bump has an assorted capacitance and inductance of only 0.1 pF and 0.01 nH, respectively. The MCM technology can also reduce power consumption significantly, since large output drivers—and associated dissipation—become superfluous due to the reduced load capacitance of the output pads. The dynamic power associated with the switching of the large load capacitances is simultaneously reduced.

While MCM technology offers some clear benefits, its main disadvantage is economic. This technology requires some advanced manufacturing steps that make the process expensive. The approach was until recently only justifiable when either dense housing or extreme performance is essential. In recent years, the economics have been shifting, and advanced multichip

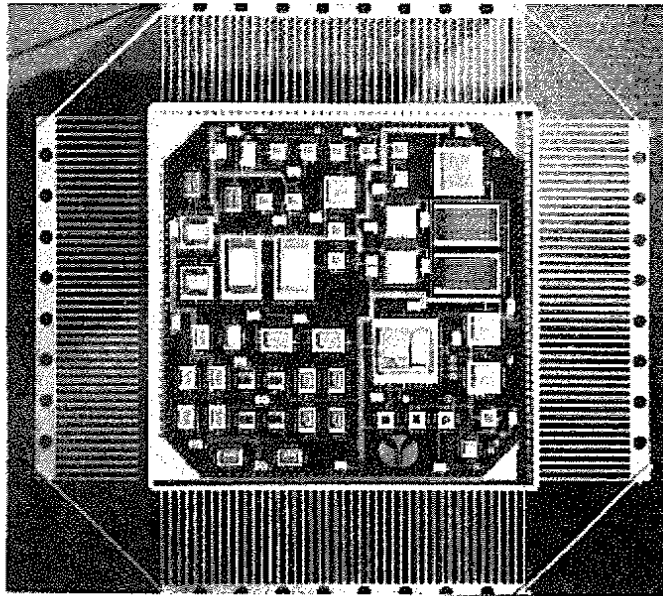


Figure 2-17 Avionics processor module. *Courtesy of Rockwell Collins, Inc.*

packaging approaches have made inroad in several low-cost high-density applications as well. This trend is called the *system-in-a-package* (SiP) strategy.

### 2.4.3 Thermal Considerations in Packaging

As the power consumption of integrated circuits rises, it becomes increasingly important to efficiently remove the heat generated by the chips. A large number of failure mechanisms in ICs are accentuated by increased temperatures. Examples are leakage in reverse-biased diodes, electromigration, and hot-electron trapping. To prevent failure, the temperature of the die must be kept within certain ranges. The supported temperature range for commercial devices during operation equals  $0^{\circ}$  to  $70^{\circ}\text{C}$ . Military parts are more demanding and require a temperature range varying from  $-55^{\circ}$  to  $125^{\circ}\text{C}$ .

The cooling effectiveness of a package depends on the thermal conduction (resistance) of the package material, which consists of the package substrate and body, the package composition, and the effectiveness of the heat transfer between package and cooling medium. Standard packaging approaches use still or circulating air as the cooling medium. The transfer efficiency can be improved by adding finned metal heat sinks to the package. More expensive packaging approaches, such as those used in mainframes or supercomputers, force air, liquids, or inert gases through tiny ducts in the package to achieve even greater cooling efficiencies.

Given the thermal resistance  $\theta$  of the package, expressed in  $^{\circ}\text{C}/\text{W}$ , we can derive the chip temperature by using the *heat flow equation*

$$\Delta T = T_{chip} - T_{env} = \theta Q, \quad (2.2)$$



with  $T_{chip}$  and  $T_{env}$  the chip and environment temperatures, respectively.  $Q$  represents the heat flow (in Watt). Observe how closely the heat flow equation resembles Ohm's Law. The heat flow and temperature differential are the equivalents of current and voltage difference, respectively. Thermal modeling of a chip, its package, and its environment is a complex task. We refer the reader to [Lau98 – Chapter 3] for a more detailed discussion on the topic.

---

### Example 2.2 Thermal Conduction of Package

As an example, a 40-pin DIP has a thermal resistance of  $38^{\circ}\text{C}/\text{W}$  and  $25^{\circ}\text{C}/\text{W}$  for natural and forced convection of air. This means that a DIP can dissipate 2 watts (3 watts) of power with natural (forced) air convection, and still keep the temperature difference between the die and the environment below  $75^{\circ}\text{C}$ . For comparison, the thermal resistance of a ceramic PGA ranges from  $15^{\circ}$  to  $30^{\circ}\text{C}/\text{W}$ .

---

Since packaging approaches with decreased thermal resistance are prohibitively expensive, keeping the power dissipation of an integrated circuit within bounds is an economic necessity. The increasing integration levels and circuit performance make this task nontrivial. An interesting relationship in this context has been derived by Nagata [Nagata92]. It provides a bound on the integration complexity and performance as a function of the thermal parameters. We write

$$\frac{N_G}{t_p} \leq \frac{\Delta T}{\theta E} \quad (2.3)$$

where  $N_G$  is the number of gates on the chip,  $t_p$  the propagation delay,  $\Delta T$  the maximum temperature difference between chip and environment,  $\theta$  the thermal resistance between them, and  $E$  the switching energy of each gate.

---

### Example 2.3 Thermal Bounds on Integration

For  $\Delta T = 100^{\circ}\text{C}$ ,  $\theta = 2.5^{\circ}\text{C}/\text{W}$  and  $E = 0.1$  pJ, this results in  $N_G/t_p \leq 4 \times 10^5$  (gates/nsec). In other words, the maximum number of gates on a chip, when all gates are operating simultaneously, must be less than 400,000 if the switching speed of each gate is 1 nsec. This is equivalent to a power dissipation of 40 W.

---

Fortunately, not all gates are operating simultaneously in real systems. The maximum number of gates can be substantially larger, based on the activity in the circuit. For example, it has been experimentally derived that the ratio between the average switching period and the propagation delay ranges from 20 to 200 in mini- and large-scale computers [Masaki92].

Nevertheless, Eq. (2.3) demonstrates that heat dissipation and thermal concerns present an important limitation on circuit integration. Design approaches for low power that reduce either  $E$  or the activity factor are rapidly gaining importance.

## 2.5 Perspective—Trends in Process Technology

Modern CMOS processes pretty much track the flow described in the previous sections, although a number of the steps might be reversed, a single well approach might be followed, a grown field oxide instead of the trench approach might be used, or extra steps such as LDD (*Lightly Doped Drain*) might be introduced. Also, it is quite common to cover the polysilicon interconnections as well as the drain and source regions with a *silicide* such as  $\text{TiSi}_2$  to improve the conductivity (see Figure 2-2). This extra operation is inserted between steps  $i$  and  $j$  of our process. Some important modifications or improvements to the technology are currently under way or are on the horizon, and deserve some attention. Beyond these, we expect no dramatic changes from the described CMOS technology in the next decade.

### 2.5.1 Short-Term Developments

#### Copper and Low-k Dielectrics

A recurring theme throughout this book will be the increasing impact of interconnect on the overall design performance. Process engineers are continuously evaluating alternative options for the traditional Aluminum-conductor- $\text{SiO}_2$ -insulator combination that has been the norm for the last several decades. In 1998, engineers at IBM introduced an approach that finally made the use of copper as an interconnect material in a CMOS process viable and economical [Geppert98]. Copper has a resistivity that is substantially lower than aluminum. It has the disadvantage of easy diffusion into silicon, which degrades the characteristics of the devices. Coating the copper with a buffer material such as titanium-nitride, preventing the diffusion, addresses this problem, but requires a special deposition process. The Dual Damascene process, introduced by IBM, (Figure 2-18) uses a metallization approach that fills trenches etched into the insulator, followed by a chemical-mechanical polishing step. This is in contrast with the traditional approach that first deposits a full metal layer, and removes the redundant material through etching.

In addition to the lower resistivity interconnections, insulator materials with a lower dielectric constant than  $\text{SiO}_2$ , and hence, lower capacitance have also found their way into the production process, starting with the 0.18- $\mu\text{m}$  CMOS process generation.

#### Silicon on Insulator

Although it has been around a long time, there seems to be a good chance that Silicon-on-Insulator (SOI) CMOS might replace the traditional CMOS process, described in the previous sections (also known as the *bulk CMOS process*). The main difference lies in the start material: the SOI transistors are constructed in a very thin layer of silicon, deposited on top of a thick layer of insulating  $\text{SiO}_2$  (see Figure 2-19). The primary advantages of the SOI process are reduced

## Dual damascene IC process

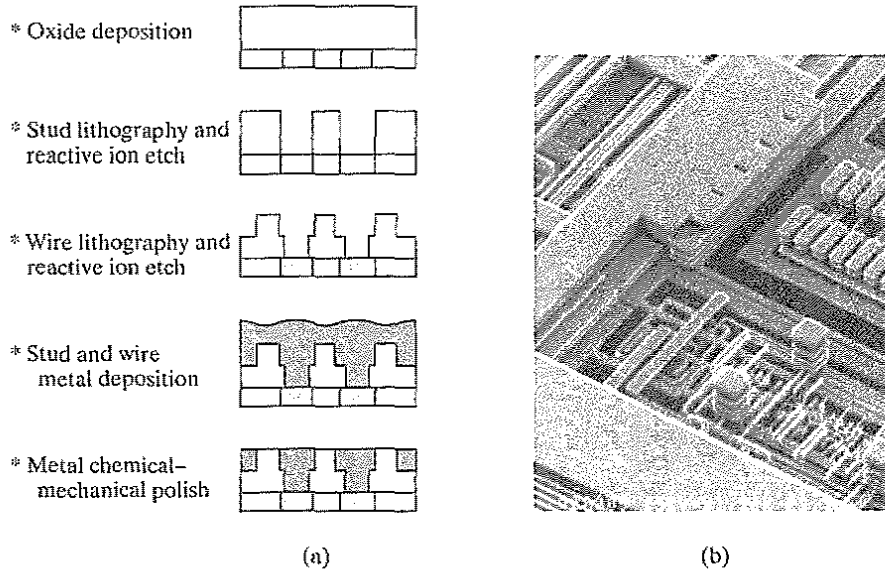


**Figure 2-18** The damascene process (from [Geppert98]): process steps (a), and microphotograph of interconnect after removal of insulator (b).

parasitics and better transistor on-off characteristics. It has, for example, been demonstrated by researchers at IBM, that the porting of a design from a bulk CMOS to an SOI process—leaving all other design and process parameters such as channel length and oxide thickness identical—yields a performance improvement of 22% [Allen99]. Preparing a high quality SOI substrate at an economical cost was long the main hindrance against a large-scale introduction of the process. This picture had changed by the end of the 1990s, and SOI is steadily moving into the mainstream.

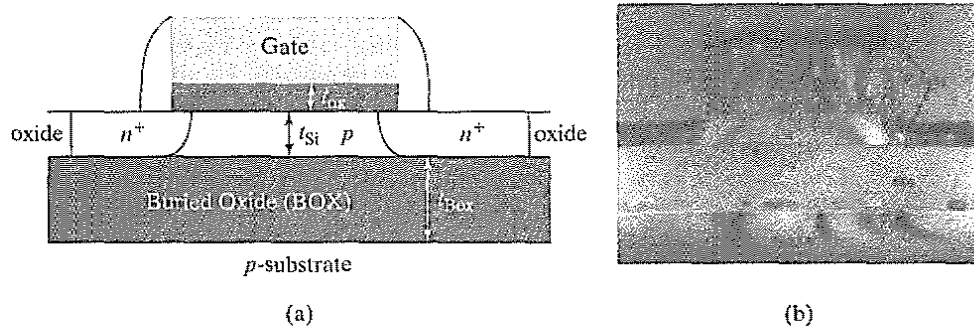


**Figure 2-19** Silicon-on-insulator process—schematic diagram (a) and SEM cross section (b). [Eaglesham99].

### 2.5.2 In the Longer Term

Extending the life of CMOS technology beyond the next decade, and going deeply below the 100 nm channel length region, however, will require redeveloping the process technology and the device structure. Already we are witnessing the emergence of a wide range of new devices (such as organic transistors, molecular switches, and quantum devices). While we cannot project what approaches will dominate in the next era, one interesting development is worth mentioning.

#### Truly Three-Dimensional Integrated Circuits

Getting signals in and out of the computation elements in a timely fashion is one of the main challenges presented by the continued increase in integration density. One way to address this problem is to introduce extra active layers, and to sandwich them between the metal interconnect layers, as shown in Figure 2-20. This enables us to position high density memory on top of the logic processors implemented in the bulk CMOS, reducing the distance between computation and storage, and thus also the delay [Souri00]. In addition, devices with different voltage, performance, or substrate material requirements can be placed in different layers. For instance, the top active layer can be reserved for the realization of optical transceivers, which may help to address the input/output requirements, or MEMS (Micro Electro-Mechanical Systems) devices providing sensing functions or radio frequency (RF) interfaces.

While this approach may seem to be promising, a number of major challenges and hindrances have to be resolved to make it truly viable. How to remove the dissipated heat is one of the more compelling questions, ensuring yield is another. Researchers are demonstrating major progress on these issues, and 3D integration might well be on the horizon. Before the true solution arrives, we might have to rely on some intermediate approaches. One alternative, called *2.5D integration*, is to bond two fully processed wafers, on which circuits are fabricated on the

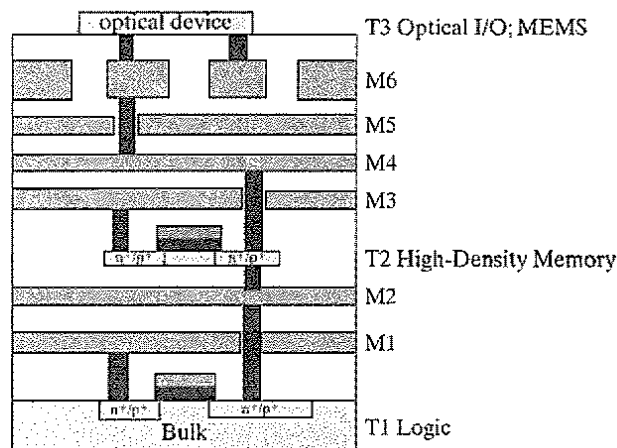


**Figure 2-20** Example of true 3D integration. Extra active layers (T\*), implementing high-density memory and I/O, are sandwiched between the metal interconnect layers (M\*).

surface such that the chips completely overlap. Vias are etched to electrically connect both chips after metallization. The advantages of this technology lie in the similar electrical properties of devices on all active levels and the independence of processing temperature since all chips can be fabricated separately and later bonded. The major limitation of this technique is its lack of precision (best case alignment:  $\pm 2 \mu\text{m}$ ), which restricts the interchip communication to global metal lines.

One picture that strongly emerges from these futuristic devices is that the line between chip, substrate, package, and board is blurring. Designers of these *systems on a die* or *systems in a package* will have to consider all these aspects simultaneously.

## 2.6 Summary

This chapter has presented a bird's-eye view of the manufacturing and packaging process of CMOS integrated circuits:

- The manufacturing process of integrated circuits requires many steps, each of which consists of a sequence of basic operations. A number of these steps and/or operations, such as photolithographical exposure and development, material deposition, and etching, are executed very repetitively in the course of the manufacturing process.
- The *optical masks* forms the central interface between the intrinsics of the manufacturing process and the design that the user wants to see transferred to the silicon fabric.
- The *design-rules set* defines the constraints in terms of minimum width and separation that the IC design has to adhere to if the resulting circuit is to be fully functional. These design rules act as the contract between the circuit designer and the process engineer.
- The *package* forms the interface between the circuit implemented on the silicon die and the outside world, and as such has a major impact on the performance, reliability, longevity, and cost of the integrated circuit.

## 2.7 To Probe Further

Many books on semiconductor manufacturing have been published in the last few decades. An excellent overview of the state of the-art in CMOS manufacturing is *Silicon VLSI Technology* by J. Plummer, M. Deal, and P. Griffin [Plummer00]. A visual overview of the different steps in the manufacturing process can be found on the Web at [Fullman99]. Other sources for information are the IEEE Transactions on Electron Devices, and the Technical Digest of the IEDM conference. A number of great compendia are available for up-to-date and in-depth information about electronic packaging. [Doane93], [Harper00], and [Lau98] are good examples of such.

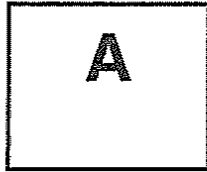
## References

- [Allen99] D. Allen, et al., "A 0.2  $\mu\text{m}$  1.8 V SOI 550 MHz PowerPC Microprocessor with Copper Interconnects," *Proceedings IEEE ISSCC Conference*, vol. XLII, pp. 438-439, February 1999.
- [Bakoglu90] H. Bakoglu, *Circuits, Interconnections and Packaging for VLSI*, Addison-Wesley, 1990.

- [Doane93] D. Doane, ed., *Multichip Module Technologies and Alternatives*, Van Nostrand-Reinhold, 1993.
- [Eaglesham 99] D. Eaglesham, "0.18  $\mu\text{m}$  CMOS and Beyond," *Proceedings 1999 Design Automation Conference*, pp. 703–708, June 1999.
- [Franzon93] P. Franzon, "Electrical Design of Digital Multichip Modules," in [Doane93], pp 525–568, 1993.
- [Fullman99] Fullman Kinetics, "The Semiconductor Manufacturing Process," <http://www.fullman-kinetics.com/semiconductors/semiconductors.html>, 1999.
- [Geppert98] L. Geppert, "Technology—1998 Analysis and Forecast," *IEEE Spectrum*, vol. 35, no. 1, p. 23, January 1998.
- [Harper00] C. Harper, Ed., *Electronic Packaging and Interconnection Handbook*, McGraw-Hill, 2000.
- [Landman71] B. Landman and R. Russo, "On a Pin versus Block Relationship for Partitions of Logic Graphs," *IEEE Trans. on Computers*, vol. C-20, pp. 1469–1479, December 1971.
- [Lau98] J. Lau et al., *Electronic Packaging—Design, Materials, Process, and Reliability*, McGraw-Hill, 1998.
- [Masaki92] A. Masaki, "Deep-Submicron CMOS Warms Up to High-Speed Logic," *Circuits and Devices Magazine*, November 1992.
- [Mead80] C. Mead and L. Conway, *Introduction to VLSI Systems*, Addison-Wesley, 1980.
- [Nagata92] M. Nagata, "Limitations, Innovations, and Challenges of Circuits and Devices into a Half Micrometer and Beyond," *IEEE Journal of Solid State Circuits*, vol. 27, no. 4, pp. 465–472, April 1992.
- [Plummer00] J. Plummer, M. Deal, and P. Griffin, *Silicon VLSI Technology*, Prentice Hall, 2000.
- [Steidel83] C. Steidel, *Assembly Techniques and Packaging*, in [Sze83], pp. 551–598, 1983.
- [Souri00] S. J. Souri, K. Banerjee, A. Mehrotra and K. C. Saraswat, "Multiple Si Layer ICs: Motivation, Performance Analysis, and Design Implications," *Proceedings 37th Design Automation Conference*, pp. 213–220, June 2000.



# DESIGN METHODOLOGY INSERT



## IC LAYOUT

*Creating a manufacturable layout*  
*Verifying the layout*

The increasing complexity of the integrated circuit has made the role of design-automation tools indispensable, and raises the abstractions the designer is working with to ever higher levels. Yet, when performance or design density is of primary importance, the designer has no other choice than to return to handcrafting the circuit topology and physical design. The labor-intensive nature of this approach, called *custom design*, translates into a high cost and a long time to market. Therefore, it can only be justified economically under the following conditions:

- The custom block can be reused many times, as a library cell, for instance.
- The cost can be amortized over a large volume. Microprocessors and semiconductor memories are examples of applications in this class.
- Cost is not among the prime design criteria.<sup>1</sup> Examples include space applications and scientific instrumentation.

With continuous progress in the design-automation arena, the share of custom design reduces from year to year. Even in high-performance microprocessors, large portions are

---

<sup>1</sup>This is becoming increasingly rare.



designed automatically using semicustom design approaches. Only the most performance-critical modules—such as the integer and floating-point execution units—are handcrafted.

Although the amount of design automation in the custom design process is minimal, some design tools have proven to be indispensable. Together with circuit simulators, these programs form the core of every design-automation environment, and they are the first tools an aspiring circuit designer will encounter.

### Layout Editor

The layout editor is the premier working tool of the designer and exists primarily for the generation of a physical representation of a design, given a circuit topology. Virtually every design-automation vendor offers an entry in this field. The most well known is the MAGIC tool developed at the University of California at Berkeley [Ousterhout84], which has been widely distributed. Even though MAGIC did not withstand the evolution of software technology and user interface, some of its offspring did. Throughout this book, we will be using a layout tool called **max**, a MAGIC descendant developed by a company called MicroMagic [mimi00]. A typical **max** display is shown in Figure A-1 and illustrates the basic function of the layout editor—placing polygons on

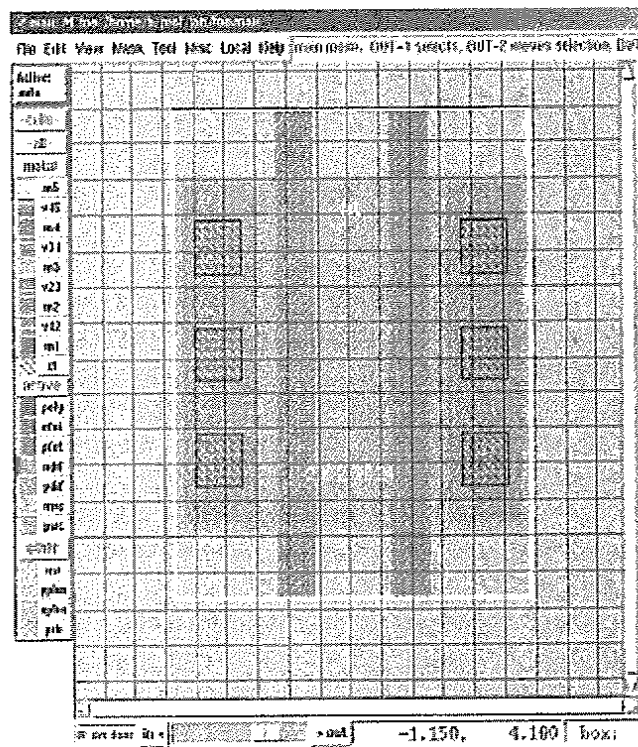


**Figure A-1** View of a **max** display window. It plots the layout of two stacked NMOS transistor. The menu on the left side allows for the selection of the layer a particular polygon will be placed on.

different mask layers so that a functional physical design is obtained (scathingly called *polygon pushing*).

### Symbolic Layout

Since physical design occupies a major fraction of the design time for a new cell or component, techniques to expedite this process have been in continual demand. The *symbolic-layout* approach has gained popularity over the years. In this design methodology, the designer only draws a shorthand notation for the layout structure. This notation indicates only the *relative* positioning of the various design components (transistors, contacts, wires). The *absolute* coordinates of these elements are determined automatically by the editor using a *compactor* [Hsueh79, Weste93]. The compactor translates the design rules into a set of constraints on the component positions, and solves a constrained optimization problem that attempts to minimize the area or another cost function.

An example of a symbolic notation for a circuit topology called a *sticks diagram* is shown in Figure A-2. The different layout entities are dimensionless, since only positioning is important. The advantage of this approach is that the designer does not have to worry about design rules, because the compactor ensures that the final layout is physically correct. Thus, she can avoid cumbersome polygon manipulations. Another plus of the symbolic approach is that cells can adjust themselves automatically to the environment. For example, automatic pitch matching of cells is an attractive feature in module generators. Consider the case of Figure A-3 (from [Croes88]), in which the original cells have different heights, and the terminal positions do not match. Connecting the cells would require extra wiring. The symbolic approach allows the cells to adjust themselves and connect without any overhead.

The disadvantage of the symbolic approach is that the outcome of the compaction phase often is unpredictable. The resulting layout can be less dense than what is obtained with the manual approach. This has prevented it from becoming a mainstream layout tool. Nonetheless, symbolic layout techniques have improved considerably over the years, and they have become very useful as a first-order drafting tool for new cells. More important, they form the solid underpinning of the automatic cell-generation techniques, described later, in Chapter 8.

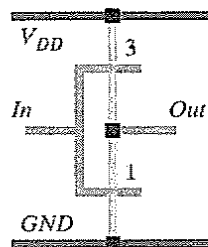


**Figure A-2** Sticks representation of CMOS inverter. The numbers represent the (*Width/Length*)-ratios of the transistors.

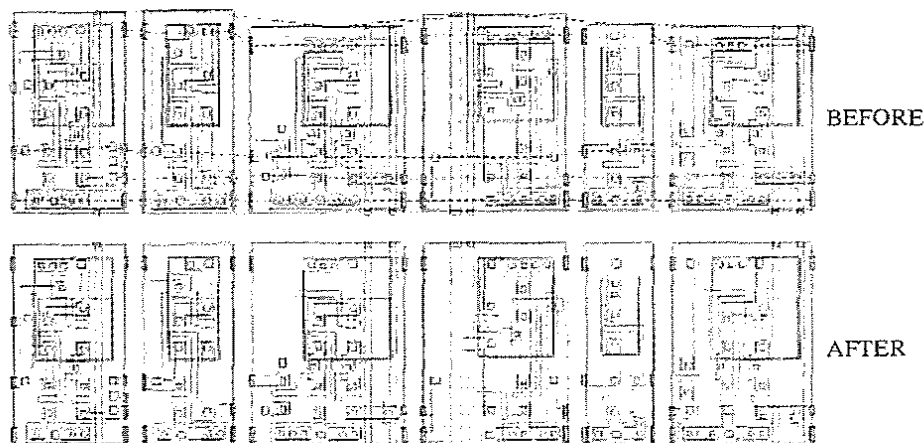


Figure A-3 Automatic pitch matching of data path cells based on symbolic layout.

### Design-Rule Checking

Design rules were introduced in Chapter 2 as a set of layout restrictions that ensure the manufactured design will operate as desired with no short or open circuits. A prime requirement of the physical layout of a design is that it adhere to these rules. This can be verified with the aid of a *design-rule checker (DRC)*, which uses as inputs the physical layout of a design and a description of the design rules presented in the form of a *technology file*. Since a complex circuit can contain millions of polygons that must be checked against each other, efficiency is the most important property of a good DRC tool. The verification of a large chip can take hours or days of computation time. One way of expediting the process is to preserve the design hierarchy at the physical level. For example, if a cell is used multiple times in a design, it should be checked only once. Besides speeding up the process, the use of hierarchy can make error messages more informative by retaining knowledge of the circuit structure.

DRC tools come in two formats: (1) The *on-line DRC* runs concurrent with the layout editor and flags design violations during the cell layout. For instance, **max** has a built-in design-rule checking facility. An example of on-line DRC is shown in Figure A-4. (2) *Batch DRC* is used as a postdesign verifier; it is run on a complete chip prior to shipping the mask descriptions to the manufacturer.

### Circuit Extraction

Another important tool in the custom-design methodology is the circuit extractor, which derives a circuit schematic from a physical layout. By scanning the various layers and their interactions, the extractor reconstructs the transistor network, including the sizes of the devices and the interconnections. The schematic produced can be used to verify that the artwork implements the intended function. Furthermore, the resulting circuit diagram contains precise information on the parasitics, such as the diffusion and wiring capacitances and resistances. This allows for a

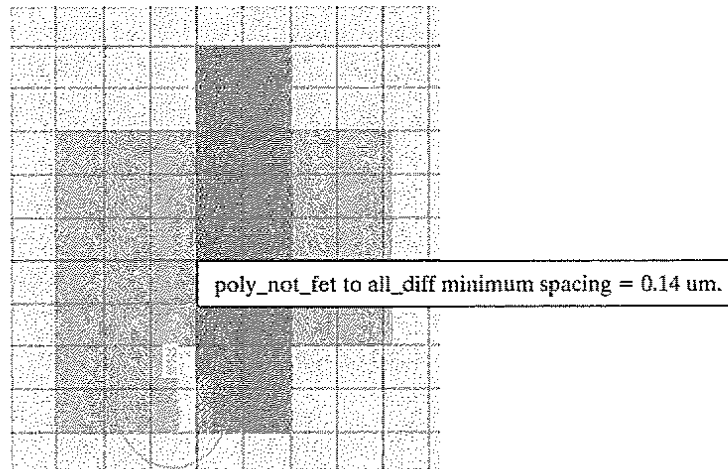


**Figure A-4** On-line design rule checking. The white dots indicate a design rule violation. The violated rule can be obtained with a simple mouse click.

more accurate simulation and analysis. The complexity of the extraction depends greatly upon the desired information. Most extractors extract the transistor network and the capacitances of the interconnect with respect to *GND* or other network nodes. Extraction of the wiring resistances already comes at a greater cost, yet it has become a necessity for virtually all high-performance circuits. Clever algorithms have helped to reduce the complexity of the resulting circuit diagrams. For very high-speed circuits, extraction of the inductance would be desirable as well. Unfortunately, this requires a three-dimensional analysis and is only feasible for small-sized circuits at present.

### A.1 To Probe Further

More detailed information regarding the *MAGIC* and *max* layout editors can be found on the web site of this book. In-depth textbooks on layout generation and verification have been published, and can be of great help to the novice designer. To mention a few of them, [Clein00], [Uyemura95], and [Wolf94] offer some comprehensive and well-illustrated treatment and discussion.

### References

- [Clein00] D. Clein, *CMOS IC Layout—Concepts, Methodologies, and Tools*, Newnes, 2000.
- [Croes88] K. Croes, H. De Man, and P. Six, "CAMELEON: A Process-Tolerant Symbolic Layout System," *Journal of Solid State Circuits*, vol. 23 no. 3, pp. 705–713, June 1988.
- [Hsueh79] M. Hsueh and D. Pederson, "Computer-Aided Layout of LSI Building Blocks," *Proceedings ISCAS Conf.*, pp. 474–477, Tokyo, 1979.
- [mimi00] MicroMagic, Inc, <http://www.micromagic.com>.

- [Ousterhout84] J. Ousterhout, G. Hamachi, R. Mayo, W. Scott, and G. Taylor, "Magic: A VLSI Layout System," *Proc. 21st Design Automation Conference*, pp. 152-159, 1984.
- [Uyemura95] J. Uyemura, *Physical Design of CMOS Integrated Circuits Using L-EDIT*, PWS Publishing Company, 1995.
- [Weste93] N. Weste and K. Eshraghian, *Principles of CMOS VLSI Design—A Systems Perspective*, Addison-Wesley, 1993.
- [Wolf94] W. Wolf, *Modern VLSI Design—A Systems Approach*, Prentice Hall, 1994.

## CHAPTER

# 5

## The CMOS Inverter

*Quantification of integrity, performance, and energy metrics of an inverter*  
*Optimization of an inverter design*

- 5.1 Introduction
- 5.2 The Static CMOS Inverter—An Intuitive Perspective
- 5.3 Evaluating the Robustness of the CMOS Inverter—The Static Behavior
  - 5.3.1 Switching Threshold
  - 5.3.2 Noise Margins
  - 5.3.3 Robustness Revisited
- 5.4 Performance of CMOS Inverter: The Dynamic Behavior
  - 5.4.1 Computing the Capacitances
  - 5.4.2 Propagation Delay: First-Order Analysis
  - 5.4.3 Propagation Delay from a Design Perspective
- 5.5 Power, Energy, and Energy Delay
  - 5.5.1 Dynamic Power Consumption
  - 5.5.2 Static Consumption
  - 5.5.3 Putting It All Together
  - 5.5.4 Analyzing Power Consumption by Using SPICE
- 5.6 Perspective: Technology Scaling and its Impact on the Inverter Metrics
- 5.7 Summary
- 5.8 To Probe Further

## 5.1 Introduction

The inverter is truly the nucleus of all digital designs. Once its operation and properties are clearly understood, designing more intricate structures such as logic gates, adders, multipliers, and microprocessors is greatly simplified. The electrical behavior of these complex circuits can be almost completely derived by extrapolating the results obtained for inverters. The analysis of inverters can be extended to explain the behavior of more complex gates such as NAND, NOR, or XOR, which in turn form the building blocks for modules such as multipliers and processors.

In this chapter, we focus on a single incarnation of the inverter gate—the static CMOS inverter. This is certainly the most popular inverter at present, and therefore deserves special attention. We analyze the gate with respect to the different design metrics that were outlined in Chapter 1:

- *cost*, expressed by the complexity and area
- *integrity and robustness*, expressed by the static (or steady-state) behavior
- *performance*, determined by the dynamic (or transient) response
- *energy efficiency*, set by the energy and power consumption

Using this analysis, we develop a model of the gate and identify its design parameters. We develop methods to choose the parameter values so that the resulting design meets the desired specifications. While each of these parameters can easily be quantified for a given technology, we also discuss how they are affected by *scaling of the technology*.

While the chapter focuses uniquely on the CMOS inverter, in the next chapter, we see that the same methodology also applies to other gate topologies.

## 5.2 The Static CMOS Inverter—An Intuitive Perspective

Figure 5-1 shows the circuit diagram of a static CMOS inverter. Its operation is readily understood with the aid of the simple switch model of the MOS transistor that we introduced in Chapter 3 (see Figure 3-26). The transistor is nothing more than a switch with an infinite off-

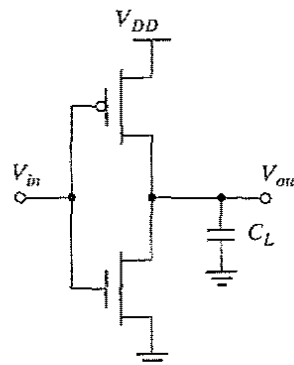


Figure 5-1 Static CMOS inverter.  $V_{DD}$  stands for the supply voltage.

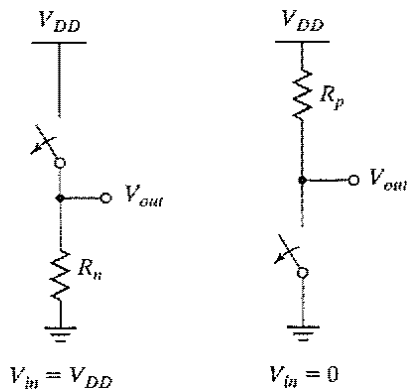


Figure 5-2 Switch models of CMOS inverter.

resistance (for  $|V_{GS}| < |V_T|$ ) and a finite on-resistance (for  $|V_{GS}| > |V_T|$ ). This leads to the following interpretation of the inverter. When  $V_{in}$  is high and equal to  $V_{DD}$ , the NMOS transistor is on and the PMOS is off. This yields the equivalent circuit of Figure 5-2a. A direct path exists between  $V_{out}$  and the ground node, resulting in a steady-state value of 0 V. On the other hand, when the input voltage is low (0 V), NMOS and PMOS transistors are off and on, respectively. The equivalent circuit of Figure 5-2b shows that a path exists between  $V_{DD}$  and  $V_{out}$ , yielding a high output voltage. The gate clearly functions as an inverter.

A number of other important properties of static CMOS can be derived from this switch level view:

- The high and low output levels equal  $V_{DD}$  and  $GND$ , respectively; in other words, the voltage swing is equal to the supply voltage. This results in high noise margins.
- The logic levels are not dependent upon the relative device sizes, so that the transistors can be minimum size. Gates with this property are called *ratioless*. This is in contrast with *ratioed logic*, where logic levels are determined by the relative dimensions of the composing transistors.
- In steady state, there always exists a path with finite resistance between the output and either  $V_{DD}$  or  $GND$ . A well-designed CMOS inverter, therefore, has a *low output impedance*, which makes it less sensitive to noise and disturbances. Typical values of the output resistance are in  $k\Omega$  range.
- The *input resistance* of the CMOS inverter is extremely high, as the gate of an MOS transistor is a virtually perfect insulator and draws no dc input current. Since the input node of the inverter only connects to transistor gates, the steady-state input current is nearly zero. A single inverter can theoretically drive an infinite number of gates (or have an infinite fan-out) and still be functionally operational; however, increasing the fan-out also increases the propagation delay, as will become clear shortly. Although fan-out does not have any effect on the steady-state behavior, it degrades the transient response.



- No direct path exists between the supply and ground rails under steady-state operating conditions (i.e., when the input and outputs remain constant). The absence of current flow (ignoring leakage currents) means that the gate does not consume any static power.

**SIDELINE:** The preceding observation, while seemingly obvious, is of crucial importance, and is one of the primary reasons CMOS is the digital technology of choice at present. The situation was very different in the 1970s and early 1980s. All early microprocessors—such as the Intel 4004—were implemented in a pure NMOS technology. The lack of complementary devices (such as the NMOS and PMOS transistor) in such a technology makes the realization of inverters with zero static power nontrivial. The resulting static power consumption puts a firm upper bound on the number of gates that can be integrated on a single die; hence, the forced move to CMOS in the 1980s, when scaling of the technology allowed for higher integration densities.

The nature and the form of the voltage-transfer characteristic (VTC) can be graphically deduced by superimposing the current characteristics of the NMOS and the PMOS devices. Such a graphical construction is traditionally called a *load-line plot*. It requires that the  $I$ - $V$  curves of the NMOS and PMOS devices are transformed onto a common coordinate set. We have selected the input voltage  $V_{in}$ , the output voltage  $V_{out}$  and the NMOS drain current  $I_{DN}$  as the variables of choice. The PMOS  $I$ - $V$  relations can be translated into this variable space by the following relations (the subscripts  $n$  and  $p$  denote the NMOS and PMOS devices, respectively):

$$\begin{aligned} I_{DSp} &= -I_{DSn} \\ V_{GSn} &= V_{in}; \quad V_{GSp} = V_{in} - V_{DD} \\ V_{DSn} &= V_{out}; \quad V_{DSp} = V_{out} - V_{DD} \end{aligned} \quad (5.1)$$

The load-line curves of the PMOS device are obtained by a mirroring around the  $x$ -axis and a horizontal shift over  $V_{DD}$ . This procedure is outlined in Figure 5-3, where the subsequent steps to adjust the original PMOS  $I$ - $V$  curves to the common coordinate set  $V_{in}$ ,  $V_{out}$ , and  $I_{Dn}$  are illustrated.

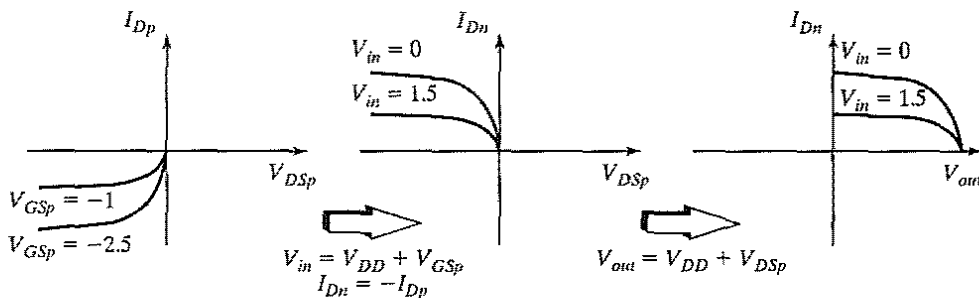


**Figure 5-3** Transforming PMOS  $I$ - $V$  characteristic to a common coordinate set (assuming  $V_{DD} = 2.5$  V).

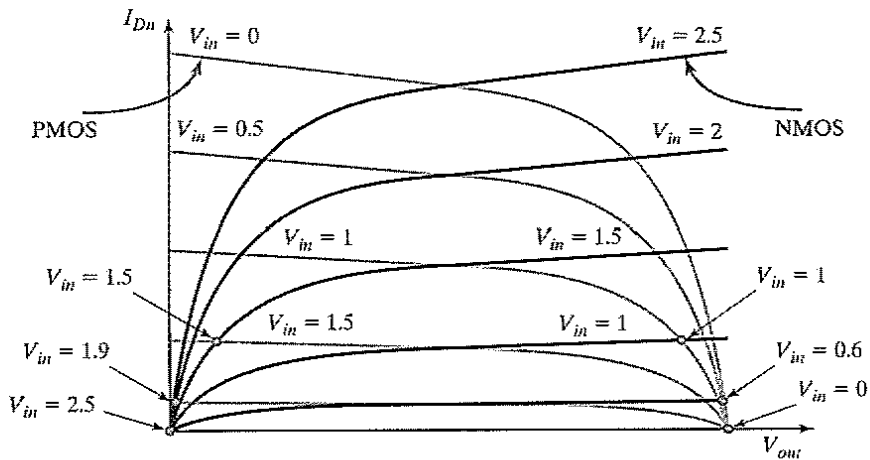


**Figure 5-4** Load curves for NMOS and PMOS transistors of the static CMOS inverter ( $V_{DD} = 2.5$  V). The dots represent the dc operation points for various input voltages.

The resulting load lines are plotted in Figure 5-4. For a dc operating point to be valid, the currents through the NMOS and PMOS devices must be equal. Graphically, this means that the dc points must be located at the intersection of corresponding load lines. A number of those points (for  $V_{in} = 0, 0.5, 1, 1.5, 2,$  and  $2.5$  V) are marked on the graph. As can be seen, all operating points are located either at the high or low output levels. The VTC of the inverter thus exhibits a very narrow transition zone. This results from the high gain during the switching transient, when both NMOS and PMOS are simultaneously on and in saturation. In that operation region, a small change in the input voltage results in a large output variation. All these observations translate into the VTC shown in Figure 5-5.

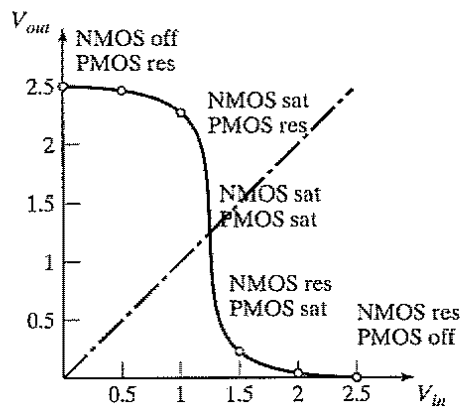


**Figure 5-5** VTC of static CMOS inverter, derived from Figure 5-4 ( $V_{DD} = 2.5$  V). For each operation region, the modes of the transistors are annotated—off, res(istive), or sat(urated).

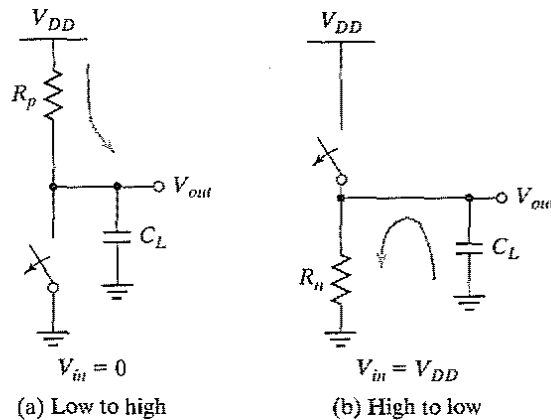


**Figure 5-6** Switch model of dynamic behavior of static CMOS inverter.

Before going into the analytical details of the operation of the CMOS inverter, a qualitative analysis of the transient behavior of the gate is appropriate. This response is dominated mainly by the output capacitance of the gate,  $C_L$ , which is composed of the drain diffusion capacitances of the NMOS and PMOS transistors, the capacitance of the connecting wires, and the input capacitance of the fan-out gates. Assuming temporarily that the transistors switch instantaneously, we can get an approximate idea of the transient response by using the simplified switch model again. Let us first consider the low-to-high transition (see Figure 5-6a). The gate response time is simply determined by the time it takes to charge the capacitor  $C_L$  through the resistor  $R_p$ . In Example 4.5, we learned that the propagation delay of such a network is proportional to the time constant  $R_p C_L$ . **Hence, a fast gate is built either by keeping the output capacitance small or by decreasing the on-resistance of the transistor.** The latter is achieved by increasing the  $W/L$  ratio of the device. Similar considerations are valid for the high-to-low transition (Figure 5-6b), which is dominated by the  $R_n C_L$  time constant. The reader should be aware that the on-resistance of the NMOS and PMOS transistor is not constant; rather, it is a nonlinear function of the voltage across the transistor. This complicates the exact determination of the propagation delay. (An in-depth analysis of how to analyze and optimize the performance of the static CMOS inverter is offered in Section 5.4.)

### 5.3 Evaluating the Robustness of the CMOS Inverter—The Static Behavior

In the preceding qualitative discussion, the overall shape of the voltage-transfer characteristic of the static CMOS inverter was sketched, and the values of  $V_{OH}$  and  $V_{OL}$ —which are evaluated to  $V_{DD}$  and  $GND$ , respectively—were derived. It remains to determine the precise values of  $V_M$ ,  $V_{IH}$ , and  $V_{IL}$ , as well as the noise margins.

### 5.3.1 Switching Threshold

The switching threshold  $V_M$  is defined as the point where  $V_{in} = V_{out}$ . Its value can be obtained graphically from the intersection of the VTC with the line given by  $V_{in} = V_{out}$  (see Figure 5-5). In this region, both PMOS and NMOS are always saturated, since  $V_{DS} = V_{GS}$ . An analytical expression for  $V_M$  is obtained by equating the currents through the transistors. We solve for the case in which the supply voltage is high enough so that the devices can be assumed to be velocity-saturated (or  $V_{DSAT} < V_M - V_T$ ). Furthermore, we ignore the channel length modulation effects. We have

$$k_n V_{DSATn} \left( V_M - V_{Tn} - \frac{V_{DSATn}}{2} \right) + k_p V_{DSATp} \left( V_M - V_{DD} - V_{Tp} \frac{V_{DSATp}}{2} \right) = 0 \quad (5.2)$$

Solving for  $V_M$  yields

$$V_M = \frac{\left( V_{Tn} + \frac{V_{DSATn}}{2} \right) + r \left( V_{DD} + V_{Tp} + \frac{V_{DSATp}}{2} \right)}{1 + r} \quad \text{with } r = \frac{k_p V_{DSATp}}{k_n V_{DSATn}} = \frac{\mu_{satp} W_p}{\mu_{satn} W_n} \quad (5.3)$$

assuming identical oxide thicknesses for PMOS and NMOS transistors. For large values of  $V_{DD}$  (compared with threshold and saturation voltages), Eq. (5.3) can be simplified:

$$V_M \approx \frac{r V_{DD}}{1 + r} \quad (5.4)$$

Equation (5.4) states that the switching threshold is set by the ratio  $r$ , which compares the relative driving strengths of the PMOS and NMOS transistors. It is generally desirable for  $V_M$  to be located around the middle of the available voltage swing (or at  $V_{DD}/2$ ), since this results in comparable values for the low and high noise margins. This requires  $r$  to be approximately 1, which is equivalent to sizing the PMOS device so that  $(W/L)_p = (W/L)_n \times (V_{DSATn} k'_n) / (V_{DSATp} k'_p)$ . To move  $V_M$  upwards, a larger value of  $r$  is required, which means making the PMOS wider. Increasing the strength of the NMOS, on the other hand, moves the switching threshold closer to GND.

From Eq. (5.2), we derive the required ratio of PMOS to NMOS transistor sizes such that the switching threshold is set to a desired value  $V_M$ :

$$\frac{(W/L)_p}{(W/L)_n} = \frac{k'_n V_{DSATn} (V_M - V_{Tn} - V_{DSATn}/2)}{k'_p V_{DSATp} (V_{DD} - V_M + V_{Tp} + V_{DSATp}/2)} \quad (5.5)$$

When using this expression, make sure that the assumption that both devices are velocity saturated still holds for the chosen operation point.

---

#### Problem 5.1 Inverter Switching Threshold for Long-Channel Devices, or Low-Supply Voltages

The preceding expressions were derived under the assumption that the transistors are velocity saturated. When the PMOS and NMOS are long-channel devices, or when the supply voltage is low,

velocity saturation does not occur ( $V_M - V_T < V_{DSAT}$ ). Under these circumstances, the following equation holds for  $V_M$ :

$$V_M = \frac{V_{Tn} + r(V_{DD} + V_{Tp})}{1 + r} \quad \text{with } r = \sqrt{\frac{-k_p}{k_n}} \quad (5.6)$$

Derive this equation.

### Design Technique—Maximizing the Noise Margins

When designing static CMOS circuits, it is advisable to balance the driving strengths of the transistors by making the PMOS section wider than the NMOS section if maximizing the noise margins and obtaining symmetrical characteristics are desired. The required ratio is given by Eq. (5.5). ■

#### Example 5.1 Switching Threshold of CMOS Inverter

We derive the sizes of PMOS and NMOS transistors such that the switching threshold of a CMOS inverter, implemented in our generic 0.25  $\mu\text{m}$  CMOS process, is located in the middle between the supply rails. We use the process parameters presented in Example 3.7, and assume a supply voltage of 2.5 V. The minimum size device has a width-to-length ratio of 1.5. With the aid of Eq. (5.5), we find that

$$\frac{(W/L)_p}{(W/L)_n} = \frac{115 \times 10^{-6}}{30 \times 10^{-6}} \times \frac{0.63}{1.0} \times \frac{(1.25 - 0.43 - 0.63/2)}{(1.25 - 0.4 - 1.0/2)} = 3.5$$

Figure 5-7 plots the values of switching threshold as a function of the PMOS-to-NMOS ratio, as obtained by circuit simulation. The simulated PMOS-to-NMOS ratio of 3.4 for a 1.25-V switching threshold confirms the value predicted by Eq. (5.5).

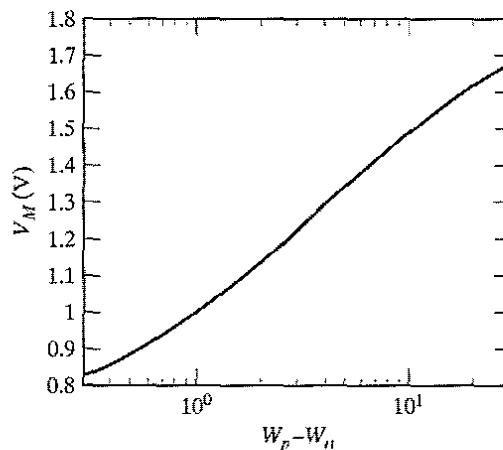


**Figure 5-7** Simulated inverter switching threshold versus PMOS-to-NMOS ratio (0.25- $\mu\text{m}$  CMOS,  $V_{DD} = 2.5$  V).

An analysis of the curve of Figure 5-7 leads to some interesting observations:

1.  $V_M$  is relatively insensitive to variations in the device ratio. This means that small variations of the ratio (e.g., making it 3 or 2.5) do not disturb the transfer characteristic that much. It is therefore an accepted practice in industrial designs to set the width of the PMOS transistor to values smaller than those required for exact symmetry. For the preceding example, setting the ratio to 3, 2.5, and 2 yields switching thresholds of 1.22 V, 1.18 V, and 1.13 V, respectively.
2. The effect of changing the  $W_p$ -to- $W_n$  ratio is to shift the transient region of the VTC. Increasing the width of the PMOS or the NMOS moves  $V_M$  toward  $V_{DD}$  or  $GND$ , respectively. This property can be very useful, as asymmetrical transfer characteristics are actually desirable in some designs. This is demonstrated by the example of Figure 5-8. The incoming signal  $V_{in}$  has a very noisy zero value. Passing this signal through a symmetrical inverter would lead to erroneous values (Figure 5-8a). This can be addressed by raising the threshold of the inverter, which results in a correct response (Figure 5-8b). Later in the text we will see other circuit instances in which inverters with asymmetrical switching thresholds are desirable. Changing the switching threshold by a considerable amount, however, is not easy, especially when the ratio of supply voltage to transistor threshold is relatively small ( $2.5/0.4 = 6$ , for our particular example). To move the threshold to 1.5 V requires a transistor ratio of 11, and further increases are prohibitively expensive. Observe that Figure 5-7 is plotted in a semilog format.

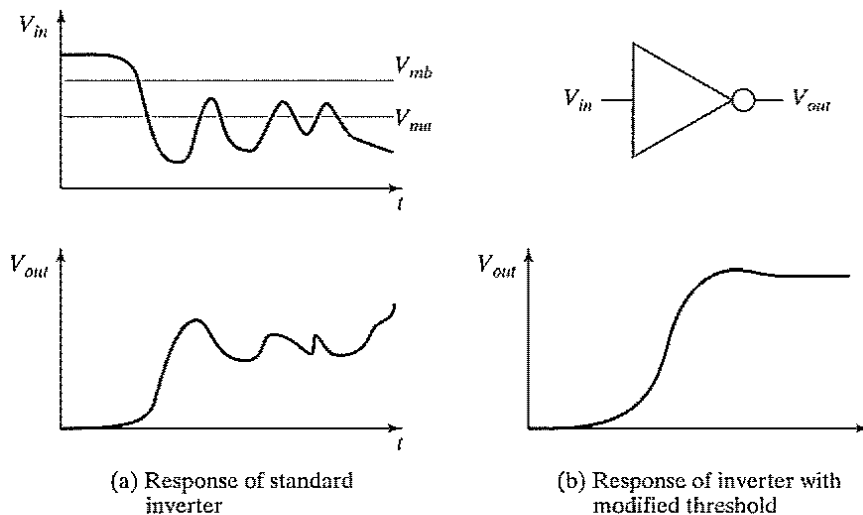


**Figure 5-8** Changing the inverter threshold can improve the circuit reliability.

### 5.3.2 Noise Margins

By definition,  $V_{IH}$  and  $V_{IL}$  are the operational points of the inverter where  $\frac{dV_{out}}{dV_{in}} = -1$ . In the terminology of the analog circuit designer, these are the points where the gain  $g$  of the amplifier, formed by the inverter, is equal to  $-1$ . While it is indeed possible to derive analytical expressions for  $V_{IH}$  and  $V_{IL}$ , these tend to be unwieldy and provide little insight in what parameters are instrumental in setting the noise margins.

A simpler approach is to use a piece-wise linear approximation for the VTC, as shown in Figure 5-9. The transition region is approximated by a straight line, the gain of which equals the gain  $g$  at the switching threshold  $V_M$ . The crossover with the  $V_{OH}$  and the  $V_{OL}$  lines is used to define  $V_{IH}$  and  $V_{IL}$  points. The error introduced is small and well within the range of what is required for an initial design. This approach yields the following expressions for the width of the transition region  $V_{IH} - V_{IL}$ ,  $V_{IH}$ ,  $V_{IL}$ , and the noise margins  $NM_H$  and  $NM_L$ :

$$\begin{aligned}
 V_{IH} - V_{IL} &= \frac{(V_{OH} - V_{OL})}{g} = \frac{-V_{DD}}{g} \\
 V_{IH} &= V_M - \frac{V_M}{g} & V_{IL} &= V_M + \frac{V_{DD} - V_M}{g} \\
 NM_H &= V_{DD} - V_{IH} & NM_L &= V_{IL}
 \end{aligned} \tag{5.7}$$

These expressions make it increasingly clear that a high gain in the transition region is very desirable. In the extreme case of an infinite gain, the noise margins simplify to  $V_{OH} - V_M$  and  $V_M - V_{OL}$  for  $NM_H$  and  $NM_L$ , respectively, and span the complete voltage swing.

It remains for us to determine the midpoint gain of the static CMOS inverter. We assume once again that both PMOS and NMOS are velocity saturated. It is apparent from Figure 5-4 that the gain is a strong function of the slopes of the currents in the saturation region. The channel-

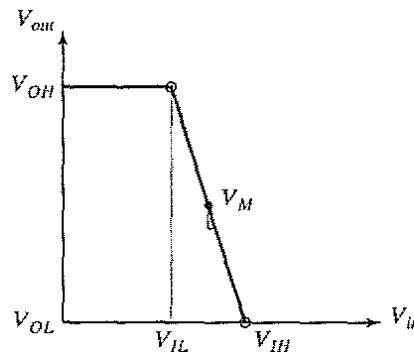


**Figure 5-9** A piecewise linear approximation of the VTC simplifies the derivation of  $V_{IL}$  and  $V_{IH}$ .

length modulation factor therefore cannot be ignored in this analysis—doing so would lead to an infinite gain. The gain can now be derived by differentiating the current Eq. (5.8), which is valid around the switching threshold, with respect to  $V_{in}$ :

$$\begin{aligned} k_n V_{DSATn} \left( V_{in} - V_{Tn} - \frac{V_{DSATn}}{2} \right) (1 + \lambda_n V_{out}) + \\ k_p V_{DSATp} \left( V_{in} - V_{DD} - V_{Tp} - \frac{V_{DSATp}}{2} \right) (1 + \lambda_p V_{out} - \lambda_p V_{DD}) = 0 \end{aligned} \quad (5.8)$$

Differentiating and solving for  $dV_{out}/dV_{in}$ , yields

$$\frac{dV_{out}}{dV_{in}} = \frac{k_n V_{DSATn} (1 + \lambda_n V_{out}) + k_p V_{DSATp} (1 + \lambda_p V_{out} - \lambda_p V_{DD})}{\lambda_n k_n V_{DSATn} (V_{in} - V_{Tn} - V_{DSATn}/2) + \lambda_p k_p V_{DSATp} (V_{in} - V_{DD} - V_{Tp} - V_{DSATp}/2)} \quad (5.9)$$

Ignoring some second-order terms and setting  $V_{in} = V_M$  produces the gain expression,

$$\begin{aligned} g &= \frac{1}{I_D(V_M)} \frac{k_n V_{DSATn} + k_p V_{DSATp}}{\lambda_n - \lambda_p} \\ &\approx \frac{1 + r}{(V_M - V_{Tn} - V_{DSATn}/2)(\lambda_n - \lambda_p)} \end{aligned} \quad (5.10)$$

with  $I_D(V_M)$  the current flowing through the inverter for  $V_{in} = V_M$ . The gain is almost purely determined by technology parameters, especially the channel-length modulation. It can only be influenced in a minor way by the designer through the choice of the supply voltage and the transistor sizes.

### Example 5.2 Voltage Transfer Characteristic and Noise Margins of CMOS Inverter

Assume an inverter in the generic 0.25- $\mu\text{m}$  CMOS technology designed with a PMOS-to-NMOS ratio of 3.4 and with the NMOS transistor minimum size ( $W = 0.375 \mu\text{m}$ ,  $L = 0.25 \mu\text{m}$ ,  $W/L = 1.5$ ). We first compute the gain at  $V_M (= 1.25 \text{ V})$ :

$$I_D(V_M) = 1.5 \times 115 \times 10^{-6} \times 0.63 \times (1.25 - 0.43 - 0.63/2) \times (1 + 0.06 \times 1.25) = 59 \times 10^{-6} \text{ A}$$

$$g = \frac{1}{59 \times 10^{-6}} \frac{1.5 \times 115 \times 10^{-6} \times 0.63 + 1.5 \times 3.4 \times 30 \times 10^{-6} \times 1.0}{0.06 + 0.1} = -27.5 \text{ (Eq. 5.10a)}$$

This yields the following values for  $V_{IL}$ ,  $V_{IH}$ ,  $NM_L$ ,  $NM_H$ :

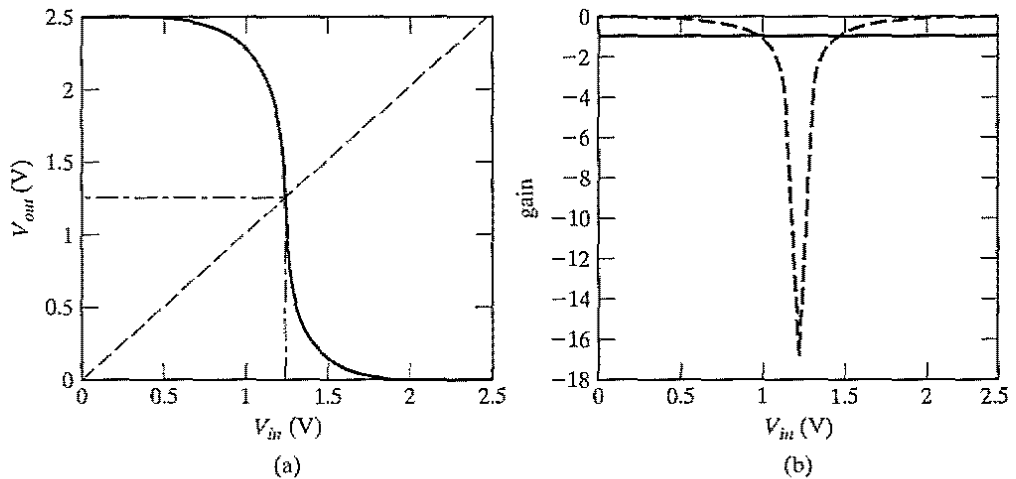
$$V_{IL} = 1.2 \text{ V}, V_{IH} = 1.3 \text{ V}, NM_L = NM_H = 1.2$$

Figure 5-10 plots the simulated VTC of the inverter, as well as its derivative, the gain. A close to ideal characteristic is obtained. The actual values of  $V_{IL}$  and  $V_{IH}$  are 1.03 V and 1.45 V, respectively, which leads to noise margins of 1.03 V and 1.05 V. These values are lower than those predicted, for two reasons:



- Eq. (5.10) overestimates the gain. As observed in Figure 5-10b, the maximum gain (at  $V_M$ ) equals only 17. This reduced gain would yield values for  $V_{IL}$  and  $V_{IH}$  of 1.17 V, and 1.33 V, respectively<sup>1</sup>.
- The most important deviation is due to the piecewise linear approximation of the VTC, which is optimistic with respect to the actual noise margins. The expressions obtained are, however, perfectly useful as first-order estimations, as well as means of identifying the relevant parameters and their impact.

To conclude this example, we also extracted from simulations the output resistance of the inverter in the low- and high-output states. Low values of 2.4 k $\Omega$  and 3.3 k $\Omega$ , respectively, were observed. The output resistance is a good measure of the sensitivity of the gate with respect to noise induced at the output, and is preferably as low as possible.



**Figure 5-10** Simulated Voltage Transfer Characteristic (a) and voltage gain (b) of CMOS inverter (0.25- $\mu$ m CMOS,  $V_{DD} = 2.5$  V).

**SIDELINE:** Surprisingly (or perhaps not so surprisingly), the static CMOS inverter can also be used as an analog amplifier, as it has a fairly high gain in its transition region. This region is very narrow, however, as is apparent in the graph of Figure 5-10b. It also receives poor marks on other amplifier properties such as supply noise rejection. Still, this observation can be used to demonstrate one of the major differences between analog and digital design. Where the analog designer would bias the amplifier in the middle of the transient region so that a maximum linearity is obtained, the digital designer will operate the device in the regions of extreme nonlinearity, resulting in well-defined and well-separated high and low signals.

<sup>1</sup>In addition, Eq. (5.10) is not entirely valid for this particular example. The attentive reader will observe that for the operating conditions at hand, the PMOS operates in saturation mode, not velocity saturation. The impact on the result is minor, however.

**Problem 5.2 Inverter Noise Margins for Long-Channel Devices**

Derive expressions for the gain and noise margins assuming that PMOS and NMOS are long-channel devices (or that the supply voltage is low), so that velocity saturation does not occur.

**5.3.3 Robustness Revisited****Device Variations**

While we design a gate for nominal operation conditions and typical device parameters, we should always be aware that the actual operating temperature might vary over a large range, and that the device parameters after fabrication probably will deviate from the nominal values we used in our design optimization process. Fortunately, the dc characteristics of the static CMOS inverter turn out to be rather insensitive to these variations, and the gate remains functional over a wide range of operating conditions. This already became apparent in Figure 5-7, which shows that variations in the device sizes have only a minor impact on the switching threshold of the inverter. To further confirm the assumed robustness of the gate, we have resimulated the voltage transfer characteristic by replacing the nominal devices by their worst or best case incarnations. Two corner cases are plotted in Figure 5-11: a better-than-expected NMOS, combined with an inferior PMOS, and the opposite scenario. Comparing the resulting curves with the nominal response shows that the operation of the gate is by no means affected, and that the variations mainly cause a shift in the switching threshold. This robust behavior, which ensures functionality of the gate over a wide range of conditions, has contributed in a big way to the popularity of the static CMOS gate.

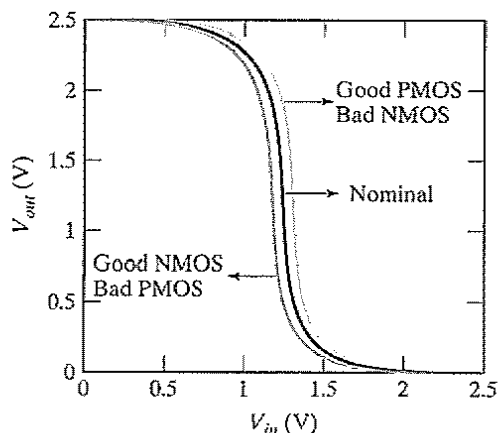


**Figure 5-11** Impact of device variations on static CMOS inverter VTC. The “good” device has a smaller oxide thickness (– 3 nm), a smaller length (– 25 nm), a higher width (+ 30 nm), and a smaller threshold (– 60 mV). The opposite is true for the “bad” transistor.

### Scaling the Supply Voltage

In Chapter 3, we observed that continuing technology scaling forces the supply voltages to reduce at rates similar to the device dimensions. At the same time, device threshold voltages are virtually kept constant. You may wonder about the impact of this trend on the integrity parameters of the CMOS inverter. Do inverters keep on working when the voltages are scaled, and are there potential limits to the supply scaling?

A first hint on what might happen was offered in Eq. (5.10), which indicates that the gain of the inverter in the transition region actually increases with a reduction of the supply voltage! Note that for a fixed transistor ratio  $r$ ,  $V_M$  is approximately proportional to  $V_{DD}$ . Plotting the (normalized) VTC for different supply voltages not only confirms this conjecture, but even shows that the inverter is well and alive for supply voltages close to the threshold voltage of the composing transistors (see Figure 5-12a). At a voltage of 0.5 V—which is just 100 mV above the threshold of the transistors—the width of the transition region measures only 10% of the supply voltage (for a maximum gain of 35), while it widens to 17% for 2.5 V. So, given this improvement in dc characteristics, why do we not choose to operate all of our digital circuits at these low supply voltages? Three important reasons come to mind:

- Reducing the supply voltage indiscriminately has a positive impact on the energy dissipation, but is absolutely detrimental to the delay of the gate, as we will learn in the next sections.
- The dc characteristic becomes increasingly sensitive to variations in the device parameters, such as the transistor threshold, once supply voltages and intrinsic voltages become comparable.
- Scaling the supply voltage means reducing the signal swing. While this typically helps to reduce the internal noise in the system (such as caused by crosstalk), it makes the design more sensitive to external noise sources that do not scale.

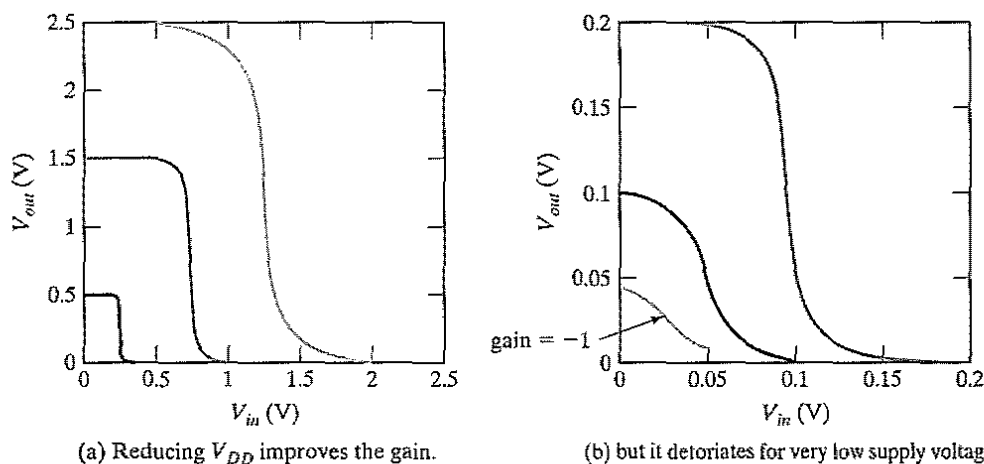


Figure 5-12 VTC of CMOS inverter as a function of supply voltage (0.25- $\mu$ m CMOS technology).

To provide an insight into the question on potential limits to the voltage scaling, we have plotted the voltage transfer characteristic of the same inverter for the even lower supply voltages of 200 mV, 100 mV, and 50 mV in Figure 5-12b. The transistor thresholds are kept at the same level. Amazingly enough, we still obtain an inverter characteristic, even though the supply voltage is not large enough to turn the transistors on! The explanation can be found in the subthreshold operation of the transistors. The subthreshold currents are sufficient to switch the gate between low and high levels, as well as to provide enough gain to produce acceptable VTCs. The low value of the switching currents ensures a very slow operation, but this might be acceptable for some applications (such as watches, for example).

At around 100 mV, we start observing a major deterioration of the gate characteristic.  $V_{OL}$  and  $V_{OH}$  are no longer at the supply rails and the transition region gain approaches 1. The latter turns out to be a fundamental showstopper. To achieve sufficient gain for use in a digital circuit, it is necessary that the supply be at least two times  $\phi_T = kT/q$  ( $= 25$  mV at room temperature), the thermal voltage introduced in Chapter 3 [Swanson72]. It turns out that below this same voltage, thermal noise becomes an issue as well, potentially resulting in unreliable operation. We express this relation as

$$V_{DDmin} > 2 \dots 4 \frac{kT}{q} \quad (5.11)$$

Equation (5.11) presents a true lower bound on supply scaling. It suggests that the only way to get CMOS inverters to operate below 100 mV is to reduce the ambient temperature—or in other words, to cool the circuit.

---

#### Problem 5.3 Minimum Supply Voltage of CMOS Inverter

Once the supply voltage drops below the threshold voltage, the transistors operate in the subthreshold region, and display an exponential current–voltage relationship (as expressed in Eq. (3.39)). Derive an expression for the gain of the inverter under these circumstances (assume symmetrical NMOS and PMOS transistors, and a maximum gain at  $V_M = V_{DD}/2$ ). The resulting expression demonstrates that the minimum voltage is a function of the slope factor  $n$  of the transistor:

$$g = - \left( \frac{1}{n} \right) (e^{V_{DD}/2\phi_T} - 1) \quad (5.12)$$

According to this expression, the gain drops to  $-1$  at  $V_{DD} = 48$  mV (for  $n = 1.5$  and  $\phi_T = 25$  mV).

---

#### 5.4 Performance of CMOS Inverter: The Dynamic Behavior

The qualitative analysis presented earlier concluded that the propagation delay of the CMOS inverter is determined by the time it takes to charge and discharge the load capacitor  $C_L$  through the PMOS and NMOS transistors, respectively. This observation suggests that **getting  $C_L$  as small as possible is crucial to the realization of high-performance CMOS circuits.** It is thus

worthwhile to first study the major components of the load capacitance before embarking on an in-depth analysis of the propagation delay of the gate. In addition to this detailed analysis, this section also presents a summary of techniques that a designer might use to optimize the performance of the inverter.

### 5.4.1 Computing the Capacitances

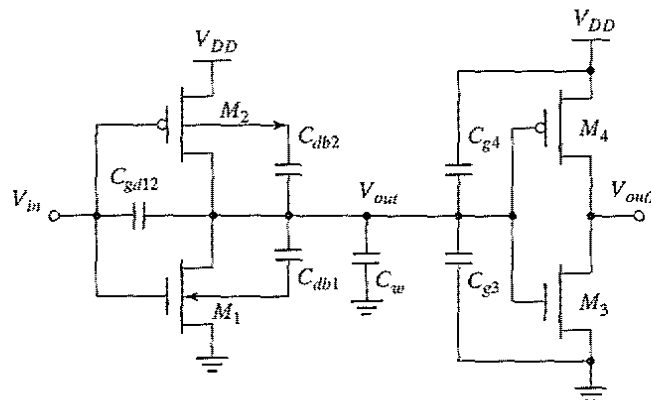
Manual analysis of MOS circuits where each capacitor is considered individually is virtually impossible. The problem is exacerbated by the many nonlinear capacitances in the MOS transistor model. To make the analysis tractable, we assume that all capacitances are lumped together into one single capacitor  $C_L$ , located between  $V_{out}$  and  $GND$ . Be aware that this is a considerable simplification of the actual situation, even in the case of a simple inverter.

Figure 5-13 shows the schematic of a cascaded inverter pair. It includes all the capacitances influencing the transient response of node  $V_{out}$ . It is initially assumed that the input  $V_{in}$  is driven by an ideal voltage source with zero rise and fall times. Accounting only for capacitances connected to the output node,  $C_L$  breaks down into the following components.

#### Gate-Drain Capacitance $C_{gd12}$

$M_1$  and  $M_2$  are either in cut-off or in the saturation mode during the first half (up to 50% point) of the output transient. Under these circumstances, the only contributions to  $C_{gd12}$  are the overlap capacitances of both  $M_1$  and  $M_2$ . The channel capacitance of the MOS transistors does not play a role here, as it is located either completely between gate and bulk (cut-off) or gate and source (saturation) (see Chapter 3).

The lumped capacitor model now requires that this floating gate-drain capacitor be replaced by a capacitance to ground. This is accomplished by taking the so-called Miller effect into account. During a low-high or high-low transition, the terminals of the gate-drain capacitor are moving in opposite directions (see Figure 5-14). The voltage change over the floating capacitor is thus twice the actual output voltage swing. To present an identical load to the out-



**Figure 5-13** Parasitic capacitances, influencing the transient behavior of the cascaded inverter pair.

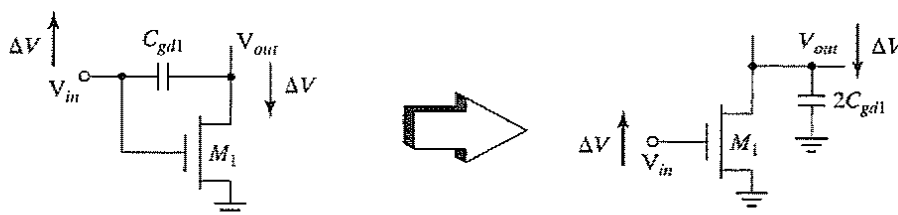


**Figure 5-14** The Miller effect—A capacitor experiencing identical but opposite voltage swings at both its terminals can be replaced by a capacitor to ground, whose value is two times the original value.

put node, the capacitance to ground must have a value that is twice as large as the floating capacitance.

We use the following equation for the gate-drain capacitors:  $C_{gd} = 2 C_{GD0} W$  (with  $C_{GD0}$  the overlap capacitance per unit width as used in the SPICE model). For an in-depth discussion of the Miller effect, please refer to textbooks such as [Sedra87, p. 57].<sup>2</sup>

#### Diffusion Capacitances $C_{db1}$ and $C_{db2}$

The capacitance between drain and bulk is due to the reverse-biased  $pn$ -junction. Such a capacitor is, unfortunately, quite nonlinear and depends heavily on the applied voltage. We argued in Chapter 3 that the best approach to simplifying the analysis is to replace the nonlinear capacitor by a linear one with the same change in charge for the voltage range of interest. A multiplication factor  $K_{eq}$  is introduced to relate the linearized capacitor to the value of the junction capacitance under zero-bias conditions.

$$C_{eq} = K_{eq} C_{j0} \quad (5.13)$$

with  $C_{j0}$  the junction capacitance per unit area under zero-bias conditions. For convenience, we repeat Eq. (3.11) here, written as

$$K_{eq} = \frac{-\phi_0^m}{(V_{high} - V_{low})(1 - m)} [(\phi_0 - V_{high})^{1-m} - (\phi_0 - V_{low})^{1-m}] \quad (5.14)$$

with  $\phi_0$  the built-in junction potential and  $m$  the grading coefficient of the junction. Observe that the junction voltage is defined to be negative for reverse-biased junctions.

#### Example 5.3 $K_{eq}$ for a 2.5-V CMOS Inverter

Consider the inverter of Figure 5-13 designed in the generic 0.25- $\mu\text{m}$  CMOS technology. The relevant capacitance parameters for this process were summarized in Table 3-5.

Let us first analyze the NMOS transistor ( $C_{db1}$  in Figure 5-13). The propagation delay is defined by the time between the 50% transitions of the input and the output. For the CMOS inverter, this is the time instance where  $V_{out}$  reaches 1.25-V, as the output

<sup>2</sup>The Miller effect discussed in this context is a simplified version of the general analog case. In a digital inverter, the large-scale gain between input and output always equals  $-1$ .

voltage swing goes from rail to rail or equals 2.5 V. We therefore linearize the junction capacitance over the interval  $\{2.5 \text{ V}, 1.25 \text{ V}\}$  for the high-to-low transition, and  $\{0, 1.25 \text{ V}\}$  for the low-to-high transition.

During the high-to-low transition at the output,  $V_{out}$  initially equals 2.5 V. Because the bulk of the NMOS device is connected to  $GND$ , this translates into a reverse voltage of 2.5 V over the drain junction or  $V_{high} = -2.5 \text{ V}$ . At the 50% point,  $V_{out} = 1.25 \text{ V}$  or  $V_{low} = -1.25 \text{ V}$ . Evaluating Eq. (5.14) for the bottom plate and sidewall components of the diffusion capacitance yields the following data:

$$\begin{aligned} \text{Bottom plate: } & K_{eq} (m = 0.5, \phi_0 = 0.9) = 0.57 \\ \text{Sidewall: } & K_{eqsw} (m = 0.44, \phi_0 = 0.9) = 0.61 \end{aligned}$$

During the low-to-high transition,  $V_{low}$  and  $V_{high}$  equal 0 V and  $-1.25 \text{ V}$ , respectively, resulting in higher values for  $K_{eq}$ :

$$\begin{aligned} \text{Bottom plate: } & K_{eq} (m = 0.5, \phi_0 = 0.9) = 0.79 \\ \text{Sidewall: } & K_{eqsw} (m = 0.44, \phi_0 = 0.9) = 0.81 \end{aligned}$$

The PMOS transistor displays a reverse behavior, as its substrate is connected to 2.5 V. Hence, for the high-to-low transition ( $V_{low} = 0, V_{high} = -1.25 \text{ V}$ ), we have

$$\begin{aligned} \text{Bottom plate: } & K_{eq} (m = 0.48, \phi_0 = 0.9) = 0.79 \\ \text{Sidewall: } & K_{eqsw} (m = 0.32, \phi_0 = 0.9) = 0.86 \end{aligned}$$

Finally, for the low-to-high transition ( $V_{low} = -1.25 \text{ V}, V_{high} = -2.5 \text{ V}$ ), we have

$$\begin{aligned} \text{Bottom plate: } & K_{eq} (m = 0.48, \phi_0 = 0.9) = 0.59 \\ \text{Sidewall: } & K_{eqsw} (m = 0.32, \phi_0 = 0.9) = 0.7 \end{aligned}$$

By using this approach, the junction capacitance can be replaced by a linear component and treated as any other device capacitance. The result of the linearization is a minor error in the voltage and current waveforms. The logic delays are not significantly influenced by this simplification.

### Wiring Capacitance $C_w$

The capacitance due to the wiring depends on the length and width of the connecting wires, and is a function of the distance of the fan-out from the driving gate and the number of fan-out gates. As argued in Chapter 4, this component is growing in importance with the scaling of the technology.

### Gate Capacitance of Fan-Out $C_{g3}$ and $C_{g4}$

We assume that the fan-out capacitance equals the total gate capacitance of the loading gates  $M_3$  and  $M_4$ . Hence,

$$\begin{aligned} C_{fan-out} &= C_{gate}(\text{NMOS}) + C_{gate}(\text{PMOS}) \\ &= (C_{GSO_n} + C_{GDO_n} + W_n L_n C_{ox}) + (C_{GSO_p} + C_{GDO_p} + W_p L_p C_{ox}) \end{aligned} \quad (5.15)$$

This expression simplifies the actual situation in two ways:

- It assumes that all components of the gate capacitance are connected between  $V_{out}$  and  $GND$  (or  $V_{DD}$ ), and it ignores the Miller effect on the gate–drain capacitances. This has a relatively minor effect on the accuracy, since we can safely assume that the connecting gate does not switch before the 50% point is reached, and  $V_{out2}$  thus remains constant in the interval of interest.
- A second approximation is that the channel capacitance of the connecting gate is constant over the interval of interest. This is not exactly the case as we discovered in Chapter 3. The total channel capacitance is a function of the operation mode of the device, and varies from approximately  $(2/3) WLC_{ox}$  (saturation) to the full  $WLC_{ox}$  (linear and cutoff). A drop in overall gate capacitance also occurs just before the transistor turns on, as in Figure 3-31. During the first half of the transient, it may be assumed that one of the load devices is always in linear mode, while the other transistor evolves from the off mode to saturation. Ignoring the capacitance variation results in a pessimistic estimation with an error of approximately 10%, which is acceptable for a first-order analysis.

#### Example 5.4 Capacitances of a 0.25- $\mu\text{m}$ CMOS Inverter

A minimum-size, symmetrical CMOS inverter has been designed in the 0.25- $\mu\text{m}$  CMOS technology. The layout is shown in Figure 5-15. The supply voltage  $V_{DD}$  is set to 2.5 V. From the layout, we derive the transistor sizes, diffusion areas, and perimeters. This data is summarized in Table 5-1. As an example, we will derive the drain area and perimeter for the NMOS transistor. The drain area is formed by the metal-diffusion contact, which has an area of  $4 \times 4 \lambda^2$ , and the rectangle between contact and gate, which has an area of  $3 \times 1 \lambda^2$ . This results in a total area of  $19 \lambda^2$ , or  $0.30 \mu\text{m}^2$  (as  $\lambda = 0.125 \mu\text{m}$ ). The perimeter of the drain area is rather involved and consists of the following components (going counterclockwise):  $5 + 4 + 4 + 1 + 1 = 15 \lambda$  or  $PD = 15 \times 0.125 = 1.875 \mu\text{m}$ . Notice that the gate side of the drain perimeter is not included, as this is not considered a part of the sidewall. The drain area and perimeter of the PMOS transistor are derived similarly (the rectangular shape makes the exercise considerably simpler):  $AD = 5 \times 9 \lambda^2 = 45 \lambda^2$ , or  $0.7 \mu\text{m}^2$ ;  $PD = 5 + 9 + 5 = 19 \lambda$ , or  $2.375 \mu\text{m}$ .

Table 5-1 Inverter transistor data.

	W/L	AD ( $\mu\text{m}^2$ )	PD ( $\mu\text{m}$ )	AS ( $\mu\text{m}^2$ )	PS ( $\mu\text{m}$ )
NMOS	0.375/0.25	0.3 ( $19 \lambda^2$ )	1.875 ( $15\lambda$ )	0.3 ( $19 \lambda^2$ )	1.875 ( $15\lambda$ )
PMOS	1.125/0.25	0.7 ( $45 \lambda^2$ )	2.375 ( $19\lambda$ )	0.7 ( $45 \lambda^2$ )	2.375 ( $19\lambda$ )



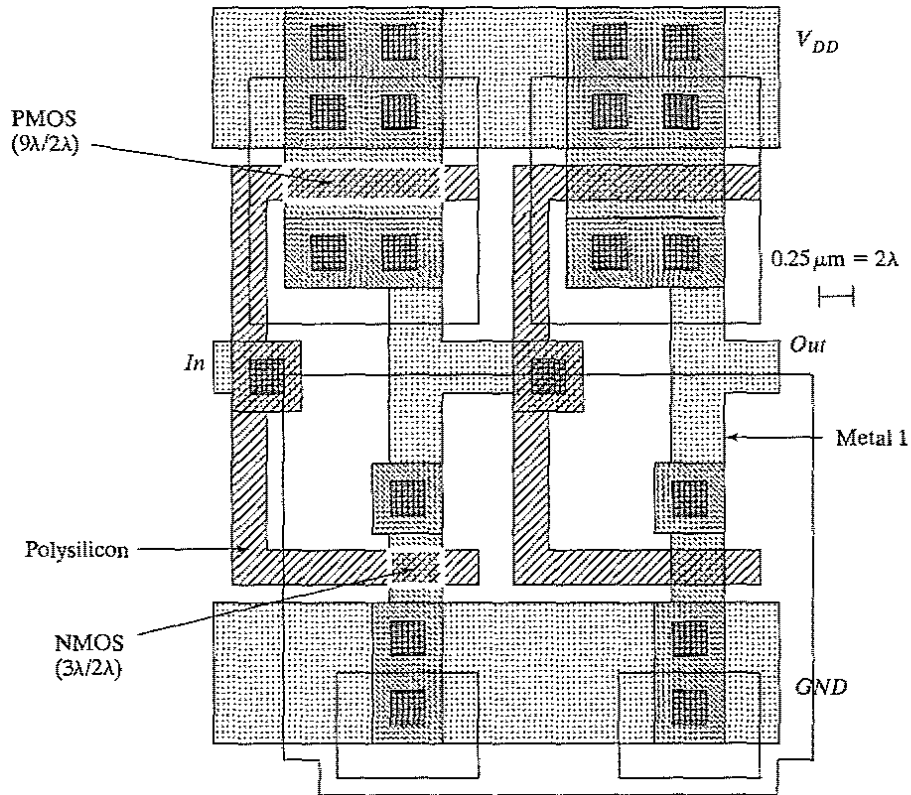


**Figure 5-15** Layout of two chained, minimum-size inverters using SCMOS Design Rules (see also Color-plate 6).

This physical information can be combined with the approximations derived earlier to come up with an estimation of  $C_L$ . The capacitor parameters for our generic process were summarized in Table 3-5 and are repeated here for convenience:

Overlap capacitance:  $CGD0(\text{NMOS}) = 0.31 \text{ fF}/\mu\text{m}$ ;  $CGD0(\text{PMOS}) = 0.27 \text{ fF}/\mu\text{m}$   
 Bottom junction capacitance:  $CJ(\text{NMOS}) = 2 \text{ fF}/\mu\text{m}^2$ ;  $CJ(\text{PMOS}) = 1.9 \text{ fF}/\mu\text{m}^2$   
 Sidewall junction capacitance:  $CJSW(\text{NMOS}) = 0.28 \text{ fF}/\mu\text{m}$ ;  $CJSW(\text{PMOS}) = 0.22 \text{ fF}/\mu\text{m}$   
 Gate capacitance:  $C_{ox}(\text{NMOS}) = C_{ox}(\text{PMOS}) = 6 \text{ fF}/\mu\text{m}^2$

Finally, we should also consider the capacitance contributed by the wire connecting the gates and implemented in metal 1 and polysilicon. A layout extraction program typically delivers precise values for this parasitic capacitance. Inspection of the layout helps us form a first-order estimate. It yields that the metal-1 and polysilicon areas of the wire, which are not over active diffusion, equal  $42 \lambda^2$  and  $72 \lambda^2$ , respectively. With the aid of the interconnect parameters of Table 4-2, we find the wire capacitance (observe that we ignore the fringing

Table 5-2 Components of  $C_L$  (for high-to-low and low-to-high transitions).

Capacitor	Expression	Value (fF) (H → L)	Value (fF) (L → H)
$C_{gd1}$	$2 CGD0_n W_n$	0.23	0.23
$C_{gd2}$	$2 CGD0_p W_p$	0.61	0.61
$C_{db1}$	$K_{eqn} AD_n CJ + K_{eqswp} PD_n CJSW$	0.66	0.90
$C_{db2}$	$K_{eqp} AD_p CJ + K_{eqswp} PD_p CJSW$	1.5	1.15
$C_{g3}$	$(CGD0_n + CGSO_n) W_n + C_{ox} W_n L_n$	0.76	0.76
$C_{g4}$	$(CGD0_p + CGSO_p) W_p + C_{ox} W_p L_p$	2.28	2.28
$C_w$	From Extraction	0.12	0.12
$C_L$	$\Sigma$	6.1	6.0

capacitance in this simple exercise; due to the short length of the wire, this contribution can be ignored compared with the other entries):

$$C_{wire} = 42/8^2 \mu\text{m}^2 \times 30 \text{ aF}/\mu\text{m}^2 + 72/8^2 \mu\text{m}^2 \times 88 \text{ aF}/\mu\text{m}^2 = 0.12 \text{ fF}$$

The results of bringing all the components together are summarized in Table 5-2. We use the values of  $K_{eq}$  derived in Example 5.3 for the computation of the diffusion capacitances. Notice that the load capacitance is almost evenly split between its two major components: the *intrinsic capacitance*, composed of diffusion and overlap capacitances, and the *extrinsic load capacitance*, contributed by wire and connecting gate.

#### 5.4.2 Propagation Delay: First-Order Analysis

One way to compute the propagation delay of the inverter is to integrate the capacitor (dis)charge current. This results in the expression

$$t_p = \int_{v_1}^{v_2} \frac{C_L(v)}{i(v)} dv \quad (5.16)$$

with  $i$  the (dis)charging current,  $v$  the voltage over the capacitor, and  $v_1$  and  $v_2$  the initial and final voltage, respectively. An exact computation of this equation is intractable, as both  $C_L(v)$  and  $i(v)$  are nonlinear functions of  $v$ . Instead, we fall back to the simplified switch model of the inverter introduced in Figure 5-6 to derive a reasonable approximation of the propagation delay adequate for manual analysis. The voltage dependencies of the “on” resistance and the load

capacitor are addressed by replacing both by a constant linear element with a value averaged over the interval of interest. The preceding section derived precisely this value for the load capacitance. An expression for the average “on” resistance of the MOS transistor was already derived in Example 3.8 and is repeated here for convenience:

$$R_{eq} = \frac{1}{V_{DD}/2} \int_{V_{DD}/2}^{V_{DD}} \frac{V}{I_{DSAT}(1 + \lambda V)} dV \approx \frac{3}{4} \frac{V_{DD}}{I_{DSAT}} \left( 1 - \frac{7}{9} \lambda V_{DD} \right) \quad (5.17)$$

$$\text{with } I_{DSAT} = k' \frac{W}{L} \left( (V_{DD} - V_T) V_{DSAT} - \frac{V_{DSAT}^2}{2} \right)$$

Deriving the propagation delay of the resulting circuit is now straightforward—it is nothing more than the analysis of a first-order linear  $RC$  network, identical to the exercise of Example 4.5. We learned there that the propagation delay of such a network, excited by a voltage step, is proportional to the time constant of the network, formed by pull-down resistor and load capacitance. Hence,

$$t_{pHL} = \ln(2) R_{eqn} C_L = 0.69 R_{eqn} C_L \quad (5.18)$$

Similarly, we can obtain the propagation delay for the low-to-high transition. We write

$$t_{pLH} = 0.69 R_{eqp} C_L \quad (5.19)$$

with  $R_{eqp}$  the equivalent on resistance of the PMOS transistor over the interval of interest. This analysis assumes that the equivalent load-capacitance is identical for both the high-to-low and low-to-high transitions. This was shown to be approximately the case in the example of the previous section. The overall propagation delay of the inverter is defined as the average of the two values:

$$t_p = \frac{t_{pHL} + t_{pLH}}{2} = 0.69 C_L \left( \frac{R_{eqn} + R_{eqp}}{2} \right) \quad (5.20)$$

Very often, it is desirable for a gate to have identical propagation delays for both rising and falling inputs. This condition can be achieved by making the “on” resistance of the NMOS and PMOS approximately equal. Remember that this condition is identical to the requirement for a symmetrical VTC.

---

### Example 5.5 Propagation Delay of a 0.25 $\mu\text{m}$ CMOS Inverter

To derive the propagation delays of the CMOS inverter of Figure 5-15, we make use of Eq. (5.18) and Eq. (5.19). The load capacitance  $C_L$  was already computed in Example 5.4, while the equivalent “on” resistances of the transistors for the generic 0.25- $\mu\text{m}$  CMOS process were derived in Table 3-3. For a supply voltage of 2.5 V, the normalized “on” resistances of NMOS and PMOS transistors equal 13  $\text{k}\Omega$  and 31  $\text{k}\Omega$ , respectively. From the layout, we determine the ( $W$ -to- $L$ ) ratios of the transistors to be 1.5 for the NMOS, and

4.5 for the PMOS. We assume that the difference between drawn and effective dimensions is small enough to be ignorable. This leads to the following values for the delays:

$$t_{pHL} = 0.69 \times \left( \frac{13 \text{ k}\Omega}{1.5} \right) \times 6.1 \text{ fF} = 36 \text{ ps}$$

$$t_{pLH} = 0.69 \times \left( \frac{31 \text{ k}\Omega}{4.5} \right) \times 6.0 \text{ fF} = 29 \text{ ps}$$

and

$$t_p = \left( \frac{36 + 29}{2} \right) = 32.5 \text{ ps}$$

The accuracy of this analysis is checked by performing a SPICE transient simulation on the circuit schematic, extracted from the layout of Figure 5-15. The computed transient response of the circuit is plotted in Figure 5-16, and determines the propagation delays to be 39.9 ps and 31.7 ps for the HL and LH transitions, respectively. The manual results are good, considering the many simplifications made during their derivation. Notice in particular the overshoots on the simulated output signals. These are caused by the gate-drain capacitances of the inverter transistors, which couple the steep voltage step at the input node directly to the output before the transistors can even start to react to the changes at the input. These overshoots clearly have a negative impact on the performance of the gate and explain why the simulated delays are larger than the estimations.

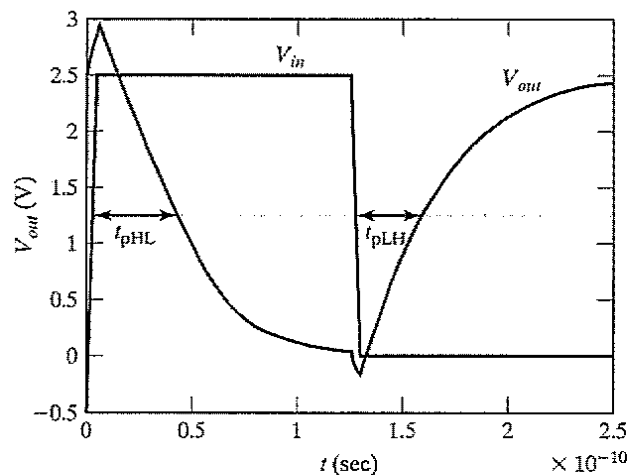


Figure 5-16 Simulated transient response of the inverter of Figure 5-15.

**WARNING:** This example might give the impression that manual analysis always leads to close approximations of the actual response, which is not necessarily the case. Large deviations often can be observed between first- and higher order models. The purpose of the manual

analysis is to get a basic insight into the behavior of the circuit and to determine the dominant parameters. A detailed simulation is indispensable when quantitative data is required. Consider the preceding example a stroke of good luck.

The obvious question a designer asks at this point is how to manipulate or optimize the delay of a gate. To provide an answer to this question, it is necessary to make the parameters governing the delay explicit by expanding  $R_{eq}$  in the delay equation. Combining Eq. (5.18) and Eq. (5.17), and assuming for the time being that the channel-length modulation factor  $\lambda$  is ignorable, yields the following expression for  $t_{pHL}$  (a similar analysis holds for  $t_{pLH}$ ):

$$t_{pHL} = 0.69 \frac{3C_L V_{DD}}{4 I_{DSATn}} = 0.52 \frac{C_L V_{DD}}{(W/L)_n k'_n V_{DSATn} (V_{DD} - V_{Th} - V_{DSATn}/2)} \quad (5.21)$$

In the majority of designs, the supply voltage is chosen high enough so that  $V_{DD} \gg V_{Th} + V_{DSATn}/2$ . Under these conditions, the delay becomes virtually independent of the supply voltage:

$$t_{pHL} \approx 0.52 \frac{C_L}{(W/L)_n k'_n V_{DSATn}} \quad (5.22)$$

Observe that this is a first-order approximation, and that increasing the supply voltage yields an observable, albeit small, improvement in performance due to a nonzero channel-length modulation factor. This analysis is confirmed in Figure 5-17, which plots the propagation delay of the inverter as a function of the supply voltage. It comes as no surprise that this curve is virtu-

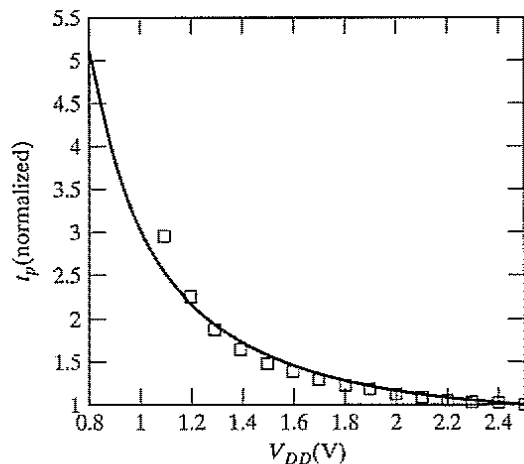


**Figure 5-17** Propagation delay of CMOS inverter as a function of supply voltage (normalized with respect to the delay at 2.5 V). The dots indicate the delay values predicted by Eq. (5.21). Observe that this equation is only valid when the devices are velocity saturated. Hence, the deviation at low supply voltages.

ally identical in shape to the one of Figure 3-28, which charts the equivalent “on” resistance of the MOS transistor as a function of  $V_{DD}$ . While the delay is relatively insensitive to supply variations for higher values of  $V_{DD}$ , a sharp increase can be observed starting around  $\approx 2V_T$ . This operation region clearly should be avoided if achieving high performance is a primary design goal.

### Design Techniques

From the preceding discussion, we deduce that the propagation delay of a gate can be minimized in the following ways:

- **Reduce  $C_L$ .** Remember that three major factors contribute to the load capacitance: the internal diffusion capacitance of the gate itself, the interconnect capacitance, and the fan-out. Careful layout helps to reduce the diffusion and interconnect capacitances. **Good design practice requires keeping the drain diffusion areas as small as possible.**
- **Increase the  $W/L$  ratio of the transistors.** This is the most powerful and effective performance optimization tool in the hands of the designer. Proceed with caution, however, when applying this approach. Increasing the transistor size also raises the diffusion capacitance and hence  $C_L$ . In fact, once the intrinsic capacitance (i.e. the diffusion capacitance) starts to dominate the extrinsic load formed by wiring and fan-out, increasing the gate size no longer helps in reducing the delay. It only makes the gate larger in area. This effect is called *self-loading*. In addition, wide transistors have a larger gate capacitance, which increases the fan-out factor of the driving gate and adversely affects its speed as well.
- **Increase  $V_{DD}$ .** As illustrated in Figure 5-17, the delay of a gate can be modulated by modifying the supply voltage. This flexibility allows the designer to trade off energy dissipation for performance, as we will see in a later section. However, increasing the supply voltage above a certain level yields only very minimal improvement and thus should be avoided. Also, reliability concerns (oxide breakdown, hot-electron effects) enforce firm upper bounds on the supply voltage in deep submicron processes. ■

#### Problem 5.4 Propagation Delay as a Function of (dis)charge Current

So far, we have expressed the propagation delay as a function of the equivalent resistance of the transistors. Another approach would be to replace the transistor by a current source with a value equal to the average (dis)charge current over the interval of interest. Derive an expression of the propagation delay using this alternative approach.

#### 5.4.3 Propagation Delay from a Design Perspective

Some interesting design considerations and trade-offs can be derived from the delay expressions we have derived so far. Most importantly, they lead to a general approach toward transistor sizing that will prove to be extremely useful.

##### NMOS-to-PMOS Ratio

So far, we have consistently widened the PMOS transistor so that its resistance matches that of the pull-down NMOS device. This typically requires a ratio of 3 to 3.5 between PMOS and

NMOS width. The motivation behind this approach is to create an inverter with a symmetrical VTC and to equate the high-to-low and low-to-high propagation delays. However, this does not imply that this ratio also yields the minimum overall propagation delay. If symmetry and reduced noise margins are not of prime concern, it is actually possible to speed up the inverter by reducing the width of the PMOS device!

The reasoning behind this statement is that, while widening the PMOS improves the  $t_{pLH}$  of the inverter by increasing the charging current, it also degrades the  $t_{pHL}$  by causing a larger parasitic capacitance. When two contradictory effects are present, a transistor ratio must exist that optimizes the propagation delay of the inverter.

This optimum ratio can be derived using a simple analysis technique. Consider two identical cascaded CMOS inverters. The approximate load capacitance of the first gate is given by

$$C_L = (C_{dp1} + C_{dn1}) + (C_{gp2} + C_{gn2}) + C_W \quad (5.23)$$

where  $C_{dp1}$  and  $C_{dn1}$  are the equivalent drain diffusion capacitances of PMOS and NMOS transistors of the first inverter and  $C_{gp2}$  and  $C_{gn2}$  are the gate capacitances of the second gate.  $C_W$  represents the wiring capacitance.

When the PMOS devices are made  $\beta$  times larger than the NMOS ones ( $\beta = (W/L)_p/(W/L)_n$ ), all transistor capacitances scale in approximately the same way, or  $C_{dp1} \approx \beta C_{dn1}$ , and  $C_{gp2} \approx \beta C_{gn2}$ . Equation (5.23) can then be rewritten as

$$C_L = (1 + \beta)(C_{dn1} + C_{gn2}) + C_W \quad (5.24)$$

Based on Eq. (5.20), the following expression for the propagation delay can be derived,

$$\begin{aligned} t_p &= \frac{0.69}{2}((1 + \beta)(C_{dn1} + C_{gn2}) + C_W) \left( R_{eqn} + \frac{R_{eqp}}{\beta} \right) \\ &= 0.345((1 + \beta)(C_{dn1} + C_{gn2}) + C_W) R_{eqn} \left( 1 + \frac{r}{\beta} \right) \end{aligned} \quad (5.25)$$

Here,  $r (= R_{eqp}/R_{eqn})$  represents the resistance ratio of identically sized PMOS and NMOS transistors. The optimal value of  $\beta$  can be found by setting  $\frac{\partial t_p}{\partial \beta}$  to 0, which yields

$$\beta_{opt} = \sqrt{r \left( 1 + \frac{C_W}{C_{dn1} + C_{gn2}} \right)} \quad (5.26)$$

This means that when the wiring capacitance is negligible ( $C_{dn1} + C_{gn2} \gg C_W$ ),  $\beta_{opt}$  equals  $\sqrt{r}$ , in contrast to the factor  $r$  normally used in the noncascaded case. If the wiring capacitance dominates, larger values of  $\beta$  should be used. The surprising result of this analysis is that smaller device sizes (and thus a smaller design area) yield a faster design at the expense of symmetry and noise margin.

**Example 5.6 Sizing of CMOS Inverter Loaded by an Identical Gate**

Consider again our standard design example. From the values of the equivalent resistances (Table 3-3), we find that a ratio  $\beta$  of 2.4 ( $= 31 \text{ k}\Omega / 13 \text{ k}\Omega$ ) would yield a symmetrical transient response. Eq. (5.26) now predicts that the device ratio for an optimal performance should equal 1.6. These results are verified in Figure 5-18, which plots the simulated propagation delay as a function of the transistor ratio  $\beta$ . The graph clearly illustrates how a changing  $\beta$  trades off between  $t_{pLH}$  and  $t_{pHL}$ . The optimum point occurs around  $\beta = 1.9$ , which is somewhat higher than predicted. Observe also that the rising and falling delays are identical at the predicted point of  $\beta$  equal to 2.4. This is the preferred operation point when the worst case delay is the prime concern.<sup>3</sup>

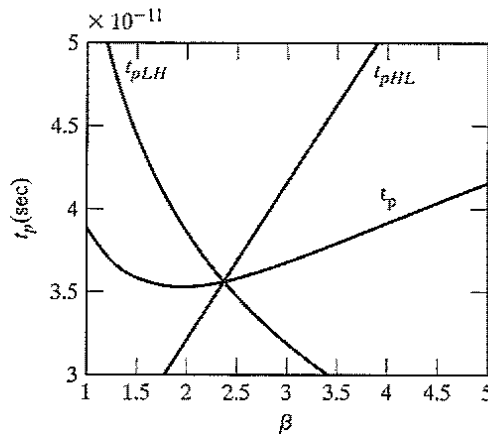


**Figure 5-18** Propagation delay of CMOS inverter as a function of the PMOS-to-NMOS transistor ratio  $\beta$ .

**Sizing Inverters for Performance**

In this analysis, we assume a symmetrical inverter, which is an inverter where PMOS and NMOS are sized such that the rise and fall delays are identical. The load capacitance of the inverter can be divided into an intrinsic and an extrinsic component, or  $C_L = C_{int} + C_{ext}$ .  $C_{int}$  represents the self-loading or intrinsic output capacitance of the inverter, and is associated with the diffusion capacitances of the NMOS and PMOS transistors as well as the gate-drain overlap (Miller) capacitances.  $C_{ext}$  is the extrinsic load capacitance, attributable to fan-out and wiring

<sup>3</sup>You probably wonder why we do not always consider the worst of the rising and falling delays as the prime performance measure of a gate. When cascading inverting gates to form a more complex logic network, you quickly realize that the average of the two is a more meaningful measure. A rising transition on one gate is followed by a falling transition on the next.



capacitance. Assuming that  $R_{eq}$  stands for the equivalent resistance of the gate, we can express the propagation delay as

$$\begin{aligned} t_p &= 0.69R_{eq}(C_{int} + C_{ext}) \\ &= 0.69R_{eq}C_{int}(1 + C_{ext}/C_{int}) = t_{p0}(1 + C_{ext}/C_{int}) \end{aligned} \quad (5.27)$$

where  $t_{p0} = 0.69 R_{eq} C_{int}$  represents the delay of the inverter only loaded by its own intrinsic capacitance ( $C_{ext} = 0$ ), and is called the *intrinsic or unloaded delay*.

The next question is how transistor sizing impacts the performance of the gate. To answer this question, we must establish the relationship between the various parameters in Eq. (5.27) and a sizing factor  $S$ , which relates the transistor sizes of our inverter to a reference gate—typically a minimum-sized inverter. The intrinsic capacitance  $C_{int}$  consists of the diffusion and Miller capacitances, both of which are proportional to the width of the transistors. Hence,  $C_{int} = SC_{iref}$ . The resistance of the gate relates to the reference gate as  $R_{eq} = R_{ref}/S$ . We can now rewrite Eq. (5.27) as

$$\begin{aligned} t_p &= 0.69(R_{ref}/S)(SC_{iref})(1 + C_{ext}/(SC_{iref})) \\ &= 0.69R_{ref}C_{iref}\left(1 + \frac{C_{ext}}{SC_{iref}}\right) = t_{p0}\left(1 + \frac{C_{ext}}{SC_{iref}}\right) \end{aligned} \quad (5.28)$$

From this analysis, we draw two important conclusions:

- The intrinsic delay of the inverter  $t_{p0}$  is independent of the sizing of the gate, and is determined purely by technology and inverter layout. When no load is present, an increase in the drive of the gate is totally offset by the increased capacitance.
- Making  $S$  infinitely large yields the maximum obtainable performance gain, eliminating the impact of any external load, and reducing the delay to the intrinsic one. Yet, any sizing factor  $S$  that is sufficiently larger than  $(C_{ext}/C_{int})$  produces similar results at a substantial gain in silicon area.

### Example 5.7 Device Sizing for Performance

Let us explore the performance improvement that can be obtained by device sizing in the design of Example 5.5. We find from Table 5-2 that  $C_{int}/C_{ext} \approx 1.05$  ( $C_{int} = 3.0$  fF,  $C_{ext} = 3.15$  fF). This would predict a maximum performance gain of 2.05. A scaling factor of 10 allows us to get within 10% of this optimal performance, while larger device sizes only yield ignorable performance gains.

This is confirmed by simulation results, which predict a maximum obtainable performance improvement of 1.9 ( $t_{p0} = 19.3$  ps). In Figure 5-19, we observe that the majority of the improvement is already obtained for  $S = 5$ , and that sizing factors larger than 10 barely yield any extra gain.

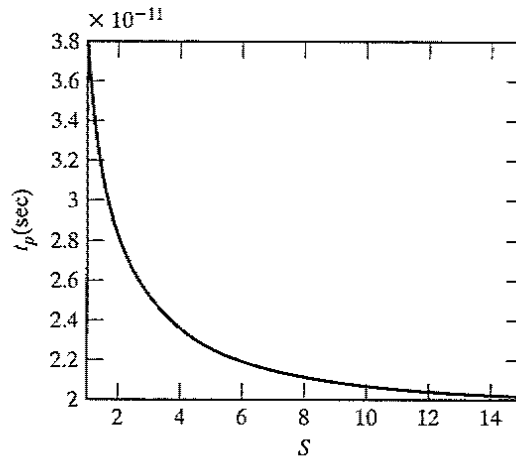


**Figure 5-19** Increasing inverter performance by sizing the NMOS and PMOS transistor with an identical factor  $S$  for a fixed fan-out (inverter of Figure 5-15).

### Sizing a Chain of Inverters

While sizing up an inverter reduces its delay, it also increases its input capacitance. Gate sizing in an isolated fashion without taking into account its impact on the delay of the preceding gates is a purely academic enterprise. Therefore, a more relevant problem is determining the optimum sizing of a gate when **embedded in a real environment**. A simple chain of inverters is a good first case to study. To determine the input loading effect, the relationship between the input gate capacitance  $C_g$  and the intrinsic output capacitance of the inverter has to be established. Both are proportional to the gate sizing. Hence, the following relationship holds, independently of gate sizing:

$$C_{int} = \gamma C_g \quad (5.29)$$

In Eq. (5.29),  $\gamma$  is a proportionality factor that is only a function of technology and is close to 1 for most submicron processes, as we observed in the preceding examples. Rewriting Eq. (5.28), we obtain

$$t_p = t_{p0} \left( 1 + \frac{C_{ext}}{\gamma C_g} \right) = t_{p0} (1 + f/\gamma) \quad (5.30)$$

which establishes that the delay of an inverter is **only a function of the ratio between its external load capacitance and its input capacitance**. This ratio is called the *effective fan-out*  $f$ .

Let us consider the circuit of Figure 5.20. The goal is to minimize the delay through the inverter chain, with the input capacitance  $C_{g1}$  of the first inverter—typically a minimally-sized gate—and the load capacitance  $C_L$  at the end of the chain fixed.

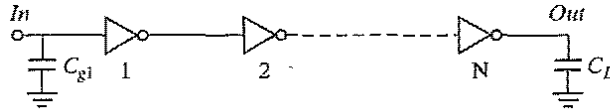


Figure 5-20 Chain of  $N$  inverters with fixed input and output capacitance.

Given the delay expression for the  $j$ -th inverter stage,<sup>4</sup>

$$t_{p,j} = t_{p0} \left( 1 + \frac{C_{g,j+1}}{\gamma C_{g,j}} \right) = t_{p0} (1 + f_j / \gamma) \quad (5.31)$$

we can derive the total delay of the chain:

$$t_p = \sum_{j=1}^N t_{p,j} = t_{p0} \sum_{j=1}^N \left( 1 + \frac{C_{g,j+1}}{\gamma C_{g,j}} \right), \text{ with } C_{g,N+1} = C_L \quad (5.32)$$

This equation has  $N - 1$  unknowns, being  $C_{g,2}, C_{g,3}, \dots, C_{g,N}$ . The minimum delay can be found by taking  $N - 1$  partial derivatives, and equating them to 0, or  $\partial t_p / \partial C_{g,j} = 0$ . The result is a set of constraints,

$$C_{g,j+1} / C_{g,j} = C_{g,j} / C_{g,j-1} \quad \text{with } (j = 2 \dots N) \quad (5.33)$$

In other words, the optimum size of each inverter is the geometric mean of its neighbors sizes:

$$C_{g,j} = \sqrt{C_{g,j-1} C_{g,j+1}} \quad (5.34)$$

This means that each inverter is sized up by the same factor  $f$  with respect to the preceding gate, has the same effective fan-out ( $f_j = f$ ), and thus the same delay. With  $C_{g,1}$  and  $C_L$  given, we can derive the sizing factor as

$$f = \sqrt[N]{C_L / C_{g,1}} = \sqrt[N]{F} \quad (5.35)$$

and the minimum delay through the chain as

$$t_p = N t_{p0} (1 + \sqrt[N]{F} / \gamma) \quad (5.36)$$

$F$  represents the *overall effective fan-out* of the circuit and equals  $C_L / C_{g,1}$ . Observe how the relationship between  $t_p$  and  $F$  is a strong function of the number of stages. As expected, the relationship is linear when only 1 stage is present. Introducing a second stage turns it into a square root function, and so on. The obvious question now is how to choose the number of stages so that the delay is minimized for a given value of  $F$ .

<sup>4</sup>This expression ignores the wiring capacitance, which is a fair assumption for the time being.

### Choosing the Right Number of Stages in an Inverter Chain

Evaluation of Eq. (5.36) reveals the trade-offs in choosing the number of stages for a given  $F$  ( $= f^N$ ). When the number of stages is too large, the first component of the equation, which represents the intrinsic delay of the stages, becomes dominant. If the number of stages is too small, the effective fan-out of each stage becomes large, and the second component is dominant. The optimum value can be found by differentiating the minimum delay expression by the number of stages and setting the result to 0. We obtain

$$\gamma + N\sqrt{F} - \frac{N\sqrt{F} \ln F}{N} = 0$$

or equivalently

$$f = e^{(1+\gamma/f)}$$

Equation (5.35) has only a closed-form solution for  $\gamma = 0$ —that is when the self-loading is ignored and the load capacitance only consists of the fan-out. Under these simplified conditions, it is found that the optimal number of stages equals  $N = \ln(F)$ , and the effective fan-out of each stage is set to  $f = e = 2.71828$ . This optimal buffer design scales consecutive stages in an exponential fashion, and is thus called an exponential horn [Mead80]. When self-loading is included, Eq. can only be solved numerically. The results are plotted in Figure 5-21a. For the typical case of  $\gamma \approx 1$ , the optimum tapering factor turns out to be close to 3.6. Figure 5-21b plots the (normalized) propagation delay of the inverter chain as a function of the effective fan-out for  $\gamma = 1$ . Choosing values of the fan-out that are higher than the optimum does not effect the delay very much and reduces the required number of buffer stages and the implementation area. A common practice is to **select an optimum fan-out of 4**. The use of too many stages ( $f < f_{opt}$ ), on the other hand, has a substantial negative impact on the delay, and should be avoided.

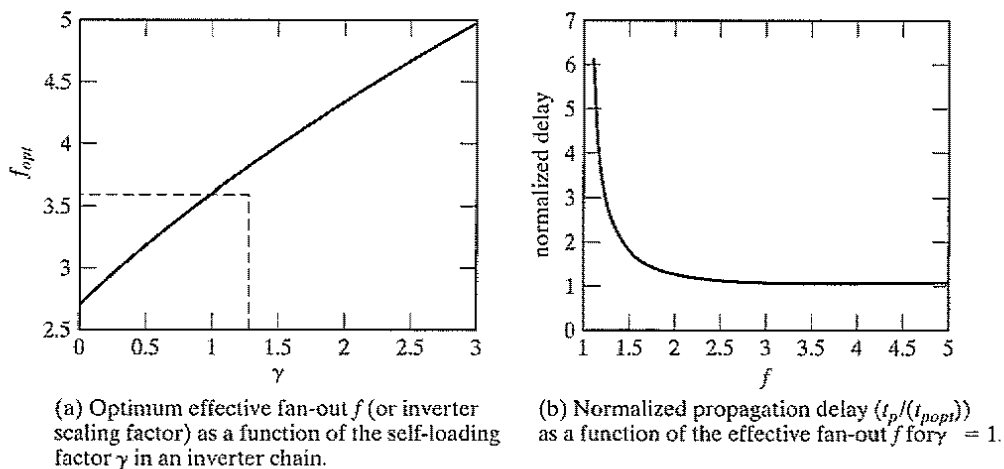


**Figure 5-21** Optimizing the number of stages in an inverter chain.

**Example 5.8 The Impact of Introducing Buffer Stages**

Table 5-3 enumerates the values of  $t_{p,opt}/t_{p0}$  for the unbuffered design, the dual stage, and optimized inverter chain for a variety of values of  $F$  (for  $\gamma = 1$ ). Observe the impressive speedup obtained with cascaded inverters when driving very large capacitive loads.

**Table 5-3**  $t_{p,opt}/t_{p0}$  versus  $x$  for various driver configurations.

F	Unbuffered	Two Stage	Inverter Chain
10	11	8.3	8.3
100	101	22	16.5
1000	1001	65	24.8
10,000	10,001	202	33.1

The preceding analysis can be extended to not only cover chains of inverters, but also networks of inverters that contain actual fan-out, an example of which is shown in Figure 5-22. We merely have to adjust the expression for  $C_{ext}$  to incorporate the additional fan-out factors.

**Problem 5.5 Sizing an Inverter Network**

Determine the sizes of the inverters in the circuit of Figure 5-22, such that the delay between nodes *Out* and *In* is minimized. You may assume that  $C_L = 64 C_{g,1}$ .

Hints: Determine first the ratios between the devices that minimize the delay. You should find that the following relationship must hold:

$$\frac{4C_{g,2}}{C_{g,1}} = \frac{4C_{g,3}}{C_{g,2}} = \frac{C_L}{C_{g,3}}$$

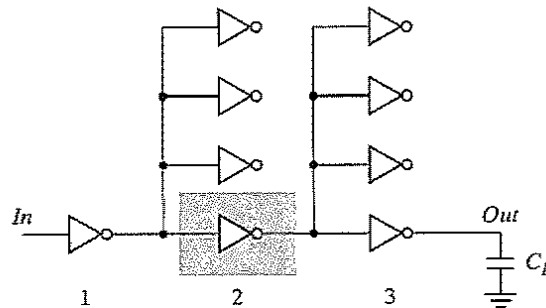


**Figure 5-22** Inverter network, in which each gate has a fan-out of 4 gates, distributing a single input to 16 output signals in a treelike fashion.

Finding the actual gate sizes ( $C_{g,3} = 2.52C_{g,2} = 6.35C_{g,1}$ ) is a relatively straightforward task (with  $2.52 = 16^{1/3}$ ). Straightforward sizing of the inverter chain, without taking the extra fan-out into account, would have led to a sizing factor of 4 instead of 2.52.

### The Rise-Fall Time of the Input Signal

All of the preceding expressions were derived under the assumption that the input signal to the inverter abruptly changed from 0 to  $V_{DD}$  or vice versa. Only one of the devices is assumed to be on during the (dis)charging process. In reality, the input signal changes gradually and, temporarily, PMOS and NMOS transistors conduct simultaneously. This affects the total current available for (dis)charging and impacts the propagation delay. Figure 5-23 plots the propagation delay of a minimum-size inverter as a function of the input signal slope—as obtained from SPICE. It can be observed that  $t_p$  increases (approximately) linearly with increasing input slope, once  $t_s > t_p$  ( $t_s = 0$ ).

While it is possible to derive an analytical expression describing the relationship between input signal slope and propagation delay, the result tends to be complex and of limited value. From a design perspective, it is more valuable to relate the impact of the finite slope on the performance directly to its cause, which is the limited driving capability of the preceding gate. If the latter would be infinitely strong, its output slope would be zero, and the performance of the gate under examination would be unaffected. The strength of this approach is that it realizes that a gate is never designed in isolation, and that its performance is affected by both the fan-out and the driving strength of the gate(s) feeding into its inputs. This leads to a revised expression for the propagation delay of an inverter  $i$  in a chain of inverters [Hedenstierna87]:

$$t_p^i = t_{step}^i + \eta t_{step}^{i-1} \quad (5.38)$$

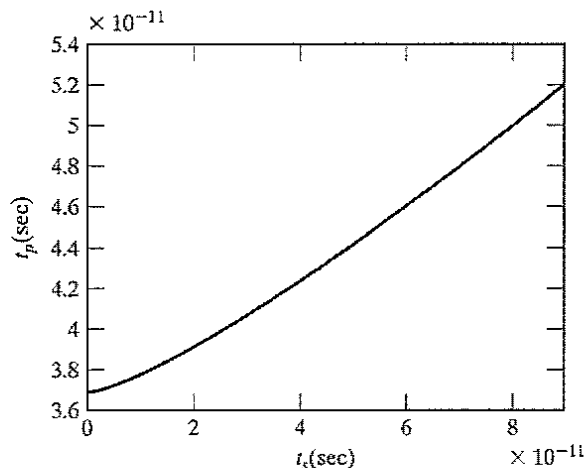


**Figure 5-23**  $t_p$  as a function of the input signal slope (10–90% rise or fall time) for minimum-size inverter with fan-out of a single gate.

Eq. (5.38) states that the propagation delay of inverter  $i$  equals the sum of the delay of the same gate for a step input ( $t_{step}^i$ ) (i.e. zero input slope) augmented with a fraction of the step-input delay of the preceding gate ( $i - 1$ ). The fraction  $\eta$  is an empirical constant, which typically has values around 0.25. This expression has the advantage of being very simple, while exposing all relationships necessary for the delay computations of complex circuits.

### Example 5.9 Delay of Inverter Embedded in Network

Consider, for example, the circuit of Figure 5-22. With the aid of Eq. (5.31) and Eq. (5.38), we can derive an expression for the delay of the stage-2 inverter, marked by the gray box:

$$t_{p,2} = t_{p0} \left( 1 + \frac{4C_{g,3}}{\gamma C_{g,2}} \right) + \eta t_{p0} \left( 1 + \frac{4C_{g,2}}{\gamma C_{g,1}} \right)$$

An analysis of the overall propagation delay in the style of Problem 5.5, leads to the following revised sizing requirements for minimum delay:

$$\frac{4(1 + \eta)C_{g,2}}{C_{g,1}} = \frac{4(1 + \eta)C_{g,3}}{C_{g,2}} = \frac{C_L}{C_{g,3}}$$

If we assume  $\eta = 0.25$ ,  $f_2$  and  $f_1$  evaluate to 2.47.

### Design Challenge

It is advantageous to keep the signal rise times smaller than or equal to the gate propagation delays. This proves to be true not only for performance, but also for power consumption considerations, as will be discussed later. Keeping the rise and fall times of the signals small and of approximately equal values is one of the major challenges in high-performance design; it is often called *slope engineering*. ■

### Problem 5.6 Impact of Input Slope

Determine if reducing the supply voltage increases or decreases the influence of the input signal slope on the propagation delay. Explain your answer.

### Delay in the Presence of (Long) Interconnect Wires

The interconnect wire has played a minimal role in our analysis thus far. When gates get farther apart, the wire capacitance and resistance can no longer be ignored, and may even dominate the transient response. Earlier delay expressions can be adjusted to accommodate these extra contributions by employing the wire modeling techniques introduced in the previous chapter. The analysis detailed in Example 4.9 is directly applicable to the problem at hand. Consider the circuit of Figure 5-24, where an inverter drives a single fan-out through a wire of length  $L$ . The driver is represented by a single resistance  $R_{dr}$ , which is the average between  $R_{eqn}$  and  $R_{eqp}$ .  $C_{int}$  and  $C_{fan}$  account for the intrinsic capacitance of the driver, and the input capacitance of the fan-out gate, respectively.

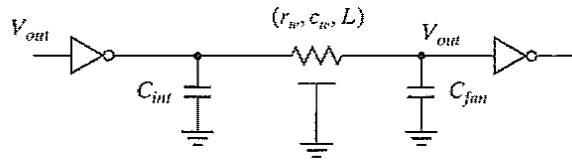


Figure 5-24 Inverter driving single gate through wire of length  $L$ .

The propagation delay of the circuit can be obtained by applying the Elmore delay expression:

$$\begin{aligned} t_p &= 0.69R_{dr}C_{int} + (0.69R_{dr} + 0.38R_w)C_w + 0.69(R_{dr} + R_w)C_{fan} \\ &= 0.69R_{dr}(C_{int} + C_{fan}) + 0.69(R_{dr}c_w + r_wC_{fan})L + 0.38r_wc_wL^2 \end{aligned} \quad (5.39)$$

The 0.38 factor accounts for the fact that the wire represents a distributed delay.  $C_w$  and  $R_w$  stand for the total capacitance and resistance of the wire, respectively. The delay expression contains a component that is linear with the wire length, as well as a quadratic one. It is the latter that causes the wire delay to rapidly become the dominant factor in the delay budget for longer wires.

#### Example 5.10 Inverter Delay in Presence of Interconnect

Consider the circuit of Figure 5-24, and assume the device parameters of Example 5.5:  $C_{int} = 3$  fF,  $C_{fan} = 3$  fF, and  $R_{dr} = 0.5(13/1.5 + 31/4.5) = 7.8$  k $\Omega$ . The wire is implemented in metal and has a width of  $0.4$   $\mu\text{m}$ —the minimum allowed. This yields the following parameters:  $c_w = 92$  aF/ $\mu\text{m}$ , and  $r_w = 0.19$   $\Omega/\mu\text{m}$  (Example 4.4). With the aid of Eq. (5.39), we can compute at what wire length the delay of the interconnect becomes equal to the intrinsic delay caused purely by device parasitics. Solving the following quadratic equation yields a single (meaningful) solution:

$$\begin{aligned} 6.6 \times 10^{-16}L^2 + 0.5 \times 10^{-12}L &= 32.29 \times 10^{-12} \\ \text{or, } L &= 65 \mu\text{m} \end{aligned}$$

Observe that the extra delay is due solely to the linear factor in the equation—more specifically, to the extra capacitance introduced by the wire. The quadratic factor (the distributed wire delay) becomes dominant only at much larger wire lengths ( $> 7$  cm). This can be attributed to the high resistance of the (minimum-size) driver transistors. A different balance emerges when wider transistors are used. Analyze, for instance, the same problem with the driver transistors 100 times wider.

## 5.5 Power, Energy, and Energy Delay

So far, we have seen that the static CMOS inverter with its almost ideal VTC—symmetrical shape, full logic swing, and high noise margins—offers a superior robustness, which simplifies the design process considerably and opens the door for design automation. Another major



attractor for static CMOS is the almost complete absence of power consumption in steady-state operation mode. It is this combination of robustness and low static power that has made static CMOS the technology of choice of most contemporary digital designs. The power dissipation of a CMOS circuit is instead dominated by the dynamic dissipation resulting from charging and discharging capacitances.

### 5.5.1 Dynamic Power Consumption

#### Dynamic Dissipation due to Charging and Discharging Capacitances

Each time the capacitor  $C_L$  gets charged through the PMOS transistor, its voltage rises from 0 to  $V_{DD}$ , and a certain amount of energy is drawn from the power supply. Part of this energy is dissipated in the PMOS device, while the remainder is stored on the load capacitor. During the high-to-low transition, this capacitor is discharged, and the stored energy is dissipated in the NMOS transistor.<sup>5</sup>

A precise measure for this energy consumption can be derived. Let us first consider the low-to-high transition. We assume, initially, that the input waveform has zero rise and fall times—in other words, the NMOS and PMOS devices are never on simultaneously. Therefore, the equivalent circuit of Figure 5-25 is valid. The values of the energy  $E_{V_{DD}}$ , taken from the supply during the transition, as well as the energy  $E_C$ , stored on the capacitor at the end of the transition, can be derived by integrating the instantaneous power over the period of interest:

$$E_{V_{DD}} = \int_0^{\infty} i_{V_{DD}}(t) V_{DD} dt = V_{DD} \int_0^{\infty} C_L \frac{dv_{out}}{dt} dt = C_L V_{DD} \int_0^{V_{DD}} dv_{out} = C_L V_{DD}^2 \quad (5.40)$$

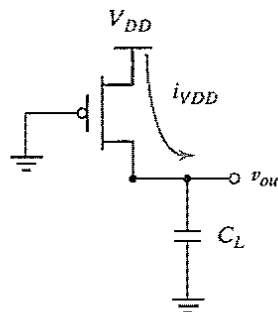


Figure 5-25 Equivalent circuit during the low-to-high transition.

<sup>5</sup>Observe that this model is a simplification of the actual circuit. In reality, the load capacitance consists of multiple components, some of which are located between the output node and GND, others between output node and  $V_{DD}$ . The latter experience a charge–discharge cycle that is out of phase with the capacitances to GND (i.e., they get charged when  $V_{out}$  goes low and discharged when  $V_{out}$  rises.) While this distributes the energy delivery by the supply over the two phases, it does not affect the overall dissipation, and the results presented in this section are still valid.

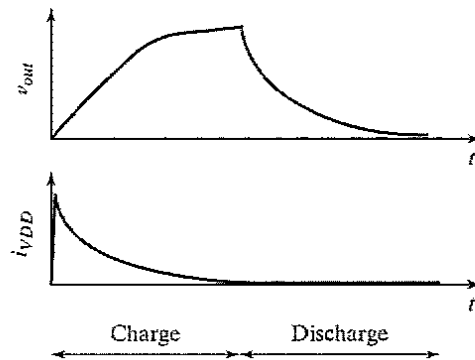


Figure 5-26 Output voltages and supply current during (dis)charge of  $C_L$ .

and

$$E_C = \int_0^{\infty} i_{VDD}(t) v_{out} dt = \int_0^{\infty} C_L \frac{dv_{out}}{dt} v_{out} dt = C_L \int_0^{V_{DD}} v_{out} dv_{out} = \frac{C_L V_{DD}^2}{2} \quad (5.41)$$

The corresponding waveforms of  $v_{out}(t)$  and  $i_{VDD}(t)$  are pictured in Figure 5-26.

These results can also be derived by observing that during the low-to-high transition,  $C_L$  is loaded with a charge  $C_L V_{DD}$ . Providing this charge requires an energy from the supply equal to  $C_L V_{DD}^2 (= Q \times V_{DD})$ . The energy stored on the capacitor equals  $C_L V_{DD}^2/2$ . This means that only half of the energy supplied by the power source is stored on  $C_L$ . The other half has been dissipated by the PMOS transistor. Notice that this energy dissipation is independent of the size (and hence the resistance) of the PMOS device! During the discharge phase, the charge is removed from the capacitor, and its energy is dissipated in the NMOS device. Once again, there is no dependence on the size of the device. In summary, each switching cycle (consisting of an L→H and an H→L transition) takes a fixed amount of energy, equal to  $C_L V_{DD}^2$ . In order to compute the power consumption, we have to take into account how often the device is switched. If the gate is switched **on and off**  $f_{0 \rightarrow 1}$  times per second, the power consumption is given by

$$P_{dyn} = C_L V_{DD}^2 f_{0 \rightarrow 1} \quad (5.42)$$

where  $f_{0 \rightarrow 1}$  represents the frequency of energy-consuming transitions (these are  $0 \rightarrow 1$  transitions for static CMOS).

Advances in technology result in ever-higher values of  $f_{0 \rightarrow 1}$  (as  $t_p$  decreases). At the same time, the total capacitance on the chip ( $C_L$ ) increases as more and more gates are placed on a single die. Consider, for instance, a 0.25- $\mu\text{m}$  CMOS chip with a clock rate of 500 MHz and an average load capacitance of 15 fF/gate, assuming a fan-out of 4. The power consumption per gate for a 2.5-V supply then equals approximately 50  $\mu\text{W}$ . For a design with 1 million gates, and assuming that a transition occurs at every clock edge, this would result in a power consumption of 50 W! This

evaluation, fortunately, presents a pessimistic perspective. In reality, not all gates in the complete IC switch at the full rate of 500 Mhz. The actual activity in the circuit is substantially lower.

---

### Example 5.11 Capacitive Power Dissipation of Inverter

The capacitive dissipation of the CMOS inverter of Example 5.4 is now easily computed. In Table 5-2, the value of the load capacitance was determined to equal 6 fF. For a supply voltage of 2.5 V, the amount of energy needed to charge and discharge that capacitance equals

$$E_{dyn} = C_L V_{DD}^2 = 37.5 \text{ fJ}$$

Assume that the inverter is switched at the (hypothetically) maximum possible rate ( $T = 1/f = t_{pLH} + t_{pHL} = 2t_p$ ). For a  $t_p$  of 32.5 ps (Example 5.5), we find that the dynamic power dissipation of the circuit is

$$P_{dyn} = E_{dyn}/(2t_p) = 580 \text{ } \mu\text{W}$$

Of course, an inverter in an actual circuit is rarely switched at this maximum rate, and even if it would be, the output does not swing from rail to rail. The power dissipation will thus be substantially lower. For a rate of 4 GHz ( $T = 250$  ps), the dissipation reduces to 150  $\mu\text{W}$ . This is confirmed by simulations, which yield a power consumption of 155  $\mu\text{W}$ .

---

Computing the dissipation of a complex circuit is complicated by the  $f_{0 \rightarrow 1}$  factor, also called the *switching activity*. While the switching activity is easily computed for an inverter, it turns out to be far more complex in the case of more complex gates and circuits. One concern is that the switching activity of a network is a function of the nature and the statistics of the input signals: If the input signals remain unchanged, no switching happens, and the dynamic power consumption is zero! On the other hand, rapidly changing signals provoke plenty of switching and therefore dissipation. Other factors influencing the activity are the overall network topology and the function to be implemented. We can accommodate this by writing

$$P_{dyn} = C_L V_{DD}^2 f_{0 \rightarrow 1} = C_L V_{DD}^2 P_{0 \rightarrow 1} f = C_{EFF} V_{DD}^2 f \quad (5.43)$$

where  $f$  now presents the maximum possible event rate of the inputs (which is often the clock rate) and  $P_{0 \rightarrow 1}$  the probability that a clock event results in a  $0 \rightarrow 1$  (or power-consuming) event at the output of the gate.  $C_{EFF} = P_{0 \rightarrow 1} C_L$  is called the *effective capacitance* and represents the average capacitance switched every clock cycle. For our example, an activity factor of 10% ( $P_{0 \rightarrow 1} = 0.1$ ) reduces the average consumption to 5 W.

**Example 5.12 Switching Activity**

Consider the waveforms in Figure 5.27, where the upper waveform represents the idealized clock signal, and the bottom one shows the signal at the output of the gate. Power consuming transitions occur 2 out of 8 times, which is equivalent to a transition probability of 0.25 (or 25%).

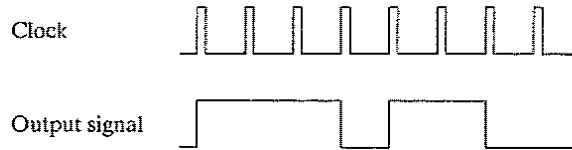


**Figure 5-27** Clock and signal waveforms.

### Low Energy–Power Design Techniques

With the increasing complexity of digital integrated circuits, it is anticipated that the power problem will only worsen in future technologies. This is one of the reasons that lower supply voltages are becoming more and more attractive. **Reducing  $V_{DD}$  has a quadratic effect on  $P_{dyn}$ .** For instance, reducing  $V_{DD}$  from 2.5 V to 1.25 V for our example drops the power dissipation from 5 W to 1.25 W. This assumes that the same clock rate can be sustained. Figure 5-17 demonstrates that this assumption is not that unrealistic as long as the supply voltage is substantially higher than the threshold voltage. A large performance penalty occurs once  $V_{DD}$  approaches  $2V_T$ .

When a lower limit on the supply voltage is set by external constraints (as often happens in real-world designs), or when the performance degradation due to lowering the supply voltage is intolerable, the only means of reducing the dissipation is by lowering the effective capacitance. This can be achieved by addressing both of its components: the physical capacitance and the switching activity.

A *reduction in the switching activity* can only be accomplished at the logic and architectural abstraction levels, and will be discussed in more detail in Chapter 11. *Lowering the physical capacitance* is a worthwhile goal overall, and it also may help to improve the performance of the circuit. As most of the capacitance in a combinational logic circuit is due to transistor capacitances (gate and diffusion), it makes sense to keep those contributions to a minimum when designing for low power. This means that transistors should be kept to *minimal size* whenever possible or reasonable. This definitely affects the performance of the circuit, but the effect can be offset by using logic or architectural speedup techniques. The only instances where transistors should be sized up is when the load capacitance is dominated by extrinsic capacitances (such as fan-out or wiring capacitance). This is contrary to common design practices used in cell libraries, where transistors are generally made large to accommodate a range of loading and performance requirements.

These observations lead to an interesting design challenge. Assume we have to minimize the energy dissipation of a circuit with a specified lower bound on the performance. An attractive approach is to lower the supply voltage as much as possible, and to compensate the loss in performance by increasing the transistor sizes. Yet, the latter causes the capacitance to increase. It may be foreseen that at a low enough supply voltage, the latter factor may start to dominate and cause energy to increase with a further drop in the supply voltage. ■

**Example 5.13 Transistor Sizing for Energy Minimization**

To analyze the transistor sizing for a minimum energy problem, we examine the simple case of a static CMOS inverter driving an external load capacitance  $C_{ext}$ , as in Figure 5.28. To take the input loading effects into account, we assume that the inverter itself is driven by a minimum-sized device. The goal is to minimize the energy dissipation of the complete circuit, while maintaining a lower bound on performance. The degrees of freedom are the size factor  $f$  of the inverter and the supply voltage  $V_{dd}$  of the circuit. The propagation delay of the optimized circuit should not be larger than that of a reference circuit, chosen to have as parameters  $f = 1$  and  $V_{dd} = V_{ref}$ .

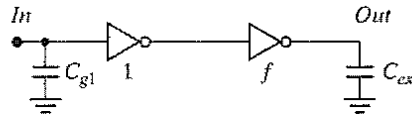


**Figure 5-28** CMOS inverter driving an external load capacitance  $C_{ext}$ , while being driven by a minimum sized gate.

Using the approach introduced in Section 5.4.3 (*Sizing a Chain of Inverters*), we can derive the following expression for the propagation delay of the circuit:

$$t_p = t_{p0} \left( \left( 1 + \frac{f}{\gamma} \right) + \left( 1 + \frac{F}{f\gamma} \right) \right) \quad (5.44)$$

here  $F = (C_{ext}/C_{g1})$  is the overall effective fan-out of the circuit, and  $t_{p0}$  is the intrinsic delay of the inverter. Its dependence upon  $V_{DD}$  is approximated by the following expression, derived from Eq. (5.21):

$$t_{p0} \sim \frac{V_{DD}}{V_{DD} - V_{TE}} \quad (5.45)$$

The energy dissipation for a single transition at the input is easily found once the total capacitance of the circuit is known:

$$E = V_{dd}^2 C_{g1} \left( (1 + \gamma)(1 + f) + F \right) \quad (5.46)$$

The performance constraint now states that the propagation delay of the scaled circuit should be equal (or smaller) to the delay of the reference circuit ( $f = 1, V_{dd} = V_{ref}$ ). To simplify the subsequent analysis, we make the assumption that the intrinsic output capacitance of the gate equals its gate capacitance, or  $\gamma = 1$ . Hence,

$$\frac{t_p}{t_{pref}} = \frac{t_{p0} \left( 2 + f + \frac{F}{f} \right)}{t_{p0ref} (3 + F)} = \left( \frac{V_{DD}}{V_{ref}} \right) \left( \frac{V_{ref} - V_{TE}}{V_{DD} - V_{TE}} \right) \left( \frac{2 + f + \frac{F}{f}}{3 + F} \right) = 1 \quad (5.47)$$

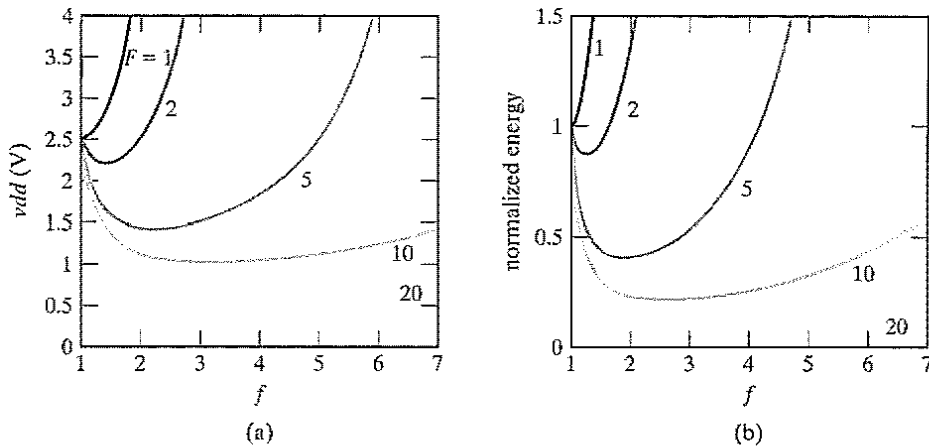


**Figure 5-29** Sizing of an inverter for energy minimization. (a) Required supply voltage as a function of the sizing factor  $f$  for different values of the overall effective fan-out  $F$ ; (b) Energy of scaled circuit (normalized with respect to the reference case) as a function of  $f$ .  $V_{ref} = 2.5$  V,  $V_{TE} = 0.5$  V.

Equation (5.47) establishes a relationship between the sizing factor  $f$  and the supply voltage, plotted in Figure 5-29a for different values of  $F$ . Those curves show a clear minimum. Increasing the size of the inverter from the minimum initially increases the performance, and hence allows for a lowering of the supply voltage. This is fruitful until the optimum sizing factor of  $f = \sqrt{F}$  is reached, which should not surprise those who read the previous sections carefully. Further increases in the device sizes only increase the self-loading factor, deteriorate the performance, and require an increase in supply voltage. Also, observe that for the case of  $F = 1$ , the reference case is the best solution; any resizing just increases the self-loading.

With the  $V_{DD}(f)$  relationship in hand, we can derive the energy of the scaled circuit (normalized with respect to the reference circuit) as a function of the sizing factor  $f$ :

$$\frac{E}{E_{ref}} = \left(\frac{V_{DD}}{V_{ref}}\right)^2 \left(\frac{2 + 2f + F}{4 + F}\right) \quad (5.48)$$

Finding an analytical expression for the optimal sizing factor is possible, but yields a complex and messy equation. A graphical approach is just as effective. The resulting charts are plotted in Figure 5-29b, from which a number of conclusions can be drawn:<sup>6</sup>

- **Device sizing, combined with supply voltage reduction, is a very effective approach in reducing the energy consumption of a logic network.** This is especially true for networks with large effective fan-outs, where energy reductions with almost a factor of 10 can be obtained. The gain is also sizable for smaller values of  $F$ . The only exception is the  $F = 1$  case, where the minimum size device is also the most effective one.

<sup>6</sup>We will revisit some of these conclusions in Chapter 11 in a broader context.

- Oversizing the transistors beyond the optimal value comes at a hefty price in energy. This is, unfortunately, a common approach in many of today's designs.
- The optimal sizing factor for energy is smaller than the one for performance, especially for large values of  $F$ . For example, for a fan-out of 20,  $f_{opt}(\text{energy}) = 3.53$ , while  $f_{opt}(\text{performance}) = 4.47$ . Increasing the device sizes only leads to a minimal supply reduction once  $V_{DD}$  starts approaching  $V_{TE}$ , thus leading to very minimal energy gains.

### Dissipation Due to Direct-Path Currents

In actual designs, the assumption of the zero rise and fall times of the input wave forms is not correct. The finite slope of the input signal causes a direct current path between  $V_{DD}$  and  $GND$  for a short period of time during switching, while the NMOS and the PMOS transistors are conducting simultaneously. This is illustrated in Figure 5-30. Under the (reasonable) assumption that the resulting current spikes can be approximated as triangles and that the inverter is symmetrical in its rising and falling responses, we can compute the energy consumed per switching period as follows:

$$E_{dp} = V_{DD} \frac{I_{peak} t_{sc}}{2} + V_{DD} \frac{I_{peak} t_{sc}}{2} = t_{sc} V_{DD} I_{peak} \quad (5.49)$$

We compute the average power consumption as

$$P_{dp} = t_{sc} V_{DD} I_{peak} f = C_{sc} V_{DD}^2 f \quad (5.50)$$

The direct-path power dissipation is proportional to the switching activity, similar to the capacitive power dissipation.  $t_{sc}$  represents the time both devices are conducting. For a linear input slope, this time is reasonably well approximated by Eq. (5.51) where  $t_s$  represents the 0–100% transition time,

$$t_{sc} = \frac{V_{DD} - 2V_T}{V_{DD}} t_s \approx \frac{V_{DD} - 2V_T}{V_{DD}} \times \frac{t_{r(f)}}{0.8} \quad (5.51)$$

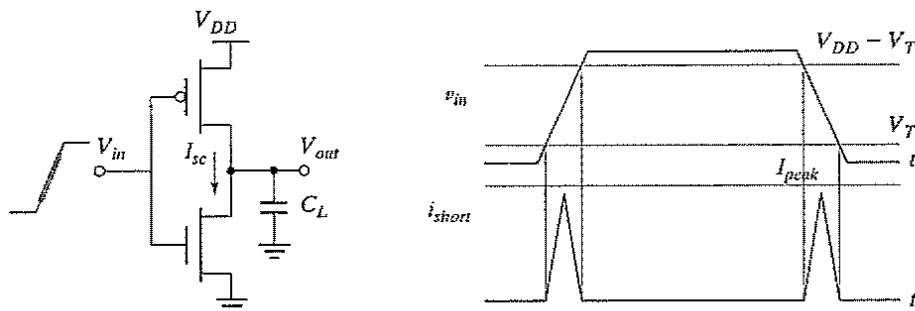


Figure 5-30 Short-circuit currents during transients.

$I_{peak}$  is determined by the saturation current of the devices and is hence directly proportional to the sizes of the transistors. The peak current is also a **strong function of the ratio between input and output slopes**. This relationship is best illustrated by the following simple analysis: Consider a static CMOS inverter with a  $0 \rightarrow 1$  transition at the input. Assume first that the load capacitance is very large, so that the output fall time is significantly larger than the input rise time (Figure 5-31a). Under those circumstances, the input moves through the transient region before the output starts to change. As the source-drain voltage of the PMOS device is approximately 0 during that period, the device shuts off without ever delivering any current. The short-circuit current is close to zero in this case. Consider now the reverse case, where the output capacitance is very small, and the output fall time is substantially smaller than the input rise time (Figure 5-31b). The drain-source voltage of the PMOS device equals  $V_{DD}$  for most of the transition period, guaranteeing the maximal short-circuit current (equal to the saturation current of the PMOS). This clearly represents the worst case condition. The conclusions of the preceding analysis are confirmed in Figure 5-32, which plots the short-circuit current through the NMOS transistor during a low-to-high transition as a function of the load capacitance.

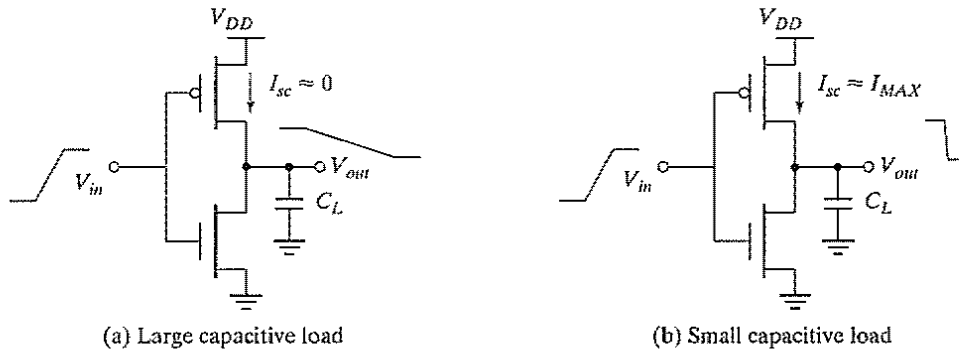


Figure 5-31 Impact of load capacitance on short-circuit current.

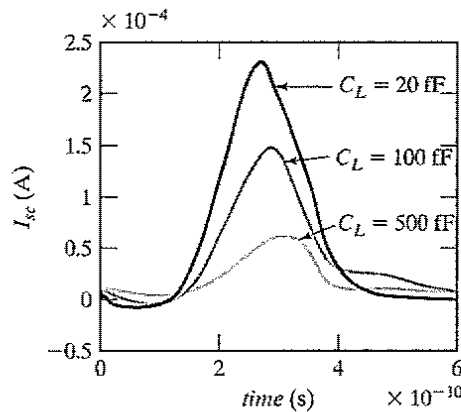


Figure 5-32 CMOS inverter short-circuit current through NMOS transistor as a function of the load capacitance (for a fixed input slope of 500 ps).



This analysis leads to the conclusion that the short-circuit dissipation is minimized by making the output rise/fall time larger than the input rise/fall time. On the other hand, making the output rise/fall time too large slows down the circuit and can cause short-circuit currents in the fan-out gates. This presents a perfect example of how local optimization and forgetting the global picture can lead to an inferior solution.

### Design Techniques

A more practical rule, which optimizes the power consumption in a global way, can be formulated ([Veendrick84]):

The power dissipation due to short-circuit currents is minimized by matching the rise/fall times of the input and output signals. At the overall circuit level, this means that rise/fall times of all signals should be kept constant within a range.

Making the input and output rise times of a gate identical is not the optimum solution for that particular gate on its own, but keeps the overall short-circuit current within bounds. This is shown in Figure 5-33, which plots the short-circuit energy dissipation of an inverter (normalized with respect to the zero-input rise time dissipation) as a function of the ratio  $r$  between input and output rise/fall times. When the load capacitance is too small for a given inverter size ( $r > 2...3$  for  $V_{DD} = 5$  V), the power is dominated by the short-circuit current. For very large capacitance values, all power dissipation is devoted to charging and discharging the load capacitance. When the rise/fall times of inputs and outputs are equalized, most power dissipation is associated with the dynamic power, and only a minor fraction ( $< 10\%$ ) is devoted to short-circuit currents.

Observe also that the impact of **short-circuit current is reduced when we lower the supply voltage**, as is apparent from Eq. (5.51). In the extreme case, when  $V_{DD} < V_{Tn} + |V_{Tp}|$ , short-circuit dissipation is completely eliminated, because both devices are never on simultaneously. With threshold voltages scaling at a slower rate than the supply voltage, short-circuit power dissipation is becoming less important

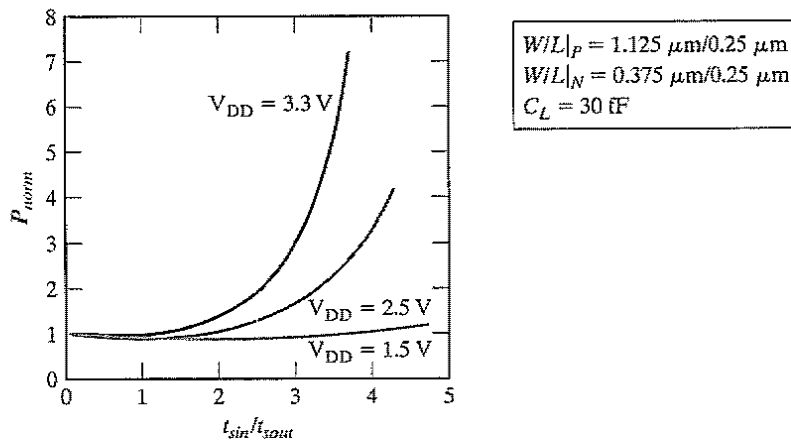


**Figure 5-33** Power dissipation of a static CMOS inverter as a function of the ratio between input and output rise/fall times. The power is normalized with respect to zero input rise-time dissipation. At low values of the slope ratio, input/output coupling leads to some extra dissipation.

in deep submicron technologies. At a supply voltage of 2.5 V and thresholds around 0.5 V, an input/output slope ratio of 2 is needed to cause a 10% degradation in dissipation. ■

Finally, it is worth observing that the short-circuit power dissipation can be modeled by adding a load capacitance  $C_{sc} = t_{sc} I_{peak} / V_{DD}$  in parallel with  $C_L$ , as is apparent in Eq. (5.50). The value of this short-circuit capacitance is a function of  $V_{DD}$ , the transistor sizes, and the input/output slope ratio.

### 5.5.2 Static Consumption

The static (or steady-state) power dissipation of a circuit is expressed by the relation

$$P_{stat} = I_{stat} V_{DD} \quad (5.52)$$

where  $I_{stat}$  is the current that flows between the supply rails in the absence of switching activity.

Ideally, the static current of the CMOS inverter is equal to zero, as the PMOS and NMOS devices are never on simultaneously in steady-state operation. There is, unfortunately, a leakage current flowing through the reverse-biased diode junctions of the transistors, located between the source or drain and the substrate, as shown in Figure 5-34. This contribution is, in general, very small and can be ignored. For the device sizes under consideration, the leakage current per unit drain area typically ranges between 10–100 pA/ $\mu\text{m}^2$  at room temperature. For a die with 1 million gates, each with a drain area of 0.5  $\mu\text{m}^2$  and operated at a supply voltage of 2.5 V, the worst case power consumption due to diode leakage equals 0.125 mW, which clearly is not much of an issue.

However, be aware that the junction leakage currents are caused by thermally generated carriers. Their value increases with increasing junction temperature, and this occurs in an exponential fashion. At 85°C (a commonly imposed upper bound for junction temperatures in commercial hardware), the leakage currents increase by a factor of 60 over their room-temperature values. Keeping the overall operation temperature of a circuit low is consequently a desirable goal. As the temperature is a strong function of the dissipated heat and its removal mechanisms, this can only be accomplished by limiting the power dissipation of the circuit or by using chip packages that support efficient heat removal.

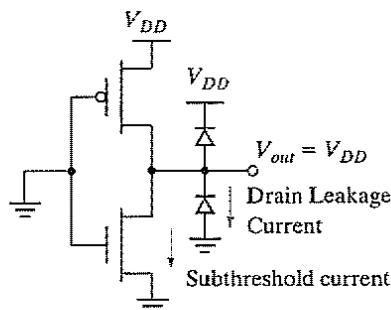
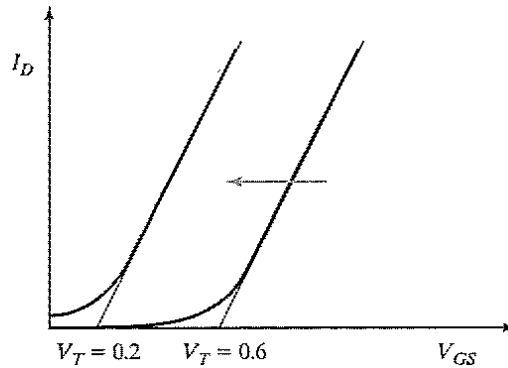


Figure 5-34 Sources of leakage currents in CMOS inverter (for  $V_{in} = 0$  V).



**Figure 5-35** Decreasing the threshold increases the subthreshold current at  $V_{GS} = 0$ .

An emerging source of leakage current is the subthreshold current of the transistors. As discussed in Chapter 3, an MOS transistor can experience a drain-source current, even when  $V_{GS}$  is smaller than the threshold voltage (see Figure 5-35). The closer the threshold voltage is to zero volts, the larger the leakage current at  $V_{GS} = 0$  V and the larger the static power consumption. To offset this effect, the threshold voltage of the device has generally been kept high enough. Standard processes feature  $V_T$  values that are never smaller than 0.5–0.6 V and that in some cases are even substantially higher ( $\sim 0.75$  V).

This approach is being challenged by the reduction in supply voltages that typically goes with deep submicron technology scaling, as became apparent in Figure 3-41. We concluded earlier (Figure 5-17) that scaling the supply voltages while keeping the threshold voltage constant results in an important loss in performance, especially when  $V_{DD}$  approaches  $2 V_T$ . One approach to address this performance issue is to scale the device thresholds down as well. This moves the curve of Figure 5-17 to the left, which means that the performance penalty for lowering the supply voltage is reduced. Unfortunately, the threshold voltages are lower bounded by the amount of allowable subthreshold leakage current, as demonstrated in Figure 5-35. The choice of the threshold voltage thus represents a trade-off between performance and static power dissipation. The continued scaling of the supply voltage predicted for the next generations of CMOS technologies, however, forces the threshold voltages ever downwards, and makes subthreshold conduction a major source of power dissipation. Process technologies that contain devices with sharper turn-off characteristics will therefore become more attractive. An example of the latter is the SOI (Silicon-on-Insulator) technology whose MOS transistors have slope factors that are close to the ideal 60 mV/decade.

---

**Example 5.14 Impact of Threshold Reduction on Performance and Static Power Dissipation**

Consider a minimum size NMOS transistor in the 0.25- $\mu\text{m}$  CMOS technology. In Chapter 3, we derived that the slope factor  $S$  for this device equals 90 mV/decade. The off-current (at  $V_{GS} = 0$ ) of the transistor for a  $V_T$  of approximately 0.5 V equals  $10^{-11}$  A

(Figure 3-22). Reducing the threshold by 200 mV to 0.3 V multiplies the off-current of the transistors with a factor of 170! Assuming a million gate design with a supply voltage of 1.5 V, this translates into a static power dissipation of  $10^6 \times 170 \times 10^{-11} \times 1.5 = 2.6$  mW. A further reduction of the threshold to 100 mV results in an unacceptable dissipation of almost 0.5 W! At that supply voltage, the threshold reductions correspond to a performance improvement of 25% and 40%, respectively.

This lower bound on the thresholds is in some sense artificial. The idea that the leakage current in a static CMOS circuit has to be zero is a misconception. Certainly, the presence of leakage currents degrades the noise margins, because the logic levels are no longer equal to the supply rails, but as long as the noise margins are within range, this is not a compelling issue. The leakage currents, of course, cause an increase in static power dissipation. This is offset by the drop in supply voltage, which is enabled by the reduced thresholds at no cost in performance, and results in a quadratic reduction in dynamic power. For a 0.25- $\mu\text{m}$  CMOS process, the following circuit configurations obtain the same performance: 3-V supply–0.7-V  $V_T$ ; and 0.45-V supply–0.1-V  $V_T$ . The dynamic power consumption of the latter is, however, 45 times smaller [Liu93]! Choosing the correct values of supply and threshold voltages once again requires a trade-off. The optimal operation point depends upon the activity of the circuit. In the presence of a sizable static power dissipation, it is essential that nonactive modules are *powered down*, lest static power dissipation would become dominant. Power-down (also called *standby*) can be accomplished by disconnecting the unit from the supply rails, or by lowering the supply voltage.

### 5.5.3 Putting It All Together

The total power consumption of the CMOS inverter is now expressed as the sum of its three components:

$$P_{tot} = P_{dyn} + P_{dp} + P_{stat} = (C_L V_{DD}^2 + V_{DD} I_{peak} t_s) f_{0 \rightarrow 1} + V_{DD} I_{leak} \quad (5.53)$$

In typical CMOS circuits, the capacitive dissipation is by far the dominant factor. The direct-path consumption can be kept within bounds by careful design, and thus should not be an issue. Leakage is ignorable at present, but this might change in the not-too-distant future.

#### The Power-Delay Product, or Energy per Operation

In Chapter 1, we introduced the *power-delay product* (PDP) as a quality measure for a logic gate:

$$PDP = P_{av} t_p \quad (5.54)$$

The PDP presents a measure of energy, as is apparent from the units ( $\text{W} \times \text{s} = \text{Joule}$ ). Assuming that the gate is switched at its maximum possible rate of  $f_{max} = 1/(2t_p)$ , and ignoring the contributions of the static- and direct-path currents to the power consumption, we find that

$$PDP = C_L V_{DD}^2 f_{max} t_p = \frac{C_L V_{DD}^2}{2} \quad (5.55)$$

Here, *PDP* stands for the **average energy consumed per switching event** (i.e., for a  $0 \rightarrow 1$ , or a  $1 \rightarrow 0$  transition). Remember that earlier we had defined  $E_{av}$  as the average energy per switching cycle (or per energy-consuming event). As each inverter cycle contains a  $0 \rightarrow 1$ , and a  $1 \rightarrow 0$  transition  $E_{av}$  thus is twice the *PDP*.

### Energy-Delay Product

The validity of the *PDP* as a quality metric for a process technology or gate topology is questionable. It measures the energy needed to switch the gate, which is an important property. For a given structure, however, this number can be made arbitrarily low by reducing the supply voltage. From this perspective, the optimum voltage to run the circuit would be the lowest possible value that still ensures functionality. This comes at the expense of performance, as discussed earlier. A more relevant metric should combine a measure of performance and energy. The energy-delay product (or *EDP*) does exactly that:

$$EDP = PDP \times t_p = P_{av} t_p^2 = \frac{C_L V_{DD}^2}{2} t_p \quad (5.56)$$

It is worth analyzing the voltage dependence of the EDP. Higher supply voltages reduce delay, but harm the energy, and the opposite is true for low voltages. An optimum operation point should therefore exist. Assuming that NMOS and PMOS transistors have comparable threshold and saturation voltages, we can simplify the propagation delay expression Eq. (5.21) as

$$t_p \approx \frac{\alpha C_L V_{DD}}{V_{DD} - V_{Te}} \quad (5.57)$$

where  $V_{Te} = V_T + V_{DSAT}/2$ , and  $\alpha$  is a technology parameter. Combining Eq. (5.56) and Eq. (5.57)<sup>7</sup> yields

$$EDP = \frac{\alpha C_L^2 V_{DD}^3}{2(V_{DD} - V_{TE})} \quad (5.58)$$

The optimum supply voltage can be obtained by taking the derivative of Eq. (5.58) with respect to  $V_{DD}$ , and equating the result to 0. The result is

$$V_{DDopt} = \frac{3}{2} V_{TE} \quad (5.59)$$

The remarkable outcome from this analysis is the low value of the supply voltage that simultaneously optimizes performance and energy. For submicron technologies with thresholds in the range of 0.5 V, the optimum supply is situated around 1 V.

<sup>7</sup>This equation is only accurate as long as the devices remain in velocity saturation, which is probably not the case for the lower supply voltages. This introduces some inaccuracy in the analysis, but will not distort the overall result.

**Example 5.15 Optimum Supply Voltage for 0.25- $\mu\text{m}$  CMOS Inverter**

From the technology parameters for our generic CMOS process presented in Chapter 3, the value of  $V_{TE}$  can be derived as follows:

$$V_{Tn} = 0.43 \text{ V}, V_{Dsatn} = 0.63 \text{ V}, V_{TEn} = 0.74 \text{ V}$$

$$V_{Tp} = -0.4 \text{ V}, V_{Dsapp} = -1 \text{ V}, V_{TEp} = -0.9 \text{ V}$$

$$V_{TE} \approx (V_{TEn} + |V_{TEp}|)/2 = 0.8 \text{ V}$$

Hence,  $V_{DDopt} = (3/2) \times 0.8 \text{ V} = 1.2 \text{ V}$ . The simulated graphs of Figure 5-36, which plot normalized delay, energy, and energy-delay product, confirm this result. The optimum supply voltage is predicted to equal 1.1 V. The charts clearly illustrate the trade-off between delay and energy.

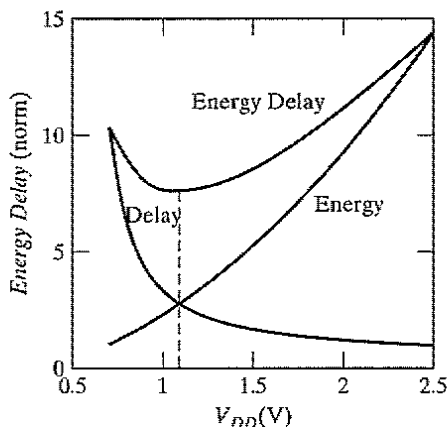


**Figure 5-36** Normalized delay, energy, and energy-delay plots for CMOS inverter in 0.25- $\mu\text{m}$  CMOS technology.

**WARNING:** While the preceding example demonstrates that a supply voltage exists that minimizes the energy-delay product of a gate, this voltage does not necessarily represent the optimum voltage for a given design problem. For instance, some designs require a minimum performance, which requires a higher voltage at the expense of energy. Similarly, a lower energy design is possible by operating at a lower voltage and by obtaining the overall system performance through the use of architectural techniques such as pipelining or concurrency.

**5.5.4 Analyzing Power Consumption by Using SPICE**

A definition of the average power consumption of a circuit was provided in Chapter 1, and is repeated here for the sake of convenience. We write

$$P_{av} = \frac{1}{T} \int_0^T p(t) dt = \frac{V_{DD}}{T} \int_0^T i_{DD}(t) dt \quad (5.60)$$

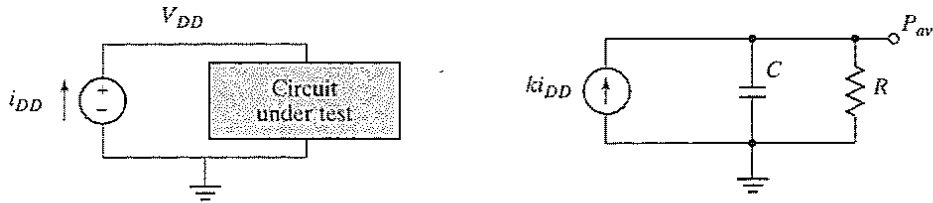


**Figure 5-37** Equivalent circuit to measure average power in SPICE.

with  $T$  the period of interest, and  $V_{DD}$  and  $i_{DD}$  the supply voltage and current, respectively. Some implementations of SPICE provide built-in functions to measure the average value of a circuit signal. For instance, the HSPICE `.MEASURE TRAN I(VDD) AVG` command computes the area under a computed transient response ( $I(VDD)$ ) and divides it by the period of interest. This is identical to the definition given in Eq. (5.60). Other implementations of SPICE are, unfortunately, not as powerful. This is not as bad as it seems, as long as one realizes that SPICE is actually a differential equation solver. A small circuit can easily be conceived that acts as an integrator and whose output signal is nothing but the average power.

Consider, for instance, the circuit of Figure 5-37. The current delivered by the power supply is measured by the current-controlled current source and integrated on the capacitor  $C$ . The resistance  $R$  is only provided for DC-convergence reasons and should be chosen as high as possible to minimize leakage. A clever choice of the element parameter ensures that the output voltage  $P_{av}$  equals the average power consumption. The operation of the circuit is summarized in Eq. under the assumption that the initial voltage on the capacitor  $C$  is zero:

$$C \frac{dP_{av}}{dt} = ki_{DD}$$

or

(5.61)

$$P_{av} = \frac{k}{C} \int_0^T i_{DD} dt$$

Equating Eq. (5.60) and Eq. yields the necessary conditions for the equivalent circuit parameters:  $k/C = V_{DD}/T$ . Under these circumstances, the equivalent circuit shown presents a convenient means of tracking the average power in a digital circuit.

### Example 5.16 Average Power of Inverter

The average power consumption of the inverter of Example 5.4 is analyzed using the above technique for a toggle period of 250 ps ( $T = 250$  ps,  $k = 1$ ,  $V_{DD} = 2.5$  V, hence  $C = 100$  pF). The resulting power consumption is plotted in Figure 5-38, showing an average power consumption of approximately 157.3  $\mu$ W. The `.MEAS AVG` command yields a value of 160.3  $\mu$ W, which demonstrates the approximate equivalence of both methods. These numbers are equivalent to an energy of 39 fJ (which is close to the 37.5 fJ derived in

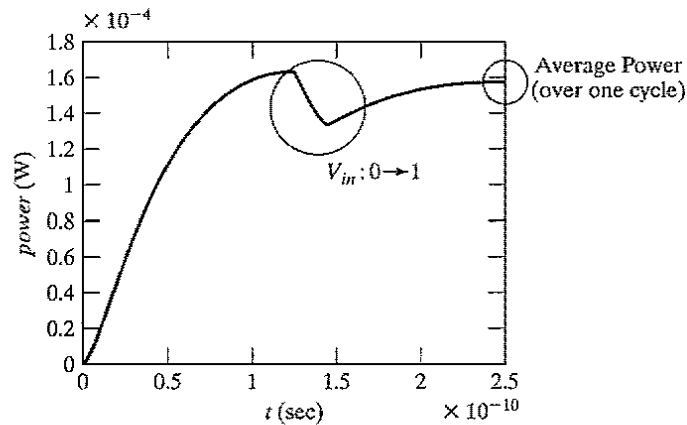


Figure 5-38 Deriving the power consumption by using SPICE.

Example 5.11). Observe the slightly negative dip during the high-to-low transition. This is due to the injection of current into the supply, when the output briefly overshoots  $V_{DD}$  as a result of the capacitive coupling between input and output (as is apparent from in the transient response of Figure 5-16).

## 5.6 Perspective: Technology Scaling and its Impact on the Inverter Metrics

In Section 3.5, we have explored the impact of the scaling of technology on some of the important design parameters, such as area, delay, and power. For the sake of clarity, we repeat here some of the most important entries of the scaling table (Table 3-8).

The validity of these theoretical projections can be verified by looking back and observing the trends during the past few decades. From Figure 5-39, we can see that the gate delay indeed decreases exponentially at a rate of 13% per year, or halving every five years. This rate is on course with the prediction of Table 5-4, since  $S$  averages approximately 1.15 as we had already

**Table 5-4** Scaling scenarios for short-channel devices ( $S$  and  $U$  represent the technology and voltage scaling parameters, respectively).

Parameter	Relation	Full Scaling	General Scaling	Fixed-Voltage Scaling
Area-Device	$W-L$	$1/S^2$	$1/S^2$	$1/S^2$
Intrinsic Delay	$R_{on}C_{gate}$	$1/S$	$1/S$	$1/S$
Intrinsic Energy	$C_{gate}V^2$	$1/S^3$	$1/SU^2$	$1/S$
Intrinsic Power	Energy-Delay	$1/S^2$	$1/U^2$	1
Power Density	$P$ -Area	1	$S^2/U^2$	$S^2$



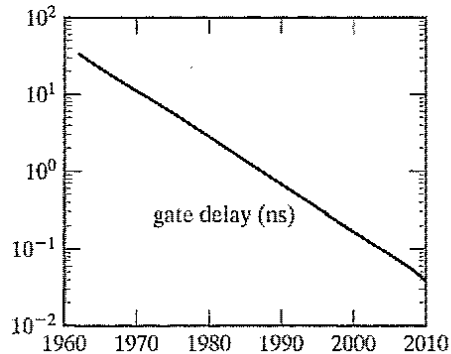


Figure 5-39 Scaling of the gate delay (from [Dally98]).

observed in Figure 3-40. The delay of a two-input NAND gate with a fan-out of four has gone from tens of nanoseconds in the 1960s to a tenth of a nanosecond in the year 2000, and is projected to be a few tens of picoseconds by 2010.

Reducing power dissipation has only been a second-order priority until recently. Hence, statistics on dissipation per gate or design are only marginally available. An interesting chart is shown in Figure 5-40, which plots the power density measured over a large number of designs produced between 1980 and 1995. Although the variation is large—even for a fixed technology—it shows the power density increasing approximately with  $S^2$ . This is in correspondence with the fixed-voltage scaling scenario presented in Table 5-4. For more recent years, we expect a scenario more in line with the full-scaling model—which predicts a constant power density—due to the accelerated supply-voltage scaling and the increased attention to power-reducing design techniques. Even under these circumstances, power dissipation per chip will continue to increase due to the ever-larger die sizes.

The scaling model presented has one major flaw, however. The performance and power predictions produce purely “intrinsic” numbers that take only device parameters into account. In Chapter 4, we concluded that the interconnect wires exhibit a different scaling behavior, and that wire parasitics may come to dominate the overall performance. Similarly, charging and discharging the wire capacitances may dominate the energy budget. To get a crisper perspective, one has to construct a combined model that considers device and wire scaling models simultaneously. The impact of the wire capacitance and its scaling behavior is summarized in Table 5-5. We adopt the fixed-resistance model introduced in Chapter 4. We furthermore assume that the resistance of the driver dominates the wire resistance, which is definitely the case for short to medium-long wires.

The model predicts that the interconnect-caused delay (and energy) gain in importance with the scaling of technology. This impact is limited to an increase with  $\epsilon c$  for short wires ( $S = S_L$ ), but it becomes increasingly more significant for medium-range and long wires ( $S_L < S$ ). These conclusions

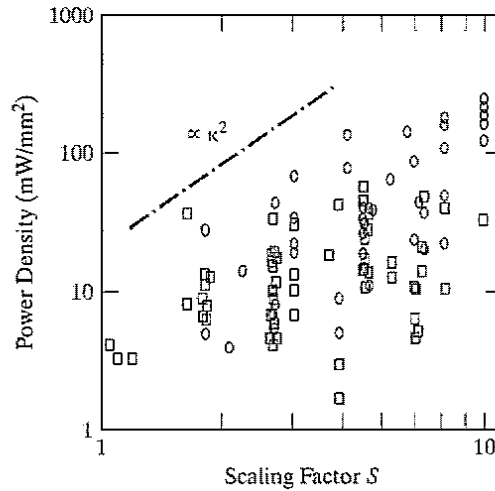


**Figure 5-40** Evolution of power density in micro- and DSP processors, as a function of the scaling factor  $S$  ([Kuroda95]).  $S$  is normalized to 1 for a 4- $\mu\text{m}$  process.

**Table 5-5** Scaling scenarios for wire capacitance.  $S$  and  $U$  represent the technology and voltage scaling parameters, respectively, while  $S_L$  stands for the wire-length scaling factor.  $\epsilon_c$  represents the impact of fringing and interwire capacitances.

Parameter	Relation	General Scaling
Wire Capacitance	$WL/t$	$\epsilon_c/S_L$
Wire Delay	$R_{on}C_{int}$	$\epsilon_c/S_L$
Wire Energy	$C_{int}V^2$	$\epsilon_c/S_L U^2$
Wire Delay / Intrinsic Delay		$\epsilon_c S/S_L$
Wire Energy / Intrinsic Energy		$\epsilon_c S/S_L$

have been confirmed by a number of studies, an example of which is shown in Figure 5-41. How the ratio of wire over intrinsic contributions will actually evolve is debatable, as it depends upon a wide range of independent parameters, such as system architecture, design methodology, transistor sizing, and interconnect materials. The doomsday scenario that interconnect may cause CMOS performance to saturate in the very near future may very well be exaggerated. Yet, it is clear that increased attention to interconnect is an absolute necessity, and may change the way the next-generation circuits are designed and optimized (e.g., [Sylvester98]).

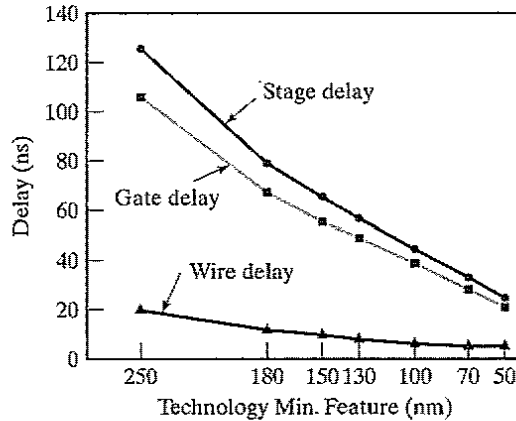


**Figure 5-41** Evolution of wire delay-to-gate delay ratio with respect to technology (from [Fisher98]).

## 5.7 Summary

This chapter presented a rigorous and in-depth analysis of the static CMOS inverter. The key characteristics of the gate are summarized as follows:

- The static CMOS inverter combines a pull-up PMOS section with a pull-down NMOS device. The PMOS is normally made wider than the NMOS due to its lower current-driving capabilities.
- The gate has an almost ideal voltage-transfer characteristic. The logic swing is equal to the supply voltage and is not a function of the transistor sizes. The noise margins of a symmetrical inverter (where PMOS and NMOS transistor have equal current-driving strength) approach  $V_{DD}/2$ . The steady-state response is not affected by fan-out.
- Its propagation delay is dominated by the time it takes to charge or discharge the load capacitor  $C_L$ . To a first order, it can be approximated as follows:

$$t_p = 0.69C_L \left( \frac{R_{eqn} + R_{eqp}}{2} \right)$$

Keeping the load capacitance small is the most effective means of implementing high-performance circuits. Transistor sizing may help to improve performance as long as the delay is dominated by the extrinsic (or load) capacitance of fan-out and wiring.

- The power dissipation is dominated by the dynamic power consumed in charging and discharging the load capacitor. It is given by  $P_{0 \rightarrow 1} C_L V_{DD}^2 f$ . The dissipation is proportional to the activity in the network. The dissipation due to the direct-path currents occurring during switching can be limited by careful tailoring of the signal slopes. The static dissipation usually can be ignored, but might become a major factor in the future as a result of sub-threshold currents.

- Scaling the technology is an effective means of reducing the area, propagation delay and power consumption of a gate. The impact is even more striking if the supply voltage is scaled simultaneously.
- The interconnect component is gradually taking a larger fraction of the delay and performance budget.

## 5.8 To Probe Further

The operation of the CMOS inverter has been the topic of numerous publications and textbooks. Virtually every book on digital design devotes a substantial number of pages to the analysis of the basic inverter gate. An extensive list of references was presented in Chapter 1. Some references of particular interest that we quoted in this chapter follow.

### References

- [Dally98] W. Dally and J. Poulton, *Digital Systems Engineering*, Cambridge University Press, 1998.
- [Fisher98] P. D. Fisher and R. Nesbitt, "The Test of Time: Clock-Cycle Estimation and Test Challenges for Future Microprocessors," *IEEE Circuits and Devices Magazine*, 14(2), pp. 37-44, 1998.
- [Hedenstierna87] N. Hedenstierna and K. Jeppson, "CMOS Circuit Speed and Buffer Optimization," *IEEE Transactions on CAD*, vol. CAD-6, no. 2, pp. 270-281, March 1987.
- [Kuroda95] T. Kuroda and T. Sakurai, "Overview of low-power ULSI circuit techniques," *IEICE Trans. on Electronics*, vol. E78-C, no. 4, pp. 334-344, April 1995.
- [Liu93] D. Liu and C. Svensson, "Trading speed for low power by choice of supply and threshold voltages," *IEEE Journal of Solid-State Circuits*, vol. 28, no.1, pp. 10-17, Jan. 1993, p.10-17.
- [Mead80] C. Mead and L. Conway, *Introduction to VLSI Systems*, Addison-Wesley, 1980.
- [Sedra87] A. Sedra and K. Smith, *MicroElectronic Circuits*, Holt, Rinehart and Winston, 1987.
- [Swanson72] R. Swanson and J. Meindl, "Ion-Implanted Complementary CMOS transistors in Low-Voltage Circuits," *IEEE Journal of Solid-State Circuits*, vol. SC-7, no. 2, pp.146-152, April 1972.
- [Sylvester98] D. Sylvester and K. Keutzer, "Getting to the Bottom of Deep Submicron," *Proceedings ICCAD Conference*, pp. 203, San Jose, November 1998.
- [Veendrick84] H. Veendrick, "Short-Circuit Dissipation of Static CMOS Circuitry and its Impact on the Design of Buffer Circuits," *IEEE Journal of Solid-State Circuits*, vol. SC-19, no. 4, pp. 468-473, 1984.

### Exercises and Design Problems

**REMINDER:** Please refer to <http://bwrc.eecs.berkeley.edu/IcBook> for up-to-date problem sets, design problems, and exercises. By making the exercises electronically available instead of in print, we can provide a dynamic environment that tracks the rapid evolution of today's digital integrated circuit design technology.



## CHAPTER

# 6

## Designing Combinational Logic Gates in CMOS

*In-depth discussion of logic families in CMOS—  
static and dynamic, pass-transistor, nonratioed and ratioed logic  
Optimizing a logic gate for area, speed, energy, or robustness  
Low-power and high-performance circuit-design techniques*

- 6.1 Introduction
- 6.2 Static CMOS Design
  - 6.2.1 Complementary CMOS
  - 6.2.2 Ratioed Logic
  - 6.2.3 Pass-Transistor Logic
- 6.3 Dynamic CMOS Design
  - 6.3.1 Dynamic Logic: Basic Principles
  - 6.3.2 Speed and Power Dissipation of Dynamic Logic
  - 6.3.3 Signal Integrity Issues in Dynamic Design
  - 6.3.4 Cascading Dynamic Gates
- 6.4 Perspectives
  - 6.4.1 How to Choose a Logic Style?
  - 6.4.2 Designing Logic for Reduced Supply Voltages
- 6.5 Summary
- 6.6 To Probe Further

## 6.1 Introduction

The design considerations for a simple inverter circuit were presented in the previous chapter. We now extend this discussion to address the synthesis of arbitrary digital gates, such as NOR, NAND, and XOR. The focus is on *combinational logic* or *nonregenerative* circuits—that is, circuits having the property that at any point in time, the output of the circuit is related to its current input signals by some Boolean expression (assuming that the transients through the logic gates have settled). No intentional connection from outputs back to inputs is present.

This is in contrast to another class of circuits, known as *sequential* or *regenerative*, for which the output is not only a function of the current input data, but also of previous values of the input signals (see Figure 6-1). This can be accomplished by connecting one or more outputs intentionally back to some inputs. Consequently, the circuit “remembers” past events and has a sense of *history*. A sequential circuit includes a combinational logic portion and a module that holds the state. Example circuits are registers, counters, oscillators, and memory. Sequential circuits are the topic of the next chapter.

There are numerous circuit styles to implement a given logic function. As with the inverter, the common design metrics by which a gate is evaluated are area, speed, energy, and power. Depending on the application, the emphasis will be on different metrics. For example, the switching speed of digital circuits is the primary metric in a high-performance processor, while in a battery operated circuit, it is energy dissipation. Recently, power dissipation also has become an important concern and considerable emphasis is placed on understanding the sources of power and approaches to dealing with power. In addition to these metrics, robustness to noise and reliability are also very important considerations. We will see that certain logic styles can significantly improve performance, but they usually are more sensitive to noise.

## 6.2 Static CMOS Design

The most widely used logic style is static complementary CMOS. The static CMOS style is really an extension of the static CMOS inverter to multiple inputs. To review, the primary advantage of the CMOS structure is robustness (i.e., low sensitivity to noise), good performance, and low power consumption with no static power dissipation. Most of those properties are carried over to large fan-in logic gates implemented using a similar circuit topology.

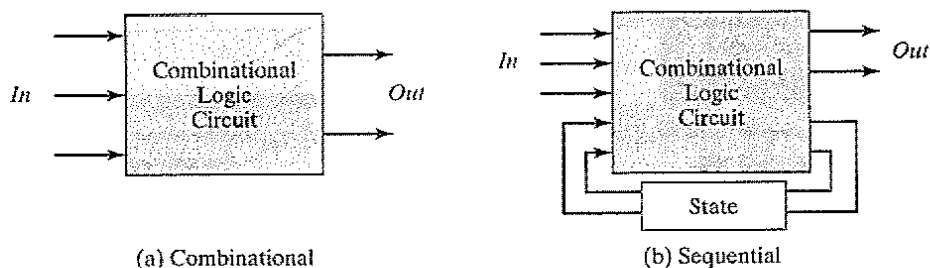


Figure 6-1 High-level classification of logic circuits.

The complementary CMOS circuit style falls under a broad class of logic circuits called *static* circuits in which **at every point in time, each gate output is connected to either  $V_{DD}$  or  $V_{SS}$  via a low-resistance path**. Also, the outputs of the gates assume at all times the value of the Boolean function implemented by the circuit (ignoring the transient effects during switching periods). This is in contrast to the *dynamic* circuit class, which relies on temporary storage of signal values on the capacitance of high-impedance circuit nodes. The latter approach has the advantage that the resulting gate is simpler and faster. Its design and operation are, however, more involved and prone to failure because of increased sensitivity to noise.

In this section, we sequentially address the design of various static circuit flavors, including complementary CMOS, ratioed logic (pseudo-NMOS and DCVSL), and pass-transistor logic. We also deal with issues of scaling to lower power supply voltages and threshold voltages.

### 6.2.1 Complementary CMOS

#### Concept

A static CMOS gate is a combination of two networks—the *pull-up network* (PUN) and the *pull-down network* (PDN), as shown in Figure 6-2. The figure shows a generic  $N$ -input logic gate where all inputs are distributed to both the pull-up and pull-down networks. The function of the PUN is to provide a connection between the output and  $V_{DD}$  anytime the output of the logic gate is meant to be 1 (based on the inputs). Similarly, the function of the PDN is to connect the output to  $V_{SS}$  when the output of the logic gate is meant to be 0. The PUN and PDN networks are constructed in a mutually exclusive fashion such that *one and only one* of the networks is conducting in steady state. In this way, once the transients have settled, a path always exists between  $V_{DD}$  and the output  $F$  for a high output (“one”), or between  $V_{SS}$  and  $F$  for a low output (“zero”). This is equivalent to stating that the output node is always a *low-impedance* node in steady state.

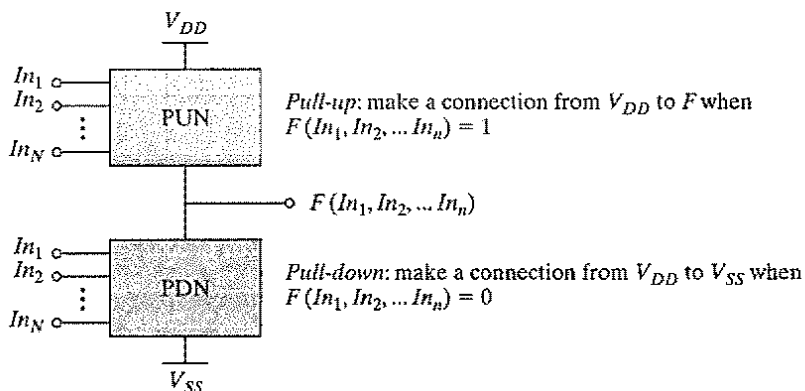


**Figure 6-2** Complementary logic gate as a combination of a PUN (pull-up network) and a PDN (pull-down network).



In constructing the PDN and PUN networks, the designer should keep the following observations in mind:

- A transistor can be thought of as a switch controlled by its gate signal. An NMOS switch is *on* when the controlling signal is high and is *off* when the controlling signal is low. A PMOS transistor acts as an inverse switch that is *on* when the controlling signal is low and *off* when the controlling signal is high.
- The PDN is constructed using NMOS devices, while PMOS transistors are used in the PUN. The primary reason for this choice is that NMOS transistors produce “strong zeros,” and PMOS devices generate “strong ones.” To illustrate this, consider the examples shown in Figure 6-3. In Figure 6-3a, the output capacitance is initially charged to  $V_{DD}$ . Two possible discharge scenarios are shown. An NMOS device pulls the output all the way down to GND, while a PMOS lowers the output no further than  $|V_{Tp}|$ —the PMOS turns *off* at that point and stops contributing discharge current. NMOS transistors are thus the preferred devices in the PDN. Similarly, two alternative approaches to charging up a capacitor are shown in Figure 6-3b, with the output initially at GND. A PMOS switch succeeds in charging the output all the way to  $V_{DD}$ , while the NMOS device fails to raise the output above  $V_{DD} - V_{Tn}$ . This explains why PMOS transistors are preferentially used in a PUN.
- A set of rules can be derived to construct logic functions (see Figure 6-4). NMOS devices connected in series correspond to an AND function. With all the inputs high, the series combination conducts and the value at one end of the chain is transferred to the other end. Similarly, NMOS transistors connected in parallel represent an OR function. A conducting path exists between the output and input terminal if at least one of the inputs is high. Using similar arguments, construction rules for PMOS networks can be formulated. A series con-

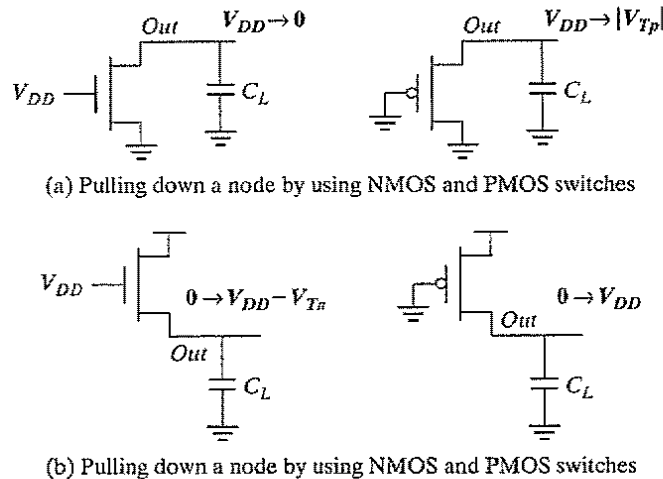


**Figure 6-3** Simple examples illustrate why an NMOS should be used as a pull-down, and a PMOS should be used as a pull-up device.

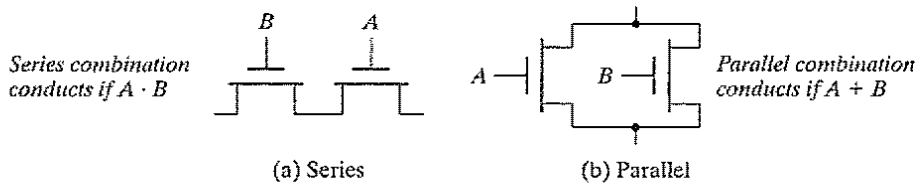


**Figure 6-4** NMOS logic rules—series devices implement an AND, and parallel devices implement an OR.

nection of PMOS conducts if both inputs are low, representing a NOR function ( $\overline{A} \cdot \overline{B} = \overline{A + B}$ ), while PMOS transistors in parallel implement a NAND ( $\overline{A} + \overline{B} = \overline{A \cdot B}$ ).

- Using De Morgan's theorems ( $\overline{A + B} = \overline{A} \cdot \overline{B}$  and  $\overline{A \cdot B} = \overline{A} + \overline{B}$ ), it can be shown that the pull-up and pull-down networks of a complementary CMOS structure are *dual* networks. This means that a parallel connection of transistors in the pull-up network corresponds to a series connection of the corresponding devices in the pull-down network, and vice versa. Therefore, to construct a CMOS gate, one of the networks (e.g., PDN) is implemented using combinations of series and parallel devices. The other network (i.e., PUN) is obtained using the duality principle by walking the hierarchy, replacing series subnets with parallel subnets, and parallel subnets with series subnets. The complete CMOS gate is constructed by combining the PDN with the PUN.
- The complementary gate is naturally *inverting*, implementing only functions such as NAND, NOR, and XNOR. The realization of a noninverting Boolean function (such as AND OR, or XOR) in a single stage is not possible, and requires the addition of an extra inverter stage.
- The number of transistors required to implement an  $N$ -input logic gate is  $2N$ .

### Example 6.1 Two-Input NAND Gate

Figure 6-5 shows a two-input NAND gate ( $F = \overline{A \cdot B}$ ). The PDN network consists of two NMOS devices in series that conduct when both  $A$  and  $B$  are high. The PUN is the dual

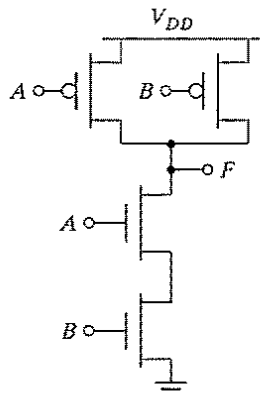


**Figure 6-5** Two-input NAND gate in complementary static CMOS style.

network, and it consists of two parallel PMOS transistors. This means that  $F$  is 1 if  $A = 0$  or  $B = 0$ , which is equivalent to  $F = \overline{A \cdot B}$ . The truth table for the simple two input NAND gate is given in Table 6-1. It can be verified that the output  $F$  is always connected to either  $V_{DD}$  or GND, but never to both at the same time.

Table 6-1 Truth Table for two-Input NAND.

$A$	$B$	$F$
0	0	1
0	1	1
1	0	1
1	1	0

### Example 6.2 Synthesis of Complex CMOS Gate

Using complementary CMOS logic, consider the synthesis of a complex CMOS gate whose function is  $F = \overline{D + A \cdot (B + C)}$ . The first step in the synthesis of the logic gate is to derive the pull-down network as shown in Figure 6-6a by using the fact that NMOS devices in series implements the AND function and parallel device implements the OR function. The next step is to use duality to derive the PUN in a hierarchical fashion. The PDN network is broken into smaller networks (i.e., subset of the PDN) called subnets that simplify the derivation of the PUN. In Figure 6-6b, the subnets (SN) for the pull-down net-

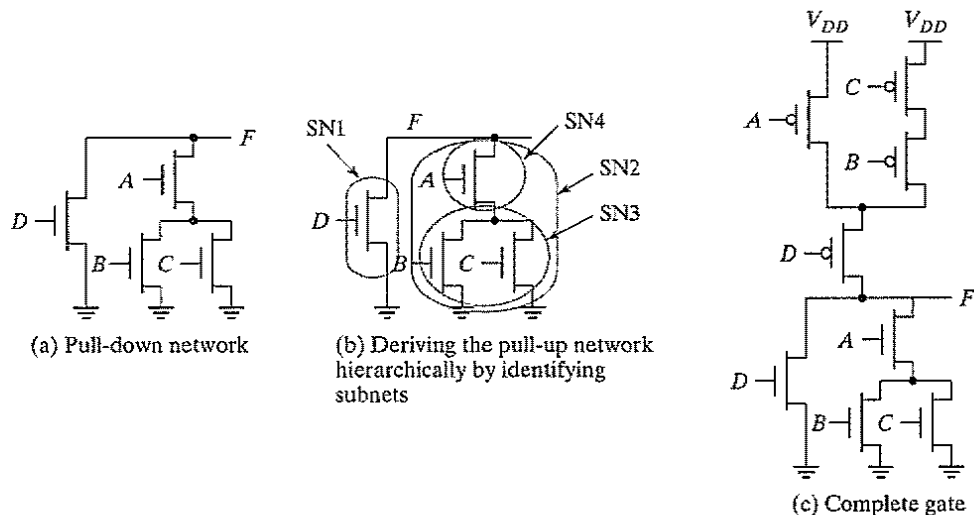


Figure 6-6 Complex complementary CMOS gate.

work are identified. At the top level, SN1 and SN2 are in parallel, so that in the dual network they will be in series. Since SN1 consists of a single transistor, it maps directly to the pull-up network. On the other hand, we need to sequentially apply the duality rules to SN2. Inside SN2, we have SN3 and SN4 in series, so in the PUN they will appear in parallel. Finally, inside SN3, the devices are in parallel, so they appear in series in the PUN. The complete gate is shown in Figure 6-6c. The reader can verify that for every possible input combination, there always exists a path to either  $V_{DD}$  or GND.

### Static Properties of Complementary CMOS Gates

Complementary CMOS gates inherit all the nice properties of the basic CMOS inverter. They exhibit rail-to-rail swing with  $V_{OH} = V_{DD}$  and  $V_{OL} = \text{GND}$ . The circuits also have no static power dissipation, since the circuits are designed such that the pull-down and pull-up networks are mutually exclusive. The analysis of the DC voltage transfer characteristics and the noise margins is more complicated than for the inverter, as these parameters **depend upon the data input patterns** applied to gate.

Consider the static two-input NAND gate shown in Figure 6-7. Three possible input combinations switch the output of the gate from high to low: (a)  $A = B = 0 \rightarrow 1$ , (b)  $A = 1, B = 0 \rightarrow 1$ , and (c)  $B = 1, A = 0 \rightarrow 1$ . The resulting voltage transfer curves display significant differences. The large variation between case (a) and the others (b and c) is explained by the fact that in the former case, both transistors in the pull-up network are on simultaneously for  $A = B = 0$ , representing a strong pull-up. In the latter cases, only one of the pull-up devices is on. The VTC is shifted to the left as a result of the weaker PUN.

The difference between (b) and (c) results mainly from the state of the internal node *int* between the two NMOS devices. For the NMOS devices to turn on, both gate-to-source voltages

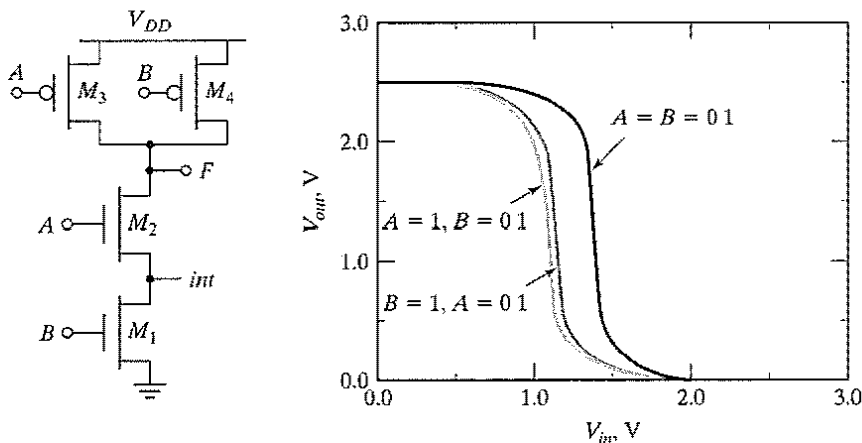


**Figure 6-7** The VTC of a two-input NAND is data dependent. NMOS devices are  $0.5 \mu\text{m}/0.25 \mu\text{m}$  while the PMOS devices are sized at  $0.75 \mu\text{m}/0.25 \mu\text{m}$ .

must be above  $V_{Tn}$ , with  $V_{GS2} = V_A - V_{DS1}$  and  $V_{GS1} = V_B$ . The threshold voltage of transistor  $M_2$  will be higher than transistor  $M_1$  due to the body effect. The threshold voltages of the two devices are given by the following equations:

$$V_{Tn2} = V_{Tn0} + \gamma(\sqrt{2\phi_f} + V_{int}) - \sqrt{2\phi_f} \quad (6.1)$$

$$V_{Tn1} = V_{Tn0} \quad (6.2)$$

For case (b),  $M_3$  is turned *off*, and the gate voltage of  $M_2$  is set to  $V_{DD}$ . To a first order,  $M_2$  may be considered as a resistor in series with  $M_1$ . Since the drive on  $M_2$  is large, this resistance is small and has only a small effect on the voltage transfer characteristics. In case (c), transistor  $M_1$  acts as a resistor, causing a  $V_T$  increase in  $M_2$  due to body effect. The overall impact is quite small, as seen from the plot.

### Design Consideration

The important point to take away from the preceding discussion is that the **noise margins are input/pattern dependent**. In Example 6.2, a glitch on only one of the two inputs has a larger chance of creating a false transition at the output than if the glitch were to occur on both inputs simultaneously. Therefore, the former condition has a lower low-noise margin. A common practice when characterizing gates such as NAND and NOR is to connect all the inputs together. Unfortunately, this does not represent the worst case static behavior; the data dependencies should be carefully modeled. ■

### Propagation Delay of Complementary CMOS Gates

The computation of propagation delay proceeds in a fashion similar to the static inverter. For the purpose of delay analysis, each transistor is modeled as a resistor in series with an ideal switch. The value of the resistance is dependent on the power supply voltage and an equivalent large signal resistance, scaled by the ratio of device width over length, must be used. The logic is transformed into an equivalent  $RC$  network that includes the effect of internal node capacitances. Figure 6-8 shows the two-input NAND gate and its equivalent  $RC$  switch level model. Note that the internal node capacitance  $C_{int}$ —attributable to the source/drain regions and the gate overlap capacitance of  $M_2$  and  $M_1$ —is included here. While complicating the analysis, the capacitance of the internal nodes can have quite an impact in some networks such as large fan-in gates. In a first pass, we ignore the effect of the internal capacitance.

A simple analysis of the model shows that, similarly to the noise margins, **the propagation delay depends on the input patterns**. Consider, for instance, the low-to-high transition. Three possible input scenarios can be identified for charging the output to  $V_{DD}$ . If both inputs are driven low, the two PMOS devices are on. The delay in this case is  $0.69 \times (R_p/2) \times C_L$ , since the two resistors are in parallel. This is not the worst case low-to-high transition, which occurs when only one device turns on, and is given by  $0.69 \times R_p \times C_L$ . For the pull-down path, the output is discharged only if both  $A$  and  $B$  are switched high, and the delay is given by  $0.69 \times (2R_n) \times C_L$  to a first order. In other words, adding devices in series slows down the circuit, and devices must be made wider to avoid a performance penalty. When sizing the transistors in a gate with multiple inputs, we should pick the combination of inputs that triggers the worst case conditions.

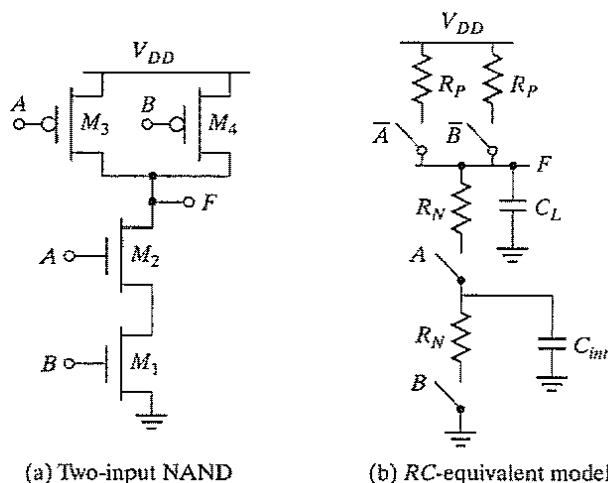


Figure 6-8 Equivalent RC model for a two-input NAND gate.

For the NAND gate to have the same pull-down delay ( $t_{pdt}$ ) as a minimum-sized inverter, the NMOS devices in the PDN stack must be made twice as wide so that the equivalent resistance of the NAND pull-down network is the same as the inverter. The PMOS devices can remain unchanged.<sup>1</sup>

This first-order analysis assumes that the extra capacitance introduced by widening the transistors can be ignored. This is not a good assumption, in general, but it allows for a reasonable first cut at device sizing.

### Example 6.3 Delay Dependence on Input Patterns

Consider the NAND gate of Figure 6-8a. Assume NMOS and PMOS devices of  $0.5 \mu\text{m}/0.25 \mu\text{m}$  and  $0.75 \mu\text{m}/0.25 \mu\text{m}$ , respectively. This sizing should result in approximately equal worst case rise and fall times (since the effective resistance of the pull-down is designed to be equal to the pull-up resistance).

Figure 6-9 shows the simulated low-to-high delay for different input patterns. As expected, the case in which both inputs transition go low ( $A = B = 1 \rightarrow 0$ ) results in a smaller delay, compared with the case in which only one input is driven low. Notice that the worst case low-to-high delay depends upon which input ( $A$  or  $B$ ) goes low. The reason for this involves the internal node capacitance of the pull-down stack (i.e., the source of  $M_2$ ). For the case in which  $B = 1$  and  $A$  transitions from  $1 \rightarrow 0$ , the pull-up PMOS device only has to charge up the output node capacitance ( $M_2$  is turned off). On the other hand, for the case in which  $A = 1$  and  $B$  transitions from  $1 \rightarrow 0$ , the pull-up PMOS device

<sup>1</sup>In deep-submicron processes, even larger increases in the width are needed due to the on-set of velocity saturation. For a two-input NAND, the NMOS transistors should be made 2.5 times as wide instead of 2 times.

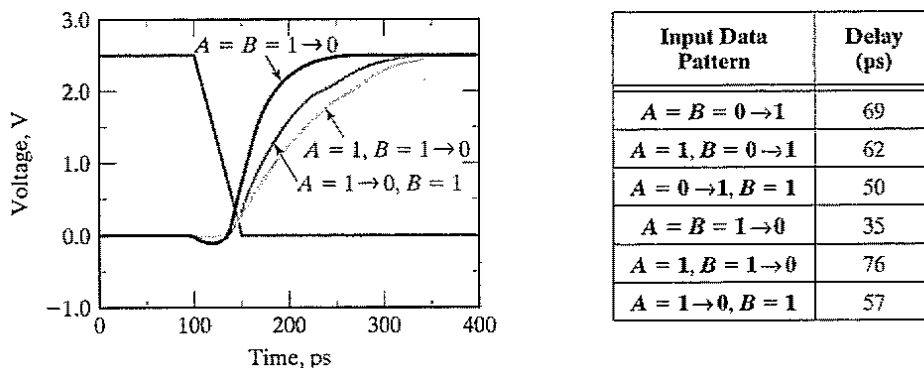


**Figure 6-9** Example showing the delay dependence on input patterns.

has to charge up the sum of the output and the internal node capacitances, which slows down the transition.

The table in Figure 6-9 shows a compilation of various delays for this circuit. The first-order transistor sizing indeed provides approximately equal rise and fall delays. An important point to note is that the high-to-low propagation delay depends on the initial state of the internal nodes. For example, when both inputs transition from  $0 \rightarrow 1$ , it is important to establish the state of the internal node. The worst case happens when the internal node is initially charged up to  $V_{DD} - V_{Th}$ , which can be ensured by pulsing the  $A$  input from  $1 \rightarrow 0 \rightarrow 1$ , while input  $B$  only makes the  $0 \rightarrow 1$  transition. In this way, the internal node is initialized properly.

The important point to take away from this example is that estimation of delay can be fairly complex, and requires a careful consideration of internal node capacitances and data patterns. Care must be taken to model the worst case scenario in the simulations. A brute force approach that applies all possible input patterns may not always work, because it is important to consider the state of internal nodes.

The CMOS implementation of a NOR gate ( $F = \overline{A + B}$ ) is shown in Figure 6-10. The output of this network is high, if and only if both inputs  $A$  and  $B$  are low. The worst case pull-down transition happens when only one of the NMOS devices turns on (i.e., if either  $A$  or  $B$  is high). Assume that the goal is to size the NOR gate such that it has approximately the same delay as an inverter with the following device sizes: NMOS of  $0.5 \mu\text{m}/0.25 \mu\text{m}$  and PMOS of  $1.5 \mu\text{m}/0.25 \mu\text{m}$ . Since the pull-down path in the worst case is a single device, the NMOS devices ( $M_1$  and  $M_2$ ) can have the same device widths as the NMOS device in the inverter. For the output to be pulled high, both devices must be turned on. Since the resistances add, the devices must be made two times larger compared with the PMOS in the inverter (i.e.,  $M_3$  and  $M_4$  must have a size of  $3 \mu\text{m}/0.25 \mu\text{m}$ ). Since PMOS devices have a lower mobility relative to NMOS devices, stacking devices in series must be avoided as much as possible. A NAND implementation is clearly preferred over a NOR implementation for implementing generic logic.

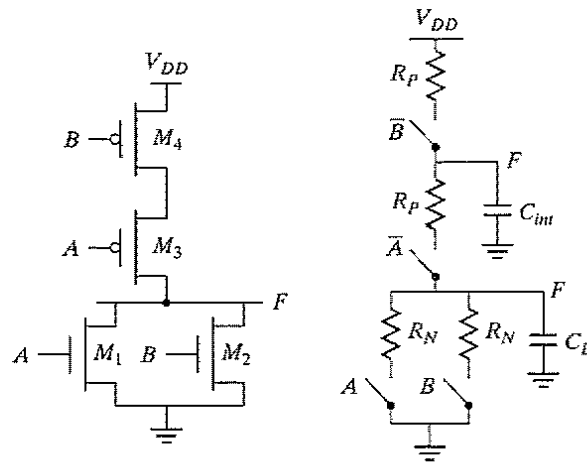


Figure 6-10 Sizing of a NOR gate.

### Problem 6.1 Transistor Sizing in Complementary CMOS Gates

Determine the sizes of the transistors in Figure 6-6c such that it has approximately the same  $t_{pth}$  and  $t_{phl}$  as an inverter with the following sizes: NMOS:  $0.5 \mu\text{m}/0.25 \mu\text{m}$  and a PMOS:  $1.5 \mu\text{m}/0.25 \mu\text{m}$ .

So far in the analysis of propagation delay, we have ignored the effect of internal node capacitances. This is often a reasonable assumption for a first-order analysis. However, in more complex logic gates with large *fan-ins*, the internal node capacitances can become significant. Consider a four-input NAND gate, as drawn in Figure 6-11, which shows the equivalent  $RC$  model of the gate, including the internal node capacitances. The internal capacitances consist of the junction capacitances of the transistors, as well as the gate-to-source and gate-to-drain capacitances. The latter are turned into capacitances to ground using the Miller equivalence. The delay analysis for such a circuit involves solving distributed  $RC$  networks, a problem we already encountered when analyzing the delay of interconnect networks. Consider the pull-down delay of the circuit. The output is discharged when all inputs are driven high. The proper initial conditions must be placed on the internal nodes (i.e., the internal nodes must be charged to  $V_{DD} - V_{TN}$ ) before the inputs are driven high.

The propagation delay can be computed by using the Elmore delay model:

$$t_{pHL} = 0.69(R_1 \cdot C_1 + (R_1 + R_2) \cdot C_2 + (R_1 + R_2 + R_3) \cdot C_3 + (R_1 + R_2 + R_3 + R_4) \cdot C_L) \quad (6.3)$$

Notice that the resistance of  $M_1$  appears in all the terms, which makes this device especially important when attempting to minimize delay. Assuming that all NMOS devices have an equal size, Eq. (6.3) simplifies to

$$t_{pHL} = 0.69R_N(C_1 + 2 \cdot C_2 + 3 \cdot C_3 + 4 \cdot C_L) \quad (6.4)$$



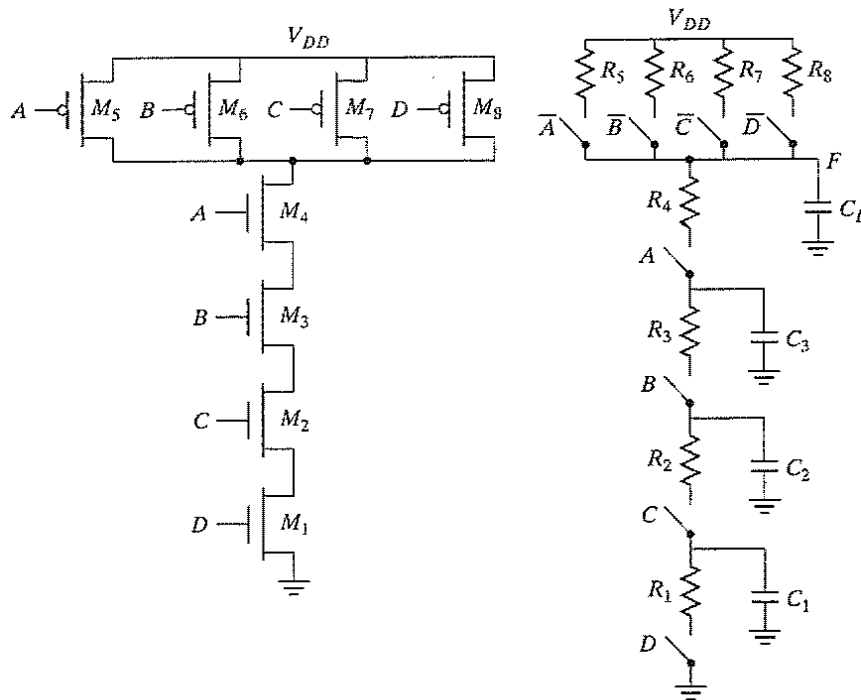


Figure 6-11 Four-input NAND gate and its  $RC$  model.

#### Example 6.4 A Four-Input Complementary CMOS NAND Gate

In this example, we evaluate the *intrinsic (or unloaded) propagation delay* of a four-input NAND gate (without any loading) is evaluated using hand analysis and simulation. The layout of the gate is shown in Figure 6-12. Assume that all NMOS devices have a  $W/L$  of  $0.5\ \mu\text{m}/0.25\ \mu\text{m}$ , and all PMOS devices have a device size of  $0.375\ \mu\text{m}/0.25\ \mu\text{m}$ . The devices are sized such that the worst case rise and fall times are approximately equal to a first order (ignoring the internal node capacitances).

By using techniques similar to those employed for the CMOS inverter in Chapter 5, the capacitance values can be computed from the layout. Notice that in the pull-up path, the PMOS devices share the drain terminal, in order to reduce the overall parasitic contribution. Using our standard design rules, we find that the area and perimeter for various devices can be easily computed, as shown in Table 6-2.

In this example, we focus on the pull-down delay, and the capacitances will be computed for the high-to-low transition at the output. While the output makes a transition from  $V_{DD}$  to 0, the internal nodes only transition from  $V_{DD} - V_{Tn}$  to GND. We need to linearize the internal junction capacitances for this voltage transition, but, to simplify the analysis, we use the same  $K_{eff}$  for the internal nodes as for the output node.

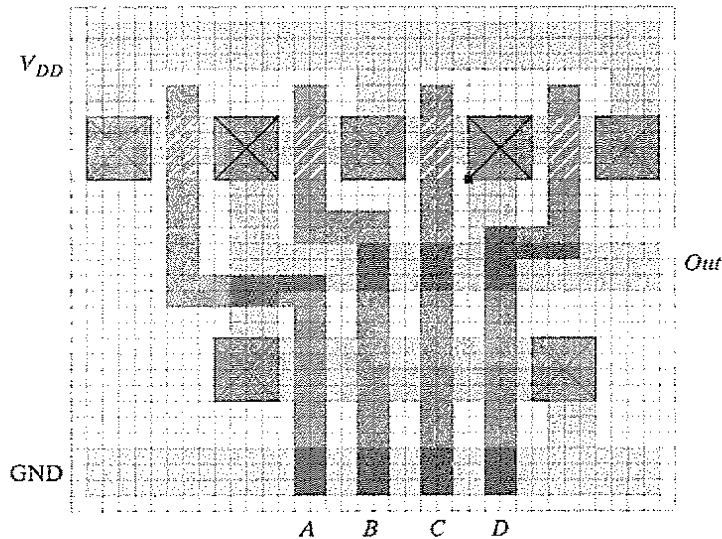


**Figure 6-12** Layout a four-input NAND gate in complementary CMOS. See also Colorplate 7.

**Table 6-2** Area and perimeter of transistors in four-input NAND gate.

Transistor	W ( $\mu\text{m}$ )	AS ( $\mu\text{m}^2$ )	AD ( $\mu\text{m}^2$ )	PS ( $\mu\text{m}$ )	PD ( $\mu\text{m}$ )
1	0.5	0.3125	0.0625	1.75	0.25
2	0.5	0.0625	0.0625	0.25	0.25
3	0.5	0.0625	0.0625	0.25	0.25
4	0.5	0.0625	0.3125	0.25	1.75
5	0.375	0.297	0.172	1.875	0.875
6	0.375	0.172	0.172	0.875	0.875
7	0.375	0.172	0.172	0.875	0.875
8	0.375	0.297	0.172	1.875	0.875

It is assumed that the output connects to a single, minimum-size inverter. The effect of intracell routing, which is small, is ignored. The various contributions are summarized in Table 6-3. For the NMOS and PMOS junctions, we use  $K_{eq} = 0.57$ ,  $K_{eqsw} = 0.61$ , and  $K_{eq} = 0.79$ ,  $K_{eqsw} = 0.86$ , respectively. Notice that the gate-to-drain capacitance is multiplied by a factor of two for all internal nodes as well as the output node, to account for the Miller effect. (This ignores the fact that the internal nodes have a slightly smaller swing due to the threshold drop.)

**Table 6-3** Computation of capacitances for high-to-low transition at the output. The table shows the intrinsic delay of the gate without extra loading. Any *fan-out* capacitance would simply be added to the  $C_L$  term.

Capacitor	Contributions (H → L)	Value (fF) (H → L)
$C1$	$C_{d1} + C_{s2} + 2 * C_{gd1} + 2 * C_{gs2}$	$(0.57 * 0.0625 * 2 + 0.61 * 0.25 * 0.28) +$ $(0.57 * 0.0625 * 2 + 0.61 * 0.25 * 0.28) +$ $2 * (0.31 * 0.5) + 2 * (0.31 * 0.5) = 0.85 \text{ fF}$
$C2$	$C_{d2} + C_{s3} + 2 * C_{gd2} + 2 * C_{gs3}$	$(0.57 * 0.0625 * 2 + 0.61 * 0.25 * 0.28) +$ $(0.57 * 0.0625 * 2 + 0.61 * 0.25 * 0.28) +$ $2 * (0.31 * 0.5) + 2 * (0.31 * 0.5) = 0.85 \text{ fF}$
$C3$	$C_{d3} + C_{s4} + 2 * C_{gd3} + 2 * C_{gs4}$	$(0.57 * 0.0625 * 2 + 0.61 * 0.25 * 0.28) +$ $(0.57 * 0.0625 * 2 + 0.61 * 0.25 * 0.28) +$ $2 * (0.31 * 0.5) + 2 * (0.31 * 0.5) = 0.85 \text{ fF}$
$CL$	$C_{d4} + 2 * C_{gd4} + C_{d5} + C_{d6} + C_{d7}$ $+ C_{d8} + 2 * C_{gd5} + 2 * C_{gd6}$ $+ 2 * C_{gd7} + 2 * C_{gd8}$ $= C_{d4} + 4 * C_{d5} + 4 * 2 * C_{gd6}$	$(0.57 * 0.3125 * 2 + 0.61 * 1.75 * 0.28) +$ $2 * (0.31 * 0.5) + 4 * (0.79 * 0.171875 * 1.9 + 0.86$ $* 0.875 * 0.22) + 4 * 2 * (0.27 * 0.375) = 3.47 \text{ fF}$

Using Eq. (6.4), we compute the propagation delay, as follows:

$$t_{pHL} = 0.69 \left( \frac{13 \text{ K}\Omega}{2} \right) (0.85 \text{ fF} + 2 \cdot 0.85 \text{ fF} + 3 \cdot 0.85 \text{ fF} + 4 \cdot 3.47 \text{ fF}) = 85 \text{ ps}$$

The simulated delay for this particular transition was found to be 86 ps! The hand analysis gives a fairly accurate estimate, given all of the assumptions and linearizations that were made. For example, we assume that the gate-source (or gate-drain) capacitance only consists of the overlap component. This is not entirely the case, because, during the transition, some other contributions come in place depending upon the operating region. Once again, the goal of hand analysis is not to provide a totally accurate delay prediction, but rather to give intuition into what factors influence the delay and to aid in initial transistor sizing. Accurate timing analysis and transistor optimization is usually done using SPICE. The simulated worst case low-to-high delay time for this gate was 106 ps.

While complementary CMOS is a very robust and simple approach for implementing logic gates, there are two major problems associated with using this style as the complexity of the gate (i.e., *fan-in*) increases. First, the number of transistors required to implement an  $N$  fan-in gate is  $2N$ . This can result in a significantly large implementation area.

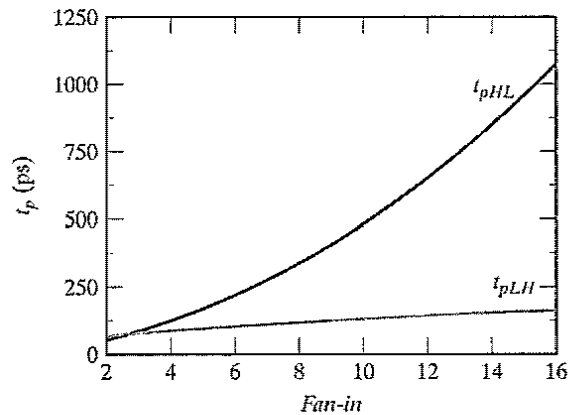


**Figure 6-13** Propagation delay of CMOS NAND gate as a function of fan-in. A fan-out of one inverter is assumed, and all pull-down transistors are minimal size.

The second problem is that propagation delay of a complementary CMOS gate deteriorates rapidly as a function of the fan-in. In fact, the *unloaded intrinsic delay* of the gate is, at worst, a *quadratic function of the fan-in*.

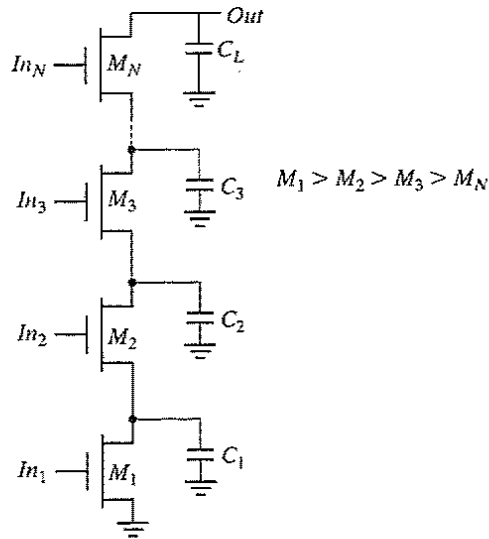
- The large number of transistors ( $2N$ ) increases the overall capacitance of the gate. For an  $N$ -input gate, the *intrinsic capacitance* increases linearly with the fan-in. Consider, for instance, the NAND gate of Figure 6-11. Given the linear increase in the number of PMOS devices connected to the output node, we expect the low-to-high delay of the gate to increase linearly with fan-in—while the capacitance goes up linearly, the pull-up resistance remains unchanged.
- The series connection of transistors in either the PUN or PDN of the gate causes an additional slowdown. We know that the *distributed RC network* in the PDN of Figure 6-11 comes with a delay that is quadratic in the number of elements in the chain. The high-to-low delay of the gate should hence be a quadratic function of the fan-in.

Figure 6-13 plots the (intrinsic) propagation delay of a NAND gate as a function of fan-in assuming a fixed fan-out of one inverter (NMOS:  $0.5\ \mu\text{m}$  and PMOS:  $1.5\ \mu\text{m}$ ). As predicted,  $t_{pLH}$  is a linear function of fan-in, while the simultaneous increase in the pull-down resistance and the load capacitance cause an approximately quadratic relationship for  $t_{pHL}$ . Gates with a *fan-in* greater than or equal to 4 become excessively slow and must be avoided.

#### Design Techniques for Large Fan-in

The designer has a number of techniques at his disposition to reduce the delay of large fan-in circuits:

- **Transistor Sizing** The most obvious solution is to increase the transistor sizes. This lowers the resistance of devices in series and lowers the time constants. However, increasing the transistor sizes results in larger parasitic capacitors, which not only affect the *propagation delay* of the gate in question, but



**Figure 6-14** Progressive sizing of transistors in large transistor chains copes with the extra load of internal capacitances.

also present a larger load to the preceding gate. This technique should therefore be used with caution. If the load capacitance is dominated by the intrinsic capacitance of the gate, widening the device only creates a “self-loading” effect, and the *propagation delay* is unaffected. Sizing is only effective when the load is dominated by the fan-out. A more comprehensive approach toward sizing transistors in complex CMOS combinational networks is discussed in the next section.

- Progressive Transistor Sizing** An alternate approach to uniform sizing (in which each transistor is scaled up uniformly), is to use progressive transistor sizing (Figure 6-14). Referring back to Eq. (6.3), we see that the resistance of  $M_1$  ( $R_1$ ) appears  $N$  times in the delay equation, the resistance of  $M_2$  ( $R_2$ ) appears  $N - 1$  times, etc. From the equation, it is clear that  $R_1$  should be made the smallest,  $R_2$  the next smallest, etc. Consequently, a progressive scaling of the transistors is beneficial:  $M_1 > M_2 > M_3 > M_N$ . This approach reduces the dominant resistance, while keeping the increase in capacitance within bounds. For an excellent treatment on the optimal sizing of transistors in a complex network, we refer the interested reader to [Shoji88, pp. 131–143]. You should be aware, however, of one important pitfall of this approach. While progressive resizing of transistors is relatively easy in a schematic diagram, it is not as simple in a real layout. Very often, design-rule considerations force the designer to push the transistors apart, which causes the internal capacitance to grow. This may offset all the gains of the resizing!
- Input Reordering** Some signals in complex combinational logic blocks might be more critical than others. Not all inputs of a gate arrive at the same time (due, for instance, to the propagation delays of the preceding logical gates). An input signal to a gate is called *critical* if it is the last signal of all inputs to assume a stable value. The path through the logic which determines the ultimate speed of the structure is called the *critical path*.

Putting the critical-path transistors closer to the output of the gate can result in a speed up, as demonstrated in Figure 6-15. Signal  $In_1$  is assumed to be a critical signal. Suppose further that  $In_2$  and  $In_3$  are high, and that  $In_1$  undergoes a  $0 \rightarrow 1$  transition. Assume also that  $C_L$  is initially charged high. In case (a), no path to GND exists until  $M_1$  is turned on, which, unfortunately, is the last event to happen. The delay between the arrival of  $In_1$  and the output is therefore determined by the time it takes to discharge  $C_L$ ,  $C_1$ , and  $C_2$ . In the second case,  $C_1$  and  $C_2$  are already

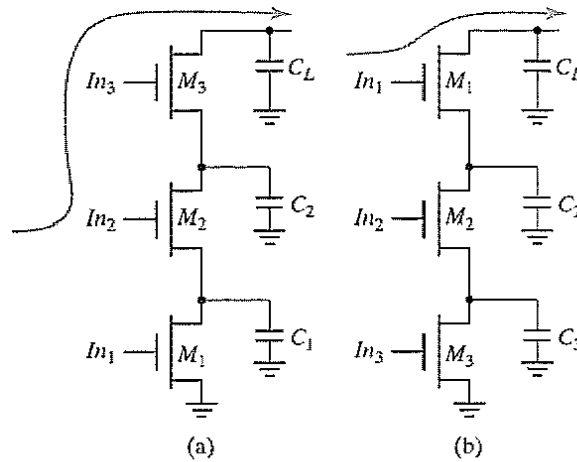


**Figure 6-15** Influence of transistor ordering on delay. Signal  $In_1$  is the critical signal.

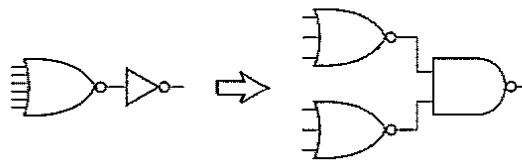


**Figure 6-16** Logic restructuring can reduce the gate fan-in.

discharged when  $In_1$  changes. Only  $C_L$  still has to be discharged, resulting in a smaller delay.

- **Logic Restructuring** Manipulating the logic equations can reduce the fan-in requirements and thus reduce the gate delay, as illustrated in Figure 6-16. The quadratic dependency of the gate delay on *fan-in* makes the six-input NOR gate extremely slow. Partitioning the NOR gate into two three-input gates results in a significant speedup, which by far offsets the extra delay incurred by turning the inverter into a two-input NAND gate. ■

### Optimizing Performance in Combinational Networks

Earlier, we established that minimization of the propagation delay of a gate in isolation is a purely academic effort. The sizing of devices should happen in its proper context. In Chapter 5, we developed a methodology to do so for inverters. We also found that an optimal fan-out for a chain of inverters driving a load  $C_L$  is  $(C_L/C_{in})^{1/N}$ , where  $N$  is the number of stages in the chain, and  $C_{in}$  the input capacitance of the first gate in the chain. If we have an opportunity to select the number of stages, we found out that we would like to keep the fan-out per stage around 4. Can this result be extended to determine the size of any combinational path for minimal delay? By extending our previous approach to address complex logic networks, we find out that this is indeed possible [Sutherland99].<sup>2</sup>

<sup>2</sup>The approach introduced in this section is commonly called logical effort, and was formally introduced in [Sutherland99], which presents an extensive treatment of the topic. The treatment offered here represents only a glance over of the overall approach.

**Table 6-4** Estimates of intrinsic delay factors of various logic types, assuming simple layout styles, and a fixed PMOS–NMOS ratio.

Gate type	$p$
Inverter	1
$n$ -input NAND	$n$
$n$ -input NOR	$n$
$n$ -way multiplexer	$2n$
XOR, NXOR	$n2^{n-1}$

To do so, we modify the basic delay equation of the inverter that we introduced in Chapter 5, namely,

$$t_p = t_{p0} \left( 1 + \frac{C_{ext}}{\gamma C_g} \right) = t_{p0} (1 + f/\gamma) \quad (6.5)$$

to

$$t_p = t_{p0} (p + gf/\gamma) \quad (6.6)$$

with  $t_{p0}$  still representing the intrinsic delay of an inverter and  $f$  the *effective fan-out*, defined as the ratio between the external load and the input capacitance of the gate. In this context,  $f$  is also called the *electrical effort*, and  $p$  represents the ratio of the intrinsic (or unloaded) delays of the complex gate and the simple inverter, and is a function of gate topology, as well as layout style. The more involved structure of the multiple-input gate causes its intrinsic delay to be higher than that of an inverter. Table 6-4 enumerates the values of  $p$  for some standard gates, assuming simple layout styles, and ignoring second-order effects such as internal node capacitances.

The factor  $g$  is called the *logical effort*, and represents the fact that, for a given load, complex gates have to work harder than an inverter to produce a similar response. In other words, the logical effort of a logic gate tells how much worse it is at producing output current than an inverter, given that each of its inputs may present only the same input capacitance as the inverter. Equivalently, logical effort is how much more input capacitance a gate presents to deliver the same output current as an inverter. Logical effort is a useful parameter, because it depends only on circuit topology. The logical efforts of some common logic gates are given in Table 6-5.

Table 6-5 Logic efforts of common logic gates, assuming a PMOS–NMOS ratio of 2.

Gate Type	Number of Inputs			
	1	2	3	n
Inverter	1			
NAND		4/3	5/3	$(n + 2)/3$
NOR		5/3	7/3	$(2n + 1)/3$
Multiplexer		2	2	2
XOR		4	12	

**Example 6.5 Logical Effort of Complex Gates**

Consider the gates shown in Figure 6-17. Assuming PMOS–NMOS ratio of 2, the input capacitance of a minimum-sized symmetrical inverter equals three times the gate capacitance of a minimum-sized NMOS (called  $C_{unit}$ ). We size the two-input NAND and NOR such that their equivalent resistances equal the resistance of the inverter (using the techniques described earlier). This increases the input capacitance of the two-input NAND to  $4 C_{unit}$ , or  $4/3$  the capacitance of the inverter. The input capacitance of the two-input NOR is  $5/3$  that of the inverter. Equivalently, for the same input capacitance, the NAND and NOR gate have  $4/3$  and  $5/3$  less driving strength than the inverter. This affects the delay component that corresponds to the load, increasing it by this same factor, called the *logical effort*. Hence,  $g_{NAND} = 4/3$ , and  $g_{NOR} = 5/3$ .

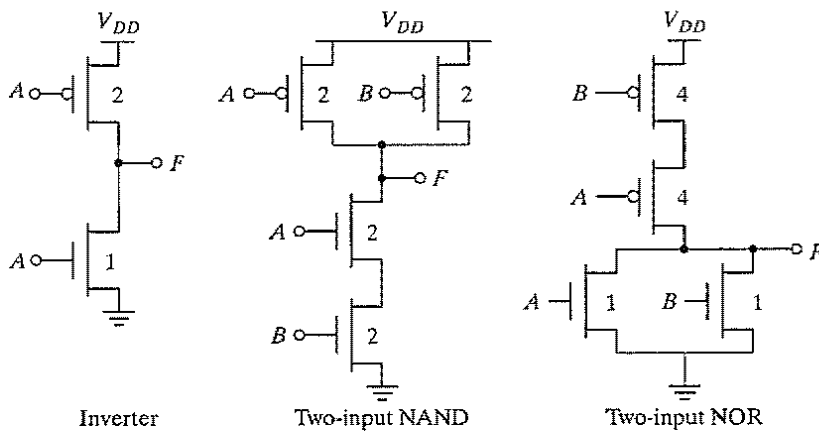
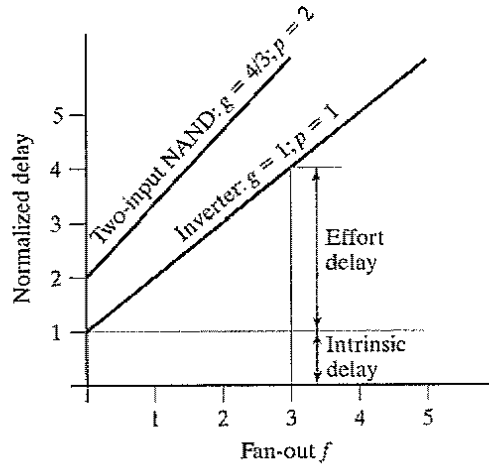


Figure 6-17 Logical effort of two-input NAND and NOR gates.





**Figure 6-18** Delay as a function of fan-out for an inverter and a two-input NAND.

The delay model of a logic gate, as represented in Eq. (6.6), is a simple linear relationship. Figure 6-18 shows this relationship graphically: the delay is plotted as a function of the fan-out for an inverter and for a two-input NAND gate. The slope of the line is the logical effort of the gate; its intercept is the intrinsic delay. The graph shows that we can adjust the delay by adjusting the effective fan-out (by transistor sizing) or by choosing a logic gate with a different logical effort. Observe also that fan-out and logical effort contribute to the delay in a similar way. We call the product of the two  $h = fg$ , the *gate effort*.

The total delay of a path through a combinational logic block can now be expressed as

$$t_p = \sum_{j=1}^N t_{p,j} = t_{p0} \sum_{j=1}^N \left( p_j + \frac{f_j g_j}{\gamma} \right) \quad (6.7)$$

We use a similar procedure as we did for the inverter chain in Chapter 5 to determine the minimum delay of the path. By finding  $N - 1$  partial derivatives and setting them to zero, we find that **each stage should bear the same gate effort**:

$$f_1 g_1 = f_2 g_2 = \dots = f_N g_N \quad (6.8)$$

The logical effort along a path in the network compounds by multiplying the logical efforts of all the gates along the path, yielding the *path logical effort*  $G$ :

$$G = \prod_1^N g_i \quad (6.9)$$

We also can define a *path effective fan-out* (or *electrical effort*)  $F$ , which relates the load capacitance of the last gate in the path to the input capacitance of the first gate:

$$F = \frac{C_L}{C_{g1}} \quad (6.10)$$

To relate  $F$  to the effective fan-outs of the individual gates, we must introduce another factor to account for the logical fan-out within the network. When fan-out occurs at the output of a node, some of the available drive current is directed along the path we are analyzing, and some is directed off the path. We define the *branching effort*  $b$  of a logical gate on a given path to be

$$b = \frac{C_{\text{on-path}} + C_{\text{off-path}}}{C_{\text{on-path}}} \quad (6.11)$$

where  $C_{\text{on-path}}$  is the load capacitance of the gate along the path we are analyzing and  $C_{\text{off-path}}$  is the capacitance of the connections that lead off the path. Note that the branching effort is, if the path does not branch (as in a chain of gates). The *path branching effort* is defined as the product of the branching efforts at each of the stages along the path, or

$$B = \prod_1^N b_i \quad (6.12)$$

The path electrical effort can now be related to the electrical and branching efforts of the individual stages:

$$F = \prod_1^N \frac{f_i}{b_i} = \frac{\prod_1^N f_i}{B} \quad (6.13)$$

Finally, the total path effort  $H$  can be defined. Using Eq. (6.13), we write

$$H = \prod_1^N h_i = \prod_1^N g_i f_i = GFB \quad (6.14)$$

From here on, the analysis proceeds along the same lines as the inverter chain. The gate effort that minimizes the path delay is

$$h = \sqrt[N]{H} \quad (6.15)$$

and the minimum delay through the path is

$$D = t_{p0} \left( \sum_{j=1}^N p_j + \frac{N(\sqrt[N]{H})}{\gamma} \right) \quad (6.16)$$

Note that the path intrinsic delay is a function of the types of logic gates in the path and is not affected by the sizing. The size factors of the individual gates in the chain  $s_i$  can then be derived by working from front to end (or vice versa). We assume that a unit-size gate has a driving capability equal to a minimum-size inverter. Based on the definition of the logical effort, this means that its input capacitance is  $g$  times larger than that of the reference inverter, which equals  $C_{\text{ref}}$ . With  $s_1$  the sizing factor of the first gate in the chain, the input capacitance of the chain  $C_{g1}$

equals  $g_1 s_1 C_{ref}$ . Including the branching effort, we know that the input capacitance of gate 2 is  $(f_1/b_1)$  larger, or

$$g_2 s_2 C_{ref} = \left(\frac{f_1}{b_1}\right) g_1 s_1 C_{ref} \quad (6.17)$$

For gate  $i$  in the chain, this yields

$$s_i = \left(\frac{g_1 s_1}{g_i}\right) \prod_{j=1}^{i-1} \left(\frac{f_j}{b_j}\right) \quad (6.18)$$

### Example 6.6 Sizing Combinational Logic for Minimum Delay

Consider the logic network of Figure 6-19, which may represent the critical path of a more complex logic block. The output of the network is loaded with a capacitance which is five times larger than the input capacitance of the first gate, which is a minimum-sized inverter. The effective fan-out of the path thus equals  $F = C_L/C_{g1} = 5$ . Using the entries in Table 6-5, we find the path logical effort as follows:

$$G = 1 \times \frac{5}{3} \times \frac{5}{3} \times 1 = \frac{25}{9}$$

Since there is no branching,  $B = 1$ . Hence,  $H = GFB = 125/9$ , and the optimal stage effort  $h$  is  $\sqrt[4]{H} = 1.93$ . Taking into account the gate types, we derive the following fan-out factors:  $f_1 = 1.93$ ;  $f_2 = 1.93 \times (3/5) = 1.16$ ;  $f_3 = 1.16$ ;  $f_4 = 1.93$ . Notice that the inverters are assigned larger than the more complex gates because they are better at driving loads.

Finally, we derive the gate sizes (with respect to the minimum-sized versions) using Eq. (6.18). This leads to the following values:  $a = f_1 g_1 / g_2 = 1.16$ ;  $b = f_1 f_2 g_1 / g_3 = 1.34$ ; and  $c = f_1 f_2 f_3 g_1 / g_4 = 2.60$ .

These calculations do not have to be very precise. As discussed in Chapter 5, sizing a gate too large or too small by a factor of 1.5 still results in circuits within 5% of minimum delay. Therefore, the “back of the envelope” hand calculations using this technique are quite effective.

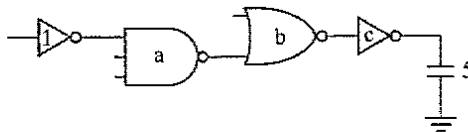


Figure 6-19 Critical path of combinational network.

**Problem 6.2 Sizing an Inverter Network**

Revisit Problem 5.5, but this time around use the branching-effort approach to produce the solution.

**Power Consumption in CMOS Logic Gates**

The sources of power consumption in a complementary CMOS inverter were discussed in detail in Chapter 5. Many of these issues apply directly to complex CMOS gates. The power dissipation is a strong function of transistor sizing (which affects physical capacitance,) input and output rise–fall times (which determine the short-circuit power,) device thresholds and temperature (which impact leakage power,) and switching activity. The dynamic power dissipation is given by  $\alpha_{0 \rightarrow 1} C_L V_{DD}^2 f$ . Making a gate more complex mostly affects the *switching activity*  $\alpha_{0 \rightarrow 1}$ , which has two components: a static component that is only a function of the topology of the logic network, and a dynamic one that results from the timing behavior of the circuit. (The latter factor is also called glitching.)

**Logic Function** The transition activity is a strong function of the logic function being implemented. For static CMOS gates with statistically independent inputs, the static transition probability is the probability  $p_0$  that the output will be in the *zero* state in one cycle, multiplied by the probability  $p_1$  that the output will be in the *one* state in the next cycle:

$$\alpha_{0 \rightarrow 1} = p_0 \cdot p_1 = p_0 \cdot (1 - p_0) \quad (6.19)$$

Assuming that the inputs are independent and uniformly distributed, any  $N$ -input static gate has a transition probability given by

$$\alpha_{0 \rightarrow 1} = \frac{N_0}{2^N} \cdot \frac{N_1}{2^N} = \frac{N_0 \cdot (2^N - N_0)}{2^{2N}} \quad (6.20)$$

where  $N_0$  is the number of *zero* entries, and  $N_1$  is the number of *one* entries in the output column of the truth table of the function. To illustrate, consider a static two-input NOR gate whose truth table is shown in Table 6-6. Assume that only one input transition is possible during a clock cycle and that the inputs to the NOR gate have a uniform input distribution (in other words, the four possible states for inputs  $A$  and  $B$ —00, 01, 10, 11—are equally likely).

**Table 6-6** Truth table of a two-input NOR gate.

A	B	Out
0	0	1
0	1	0
1	0	0
1	1	0

From Table 6-6 and Eq. (6.20), the output transition probability of a two-input static CMOS NOR gate can be derived:

$$\alpha_{0 \rightarrow 1} = \frac{N_0 \cdot (2^N - N)}{2^{2N}} = \frac{3 \cdot (2^2 - 3)}{2^{2 \cdot 2}} = \frac{3}{16} \quad (6.21)$$

### Problem 6.3 $N$ -Input XOR Gate

Assuming the inputs to an  $N$ -input XOR gate are uncorrelated and uniformly distributed, derive the expression for the switching activity factor.

**Signal Statistics** The switching activity of a logic gate is a strong function of the input signal statistics. Using a uniform input distribution to compute activity is not a good technique, since the propagation through logic gates can significantly modify the signal statistics. For example, consider once again a two-input static NOR gate, and let  $p_a$  and  $p_b$  be the probabilities that the inputs  $A$  and  $B$  are *one*. Assume further that the inputs are not correlated. The probability that the output node is 1 is given by

$$p_1 = (1 - p_a)(1 - p_b) \quad (6.22)$$

Therefore, the probability of a transition from 0 to 1 is

$$\alpha_{0 \rightarrow 1} = p_0 p_1 = (1 - (1 - p_a)(1 - p_b))(1 - p_a)(1 - p_b) \quad (6.23)$$

Figure 6-20 shows the transition probability as a function of  $p_a$  and  $p_b$ . Observe how this graph degrades into the simple inverter case when one of the input probabilities is set to 0. From

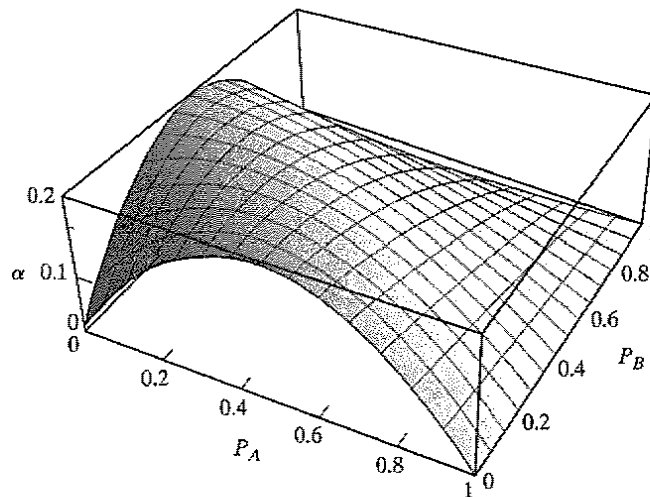


**Figure 6-20** Transition activity of a two-input NOR gate as a function of the input probabilities ( $p_A$ ,  $p_B$ ).

this plot, it is clear that understanding the signal statistics and their impact on switching events can be used to significantly impact the power dissipation.

**Problem 6.4 Power Dissipation of Basic Logic Gates**

Derive the  $0 \rightarrow 1$  output transition probabilities for the basic logic gates (AND, OR, XOR). The results to be obtained are given in Table 6-7.

**Table 6-7** Output transition probabilities for static logic gates.

	$\alpha_{0 \rightarrow 1}$
AND	$(1 - p_A p_B) p_A p_B$
OR	$(1 - p_A)(1 - p_B)[1 - (1 - p_A)(1 - p_B)]$
XOR	$[1 - (p_A + p_B - 2p_A p_B)](p_A + p_B - 2p_A p_B)$

**Intersignal Correlations** The evaluation of the switching activity is further complicated by the fact that signals exhibit correlation in space and time. Even if the primary inputs to a logic network are uncorrelated, the signals become correlated or “colored,” as they propagate through the logic network. This is best illustrated with a simple example. Consider first the circuit shown in Figure 6-21a, and assume that the primary inputs *A* and *B* are uncorrelated and uniformly distributed. Node *C* has a 1 (0) probability of 1/2, and a  $0 \rightarrow 1$  transition probability of 1/4. The probability that the node *Z* undergoes a power consuming transition is then determined using the AND-gate expression of Table 6-7:

$$p_{0 \rightarrow 1} = (1 - p_a p_b) p_a p_b = (1 - 1/2 \cdot 1/2) 1/2 \cdot 1/2 = 3/16 \tag{6.24}$$

The computation of the probabilities is straightforward: signal and transition probabilities are evaluated in an ordered fashion, progressing from the input to the output node. This approach, however, has two major limitations: (1) it does not deal with circuits with feedback as found in sequential circuits, and (2) it assumes that the signal probabilities at the input of each gate are independent. This is rarely the case in actual circuits, where reconvergent fan-out often causes intersignal dependencies. For instance, the inputs to the AND gate in Figure 6-21b (*C* and *B*) are interdependent because both are a function of *A*. The approach to computing

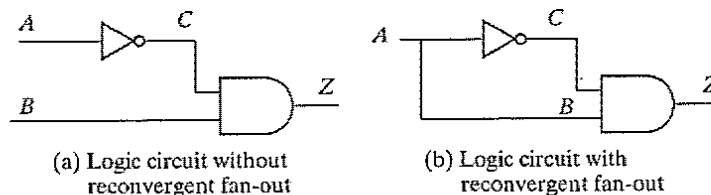


**Figure 6-21** Example illustrating the effect of signal correlations.

probabilities that we presented previously fails under these circumstances. Traversing from inputs to outputs yields a transition probability of 3/16 for node  $Z$ , similar to the previous analysis. This value clearly is false, as logic transformations show that the network can be reduced to  $Z = C \cdot B = A \cdot \bar{A} = 0$ , and thus no transition will ever take place.

To get the precise results in the progressive analysis approach, it is essential to take signal interdependencies into account. This can be accomplished with the aid of conditional probabilities. For an AND gate,  $Z$  equals 1 if and only if  $B$  and  $C$  are equal to 1. Thus,

$$p_Z = p(Z = 1) = p(B = 1, C = 1) \quad (6.25)$$

where  $p(B = 1, C = 1)$  represents the probability that  $B$  and  $C$  are equal to 1 simultaneously. If  $B$  and  $C$  are independent,  $p(B = 1, C = 1)$  can be decomposed into  $p(B = 1) \cdot p(C = 1)$ , and this yields the expression for the AND gate derived earlier:  $p_Z = p(B = 1) \cdot p(C = 1) = p_B p_C$ . If a dependency between the two exists (as is the case in Figure 6-21b), a conditional probability has to be employed, such as the following:

$$p_Z = p(C = 1|B = 1) \cdot p(B = 1) \quad (6.26)$$

The first factor in Eq. (6.26) represents the probability that  $C = 1$  given that  $B = 1$ . The extra condition is necessary because  $C$  is dependent upon  $B$ . Inspection of the network shows that this probability is equal to 0, since  $C$  and  $B$  are logical inversions of each other, resulting in the signal probability for  $Z$ ,  $p_Z = 0$ .

Deriving those expressions in a structured way for large networks with reconvergent fan-out is complex, especially when the networks contain feedback loops. Computer support is therefore essential. To be meaningful, the analysis program has to process a typical sequence of input signals, because the power dissipation is a strong function of statistics of those signals.

**Dynamic or Glitching Transitions** When analyzing the transition probabilities of complex, multistage logic networks in the preceding section, we ignored the fact that the gates have a non-zero propagation delay. In reality, the finite propagation delay from one logic block to the next can cause spurious transitions known as *glitches* or *dynamic hazards* to occur: a node can exhibit multiple transitions in a single clock cycle before settling to the correct logic level.

A typical example of the effect of glitching is shown in Figure 6-22, which displays the simulated response of a chain of NAND gates for all inputs going simultaneously from 0 to 1. Initially, all the outputs are 1 since one of the inputs was 0. For this particular transition, all the odd bits must transition to 0, while the even bits remain at the value of 1. However, due to the finite propagation delay, the even output bits at the higher bit positions start to discharge, and the voltage drops. When the correct input ripples through the network, the output goes high. The glitch on the even bits causes extra power dissipation beyond what is required to strictly implement the logic function. Although the glitches in this example are only partial (i.e., not from rail to rail), they contribute significantly to the power dissipation. Long chains of gates often occur in important structures such as adders and multipliers, and the glitching component can easily dominate the overall power consumption.

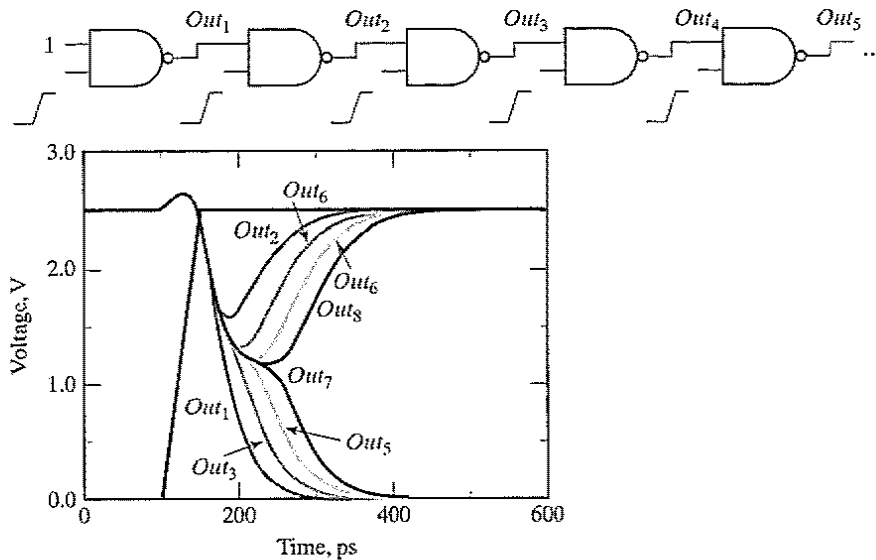


Figure 6-22 Glitching in a chain of NAND gates.

### Design Techniques to Reduce Switching Activity

The dynamic power of a logic gate can be reduced by minimizing the physical capacitance and the switching activity. The physical capacitance can be minimized in a number of ways, including circuit style selection, transistor sizing, placement and routing, and architectural optimizations. The switching activity, on the other hand, can be minimized at all levels of the design abstraction, and is the focus of this section. Logic structures can be optimized to minimize both the fundamental transitions required to implement a given function and the spurious transitions.

- Logic Restructuring** Changing the topology of a logic network may reduce its power dissipation. Consider, for example, two alternative implementations of  $F = A \cdot B \cdot C \cdot D$ , as shown in Figure 6-23. Ignore glitching and assume that all primary inputs ( $A, B, C, D$ ) are uncorrelated and uniformly distributed (this is,  $p_{1(a,b,c,d)} = 0.5$ ). Using the expressions from Table 6-7, the activity can be computed for the two topologies, as shown in Table 6-8. The results indicate that the chain implementation has an overall lower switching activity than the tree implementation for random inputs. However, as mentioned before, it is also important to consider the timing behavior to

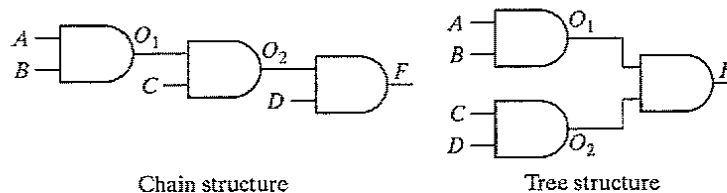


Figure 6-23 Simple example to demonstrate the influence of circuit topology on activity.



Table 6-8 Probabilities for tree and chain topologies.

	$O_1$	$O_2$	F
$p_1$ (chain)	1/4	1/8	1/16
$p_0 = 1-p_1$ (chain)	3/4	7/8	15/16
$p_{0 \rightarrow 1}$ (chain)	3/16	7/64	15/256
$p_1$ (tree)	1/4	1/4	1/16
$p_0 = 1-p_1$ (tree)	3/4	3/4	15/16
$p_{0 \rightarrow 1}$ (tree)	3/16	3/16	15/256

accurately make power trade-offs. In this example, the tree topology experiences (virtually) no glitching activity since the signal paths are balanced to all the gates.

2. **Input ordering** Consider the two static logic circuits of Figure 6-24. The probabilities that  $A$ ,  $B$ , and  $C$  are equal to 1 are listed in the Figure. Since both circuits implement identical logic functionality, it is clear that the activity at the output node  $Z$  is equal in both cases. The difference is in the activity at the intermediate node. In the first circuit, this activity equals  $(1 - 0.5 \times 0.2) (0.5 \times 0.2) = 0.09$ . In the second case, the probability that a  $0 \rightarrow 1$  transition occurs equals  $(1 - 0.2 \times 0.1) (0.2 \times 0.1) = 0.0196$ , a substantially lower value. From this, we learn that it is beneficial to postpone the introduction of signals with a high transition rate (i.e., signals with a signal probability close to 0.5). A simple reordering of the input signals is often sufficient to accomplish that goal.

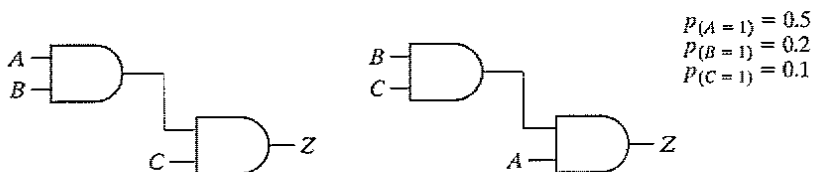
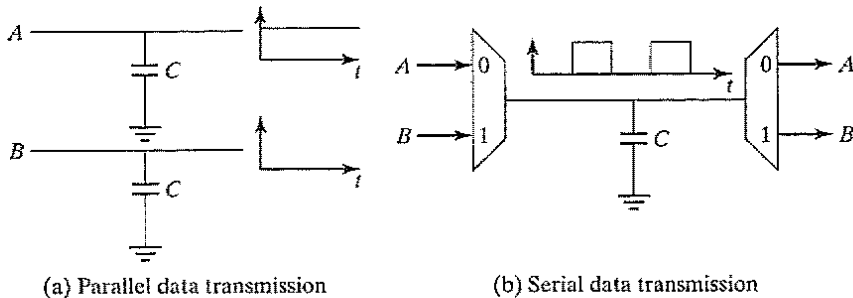


Figure 6-24 Reordering of inputs affects the circuit activity.

3. **Time-multiplexing resources** Time-multiplexing a single hardware resource—such as a logic unit or a bus—over a number of functions is a technique often used to minimize the implementation area. Unfortunately, the minimum area solution does not always result in the lowest switching activity. For example, consider the transmission of two input bits ( $A$  and  $B$ ) using either dedicated resources or a time-multiplexed approach, as shown in Figure 6-25. To the first order, ignoring the multiplexer overhead, it would seem that the degree of time multiplexing should not affect the switched capacitance, since the time-multiplexed solution has half the physical capacitance switched at twice the frequency (for a fixed throughput).

If the data being transmitted are random, it will make no difference which architecture is used. However, if the data signals have some distinct properties (such as temporal correlation), the power dissipation of the time-multiplexed solution can be significantly higher. Suppose, for instance, that  $A$  is always (or mostly) 1, and  $B$  is (mostly) 0. In the parallel solution, the switched capacitance is very low since there are very few transitions on the data bits. However, in the time-multiplexed solution,



**Figure 6-25** Parallel versus time-multiplexed data busses.

the bus toggles between 0 and 1. Care must be taken in digital systems to avoid time-multiplexing data streams with very distinct data characteristics.

4. **Glitch Reduction by balancing signal paths** The occurrence of glitching in a circuit is mainly due to a mismatch in the path lengths in the network. If all input signals of a gate change simultaneously, no glitching occurs. On the other hand, if input signals change at different times, a dynamic hazard might develop. Such a mismatch in signal timing is typically the result of different path lengths with respect to the primary inputs of the network. This is illustrated in Figure 6-26. Assume that the XOR gate has a unit delay. The first network (a) suffers from glitching as a result of the wide disparity between the arrival times of the input signals for a gate. For example, for gate  $F_3$ , one input settles at time 0, while the second one only arrives at time 2. Redesigning the network so that all arrival times are identical can dramatically reduce the number of superfluous transitions (network b).

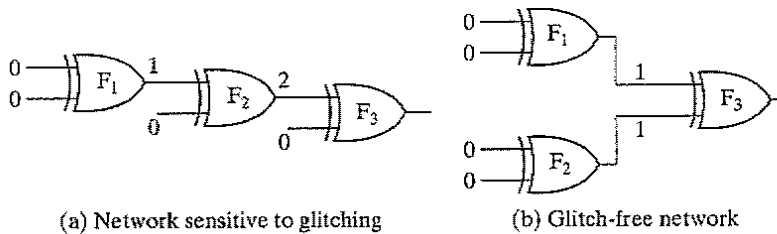


**Figure 6-26** Glitching is influenced by matching of signal path lengths. The annotated numbers indicate the signal arrival times.

## Summary

The CMOS logic style described in the previous section is highly robust and scalable with technology, but requires  $2N$  transistors to implement an  $N$ -input logic gate. Also, the load capacitance is significant, since each gate drives two devices (a PMOS and an NMOS) per *fan-out*. This has opened the door for alternative logic families that either are simpler or faster.

### 6.2.2 Ratioed Logic

#### Concept

Ratioed logic is an attempt to reduce the number of transistors required to implement a given logic function, often at the cost of reduced robustness and extra power dissipation. The purpose

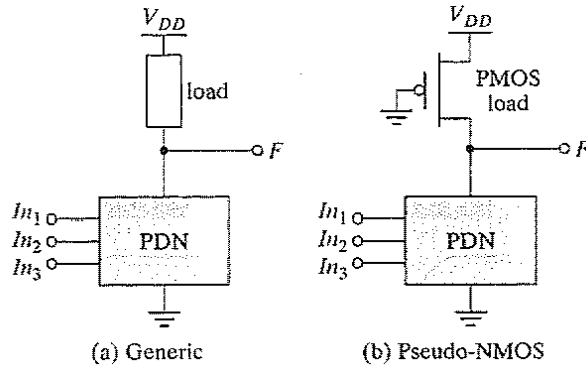


Figure 6-27 Ratioed logic gate.

of the PUN in complementary CMOS is to provide a conditional path between  $V_{DD}$  and the output when the PDN is turned *off*. In ratioed logic, the entire PUN is replaced with a single unconditional load device that pulls up the output for a high output as in Figure 6-27a. Instead of a combination of active pull-down and pull-up networks, such a gate consists of an NMOS pull-down network that realizes the *logic function*, and a simple *load device*. Figure 6-27b shows an example of ratioed logic, which uses a grounded PMOS load and is referred to as a pseudo-NMOS gate.

The clear advantage of a pseudo-NMOS gate is the reduced number of transistors ( $N + 1$ , versus  $2N$  for complementary CMOS). The nominal high output voltage ( $V_{OH}$ ) for this gate is  $V_{DD}$  since the pull-down devices are turned *off* when the output is pulled high (assuming that  $V_{OL}$  is below  $V_{Tn}$ ). On the other hand, the **nominal low output voltage is not 0 V**, since there is contention between the devices in the PDN and the grounded PMOS load device. This results in reduced noise margins and, more importantly, static power dissipation. The sizing of the load device relative to the pull-down devices can be used to trade off parameters such as *noise margin*, *propagation delay*, and *power dissipation*. Since the voltage swing on the output and the overall functionality of the gate depend on the ratio of the NMOS and PMOS sizes, the circuit is called *ratioed*. This is in contrast to the *ratioless* logic styles, such as complementary CMOS, where the low and high levels do not depend on transistor sizes.

Computing the dc-transfer characteristic of the pseudo-NMOS proceeds along paths similar to those used for its complementary CMOS counterpart. The value of  $V_{OL}$  is obtained by equating the currents through the driver and load devices for  $V_{in} = V_{DD}$ . At this operation point, it is reasonable to assume that the NMOS device resides in linear mode (since, ideally, the output should be close to 0V), while the PMOS load is saturated:

$$k_n \left( (V_{DD} - V_{Tn}) V_{OL} - \frac{V_{OL}^2}{2} \right) + k_p \left( (-V_{DD} - V_{Tp}) \cdot V_{DSATp} - \frac{V_{DSATp}^2}{2} \right) = 0 \quad (6.27)$$

Assuming that  $V_{OL}$  is small relative to the gate drive ( $V_{DD} - V_T$ ), and that  $V_{Tn}$  is equal to  $V_{Tp}$  in magnitude,  $V_{OL}$  can be approximated as

$$V_{OL} \approx \frac{k_p(V_{DD} + V_{Tp}) \cdot V_{DSATp}}{k_n(V_{DD} - V_{Tn})} \approx \frac{\mu_p \cdot W_p}{\mu_n \cdot W_n} \cdot V_{DSATp} \quad (6.28)$$

In order to make  $V_{OL}$  as small as possible, the PMOS device should be sized much smaller than the NMOS pull-down devices. Unfortunately, this has a negative impact on the *propagation delay* for charging up the output node since the current provided by the PMOS device is limited.

A major disadvantage of the pseudo-NMOS gate is the static power that is dissipated when the output is low through the direct current path that exists between  $V_{DD}$  and GND. The static power consumption in the low-output mode is easily derived:

$$P_{low} = V_{DD} I_{low} \approx V_{DD} \cdot \left| k_p \left( (-V_{DD} - V_{Tp}) \cdot V_{DSATp} - \frac{V_{DSATp}^2}{2} \right) \right| \quad (6.29)$$

### Example 6.7 Pseudo-NMOS Inverter

Consider a simple pseudo-NMOS inverter (where the PDN network in Figure 6-27 degenerates to a single transistor) with an NMOS size of  $0.5 \mu\text{m}/0.25 \mu\text{m}$ . In this example, we study the effect of sizing the PMOS device to demonstrate the impact on various parameters. The  $W$ - $L$  ratio of the grounded PMOS is varied over values from 4, 2, 1, 0.5 to 0.25. Devices with a  $W$ - $L < 1$  are constructed by making the length greater than the width. The voltage transfer curve for the different sizes is plotted in Figure 6-28.

Table 6-9 summarizes the nominal output voltage ( $V_{OL}$ ), static power dissipation, and the low-to-high propagation delay. The low-to-high delay is measured as the time it takes to reach 1.25 V from  $V_{OL}$  (which is not 0V for this inverter)—by definition. The trade-off between the static and dynamic properties is apparent. A larger pull-up device not only improves performance, but also increases static power dissipation and lowers noise margins by increasing  $V_{OL}$ .

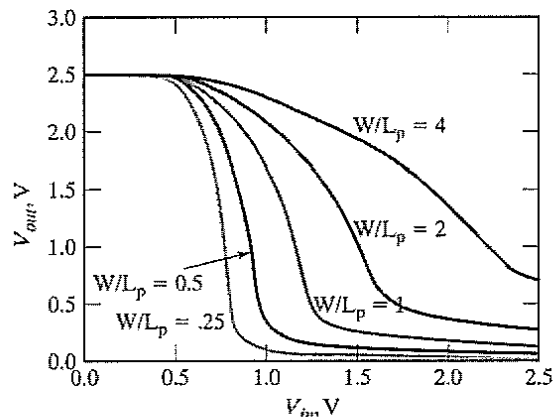


**Figure 6-28** Voltage-transfer curves of the pseudo-NMOS inverter as a function of the PMOS size.

Table 6-9 Performance of a pseudo-NMOS inverter.

Size	$V_{OL}$	Static Power Dissipation	$t_{pth}$
4	0.693 V	564 $\mu$ W	14 ps
2	0.273 V	298 $\mu$ W	56 ps
1	0.133 V	160 $\mu$ W	123 ps
0.5	0.064 V	80 $\mu$ W	268 ps
0.25	0.031 V	41 $\mu$ W	569 ps

Notice that the simple first-order model to predict  $V_{OL}$  is quite effective. For a PMOS  $W-L$  of 4,  $V_{OL}$  is given by  $(30/115)(4)(0.63V) = 0.66V$ .

The static power dissipation of pseudo-NMOS limits its use. When area is most important however, its reduced transistor count compared with complementary CMOS is quite attractive. Pseudo-NMOS thus still finds occasional use in large fan-in circuits. Figure 6-29 shows the schematics of pseudo-NMOS NOR and NAND gates.

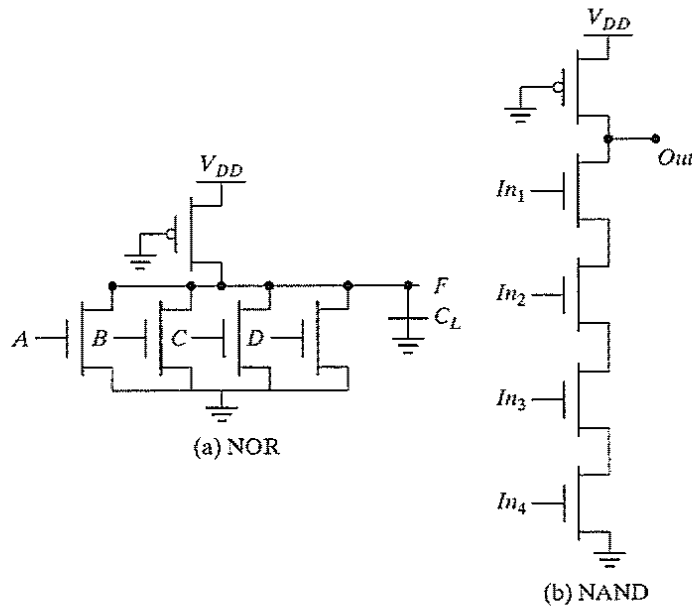


Figure 6-29 Four-input pseudo-NMOS NOR and NAND gates.

**Problem 6.5 NAND versus NOR in Pseudo-NMOS**

Given the choice between NOR or NAND logic, which one would you prefer for implementation in pseudo-NMOS?

**How to Build Even Better Loads**

It is possible to create a ratioed logic style that completely eliminates static currents and provides rail-to-rail swing. Such a gate combines two concepts: *differential logic* and *positive feedback*. A differential gate requires that each input is provided in complementary format, and it produces complementary outputs in turn. The feedback mechanism ensures that the load device is turned off when not needed. An example of such a logic family, called *Differential Cascode Voltage Switch Logic* (or DCVSL), is presented conceptually in Figure 6-30a [Heller84].

The pull-down networks PDN1 and PDN2 use NMOS devices and are mutually exclusive—that is, when PDN1 conducts, PDN2 is off, and when PDN1 is off, PDN2 conducts—such that the required logic function and its inverse are simultaneously implemented. Assume now that, for a given set of inputs, PDN1 conducts while PDN2 does not, and that *Out* and  $\overline{Out}$  are initially high and low, respectively. Turning on PDN1, causes *Out* to be pulled down, although there is still contention between  $M_1$  and PDN1.  $\overline{Out}$  is in a high impedance state, as  $M_2$  and PDN2 are both turned off. PDN1 must be strong enough to bring *Out* below  $V_{DD} - |V_{Tp}|$ , the point at which  $M_2$  turns on and starts charging  $\overline{Out}$  to  $V_{DD}$ , eventually turning off  $M_1$ . This in turn enables *Out* to discharge all the way to GND. Figure 6-30b shows an example of an XOR–XNOR gate. Notice that it is possible to share transistors among the two pull-down networks, which reduces the implementation overhead.

The resulting circuit exhibits a rail-to-rail swing, and the static power dissipation is eliminated; in steady state, none of the stacked pull-down networks and load devices are

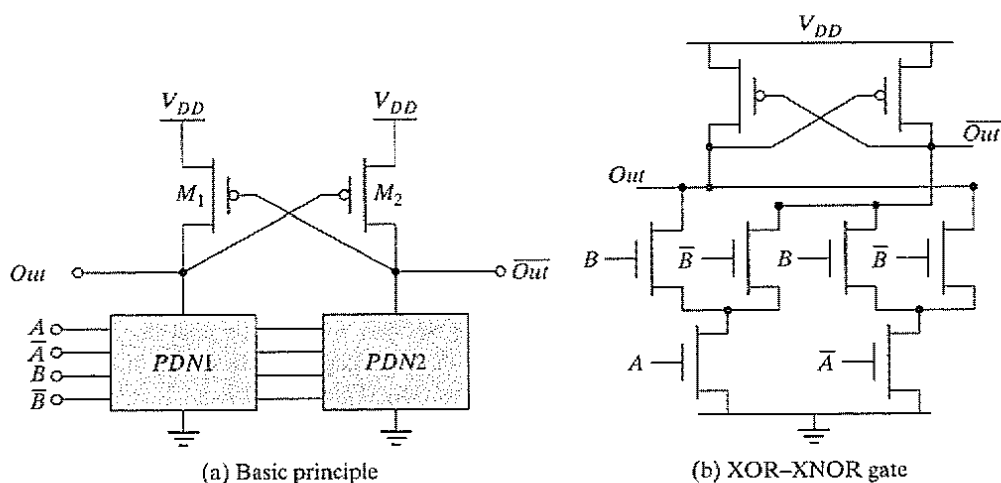


**Figure 6-30** DCVSL logic gate.

simultaneously conducting. However, the circuit is still ratioed since the sizing of the PMOS devices relative to the pull-down devices is critical to functionality, not just performance. In addition to the problem of increased design complexity, this circuit style has a power-dissipation problem that is due to cross-over currents. During the transition, there is a period of time when PMOS and PDN are turned on simultaneously, producing a short circuit path.

### Example 6.8 DCVSL Transient Response

An example transient response is shown in Figure 6.31 for an AND/NAND gate in DCVSL. Notice that as  $Out$  is pulled down to  $V_{DD} - |V_{Tp}|$ ,  $\overline{Out}$  starts to charge up to  $V_{DD}$  quickly. The delay from the input to  $Out$  is 197 ps and to  $\overline{Out}$  is 321 ps. A static CMOS AND gate (NAND followed by an inverter) has a delay of 200 ps.

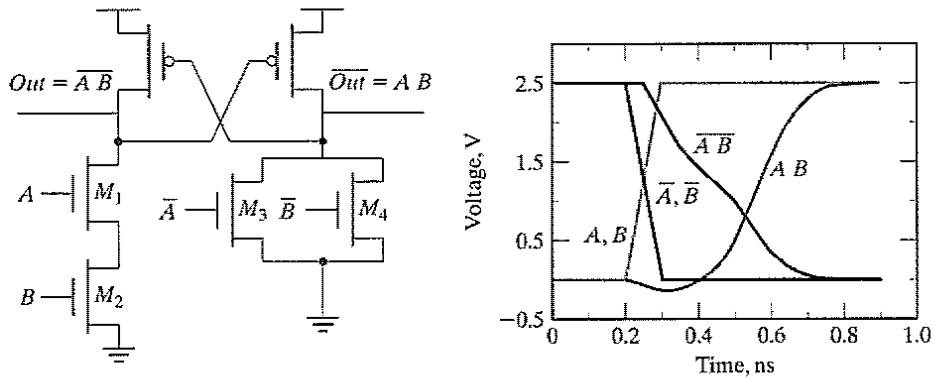


**Figure 6-31** Transient response of a simple AND/NAND DCVSL gate.  $M_1$  and  $M_2$   $1 \mu\text{m}/0.25 \mu\text{m}$ ,  $M_3$  and  $M_4$  are  $0.5 \mu\text{m}/0.25 \mu\text{m}$  and the cross-coupled PMOS devices are  $1.5 \mu\text{m}/0.25 \mu\text{m}$ .

### Design Consideration—Single-Ended versus Differential

The DCVSL gate provides *differential* (or *complementary*) outputs. Both the output signal ( $V_{out}$ ) and its inverted value ( $\overline{V}_{out}$ ) are simultaneously available. This is a distinct advantage, because it eliminates the need for an extra inverter to produce the complementary signal. It has been observed that a differential implementation of a complex function may reduce the number of gates required by a factor of two! The number of gates in the critical timing path is often reduced as well. Finally, the approach prevents some of the time-differential problems introduced by additional inverters. For example, in logic design, it often happens that both a signal and its complement are needed simultaneously. When the complementary signal is generated using an inverter, the inverted signal is delayed with respect to the original (Figure 6-32a). This causes timing problems, especially in very high-speed designs. Logic families with differential output capability avoid this problem to a major extent, if not completely (Figure 6-32b).

With all these positive properties, why not always use differential logic? The reason is that the differential nature virtually doubles the number of wires that have to be routed, often leading to unwieldy designs on top of the additional implementation overhead in the individual gates. The dynamic power dissipation also is high.

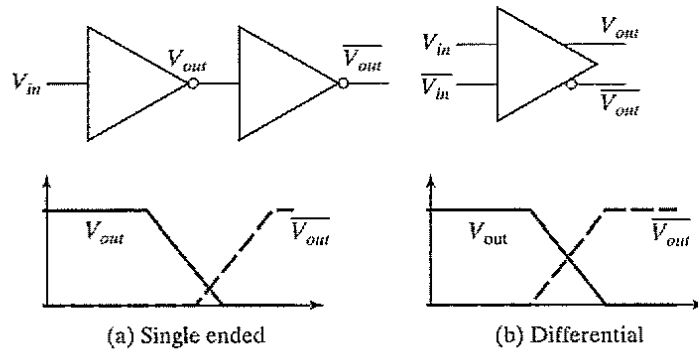


Figure 6-32 Advantage of over single-ended (a) differential (b) gate. ■

### 6.2.3 Pass-Transistor Logic

#### Pass-Transistor Basics

A popular and widely used alternative to complementary CMOS is *pass-transistor logic*, which attempts to reduce the number of transistors required to implement logic by allowing the primary inputs to drive gate terminals as well as source–drain terminals [Radhakrishnan85]. This is in contrast to logic families that we have studied so far, which only allow primary inputs to drive the gate terminals of MOSFETS.

Figure 6-33 shows an implementation of the AND function constructed that way, using only NMOS transistors. In this gate, if the  $B$  input is high, the top transistor is turned on and copies the input  $A$  to the output  $F$ . When  $B$  is low, the bottom pass-transistor is turned on and passes a 0. The switch driven by  $\bar{B}$  seems to be redundant at first glance. Its presence is essential to ensure that the gate is static—a low-impedance path must exist to the supply rails under all circumstances (in this particular case, when  $B$  is low).

The promise of this approach is that fewer transistors are required to implement a given function. For example, the implementation of the AND gate in Figure 6-33 requires 4 transistors (including the inverter required to invert  $B$ ), while a complementary CMOS implementation would require 6 transistors. The reduced number of devices has the additional advantage of lower capacitance.

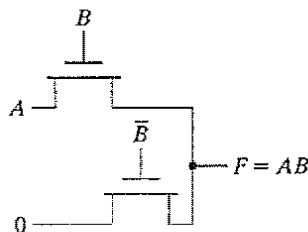


Figure 6-33 Pass-transistor implementation of an AND gate.



Unfortunately, as discussed earlier, an NMOS device is effective at passing a 0, but it is poor at pulling a node to  $V_{DD}$ . When the pass-transistor pulls a node high, the output only charges up to  $V_{DD} - V_{Th}$ . In fact, the situation is worsened by the fact that the devices experience body effect, because a significant source-to-body voltage is present when pulling high. Consider the case in which the pass-transistor is charging up a node with the gate and drain terminals set at  $V_{DD}$ . Let the source of the NMOS pass-transistor be labeled  $x$ . The node  $x$  will charge up to  $V_{DD} - V_{Th}(V_x)$ . We obtain

$$V_x = V_{DD} - (V_{Th0} + \gamma(\sqrt{|2\phi_f| + V_x} - \sqrt{|2\phi_f|})) \quad (6.30)$$

### Example 6.9 Voltage Swing for Pass-Transistors Circuits

The transient response of Figure 6-34 shows an NMOS charging up a capacitor. The drain voltage of the NMOS is at  $V_{DD}$ , and its gate voltage is being ramped from 0 V to  $V_{DD}$ . Assume that node  $x$  is initially at 0 V. We observe that the output initially charges up quickly, but the tail end of the transient is slow. The current drive of the transistor (gate-to-source voltage) is reduced significantly as the output approaches  $V_{DD} - V_{Th}$ , and the current available to charge up node  $x$  is reduced drastically. Manual calculation using Eq. (6.30) results in an output voltage of 1.8 V, which is close to the simulated value.

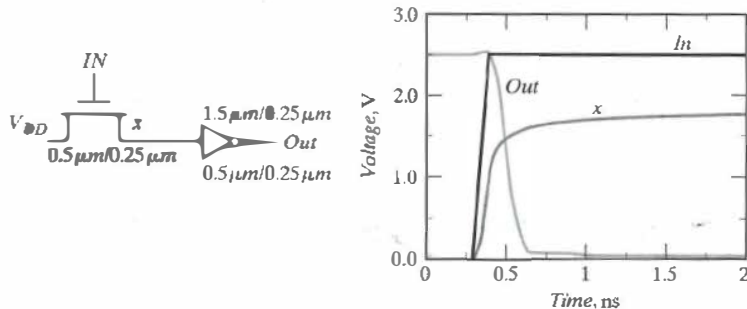


**Figure 6-34** Transient response of charging up a node using an  $N$  device. Notice the slow tail after an initial quick response.  $V_{DD} = 2.5$  V.

**WARNING:** The preceding example demonstrates that **pass-transistor gates cannot be cascaded by connecting the output of a pass gate to the gate input of another pass-transistor**. This is illustrated in Figure 6-35a, where the output of  $M_1$  (node  $x$ ) drives the gate of another MOS device. Node  $x$  can charge up to  $V_{DD} - V_{Th1}$ . If node  $C$  has a rail-to-rail swing, node  $Y$  only charges up to the voltage on node  $x - V_{Th2}$ , which works out to  $V_{DD} - V_{Th1} - V_{Th2}$ . Figure 6-35b, on the other hand, has the output of  $M_1$  ( $x$ ) driving the junction of  $M_2$ , and there is only one threshold drop. This is the proper way of cascading pass gates.

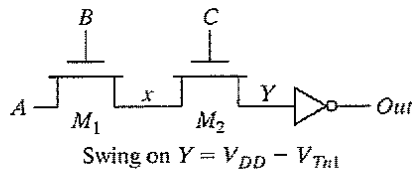


**Figure 6-35** Pass-transistor output (drain–source) terminal should not drive other gate terminals to avoid multiple threshold drops.

### Example 6.10 VTC of the Pass-Transistor AND Gate

The voltage transfer curve of a pass-transistor gate shows little resemblance to complementary CMOS. Consider the AND gate shown in Figure 6-36. Similar to complementary CMOS, the VTC of pass-transistor logic is data dependent. For the case when  $B = V_{DD}$ , the top pass-transistor is turned *on*, while the bottom one is turned *off*. In this case, the output just follows the input  $A$  until the input is high enough to turn *off* the top pass-transistor (i.e., reaches  $V_{DD} - V_{Th}$ ). Next, consider the case in which  $A = V_{DD}$ , and  $B$  makes a transition from  $0 \rightarrow 1$ . Since the inverter has a threshold of  $V_{DD}/2$ , the bottom pass-transistor is turned *on* until then and the output remains close to zero. Once the bottom pass-transistor turns *off*, the output follows the input  $B$  minus a threshold drop. A similar behavior is observed when both inputs  $A$  and  $B$  transition from  $0 \rightarrow 1$ .

Observe that a pure pass-transistor gate is not regenerative. A gradual signal degradation will be observed after passing through a number of subsequent stages. This can be remedied by the occasional insertion of a CMOS inverter. With the inclusion of an inverter in the signal path, the VTC resembles one of the CMOS gates.

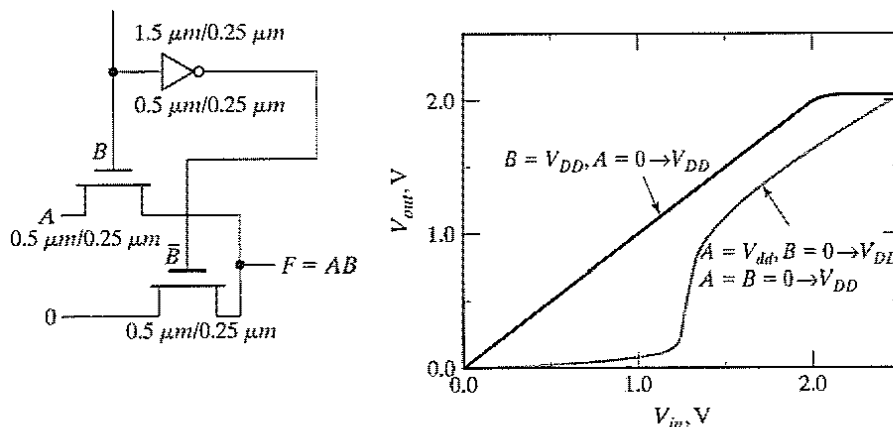


**Figure 6-36** Voltage transfer characteristic for the pass-transistor AND gate of Figure 6-33.

Pass-transistors require lower switching energy to charge up a node, due to the reduced voltage swing. For the pass-transistor circuit in Figure 6-34, assume that the drain voltage is at

$V_{DD}$  and the gate voltage transitions to  $V_{DD}$ . The output node charges from 0V to  $V_{DD} - V_{Th}$  (assuming that node  $x$  was initially at 0V), and the energy drawn from the power supply for charging the output of a pass-transistor is given by

$$\begin{aligned}
 E_{0 \rightarrow 1} &= \int_0^T P(t) dt = V_{DD} \int_0^T i_{supply}(t) dt \\
 &= V_{DD} \int_0^{(V_{DD} - V_{Th})} C_L dV_{out} = C_L \cdot V_{DD} \cdot (V_{DD} - V_{Th})
 \end{aligned}
 \tag{6.31}$$

While the circuit exhibits lower switching power, it may also consume static power when the output is high—the reduced voltage level may be insufficient to turn off the PMOS transistor of the subsequent CMOS inverter.

**Differential Pass-Transistor Logic**

For high performance design, a differential pass-transistor logic family, called *CPL* or *DPL*, is commonly used. The basic idea (similar to DCVSL) is to accept true and complementary inputs and produce true and complementary outputs. Several CPL gates (AND/NAND, OR/NOR, and XOR/NXOR) are shown in Figure 6-37. These gates possess some interesting properties:

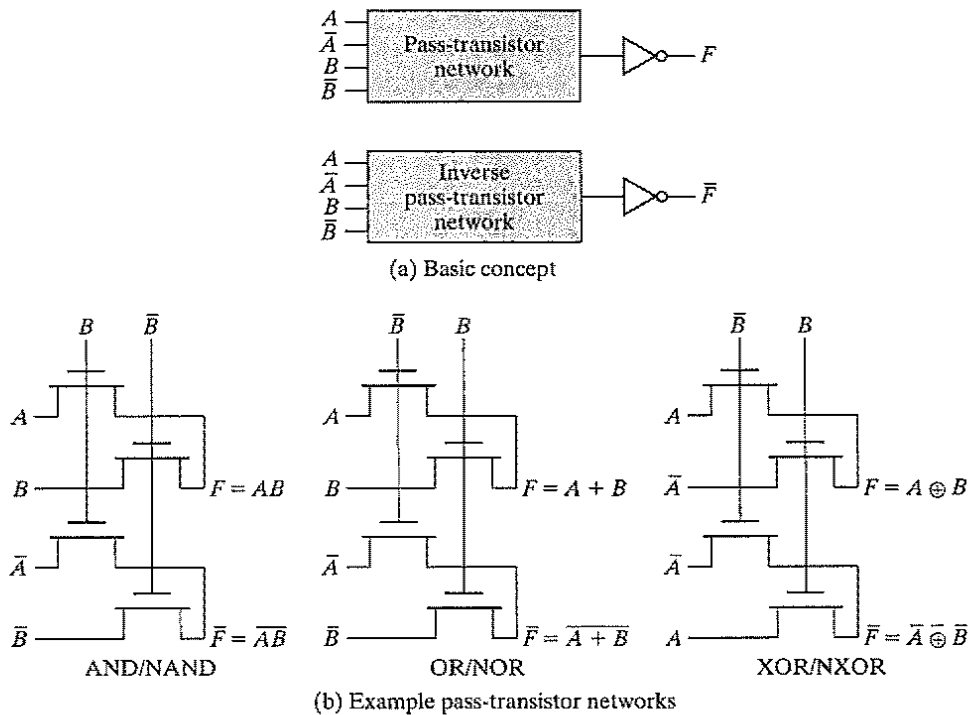


**Figure 6-37** Complementary pass-transistor logic (CPL).

- Since the circuits are *differential*, complementary data inputs and outputs are always available. Although generating the differential signals requires extra circuitry, the differential style has the advantage that some complex gates such as XORs and adders can be realized efficiently with a small number of transistors. Furthermore, the availability of both polarities of every signal eliminates the need for extra inverters, as is often the case in static CMOS or pseudo-NMOS.
- CPL belongs to the class of *static* gates, because the output-defining nodes are always connected to either  $V_{DD}$  or GND through a low-resistance path. This is advantageous for the noise resilience.
- The design is very modular. In effect, all gates use exactly the same topology. Only the inputs are permuted. This makes the design of a library of gates very simple. More complex gates can be built by cascading the standard pass-transistor modules.

### Example 6.11 Four-Input NAND in CPL

Consider the implementation of a four-input AND/NAND gate using CPL. Based on the associativity of the boolean AND operation [ $A \cdot B \cdot C \cdot D = (A \cdot B) \cdot (C \cdot D)$ ], a two-stage approach has been adopted to implement the gate (Figure 6-38). The total number of transistors in the gate (including the final buffer) is 14. This is substantially higher than previously discussed gates.<sup>3</sup> This factor, combined with the complicated routing requirements, makes this circuit style not particularly efficient for this gate. One should, however, be aware of the fact that the structure simultaneously implements the AND and the NAND functions, which might reduce the transistor count of the overall circuit.

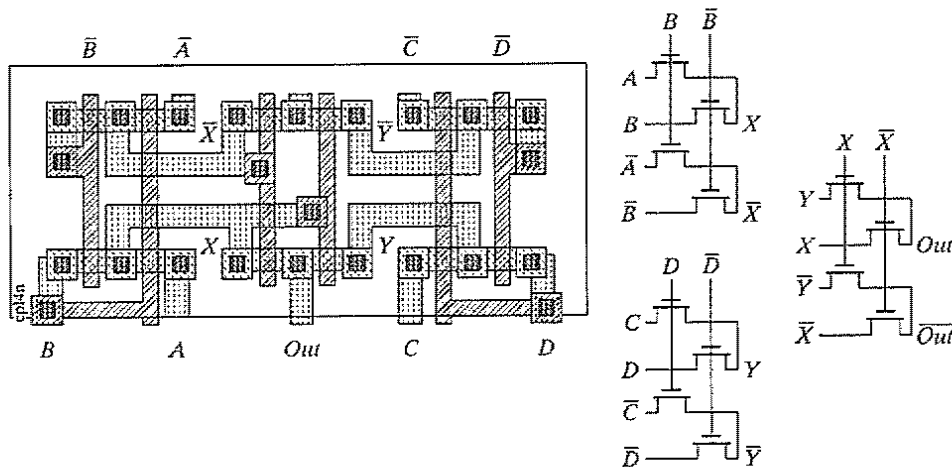


**Figure 6-38** Layout and schematics of four-input NAND gate using CPL. The final inverter stage is omitted.

<sup>3</sup>This particular circuit configuration is only acceptable when zero-threshold pass-transistors are used. If not, it directly violates the concepts introduced in Figure 6-35.

In sum, CPL is a conceptually simple and modular logic style. Its applicability depends strongly on the logic function to be implemented. The availability of a simple XOR and the ease of implementing multiplexers makes it attractive for structures such as adders and multipliers. Some extremely fast and efficient implementations have been reported in that application domain [Yano90]. When considering CPL, the designer should not ignore the implicit routing overhead of the complementary signals, which is apparent in the layout of Figure 6-38.

### Robust and Efficient Pass-Transistor Design

Unfortunately, differential pass-transistor logic, like single-ended pass-transistor logic, suffers from static power dissipation and reduced noise margins, since the high input to the signal-restoring inverter only charges up to  $V_{DD} - V_{Th}$ . There are several solutions proposed to deal with this problem, outlined as follows:

**Solution 1: Level Restoration** A common solution to the voltage drop problem is the use of a *level restorer*, which is a single PMOS configured in a feedback path (see Figure 6-39). The gate of the PMOS device is connected to the output of the inverter its drain is connected to the input of the inverter and the source is connected to  $V_{DD}$ . Assume that node  $X$  is at  $0V$  (*out* is at  $V_{DD}$  and the  $M_r$  is turned *off*) with  $B = V_{DD}$  and  $A = 0$ . If input  $A$  makes a  $0$  to  $V_{DD}$  transition,  $M_n$  only charges up node  $X$  to  $V_{DD} - V_{Th}$ . This is, however, enough to switch the output of the inverter low, turning on the feedback device  $M_r$  and pulling node  $X$  all the way to  $V_{DD}$ . This eliminates any static power dissipation in the inverter. Furthermore, no static current path can exist through the level restorer and the pass-transistor, since the restorer is only active when  $A$  is high. In sum, this circuit has the advantage that all voltage levels are either at GND or  $V_{DD}$ , and no static power is consumed.

While this solution is appealing in terms of eliminating static power dissipation, it adds complexity since the circuit is ratioed. The problem arises during the transition of node  $X$  from high to low (see Figure 6-40). The pass-transistor network attempts to pull down node  $X$ , while

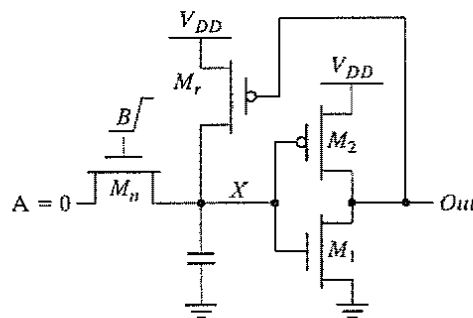


Figure 6-39 Transistor-sizing problem in level-restoring circuits.

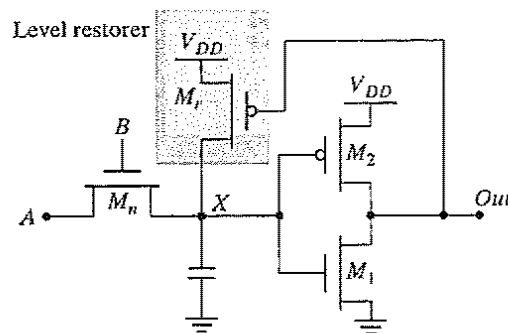


Figure 6-40 Level-restoring circuit.

the level restorer pulls  $X$  to  $V_{DD}$ . Therefore, the pull-down network, represented by  $M_n$ , must be stronger than the pull-up device  $M_r$  to switch node  $X$  (and the output). Careful transistor sizing is necessary to make the circuit function correctly. Assume the notation  $R_1$  to denote the equivalent on-resistance of transistor  $M_1$ ,  $R_2$  for  $M_2$ , and  $R_r$  for  $M_r$ . When  $R_r$  is too small, it is impossible to bring the voltage at node  $X$  below the switching threshold of the inverter. Hence, the inverter output never switches to  $V_{DD}$ , and the gate is locked in a single state. The problem can be resolved by sizing transistors  $M_n$  and  $M_r$  such that the voltage at node  $X$  drops below the threshold of the inverter  $V_M$ , which is a function of  $R_1$  and  $R_2$ . This condition is sufficient to guarantee the switching of the output voltage  $V_{out}$  to  $V_{DD}$  and the turning off of the level-restoring transistor.

### Example 6.12 Sizing of a Level Restorer

Analyzing the circuit as a whole is nontrivial, because the restoring transistor acts as a feedback device. One way to simplify the circuit for manual analysis is to open the feedback loop and to ground the gate of the restoring transistor when determining the switching point (this is a reasonable assumption, as the feedback only becomes active once the inverter starts to switch). Hence,  $M_r$  and  $M_n$  form a configuration that resembles pseudo-NMOS with  $M_r$  the load transistor, and  $M_n$  acting as a pull-down network to GND. Assume that the inverter  $M_1, M_2$  is sized to have its switching threshold at  $V_{DD}/2$  (NMOS:  $0.5 \mu\text{m}/0.25 \mu\text{m}$  and PMOS:  $1.5 \mu\text{m}/0.25 \mu\text{m}$ ). Therefore, node  $X$  must be pulled below  $V_{DD}/2$  to switch the inverter and to shut off  $M_r$ .

This is confirmed in Figure 6-41, which shows the transient response as the size of the level restorer is varied, while keeping the size of  $M_n$  fixed ( $0.5 \mu\text{m}/0.25 \mu\text{m}$ ). As the simulation indicates, for sizes above  $1.5 \mu\text{m}/0.25 \mu\text{m}$ , node  $X$  cannot be brought below the switching threshold of the inverter, and can't switch the output.

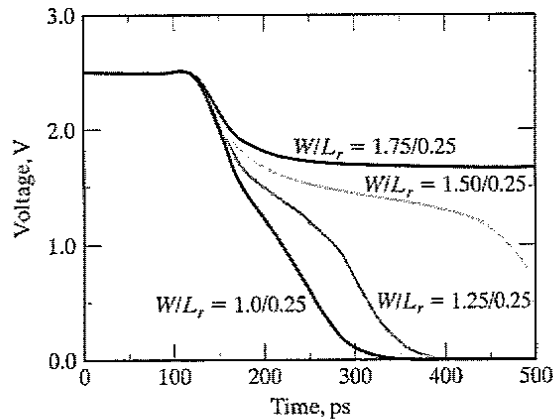


**Figure 6-41** Transient response of the circuit in Figure 6-39. A level restorer that is too large results in incorrect evaluation.

Another concern is the influence of the level restorer on the switching speed of the device. Adding the restoring device increases the capacitance at the internal node  $X$ , slowing down the gate. In addition, the rise time of the gate is affected negatively. The level restoring transistor  $M_r$  fights the decrease in voltage at node  $X$  before being switched off. On the other hand, the level restorer reduces the fall time, since the PMOS transistor, once turned on, accelerates the pull-up action.

#### Problem 6.6 Device Sizing in Pass-Transistors

For the circuit shown in Figure 6-39, assume that the pull-down device consists of six pass-transistors in series each with a device size of  $0.5\ \mu\text{m}/0.25\ \mu\text{m}$  (replacing transistor  $M_n$ ). Determine the maximum  $W-L$  size for the level restorer transistor for correct functionality.

A modification of the level restorer concept is shown in Figure 6-42. It is applicable in differential networks and is known as *swing-restored pass-transistor logic*. Instead of a simple inverter at the output of the pass-transistor network, two back-to-back inverters configured in a cross-coupled fashion are used for level restoration and performance improvement. Inputs are fed to both the gate and source-drain terminals, as in the case of conventional pass-transistor networks. Figure 6-42 shows a simple XOR/XNOR gate of three variables  $A$ ,  $B$ , and  $C$ . The complementary network can be optimized by sharing transistors between the true and complementary outputs. This logic family comes with a major caveat: When cascading gates, buffers may have to be included in between the gates. If not, contention between the level-restoring devices of the cascaded gates negatively impacts the performance.

**Solution 2: Multiple-Threshold Transistors** A technology solution to the voltage-drop problem associated with pass-transistor logic is the use of multiple-threshold devices. Using *zero-*

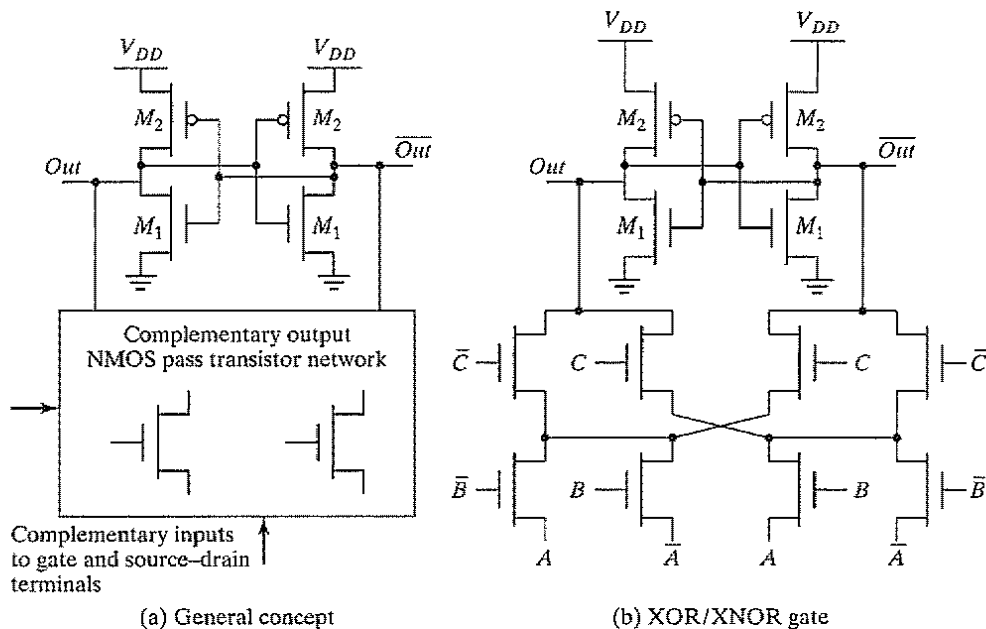


**Figure 6-42** Swing-restored pass-transistor logic [Landman91, Parameswar96].

*threshold* devices for the NMOS pass-transistors eliminates most of the threshold drop, and passes a signal close to  $V_{DD}$ . All devices other than the pass-transistors (i.e., the inverters) are implemented using standard high-threshold devices. The use of multiple-threshold transistors is becoming more common, and involves simple modifications to existing process flows. Observe that even if the device implants were carefully calibrated to yield thresholds of exactly zero, the body effect of the device still would prevent a full swing to  $V_{DD}$ .

The use of zero-threshold transistors has some negative impact on the power consumption due to the subthreshold currents flowing through the pass-transistors, even if  $V_{GS}$  is below  $V_T$ . This is demonstrated in Figure 6-43, which points out a potential sneak dc-current path. While these leakage paths are not critical when the device is switching constantly, they do pose a significant energy overhead when the circuit is in the idle state.

**Solution 3: Transmission-Gate Logic** The most widely used solution to deal with the voltage-drop problem is the use of *transmission gates*.<sup>4</sup> This technique builds on the complementary properties of NMOS and PMOS transistors: NMOS devices pass a strong 0, but a weak 1, while PMOS transistors pass a strong 1 but a weak 0. The ideal approach is to use an NMOS to pull down and a PMOS to pull up. The transmission gate combines the best of both device flavors by placing an NMOS device in parallel with a PMOS device as in Figure 6-44a. The control

<sup>4</sup>The transmission gate is only one of the possible solutions. Other styles of pass-transistor networks that combine NMOS and PMOS transistors have been devised. Double pass-transistor logic (DPL) is an example of such [Bernstein98, pp. 84].



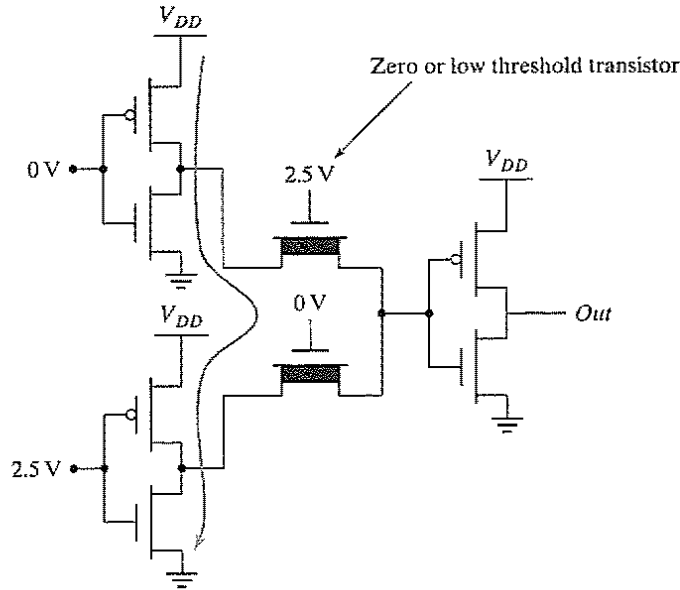


**Figure 6-43** Static power consumption when using zero-threshold pass-transistors.

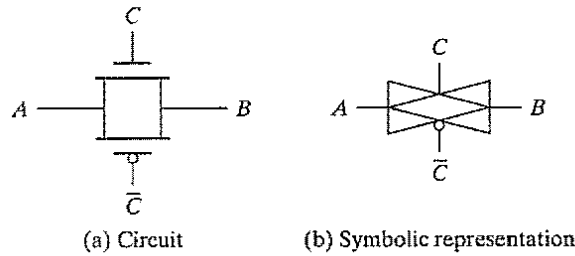


**Figure 6-44** CMOS transmission gate.

signals to the transmission gate ( $C$  and  $\bar{C}$ ) are complementary. The transmission gate acts as a bidirectional switch controlled by the gate signal  $C$ . When  $C = 1$ , both MOSFETs are on, allowing the signal to pass through the gate. In short,

$$A = B \quad \text{if} \quad C = 1 \tag{6.32}$$

On the other hand,  $C = 0$  places both transistors in cutoff, creating an open circuit between nodes  $A$  and  $B$ . Figure 6-44b shows a commonly used transmission-gate symbol.

Consider the case of charging node  $B$  to  $V_{DD}$  for the transmission-gate circuit in Figure 6-45a. Node  $A$  is set at  $V_{DD}$ , and the transmission gate is enabled ( $C = 1$  and  $\bar{C} = 0$ ). If only the NMOS pass device were present, node  $B$  would only charge up to  $V_{DD} - V_{Tn}$ , at which point the NMOS device would turn off. However, since the PMOS device is present

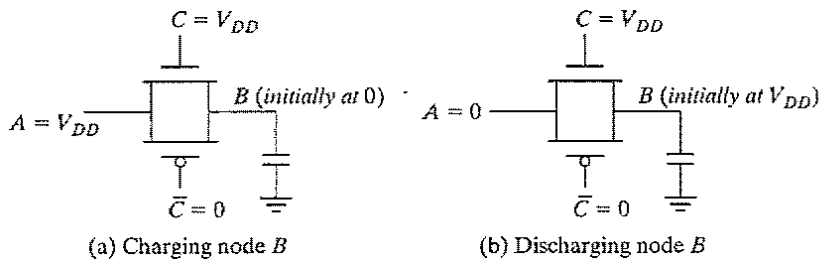


Figure 6-45 Transmission gates enable rail-to-rail switching.

and is “on” ( $V_{GSp} = -V_{DD}$ ), the output charges all the way up to  $V_{DD}$ . Figure 6-45b shows the opposite case—that is, discharging node  $B$  to 0.  $B$  is initially at  $V_{DD}$  when node  $A$  is driven low. The PMOS transistor by itself can only pull-down node  $B$  to  $V_{Tp}$  at which point it turns off. The parallel NMOS device stays turned on, however (since its  $V_{GSn} = V_{DD}$ ), and pulls node  $B$  all the way to GND. Although the transmission gate requires two transistors and more control signals, it enables rail-to-rail swing.

Transmission gates can be used to build some complex gates very efficiently. Figure 6-46 shows an example of a simple inverting two-input multiplexer. This gate either selects input  $A$  or  $B$  on the basis of the value of the control signal  $S$ , which is equivalent to implementing the following Boolean function:

$$\bar{F} = (A \cdot S + B \cdot \bar{S}) \tag{6.33}$$

A complementary implementation of the gate requires eight transistors instead of six.

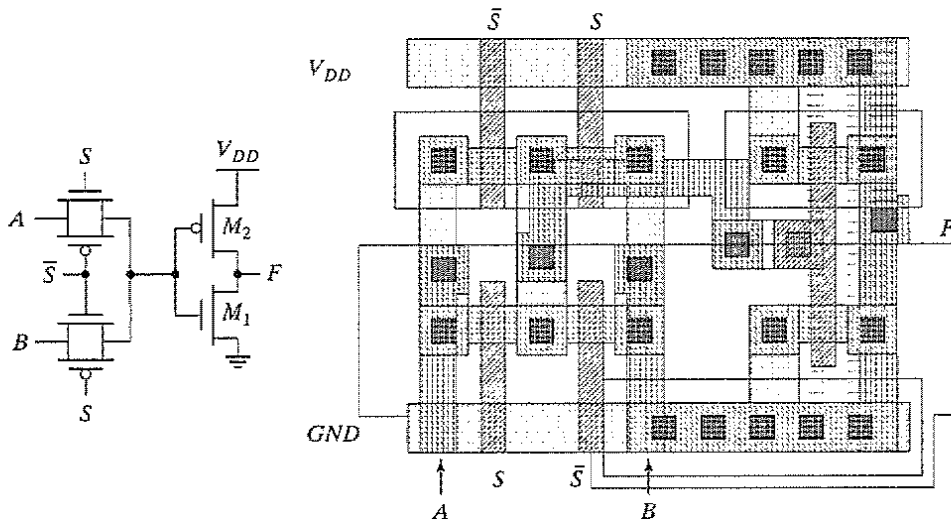


Figure 6-46 Transmission-gate multiplexer and its layout.

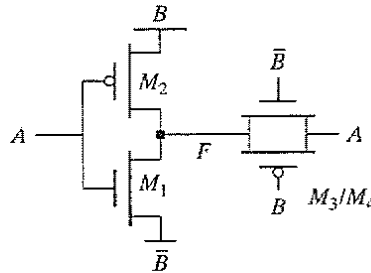


Figure 6-47 Transmission-gate XOR.

Another example of the effective use of transmission gates is the popular XOR circuit shown in Figure 6-47. The complete implementation of this gate requires only 6 transistors (including the inverter used for the generation of  $\bar{B}$ ), compared with the 12 transistors required for a complementary implementation. To understand the operation of this circuit, we need only analyze the  $B = 0$  and  $B = 1$  cases separately. For  $B = 1$ , transistors  $M_1$  and  $M_2$  act as an inverter, while the transmission gate  $M_3/M_4$  is off; hence,  $F = \bar{A}B$ . In the opposite case,  $M_1$  and  $M_2$  are disabled, and the transmission gate is operational, or  $F = A\bar{B}$ . The combination of both leads to the XOR function. Notice that regardless of the values of  $A$  and  $B$ , node  $F$  always has a connection to either  $V_{DD}$  or GND and thus is a low-impedance node. When designing static-pass-transistor networks, it is essential to adhere to the low-impedance rule under all circumstances. Other examples in which transmission-gate logic is effectively used are fast adder circuits and registers.

### Performance of Pass-Transistor and Transmission-Gate Logic

The pass-transistor and the transmission gate are, unfortunately, not ideal switches, and they have a series resistance associated with them. To quantify the resistance, consider the circuit in Figure 6-48, which involves charging a node from 0 V to  $V_{DD}$ . In this discussion, we use the large-signal definition of resistance, which involves dividing the voltage across the switch by the drain current. The effective resistance of the switch is modeled as a parallel connection of the resistances  $R_n$  and  $R_p$  of the NMOS and PMOS devices, defined as  $(V_{DD} - V_{out})/I_{Dn}$  and  $(V_{DD} - V_{out})/(-I_{Dp})$ , respectively. The currents through the devices obviously are dependent on the value of  $V_{out}$  and the operating mode of the transistors. During the low-to-high transition, the pass-transistors traverse through a number of operation modes. For low values of  $V_{out}$ , the NMOS device is saturated and the resistance is approximated as

$$R_p = \frac{V_{out} - V_{DD}}{I_{Dp}} = \frac{V_{out} - V_{DD}}{k_p \cdot \left( (-V_{DD} - V_{Tp})(V_{out} - V_{DD}) - \frac{(V_{out} - V_{DD})^2}{2} \right)} \quad (6.34)$$

$$\approx \frac{1}{k_p(-V_{DD} - V_{Tp})}$$

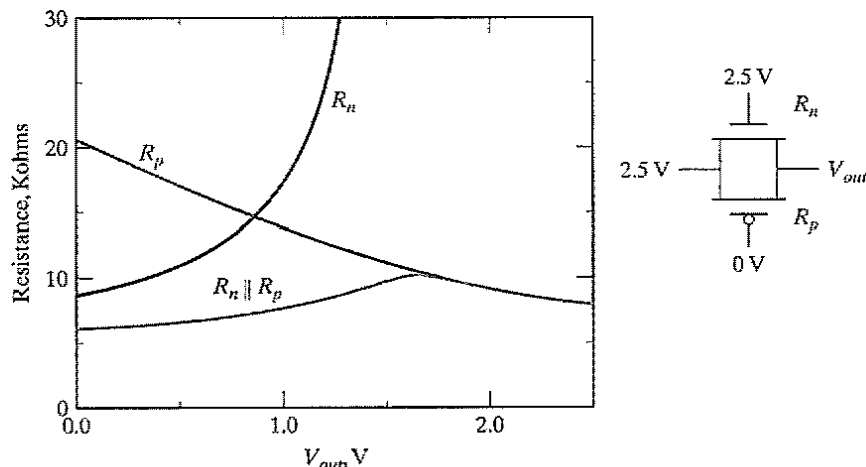


**Figure 6-48** Simulated equivalent resistance of transmission gate for low-to-high transition (for  $(W-L)_n = (W-L)_p = 0.5 \mu\text{m}/0.25 \mu\text{m}$ ). A similar response for overall resistance is obtained for the high-to-low transition.

The resistance goes up for increasing values of  $V_{out}$  and approaches infinity when  $V_{out}$  reaches  $V_{DD} - V_{Tn}$  and the device shuts off. Similarly, we can analyze the behavior of the PMOS transistor. When  $V_{out}$  is small, the PMOS is saturated, but it enters the linear mode of operation for  $V_{out}$  approaching  $V_{DD}$ . This gives the following approximated resistance:

$$R_p = \frac{V_{out} - V_{DD}}{I_{Dp}} = \frac{V_{out} - V_{DD}}{k_p \cdot \left( (-V_{DD} - V_{Tp})(V_{out} - V_{DD}) - \frac{(V_{out} - V_{DD})^2}{2} \right)} \quad (6.35)$$

$$\approx \frac{1}{k_p(-V_{DD} - V_{Tp})}$$

The simulated value of  $R_{eq} = R_p \parallel R_n$  as a function of  $V_{out}$  is plotted in Figure 6-48. It can be observed that  $R_{eq}$  is relatively constant ( $\approx 8 \text{ k}\Omega$  in this particular case). The same is true in other design instances (for example, when discharging  $C_L$ ). When analyzing transmission-gate networks, the simplifying assumption that the switch has a constant resistive value is therefore acceptable.

---

### Problem 6.7 Equivalent Resistance during Discharge

Determine the equivalent resistance by simulation for the high-to-low transition of a transmission gate. (In other words, produce a plot similar to the one presented in Figure 6-48).

---

An important consideration is the delay associated with a chain of transmission gates. Figure 6-49 shows a chain of  $n$  transmission gates. Such a configuration often occurs in circuits such as adders or deep multiplexors. Assume that all transmission gates are turned on and a step

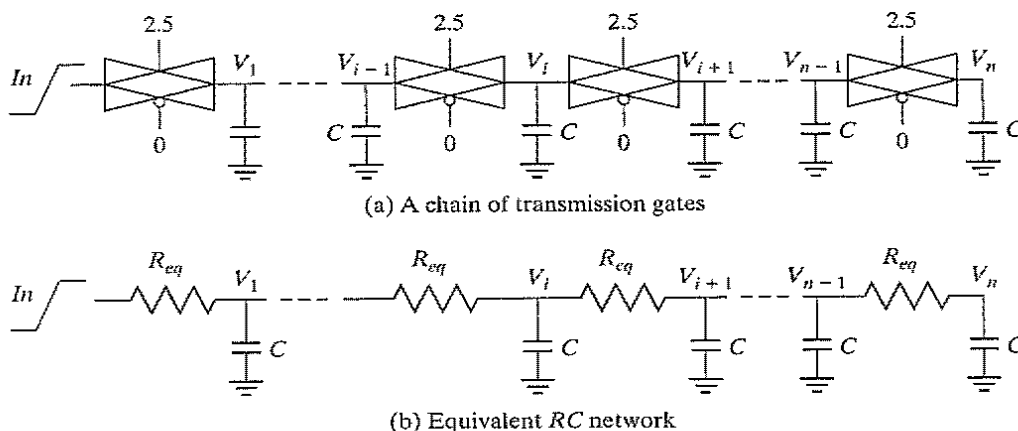


**Figure 6-49** Speed optimization in transmission-gate networks.

is applied at the input. To analyze the propagation delay of this network, the transmission gates are replaced by their equivalent resistances  $R_{eq}$ . This produces the network of Figure 6-49b.

The delay of a network of  $n$  transmission gates in sequence can be estimated by using the Elmore approximation (see Chapter 4):

$$t_p(V_n) = 0.69 \sum_{k=0}^n CR_{eq}k = 0.69CR_{eq} \frac{n(n+1)}{2} \quad (6.36)$$

This means that the propagation delay is proportional to  $n^2$  and increases rapidly with the number of switches in the chain.

### Example 6.13 Delay of Transmission-Gate Chain

Consider 16 cascaded minimum-sized transmission gates, each with an average resistance of 8 k $\Omega$ . The node capacitance consists of the capacitance of two NMOS and PMOS devices (junction and gate). Since the gate inputs are assumed to be fixed, there is no Miller multiplication. The capacitance can be calculated to be approximately 3.6 fF for the low-to-high transition. The delay is given by

$$t_p = 0.69 \cdot CR_{eq} \frac{n(n+1)}{2} = 0.69 \cdot (3.6 \text{ fF})(8 \text{ k}\Omega) \left( \frac{16(16+1)}{2} \right) \approx 2.7 \text{ ns} \quad (6.37)$$

The transient response for this particular example is shown in Figure 6-50. The simulated delay is 2.7 ns. It is remarkable that a simple RC model predicts the delay so accurately. It is also clear that the use of long pass-transistor chains causes significant delay degradation.

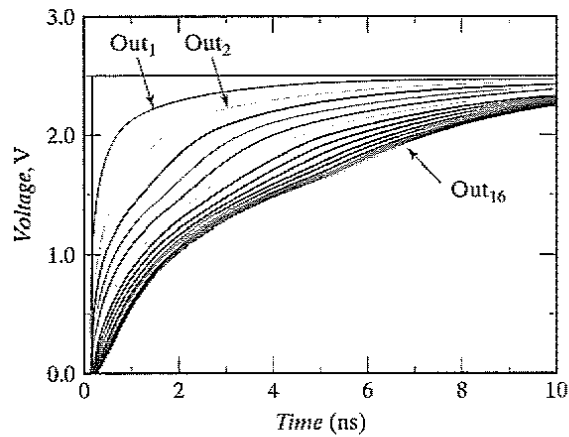


Figure 6-50 Speed optimization in transmission-gate networks.

The most common approach for dealing with the long delay is to break the chain and insert buffers every  $m$  switches (Figure 6-51). Assuming a propagation delay  $t_{buf}$  for each buffer, the overall propagation delay of the transmission gate–buffer network is then computed as follows:

$$\begin{aligned}
 t_p &= 0.69 \left[ \frac{n}{m} CR_{eq} \frac{m(m+1)}{2} \right] + \left( \frac{n}{m} - 1 \right) t_{buf} \\
 &= 0.69 \left[ CR_{eq} \frac{n(m+1)}{2} \right] + \left( \frac{n}{m} - 1 \right) t_{buf}
 \end{aligned}
 \tag{6.38}$$

The resulting delay exhibits only a linear dependence on the number of switches  $n$ , in contrast to the unbuffered circuit, which is quadratic in  $n$ . The optimal number of switches  $m_{opt}$  between buffers can be found by setting the derivative  $\frac{\partial t_p}{\partial m}$  to 0, which yields

$$m_{opt} = 1.7 \sqrt{\frac{t_{pbuf}}{CR_{eq}}}
 \tag{6.39}$$

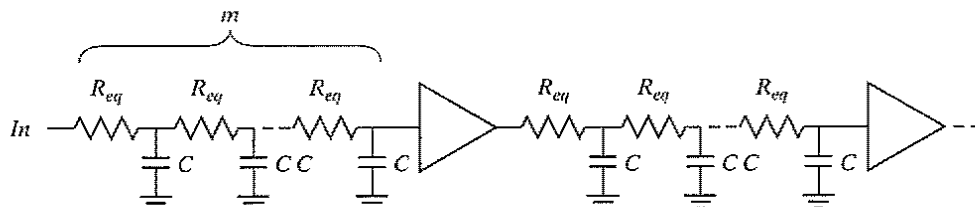


Figure 6-51 Breaking up long transmission-gate chains by inserting buffers.

Obviously, the number of switches per segment grows with increasing values of  $t_{bif}$ . In current technologies,  $m_{opt}$  typically equals 3 or 4. The presented analysis ignores that  $t_{p_{bif}}$  itself is a function of the load  $m$ . A more accurate analysis taking this factor into account is presented in Chapter 9.

#### Example 6.14 Transmission-Gate Chain

Consider the same 16-transmission-gate chain. The buffers shown in Figure 6-51 can be implemented as inverters (instead of two cascaded inverters). In some cases, it might be necessary to add an extra inverter to produce the correct polarity. Assuming that each inverter is sized such that the NMOS is  $0.5 \mu\text{m}/0.25 \mu\text{m}$  and PMOS is  $0.5 \mu\text{m}/0.25 \mu\text{m}$ , Eq. (6.39) predicts that an inverter must be inserted every 3 transmission gates. The simulated delay when placing an inverter every two transmission gates is 154 ps; for every three transmission gates, the delay is 154 ps; and for four transmission gates, it is 164 ps. The insertion of buffering inverters reduces the delay by a factor of almost 2.

**CAUTION:** Although many of the circuit styles discussed in the previous sections sound very interesting, and might be superior to static CMOS in many respects, none has the *robustness and ease of design* of complementary CMOS. Therefore, use them sparingly and with caution. For designs that have no extreme area, complexity, or speed constraints, complementary CMOS is the recommended design style.

### 6.3 Dynamic CMOS Design

It was noted earlier that static CMOS logic with a fan-in of  $N$  requires  $2N$  devices. A variety of approaches were presented to reduce the number of transistors required to implement a given logic function including pseudo-NMOS, pass-transistor logic, etc. The pseudo-NMOS logic style requires only  $N + 1$  transistors to implement an  $N$  input logic gate, but unfortunately it has static power dissipation. In this section, an alternate logic style called *dynamic logic* is presented that obtains a similar result, while avoiding static power consumption. With the addition of a clock input, it uses a sequence of *precharge* and conditional *evaluation* phases.

#### 6.3.1 Dynamic Logic: Basic Principles

The basic construction of an ( $n$ -type) dynamic logic gate is shown in Figure 6-52a. The PDN (pull-down network) is constructed exactly as in complementary CMOS. The operation of this circuit is divided into two major phases—*precharge* and *evaluation*—with the mode of operation determined by the *clock signal CLK*.

##### Precharge

When  $CLK = 0$ , the output node *Out* is precharged to  $V_{DD}$  by the PMOS transistor  $M_p$ . During that time, the evaluate NMOS transistor  $M_e$  is off, so that the pull-down path is disabled. The

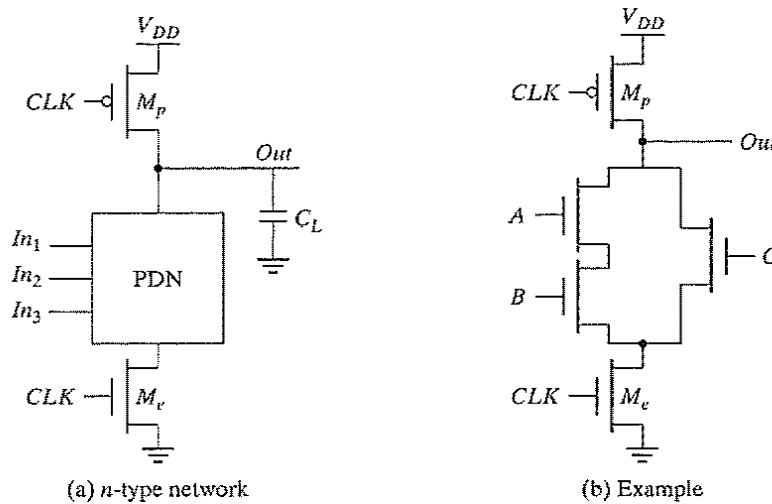


Figure 6-52 Basic concepts of a dynamic gate.

evaluation FET eliminates any static power that would be consumed during the precharge period (i.e., static current would flow between the supplies if both the pull-down and the precharge device were turned on simultaneously).

### Evaluation

For  $CLK = 1$ , the precharge transistor  $M_p$  is off, and the evaluation transistor  $M_e$  is turned on. The output is conditionally discharged based on the input values and the pull-down topology. If the inputs are such that the PDN conducts, then a low resistance path exists between  $Out$  and GND, and the output is discharged to GND. If the PDN is turned off, the precharged value remains stored on the output capacitance  $C_L$ , which is a combination of junction capacitances, the wiring capacitance, and the input capacitance of the fan-out gates. During the evaluation phase, the only possible path between the output node and a supply rail is to GND. Consequently, once  $Out$  is discharged, it cannot be charged again until the next precharge operation. **The inputs to the gate can thus make at most one transition during evaluation.** Notice that the output can be in the *high-impedance state* during the evaluation period if the pull-down network is turned off. This behavior is fundamentally different from the static counterpart that always has a low resistance path between the output and one of the power rails.

As an example, consider the circuit shown in Figure 6-52b. During the precharge phase ( $CLK = 0$ ), the output is precharged to  $V_{DD}$  regardless of the input values, because the evaluation device is turned off. During evaluation ( $CLK = 1$ ), a conducting path is created between  $Out$  and GND if (and only if)  $A \cdot B + C$  is TRUE. Otherwise, the output remains at the precharged state of  $V_{DD}$ . The following function is thus realized:

$$Out = \overline{CLK} + \overline{(A \cdot B + C)} \cdot CLK \quad (6.40)$$



A number of important properties can be derived for the dynamic logic gate:

- The logic function is implemented by the NMOS pull-down network. The construction of the PDN proceeds just as it does for static CMOS.
- The *number of transistors* (for complex gates) is substantially lower than in the static case:  $N + 2$  versus  $2N$ .
- It is *nonratioed*. The sizing of the PMOS precharge device is not important for realizing proper functionality of the gate. The size of the precharge device can be made large to improve the low-to-high transition time (of course, at a cost to the high-to-low transition time). There is, however, a trade-off with power dissipation, since a larger precharge device directly increases clock-power dissipation.
- It only consumes *dynamic power*. Ideally, no static current path ever exists between  $V_{DD}$  and GND. The overall power dissipation, however, can be significantly higher compared with a static logic gate.
- The logic gates have *faster switching speeds*, for two main reasons. The first (obvious) reason is due to the reduced load capacitance attributed to the lower number of transistors per gate and the single-transistor load per *fan-in*. This translates in a *reduced logical effort*. For instance, the logical effort of a two-input dynamic NOR gate equals  $2/3$ , which is substantially smaller than the  $5/3$  of its static CMOS counterpart. The second reason is that the dynamic gate does not have short circuit current, and all the current provided by the pull-down devices goes towards discharging the load capacitance.

The low and high output levels of  $V_{OL}$  and  $V_{OH}$  are easily identified as GND and  $V_{DD}$ , and they are not dependent on the transistor sizes. The other VTC parameters are dramatically different from static gates. Noise margins and switching thresholds have been defined as static quantities that are not a function of time. To be functional, a dynamic gate requires a periodic sequence of precharges and evaluations. Pure static analysis, therefore, does not apply. During the evaluation period, the pull-down network of a dynamic inverter starts to conduct when the input signal exceeds the threshold voltage ( $V_{Th}$ ) of the NMOS pull-down transistor. Therefore, it is reasonable to assume that the switching threshold ( $V_M$ ) as well as  $V_{IH}$  and  $V_{IL}$  are equal to  $V_{Th}$ . This translates to a low value for the  $NM_L$ .

#### Design Consideration

It is also possible to implement dynamic logic using the dual approach, where the output node is connected by a precharge NMOS transistor to GND, and the evaluation PUN network is implemented in PMOS. The operation is similar: During precharge, the output node is discharged to GND; during evaluation, the output is conditionally charged to  $V_{DD}$ . This *p*-type dynamic gate has the disadvantage of being slower than the *n*-type because of the lower current drive of the PMOS transistors. ■

### 6.3.2 Speed and Power Dissipation of Dynamic Logic

The main advantages of dynamic logic are increased speed and reduced implementation area. Fewer devices to implement a given logic function implies that the overall load capacitance is much smaller. The analysis of the switching behavior of the gate has some interesting peculiarities to it. After the precharge phase, the output is high. For a low input signal, no additional switching occurs. As a result,  $t_{pLH} = 0$ ! The high-to-low transition, on the other hand, requires the discharging of the output capacitance through the pull-down network. Therefore,  $t_{pHL}$  is proportional to  $C_L$  and the current-sinking capabilities of the pull-down network. The presence of the evaluation transistor slows the gate somewhat, as it presents an extra series resistance. Omitting this transistor, while functionally not forbidden, may result in static power dissipation and potentially a performance loss.

The preceding analysis is somewhat unfair because it ignores the influence of the precharge time on the switching speed of the gate. The precharge time is determined by the time it takes to charge  $C_L$  through the PMOS precharge transistor. During this time, the logic in the gate cannot be utilized. Very often, however, the overall digital system can be designed in such a way that the precharge time coincides with other system functions. For instance, the precharge of the arithmetic unit in a microprocessor could coincide with the instruction decode. The designer has to be aware of this “dead zone” in the use of dynamic logic and thus should carefully consider the pros and cons of its usage, taking the overall system requirements into account.

#### Example 6.15 A Four-Input Dynamic NAND Gate

Figure 6-53 shows the design of a four-input NAND example designed using the dynamic-circuit style. Due to the dynamic nature of the gate, the derivation of the voltage-transfer

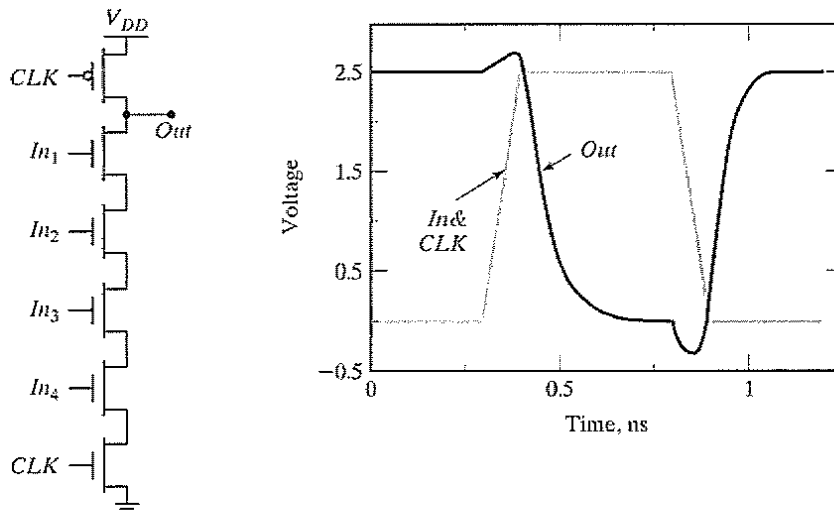


Figure 6-53 Schematic and transient response of a four-input dynamic NAND gate.

characteristic diverges from the traditional approach. As discussed earlier, we assume that the switching threshold of the gate equals the threshold of the NMOS pull-down transistor. This results in asymmetrical noise margins, as shown in Table 6-10.

**Table 6-10** The dc and ac parameters of a four-input dynamic NAND.

Transistors	$V_{OH}$	$V_{OL}$	$V_M$	$NM_H$	$NM_L$	$t_{pHL}$	$t_{pLH}$	$t_{pre}$
6	2.5 V	0 V	$V_{TN}$	$2.5 - V_{TN}$	$V_{TN}$	110 ps	0 ps	83 ps

The dynamic behavior of the gate is simulated with SPICE. It is assumed that all inputs are set high when the clock goes high. On the rising edge of the clock, the output node is discharged. The resulting transient response is plotted in Figure 6-53, and the propagation delays are summarized in Table 6-10. The duration of the precharge cycle can be adjusted by changing the size of the PMOS precharge transistor. Making the PMOS too large should be avoided, however, as it both slows down the gate and increases the capacitive load on the clock line. For large designs, the latter factor might become a major design concern because the clock load can become excessive and hard to drive.

As mentioned earlier, the static gate parameters are time dependent. To illustrate this, consider a four-input NAND gate with all the partial inputs tied together, and are making a low-to-high transition. Figure 6-54 shows a transient simulation of the output voltage for three different input transitions—from 0 to 0.45 V, 0.5 V and 0.55 V, respectively. In the preceding discussion, we have defined the switching threshold of the dynamic gate as the device threshold. However, notice that the amount by which the output voltage drops is a strong function of the input voltage and the *available evaluation time*. The noise voltage needed to corrupt the signal has to be larger if the evaluation time is short. In other words, the switching threshold is truly time dependent.

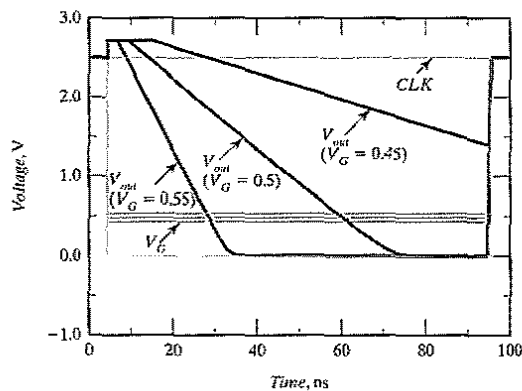


**Figure 6-54** Effect of an input glitch on the output. The switching threshold depends on the time for evaluation. A larger glitch is acceptable if the evaluation phase is shorter.

It would appear that dynamic logic presents a significant advantage from a power perspective. There are three reasons for this. First, the physical capacitance is lower since dynamic logic uses fewer transistors to implement a given function. Also, the load seen for each fan-out is one transistor instead of two. Second, dynamic logic gates *by construction* can have at most one transition per clock cycle. Glitching (or dynamic hazards) does not occur in dynamic logic. Finally, dynamic gates do not exhibit short-circuit power since the pull-up path is not turned on when the gate is evaluating.

While these arguments generally are true, they are offset by other considerations: (1) the clock power of dynamic logic can be significant, particularly since the clock node has a guaranteed transition on every single clock cycle; (2) the number of transistors is greater than the minimal set required for implementing the logic; (3) short-circuit power may exist when leakage-combatting devices are added (as will be discussed further); and (4), most importantly, dynamic logic generally displays a higher switching activity due to the periodic *precharge* and *discharge* operations. Earlier, the transition probability for a static gate was shown to be  $p_0 p_1 = p_0 (1 - p_0)$ . For dynamic logic, the output transition probability does not depend on the state (history) of the inputs, but rather on the signal probabilities. For an  $n$ -tree dynamic gate, the output makes a  $0 \rightarrow 1$  transition during the precharge phase only if the output was discharged during the preceding evaluate phase. Hence, the  $0 \rightarrow 1$  transition probability for an  $n$ -type dynamic gate is given by

$$a_{0 \rightarrow 1} = p_0 \quad (6.41)$$

where  $p_0$  is the probability that the output is zero. This number is always greater than or equal to  $p_0 p_1$ . For uniformly distributed inputs, the transition probability for an  $N$ -input gate is

$$a_{0 \rightarrow 1} = \frac{N_0}{2^N} \quad (6.42)$$

where  $N_0$  is the number of zero entries in the truth table of the logic function.

---

#### Example 6.16 Activity Estimation in Dynamic Logic

To illustrate the increased activity for a dynamic gate, consider again a two-input NOR gate. An  $n$ -tree dynamic implementation is shown in Figure 6-55, along with its static counterpart. For equally probable inputs, there is a 75% probability that the output node of the dynamic gate discharges immediately after the precharge phase, implying that the activity for such a gate equals 0.75 (i.e.,  $P_{NOR} = 0.75 C_L V_{dd}^2 f_{clk}$ ). The corresponding activity is a lot smaller, 3/16, for a static implementation. For a dynamic NAND gate, the transition probability is 1/4 (since there is a 25% probability the output will be discharged) while it is 3/16 for a static implementation. Although these examples illustrate that the switching activity of dynamic logic is generally higher, it should be noted that dynamic logic has lower physical capacitance. Both factors must be accounted for when analyzing dynamic power dissipation.

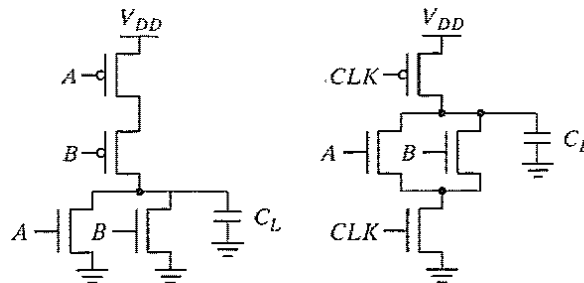


Figure 6-55 Static NOR versus  $n$ -type dynamic NOR.

### Problem 6.8 Activity Computation

For the four-input dynamic NAND gate, compute the activity factor with the following assumption for the inputs: They are independent, and  $p_{A=1} = 0.2$ ,  $p_{B=1} = 0.3$ ,  $p_{C=1} = 0.5$ , and  $p_{D=1} = 0.4$ .

### 6.3.3 Signal Integrity Issues in Dynamic Design

Dynamic logic clearly can result in high-performance solutions compared to static circuits. However, there are several important considerations that must be taken into account if one wants dynamic circuits to function properly. These include charge leakage, charge sharing, capacitive coupling, and clock feedthrough. These issues are discussed in some detail in this section.

#### Charge Leakage

The operation of a dynamic gate relies on the dynamic storage of the output value on a capacitor. If the pull-down network is *off*, ideally, the output should remain at the precharged state of  $V_{DD}$  during the evaluation phase. However, this charge gradually leaks away due to leakage currents, eventually resulting in a malfunctioning of the gate. Figure 6-56a shows the sources of leakage for the basic dynamic inverter circuit.

Source 1 and 2 are the *reverse-biased diode* and *subthreshold leakage* of the NMOS pull-down device  $M_1$ , respectively. The charge stored on  $C_L$  will slowly leak away through these leakage channels, causing a degradation in the high level (Figure 6-56b). Dynamic circuits therefore require a minimal clock rate, which is typically on the order of a few kHz. This makes the usage of dynamic techniques unattractive for low-performance products such as watches, or processors that use conditional clocks (where there are no guarantees on minimum clock rates). Note that the PMOS precharge device also contributes some leakage current due to the reverse bias diode (source 3) and the subthreshold conduction (source 4). To some extent, the leakage current of the PMOS counteracts the leakage of the pull-down path. As a result, the output voltage is going to be set by the resistive divider composed of the pull-down and pull-up paths.

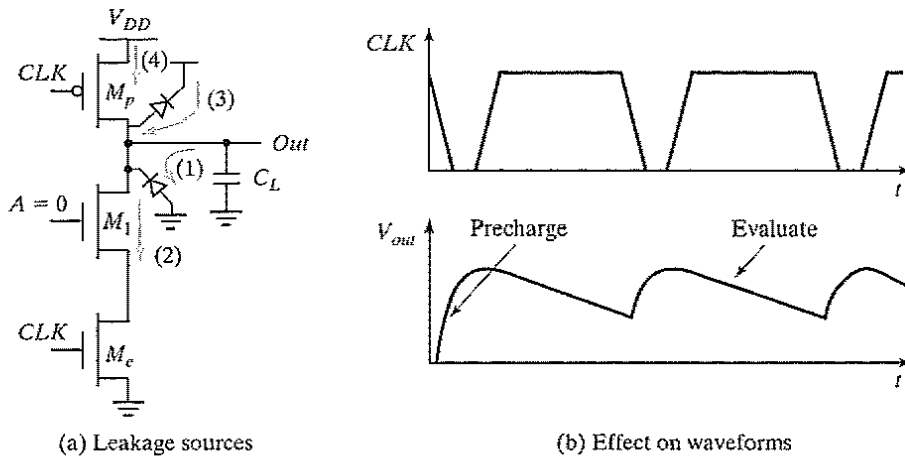


Figure 6-56 Leakage issues in dynamic circuits.

**Example 6.17 Leakage in Dynamic Circuits**

Consider the simple inverter with all devices set at  $0.5 \mu\text{m}/0.25 \mu\text{m}$ . Assume that the input is low during the evaluation period. Ideally, the output should remain at the precharged state of  $V_{DD}$ . However, as seen from Figure 6-57, the output voltage drops. Once the output drops below the switching threshold of the fan-out logic gate, the output is interpreted as a low voltage. Notice that the output settles to an intermediate voltage, due to the leakage current provided by the PMOS pull-up.

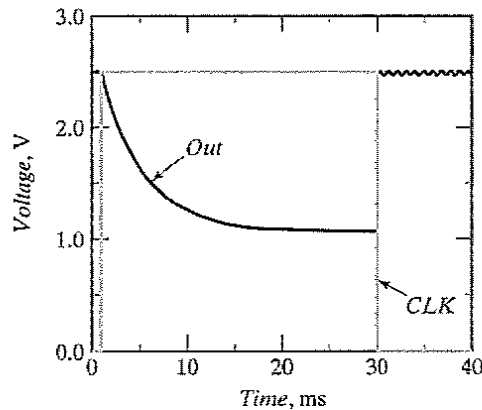
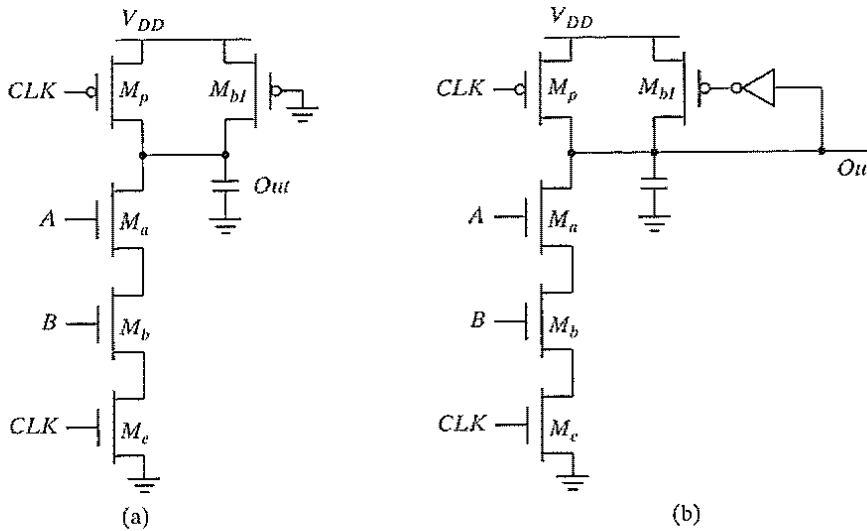


Figure 6-57 Impact of charge leakage. The output settles to an intermediate voltage determined by a resistive divider of the pull-down and pull-up devices.

Leakage is caused by the high-impedance state of the output node during the evaluate mode, when the pull-down path is turned off. The leakage problem may be counteracted by reducing the output impedance on the output node during evaluation. This often is done by



**Figure 6-58** Static bleeders compensate for the charge leakage.

adding a *bleeder transistor*, as shown in Figure 6-58a. The only function of the bleeder—an NMOS style pull-up device—is to compensate for the charge lost due to the pull-down leakage paths. To avoid the ratio problems associated with this style of circuit and the associated static power consumption, the bleeder resistance is made high (in other words, the device is kept small). This allows the (strong) pull-down devices to lower the *Out* node substantially below the switching threshold of the next gate. Often, the bleeder is implemented in a feedback configuration to eliminate the static power dissipation altogether (Figure 6-58b).

### Charge Sharing

Another important concern in dynamic logic is the impact of charge sharing. Consider the circuit in Figure 6-59. During the precharge phase, the output node is precharged to  $V_{DD}$ . Assume that all inputs are set to 0 during precharge, and that the capacitance  $C_a$  is discharged. Assume further that input *B* remains at 0 during evaluation, while input *A* makes a  $0 \rightarrow 1$  transition, turning transistor  $M_a$  on. The charge stored originally on capacitor  $C_L$  is redistributed over  $C_L$  and  $C_a$ . This causes a drop in the output voltage, which cannot be recovered due to the dynamic nature of the circuit.

The influence on the output voltage is readily calculated. Under the assumptions given previously, the following initial conditions are valid:  $V_{out}(t=0) = V_{DD}$  and  $V_X(t=0) = 0$ . As a result, two possible scenarios must be considered:

1.  $\Delta V_{out} < V_{Th}$ . In this case, the final value of  $V_X$  equals  $V_{DD} - V_{Th}(V_X)$ . Charge conservation then yields

$$\begin{aligned}
 C_L V_{DD} &= C_L V_{out}(\text{final}) + C_a [V_{DD} - V_{Th}(V_X)] \\
 \text{or} & \\
 \Delta V_{out} &= V_{out}(\text{final}) - V_{DD} = -\frac{C_a}{C_L} [V_{DD} - V_{Th}(V_X)]
 \end{aligned}
 \tag{6.43}$$

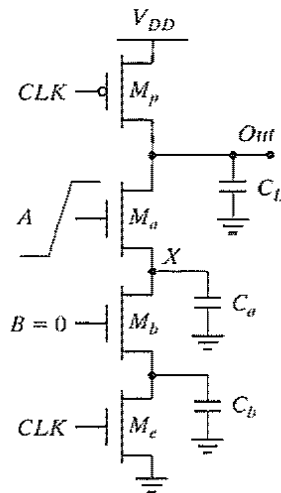


Figure 6-59 Charge sharing in dynamic networks.

2.  $\Delta V_{out} > V_{Tn}$ .  $V_{out}$  and  $V_X$  then reach the same value:

$$\Delta V_{out} = -V_{DD} \left( \frac{C_a}{C_a + C_L} \right) \quad (6.44)$$

We determine which of these scenarios is valid by the capacitance ratio. The boundary condition between the two cases can be determined by setting  $\Delta V_{out}$  equal to  $V_{Tn}$  in Eq. (6.44), yielding

$$\frac{C_a}{C_L} = \frac{V_{Tn}}{V_{DD} - V_{Tn}} \quad (6.45)$$

Case 1 holds when the  $(C_a/C_L)$  ratio is smaller than the condition defined in Eq. (6.45). If not, Eq. (6.44) is valid. Overall, it is desirable to keep the value of  $\Delta V_{out}$  below  $|V_{Tp}|$ . The output of the dynamic gate might be connected to a static inverter, in which case the low level of  $V_{out}$  would cause static power consumption. One major concern is a circuit malfunction if the output voltage is brought below the switching threshold of the gate it drives.

### Example 6.18 Charge Sharing

Let us consider the impact of charge sharing on the dynamic logic gate shown in Figure 6-60, which implements a three-input EXOR function  $y = A \oplus B \oplus C$ . The first question to be resolved is what conditions cause the worst case voltage drop on node  $y$ . For simplicity, ignore the load inverter, and assume that all inputs are low during the precharge operation and that all isolated internal nodes ( $V_a$ ,  $V_b$ ,  $V_c$ , and  $V_d$ ) are initially at 0 V.

Inspection of the truth table for this particular logic function shows that the output stays high for 4 out of 8 cases. The worst case change in output is obtained by exposing the maximum amount of internal capacitance to the output node during the evaluation



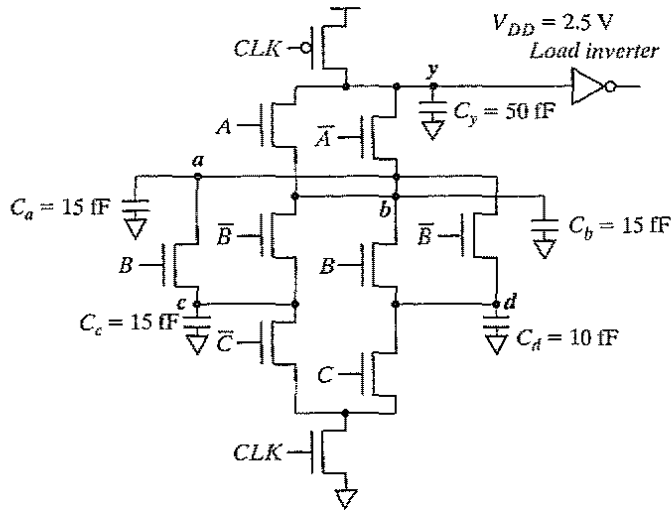


**Figure 6-60** Example illustrating the charge-sharing effect in dynamic logic.

period. This happens for  $\bar{A} B C$  or  $A \bar{B} C$ . The voltage change can then be obtained by equating the initial charge with the final charge as done with equation Eq. (6.44), yielding a worst case change of  $30/(30 + 50) * 2.5 \text{ V} = 0.94 \text{ V}$ . To ensure that the circuit functions correctly, the switching threshold of the connecting inverter should be placed below  $2.5 - 0.94 = 1.56 \text{ V}$ .

The most common and effective approach to deal with the charge redistribution is to also precharge critical internal nodes, as shown in Figure 6-61. Since the internal nodes are charged

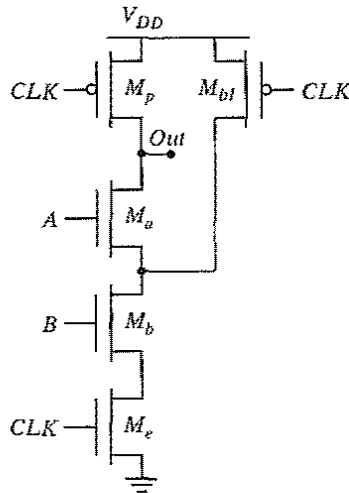


**Figure 6-61** Dealing with charge sharing by precharging internal nodes. An NMOS precharge transistor may also be used, but this requires an inverted clock.

to  $V_{DD}$  during precharge, charge sharing does not occur. This solution obviously comes at the cost of increased area and capacitance.

### Capacitive Coupling

The relatively high impedance of the output node makes the circuit very sensitive to crosstalk effects. A wire routed over or next to a dynamic node may couple capacitively and destroy the state of the floating node. Another equally important form of capacitive coupling is *backgate* (or *output-to-input*) *coupling*. Consider the circuit shown in Figure 6-62a, in which a dynamic two-input NAND gate drives a static NAND gate. A transition in the input  $In$  of the static gate may cause the output of the gate ( $Out_2$ ) to go low. This output transition couples capacitively to the other input of the gate (the dynamic node  $Out_1$ ) through the gate-source and gate-drain capacitances of transistor  $M_4$ . A simulation of this effect is shown in Figure 6-62b. It demonstrates how the coupling causes the output of the dynamic gate  $Out_1$  to drop significantly. This further causes the output of the static NAND gate not to drop all the way down to 0 V and a small amount of static power to be dissipated. If the voltage drop is large enough, the circuit can evaluate incorrectly, and the NAND output may not go low. When designing and laying out dynamic circuits, special care is needed to minimize capacitive coupling.

### Clock Feedthrough

A special case of capacitive coupling is clock feedthrough, an effect caused by the capacitive coupling between the clock input of the precharge device and the dynamic output node. The coupling capacitance consists of the gate-to-drain capacitance of the precharge device, and includes both the overlap and channel capacitances. This capacitive coupling causes the output of the dynamic node to rise above  $V_{DD}$  on the low-to-high transition of the clock, assuming that the pull-down network is turned off. Subsequently, the fast rising and falling edges of the clock couple onto the signal node, as is quite apparent in the simulation of Figure 6-62b.

The danger of clock feedthrough is that it may cause the normally reverse-biased junction diodes of the precharge transistor to become forward biased. This causes electron injection into the substrate, which can be collected by a nearby high-impedance node in the 1 state, eventually resulting in faulty operation. CMOS latchup might be another result of this injection. For all purposes, high-speed dynamic circuits should be carefully simulated to ensure that clock feedthrough effects stay within bounds.

All of the preceding considerations demonstrate that the design of dynamic circuits is rather tricky and requires extreme care. It should therefore be attempted only when high performance is required, or high quality design-automation tools are available.

#### 6.3.4 Cascading Dynamic Gates

Besides the signal integrity issues, there is one major catch that complicates the design of dynamic circuits: Straightforward cascading of dynamic gates to create multilevel logic structures does not work. The problem is best illustrated with two cascaded  $n$ -type dynamic

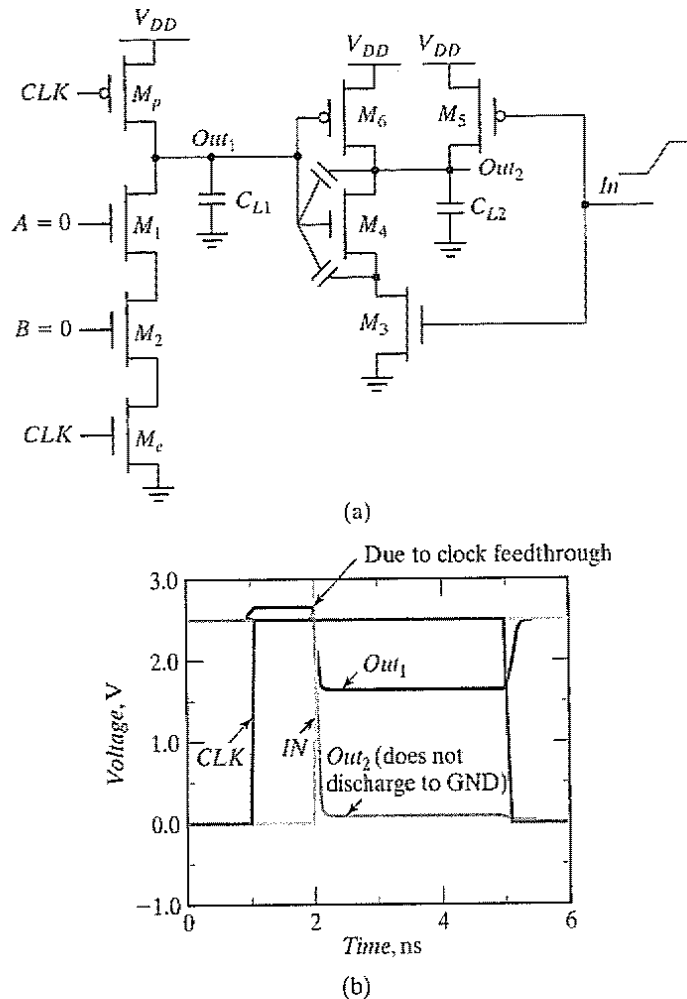


**Figure 6-62** Example demonstrating the effect of backgate coupling: (a) circuit schematics; (b) simulation results.

inverters, shown in Figure 6-63a. During the precharge phase (i.e.,  $CLK = 0$ ), the outputs of both inverters are precharged to  $V_{DD}$ . Assume that the primary input  $In$  makes a  $0 \rightarrow 1$  transition (Figure 6-63b). On the rising edge of the clock, output  $Out_1$  starts to discharge. The second output should remain in the precharged state of  $V_{DD}$  as its expected value is 1 ( $Out_1$  transitions to 0 during evaluation). However, there is a finite propagation delay for the input to discharge  $Out_1$  to GND. Therefore, the second output also starts to discharge. As long as  $Out_1$  exceeds the switching threshold of the second gate, which approximately equals  $V_{Th}$ , a conducting path exists between  $Out_2$  and GND, and precious charge is lost at  $Out_2$ . The conducting path is only disabled once  $Out_1$  reaches  $V_{Th}$ , and turns off the NMOS pull-down transistor. This leaves  $Out_2$  at an intermediate voltage level. The correct level will not be recovered, because dynamic gates rely on capacitive storage, in contrast to static gates, which have dc restoration. The charge loss leads to reduced noise margins and potential malfunctioning.

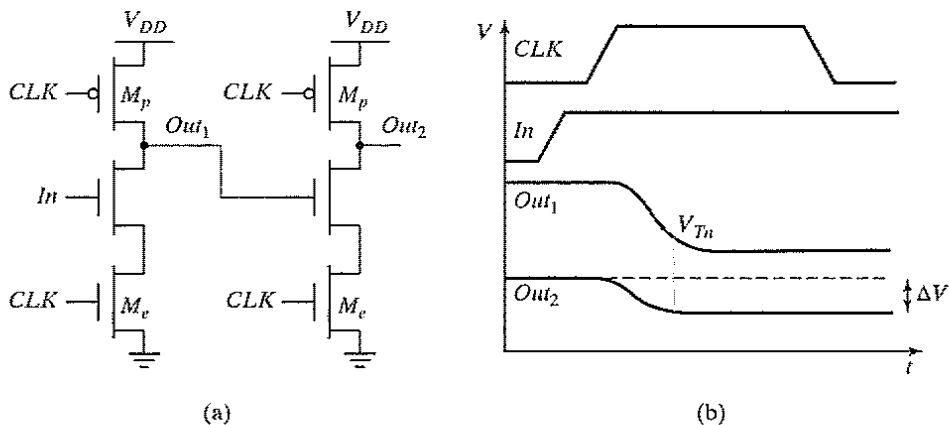


Figure 6-63 Cascade of dynamic  $n$ -type blocks.

The cascading problem arises because the outputs of each gate—and thus the inputs to the next stages—are precharged to 1. This may cause inadvertent discharge in the beginning of the evaluation cycle. Setting all the inputs to 0 during precharge addresses that concern. When doing so, all transistors in the pull-down network are turned off after precharge, and no inadvertent discharging of the storage capacitors can occur during evaluation. In other words, correct operation is guaranteed as long as **the inputs can only make a single  $0 \rightarrow 1$  transition during the evaluation period.**<sup>5</sup> Transistors are turned on only when needed—and at most, once per cycle. A number of design styles complying with this rule have been conceived, but the two most important ones are discussed next.

### Domino Logic

**Concept** A domino logic module [Krambeck82] consists of an  $n$ -type dynamic logic block followed by a static inverter (Figure 6-64). During precharge, the output of the  $n$ -type dynamic gate is charged up to  $V_{DD}$ , and the output of the inverter is set to 0. During evaluation, the dynamic gate conditionally discharges, and the output of the inverter makes a conditional transition from  $0 \rightarrow 1$ . If one assumes that all the inputs of a domino gate are outputs of other domino gates,<sup>6</sup> then it is ensured that all inputs are set to 0 at the end of the precharge phase, and that the only transitions during evaluation are  $0 \rightarrow 1$  transitions. Hence, the formulated rule is obeyed. The introduction of the static inverter has the additional advantage that the fan-out of the gate is driven by a static inverter with a low-impedance output, which increases noise immunity. Also, the buffer reduces the capacitance of the dynamic output node by separating internal and load capacitances. Finally, the inverter can be used to drive a bleeder device to combat leakage and charge redistribution, as shown in the second stage of Figure 6-64.

<sup>5</sup>This ignores the impact of charge distribution and leakage effects, discussed earlier.

<sup>6</sup>It is required that all other inputs that do not fall under this classification (for instance, primary inputs) stay constant during evaluation.

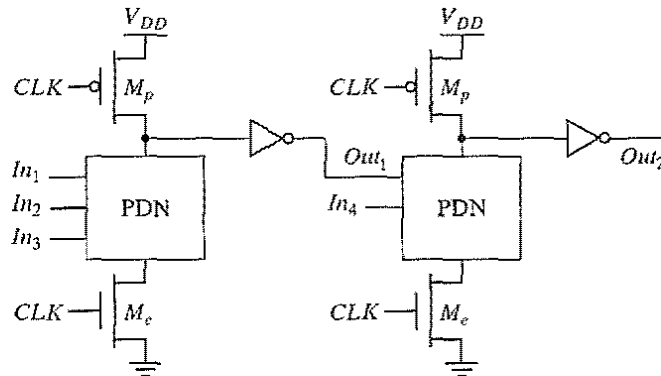
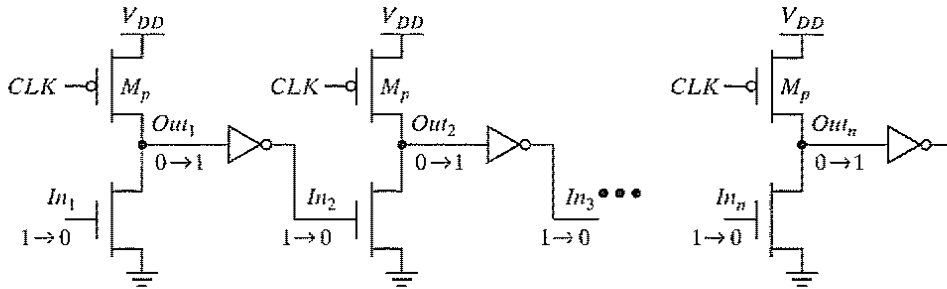


Figure 6-64 Domino CMOS logic.

Consider now the operation of a chain of domino gates. During precharge, all inputs are set to 0. During evaluation, the output of the first domino block either stays at 0 or makes a  $0 \rightarrow 1$  transition, affecting the second gate. This effect might ripple through the whole chain, one after the other, similar to a line of falling dominoes—hence the name. Domino CMOS has the following properties:

- Since each dynamic gate has a static inverter, only noninverting logic can be implemented. Although there are ways to deal with this, as discussed in a subsequent section, this is a major limiting factor, and pure domino design has thus become rare.
- Very high speeds can be achieved: only a rising edge delay exists, while  $t_{pHL}$  equals zero. The inverter can be sized to match the fan-out, which is already much smaller than in the complimentary static CMOS case, as only a single gate capacitance has to be accounted for per fan-out gate.

Since the inputs to a domino gate are low during precharge, it is tempting to eliminate the evaluation transistor because this reduces clock load and increases pull-down drive. However, eliminating the evaluation device extends the precharge cycle—the precharge now has to ripple through the logic network as well. Consider the logic network shown in Figure 6-65, where the evaluation devices have been eliminated. If the primary input  $In_1$  is 1 during evaluation, the output of each dynamic gate evaluates to 0, and the output of each static inverter is 1. On the falling edge of the clock, the precharge operation is started. Assume further that  $In_1$  makes a high-to-low transition. The input to the second gate is initially high, and it takes two gate delays before  $In_2$  is driven low. During that time, the second gate cannot precharge its output, as the pull-down network is fighting the precharge device. Similarly, the third gate has to wait until the second gate precharges before it can start precharging, etc. Therefore, the time taken to precharge the logic circuit is equal to its critical path. Another important negative is the extra power dissipation when both pull-up and pull-down devices are on. Therefore, it is good practice to always utilize evaluation devices.



**Figure 6-65** Effect of ripple precharge when the evaluation transistor is removed. The circuit also exhibits static power dissipation.

**Dealing with the Noninverting Property of Domino Logic** A major limitation in domino logic is that only noninverting logic can be implemented. This requirement has limited the widespread use of pure domino logic. There are several ways to deal with it, though. Figure 6-66 shows one approach to the problem—reorganizing the logic using simple boolean transforms such as De Morgan’s Law. Unfortunately, this sort of optimization is not always possible, and more general schemes may have to be used.

A general (but expensive) approach to solving the problem is the use of differential logic. *Dual-rail domino* is similar in concept to the DCVSL structure discussed earlier, but it uses a precharged load instead of a static cross-coupled PMOS load. Figure 6-67 shows the circuit schematic of an AND/NAND differential logic gate. Note that all inputs come from other differential domino gates. They are low during the precharge phase, while making a conditional  $0 \rightarrow 1$  transition during evaluation. Using differential domino, it is possible to implement any arbitrary function. This comes at the expense of an increased power dissipation, since a transition is guaranteed every single clock cycle regardless of the input values—either  $0$  or  $\bar{0}$  must make a  $0 \rightarrow 1$  transition. The function of transistors  $M_{f1}$  and  $M_{f2}$  is to keep the circuit static when the clock is high for extended periods of time (*bleeder*). Notice that this circuit is not ratioed, even in the presence of the PMOS pull-up devices! Due to its high performance, this differential approach is very popular, and is used in several commercial microprocessors.

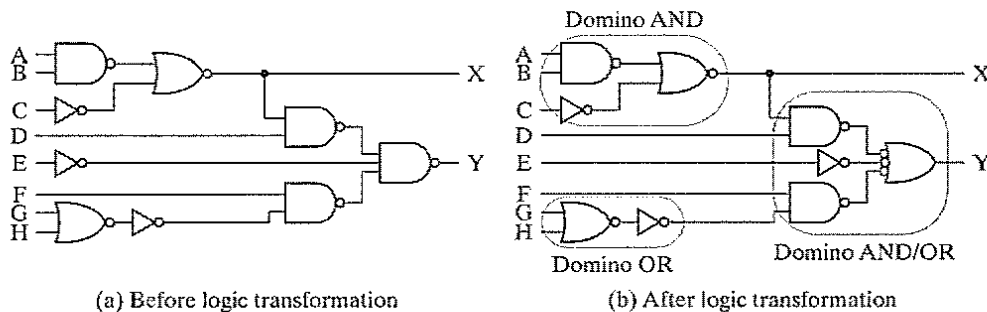


**Figure 6-66** Restructuring logic to enable implementation by using noninverting domino logic.

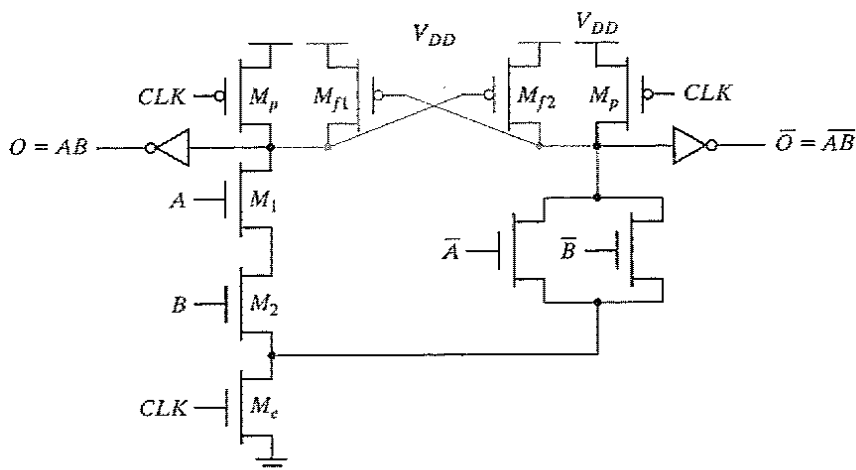


Figure 6-67 Simple dual rail (differential) domino logic gate.

**Optimization of Domino Logic Gates** Several optimizations can be performed on domino logic gates. The most obvious performance optimization involves the sizing of the transistors in the static inverter. With the inclusion of the evaluation devices in domino circuits, all gates precharge in parallel, and the precharge operation takes only two gate delays—charging the output of the dynamic gate to  $V_{DD}$ , and driving the inverter output low. The critical path during evaluation goes through the pull-down path of the dynamic gate and through the PMOS pull-up transistor of the static inverter. Therefore, to speed up the circuit during evaluation, the beta ratio of the static inverter should be made high so that its switching threshold is close to  $V_{DD}$ . This can be accomplished by using a small (minimum-sized) NMOS and a large PMOS device. The minimum-sized NMOS only affects the precharge time, which is generally limited due to the parallel precharging of all gates. The only disadvantage of using a large beta ratio is a reduction in noise margin. Hence, a designer should consider reduced noise margin and performance impact simultaneously during the device sizing.

Numerous variations of domino logic have been proposed [Bernstein98]. One optimization that reduces area is *multiple-output domino logic*. The basic concept is illustrated in Figure 6-68. It exploits the fact that certain outputs are subsets of other outputs to generate a number of logical functions in a single gate. In this example,  $O3 = C + D$  is used in all three outputs, and thus it is implemented at the bottom of the pull-down network. Since  $O2$  equals  $B \cdot O3$ , it can reuse the logic for  $O3$ . Notice that the internal nodes have to be precharged to  $V_{DD}$  to produce the correct results. Given that the internal nodes precharge to  $V_{DD}$ , the number of devices driving precharge devices is not reduced. However, the number of evaluation transistors is drastically reduced because they are amortized over multiple outputs. Additionally, this approach results in a reduction of the fan-out factor, again due to the reuse of transistors over multiple functions.

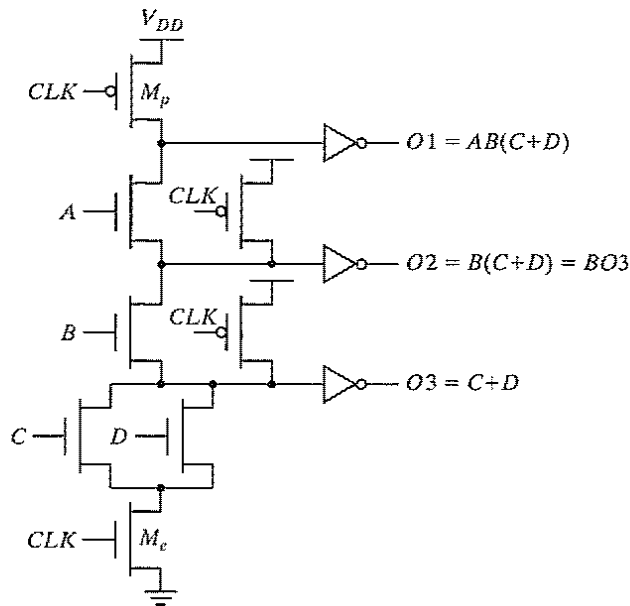


Figure 6-68 Multiple-output domino.

*Compound domino* (Figure 6-69) represents another optimization of the generic domino gate, once again minimizing the number of transistors. Instead of each dynamic gate driving a static inverter, it is possible to combine the outputs of multiple dynamic gates with the aid of a complex static CMOS gate, as shown in Figure 6-69. The outputs of three dynamic structures (implementing  $O1 = \overline{A B C}$ ,  $O2 = \overline{D E F}$  and  $O3 = \overline{G H}$ ) are combined using a single complex CMOS static gate that implements  $O = \overline{(O1 + O2) O3}$ . The total logic function realized this way is  $O = A B C D E F + G H$ .

Compound domino is a useful tool for constructing complex dynamic logic gates. Large dynamic stacks are replaced by parallel structures with small fan-in and complex CMOS gates. For example, a large *fan-in* domino AND can be implemented as a set of parallel dynamic NAND structures with lower *fan-in*, combined with a static NOR gate. One important consideration in Compound domino is the problem associated with backgate coupling. Care must be taken to ensure that the dynamic nodes are not affected by the coupling between the output of the static gates and the output of dynamic nodes.

### *np*-CMOS

An alternative approach to cascading dynamic logic is provided by *np*-CMOS, which uses two flavors (*n*-tree and *p*-tree) of dynamic logic, and avoids the extra static inverter in the critical path that comes with domino logic. In a *p*-tree logic gate, PMOS devices are used to build a pull-up logic network, including a PMOS evaluation transistor ([Gonçalvez83, Friedman84, Lee86]).



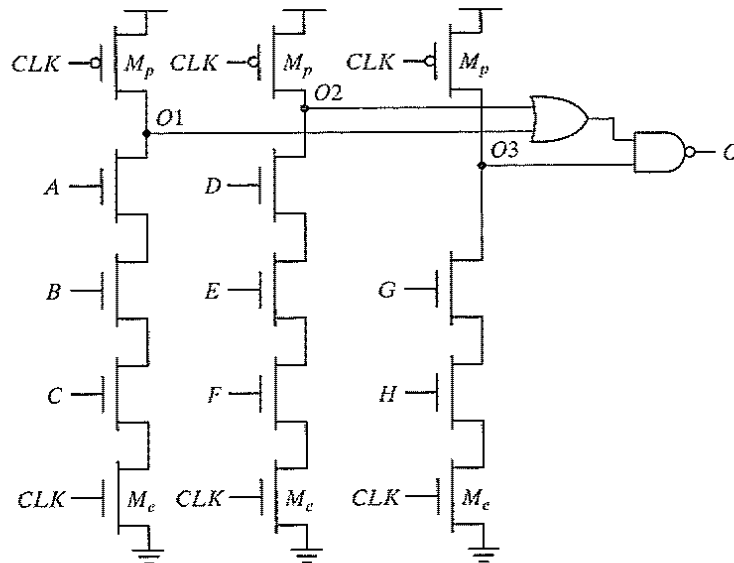


**Figure 6-69** Compound domino logic uses complex static gates at the output of the dynamic gates.

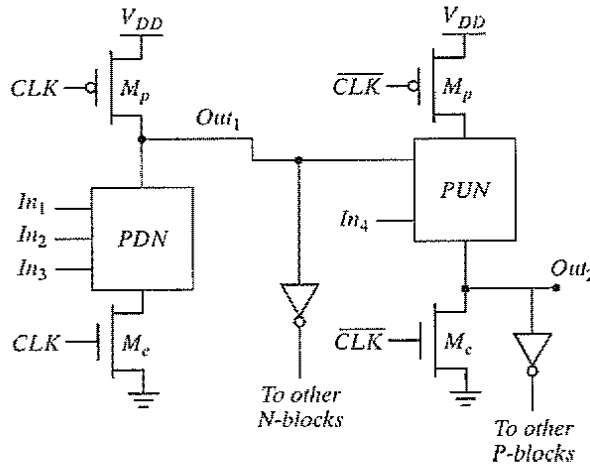


**Figure 6-70** The *np*-CMOS logic circuit style.

(see Figure 6-70). The NMOS precharge transistor drives the output low during precharge. The output conditionally makes a  $0 \rightarrow 1$  transition during evaluation depending on its inputs.

*np*-CMOS logic exploits the duality between *n*-tree and *p*-tree logic gates to eliminate the cascading problem. If the *n*-tree gates are controlled by *CLK*, and *p*-tree gates are controlled using  $\overline{CLK}$ , *n*-tree gates can directly drive *p*-tree gates, and vice versa. Similar to domino, *n*-tree outputs must go through an inverter when connecting to another *n*-tree gate. During the

precharge phase ( $CLK = 0$ ), the output of the  $n$ -tree gate,  $Out_1$ , is charged to  $V_{DD}$ , while the output of the  $p$ -tree gate,  $Out_2$ , is precharged to 0 V. Since the  $n$ -tree gate connects PMOS pull-up devices, the PUN of the  $p$ -tree is turned off at that time. During evaluation, the output of the  $n$ -tree gate can only make a  $1 \rightarrow 0$  transition, conditionally turning on some transistors in the  $p$ -tree. This ensures that no accidental discharge of  $Out_2$  can occur. Similarly,  $n$ -tree blocks can follow  $p$ -tree gates without any problems, because the inputs to the  $n$ -gate are precharged to 0. A disadvantage of the  $np$ -CMOS logic style is that the  $p$ -tree blocks are slower than the  $n$ -tree modules, due to the lower current drive of the PMOS transistors in the logic network. Equalizing the propagation delays requires extra area. Also, the lack of buffers requires that dynamic nodes are routed between gates.

## 6.4 Perspectives

### 6.4.1 How to Choose a Logic Style?

In the preceding sections, we have discussed several gate-implementation approaches using the CMOS technology. Each of the circuit styles has its advantages and disadvantages. Which one to select depends upon the primary requirement: ease of design, robustness, area, speed, or power dissipation. No single style optimizes all these measures at the same time. Even more, the approach of choice may vary from logic function to logic function.

The static approach has the advantage of being robust in the presence of noise. This makes the design process rather trouble free and amenable to a high degree of automation. It is clearly the best general-purpose logic design style. This ease of design does come at a cost: For complex gates with a large fan-in, complementary CMOS becomes expensive in terms of area and performance. Alternative static logic styles have therefore been devised. Pseudo-NMOS is simple and fast at the expense of a reduced noise margin and static power dissipation. Pass-transistor logic is attractive for the implementation of a number of specific circuits, such as multiplexers and XOR-dominated logic like adders.

Dynamic logic, on the other hand, makes it possible to implement fast and small complex gates. This comes at a price, however. Parasitic effects such as charge sharing make the design process a precarious job. Charge leakage forces a periodic refresh, which puts a lower bound on the operating frequency of the circuit.

The current trend is towards an increased use of complementary static CMOS. This tendency is inspired by the increased use of design-automation tools at the logic design level. These tools emphasize optimization at the logic level, rather than at the circuit level, and they put a premium on robustness. Another argument is that static CMOS is more amenable to voltage scaling than some of the other approaches discussed in this chapter.

### 6.4.2 Designing Logic for Reduced Supply Voltages

In Chapter 3, we projected that the supply voltage for CMOS processes will continue to drop over the coming decade, and may go as low as 0.6 V by 2010. To maintain performance under

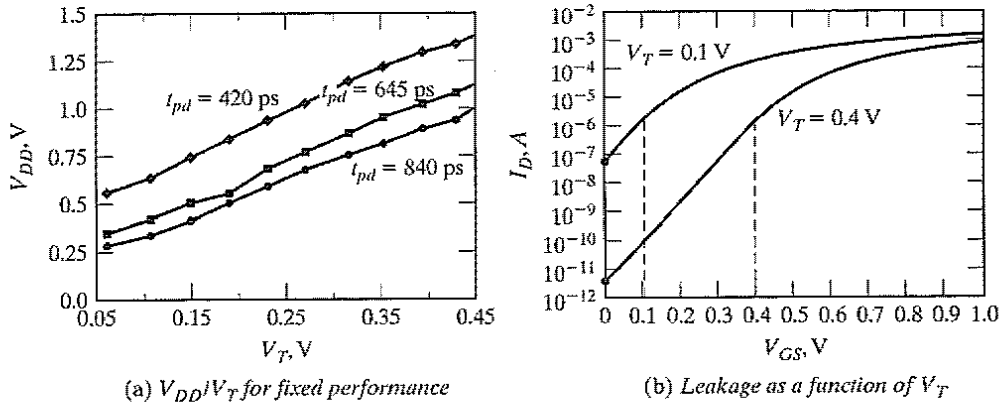


Figure 6-71 Voltage Scaling ( $V_{DD}/V_T$  on delay and leakage).

those conditions, it is essential that the device thresholds scale as well. Figure 6-71a shows a plot of the ( $V_T$ ,  $V_{DD}$ ) ratio required to maintain a given performance level (assuming that other device characteristics remain identical).

This trade-off is not without penalty. Reducing the threshold voltage increases the subthreshold leakage current exponentially, as we derived in Eq. (3.39) (repeated here for the sake of clarity):

$$I_{leakage} = I_S 10^{\frac{V_{GS} - V_{th}}{S}} \left( 1 - 10^{-\frac{nV_{DS}}{S}} \right) \quad (6.46)$$

In Eq. (6.46),  $S$  is the *slope factor* of the device. The subthreshold leakage of an inverter is the current of the NMOS for  $V_{in} = 0$  V and  $V_{out} = V_{DD}$  (or the PMOS current for  $V_{in} = V_{DD}$  and  $V_{out} = 0$ ). The exponential increase in inverter leakage for decreasing thresholds is illustrated in Figure 6-71b.

These leakage currents are a concern particularly for designs that feature intermittent computational activity separated by long periods of inactivity. For example, the processor in a cellular phone remains in idle mode for a majority of the time. While the processor is in idle mode, ideally, the system should consume zero or near-zero power. This is only possible if leakage is low—that is, the devices have a high threshold voltage. This is in contrast to the scaling scenario that we just depicted, where high performance under low supply voltage means reduced thresholds. To satisfy the contradicting requirements of high performance during active periods and low leakage during standby, several process modifications or leakage-control techniques have been introduced in CMOS processes. Most processes with feature sizes at or below  $0.18 \mu\text{m}$  CMOS support devices with different thresholds—typically a device with low threshold for high-performance circuits, and a transistor with high threshold for leakage control. Another approach gaining popularity is the

dynamic control of the threshold voltage of a device by exploiting the body effect of the transistor. Use of this approach to control individual devices requires a dual-well process (see Figure 2-2).

Clever circuit design can also help reduce the leakage current, which is a function of the circuit topology and the value of the inputs applied to the gate. Since  $V_T$  depends on body bias ( $V_{BS}$ ), the subthreshold leakage of an MOS transistor depends not only on the gate drive ( $V_{GS}$ ), but also on the body bias. In an inverter with  $In = 0$ , the subthreshold leakage of the inverter is set by the NMOS transistor with its  $V_{GS} = V_{BS} = 0$  V. In more complex CMOS gates, such as the two-input NAND gate of Figure 6-72, the leakage current depends on the input vector. The subthreshold leakage current of this gate is the least when  $A = B = 0$ . Under these conditions, the intermediate node  $X$  settles to

$$V_X \approx V_{th} \ln(1 + n) \quad (6.47)$$

The leakage current of the gate is then determined by the topmost NMOS transistor with  $V_{GS} = V_{BS} = -V_X$ . Clearly, the subthreshold leakage under this condition is smaller than that of the inverter. This reduction due to stacked transistors is called the *stack effect*. The Table in Figure 6-72 analyzes the leakage components for the two-input NAND gate under different input conditions.

The reality is even better. In short-channel MOS transistors, the subthreshold leakage current depends not only on the gate drive ( $V_{GS}$ ) and the body bias ( $V_{BS}$ ), but also on the drain voltage ( $V_{DS}$ ). The threshold voltage of a short-channel MOS transistor decreases with increasing  $V_{DS}$  due to *drain-induced barrier lowering* (DIBL). Typical values for DIBL can range from a 20- to a 150-mV change in  $V_T$  per voltage change in  $V_{DS}$ . Because of this, the impact of the stack effect is even more significant for short-channel transistors. The intermediate voltage reduces the drain-source voltage of the topmost device, increases its threshold, and thus lowers its leakage.

---

#### Example 6.19 Stack Effect in Two-Input NAND Gate

Consider again the two-input NAND gate of Figure 6-72a, when both  $N_1$  and  $N_2$  are *off* ( $A = B = 0$ ). From the simulated load lines shown in Figure 6-72c, we see that  $V_X$  settles to approximately 100 mV in steady state. The steady-state subthreshold leakage in the gate is therefore due to  $V_{GS} = V_{BS} = -100$  mV and  $V_{DS} = V_{DD} - 100$  mV, which is 20 times smaller than the leakage of a stand-alone NMOS transistor with  $V_{GS} = V_{BS} = 0$  mV and  $V_{DS} = V_{DD}$  [Ye98].

---

In sum, the subthreshold leakage in complex stacked circuits can be significantly lower than in individual devices. Observe that the maximum leakage reduction occurs when all the transistors in the stack are *off*, and the intermediate node voltage reaches its steady-state value. Exploiting this effect requires a careful selection of the input signals to every gate during standby or sleep mode.

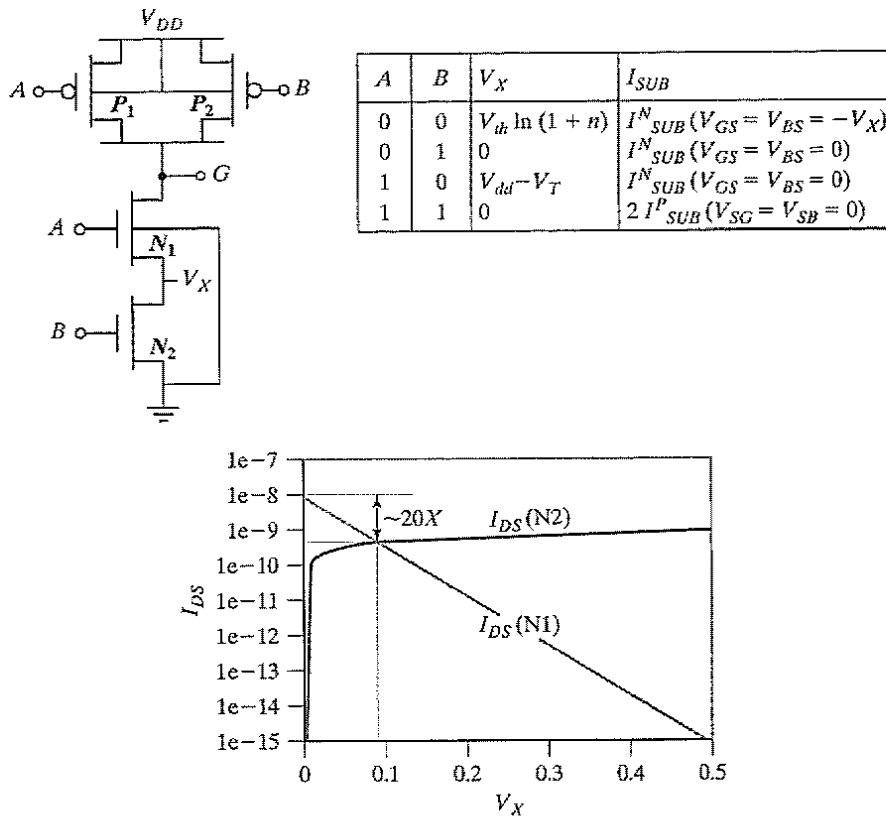


**Figure 6-72** Subthreshold leakage reduction in a two-input NAND gate (a) due to stack effect for different input conditions (b). Figure (c) plots the simulated load lines of the gate for  $A = B = 0$ .

### Problem 6.9 Computing $V_X$

Equation (6.47) calculates the intermediate node voltage for a two-input NAND with less than 10% error, for  $A = B = 0$ . Derive Eq. (6.47) assuming (1)  $V_T$  and  $I_S$  of  $N_1$  and  $N_2$  are approximately equal, (2) NMOS transistors are identically sized, and (3)  $n < 1.5$ .

## 6.5 Summary

In this chapter, we have extensively analyzed the behavior and performance of combinational CMOS digital circuits with regard to area, speed, and power. We summarize the major points as follows:

- *Static complementary CMOS* combines dual pull-down and pull-up networks, only one of which is enabled at any time.

- The performance of a CMOS gate is a strong function of the *fan-in*. Techniques to deal with fan-in include transistor sizing, input reordering, and partitioning. The speed is also a linear function of the fan-out. Extra buffering is needed for large fan-outs.
- The *ratioed logic* style consists of an active pull-down (-up) network connected to a load device. This results in a substantial reduction in gate complexity at the expense of static power consumption and an asymmetrical response. Careful transistor sizing is necessary to maintain sufficient noise margins. The most popular approaches in this class are the pseudo-NMOS techniques and differential DCVSL, which require complementary signals.
- *Pass-transistor logic* implements a logic gate as a simple switch network. This results in very simple implementations for some logic functions. Long cascades of switches are to be avoided due to a quadratic increase in delay with respect to the number of elements in the chain. NMOS-only pass-transistor logic produces even simpler structures, but might suffer from static power consumption and reduced noise margins. This problem can be addressed by adding a level-restoring transistor.
- The operation of *dynamic logic* is based on the storage of charge on a capacitive node and the conditional discharging of that node as a function of the inputs. This calls for a two-phase scheme, consisting of a precharge followed by an evaluation step. Dynamic logic trades off noise margin for performance. It is sensitive to parasitic effects such as leakage, charge redistribution, and clock feedthrough. Cascading dynamic gates can cause problems and thus should be addressed carefully.
- The *power consumption* of a logic network is strongly related to the switching activity of the network. This activity is a function of the input statistics, the network topology, and the logic style. Sources of power consumption such as glitches and short-circuit currents can be minimized by careful circuit design and transistor sizing.
- Threshold voltage scaling is required for *low-voltage operation*. Leakage control is critical for low-voltage operation.

## 6.6 To Probe Further

The topic of (C)MOS logic styles is treated extensively in the literature. Numerous texts have been devoted to the issue. Some of the most comprehensive treatments can be found in [Weste93] and [Chandrakasan01]. Regarding the intricacies of high-performance design, [Shoji96] and [Bernstein98] offer the most in-depth discussion of the optimization and analysis of digital MOS circuits. The topic of power minimization is relatively new, but comprehensive reference works are available in [Chandrakasan95], [Rabaey95], and [Pedram02].

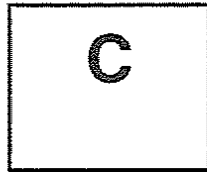
Innovations in the MOS logic area are typically published in the proceedings of the ISSCC Conference and the VLSI circuits symposium, as well as the *IEEE Journal of Solid State Circuits* (especially the November issue).

## References

- [Bernstein98] K. Bernstein et al., *High-Speed CMOS Design Styles*, Kluwer Academic Publishers, 1998.
- [Chandrakasan95] A. Chandrakasan and R. Brodersen, *Low Power Digital CMOS Design*, Kluwer Academic Publishers, 1995.
- [Chandrakasan01] A. Chandrakasan, W. Bowhill, and F. Fox, ed., *Design of High-Performance Microprocessor Circuits*, IEEE Press, 2001.
- [Gonçalvez83] N. Gonçalvez and H. De Man, "NORA: A Racefree Dynamic CMOS Technique for Pipelined Logic Structures," *IEEE Journal of Solid State Circuits*, vol. SC-18, no. 3, pp. 261–266, June 1983.
- [Heller84] L. Heller et al., "Cascade Voltage Switch Logic: A Differential CMOS Logic Family," *Proc. IEEE ISSCC Conference*, pp. 16–17, February 1984.
- [Krambeck82] R. Krambeck et al., "High-Speed Compact Circuits with CMOS," *IEEE Journal of Solid State Circuits*, vol. SC-17, no. 3, pp. 614–619, June 1982.
- [Landman91] P. Landman and J. Rabaey, "Design for Low Power with Applications to Speech Coding," *Proc. International Micro-Electronics Conference*, Cairo, December 1991.
- [Parameswar96] A. Parameswar, H. Hara, and T. Sakurai, "A Swing Restored Pass-Transistor Logic-Based Multiply and Accumulate Circuit for Multimedia Applications," *IEEE Journal of Solid State Circuits*, vol. SC-31, no. 6, pp. 805–809, June 1996.
- [Pedram02] M. Pedram and J. Rabaey, ed., *Power-Aware Design Methodologies*, Kluwer, 2002.
- [Rabaey95] J. Rabaey and M. Pedram, ed., *Low Power Design Methodologies*, Kluwer, 1995.
- [Radhakrishnan85] D. Radhakrishnan, S. Whittaker, and G. Maki, "Formal Design Procedures for Pass-Transistor Switching Circuits," *IEEE Journal of Solid State Circuits*, vol. SC-20, no. 2, pp. 531–536, April 1985.
- [Shoji88] M. Shoji, *CMOS Digital Circuit Technology*, Prentice Hall, 1988.
- [Shoji96] M. Shoji, *High-Speed Digital Circuits*, Addison-Wesley, 1996.
- [Sutherland99] I. Sutherland, B. Sproull, and D. Harris, *Logical Effort*, Morgan Kaufmann, 1999.
- [Weste93] N. Weste and K. Eshragian, *Principles of CMOS VLSI Design: A Systems Perspective*, Addison-Wesley, 1993.
- [Yano90] K. Yano et al., "A 3.8 ns CMOS 16 × 16 b Multiplier Using Complimentary Pass-Transistor Logic," *IEEE Journal of Solid State Circuits*, vol. SC-25, no. 2, pp. 388–395, April 1990.
- [Ye98] Y. Ye, S. Borkar, and V. De, "A New Technique for Standby Leakage Reduction in High-Performance Circuits," *Symposium on VLSI Circuits*, pp. 40–41, 1998.

## Exercises

For the latest problem sets and design challenges in CMOS digital logic, log in to <http://bwrc.eecs.berkeley.edu/IcBook>.



## How to Simulate Complex Logic Circuits

*Timing- and Switch-Level Simulation*

*Logic and Functional Simulation*

*Behavioral Simulation*

*Register-Transfer Languages*

While circuit simulation in the SPICE style proves to be an extremely valuable element of the designers tool box, it has one major deficiency. By taking into account all the peculiarities and second-order effects of the semiconductor devices, it tends to be time consuming. It rapidly becomes unwieldy when designing complex circuits, unless one is willing to spend days of computer time. Even though computers are always getting faster and simulators are getting better, circuits are getting complex even faster. The designer can address the complexity issue by giving up modeling accuracy and resorting to higher representation levels. A discussion of the different abstraction levels available to the designer and their impact on simulation accuracy is the topic of this insert.

The best way of differentiating among the myriad of simulation approaches and abstraction levels is to identify how the data and time variables are represented—as analog, continuous variables, as discrete signals, or as abstract data models.



## C.1 Representing Digital Data as a Continuous Entity

### Circuit Simulation and Derivatives

In Design Methodology Insert B, we established that a circuit simulator is “digitally agnostic,” meaning that it is, in essence, an analog simulator. Voltage, current, and time are treated as analog variables. This accurate modeling, combined with the nonlinearity of most of the devices leads to a high overhead in simulation time.

Substantial effort has been invested to decrease the computation time at the expense of generality. Consider an MOS digital circuit. Due to the excellent isolation property of the MOS gate, it is often possible to partition the circuit into a number of sections that have limited interaction. A possible approach is to solve each of these partitions individually over a given period, assuming that the inputs from other sections are known or constant. The resulting waveforms can then be iteratively refined. This *relaxation-based* approach has the advantage of being computationally more effective than the traditional technique by avoiding expensive matrix inversions, but it is restricted to MOS circuits [White87]. When the circuit contains feedback paths, the partitions can become large, and simulation performance degrades.

Another approach is to reduce the complexity of the transistor models used. For example, linearization of the model leads to a dramatic reduction in the computational complexity. Yet another approach is to employ a simplified table-lookup model. While this approach, by necessity, leads to a decreased accuracy of the waveforms, it still allows for a good estimation of timing parameters such as propagation delay and rise and fall times. This explains why these tools often are called *timing simulators*. The big advantage is in the execution speed, which can be one or two orders of magnitude higher than that of SPICE-like tools. Another advantage is that, in contrast to the tools that are discussed next, timing simulators still can incorporate second-order effects such as leakage, threshold drops, and signal glitches. Examples of an offering in this class is the NanoSim (formerly TimeMill/PowerMill) tool set from Synopsys [TimeMill]. As a point of reference, simulators in this class typically give up 5 to 10% in accuracy on timing parameters, with respect to full-blown circuit simulators.

## C.2 Representing Data as a Discrete Entity

In digital circuits, we generally are not interested in the actual value of the voltage variable, but only in the digital value it represents. Therefore, it is possible to envision a simulator in which data signals are either in the 0 or 1 range. Signals that do not comply with either condition are denoted as  $X$ , or undefined.

This tertiary representation  $\{0, 1, X\}$  is used extensively in simulators at both the device and gate level. By augmenting this set of allowable data values, we can obtain more detailed information, while retaining the capability of handling complex designs. Possible extensions are the  $Z$ -value for a tristate node in the high-impedance state, and  $R$ - and  $F$ -values for the rising and falling transients. Some commercially offered simulators provide as many as a dozen possible signal states.

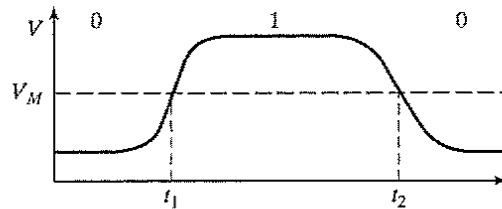


Figure C-1 Discretizing the time variable.

While substantial performance improvement is obtained by making the data representation space discrete, similar benefits can be obtained by making time a discrete variable as well. Consider the voltage waveform of Figure C-1, which represents the signal at the input of an inverter with a switching threshold  $V_M$ . It is reasonable to assume that the inverter output changes its value one propagation delay after its input crossed  $V_M$ . When one is not strictly interested in the exact shape of the signal waveforms, it is sufficient to evaluate the circuit only at the interesting time points,  $t_1$  and  $t_2$ .

Similarly, the interesting points of the output waveform are situated at  $t_1 + t_{pHL}$  and  $t_2 + t_{pLH}$ . A simulator that only evaluates a gate at the time an event happens at one of its inputs is called an *event-driven* simulator. The evaluation order is determined by putting projected events on a time queue and processing them in a time-ordered fashion. Suppose that the waveform of Figure C-1 acts as the input waveform to a gate. An event is scheduled to occur at time  $t_1$ . Upon processing that event, a new event is scheduled for the fan-out nodes at  $t_1 + t_{pHL}$  and is put on the time queue. This event-driven approach is evidently more efficient than the time-step-driven approach of the circuit simulators. To take the impact of fan-out into account, the propagation delay of a circuit can be expressed in terms of an intrinsic delay ( $t_{in}$ ) and a load-dependent factor ( $t_f$ ), and it can differ over edge transitions:

$$t_{pLH} = t_{inLH} + t_{fLH} \times C_L \quad (\text{C.1})$$

The load  $C_L$  can be entered in absolute terms (in pF) or as a function of the number of fan-out gates. Observe how closely this equation resembles the *logical-effort* model we introduced in the preceding chapter.

While offering a substantial performance benefit, the preceding approach still has the disadvantage that events can happen any time. Another simplification could be to make the time even more discrete and allow events to happen only at integer multiples of a *unit time* variable. An example of such an approach is the *unit-delay* model, where each circuit has a single delay of one unit. Finally, the simplest model is the *zero-delay* model, in which gates are assumed to be free of delay. Under this paradigm, time proceeds from one clock event to the next, and all events are assumed to occur instantaneously upon arrival of a clocking event. These concepts can be applied on a number of abstraction levels, resulting in the simulation approaches discussed next.

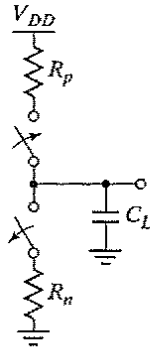


Figure C-2 Switch-level model of CMOS inverter.

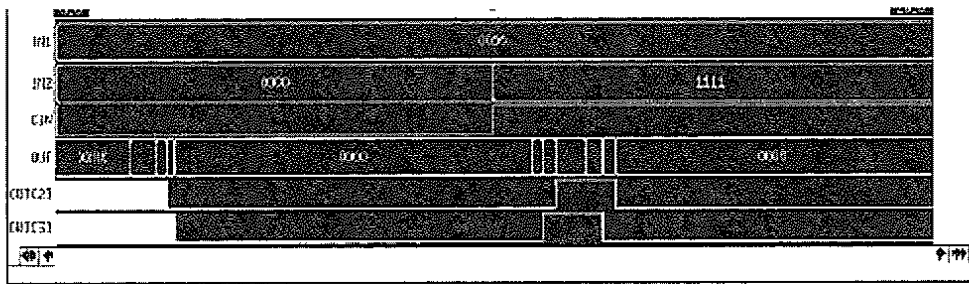
### Switch-Level Simulation

The nonlinear nature of semiconductor devices is one of the major impediments to higher simulation speeds. The switch-level model [Bryant81] overcomes this hurdle by approximating the transistor behavior with a linear resistance whose value is a function of the operating conditions. In the off-mode, the resistance is set to infinity, while in the on-mode, it is set to the average “on” resistance of the device (Figure C-2). The resulting network is a time-variant, linear network of resistors and capacitors that can be more efficiently analyzed. Evaluation of the resistor network determines the steady-state values of the signals and typically employs a {0, 1, X} model. For instance, if the total resistance between a node and GND is substantially smaller than the resistance to  $V_{DD}$ , the node is set to the 0-state. The timing of the events can be resolved by analyzing the  $RC$  network. Simpler timing models such as the unit-delay model are also employed.

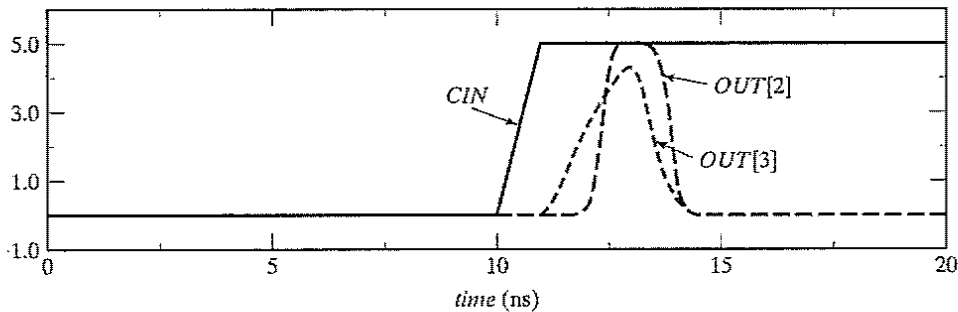
---

### Example C.1 Switch versus Circuit-Level Simulation

A four-bit adder is simulated using the switch-level simulator IRSIM ([Salz89]). The simulation results are plotted in Figure C-3. Initially, all inputs ( $IN1$  and  $IN2$ ) and the carry-input  $CIN$  are set to 0. After 10 nsec, all inputs  $IN2$  as well as  $CIN$  are set to 1. The display window plots the input signals, the output vector  $OUT[0-3]$ , and the most significant output bits  $OUT[2]$  and  $OUT[3]$ . The output converges to the correct value 0000 after a transition period. Notice how the data assumes only 0 and 1 levels. The glitches in the output signals go rail to rail, although in reality they might represent only partial excursions. During transients, the signal is marked X, which means “undefined.” To put this result in perspective, Figure C-3 plots the SPICE results for the same input vectors. Notice the partial glitches. Also, it shows that the IRSIM timing, which is based on an  $RC$  model, is relatively accurate and sufficient to get a first-order impression.



(a) IRSIM results.



(b) SPICE results.

**Figure C-3** Comparison between circuit and switch-level simulations.

### Gate-Level (or Logic) Simulation

Gate-level simulators use the same signal values as the switch-level tools, but the simulation primitives are gates instead of transistors. This approach enables the simulation of more complex circuits at the expense of detail and generality. For example, some common VLSI structures such as tristate busses and pass transistors are hard to deal with at this level. Since gate level is the preferred entry level for many designers, this simulation approach remained extremely popular until the introduction of logic synthesis tools, which moved the focus to the functional or behavioral abstraction layer. The interest in logic simulation was so great that special and expensive hardware accelerators were developed to expedite the simulation process (e.g., [Agrawal90]).

### Functional Simulation

Functional simulation can be considered as a simple extension of logic simulation. The primitive elements of the input description can be of an arbitrary complexity. For instance, a simulation element can be a NAND gate, a multiplier, or an SRAM memory. The functionality of one of these complex units can be described using a modern programming language or a dedicated hardware description language. For instance, the THOR simulator uses the C programming language to determine the output values of a module as a function of its inputs [Thor88].

The *SystemC* language [SystemC] uses most of the syntax and semantics of C, but adds a number of constructs and data types to deal with the peculiarities of hardware design—such as the presence of concurrency. On the other hand, *VHDL* (*VHSIC Hardware Description Language*) [VHDL88] is a specially developed language for the description of hardware designs.

In the *structural mode*, VHDL describes a design as a connection of functional modules. Such a description often is called a *netlist*. For example, Figure C-4 shows a description of a 16-bit accumulator consisting of a register and adder.

The adder and register can in turn be described as a composition of components such as full-adder or register cells. An alternative approach is to use the *behavioral mode* of the language that describes the functionality of the module as a set of input/output relations regardless of the chosen implementation. As an example, Figure C-5 describes how the output of the adder is the two's-complement sum of its inputs.

```

entity accumulator is
  port ( -- definition of input and output terminals
    DI: in bit_vector(15 downto 0) -- a vector of 16 bit wide
    DO: inout bit_vector(15 downto 0);
    CLK: in bit
  );
end accumulator;

architecture structure of accumulator is
  component reg -- definition of register ports
    port (
      DI : in bit_vector(15 downto 0);
      DO : out bit_vector(15 downto 0);
      CLK : in bit
    );
  end component;
  component add -- definition of adder ports
    port (
      IN0 : in bit_vector(15 downto 0);
      IN1 : in bit_vector(15 downto 0);
      OUT0 : out bit_vector(15 downto 0)
    );
  end component;
  -- definition of accumulator structure
  signal X : bit_vector(15 downto 0);
begin
  add1 : add
    port map (DI, DO, X); -- defines port connectivity
  reg1 : reg
    port map (X, DO, CLK);
end structure;

```

**Figure C-4** Functional description of an accumulator in VHDL.

```

entity add is
  port (
    IN0 : in bit_vector(15 downto 0);
    IN1 : in bit_vector(15 downto 0);
    OUT0 : out bit_vector(15 downto 0)
  );
end add;

architecture behavior of add is
begin
  process(IN0, IN1)
    variable C : bit_vector(16 downto 0);
    variable S : bit_vector(15 downto 0);
  begin
    loop1:
    for j in 0 to 15 loop
      S(j) := IN0(j) xor IN1(j) xor C(j);
      C(j+1) := IN0(j) and IN1(j) or C(j) and (IN0(j) or IN1(j));
    end loop loop1;
    OUT0 <= S;
  end process;
end behavior;

```

**Figure C-5** Behavioral description of 16-bit adder.

The signal levels of the functional simulator are similar to the switch and logic levels. A variety of timing models can be used—for example, the designer can describe the delay between input and output signals as part of the behavioral description of a module. Most often the zero-delay model is employed, since it yields the highest simulation speed.

### C.3 Using Higher-Level Data Models

When conceiving a digital system such as a compact disk player or an embedded microcontroller, the designer rarely thinks in terms of bits. Instead, she envisions data moving over busses as integer or floating-point words, and patterns transmitted over the instruction bus as members of an enumerated set of instruction words (such as {*ACC*, *RD*, *WR*, or *CLR*}). Modeling a discrete design at this level of abstraction has the distinct advantage of being more understandable, and it also results in a substantial benefit in simulation speed. Since a 64-bit bus is now handled as a single object, analyzing its value requires only one action instead of the 64 evaluations it formerly took to determine the current state of the bus at the logic level. The disadvantage of this approach is another sacrifice of timing accuracy. Since a bus is now considered to be a single entity, only one global delay can be annotated to it, while the delay of bus elements can vary from bit to bit at the logic level.

It also is common to distinguish between *functional* (or *structural*) and *behavioral* descriptions. In a functional-level specification, the description mirrors the intended hardware

structure. Behavioral-level specifications only mimic the input/output functionality of a design. Hardware delay loses its meaning, and simulations are normally performed on a per clock-cycle (or higher) basis. For instance, the behavioral models of a microprocessor that are used to verify the completeness and the correctness of the instruction set are performed on a per instruction basis.

The most popular languages at this level of abstraction are the VHDL and VERILOG hardware-description languages. VHDL allows for the introduction of user-defined data types such as 16-bit, two's-complement words or enumerated instruction sets. Many designers tend to use traditional programming approaches such as C or C++ for their first-order behavioral models. This approach has the advantage of offering more flexibility, but it requires the user to define all data types and to essentially write the complete simulation scenario.

---

### Example C.2 Behavioral-Level VHDL Description

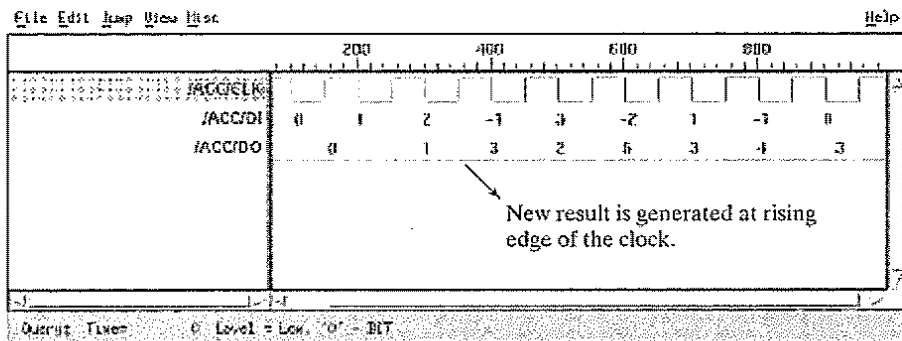
To contrast the functional and behavioral description modes and the use of higher level data models, consider again the example of the accumulator (see Figure C-6). In this case, we use a fully behavioral description that employs integer data types to describe the module operation.

Figure C-7 shows the results of a simulation performed at this level of abstraction. Even for this small example, the simulation performance in terms of CPU time is three times better than what is obtained with the structural description of Figure C-4.

```
entity accumulator is
  port (
    DI : in integer;
    DO : inout integer := 0;
    CLK : in bit
  );
end accumulator;

architecture behavior of accumulator is
begin
  process(CLK)
    variable X : integer := 0; -- intermediate variable
  begin
    if CLK = '1' then
      X <= DO + DI;
      DO <= X;
    end if;
  end process;
end behavior;
```

**Figure C-6** Accumulator for Example C.2.



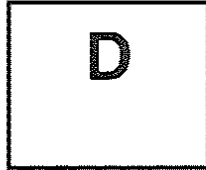
**Figure C-7** Display of simulation results for accumulator example as obtained at the behavioral level. The WAVES display tool (and VHDL simulator) are part of the Synopsys VHDL tool suite (Courtesy of Synopsys.).

## References

- [Agrawal90] P. Agrawal and W. Dally, "A Hardware Logic Simulation System," *IEEE Trans. Computer-Aided Design*, CAD-9, no. 9, pp. 19–29, January 1990.
- [Bryant81] R. Bryant, *A Switch-Level Simulation Model for Integrated Logic Circuits*, Ph. D. diss., MIT Laboratory for Computer Science, report MIT/LCS/TR-259, March 1981.
- [Salz89] A. Salz and M. Horowitz, "IRSIM: An Incremental MOS Switch-Level Simulator," *Proceedings of the 26th Design Automation Conference*, pp. 173–178, 1989.
- [SystemC] *Everything You Wanted to Know about SystemC*, <http://www.systemc.org/>
- [Thor88] R. Alverson et al., "THOR User's Manual," Technical Report CSL-TR-88-348 and 349, Stanford University, January 1988.
- [TimeMill] <http://www.synopsys.com/products/mixedsignal/mixedsignal.html>
- [VHDL88] VHDL Standards Committee, *IEEE Standard VHDL Language Reference Manual*, IEEE standard 1076–1077, 1978.
- [White87] J. White and A. Sangiovanni-Vincentelli, *Relaxation Techniques for the Simulation of VLSI Circuits*, Kluwer Academic, 1987.







## Layout Techniques for Complex Gates

*Weinberger and standard-cell layout techniques*

*Euler graph approach*

In Chapter 6, we discussed in detail how to construct the schematics of complex gates and how to size the transistors. The last step in the design process is to derive a layout for the gate or cell; in other words, we must determine the exact shape of the various polygons composing the gate layout. The composition of a layout is strongly influenced by the *interconnect approach*. How does the cell fit in the overall chip layout, and how does it communicate with neighboring cells? Keeping these questions in mind from the start results in denser designs with less parasitic capacitance.

### **Weinberger and Standard-Cell Layout Techniques**

We now examine two important layout approaches, although many others can be envisioned. In the *Weinberger approach* [Weinberger67], the data wires (inputs and outputs) are routed (in metal) parallel to the supply rails and perpendicular to the diffusion areas, as illustrated in Figure D-1. Transistors are formed at the cross points of the polysilicon signal wires (connected to the horizontal metal wires) and the diffusion zones. The “over-the-cell” wiring approach makes the Weinberger technique particularly suited for bit-sliced datapaths. While it is still used on an occasional base, the Weinberger technique has lost its appeal over the years in favor of the standard-cell style.

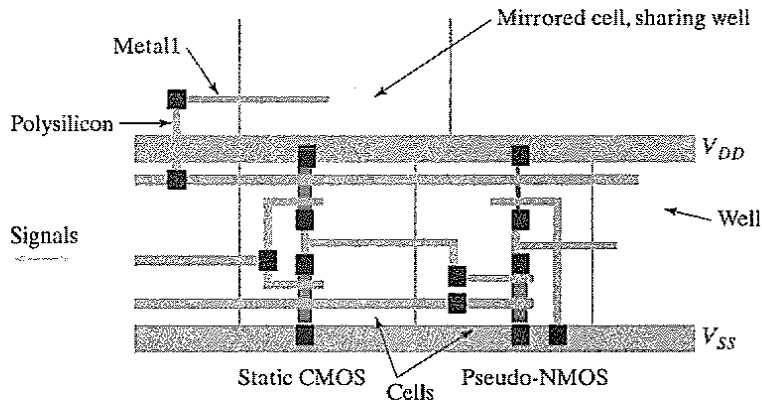


**Figure D-1** The Weinberger approach for complex gate layout (using a single metal layer).

In the *standard-cell technique*, signals are routed in polysilicon perpendicular to the power distribution (Figure D-2). This approach tends to result in a dense layout for static CMOS gates, as the vertical polysilicon wire can serve as the input to both the NMOS and the PMOS transistors. An example of a cell implemented using the standard-cell approach is shown in Figure 6-12. Interconnections between cells generally are established in so-called routing channels, as demonstrated in Figure D-2. The standard-cell approach is very popular at present due to its high degree of automation. (For a detailed description of the design automation tools supporting the standard-cell approach, see Chapter 8.)

#### Layout Planning using the Euler Path Approach

The common use of this layout strategy makes it worth analyzing how a complex Boolean function can be mapped efficiently onto such a structure. For density reasons, it is desirable to realize the NMOS and PMOS transistors as an unbroken row of devices with abutting source-drain con-

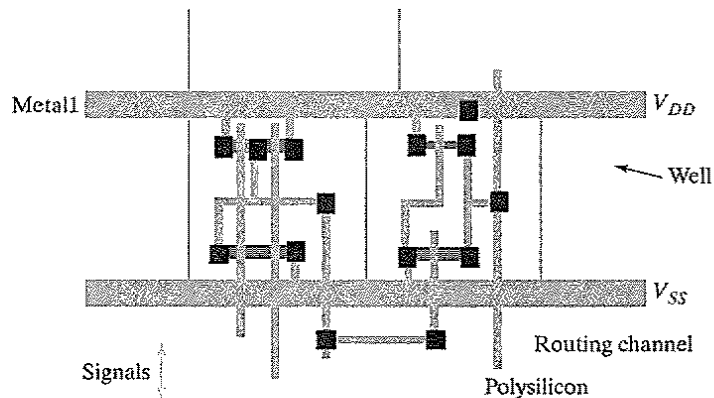


**Figure D-2** The standard-cell approach for complex gate layout.

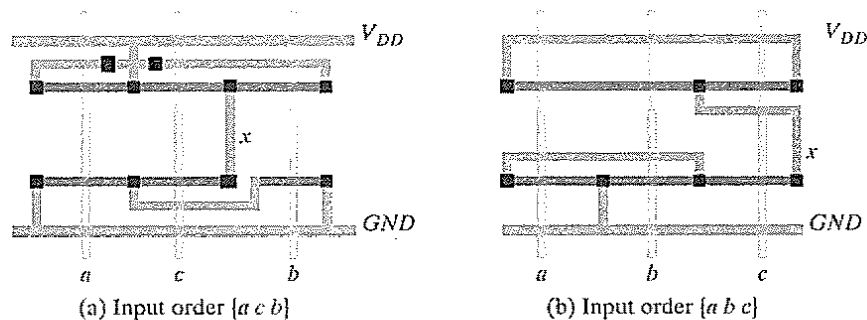


**Figure D-3** Stick Diagram for  $x = (a + b) \cdot c$ .

nections, and with the gate connections of the corresponding NMOS and PMOS transistors aligned. This approach requires only a single strip of diffusion in both wells. To achieve this goal, a careful ordering of the input terminals is necessary. This is illustrated in Figure D-3, where the logical function  $\bar{x} = (a + b) \cdot c$  is implemented. In the first version, the order  $\{a c b\}$  is adopted. It can easily be seen that no solution will be found using only a single diffusion strip. A reordering of the terminals (for instance, using  $\{a b c\}$ ), generates a feasible solution, as shown in Figure D-3b. Observe that the “layouts” in Figure D-3 do not represent actual mask geometries, but are rather symbolic diagrams of the gate topologies. Wires and transistors are represented as dimensionless objects, and positioning is relative, not absolute. Such conceptual representations are called *stick diagrams*, and often are used at the conception time of the gate, before determining the actual dimensions. We use stick diagrams whenever we want to discuss gate topologies or layout strategies.

Fortunately, a systematic approach has been developed to derive the permutation of the input terminals so that complex functions can be realized by uninterrupted diffusion strips that minimize the area [Uehara81]. The systematic nature of the technique also has the advantage that it is easily automated. It consists of the following two steps:

1. **Construction of logic graph.** The logic graph of a transistor network (or a switching function) is the graph of which the vertices are the nodes (signals) of the network, and the edges represent the transistors. Each edge is named for the signal controlling the corresponding transistor. Since the PUN and PDN networks of a static CMOS gate are dual, their corresponding graphs are dual as well—that is, a parallel connection is replaced by a series one and vice versa. This is demonstrated in Figure D-4, where the logic graphs for the PDN and PUN networks of the Boolean function  $\bar{x} = (a + b) \cdot c$  are overlaid (notice that this approach can be used to derive dual networks).
2. **Identification of Euler paths.** An Euler path in a graph is defined as a path through all nodes in the graph such that each edge in the graph is only visited once. Identification of such a path is important, because an ordering of the inputs leading to an uninterrupted diffusion strip of NMOS (PMOS) transistors is possible only if there exists an Euler path in

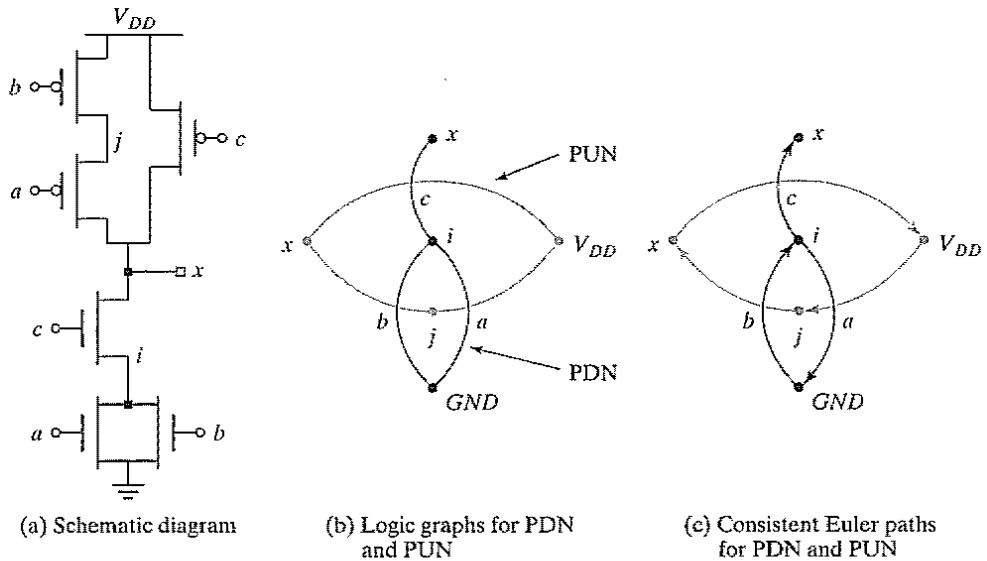


**Figure D-4** Schematic diagram, logic graph, and Euler paths for  $x = (a + b) \cdot c$ .

the logic graph of the PDN (PUN) network. The reasoning behind this finding is as follows:

To form an interrupted strip of diffusion, all transistors must be visited in sequence; that is, the drain of one device is the source of the next one. This is equivalent to traversing the logic graph along an Euler path. Be aware that Euler paths are not unique: many different solutions may exist.

The sequence of edges in the Euler path equals the ordering of the inputs in the gate layout. To obtain the same ordering in both the PUN and PDN networks, as is necessary if we want to use a single poly strip for every input signal, the Euler paths must be *consistent*—that is, they must have the same sequence.

Consistent Euler paths for the example of Figure D-4a are shown in Figure D-4c. The layout associated with this solution is shown in Figure D-3b. An inspection of the logic diagram of the function shows that  $\{a c b\}$  is an Euler path for the PUN, but not for the PDN. A single-diffusion-strip solution is, hence, nonexistent (Figure D-3a).

**Example D.1 Derivation of Layout Topology of Complex Logic Gate**

As an example, let us derive the layout topology of the following logical function:

$$x = \overline{ab + cd}$$

The logical function and one consistent Euler path are shown in Figure D-5a and Figure D-5b. The corresponding layout is shown in Figure D-5c.

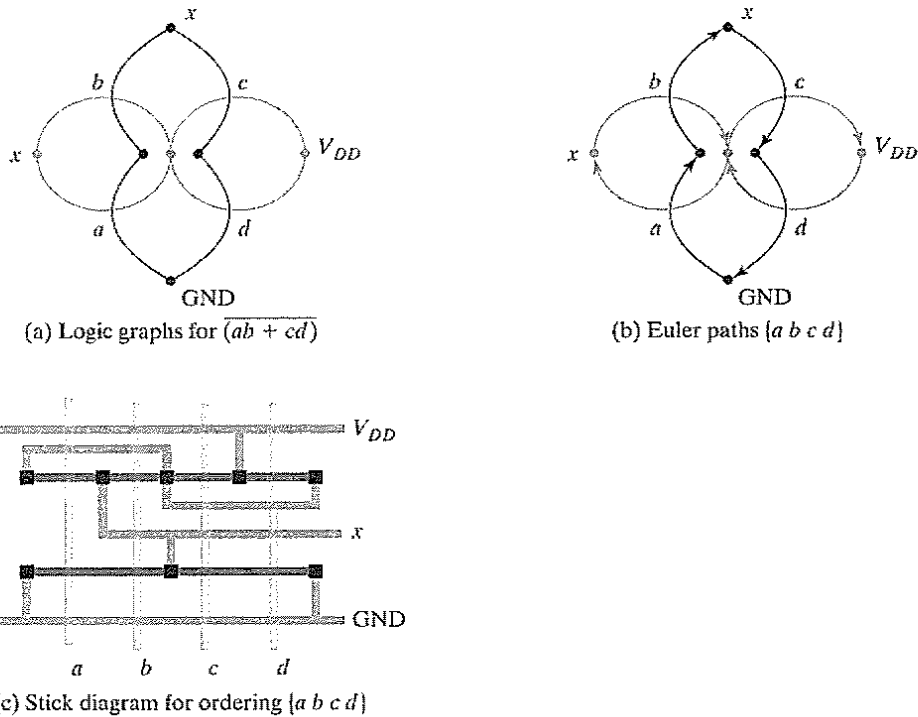


**Figure D-5** Deriving the layout topology for  $x = (ab + cd)$ .

The reader should be aware that the existence of consistent Euler paths depends on the way the Boolean expressions (and the corresponding logic graphs) are constructed. For example, no consistent Euler paths can be found for  $\bar{x} = a + b \cdot c + d \cdot e$ , but the function  $\bar{x} = b \cdot c + a + d \cdot e$  has a simple solution (confirm that this is true by preserving the ordering of the function when constructing the logic graphs). A restructuring of the function is sometimes necessary before a set of consistent paths can be identified. This could lead to an exhaustive search over all possible path combinations. Fortunately, a simple algorithm to avoid this plight has been proposed [Uehara81]. A discussion of this is beyond our scope, however, and we refer the interested reader to that text.

Finally, it is worth mentioning that the layout strategies presented are not the only possibilities. For example, sometimes it might be more effective to provide multiple diffusion strips stacked vertically. In this case, a single polysilicon input line can serve as the input for multiple transistors. This might be beneficial for certain gate structures, such as the NXOR gate, and therefore, case-by-case analysis is recommended.

**To Probe Further**

A good overview of cell-generation techniques can be found in [Rubin87, pp. 116–128]. Some of the landmark papers in this area include the following:

[Clein00] D. Clein, *CMOS IC Layout*, Newnes, 2000.

[Rubin87] S. Rubin, *Computer Aids for VLSI Design*, Addison-Wesley, 1987.

[Uehara81] T. Uehara and W. Van Cleemput, "Optimal Layout of CMOS Functional Arrays," *IEEE Trans. on Computers*, vol. C-30, no. 5, pp. 305-311, May 1981.

[Weinberger67] A. Weinberger, "Large Scale Integration of MOS Complex Logic: A Layout Method," *IEEE Journal of Solid State Circuits*, vol. 2, no. 4, pp. 182-190, 1967.

## CHAPTER

# 7

## Designing Sequential Logic Circuits

*Implementation techniques for registers, latches, flip-flops, oscillators, pulse generators, and Schmitt triggers*

*Static versus dynamic realization*

*Choosing clocking strategies*

- 7.1 Introduction
  - 7.1.1 Timing Metrics for Sequential Circuits
  - 7.1.2 Classification of Memory Elements
- 7.2 Static Latches and Registers
  - 7.2.1 The Bistability Principle
  - 7.2.2 Multiplexer-Based Latches
  - 7.2.3 Master–Slave Edge-Triggered Register
  - 7.2.4 Low-Voltage Static Latches
  - 7.2.5 Static SR Flip-Flops—Writing Data by Pure Force
- 7.3 Dynamic Latches and Registers
  - 7.3.1 Dynamic Transmission-Gate Edge-Triggered Registers
  - 7.3.2 C<sup>2</sup>MOS—A Clock-Skew Insensitive Approach
  - 7.3.3 True Single-Phase Clocked Register (TSPCR)
- 7.4 Alternative Register Styles\*
  - 7.4.1 Pulse Registers
  - 7.4.2 Sense-Amplifier-Based Registers
- 7.5 Pipelining: An Approach to Optimize Sequential Circuits
  - 7.5.1 Latch- versus Register-Based Pipelines
  - 7.5.2 NORA–CMOS—A Logic Style for Pipelined Structures



- 7.6 Nonbistable Sequential Circuits
  - 7.6.1 The Schmitt Trigger
  - 7.6.2 Monostable Sequential Circuits
  - 7.6.3 Astable Circuits
- 7.7 Perspective: Choosing a Clocking Strategy
- 7.8 Summary
- 7.9 To Probe Further

## 7.1 Introduction

As described earlier, combinational logic circuits have the property that the output of a logic block is only a function of the *current* input values, assuming that enough time has elapsed for the logic gates to settle. Still, virtually all useful systems require storage of state information, leading to another class of circuits called *sequential logic* circuits. In these circuits, the output depends not only on the *current* values of the inputs, but also on *preceding* input values. In other words, a sequential circuit remembers some of the past history of the system—it has memory.

Figure 7-1 shows a block diagram of a generic *finite-state machine* (FSM) that consists of combinational logic and registers, which hold the system state. The system depicted here belongs to the class of *synchronous* sequential systems, in which all registers are under control of a single global clock. The outputs of the FSM are a function of the current *Inputs* and the *Current State*. The *Next State* is determined based on the *Current State* and the current *Inputs* and is fed to the inputs of registers. On the rising edge of the clock, the *Next State* bits are copied to the outputs of the registers (after some propagation delay), and a new cycle begins. The register then ignores changes in the input signals until the next rising edge. In general, registers can be *positive edge triggered* (where the input data is copied on the rising edge of the clock) or *negative edge triggered* (where the input data is copied on the falling edge, as indicated by a small circle at the clock input).

This chapter discusses the CMOS implementation of the most important sequential building blocks. A variety of choices in sequential primitives and clocking methodologies exist; making the correct selection is getting increasingly important in modern digital circuits, and can

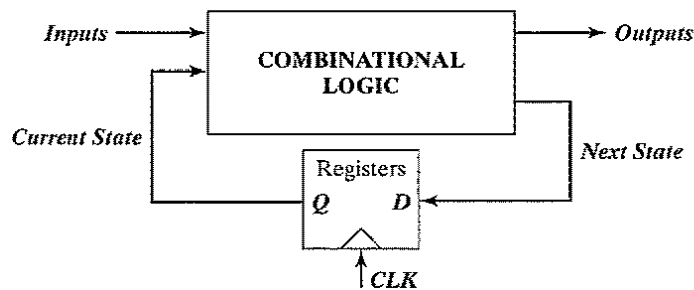


**Figure 7-1** Block diagram of a finite-state machine, using *positive edge-triggered* registers.

have a great impact of performance, power, and/or design complexity. Before embarking on a detailed discussion of the various design options, a review of the relevant design metrics and a classification of the sequential elements is necessary.

### 7.1.1 Timing Metrics for Sequential Circuits

There are three important timing parameters associated with a register. They are shown in Figure 7-2. The *setup time* ( $t_{su}$ ) is the time that the data inputs ( $D$ ) must be valid before the clock transition (i.e., the  $0 \rightarrow 1$  transition for a *positive edge-triggered register*). The *hold time* ( $t_{hold}$ ) is the time the data input must remain valid after the clock edge. Assuming that the *setup* and *hold* times are met, the data at the  $D$  input is copied to the  $Q$  output after a worst case *propagation delay* (with reference to the clock edge) denoted by  $t_{c-q}$ .

Once we know the timing information for the registers and the combinational logic blocks, we can derive the system-level timing constraints (see Figure 7-1 for a simple system view). In synchronous sequential circuits, switching events take place concurrently in response to a clock stimulus. Results of operations await the next clock transitions before progressing to the next stage. In other words, the next cycle cannot begin unless all current computations have completed and the system has come to rest. The *clock period*  $T$ , at which the sequential circuit operates, must thus accommodate the longest delay of any stage in the network. Assume that the worst case propagation delay of the logic equals  $t_{plogic}$ , while its minimum delay—also called the *contamination delay*—is  $t_{cd}$ . The minimum clock period  $T$  required for proper operation of the sequential circuit is given by

$$T \geq t_{c-q} + t_{plogic} + t_{su} \quad (7.1)$$

The *hold time* of the register imposes an extra constraint for proper operation, namely

$$t_{cdregister} + t_{cdlogic} \geq t_{hold} \quad (7.2)$$

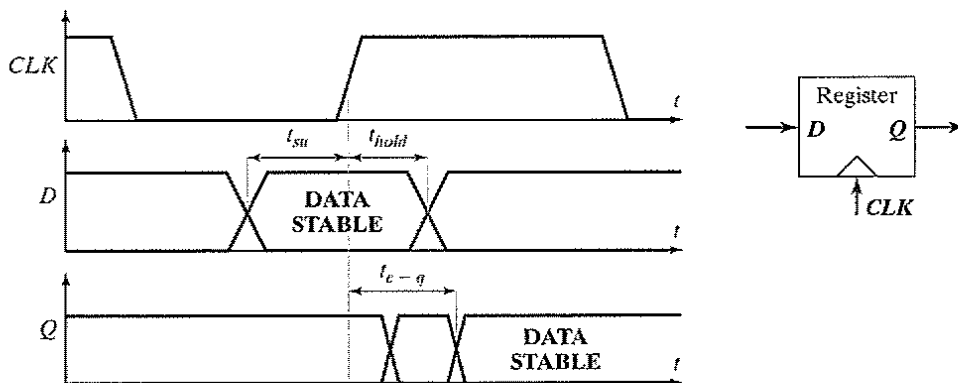


**Figure 7-2** Definition of *setup time*, *hold time*, and *propagation delay* of a synchronous register.

where  $t_{cdregister}$  is the minimum *propagation delay* (or *contamination delay*) of the register. This constraint ensures that the input data of the sequential elements is held long enough after the clock edge and is not modified too soon by the new wave of data coming in.

As seen from Eq. (7.1), it is important to minimize the values of the timing parameters associated with the register, as these directly affect the rate at which a sequential circuit can be clocked. In fact, modern high-performance systems are characterized by a very low logic depth, and the register *propagation delay* and *setup* times account for a significant portion of the clock period. For example, the DEC Alpha EV6 microprocessor [Gieseke97] has a maximum logic depth of 12 gates, and the register overhead stands for approximately 15% of the clock period. In general, the requirement of Eq. (7.2) is not difficult to meet, although it becomes an issue when there is little or no logic between registers.<sup>1</sup>

### 7.1.2 Classification of Memory Elements

#### Foreground versus Background Memory

At a high level, memory is classified into background and foreground memory. Memory that is embedded into logic is *foreground memory* and is most often organized as individual registers or register banks. Large amounts of centralized memory core are referred to as *background memory*. Background memory, discussed in Chapter 12, achieves higher area densities through efficient use of array structures and by trading off performance and robustness for size. In this chapter, we focus on foreground memories.

#### Static versus Dynamic Memory

Memories can be either static or dynamic. Static memories preserve the state as long as the power is turned on. They are built by using *positive feedback* or regeneration, where the circuit topology consists of intentional connections between the output and the input of a combinational circuit. Static memories are most useful when the register will not be updated for extended periods of time. Configuration data, loaded at power-up time, is a good example of static data. This condition also holds for most processors that use conditional clocking (i.e., gated clocks) where the clock is turned off for unused modules. In that case, there are no guarantees on how frequently the registers will be clocked, and static memories are needed to preserve the state information. Memory based on positive feedback falls under the class of elements called *multivibrator circuits*. The *bistable* element is its most popular representative, but other elements such as *monostable* and *astable* circuits also are frequently used.

Dynamic memories store data for a short period of time, perhaps milliseconds. They are based on the principle of temporary *charge storage* on parasitic capacitors associated with MOS devices. As with dynamic logic, discussed earlier, the capacitors have to be refreshed periodically to compensate for charge leakage. Dynamic memories tend to be simpler, resulting in significantly higher performance and lower power dissipation. They are most useful in datapath

---

<sup>1</sup>Or when the clocks at different registers are somewhat out of phase due to clock skew. We discuss this topic in Chapter 10.

circuits that require high performance levels and are periodically clocked. It is possible to use dynamic circuitry even when circuits are conditionally clocked, if the state can be discarded when a module goes into idle mode.

### Latches versus Registers

A latch is an essential component in the construction of an *edge-triggered* register. It is a *level-sensitive* circuit that passes the  $D$  input to the  $Q$  output when the clock signal is high. This latch is said to be in *transparent* mode. When the clock is low, the input data sampled on the falling edge of the clock is held stable at the output for the entire phase, and the latch is in *hold* mode. The inputs must be stable for a short period around the falling edge of the clock to meet setup and hold requirements. A latch operating under these conditions is a *positive latch*. Similarly, a *negative latch* passes the  $D$  input to the  $Q$  output when the clock signal is low. Positive and negative latches are also called *transparent high* or *transparent low*, respectively. The signal waveforms for a positive and negative latch are shown in Figure 7-3. A wide variety of static and dynamic implementations exists for the realization of latches.

Contrary to *level-sensitive* latches, *edge-triggered* registers only sample the input on a clock transition—that is,  $0 \rightarrow 1$  for a *positive edge-triggered* register, and  $1 \rightarrow 0$  for a *negative edge-triggered* register. They are typically built to use the latch primitives of Figure 7-3. An often-recurring configuration is the *master-slave* structure, that cascades a positive and negative latch. Registers also can be constructed by using one-shot generators of the clock signal (“glitch” registers), or by using other specialized structures. Examples of these are shown later in this chapter.

The literature on sequential circuits has been plagued by ambiguous definitions for the different types of storage elements (i.e., register, flip-flop, and latch). To avoid confusion, we adhere strictly to the following set of definitions in this book:

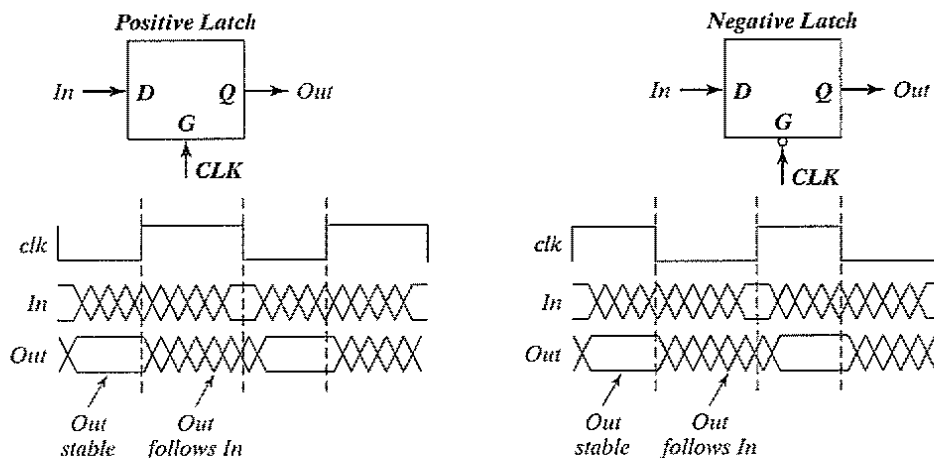


Figure 7-3 Timing of positive and negative latches.

- An *edge-triggered* storage element is called a *register*;
- A *latch* is a *level-sensitive* device;
- and any *bistable* component, formed by the cross coupling of gates, is called a *flip-flop*.<sup>2</sup>

## 7.2 Static Latches and Registers

### 7.2.1 The Bistability Principle

Static memories use positive feedback to create a *bistable circuit*—a circuit having two stable states that represent 0 and 1. The basic idea is shown in Figure 7-4a, which shows two inverters connected in cascade along with a voltage-transfer characteristic typical of such a circuit. Also plotted are the VTCs of the first inverter—that is,  $V_{o1}$  versus  $V_{i1}$ —and the second inverter ( $V_{o2}$  versus  $V_{o1}$ ). The latter plot is rotated to accentuate that  $V_{i2} = V_{o1}$ . Assume now that the output of the second inverter  $V_{o2}$  is connected to the input of the first  $V_{i1}$ , as shown by the dotted lines in Figure 7-4a. The resulting circuit has only three possible operation points (*A*, *B*, and *C*), as demonstrated on the combined VTC. It is easy to prove the validity of the following important conjecture:

**When the gain of the inverter in the transient region is larger than 1, *A* and *B* are the only stable operation points, and *C* is a metastable operation point.**

Suppose that the cross-coupled inverter pair is biased at point *C*. A small deviation from this bias point, possibly caused by noise, is amplified and *regenerated* around the circuit loop.

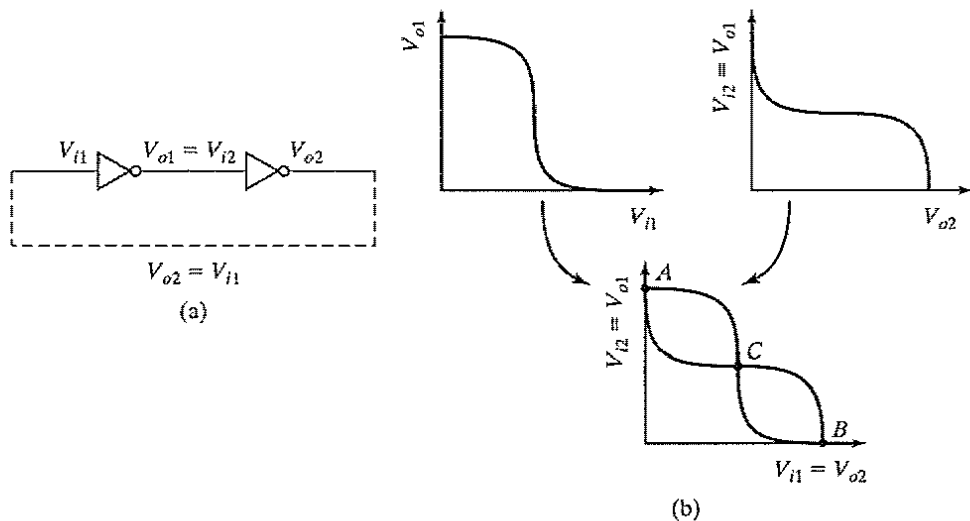


**Figure 7-4** Two cascaded inverters (a) and their VTCs (b).

<sup>2</sup>An edge-triggered register is often referred to as a flip-flop as well. In this text, flip-flop is used to **uniquely** mean bistable element.

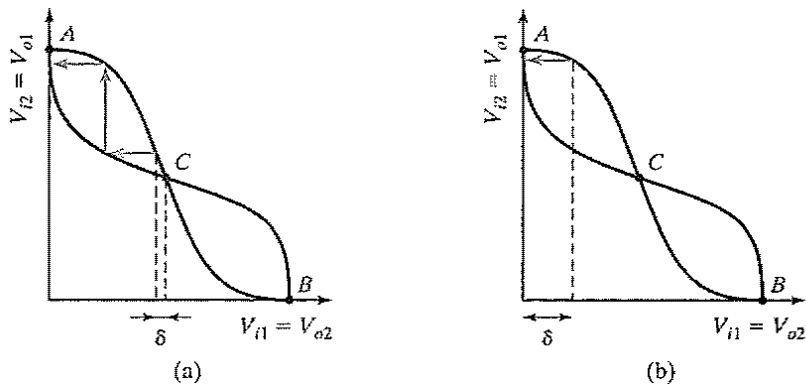


Figure 7-5 Metastable versus stable operation points.

This is a result of the gain around the loop being larger than 1. The effect is demonstrated in Figure 7-5a. A small deviation  $\delta$  is applied to  $V_{i1}$  (biased in C). This deviation is amplified by the gain of the inverter. The enlarged divergence is applied to the second inverter and amplified once more. The bias point moves away from C until one of the operation points A or B is reached. In conclusion, C is an unstable operation point. Every deviation (even the smallest one) causes the operation point to run away from its original bias. The chance is indeed very small that the cross-coupled inverter pair is biased at C and stays there. Operation points with this property are termed *metastable*.

On the other hand, A and B are stable operation points, as demonstrated in Figure 7-5b. In these points, the **loop gain is much smaller than unity**. Even a rather large deviation from the operation point reduces in size and disappears.

Hence, the cross coupling of two inverters results in a *bistable* circuit—that is, a circuit with two stable states, each corresponding to a logic state. The circuit serves as a memory, storing either a 1 or a 0 (corresponding to positions A and B).

In order to change the stored value, we must be able to bring the circuit from state A to B and vice versa. Since the precondition for stability is that the loop gain  $G$  is smaller than unity, we can achieve this by making A (or B) temporarily unstable by increasing  $G$  to a value larger than 1. This is generally done by applying a trigger pulse at  $V_{i1}$  or  $V_{i2}$ . For example, assume that the system is in position A ( $V_{i1} = 0$ ,  $V_{i2} = 1$ ). Forcing  $V_{i1}$  to 1 causes both inverters to be on simultaneously for a short time and the loop gain  $G$  to be larger than 1. The positive feedback regenerates the effect of the trigger pulse, and the circuit moves to the other state (B, in this case). The width of the trigger pulse need be only a little larger than the total propagation delay around the circuit loop, which is twice the average propagation delay of the inverters.

In summary, a bistable circuit has two stable states. In absence of any triggering, the circuit remains in a single state (assuming that the power supply remains applied to the circuit) and thus remembers a value. Another common name for a bistable circuit is *flip-flop*. A flip-flop is useful only if there also exists a means to bring it from one state to the other one. In general, two different approaches may be used to accomplish the following:

- **Cutting the feedback loop.** Once the feedback loop is open, a new value can easily be written into *Out* (or *Q*). Such a latch is called *multiplexer based*, as it realizes that the logic expression for a synchronous latch is identical to the multiplexer equation:

$$Q = \overline{Clk} \cdot Q + Clk \cdot In \quad (7.3)$$

This approach is the most popular in today's latches, and thus forms the bulk of this section.

- **Overpowering the feedback loop.** By applying a trigger signal at the input of the flip-flop, a new value is forced into the cell by overpowering the stored value. A careful sizing of the transistors in the feedback loop and the input circuitry is necessary to make this possible. A weak trigger network may not succeed in overruling a strong feedback loop. This approach used to be in vogue in the earlier days of digital design, but has gradually fallen out of favor. It is, however, the dominant approach to the implementation of static background memories (which we discuss more fully in Chapter 12). A short introduction will be given later in the chapter.

### 7.2.2 Multiplexer-Based Latches

The most robust and common technique to build a latch involves the use of transmission-gate multiplexers. Figure 7-6 shows an implementation of positive and negative static latches based on multiplexers. For a negative latch, input 0 of the multiplexer is selected when the clock is low, and the *D* input is passed to the output. When the clock signal is high, input 1 of the multiplexer, which connects to the output of the latch, is selected. The feedback ensures a stable output as long as the clock is high. Similarly in the positive latch, the *D* input is selected when the clock signal is high, and the output is held (using feedback) when the clock signal is low.

A transistor-level implementation of a positive latch based on multiplexers is shown in Figure 7-7. When *CLK* is high, the bottom transmission gate is on and the latch is transparent—that is, the *D* input is copied to the *Q* output. During this phase, the feedback loop is open, since the top transmission gate is off. Sizing of the transistors therefore is not critical for realizing correct functionality. The number of transistors that the clock drives is an important metric from a power perspective, because the clock has an *activity factor* of 1. This particular latch implemen-

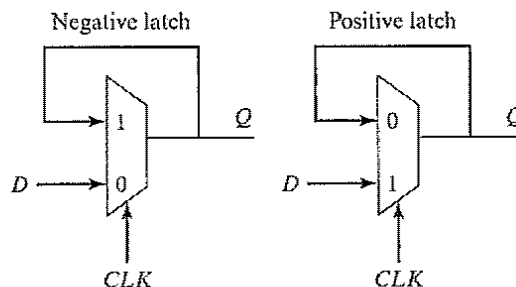
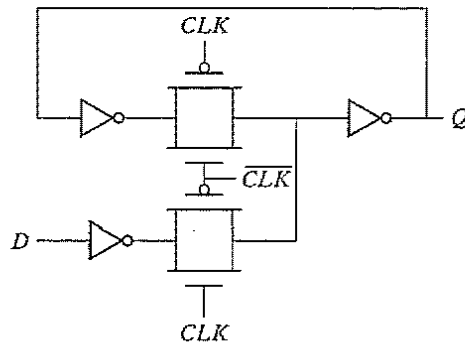
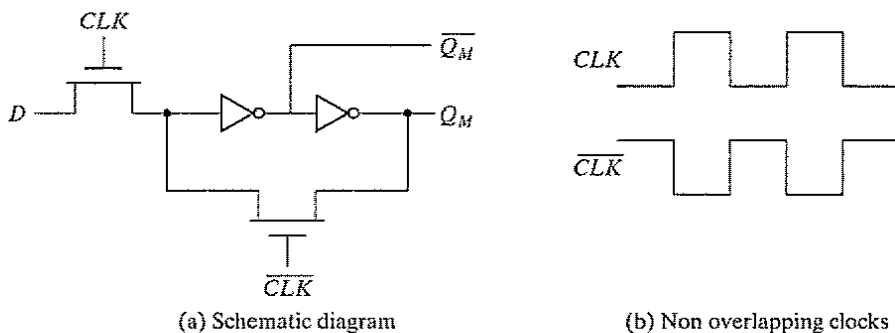


Figure 7-6 Negative and positive latches based on multiplexers.



**Figure 7-7** Transistor-level implementation of a positive latch built by using transmission gates.



**Figure 7-8** Multiplexer-based NMOS latch by using NMOS-only pass transistors for multiplexers.

tation is not very efficient from this perspective: It presents a load of four transistors to the  $CLK$  signal.

It is possible to reduce the clock load to two transistors by implementing multiplexers that use as NMOS-only pass transistors, as shown in Figure 7-8. When  $CLK$  is high, the latch samples the  $D$  input, while a low clock signal enables the feedback loop, and puts the latch in the hold mode. While attractive for its simplicity, the use of NMOS-only pass transistors results in the passing of a degraded high voltage of  $V_{DD} - V_{Th}$  to the input of the first inverter. This impacts both noise margin and the switching performance, especially in the case of low values of  $V_{DD}$  and high values of  $V_{Th}$ . It also causes static power dissipation in the first inverter, because the maximum input voltage to the inverter equals  $V_{DD} - V_{Th}$ , and the PMOS device of the inverter is never fully turned off.

### 7.2.3 Master–Slave Edge-Triggered Register

The most common approach for constructing an *edge-triggered* register is to use a *master–slave* configuration, as shown in Figure 7-9. The register consists of cascading a negative latch (master stage) with a positive one (slave stage). A multiplexer-based latch is used in this particular



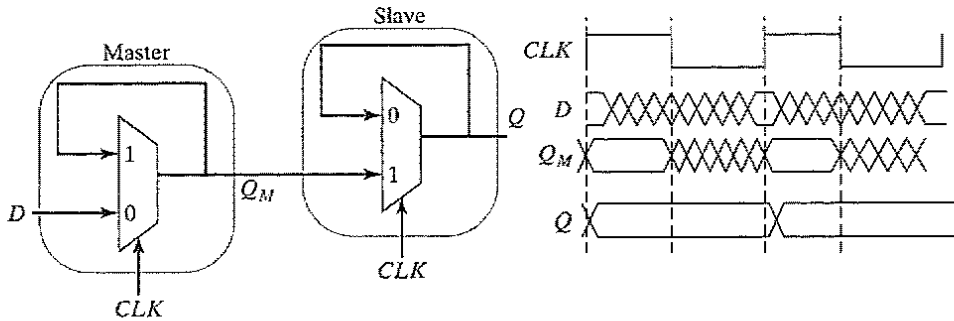


Figure 7-9 Positive edge-triggered register based on a master–slave configuration.

implementation, although any latch could be used. On the low phase of the clock, the master stage is transparent, and the  $D$  input is passed to the master stage output,  $Q_M$ . During this period, the slave stage is in the hold mode, keeping its previous value by using feedback. On the rising edge of the clock, the master stage stops sampling the input, and the slave stage starts sampling. During the high phase of the clock, the slave stage samples the output of the master stage ( $Q_M$ ), while the master stage remains in a hold mode. Since  $Q_M$  is constant during the high phase of the clock, the output  $Q$  makes only one transition per cycle. The value of  $Q$  is the value of  $D$  right before the rising edge of the clock, achieving the *positive edge-triggered* effect. A negative edge-triggered register can be constructed by using the same principle by simply switching the order of the positive and negative latches (i.e., placing the positive latch first).

A complete transistor-level implementation of the master–slave positive edge-triggered register is shown in Figure 7-10. The multiplexer is implemented by using transmission gates as discussed in the previous section. When the clock is low ( $\overline{CLK} = 1$ ),  $T_1$  is on and  $T_2$  is off, and the  $D$  input is sampled onto node  $Q_M$ . During this period,  $T_3$  and  $T_4$  are off and on, respectively. The cross-coupled inverters ( $I_5, I_6$ ) hold the state of the slave latch. When the clock goes high, the master stage stops sampling the input and goes into a hold mode.  $T_1$  is off and  $T_2$  is on, and the cross-coupled inverters  $I_2$  and  $I_3$  hold the state of  $Q_M$ . Also,  $T_3$  is on and  $T_4$  is off, and  $Q_M$  is copied to the output  $Q$ .

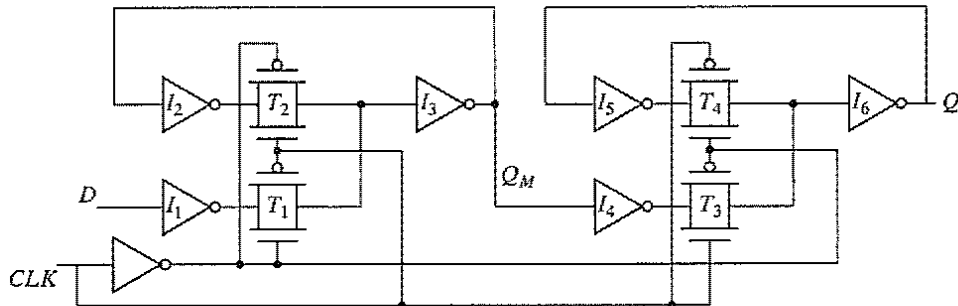


Figure 7-10 Master–slave positive edge-triggered register, using multiplexers.

**Problem 7.1 Optimization of the Master–Slave Register**

It is possible to remove the inverters  $I_1$  and  $I_4$  from Figure 7-10 without loss of functionality. Is there any advantage to including these inverters in the implementation?

**Timing Properties of Multiplexer-Based Master–Slave Registers**

Registers are characterized by three important timing parameters: the setup time, the hold time and the propagation delay. It is important to understand the factors that affect these timing parameters and develop the intuition to manually estimate them. Assume that the propagation delay of each inverter is  $t_{pd\_inv}$ , and the propagation delay of the transmission gate is  $t_{pd\_tx}$ . Also assume that the contamination delay is 0, and that inverter, deriving  $\overline{CLK}$  from  $CLK$ , has a delay of 0 as well.

The setup time is the time before the rising edge of the clock that the input data  $D$  must be valid. This is similar to asking the question, how long before the rising edge of the clock must the  $D$  input be stable such that  $Q_M$  samples the value reliably? For the transmission gate multiplexer-based register, the input  $D$  has to propagate through  $I_1$ ,  $T_1$ ,  $I_3$ , and  $I_2$  before the rising edge of the clock. This ensures that the node voltages on both terminals of the transmission gate  $T_2$  are at the same value. Otherwise, it is possible for the cross-coupled pair  $I_2$  and  $I_3$  to settle to an incorrect value. The setup time is therefore equal to  $3 \times t_{pd\_inv} + t_{pd\_tx}$ .

The propagation delay is the time it takes for the value of  $Q_M$  to propagate to the output  $Q$ . Note that, since we included the delay of  $I_2$  in the setup time, the output of  $I_4$  is valid before the rising edge of the clock. Therefore, the delay  $t_{c-q}$  is simply the delay through  $T_3$  and  $I_6$  ( $t_{c-q} = t_{pd\_tx} + t_{pd\_inv}$ ).

The hold time represents the time that the input must be held stable after the rising edge of the clock. In this case, the transmission gate  $T_1$  turns off when the clock goes high. Since both the  $D$  input and the CLK pass through inverters before reaching  $T_1$ , any changes in the input after the clock goes high do not affect the output. Therefore, the hold time is 0.

**Example 7.1 Timing Analysis, Using SPICE**

To obtain the setup time of the register while using SPICE, we progressively skew the input with respect to the clock edge until the circuit fails. Figure 7-11 shows the setup-time simulation assuming a skew of 210 ps and 200 ps. For the 210 ps case, the correct value of input  $D$  is sampled (in this case, the  $Q$  output remains at the value of  $V_{DD}$ ). For a skew of 200 ps, an incorrect value propagates to the output, as the  $Q$  output transitions to 0. Node  $Q_M$  starts to go high, and the output of  $I_2$  (the input to transmission gate  $T_2$ ) starts to fall. However, the clock is enabled before the two nodes across the transmission gate  $T_2$  settle to the same value. This results in an incorrect value being written into the master latch. The setup time for this register is 210 ps.

In a similar fashion, the hold time can be simulated. The  $D$ -input edge is once again skewed relative to the clock signal until the circuit stops functioning. For this design, the

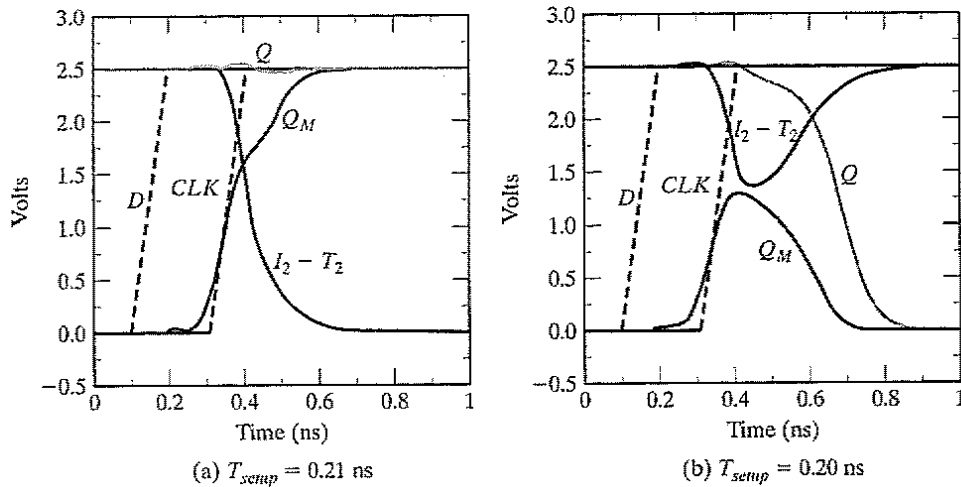


Figure 7-11 Setup time simulation.

hold time is 0 (i.e., the inputs can be changed on the clock edge). Finally, for the propagation delay, the inputs transition at least one setup time before the rising edge of the clock, and the delay is measured from the 50% point of the *CLK* edge to the 50% point of the *Q* output. From this simulation (Figure 7-12),  $t_{c-q(th)}$  was 160 ps, and  $t_{c-q(hl)}$  was 180 ps.

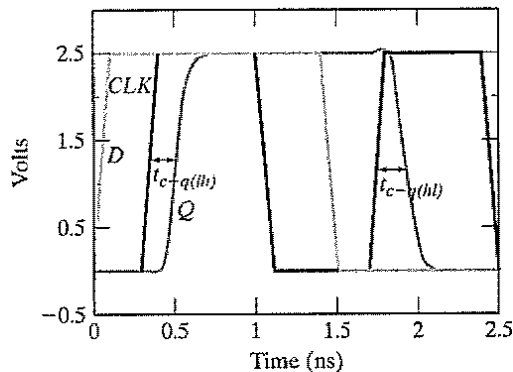


Figure 7-12 Simulation of propagation delay of transmission gate register.

The drawback of the transmission-gate register is the high capacitive load presented to the clock signal. The clock load per register is important, since it directly impacts the power dissipation of the clock network. Ignoring the overhead required to invert the clock signal—since the inverter overhead can be amortized over multiple register bits—each register has a clock load of eight transistors. One approach to reduce the clock load at the cost of robustness is to make the circuit

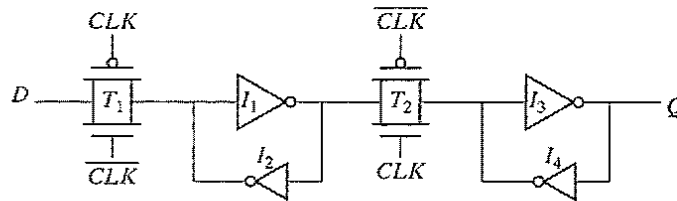


Figure 7-13 Reduced load clock load static master-slave register.

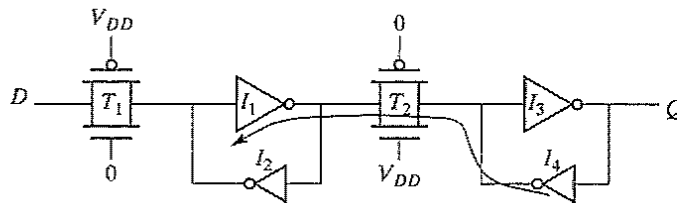


Figure 7-14 Reverse conduction possible in the transmission gate.

ratioed. Figure 7-13 shows that the feedback transmission gate can be eliminated by directly cross-coupling the inverters.

The penalty paid for the reduced in clock load is an increased design complexity. The transmission gate ( $T_1$ ) and its source driver must overpower the feedback inverter ( $I_2$ ) to switch the state of the cross-coupled inverter. The sizing requirements for the transmission gates can be derived by using an analysis similar to the one used for the sizing of the level-restoring device in Chapter 6. The input to the inverter  $I_1$  must be brought below its switching threshold in order to make a transition. If minimum-sized devices are to be used in the transmission gates, it is essential that the transistors of inverter  $I_2$  should be made even weaker. This can be accomplished by making their channel lengths larger than minimum. Using minimum or close-to-minimum size devices in the transmission gates is desirable to reduce the power dissipation in the latches and the clock distribution network.

Another problem with this scheme is *reverse conduction*—the second stage can affect the state of the first latch. When the slave stage is on (Figure 7-14), it is possible for the combination of  $T_2$  and  $I_4$  to influence the data stored in the  $I_1$ - $I_2$  latch. As long as  $I_4$  is a weak device, this fortunately not a major problem.

### Non-Ideal Clock Signals

So far, we have assumed that  $\overline{CLK}$  is a perfect inversion of  $CLK$ , or in other words, that the delay of the generating inverter is zero. Even if this were possible, this still would not be a good assumption. Variations can exist in the wires used to route the two clock signals, or the load capacitances can vary based on data stored in the connecting latches. This effect, known as *clock skew*, is a major problem, causing the two clock signals to overlap, as shown in Figure 7-15b. *Clock overlap* can cause two types of failures, which we illustrate for the NMOS-only negative master-slave register of Figure 7-15a.

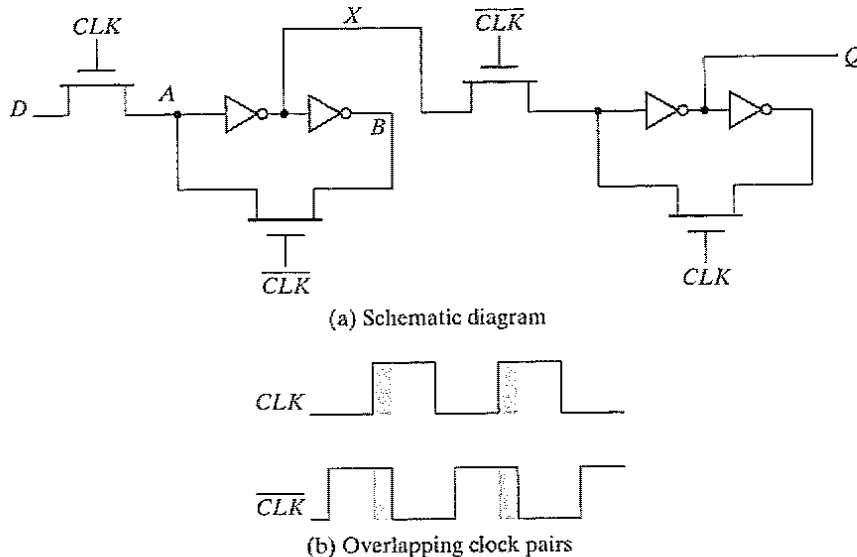


**Figure 7-15** Master-slave register based on NMOS-only pass transistors.

1. When the clock goes high, the slave stage should stop sampling the master stage output and go into a hold mode. However, since  $CLK$  and  $\overline{CLK}$  are both high for a short period of time (the *overlap period*), both sampling pass transistors conduct, and there is a direct path from the  $D$  input to the  $Q$  output. As a result, data at the output can change on the rising edge of the clock, which is undesired for a negative edge-triggered register. This is known as a *race condition* in which the value of the output  $Q$  is a function of whether the input  $D$  arrives at node  $X$  before or after the falling edge of  $\overline{CLK}$ . If node  $X$  is sampled in the metastable state, the output will switch to a value determined by noise in the system.
2. The primary advantage of the multiplexer-based register is that the feedback loop is open during the sampling period, and therefore the sizing of the devices is not critical to functionality. However, if there is clock overlap between  $CLK$  and  $\overline{CLK}$ , node  $A$  can be driven by both  $D$  and  $B$ , resulting in an undefined state.

These problems can be avoided by using two *nonoverlapping clocks* instead,  $PHI_1$  and  $PHI_2$  (Figure 7-16), and by keeping the nonoverlap time  $t_{non\_overlap}$  between the clocks large enough so that no overlap occurs even in the presence of clock-routing delays. During the nonoverlap time, the  $FF$  is in the high-impedance state—the feedback loop is open, the loop gain is zero, and the input is disconnected. Leakage will destroy the state if this condition holds for too long—hence the name *pseudostatic*: The register employs a combination of static and dynamic storage approaches, depending upon the state of the clock.

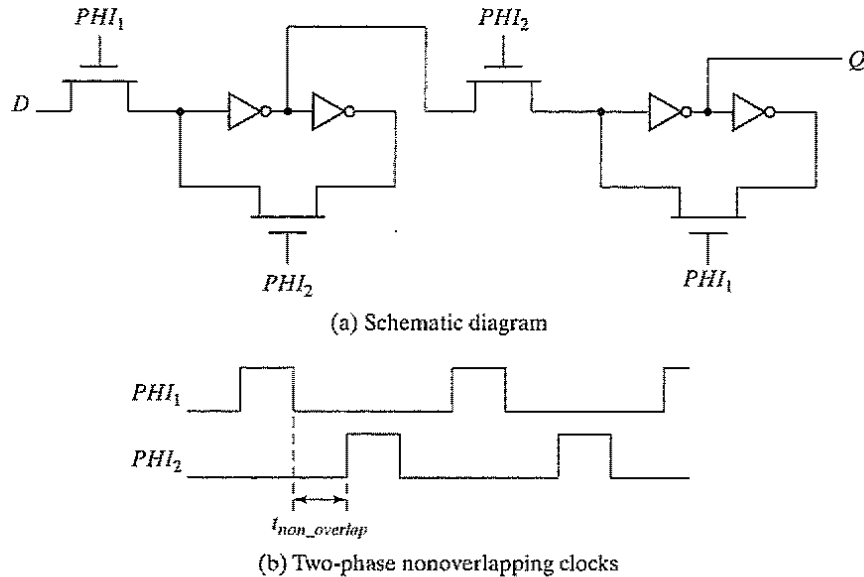


Figure 7-16 Pseudostatic two-phase  $D$  register.

### Problem 7.2 Generating Nonoverlapping Clocks

Figure 7-17 shows one possible implementation of the clock generation circuitry for generating a two-phase nonoverlapping clock. Assuming that each gate has a unit gate delay, derive the timing relationship between the input clock and the two output clocks. What is the nonoverlap period? How can this period be increased if needed?

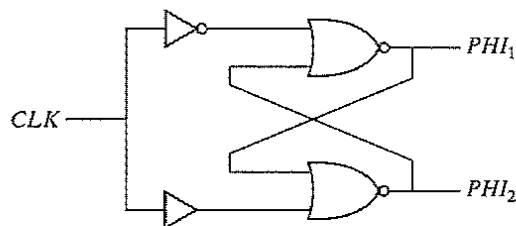


Figure 7-17 Circuitry for generating a two-phase nonoverlapping clock.

### 7.2.4 Low-Voltage Static Latches

The scaling of supply voltages is critical for low-power operation. Unfortunately, certain latch structures do not function at reduced supply voltages. For example, without the scaling of device thresholds, NMOS-only pass transistors (e.g., Figure 7-16) don't scale well with supply voltage

due to its inherent threshold drop. At very low power supply voltages, the input to the inverter cannot be raised above the switching threshold, resulting in incorrect evaluation. Even with the use of transmission gates, performance degrades significantly at reduced supply voltages.

Scaling to low supply voltages thus requires the use of reduced threshold devices. However, this has the negative effect of exponentially increasing the subthreshold leakage power (as discussed in Chapter 6). When the registers are constantly accessed, the leakage energy typically is insignificant compared with the switching power. However, with the use of conditional clocks, it is possible that registers are idle for extended periods, and the leakage energy expended by registers can be quite significant.

Many solutions are being explored to address the problem of high leakage during idle periods. One approach involves the use of Multiple Threshold devices, as shown in Figure 7-18 [Mutoh95]. Only the negative latch is shown. The shaded inverters and transmission gates are implemented in low-threshold devices. The low-threshold inverters are gated by using high-threshold devices to eliminate leakage.

During the normal mode of operation, the sleep devices are turned on. When the clock is low, the  $D$  input is sampled and propagates to the output. The latch is in the hold mode when the clock is high. The feedback transmission gate conducts and the cross-coupled feedback is enabled. An extra inverter, in parallel with the low-threshold one, is added to store the state when the latch is in *idle* (or *sleep*) mode. Then, the high-threshold devices in series with the low-threshold inverter are turned off (the  $SLEEP$  signal is high), eliminating leakage. It is assumed that clock

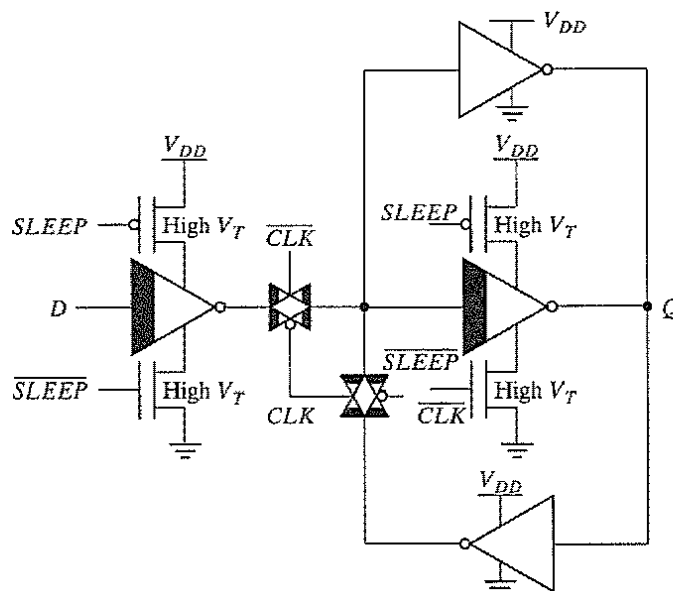


Figure 7-18 Solving the leakage problem, using multiple-threshold CMOS.

is held high when the latch is in the sleep state. The feedback low-threshold transmission gate is turned on and the cross-coupled high-threshold devices maintain the state of the latch.

### Problem 7.3 Transistor Minimization in the MTCMOS Register

Unlike combinational logic, both NMOS and PMOS high-threshold devices are required to eliminate the leakage in low-threshold latches. Explain why this is the case.

Hint: Eliminate the high- $V_T$  NMOS or high- $V_T$  PMOS of the low-threshold inverter on the right of Figure 7-18, and investigate potential leakage paths.

## 7.2.5 Static SR Flip-Flops—Writing Data by Pure Force

The traditional way of causing a bistable element to change state is to overpower the feedback loop. The simplest incarnation accomplishing this is the well-known *SR*, or *set-reset, flip-flop*, an implementation of which is shown in Figure 7-19a. This circuit is similar to the cross-coupled inverter pair with NOR gates replacing the inverters. The second input of the NOR gates is connected to the trigger inputs (*S* and *R*) that make it possible to force the outputs *Q* and  $\bar{Q}$  to a given state. These outputs are complimentary (except for the  $SR = 11$  state). When both *S* and *R* are 0, the flip-flop is in a quiescent state and both outputs retain their values. (A NOR gate with one of its inputs being 0 looks like an inverter, and the structure looks like a cross-coupled inverter.) If a positive (or 1) pulse is applied to the *S* input, the *Q* output is forced into the 1 state (with  $\bar{Q}$  going to 0) and vice versa: A 1-pulse on *R* resets the flip-flop, and the *Q* output goes to 0.

These results are summarized in the *characteristic table* of the flip-flop, shown in Figure 7-19c. The characteristic table is the truth table of the gate and lists the output states as functions of all possible input conditions. When both *S* and *R* are high, both *Q* and  $\bar{Q}$  are forced to zero. Since this does not correspond with our constraint that *Q* and  $\bar{Q}$  must be complementary, this input mode is considered forbidden. An additional problem with this condition is that when the input triggers return to their zero levels, the resulting state of the latch is unpredictable, and depends on whatever input is last to go low. Finally, Figure 7-19b shows the schematic symbol of the *SR* flip-flop.

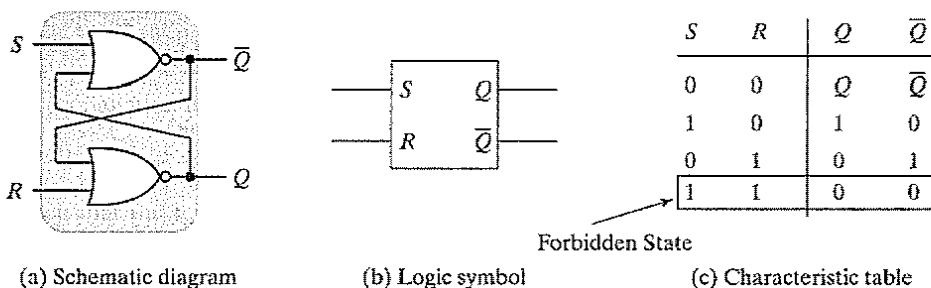
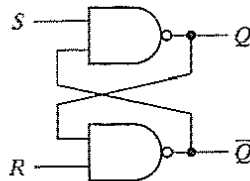


Figure 7-19 NOR-based *SR* flip-flop.



**Problem 7.4 SR Flip-Flop, Using NAND Gates**

An SR flip-flop can also be implemented by using a cross-coupled NAND structure, as shown in Figure 7-20. Derive the truth table for a such an implementation.



**Figure 7-20** NAND-based SR flip-flop.

The SR flip-flop shown so far is purely asynchronous, which does not match well with the synchronous design methodology, the preferred strategy for more than 99% of today's integrated circuits. A clocked version of the latch is shown in Figure 7-21. It consists of a cross-coupled inverter pair, plus four extra transistors to drive the flip-flop from one state to another, and to provide synchronization. In steady state, one inverter resides in the high state, while the other one is low. No static paths between  $V_{DD}$  and GND exist. Transistor sizing is, however, essential to ensure that the flip-flop can transition from one state to the other when requested.

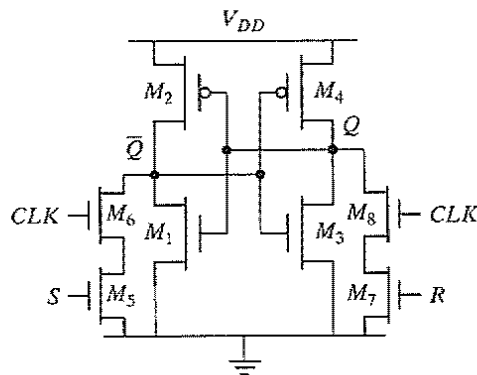


**Figure 7-21** Ratioed CMOS SR latch.

**Example 7.2 Transistor Sizing of Clocked SR Latch**

Consider the case in which  $Q$  is high and an  $R$  pulse is applied. In order to make the latch switch, we must succeed in bringing  $Q$  below the switching threshold of the inverter  $M_1$ – $M_2$ . Once this is achieved, the positive feedback causes the flip-flop to invert states. This requirement forces us to increase the sizes of transistors  $M_5$ ,  $M_6$ ,  $M_7$ , and  $M_8$ . The combination of transistors  $M_4$ ,  $M_7$ , and  $M_8$  forms a ratioed inverter. Assume that the cross-coupled inverter pair is designed such that the inverter threshold  $V_M$  is located at  $V_{DD}/2$ . For a 0.25- $\mu\text{m}$  CMOS technology, the following transistor sizes

were selected:  $(W/L)_{M_1} = (W/L)_{M_3} = (0.5 \mu\text{m}/0.25 \mu\text{m})$ , and  $(W/L)_{M_2} = (W/L)_{M_4} = (1.5 \mu\text{m}/0.25 \mu\text{m})$ . Assuming  $Q = 0$ , we determine the minimum sizes of  $M_5$ ,  $M_6$ ,  $M_7$ , and  $M_8$  to make the device switchable.

To switch the latch from the  $Q = 0$  to the  $Q = 1$  state, it is essential that the low level of the ratioed, pseudo-NMOS inverter  $(M_5-M_6)-M_2$  be below the switching threshold of the inverter  $M_3-M_4$  that equals  $V_{DD}/2$ . It is reasonable to assume that as long as  $V_{\bar{Q}} > V_M$ ,  $V_Q$  equals 0 and the gate of transistor  $M_2$  is grounded. The boundary conditions on the transistor sizes can be derived by equating the currents in the inverter for  $V_{\bar{Q}} = V_{DD}/2$ , as given in Eq. (7.4) (this ignores channel-length modulation). The currents are determined by the saturation current, since  $V_S = V_{DD} = 2.5 \text{ V}$  and  $V_M = 1.25 \text{ V}$ . We assume that  $M_5$  and  $M_6$  have identical sizes and that  $W/L_{5-6}$  is the effective ratio of the series-connected devices. Under this condition, the pull-down network can be modeled by a single transistor  $M_{5-6}$ , whose length is twice the length of the individual devices:

$$k'_n \left( \frac{W}{L} \right)_{5-6} \left( (V_{DD} - V_{Tn}) V_{DSATn} - \frac{V_{DSATn}^2}{2} \right) = -k'_p \left( \frac{W}{L} \right)_2 \left( (-V_{DD} - V_{Tp}) V_{DSATp} - \frac{V_{DSATp}^2}{2} \right) \quad (7.4)$$

Using the parameters for the 0.25- $\mu\text{m}$  process, Eq. (7.4) results in the constraint that the effective  $(W/L)_{M_{5-6}} \geq 2.26$ . This implies that the individual device ratio for  $M_5$  or  $M_6$  must be larger than approximately 4.5. Figure 7-22a shows the DC plot of  $V_{\bar{Q}}$  as a function of the individual device sizes of  $M_5$  and  $M_6$ . We notice that the individual device ratio of greater than 3 is sufficient to bring the  $\bar{Q}$  voltage to the inverter switching threshold. The difference between the manual analysis and simulation arises from second-order effects

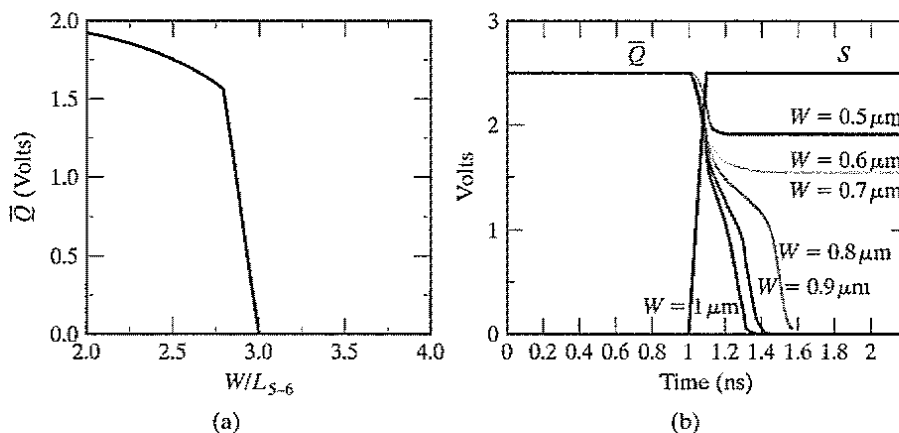


**Figure 7-22** Sizing issues for SR flip-flop. (a) DC output voltage versus pull-down device size  $M_{5-6}$  (with  $W/L_2 = 1.5 \mu\text{m}/0.25 \mu\text{m}$ ). (b) Transient response showing that  $M_5$  and  $M_6$  must each have a  $W/L$  larger than 3 to switch the SR flip-flop.

such as channel length modulation and DIBL. Figure 7-22b plots the transient response for different device sizes and confirms that an individual  $W/L$  ratio of greater than 3 is required to overpower the feedback and switch the state of the latch.

### 7.3 Dynamic Latches and Registers

Storage in a static sequential circuit relies on the concept that a cross-coupled inverter pair produces a bistable element and can thus be used to memorize binary values. This approach has the useful property that a stored value remains valid as long as the supply voltage is applied to the circuit—hence the name *static*. The major disadvantage of the static gate, however, is its complexity. When registers are used in computational structures that are constantly clocked (such as a pipelined datapath), the requirement that the memory should hold state for extended periods of time can be significantly relaxed.

This results in a class of circuits based on temporary storage of charge on parasitic capacitors. The principle is exactly identical to the one used in dynamic logic—charge stored on a capacitor can be used to represent a logic signal. The absence of charge denotes a 0, while its presence stands for a stored 1. No capacitor is ideal, unfortunately, and some charge leakage is always present. A stored value can thus only be kept for a limited amount of time, typically in the range of milliseconds. If one wants to preserve signal integrity, a periodic *refresh* of the value is necessary; hence, the name *dynamic* storage. Reading the value of the stored signal from a capacitor without disrupting the charge requires the availability of a device with a high-input impedance.

#### 7.3.1 Dynamic Transmission-Gate Edge-Triggered Registers

A fully dynamic positive edge-triggered register based on the master–slave concept is shown in Figure 7-23. When  $CLK = 0$ , the input data is sampled on storage node 1, which has an equivalent capacitance of  $C_1$ , consisting of the gate capacitance of  $I_1$ , the junction capacitance of  $T_1$ , and the overlap gate capacitance of  $T_1$ . During this period, the slave stage is in a hold mode, with node 2 in a high-impedance (floating) state. On the rising edge of clock, the transmission gate  $T_2$  turns on, and the value sampled on node 1 right before the rising edge propagates to the output  $Q$  (note that node 1 is stable during the high phase of the clock, since the first transmission gate is

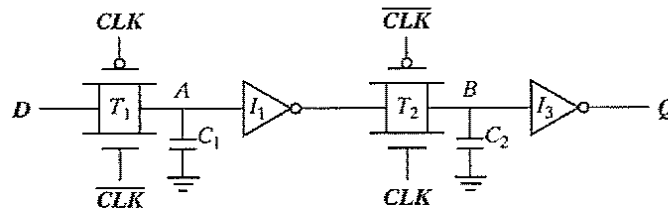


Figure 7-23 Dynamic edge-triggered register.

turned off). Node 2 now stores the inverted version of node 1. This implementation of an edge-triggered register is very efficient because it requires only eight transistors. The sampling switches can be implemented using NMOS-only pass transistors, resulting in an even simpler six transistor implementation. The reduced transistor count is attractive for high-performance and low-power systems.

The setup time of this circuit is simply the delay of the transmission gate, and it corresponds to the time it takes node 1 to sample the  $D$  input. The hold time is approximately zero, since the transmission gate is turned off on the clock edge and further inputs changes are ignored. The propagation delay ( $t_{c-q}$ ) is equal to two inverter delays plus the delay of the transmission gate  $T_2$ .

One important consideration for such a dynamic register is that the storage nodes (i.e., the state) have to be refreshed at periodic intervals to prevent losses due to charge leakage, diode leakage, or subthreshold currents. In datapath circuits, the refresh rate is not an issue, since the registers are periodically clocked, and the storage nodes are constantly updated.

Clock overlap is an important concern for this register. Consider the clock waveforms shown in Figure 7-24. During the 0–0 overlap period, the NMOS of  $T_1$  and the PMOS of  $T_2$  are simultaneously on, creating a direct path for data to flow from the  $D$  input of the register to the  $Q$  output. In other words, a *race condition* occurs. The output  $Q$  can change on the falling edge if the overlap period is large—obviously an undesirable effect for a positive edge-triggered register. The same is true for the 1–1 overlap region, where an input-output path exists through the PMOS of  $T_1$  and the NMOS of  $T_2$ . The latter case is taken care of by enforcing a *hold time* constraint. That is, the data must be stable during the high-overlap period. The former situation (0–0 overlap) can be addressed by making sure that there is enough delay between the  $D$  input and node  $B$ , ensuring that new data sampled by the master stage does not propagate through to the slave stage. Generally, the built-in single inverter delay should be sufficient. The overlap period constraint is given by

$$t_{\text{overlap}0-0} < t_{T1} + t_{f1} + t_{T2} \quad (7.5)$$

Similarly, the constraint for the 1–1 overlap is given as:

$$t_{\text{hold}} > t_{\text{overlap}1-1} \quad (7.6)$$

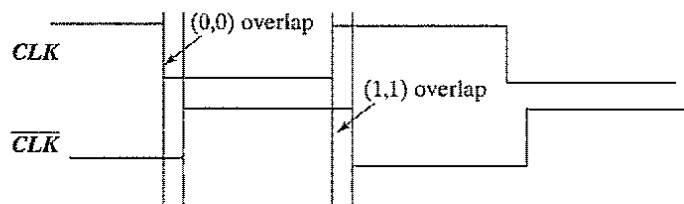


Figure 7-24 Impact of nonoverlapping clocks.

**WARNING:** The dynamic circuits shown in this section are very appealing from the perspective of complexity, performance, and power. Unfortunately, robustness considerations limit their use. In a fully dynamic circuit like that shown in Figure 7-23, a signal net that is capacitively coupled to the internal storage node can inject significant noise and destroy the state. This is especially important in ASIC flows, where there is little control over coupling between signal nets and internal dynamic nodes. Leakage currents cause another problem: Most modern processors require that the clock can be slowed down or completely halted, to conserve power in low-activity periods. Finally, the internal dynamic nodes do not track variations in power supply voltage. For example, when  $CLK$  is high for the circuit in Figure 7-23, node  $A$  holds its state, but it does not track variations in the power supply seen by  $I_1$ . This results in reduced noise margins.

Most of these problems can be adequately addressed by adding a weak feedback inverter and making the circuit *pseudostatic* (Figure 7-25). While this comes at a slight cost in delay, it improves the noise immunity significantly. Unless registers are used in a highly-controlled environment (for instance, a custom-designed high-performance datapath), they should be made pseudostatic or static. This holds for all latches and registers discussed in this section.

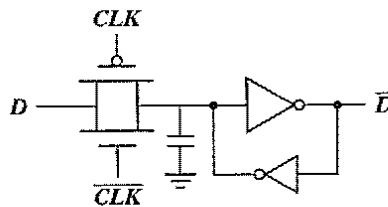


Figure 7-25 Making a dynamic latch pseudostatic.

### 7.3.2 C<sup>2</sup>MOS—A Clock-Skew Insensitive Approach

#### The C<sup>2</sup>MOS Register

Figure 7-26 shows an ingenious positive edge-triggered register that is based on a master–slave concept insensitive to clock overlap. This circuit is called the *C<sup>2</sup>MOS* (Clocked CMOS) register [Suzuki73], and operates in two phases:

1.  $CLK = 0$  ( $\overline{CLK} = 1$ ): The first tristate driver is turned on, and the master stage acts as an inverter sampling the inverted version of  $D$  on the internal node  $X$ . The master stage is in the evaluation mode. Meanwhile, the slave section is in a high-impedance mode, or in a hold mode. Both transistors  $M_7$  and  $M_8$  are off, decoupling the output from the input. The output  $Q$  retains its previous value stored on the output capacitor  $C_{L2}$ .
2. The roles are reversed when  $CLK = 1$ : The master stage section is in hold mode ( $M_3$ – $M_4$  off), while the second section evaluates ( $M_7$ – $M_8$  on). The value stored on  $C_{L1}$  propagates to the output node through the slave stage, which acts as an inverter.

The overall circuit operates as a positive edge-triggered master–slave register very similar to the transmission-gate-based register presented earlier. However, there is an important difference:

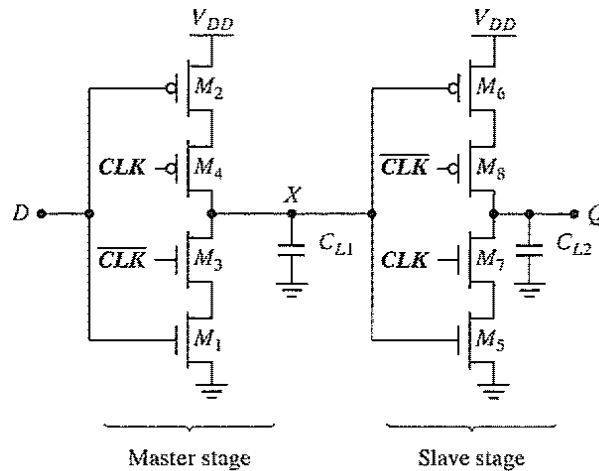


Figure 7-26 C<sup>2</sup>MOS master-slave positive edge-triggered register.

**A C<sup>2</sup>MOS register with  $CLK-\overline{CLK}$  clocking is insensitive to overlap, as long as the rise and fall times of the clock edges are sufficiently small.**

To prove this statement, we examine both the (0-0) and (1-1) overlap cases (see Figure 7-24). In the (0-0) overlap case, the circuit simplifies to the network shown in Figure 7-27a in which both PMOS devices are *on* during this period. To operate correctly, none of the new data sampled during the overlap window should propagate to the output  $Q$ , since data should not change on the negative edge of a positive edge-triggered register. Indeed, new data is sampled on node  $X$  through the series PMOS devices  $M_2$ - $M_4$ , and node  $X$  can make a 0-to-1 transition during the overlap period. However, this data cannot propagate to the output since the NMOS device  $M_7$  is turned off. At the end of the overlap period,  $\overline{CLK} = 1$  and both  $M_7$  and  $M_8$  turn off, putting the slave stage in the hold mode. Therefore, any new data sampled on the falling clock edge is not seen at the slave output  $Q$ , since the slave state is off till the next rising edge of the clock. As the circuit consists of a cascade of inverters, signal propagation requires one pull-up followed by a pull-down, or vice versa, which is not feasible in the situation presented.

The (1-1) overlap case where both NMOS devices  $M_3$  and  $M_7$  are turned on, is somewhat more contentious (see Figure 7-27b). The question is again if new data sampled during the overlap period (right after clock goes high) propagates to the  $Q$  output. A positive edge-triggered register may only pass data that is presented at the input before the rising edge. If the  $D$  input changes during the overlap period, node  $X$  can make a 1-to-0 transition, but cannot propagate further. However, as soon as the overlap period is over, the PMOS  $M_8$  turns on and the 0 propagates to output, which is not desirable. The problem is fixed by imposing a hold-time constraint on the input data,  $D$ ; or, in other words, the data  $D$  should be stable during the overlap period.

In sum, it can be stated that the C<sup>2</sup>MOS latch is insensitive to clock overlaps because those overlaps activate either the pull-up or the pull-down networks of the latches, but never both of them simultaneously. If the rise and fall times of the clock are sufficiently slow, however, there

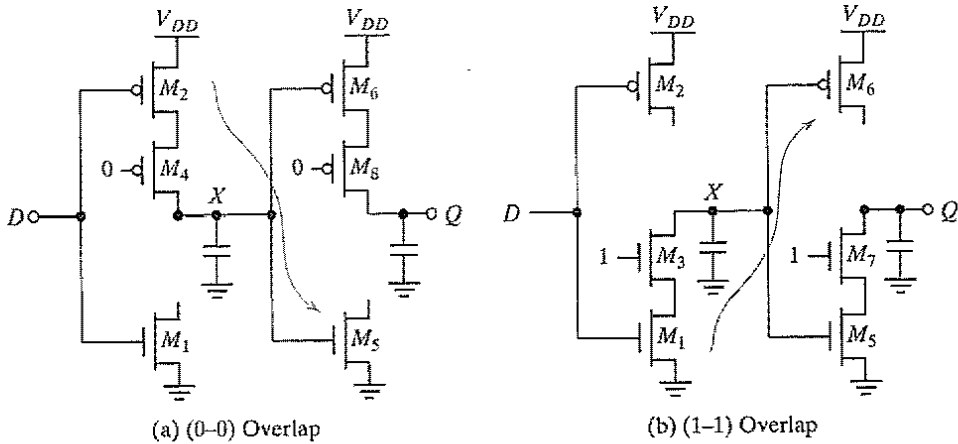


**Figure 7-27** C<sup>2</sup>MOS D FF during overlap periods. No feasible signal path can exist between *in* and *D*, as illustrated by the arrows.

exists a time slot where both the NMOS and PMOS transistors are conducting. This creates a path between input and output that can destroy the state of the circuit. Simulations have shown that the circuit operates correctly as long as the clock rise time (or fall time) is smaller than approximately five times the propagation delay of the register. This criterion is not too stringent, and it is easily met in practical designs. The impact of the rise and fall times is illustrated in Figure 7-28, which plots the simulated transient response of a C<sup>2</sup>MOS D FF for clock slopes of, respectively, 0.1 and 3 ns. For slow clocks, the potential for a *race condition* exists.

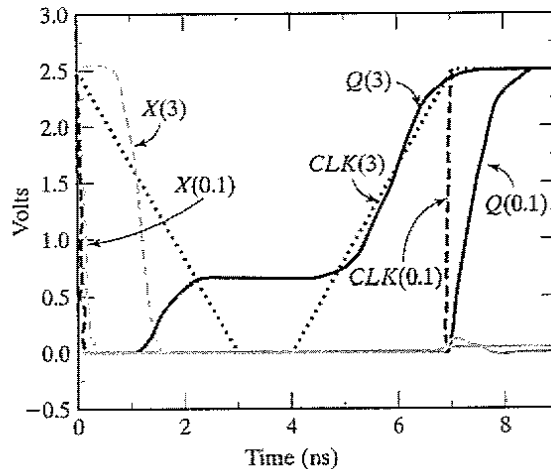


**Figure 7-28** Transient response of C<sup>2</sup>MOS FF for 0.1-ns and 3-ns clock rise/fall times, assuming *ln* = 1.

### Dual-Edge Registers

So far, we have focused on edge-triggered registers that sample the input data on only one of the clock edges (rising or falling). It also is possible to design sequential circuits that sample the input on both edges. The advantage of this scheme is that a lower frequency clock—half the original rate—is distributed for the same functional throughput, resulting in power savings in the clock distribution network. Figure 7-29 shows a modification of the C<sup>2</sup>MOS register enabling sampling on both edges. It consists of two parallel master–slave edge-triggered registers, whose outputs are multiplexed by using tristate drivers.

When clock is high, the positive latch composed of transistors  $M_1$ – $M_4$  is sampling the inverted  $D$  input on node  $X$ . Node  $Y$  is held stable, since devices  $M_9$  and  $M_{10}$  are turned off. On the falling edge of the clock, the top slave latch  $M_5$ – $M_8$  turns on, and drives the inverted value of  $X$  to the  $Q$  output. During the low phase, the bottom master latch ( $M_1, M_4, M_9, M_{10}$ ) is turned on, sampling the inverted  $D$  input on node  $Y$ . Note that the devices  $M_1$  and  $M_4$  are reused, reducing the load on the  $D$  input. On the rising edge, the bottom slave latch conducts and drives the inverted version of  $Y$  on node  $Q$ . Data thus changes on both edges. Note that the slave latches operate in a complementary fashion—that is, only one of them is turned on during each phase of the clock.

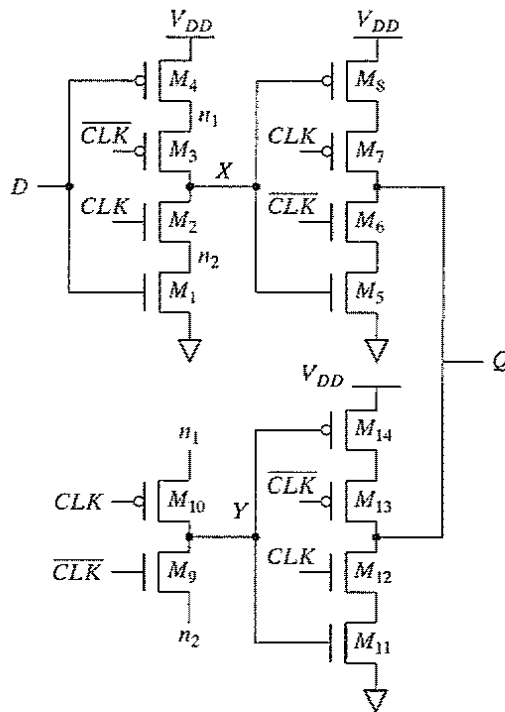


Figure 7-29 C<sup>2</sup>MOS-based dual-edge triggered register.



**Problem 7.5 Dual-Edge Registers**

Determine how the adoption of dual-edge registers influences the power dissipation in the clock-distribution network.

**7.3.3 True Single-Phase Clocked Register (TSPCR)**

In the two-phase clocking schemes described earlier, care must be taken in routing the two clock signals to ensure that overlap is minimized. While the  $C^2$ MOS provides a skew-tolerant solution, it is possible to design registers that only use a single phase clock. The *True Single-Phase Clocked Register (TSPCR)*, proposed by Yuan and Svensson, uses a **single clock** [Yuan89]. The basic single-phase positive and negative latches are shown in Figure 7-30. For the positive latch, when  $CLK$  is high, the latch is in the transparent mode and corresponds to two cascaded inverters; the latch is noninverting, and propagates the input to the output. On the other hand, when  $CLK = 0$ , both inverters are disabled, and the latch is in hold mode. Only the pull-up networks are still active, while the pull-down circuits are deactivated. As a result of the dual-stage approach, no signal can ever propagate from the input of the latch to the output in this mode. A register can be constructed by cascading positive and negative latches. The clock load is similar to a conventional transmission gate register, or  $C^2$ MOS register. The main advantage is the use of a single clock phase. The disadvantage is the slight increase in the number of transistors—12 transistors are now required.

As a reminder, note that a dynamic circuit in the style of Figure 7-30 must be used with caution. When the clock is low (for the positive latch), the output node may be floating, and it is exposed to coupling from other signals. Also, charge sharing can occur if the output node drives transmission gates. Dynamic nodes should be isolated with the aid of static inverters, or made pseudostatic for improved noise immunity.

As with many other latch families, TSPC offers an additional advantage that we have not explored so far: The possibility of embedding logic functionality into the latches. This reduces

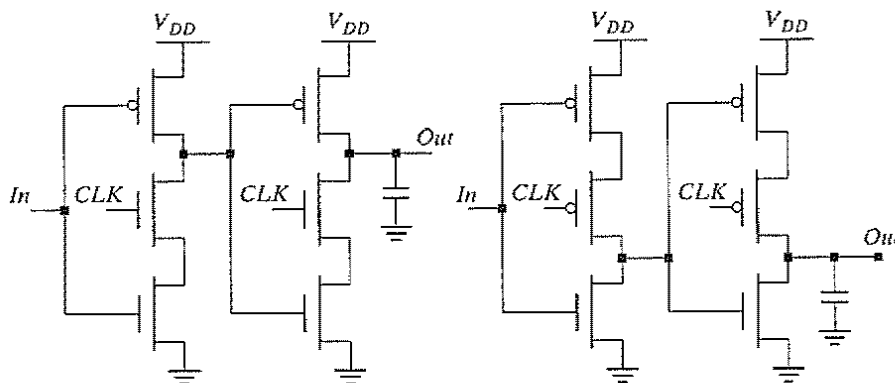


Figure 7-30 True Single-Phase Latches.

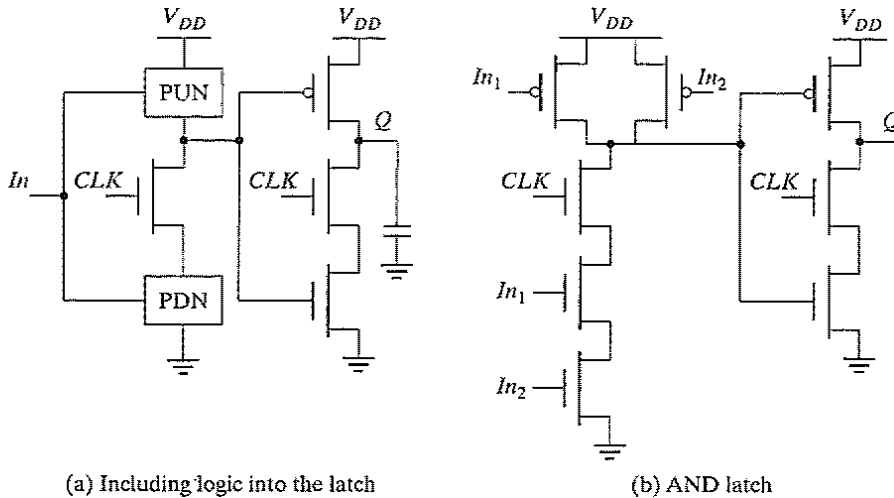


Figure 7-31 Adding logic to the TSPC approach.

the delay overhead associated with the latches. Figure 7-31a outlines the basic approach for embedding logic, while Figure 7-31b shows an example of a positive latch that implements the AND of  $In_1$  and  $In_2$  in addition to performing the latching function. While the setup time of this latch has increased over the one shown in Figure 7-30, the overall performance of the digital circuit (that is, the clock period of a sequential circuit) has improved: The increase in setup time typically is smaller than the delay of an AND gate. This approach of embedding logic into latches has been used extensively in the design of the EV4 DEC Alpha microprocessor [Dobberpuhl92] and many other high-performance processors.

### Example 7.3 Impact of Embedding Logic into Latches on Performance

Consider embedding an AND gate into the TSPC latch, as shown in Figure 7-31b. In a 0.25- $\mu\text{m}$  technology, the setup time of such a circuit, using minimum-size devices is 140 ps. A conventional approach, composed of an AND gate followed by a positive latch, has an effective setup time of 600 ps (we treat the AND plus latch as a black box that performs both functions). The embedded logic approach thus results in significant performance improvements.

The TSPC latch circuits can be further reduced in complexity, as illustrated in Figure 7-32, where only the first inverter is controlled by the clock. Besides the reduced number of transistors, these circuits have the advantage that the clock load is reduced by half. On the other hand, not all node voltages in the latch experience the full logic swing. For instance, the voltage at node A (for  $V_{in} = 0$  V) for the positive latch maximally equals  $V_{DD} - V_{Tn}$ , which results in a reduced drive for the output NMOS transistor and a loss in performance. Similarly, the voltage

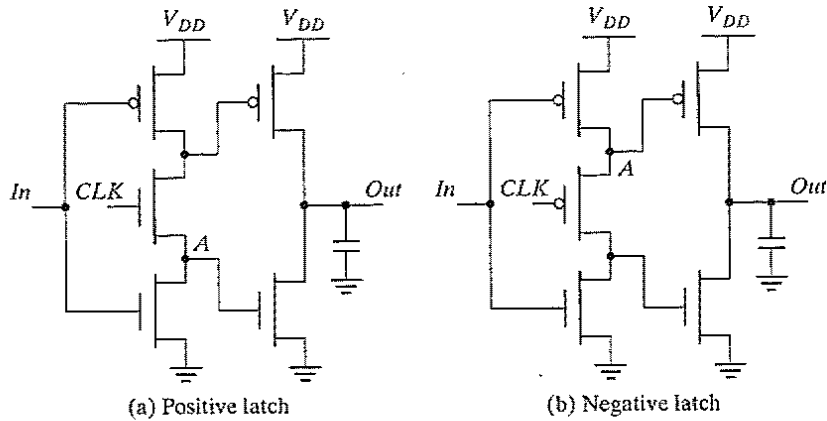


Figure 7-32 Simplified TSPC latch (also called split output).

on node  $A$  (for  $V_{in} = V_{DD}$ ) for the negative latch is only driven down to  $|V_{TP}|$ . This also limits the amount of  $V_{DD}$  scaling possible on the latch.

Figure 7-33 shows the design of a specialized single-phase edge-triggered register. When  $CLK = 0$ , the input inverter is sampling the inverted  $D$  input on node  $X$ . The second (dynamic) inverter is in the precharge mode, with  $M_6$  charging up node  $Y$  to  $V_{DD}$ . The third inverter is in the hold mode, since  $M_8$  and  $M_9$  are off. Therefore, during the low phase of the clock, the input to the final (static) inverter is holding its previous value and the output  $Q$  is stable. On the rising edge of the clock, the dynamic inverter  $M_4$ – $M_6$  evaluates. If  $X$  is high on the rising edge, node  $Y$  discharges. The third inverter  $M_7$ – $M_9$  is on during the high phase, and the node value on  $Y$  is passed to the output  $Q$ . On the positive phase of the clock, note that node  $X$  transitions to a low if the  $D$  input transitions to a high level. Therefore, the input must be kept stable until the value on node  $X$  before the rising edge of the clock propagates to  $Y$ . This represents the hold time of the register (note that the hold time is less than 1 inverter delay, since it takes 1 delay for the input to affect node  $X$ ). The propagation delay of the register is essentially three inverters, because the

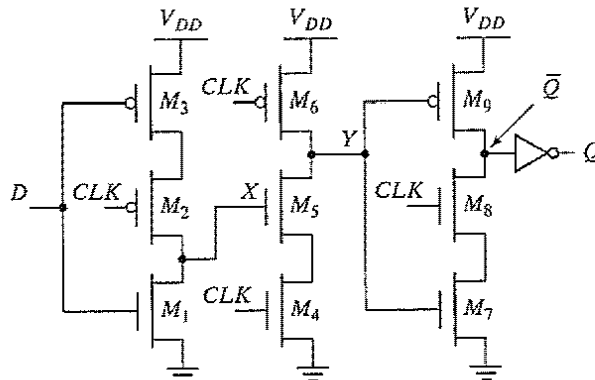


Figure 7-33 Positive edge-triggered register in TSPC.

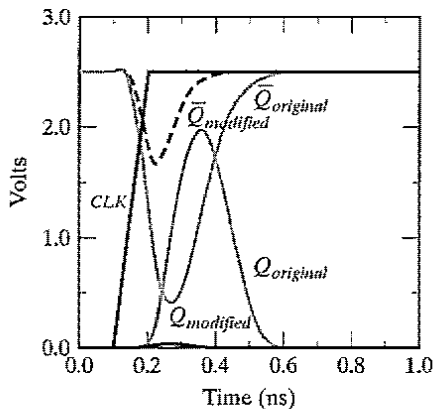
value on node  $X$  must propagate to the output  $Q$ . Finally, the setup time is the time for node  $X$  to be valid, which is one inverter delay.

**WARNING:** Similar to the  $C^2$ MOS latch, the TSPC latch malfunctions when the *slope of the clock* is not sufficiently steep. Slow clocks cause both the NMOS and PMOS clocked transistors to be on simultaneously, resulting in undefined values of the states and race conditions. The clock slopes should therefore be carefully controlled. If necessary, local buffers must be introduced to ensure the quality of the clock signals.

#### Example 7.4 TSPC Edge-Triggered Register

Transistor sizing is critical for achieving correct functionality in the TSPC register. With improper sizing, glitches may occur at the output due to a *race condition* when the clock transitions from low to high. Consider the case where  $D$  is low and  $\overline{Q} = 1$  ( $Q = 0$ ). While  $CLK$  is low,  $Y$  is precharged high turning on  $M_7$ . When  $CLK$  transitions from low to high, nodes  $Y$  and  $\overline{Q}$  start to discharge simultaneously (through  $M_4$ – $M_5$  and  $M_7$ – $M_8$ , respectively). Once  $Y$  is sufficiently low, the trend on  $\overline{Q}$  is reversed and the node is pulled high again through  $M_9$ . In a sense, this sequence of events is comparable to what happens when we chain dynamic logic gates. Figure 7-34 shows the transient response of the circuit of Figure 7-33 for different sizes of devices in the final two stages.

This glitch may be the cause of fatal errors, because it may create unwanted events (for instance, when the output of the latch is used as a clock signal input to another register). It also reduces the contamination delay of the register. The problem can be corrected by resizing the relative strengths of the pull-down paths through  $M_4$ – $M_5$  and  $M_7$ – $M_8$ , so that  $Y$  discharges much faster than  $\overline{Q}$ . This is accomplished by reducing the strength of the  $M_7$ – $M_8$  pull-down path, and by speeding up the  $M_4$ – $M_5$  pull-down path.



	$M_4, M_5$	$M_7, M_8$
Original Width	$0.5 \mu\text{m}$	$2 \mu\text{m}$
Modified Width	$1 \mu\text{m}$	$1 \mu\text{m}$

Figure 7-34 Transistor sizing issues in TSPC (for the register of Figure 7-33).

## 7.4 Alternative Register Styles\*

### 7.4.1 Pulse Registers

Until now, we have used the master–slave configuration to create an edge-triggered register. A fundamentally different approach for constructing a register uses *pulse signals*. The idea is to construct a short pulse around the rising (or falling) edge of the clock. This pulse acts as the clock input to a latch (for example, Figure 7-35a), sampling the input only in a short window. Race conditions are thus avoided by keeping the opening time (i.e., the transparent period) of the latch very short. The combination of the glitch-generation circuitry and the latch results in a positive edge-triggered register.

Figure 7-35b shows an example circuit for constructing a short intentional glitch on each rising edge of the clock [Kozu96]. When  $CLK = 0$ , node  $X$  is charged up to  $V_{DD}$  ( $M_N$  is off since  $CLKG$  is low). On the rising edge of the clock, there is a short period of time when both inputs of the AND gate are high, causing  $CLKG$  to go high. This in turn activates  $M_N$ , pulling  $X$  and eventually  $CLKG$  low (Figure 7-35c). The length of the pulse is controlled by the delay of the AND gate and the two inverters. Note that there exists also a delay between the rising edges of the input clock ( $CLK$ ) and the glitch clock ( $CLKG$ ), which also is equal to the delay of the AND gate and the two inverters. If every register on the chip uses the same clock generation mechanism, this sampling delay does not matter. However, process variations and load variations may

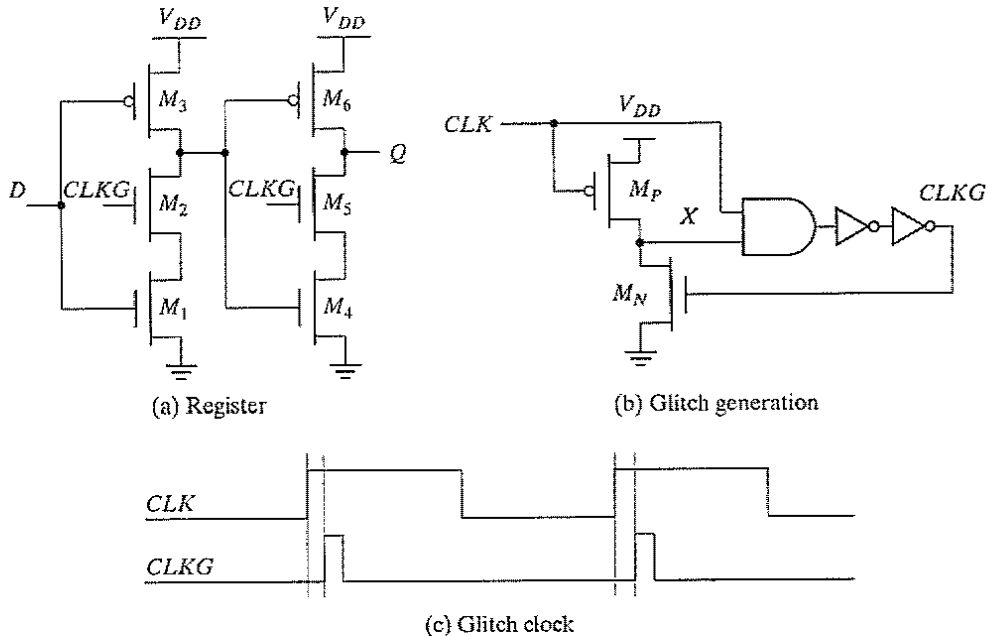


Figure 7-35 TSPC-based glitch latch-timing generation and register.

cause the delays through the glitch clock circuitry to be different. This must be taken into account when performing timing verification and clock skew analysis (the topics of Chapter 10).

If the setup time and hold time are measured in reference to the rising edge of the glitch clock, the setup time is essentially zero, the hold time is essentially equal to the length of the pulse, and the propagation delay ( $t_{c-q}$ ) equals two gate delays. The advantage of the approach is the **reduced clock load and the small number of transistors** required. The glitch-generation circuitry can be amortized over multiple register bits. The disadvantage is a substantial increase in verification complexity. For this circuit to function properly, simulations must be performed across all corners to ensure that the clock pulse always exists (i.e., that the glitch-generation circuit works reliably). Despite the increased complexity, such registers do provide an alternate approach to conventional schemes, and they have been adopted in a number of high-performance processors (e.g., [Kozu96]).

Another version of the pulsed register is shown in Figure 7-36 (as used in the AMD-K6 processor [Partovi96]). When the clock is low,  $M_3$  and  $M_6$  are off, and device  $P_1$  is turned on. Node  $X$  is precharged to  $V_{DD}$ , the output node ( $Q$ ) is decoupled from  $X$  and is held at its previous state.  $\overline{CLKD}$  is a delay-inverted version of  $CLK$ . On the rising edge of the clock,  $M_3$  and  $M_6$  turn on while devices  $M_1$  and  $M_4$  stay on for a short period, determined by the delay of the three inverters. During this interval, the circuit is transparent and the input data  $D$  is sampled by the latch. Once  $\overline{CLKD}$  goes low, node  $X$  is decoupled from the  $D$  input and is either held or starts to precharge to  $V_{DD}$  through PMOS device  $P_2$ . On the falling edge of the clock, node  $X$  is held at  $V_{DD}$  and the output is held stable by the cross-coupled inverters.

Note that this circuit also uses a *pulse generator*, but it is integrated into the register. The transparency period also determines the hold time of the register. The window must be wide enough for the input data to propagate to the  $Q$  output. In this particular circuit, the setup time can be negative. This is the case if the transparency window is longer than the delay from input to output. This is attractive, as data can arrive at the register even after the clock goes high, which means that time is borrowed from the previous cycle.

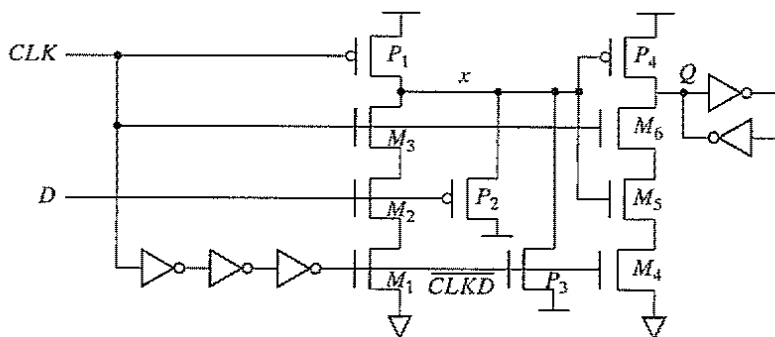


Figure 7-36 Flow-through positive edge-triggered register.

### Example 7.5 Setup Time of Glitch Register

The glitch register of Figure 7-36 is transparent during the (1–1) overlap of  $CLK$  and  $\overline{CLKD}$ . As a result, the input data can actually change after the rising edge of the clock, resulting in a negative setup time (Figure 7-37). The  $D$ -input transitions to low after the rising edge of the clock, and transitions to high before the falling edge of  $\overline{CLKD}$  (i.e., during the transparency period). Observe how the output follows the input. The output  $Q$  does go to the correct value of  $V_{DD}$  as long as the input  $D$  is set up correctly some time before the falling edge of  $\overline{CLKD}$ . When the negative setup time is exploited, there can be no guarantees on the monotonic behavior of the output. That is, the output can have multiple transitions around the rising edge, and therefore, the output of the register should not be used for driving dynamic logic or as a clock as a clock to other registers.

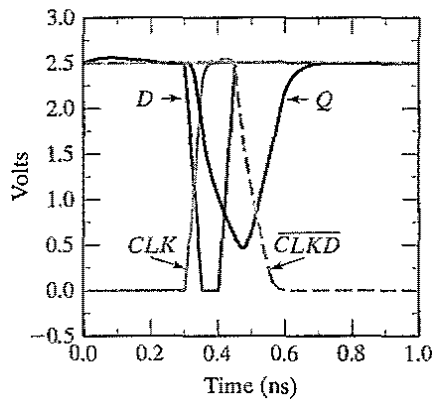


Figure 7-37 Simulation showing a negative setup time for the glitch register.

### Problem 7.6 Converting a Glitch Register to a Conditional Glitch Register

Modify the circuit in Figure 7-36 so that it takes an additional *Enable* input. The goal is to convert the register to a conditional register which latches only when the enable signal is asserted.

### 7.4.2 Sense-Amplifier-Based Registers

In addition to the *master-slave* and the *glitch* approaches to implement an edge-triggered register, a third technique based on *sense amplifiers* can be used, as introduced in Figure 7-38 [Montanaro96].<sup>3</sup> Sense-amplifier circuits accept small input signals and amplify them to generate rail-to-rail swings. They are used extensively in memory cores and in low-swing bus drivers to either improve performance or reduce power dissipation. There are many techniques to construct these amplifiers. A common approach is to use feedback—for instance, through a set of

<sup>3</sup>In a sense, these sense-amplifier-based registers are similar in operation to the glitch registers—that is, the first stage generates the pulse, and the second latches it.

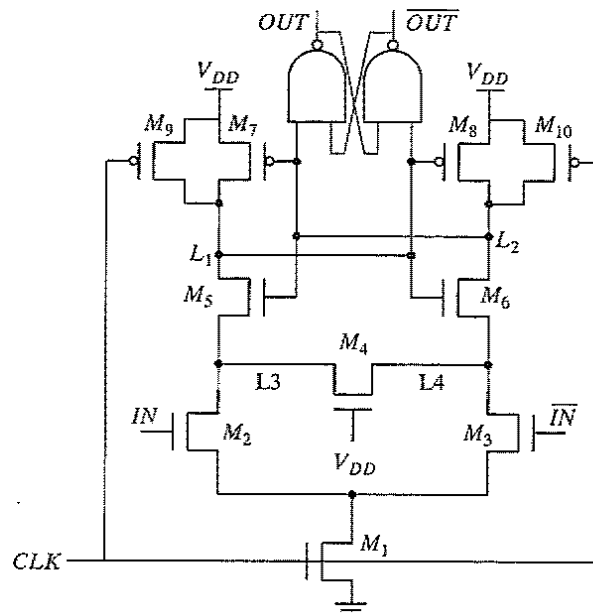


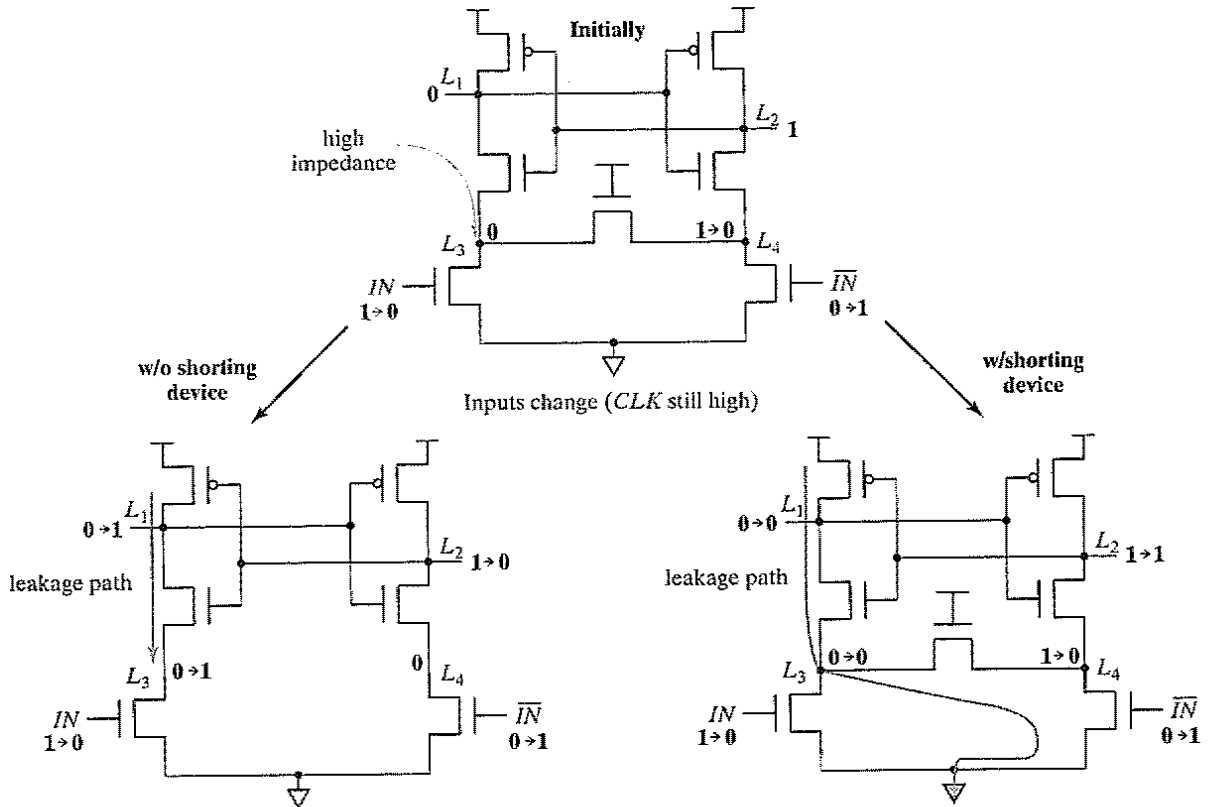
Figure 7-38 Positive edge-triggered register based on sense amplifier.

cross-coupled inverters. The circuit shown in Figure 7-38 uses a precharged front-end amplifier that samples the differential input signal on the rising edge of the clock signal. The outputs of front end are fed into a NAND cross-coupled SR *flip-flop* that holds the data and guarantees that the differential outputs switch only once per clock cycle. The differential inputs in this implementation don't have to have rail-to-rail swing.

The core of the front end consists of a cross-coupled inverter ( $M_5$ – $M_6$ ), whose outputs ( $L_1$  and  $L_2$ ) are precharged by using devices  $M_9$  and  $M_{10}$  during the low phase of the clock. As a result, PMOS transistors  $M_7$  and  $M_8$  are turned off and the NAND flip-flop is holding its previous state. Transistor  $M_1$  is similar to an evaluate switch in dynamic circuits and is turned off to ensure that the differential inputs do not affect the output during the low phase of the clock. On the rising edge of the clock, the evaluate transistor turns on and the differential input pair ( $M_2$  and  $M_3$ ) is enabled, and the difference between the input signals is amplified on the output nodes on  $L_1$  and  $L_2$ . The cross-coupled inverter pair flips to one of its stable states based on the value of the inputs. For example, if  $IN$  is 1,  $L_1$  is pulled to 0, and  $L_2$  remains at  $V_{DD}$ . Due to the amplifying properties of the input stage, it is not necessary for the input to swing all the way up to  $V_{DD}$ , which enables the use of low-swing signaling on the input wires.

The shorting transistor,  $M_4$ , is used to provide a DC-leakage path from either node  $L_3$ , or  $L_4$ , to ground. This is necessary to accommodate the case in which the inputs change their value after the positive edge of  $CLK$  has occurred, resulting in either  $L_3$  or  $L_4$  being left in a high-impedance state with a logical low-voltage level stored on the node. Without the leakage path, that node would be susceptible to charging by leakage currents. The latch could then actually change state prior to the next rising edge of  $CLK$ ! This is best illustrated graphically, as in Figure 7-39.





$L_3$  is isolated so charge accumulates until  $L_1/L_3$  change state, causing  $L_2$  to change state as well. As a result, the flip-flop outputs change.

The leakage current attempts to charge  $L_1/L_3$ , but the DC path through the shorting transistor allows it to leak away to ground.

Figure 7-39 The need for the shorting transistor  $M_4$ .

### 7.5 Pipelining: An Approach to Optimize Sequential Circuits

*Pipelining* is a popular design technique often used to accelerate the operation of datapaths in digital processors. The concept is explained with the example of Figure 7-40a. The goal of the presented circuit is to compute  $\log(|a + b|)$ , where both  $a$  and  $b$  represent streams of numbers (i.e., the computation must be performed on a large set of input values). The minimal clock period  $T_{min}$  necessary to ensure correct evaluation is given as

$$T_{min} = t_{c-q} + t_{pd,logic} + t_{su} \tag{7.7}$$

where  $t_{c-q}$  and  $t_{su}$  are the propagation delay and the setup time of the register, respectively. We assume that the registers are edge-triggered  $D$  registers. The term  $t_{pd,logic}$  stands for the worst case delay path through the combinational network, which consists of the adder, absolute value, and logarithm functions. In conventional systems (that don't push the edge of technology), the

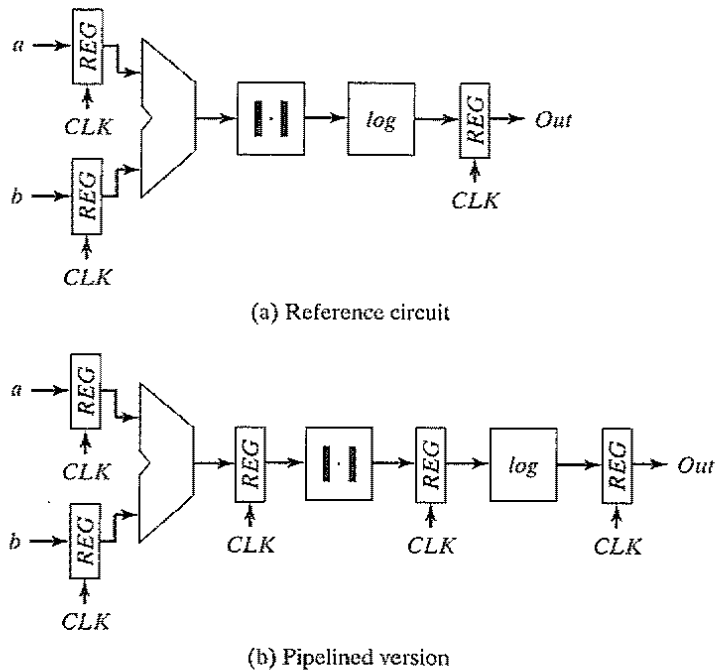


Figure 7-40 Datapath for the computation of  $\log(|a + b|)$ .

latter delay is generally much larger than the delays associated with the registers and dominates the circuit performance. Assume that each logic module has an equal propagation delay. We note that each logic module is then active for only one-third of the clock period (if the delay of the register is ignored). For example, the adder unit is active during the first third of the period and remains idle (no useful computation) during the other two-thirds of the period. Pipelining is a technique to improve the resource utilization, and increase the functional through-put. Assume that we introduce registers between the logic blocks, as shown in Figure 7-40b. This causes the computation for one set of input data to spread over a number of clock-periods, as shown in Table 7-1. The result for the data set  $(a_1, b_1)$  only appears at the output after three clock periods.

Table 7-1 Example of pipelined computations.

Clock Period	Adder	Absolute Value	Logarithm
1	$a_1 + b_1$		
2	$a_2 + b_2$	$ a_1 + b_1 $	
3	$a_3 + b_3$	$ a_2 + b_2 $	$\log( a_1 + b_1 )$
4	$a_4 + b_4$	$ a_3 + b_3 $	$\log( a_2 + b_2 )$
5	$a_5 + b_5$	$ a_4 + b_4 $	$\log( a_3 + b_3 )$

At that time, the circuit has already performed parts of the computations for the next data sets,  $(a_2, b_2)$  and  $(a_3, b_3)$ . The computation is performed in an assembly-line fashion—hence the name *pipeline*.

The advantage of pipelined operation becomes apparent when examining the minimum clock period of the modified circuit. The combinational circuit block has been partitioned into three sections, each of which has a smaller propagation delay than the original function. This effectively reduces the value of the minimum allowable clock period:

$$T_{min,pipe} = t_{c-q} + \max(t_{pd,add}, t_{pd,abs}, t_{pd,log}) + t_{su} \quad (7.8)$$

Suppose that all logic blocks have approximately the same propagation delay, and that the register overhead is small with respect to the logic delays. The pipelined network outperforms the original circuit by a factor of three under these assumptions (i.e.,  $T_{min,pipe} = T_{min}/3$ ). The increased performance comes at the relatively small cost of two additional registers and an increased latency.<sup>4</sup> This explains why pipelining is popular in the implementation of very high-performance datapaths.

### 7.5.1 Latch- versus Register-Based Pipelines

Pipelined circuits can be constructed by using level-sensitive latches instead of edge-triggered registers. Consider the pipelined circuit of Figure 7-41. The pipeline system is implemented using pass-transistor-based positive and negative latches instead of edge-triggered registers. That is, logic is introduced between the master and slave latches of a master–slave system. In the following discussion, we use the  $CLK-\overline{CLK}$  notation to denote a two-phase clock system without loss of generality. Latch-based systems give significantly more flexibility in implementing a pipelined system, and they often offer higher performance. When the  $CLK$  and  $\overline{CLK}$  clocks are nonoverlapping, correct pipeline operation is obtained. Input data is sampled on  $C_1$  at the negative edge of  $CLK$  and the computation of logic block  $F$  starts; the result of the logic block  $F$  is stored on  $C_2$  on the falling edge of  $\overline{CLK}$ , and the computation of logic block  $G$  starts. The nonoverlapping of the clocks ensures correct operation. The value stored on  $C_2$  at the end of the  $CLK$  low phase is the result of passing the previous input (stored on the falling edge of  $CLK$  on  $C_1$ ) through the logic function  $F$ . When overlap exists between  $CLK$  and  $\overline{CLK}$ , the next input is already being applied to  $F$ , and its effect might propagate to  $C_2$  before  $\overline{CLK}$  goes low (assuming that the contamination delay of  $F$  is small). In other words, a *race* develops between the previous input and the current one. Which value wins depends upon the logic and is often a function of the applied inputs. The latter factor makes the detection and elimination of race conditions non-trivial in nature.

<sup>4</sup>*Latency* is defined here as the number of clock cycles it takes for the data to propagate from the input to the output. For the example at hand, pipelining increases the latency from 1 to 3. An increased latency is generally acceptable, but it can cause a global performance degradation if not treated with care.

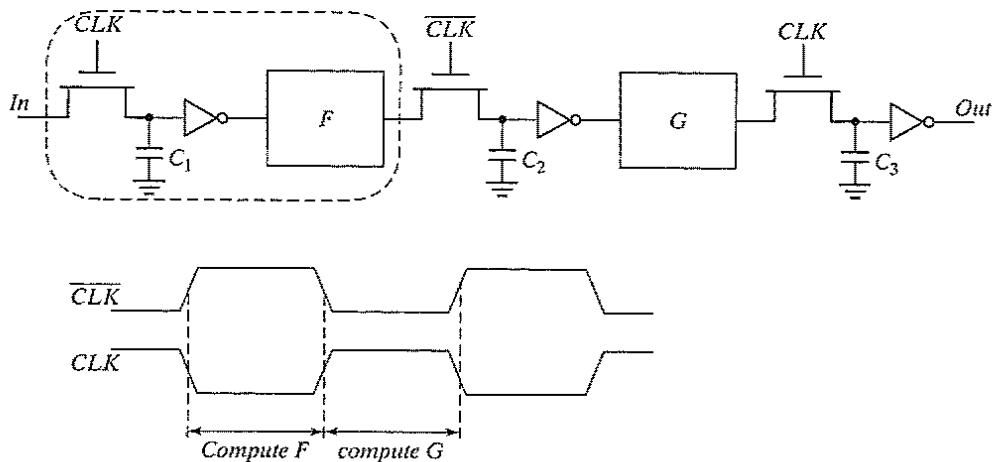


Figure 7-41 Operation of two-phase pipelined circuit, using dynamic registers.

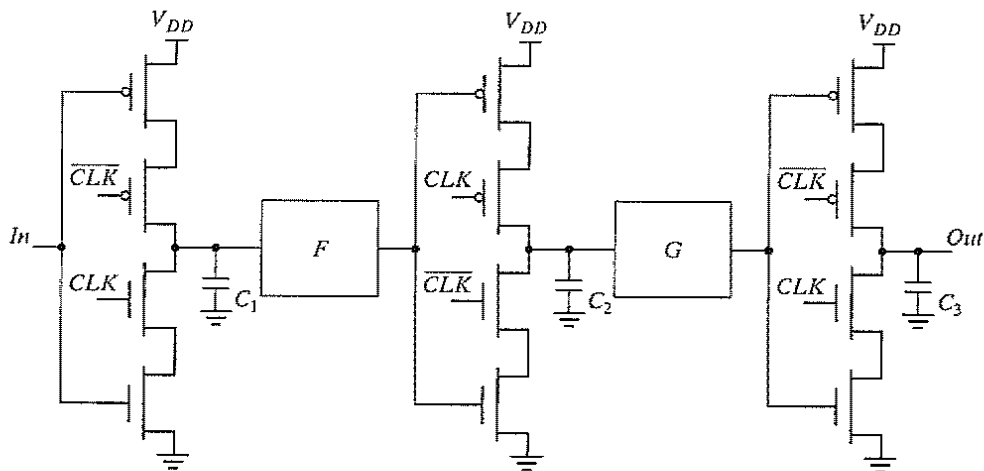


Figure 7-42 Pipelined datapath, using  $C^2MOS$  latches.

### 7.5.2 NORA-CMOS—A Logic Style for Pipelined Structures

The latch-based pipeline circuit can also be implemented by using  $C^2MOS$  latches, as shown in Figure 7-42. The operation is similar to the one discussed in Section 7.5.1. This topology has one additional important property:

**A  $C^2MOS$ -based pipelined circuit is race free as long as all the logic functions  $F$  (implemented by using static logic) between the latches are noninverting.**

The reasoning for the preceding argument is similar to the argument made in the construction of a  $C^2MOS$  register. During a (0-0) overlap between  $CLK$  and  $\overline{CLK}$ , all  $C^2MOS$  latches simplify to pure pull-up networks (see Figure 7-27). The only way a signal can race

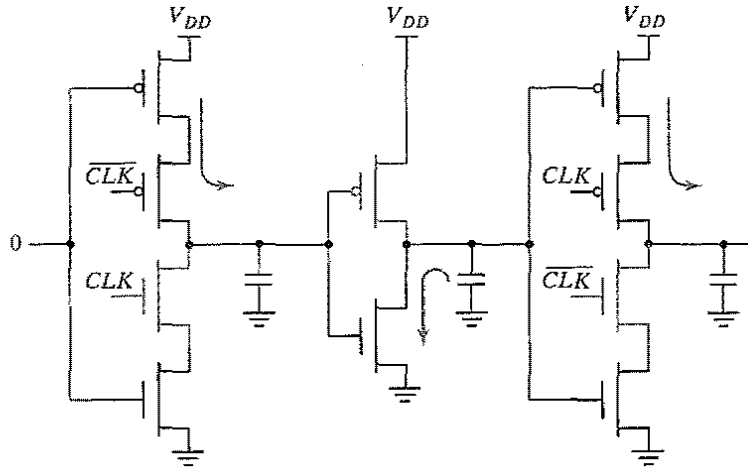


**Figure 7-43** Potential race condition during (0-0) overlap in C<sup>2</sup>MOS-based design.

from stage to stage under this condition is when the logic function  $F$  is inverting, as illustrated in Figure 7-43, where  $F$  is replaced by a single, static CMOS inverter. Similar considerations are valid for the (1-1) overlap.

Based on this concept, a logic circuit style called NORA-CMOS was conceived [Gonçalves83]. It combines C<sup>2</sup>MOS pipeline registers and NORA dynamic logic function blocks. Each module consists of a block of combinational logic that can be a mixture of static and dynamic logic, followed by a C<sup>2</sup>MOS latch. Logic and latch are clocked in such a way that both are simultaneously in either evaluation, or hold (precharge) mode. A block that is in evaluation during  $CLK = 1$  is called a  $CLK$  module, while the inverse is called a  $\overline{CLK}$  module. Examples of both classes are shown in Figure 7-44a and 7-44b, respectively. The operation modes of the modules are summarized in Table 7-2.

A NORA datapath consists of a chain of alternating  $CLK$  and  $\overline{CLK}$  modules. While one class of modules is precharging with its output latch in hold mode, preserving the previous output value, the other class is evaluating. Data is passed in a pipelined fashion from module to module. NORA offers designers a wide range of design choices. Dynamic and static logic

**Table 7-2** Operation modes for NORA logic modules.

	$CLK$ block		$\overline{CLK}$ block	
	Logic	Latch	Logic	Latch
$CLK = 0$	Precharge	Hold	Evaluate	Evaluate
$CLK = 1$	Evaluate	Evaluate	Precharge	Hold

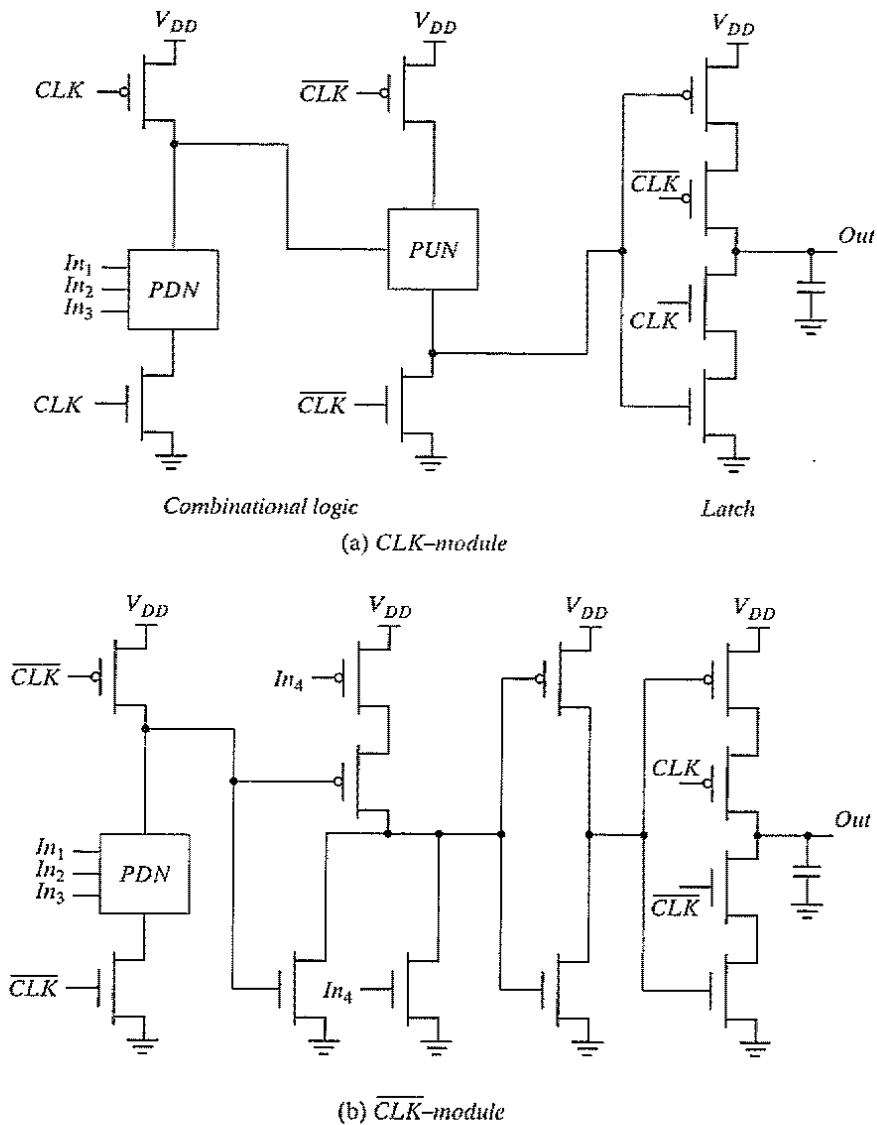


**Figure 7-44** Examples of NORA-CMOS modules.

can be mixed freely, and both  $CLK_p$  and  $CLK_n$  dynamic blocks can be used in cascaded or in pipelined form. Although this style of logic avoids the extra inverter required in domino CMOS, there are many rules that must be followed to achieve reliable and race-free operation. As a result of this added complexity, the use of NORA has been limited to high-performance applications.

## 7.6 Nonbistable Sequential Circuits

In the preceding sections, we have focused on a single type of sequential element: the latch (and its sibling, the register). The most important property of such a circuit is that it has two stable states—hence, the term *bistable*. The bistable element is not the only sequential circuit of interest. Other regenerative circuits can be catalogued as *astable* and *monostable*. The former act as oscillators and can, for instance, be used for on-chip clock generation. The latter serve as pulse generators, also called *one-shot circuits*. Another interesting regenerative circuit is the *Schmitt trigger*. This component has the useful property of showing hysteresis in its dc characteristics—its switching threshold is variable and depends upon the direction of the transition (low to high or high to low). This peculiar feature can come in handy in noisy environments.

### 7.6.1 The Schmitt Trigger

#### Definition

A *Schmitt trigger* [Schmitt38] is a device with two important properties:

1. It responds to a slowly changing input waveform with a **fast transition time at the output**.
2. The voltage-transfer characteristic of the device displays *different switching thresholds for positive- and negative-going input signals*. This is demonstrated in Figure 7-45, where a typical voltage-transfer characteristic of the Schmitt trigger is shown (and its schematics symbol). The switching thresholds for the low-to-high and high-to-low transitions are called  $V_{M+}$  and  $V_{M-}$ , respectively. The *hysteresis voltage* is defined as the difference between the two.

One of the main uses of the Schmitt trigger is to turn a noisy or slowly varying input signal into a clean digital output signal. This is illustrated in Figure 7-46. Notice how the hysteresis suppresses the ringing on the signal. At the same time, the fast low-to-high (and high-to-low) transi-

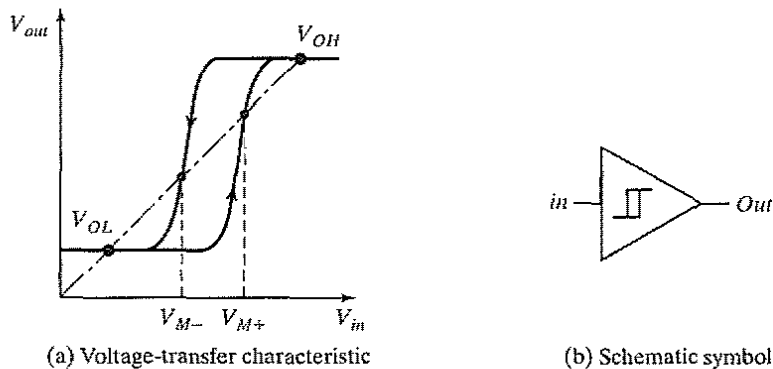
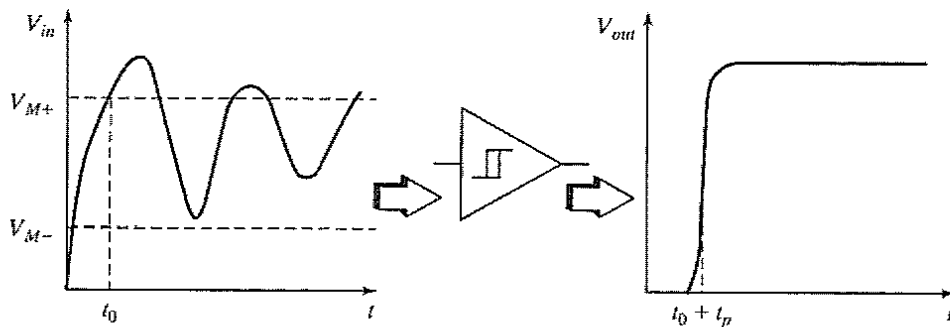


Figure 7-45 Noninverting Schmitt trigger.



**Figure 7-46** Noise suppression, using a Schmitt trigger.

tions of the output signal should be observed. Steep signal slopes are beneficial in general, for instance for reducing power consumption by suppressing direct-path currents. The “secret” behind the Schmitt trigger concept is the use of positive feedback.

### CMOS Implementation

One possible CMOS implementation of the Schmitt trigger is shown in Figure 7-47. The idea behind this circuit is that the switching threshold of a CMOS inverter is determined by the ( $k_n/k_p$ ) ratio between the PMOS and NMOS transistors. Increasing the ratio raises the threshold, while decreasing it lowers  $V_M$ . Adapting the ratio depending upon the direction of the transition results in a shift in the switching threshold and a hysteresis effect. This adaptation is achieved with the aid of feedback.

Suppose that  $V_{in}$  is initially equal to 0, so that  $V_{out} = 0$  as well. The feedback loop biases the PMOS transistor  $M_4$  in the conductive mode, while  $M_3$  is off. The input signal effectively connects to an inverter consisting of two PMOS transistors in parallel ( $M_2$  and  $M_4$ ) as a pull-up network, and a single NMOS transistor ( $M_1$ ) in the pull-down chain. This modifies the effective transistor ratio of the inverter to  $k_{M1}/(k_{M2} + k_{M4})$ , which moves the switching threshold upwards.

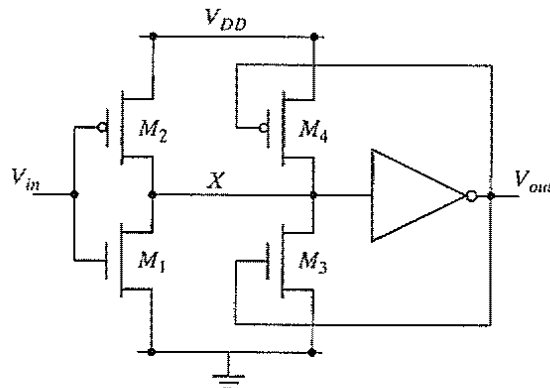


**Figure 7-47** CMOS Schmitt trigger.



Once the inverter switches, the feedback loop turns off  $M_4$ , and the NMOS device  $M_3$  is activated. This extra pull-down device speeds up the transition and produces a clean output signal with steep slopes.

A similar behavior can be observed for the high-to-low transition. In this case, the pull-down network originally consists of  $M_1$  and  $M_3$  in parallel, while the pull-up network is formed by  $M_2$ . This reduces the value of the switching threshold to  $V_{M-}$ .

### Example 7.6 CMOS Schmitt Trigger

Consider the Schmitt trigger of Figure 7-47, with  $M_1$  and  $M_2$  sized at  $1\ \mu\text{m}/0.25\ \mu\text{m}$ , and  $3\ \mu\text{m}/0.25\ \mu\text{m}$ , respectively. The inverter is designed such that the switching threshold is around  $V_{DD}/2$  ( $= 1.25\ \text{V}$ ). Figure 7-48a shows the simulation of the Schmitt trigger assuming that devices  $M_3$  and  $M_4$  are  $0.5\ \mu\text{m}/0.25\ \mu\text{m}$  and  $1.5\ \mu\text{m}/0.25\ \mu\text{m}$ , respectively. As apparent from the plot, the circuit exhibits hysteresis. The high-to-low switching point ( $V_{M-} = 0.9\ \text{V}$ ) is lower than  $V_{DD}/2$ , while the low-to-high switching threshold ( $V_{M+} = 1.6\ \text{V}$ ) is larger than  $V_{DD}/2$ .

It is possible to shift the switching point by changing the sizes of  $M_3$  and  $M_4$ . For example, to modify the low-to-high transition, we need to vary the PMOS device. The high-to-low threshold is kept constant by keeping the device width of  $M_3$  at  $0.5\ \mu\text{m}$ . The device width of  $M_4$  is varied as  $k \times 0.5\ \mu\text{m}$ . Figure 7-48b demonstrates how the switching threshold increases with raising values of  $k$ .

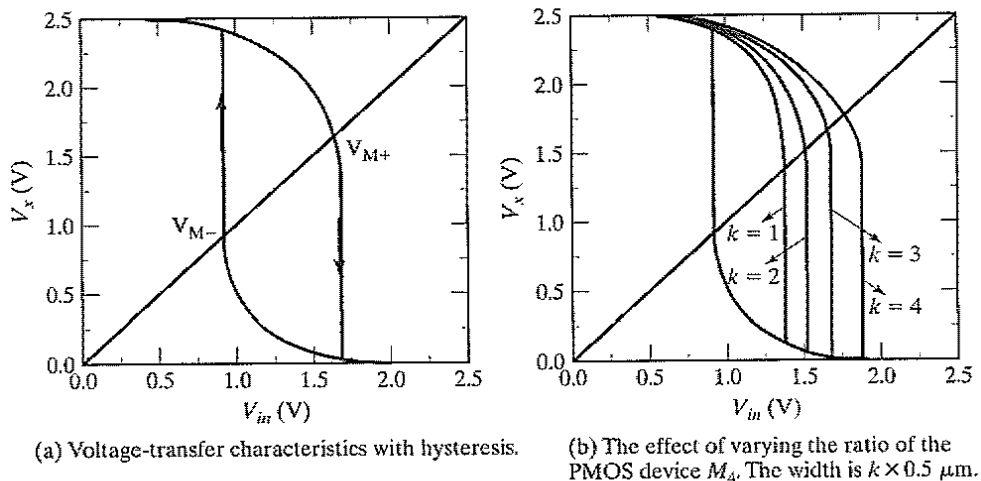


Figure 7-48 Schmitt trigger simulations.

**Problem 7.7 An Alternative CMOS Schmitt Trigger**

Another CMOS Schmitt trigger is shown in Figure 7-49. Discuss the operation of the gate, and derive expressions for  $V_{M-}$  and  $V_{M+}$ .

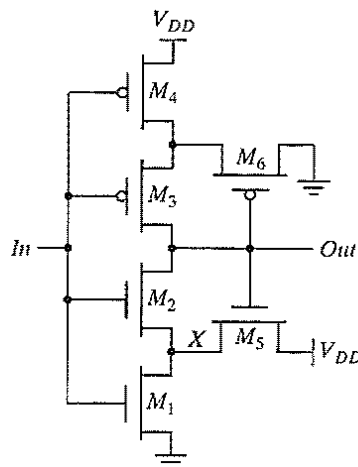
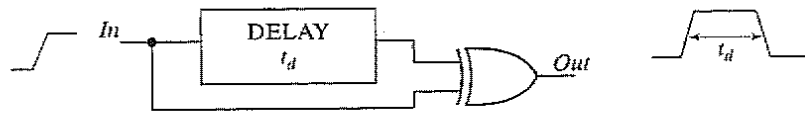


Figure 7-49 Alternate CMOS Schmitt trigger.

### 7.6.2 Monostable Sequential Circuits

A monostable element is a circuit that generates a pulse of a predetermined width every time the quiescent circuit is triggered by a pulse or transition event. It is called *monostable* because it has only one stable state (the quiescent one). A trigger event, which is either a signal transition or a pulse, causes the circuit to go temporarily into another quasi-stable state. This means that it eventually returns to its original state after a time period determined by the circuit parameters. This circuit, also called a *one-shot*, is useful in generating pulses of a known length. This functionality is required in a wide range of applications. We have already seen the use of a one-shot in the construction of glitch registers. Another well-known example is the *address transition detection* (ATD) circuit, used for the timing generation in static memories. This circuit detects a change in a signal or group of signals, such as the address or data bus, and produces a pulse to initialize the subsequent circuitry.

The most common approach to the implementation of one-shots is the use of a simple delay element to control the duration of the pulse. The concept is illustrated in Figure 7-50. In the quiescent state, both inputs to the XOR are identical, and the output is low. A transition on the input causes the XOR inputs to differ temporarily and the output to go high. After a delay  $t_d$  (of the delay element), this disruption is removed, and the output goes low again. A pulse of length  $t_d$  is created. The delay circuit can be realized in many different ways, such as an *RC*-network or a chain of basic gates.



**Figure 7-50** Transition-triggered one shot.

### 7.6.3 Astable Circuits

An astable circuit has no stable states. The output oscillates back and forth between two quasi-stable states, with a period determined by the circuit topology and parameters (delay, power supply, etc.). One of the main applications of oscillators is the on-chip generation of clock signals. (This application is discussed in detail in a later chapter on timing.)

The ring oscillator is a simple example of an astable circuit. It consists of an odd number of inverters connected in a circular chain. Due to the odd number of inversions, no stable operation point exists, and the circuit oscillates with a period equal to  $2 \times t_p \times N$ , where  $N$  is the number of inverters in the chain and  $t_p$  is the propagation delay of each inverter.

#### Example 7.7 Ring Oscillator

The simulated response of a ring oscillator with five stages is shown in Figure 7-51 (all gates use minimum-size devices). The observed oscillation period approximately equals 0.5 ns, which corresponds to a gate propagation delay of 50 ps. By tapping the chain at various points, different phases of the oscillating waveform are obtained. (Phases 1, 3, and 5 are displayed in the plot.) A wide range of clock signals with different duty-cycles and phases can be derived from those elementary signals, using simple logic operations.

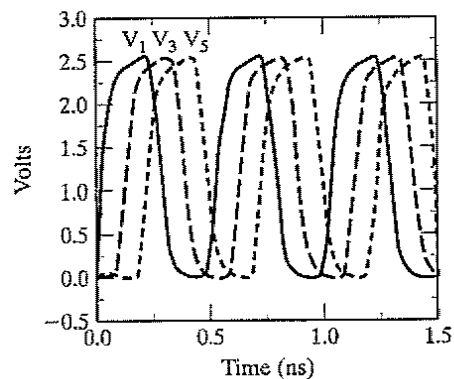


**Figure 7-51** Simulated waveforms of five-stage ring oscillator. The outputs of stages 1, 3, and 5 are shown.

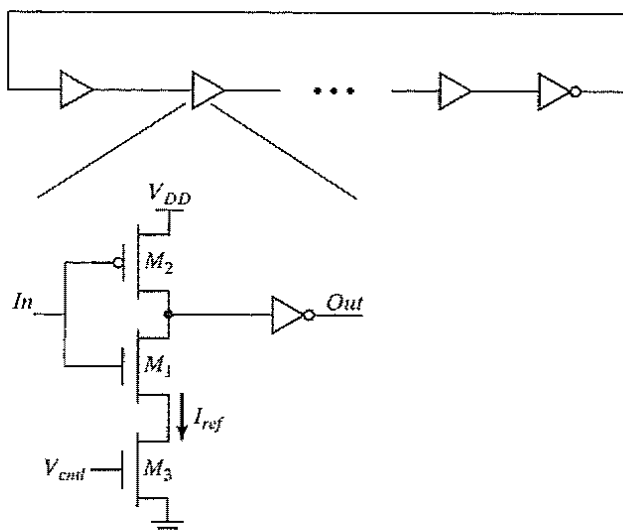


Figure 7-52 Voltage-controlled oscillator based on current-starved inverters.

The ring oscillator composed of cascaded inverters produces a waveform with a fixed oscillating frequency determined by the delay of an inverter in the CMOS process. In many applications, it is necessary to control the frequency of the oscillator. An example of such a circuit is the *voltage-controlled oscillator (VCO)*, whose oscillation frequency is a function (typically, nonlinear) of a control voltage. The standard ring oscillator can be modified into a *VCO* by replacing the standard inverter with a *current-starved inverter* like the one shown in Figure 7-52 [Jeong87]. The mechanism for controlling the delay of each inverter is to limit the current available to discharge the load capacitance of the gate.

In this modified inverter circuit, the maximal discharge current of the inverter is limited by adding an extra series device. Note that the low-to-high transition on the inverter can also be controlled by adding a PMOS device in series with  $M_2$ . The added NMOS transistor  $M_3$ , is controlled by an analog control voltage  $V_{ctrl}$ , which determines the available discharge current. Lowering  $V_{ctrl}$  reduces the discharge current and, hence, increases  $t_{pHL}$ . The ability to alter the propagation delay per stage allows us to control the frequency of the ring structure. The control voltage is generally set by using feedback techniques. Under low-operating current levels, the current-starved inverter suffers from slow fall times at its output. This can result in significant short-circuit current. We solve this problem by feeding its output into a CMOS inverter or, better yet, a Schmitt trigger. An extra inverter is needed at the end to ensure that the structure oscillates.

### Example 7.8 Current-Starved Inverter Simulation

Figure 7-53 shows the simulated delay of the current-starved inverter as a function of the control voltage  $V_{ctrl}$ . The delay of the inverter can be varied over a large range. When the control voltage is smaller than the threshold, the device enters the subthreshold region.

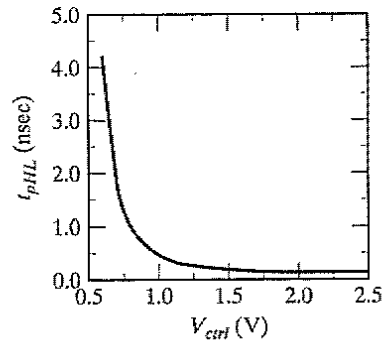


**Figure 7-53**  $t_{pHL}$  of current-starved inverter as a function of the control voltage.

This results in large variations of the propagation delay, as the drive current is exponentially dependent on the drive voltage. When operating in this region, the delay is very sensitive to variations in the control voltage and hence to noise.

Another approach to implement the delay cell is to use a differential element as shown in Figure 7-54a. Since the delay cell provides both inverting and noninverting outputs, an oscillator with an even number of stages can be implemented. Figure 7-54b shows a two-stage differential *VCO*, where the feedback loop provides  $180^\circ$  phase shift through two gate delays, one noninverting and the other inverting, therefore forming an oscillation. The simulated waveforms of this two-stage *VCO* are shown in Figure 7-54c. The in-phase and quadrature phase outputs are available simultaneously. The differential-type *VCO* has better immunity to common mode noise (for example, supply noise) compared with the common ring oscillator. However, it consumes more power due to its increased complexity and its static current.

## 7.7 Perspective: Choosing a Clocking Strategy

A crucial decision that must be made in the earliest phases of chip design is to select the appropriate clocking methodology. The reliable synchronization of the various operations occurring in a complex circuit is one of the most intriguing challenges facing the digital designer of the next decade. Choosing the right clocking scheme affects the functionality, speed, and power of a circuit.

A number of widely used clocking schemes were introduced in this chapter. The most robust and conceptually simple scheme is the two-phase master-slave design. The predominant approach is to use the multiplexer-based register, and to generate the two clock phases locally by simply inverting the clock. More exotic schemes such as the glitch register are also used in practice. However, these schemes require significant fine-tuning and must only be used in specific situations. An example of such is the need for a negative setup time to cope with clock skew.

The general trend in high-performance CMOS VLSI design is therefore to use **simple clocking schemes**, even at the expense of performance. Most automated design methodologies

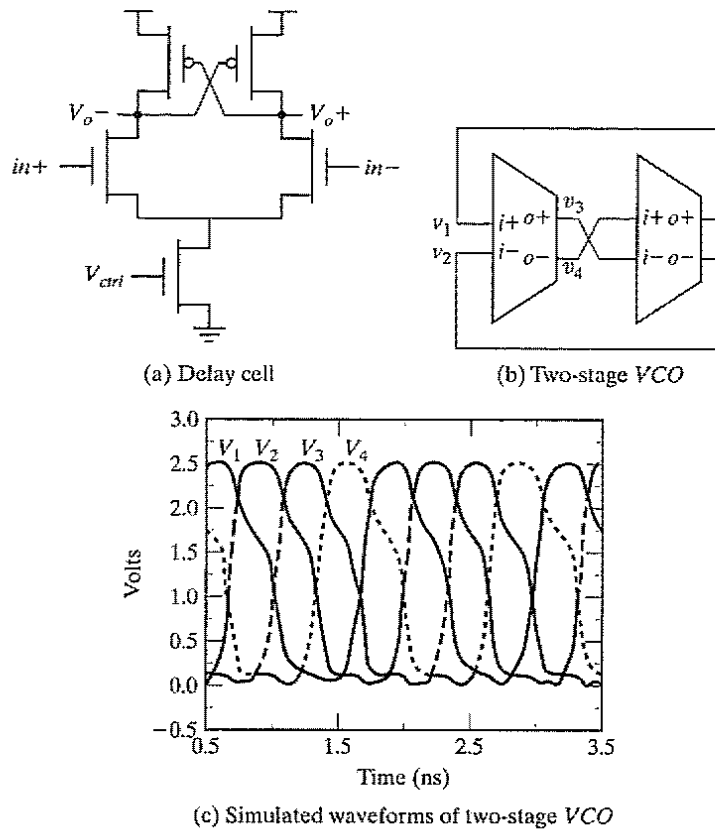


**Figure 7-54** Differential delay element and VCO topology.

such as standard cell employ a single-phase, edge-triggered approach, based on static flip-flops. Nevertheless, the tendency towards simpler clocking approaches also is apparent in high-performance designs such as microprocessors. The use of latches between logic to improve circuit performance is common as well.

## 7.8 Summary

This chapter has explored the subject of sequential digital circuits. The following topics were discussed:

- The cross coupling of two inverters creates a *bistable* circuit, also known as a *flip-flop*. A third potential operation point turns out to be metastable; that is, any diversion from this bias point causes the flip-flop to converge to one of the stable states.
- A latch is a *level-sensitive* memory element that samples data on one phase and holds data on the other phase. A register, on the other hand, samples the data on the rising or falling edge. A register has three important parameters: *the setup time, the hold time, and the*

*propagation delay*. These parameters must be carefully optimized, because they may account for a significant portion of the clock period.

- Registers can be *static* or *dynamic*. A static register holds state as long as the power supply is turned on. It is ideal for memory that is accessed infrequently (e.g., reconfiguration registers or control information). Static registers use either multiplexers or overpowering to enable the writing of data.
- Dynamic memory is based on temporary charge storage on capacitors. The primary advantage is reduced complexity, higher performance, and lower power consumption. However, charge on a dynamic node leaks away with time, and dynamic circuits thus have a minimum clock frequency. Pure dynamic memory is hardly used anymore. Register circuits are made pseudostatic to provide immunity against capacitive coupling and other sources of circuit induced noise.
- Registers can also be constructed by using the *pulse or glitch concept*. An intentional pulse (using a one-shot circuit) is used to sample the input around an edge. Sense-amplifier-based schemes also are used to construct registers; they should be used as well when high-performance or low-signal-swing signalling is required.
- Choice of *clocking style* is an important consideration. Two-phase design can result in race problems. Circuit techniques such as C<sup>2</sup>MOS can be used to eliminate race conditions in two-phase clocking. Another option is to use true single-phase clocking. However, the rise time of clocks must be carefully optimized to eliminate races.
- The combination of dynamic logic with dynamic latches can produce extremely fast computational structures. An example of such an approach, the NORA logic style, is very effective in *pipelined datapaths*.
- *Monostable structures* have only one stable state; thus, they are useful as pulse generators.
- *Astable multivibrators*, or oscillators, possess no stable state. The ring oscillator is the best-known example of a circuit of this class.
- *Schmitt triggers* display hysteresis in their dc characteristic and fast transitions in their transient response. They are mainly used to suppress noise.

## 7.9 To Probe Further

The basic concepts of sequential gates can be found in many logic design textbooks (e.g., [Mano82] and [Hill74]). The design of sequential circuits is amply documented in most of the traditional digital circuit handbooks. [Partovi01] and [Bernstein98] provide in-depth overviews of the issues and solutions in the design of high-performance sequential elements.

## References

- [Bernstein98] K. Bernstein et al., *High-Speed CMOS Design Styles*, Kluwer Academic Publishers, 1998.
- [Dopperpuhl92] D. Dopperpuhl et al., "A 200 MHz 64-b Dual Issue CMOS Microprocessor," *IEEE Journal of Solid-State Circuits*, vol. 27, no. 11, Nov. 1992, pp. 1555–1567.
- [Gieseke97] B. Gieseke et al., "A 600 MHz Superscalar RISC Microprocessor with Out-of-Order Execution," *IEEE International Solid-State Circuits Conference*, pp. 176–177, Feb. 1997.

- [Gonçalves83] N. Gonçalves and H. De Man, "NORA: a racefree dynamic CMOS technique for pipelined logic structures," *IEEE Journal of Solid-State Circuits*, vol. SC-18, no. 3, June 1983, pp. 261–266.
- [Hill74] F. Hill and G. Peterson, *Introduction to Switching Theory and Logical Design*, Wiley, 1974.
- [Jeong87] D. Jeong et al., "Design of PLL-based clock generation circuits," *IEEE Journal of Solid-State Circuits*, vol. SC-22, no. 2, April 1987, pp. 255–261.
- [Kozu96] S. Kozu et al., "A 100 MHz 0.4 W RISC Processor with 200 MHz Multiply-Adder, using Pulse-Register Technique," *IEEE ISSCC*, pp. 140–141, February 1996.
- [Mano82] M. Mano, *Computer System Architecture*, Prentice-Hall, 1982.
- [Montanaro96] J. Montanaro et al., "A 160-MHz, 32-b, 0.5-W CMOS RISC Microprocessor," *IEEE Journal of Solid-State Circuits*, pp. 1703–1714, November 1996.
- [Mutoh95] S. Mutoh et al., "1-V Power Supply High-Speed Digital Circuit Technology with Multithreshold-Voltage CMOS," *IEEE Journal of Solid State Circuits*, pp. 847–854, August 1995.
- [Partovi96] H. Partovi, "Flow-Through Latch and Edge-Triggered Flip-Flop Hybrid Elements," *IEEE ISSCC*, pp. 138–139, February 1996.
- [Partovi01] H. Partovi, "Clocked Storage Elements," in *Design of High-Performance Microprocessor Circuits*, Chandakasan et al., ed., Chapter 11, pp. 207–233, 2001.
- [Schmitt38] O. H. Schmitt, "A Thermionic Trigger," *Journal of Scientific Instruments*, vol. 15, January 1938, pp. 24–26.
- [Suzuki73] Y. Suzuki, K. Odagawa, and T. Abe, "Clocked CMOS calculator circuitry," *IEEE Journal of Solid State Circuits*, vol. SC-8, December 1973, pp. 462–469.
- [Yuan89] J. Yuan and Svensson C., "High-Speed CMOS Circuit Technique," *IEEE JSSC*, vol. 24, no. 1, February 1989, pp. 62–70.





PART

3

# A System Perspective

*"Art, it seems to me, should simplify. That, indeed, is very nearly the whole of the higher artistic process; finding what conventions of form and what of detail one can do without and yet preserve the spirit of the whole."*

Willa Sibert Cather,  
On the Art of Fiction (1920).

*"Simplicity and repose are the qualities that measure the true value of any work of art"*

Frank Lloyd Wright.



## CHAPTER

# 8

## Implementation Strategies for Digital ICs

*Semicustom and structured design methodologies*

*ASIC and system-on-a-chip design flows*

*Configurable hardware*

- 8.1 Introduction
- 8.2 From Custom to Semicustom and Structured-Array Design Approaches
- 8.3 Custom Circuit Design
- 8.4 Cell-Based Design Methodology
  - 8.4.1 Standard Cell
  - 8.4.2 Compiled Cells
  - 8.4.3 Macrocells, Megacells, and Intellectual Property
  - 8.4.4 Semicustom Design Flow
- 8.5 Array-Based Implementation Approaches
  - 8.5.1 Prediffused (or Mask-Programmable) Arrays
  - 8.5.2 Prewired Arrays
- 8.6 Perspective—The Implementation Platform of the Future
- 8.7 Summary
- 8.8 To Probe Further

## 8.1 Introduction

The dramatic increase in complexity of contemporary integrated circuits poses an enormous design challenge. Designing a multimillion-transistor circuit and ensuring that it operates correctly when the first silicon returns is a daunting task that is virtually impossible without the help of computer aids and well-established design methodologies. In fact, it has often been suggested that technology advancements might be outpacing the absorption bandwidth of the design community. This is articulated in Figure 8-1, which shows how IC complexity (in logic transistors) is growing faster than the productivity of a design engineer, creating a “design gap.” One way to address this gap is to increase steadily the size of the design teams working on a single project. We observe this trend in the high-performance processor world, where teams of more than 500 people are no longer a surprise.

Obviously, this approach cannot be sustained in the long term—just imagine all the design engineers in the world working on a single design. Fortunately, about once in a decade we witness the introduction of a novel design methodology that creates a step function in design productivity, helping to bridge the gap temporarily. Looking back over the past four decades, we can identify a number of these productivity leaps. Pure custom design was the norm in the early integrated circuits of the 1970s. Since then, programmable logic arrays (PLAs), standard cells, macrocells, module compilers, gate arrays, and reconfigurable hardware have steadily helped to ease the time and cost of mapping a function onto silicon. In this chapter, we provide a description of some commonly used design implementation approaches. Due to the extensive nature of the field, we cannot be comprehensive—doing so would require a textbook of its own. Instead, we present *a user perspective* that provides a basic perception and insight into what is offered and can be expected from the different design methodologies.

The preferred approach to mapping a function onto silicon depends largely upon the function itself. Consider, for instance, the simple digital processor of Figure 8-2. Such a processor

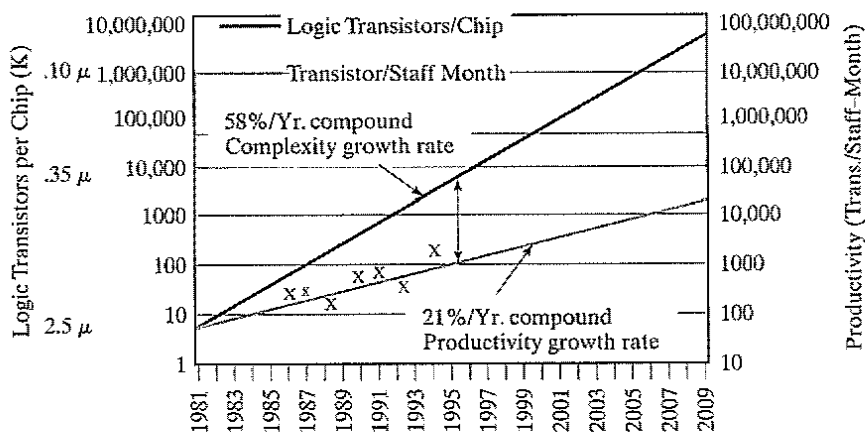


**Figure 8-1** The design productivity gap. Technology (in logic transistors/chip) outpaces the design productivity (in transistors designed by a single design engineer per month). Source: SIA [SIA97].

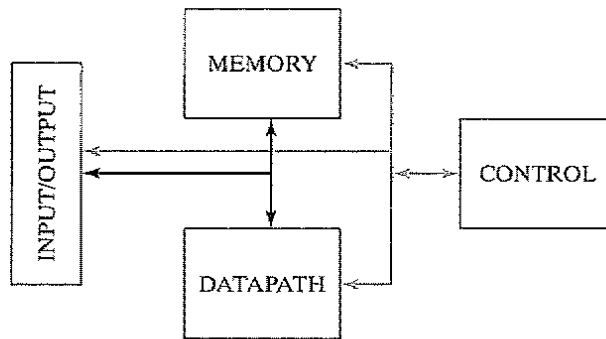


**Figure 8-2** Composition of a generic digital processor. The arrows represent the possible interconnections.

could be the brain of a personal computer (PC), or the heart of a compact-disc player or cellular phone. It is composed of a number of building blocks that occur in one form or another in almost every digital processor:

- **The datapath** is the core of the processor; it is where all computations are performed. The other blocks in the processor are support units that either store the results produced by the datapath or help to determine what will happen in the next cycle. A typical datapath consists of an interconnection of basic combinational functions, such as logic (AND, OR, EXOR) or arithmetic operators (addition, multiplication, comparison, shift). Intermediate results are stored in registers. Different strategies exist for the implementation of datapaths—structured custom cells versus automated standard cells, or fixed hard-wired versus flexible field-programmable fabric. The choice of the implementation platform is mostly influenced by the trade-off between different design metrics such as area, speed, energy, design time, and reusability.
- **The control module** determines what actions happen in the processor at any given point in time. A controller can be viewed as a finite state machine (FSM). It consists of registers and logic, and thus is a sequential circuit. The logic can be implemented in different ways—either as an interconnection of basic logic gates (standard cells), or in a more structured fashion using programmable logic arrays (PLAs) and instruction memories.
- **The memory module** serves as the centralized data storage area. A broad range of different memory classes exist. The main difference between those classes is in the way data can be accessed, such as “read only” versus “read–write,” sequential versus random access, or single-ported versus multiported access. Another way of differentiating between memories is related to their data-retention capabilities. Dynamic memory structures must be refreshed periodically to keep their data, while static memories keep their data as long as the power source is turned on. Finally, nonvolatile memories such as flash memories conserve the stored data even when the supply voltage is removed. A single processor might combine different memory classes. For example, random access memory can be used to store data, and read-only memory may store instructions.

- The **interconnect** network joins the different processor modules to one another, while the **input/output circuitry** connects to the outside world. For a long time, interconnections were an afterthought in the design process. Unfortunately, the wires composing the interconnect network are less than ideal and present a capacitive, resistive, and inductive load to the driving circuitry. As die sizes grow larger, the length of the interconnect wires also tends to grow, resulting in increasing values for these parasitics. Today, automated or structured design methodologies are being introduced that ease the deployment of these interconnect structures. Examples include *on-chip busses*, *mesh interconnect* structures, and even complete *networks on a chip*. Some components of the interconnect network typically are abstracted away on schematic block diagrams, such as the one shown in Figure 8-2, yet are of critical importance to the well-being of the design. These include the power- and clock-distribution networks. Early planning of these “service” networks can go a long way toward ensuring the correct operation of the integrated circuit.

The structure of Figure 8-2 may be repeated many times on a single die. Figure 8-3 shows an example of a *system on a chip*, which combines all the functions needed for the realization of a complete high-definition digital TV set. It combines two processors, memory units, specialized accelerators for functions such as MPEG (de)coding and data filtering, as well as a range of

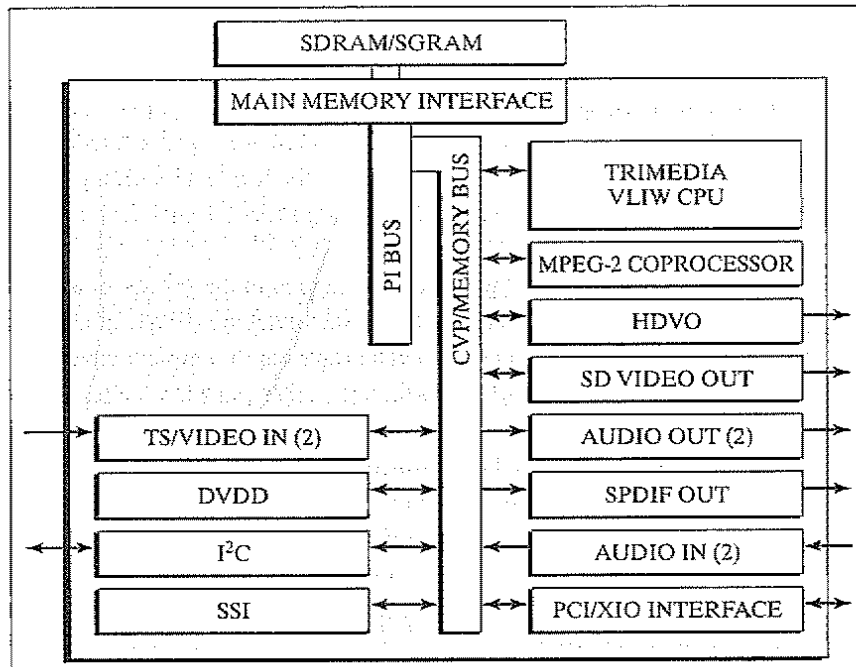


**Figure 8-3** The “Nexperia” system on a chip [Philips99]. This single chip combines a general-purpose microprocessor core, a VLIW (very large instruction word) signal processor, a memory system, an MPEG coprocessor, multiple accelerator units, and input/output peripherals, as well as two system busses.

peripheral units. Other applications such as wireless transceivers or hard-disk read/write units may even include some sizable analog modules.

Choosing an effective implementation approach strongly depends upon the function of the modules under consideration. For example, memory units tend to be very regular and structured. A module compiler that stacks cells in an arraylike fashion is thus the preferred implementation approach. Controllers, on the other hand, tend to be unstructured, and other implementation approaches are desirable. The choice of the implementation strategy can have a tremendous effect on the quality of the final product. The challenge for the designer is to pick the style that meets the product specifications and constraints. What works well for one design may well be a disaster for another one.

### Example 8.1 Trading Off Energy Efficiency and Flexibility

A design that embraces flexibility (or programmability) is very attractive from an application perspective. It allows for “late binding,” in which the application can still be changed after the chip has gone to fabrication. Flexibility makes it possible to reuse a single design for multiple applications, or to upgrade the firmware of a component in the field, reducing the risk for the manufacturer. In contrast, a hard-wired component is totally fixed at manufacturing time and cannot be modified afterwards.

So, why not use flexible or programmable components for every possible design? As always, there is no free lunch. Flexibility comes at a price in both performance and energy efficiency. Providing programmability means adding overhead to implementation. For example, a programmable processor uses stored instructions and an instruction decoder to make a single datapath perform multiple functions. Most designers are not aware of the large cost of flexibility. The impact is illustrated in Figure 8-4, which compares the *energy*

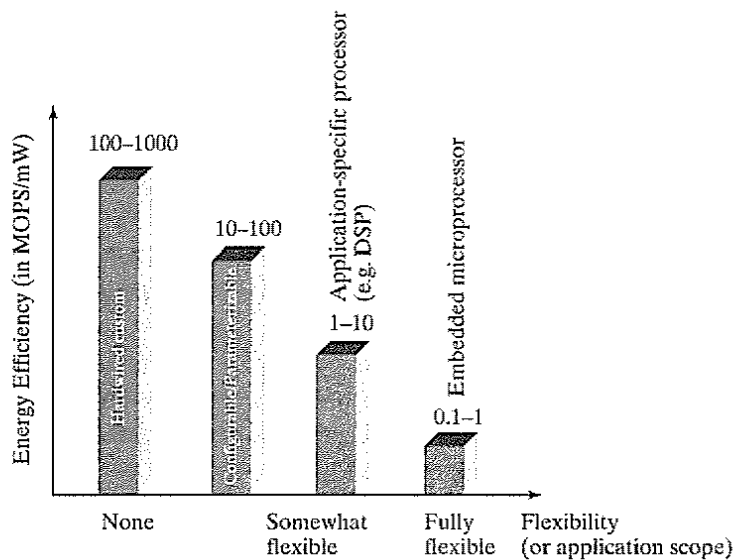


**Figure 8-4** Trading off flexibility versus energy efficiency (in MOPS/mW or millions of operations per mJ of energy) for different implementation styles. The numbers were collected for a 0.25  $\mu\text{m}$  CMOS process [Rabaey00].



*efficiency*—the number of operations that can be performed for a given amount of energy—of various implementation styles versus their *flexibility*—that is, the range of applications that can be mapped onto them. A staggering **three orders of magnitude** in variation can be observed. This clearly demonstrates that hard-wired or implementation styles with limited flexibility (such as configurable or parameterizable modules) are preferable when energy efficiency is a must.

In this and the following three chapters, we discuss, respectively, implementation techniques for random logic and controllers (this chapter), interconnect (Chapter 9), datapaths (Chapter 11), and memories (Chapter 12). Observe that the choice of the implementation approach can have a tremendous effect on the quality of the final product. Important aspects in the design of complex systems consisting of multiple blocks and thus deserving special attention are synchronization and timing (Chapter 10) and the power distribution network (Chapter 9). The distribution of clock signals and supply current has become one of the dominant problems in the design of state-of-the-art processors. A number of Design Methodology Inserts, interspersed between the chapters, address the design challenge posed by these complex components, and introduce the advanced design automation tools that are available to the designer. Inserts F, G, and H discuss design synthesis, verification, and test, respectively.

## 8.2 From Custom to Semicustom and Structured-Array Design Approaches

The viability of a microelectronics design depends on a number of (often) conflicting factors, such as performance in terms of speed or power consumption, cost, and production volume. For example, to be competitive in the market, a microprocessor has to excel in performance at a low cost to the customer. Achieving both goals simultaneously is only possible through large sales volumes. The high development cost associated with high-performance design is then amortized over many parts. Applications such as supercomputing and some defense applications present another scenario. With ultimate performance as the primary design goal, high-performance custom design techniques often are desirable. The production volume is small, but the cost of electronic parts is only a fraction of the overall system costs and thus not much of an issue. Finally, reducing the system size through integration, not performance, is the major objective in most consumer applications. Under these circumstances, the design cost can be reduced substantially by using advanced design-automation techniques, which compromise performance, but minimize design time. As noted in Chapter 1, the cost of a semiconductor device is the sum of two components:

- The *nonrecurring expense* (NRE), which is incurred only once for a design and includes the cost of designing the part.
- The *production cost per part*, which is a function of the process complexity, design area, and process yield.

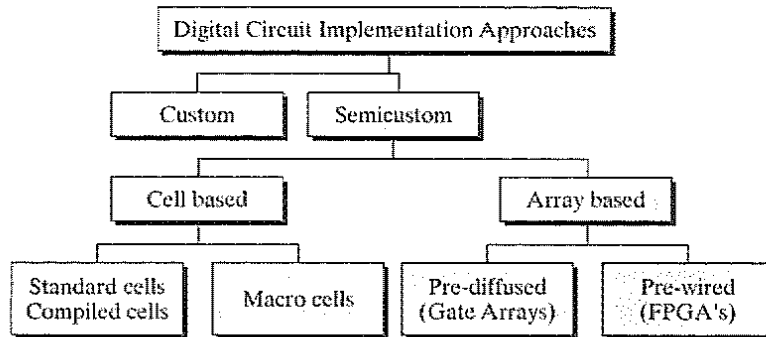


Figure 8-5 Overview of implementation approaches for digital integrated circuits (after [DeMicheli94]).

These economic considerations have spurred the development of a number of distinct implementation approaches ranging from high-performance, handcrafted design to fully programmable, medium-to-low performance designs. Figure 8-5 provides an overview of the different methodologies. In the sections that follow, we discuss first the custom design methodology, followed by the semicustom and array-based approaches.

### 8.3 Custom Circuit Design

When performance or design density is of primary importance, handcrafting the circuit topology and physical design seems to be the only option. Indeed, this approach was the only option in the early days of digital microelectronics, as is adequately demonstrated in the design of the Intel 4004 microprocessor (see Figure 8-5a). The labor-intensive nature of custom design translates into a high cost and a long *time to market*. Therefore, it can only be justified economically under the following conditions:

- The custom block can be reused many times (for example, as a library cell).
- The cost can be amortized over a large volume. Microprocessors and semiconductor memories are examples of applications in this class.
- Cost is not the prime design criterion, as it is in supercomputers or hypersupercomputers.

With continuous progress in the design-automation arena, the share of custom design reduces from year to year. Even in the most advanced high-performance microprocessors, such as the Intel Pentium<sup>®</sup> 4 processor (see Figure 8-6), virtually all portions are designed automatically using semicustom design approaches. Only the most performance-critical modules such as the phase locked-loops and the clock buffers are designed manually. In fact, library cell design is the only area where custom design still thrives today.

The amount of design automation in the custom-design process is minimal, yet some design tools have proven indispensable. In concert with a wide range of verification, simulation, extraction and modeling tools, layout editors, design-rule and electrical-rule checkers—as

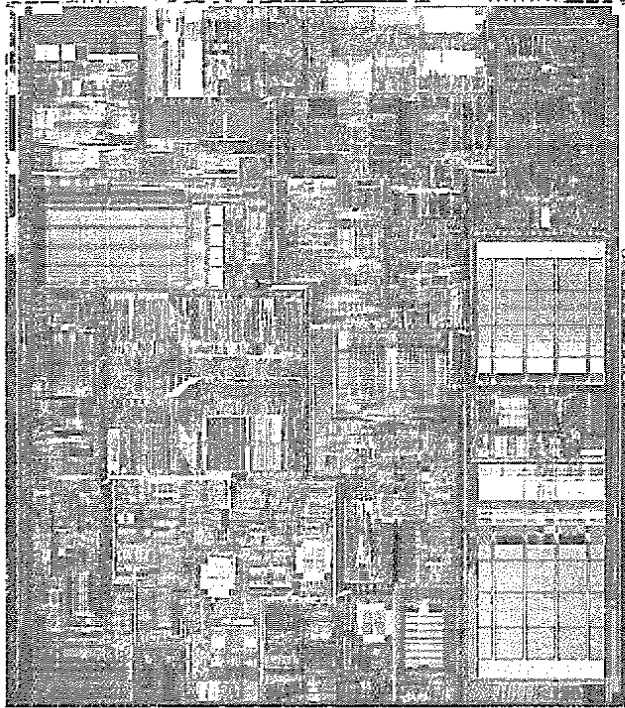


**Figure 8-6** Chip microphotograph of Intel Pentium® 4 processor. It contains 42 million transistors, designed in a 0.18- $\mu\text{m}$  CMOS technology. Its first generation runs at a clock speed of 1.5 GHz (Courtesy Intel Corp.).

described earlier in Design Methodology Insert A—are at the core of every custom-design environment. A excellent discussion of the opportunities and challenges of custom design can be found in [Grundman97].

#### 8.4 Cell-Based Design Methodology

Since the custom-design approach proves to be prohibitively expensive, a wide variety of design approaches have been introduced over the years to shorten and automate the design process. This automation comes at the price of reduced integration density and/or performance. The following rule tends to hold: **the shorter the design time, the larger is the penalty incurred.** In this section, we discuss a number of design approaches that still require a full run through the manufacturing process for every new design. The *array-based design* approach discussed in the next section cuts the design time and cost even further by requiring only a limited set of extra processing steps or by eliminating processing completely.

The idea behind cell-based design is to reduce the implementation effort by *reusing* a limited library of cells. The advantage of this approach is that the cells only need to be designed and verified once for a given technology, and they can be reused many times, thus amortizing the design cost. The disadvantage is that the constrained nature of the library reduces the possibility

of fine-tuning the design. Cell-based approaches can be partitioned into a number of classes depending on the granularity of the library elements.

### 8.4.1 Standard Cell

The standard-cell approach standardizes the design entry level at the logic gate. A library containing a wide selection of logic gates over a range of fan-in and fan-out counts is provided. Besides the basic logic functions, such as inverter, AND/NAND, OR/NOR, XOR/XNOR, and flip-flops, a typical library also contains more complex functions, such as AND-OR-INVERT, MUX, full adder, comparator, counter, decoders, and encoders. A design is captured as a schematic containing only cells available in the library, or is generated automatically from a higher level description language. The layout is then automatically generated. This high degree of automation is made possible by placing strong restrictions on the layout options. In the standard-cell philosophy, cells are placed in rows that are separated by routing channels, as illustrated in Figure 8-7. To be effective, this requires that all cells in the library have identical heights. The width of the cell can vary to accommodate for the variation in complexity between the cells. As illustrated in the drawing, the standard-cell technique can be intermixed with other layout approaches to allow for the introduction of modules such as memories and multipliers that do not adapt easily or efficiently to the logic-cell paradigm.

An example of a design implemented in an early standard-cell design style is shown in Figure 8-8a. A substantial fraction of the area is devoted to signal routing. The minimization of the interconnect overhead is the most important goal of the standard-cell placement and routing tools. One approach to minimizing the wire length is to introduce feed-through cells (Figure 8-7) that make it possible to connect between cells in different rows without having to route around a complete row. A far more important reduction in wiring overhead is obtained by adding more

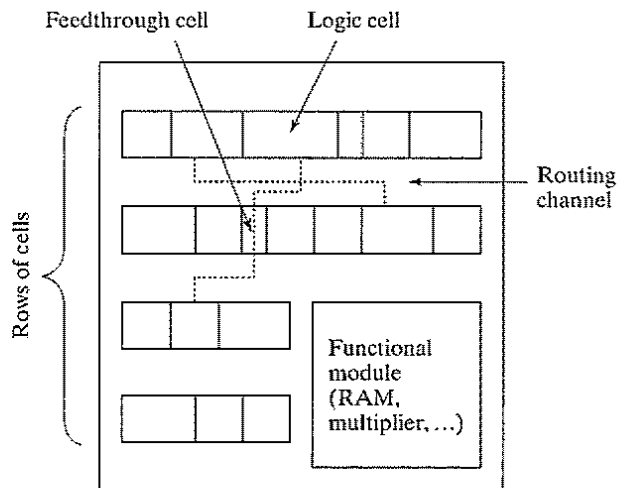
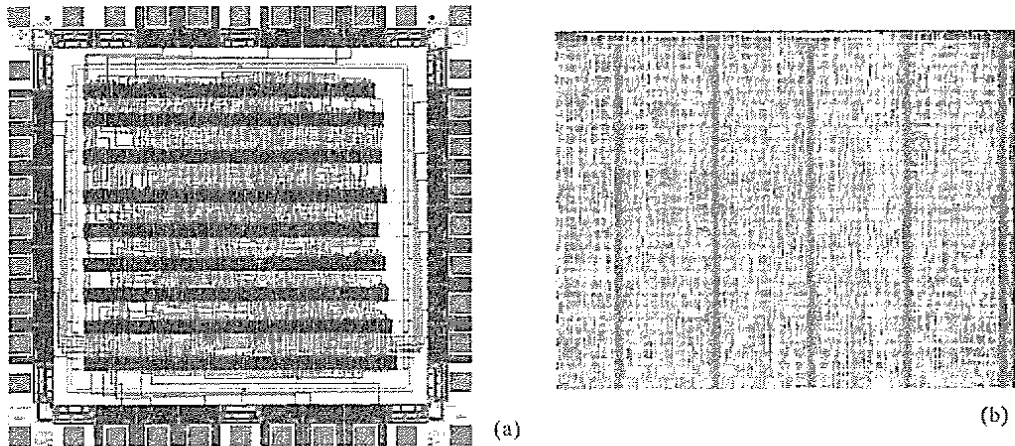


Figure 8-7 Standard-cell layout methodology.



**Figure 8-8** The evolution of standard-cell design. (a) Design in a three-layer metal technology. Wiring channels represent a substantial amount of the chip area. (b) Design in a seven-layer metal technology. Routing channels have virtually disappeared, and all interconnection is laid on top of the logic cells.

interconnect layers. The seven or more metal layers that are available in contemporary CMOS processes make it possible to all but eliminate the need for routing channels. Virtually all signals can be routed on top of the cells, creating a truly three-dimensional design. Figure 8-8b shows a fraction of a standard-cell design, implemented by using seven metal layers. The design achieves more than 90% density, which means that virtually all of the chip area is covered by logic cells, and that only a limited amount of the area is wasted for interconnect.

The design of a standard-cell library is a time-intensive undertaking that, fortunately, can be amortized over a large number of designs. Determining the composition of the library is a nontrivial task. A pertinent question is, Are we better off with a small library in which most cells have a limited fan-in, or is it more beneficial to have a large library with many versions of every gate (e.g., containing two-, three-, and four-input NAND gates, and different sizes for each of these gates)? Since the fan-out and load capacitance due to wiring are not known in advance, it used to be common practice to ensure that each gate had large current-driving capabilities, (i.e., employs large output transistors). While this simplifies the design procedure, it has a detrimental effect on area and power consumption. Today's libraries employ many versions of each cell, sized for different driving strengths, as well as performance and power consumption levels. It is left to the synthesis tool to select the correct cells, given speed and area requirements.

To make the library-based approach work, a detailed documentation of the cell library is an absolute necessity. The information should not only contain the layout, a description of functionality and terminal positioning, but it also must accurately characterize the delay and power consumption of the cell as a function of load capacitance and the input rise and fall times. Gen-

erating this information accounts for a large portion of the library generation effort. How to characterize logic and sequential cells is the topic of “Design Methodology Insert E.”

### Example 8.2 A Three-Input NAND-Gate Cell

To illustrate some of the preceding observations, the design of a three-input NAND standard-cell gate, implemented in a 0.18  $\mu\text{m}$  CMOS technology, is depicted in Figure 8-9. The library actually contains five versions of the cell, supporting capacitive loads from 0.18 pF up to 0.72 pF and ranging in area from 16.4  $\mu\text{m}^2$  to 32.8  $\mu\text{m}^2$ . The cell shown represents the low-performance, energy-efficient design corner, and uses high-threshold transistors to reduce leakage. The NMOS and PMOS transistors in the pull-down (-up) networks are both sized at a (W/L) ratio of approximately 8.

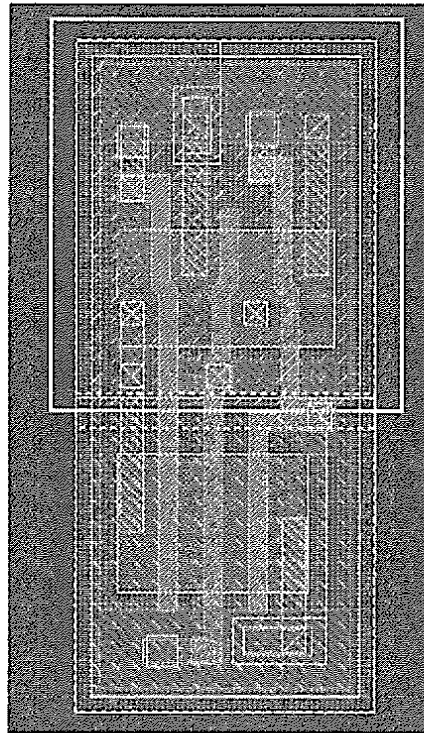


**Figure 8-9** Three-input NAND standard cell (Courtesy ST Microelectronics).

Observe how the layout strategy follows the approach outlined in Figure D-2. Supply lines are distributed horizontally and shared between cells in the same row. Input signals are wired vertically using polysilicon. The input/output terminals are located throughout the cell body (as exemplified by the *pin* terminal in the layout drawing), in line with the over-the-cell wiring approach of today's standard-cell methodology.

The standard-cell approach has become immensely popular, and is used for the implementation of virtually all logic elements in today's integrated circuits. The only exceptions are when extreme high performance or low energy consumption is needed, or when the structure of the targeted function is very regular (such as a memory or a multiplier). The success of the standard-cell approach can be attributed to a number of developments, including the following:

- **The increased quality of the automatic cell placement and routing tools** in conjunction with the availability of multiple routing layers. In fact, it has been shown in a number of studies that the automated approach of today rivals if not surpasses manual design for complex, irregular logic circuits. This is a major departure from a couple of years ago, when automated layout carried a large overhead.
- **The advent of sophisticated logic-synthesis tools.** The logic-synthesis approach allows for the design to be entered at a high level of abstraction using Boolean equations, state machines, or register-transfer languages such as VHDL or Verilog. The synthesis tools automatically translate this specification into a gate netlist, minimizing a specific cost function such as area, delay, or power. Early synthesis tools—such as those used in the first half of the 1980s—focused mostly on two-level logic minimization. While this enabled automatic design mapping for the first time, it limited the area efficiency and the performance of the generated circuits. It is only with the arrival of *multilevel logic synthesis* in the late 1980s that automated design generation has really taken off. Today, virtually no designer uses the standard-cell approach without resorting to automatic synthesis. A more detailed description of the design synthesis process can be found in “Design Methodology Insert F” which follows this chapter.

#### Historical Perspective: The Programmable Logic Array

In the early days of MOS integrated circuit design, logic design and optimization was a manual and labor-intensive task. Karnaugh maps and Quine–McCluskey tables were the techniques of choice at that time. In the late 1970s, a first approach toward automating the tedious process of designing logic circuits emerged, triggered by two important developments:

- Rather than using the ad hoc approach to laying out logic circuits, a regular structured design approach was adopted called the *Programmable Logic Array* or PLA. This methodology enabled the automatic layout generation of two-level logic circuits, and, more importantly, it did so in a predictable fashion in terms of area and performance.
- The emergence of automated logic synthesis tools for two-level logic [Brayton84] made it possible to translate any possible Boolean expression into an optimized two-level (sum-of-products or product-of-sums) logic structure. Tools for the synthesis of sequential circuits followed shortly thereafter.

The idea of structured logic design gained a rapid foothold, and already in the mid-1980s it was adopted by major microprocessor design companies such as Intel and DEC. While PLAs are only sparingly used in today's semicustom logic design, the topic deserves some discussion (especially since PLAs might be poised for a come-back).

The concept is best explained with the aid of an example. Consider the following logic functions, for which we have transformed the equations into the sum-of-products format by using logic manipulations:

$$\begin{aligned}
 f_0 &= x_0x_1 + \bar{x}_2 \\
 f_1 &= x_0x_1x_2 + \bar{x}_2 + \bar{x}_0\bar{x}_1
 \end{aligned}
 \tag{8.1}$$

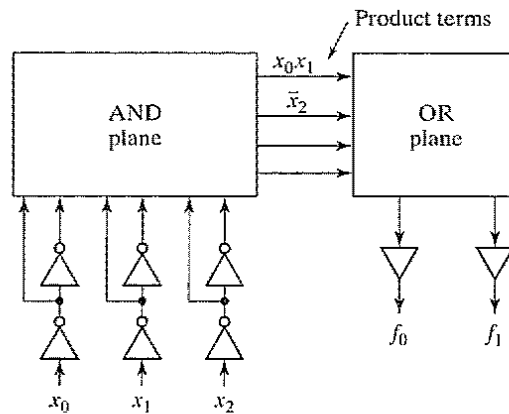


**Figure 8-10** Regular two-level implementation of Boolean functions.

One important advantage of this representation is that a regular realization is easily conceived, as illustrated in Figure 8-10. A first layer of gates implements the AND operations—also called *product terms* or *minterms*—while a second layer realizes the OR functions, called the *sumterms*. Hence, a PLA is a rectangular macrocell, consisting of an array of transistors aligned to form rows in correspondence with product terms, and columns in correspondence with inputs and outputs. The input and output columns partition the array into two subarrays, called AND and OR planes, respectively.

The schematic of Figure 8-10 is not directly realizable since single-layer logic functions in CMOS are always inverting. With a few simple Boolean manipulations, Eq. (8.1) can be rewritten into a NOR–NOR format:

$$\begin{aligned}
 \bar{f}_0 &= \overline{(\bar{x}_0 + \bar{x}_1) + x_2} \\
 \bar{f}_1 &= \overline{(\bar{x}_0 + \bar{x}_1 + \bar{x}_2) + x_2 + (x_0 + x_1)}
 \end{aligned}
 \tag{8.2}$$

### Problem 8.1 Two-Level Logic Representations

It is equally conceivable to represent Eq. (8.1) in a NAND–NAND format. In general, the NOR–NOR representation is preferred due to the prohibitively slow speed of large fan-in NAND gates. The NAND–NAND configuration is very dense, however, and thus can help to reduce power consumption. Derive the NAND–NAND representation for the example of Eq. (8.2).

Translating a set of two-level logic functions into a physical design now boils down to a “programming” task—that is, deciding where to place transistors in both the AND and the OR planes. This task is easily automated—hence, the early success of PLAs. An automatically generated PLA implementation of the logic functions described by Eq. (8.2) is shown in Figure 8-11. Unfortunately, the regular structure, while predictable,



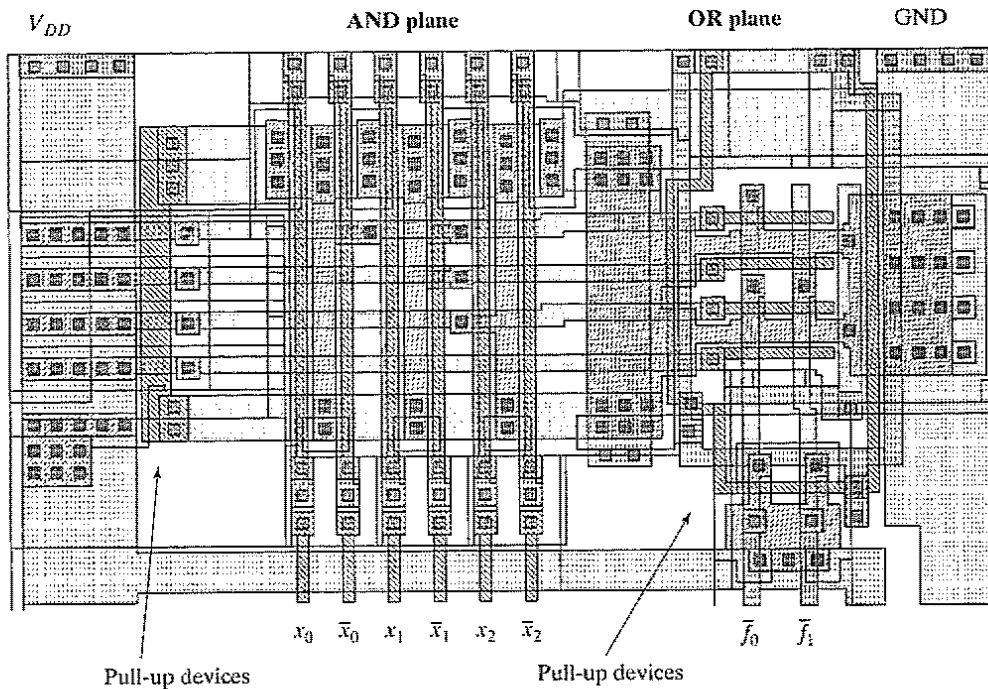


**Figure 8-11** PLA layout implementing Eq. (8.2).

brings with it a lot of overhead in area and delay (as is quite visible in the layout), which was its ultimate demise in the semicustom design world. Those who are curious on how these AND and OR planes are actually implemented must wait until we get to Chapter 12, where we discuss the transistor-level implementation of PLAs. ■

### 8.4.2 Compiled Cells

The cost of implementing and characterizing a library of cells should not be underestimated. Today's libraries contain from several hundred to more than a thousand cells. These cells have to be redesigned with every migration to a new technology. Moreover, changes happen during the development of a single technology generation. For example, minimum metal widths or contact rules often are changed to improve yield. As a result, the complete library has to be laid out and characterized again. In addition, even an extensive library has the disadvantage of being discrete, which means that the number of design options is limited. When targeting performance or power, customized cells with optimized transistor sizes are attractive. With the increased impact of interconnect load, providing cells with adjusted driver sizes is an absolute necessity from both a performance and a power perspective [Sylvester98]—hence, the quest for automated (or compiled) cell generation.

A number of automated approaches have been devised that generate cell layouts on the fly, given the transistor netlists, but high-quality automatic cell layout has remained elusive. Earlier approaches relied on fixed topologies. Later approaches allowed for more flexibility in the transistor placement (e.g., [Hill85]). Layout densities close to what can be accomplished by a human

designer are now within reach, and a number of cell-generation tools are commercially available—for example [Cadabra01, Prolific01]:

### Example 8.3 Automatic Cell Generation

The flow of a typical cell-generation process is illustrated with the example of a simple inverter (using the Abracad tool [Cadabra01]).

- The cell schematics are developed first. The Spice netlist is the starting point for the automatic layout generation. The generator examines the netlist and starts with transistor geometries. In case of a CMOS inverter, the cell contains just two transistors (see Figure 8-12a).
- The tool proceeds along the same lines that a designer would follow. The transistors are placed in a cell architecture with predefined topology rules (Figure 8-12b). This architecture is common for all the cells in the library, including the cell height, power rails, pin placements, routing and contact styles.
- The cell is routed symbolically (Figure 8-12c).
- The routing is rearranged, and the cell is compacted to meet design rules and library preferences (Figure 8-12d).
- The final step cleans the cell of any remaining design rule errors and produces the final layout (Figure 8-12e).

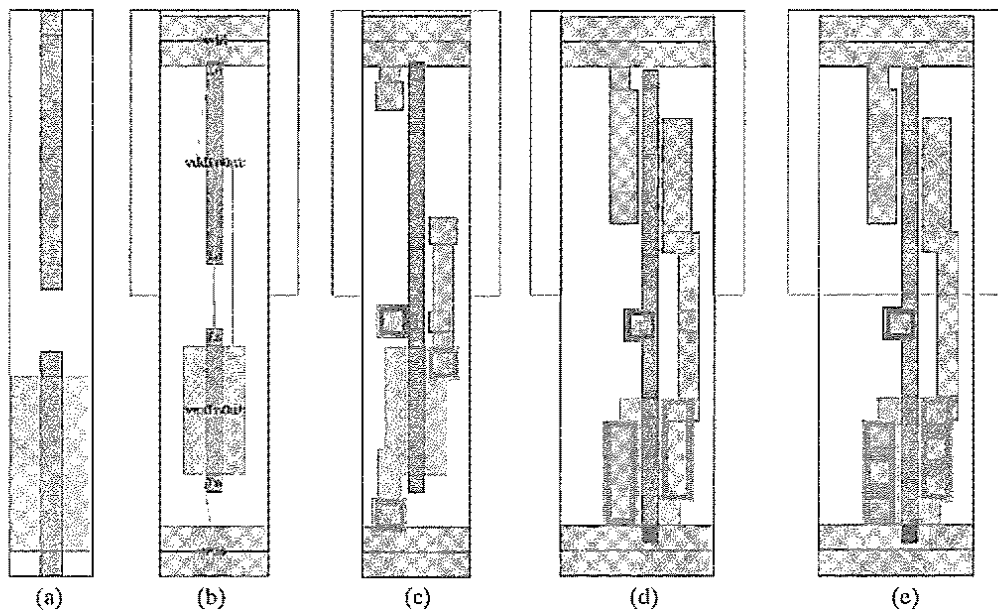


**Figure 8-12** Automatic cell layout (a) initial transistor geometries, (b) placed transistors with flylines indicating intended interconnections, (c) initially routed cell, and (d) compacted cell, (e) finished cell.

### 8.4.3 Macrocells, Megacells and Intellectual Property

Standardizing at the logic-gate level is attractive for random logic functions, but it turns out to be inefficient for more complex structures such as multipliers, data paths, memories, and embedded microprocessors and DSPs. By capturing the specific nature of these blocks, implementations can be obtained that outperform the results of the standard ASIC design process by a wide margin. Cells that contain a complexity that surpasses what is found in a typical standard-cell library are called *macrocells* (or, sometimes, *megacells*). Two types of macrocells can be identified:

**The Hard Macro** represents a module with a given functionality and a predetermined physical design. The relative location of the transistors and the wiring within the module is fixed. In essence, a hard macro represents a custom design of the requested function. In some cases, the macro is parameterized, which means that versions with slightly different properties are available or can be generated. Multipliers and memories are examples: A hard multiplier macro may not only generate a  $32 \times 16$  multiplier, but also an  $8 \times 8$  one.

The advantage of the hard macro is that it brings with it all the good properties of custom design: dense layout, and optimized and predictable performance and power dissipation. By encapsulating the function into a macromodule, it can be reused over and over in different designs. This reuse helps to offset the initial design cost. The disadvantage of the hard macro is that it is hard to port the design to other technologies or to other manufacturers. For every new technology, a major redesign of the block is necessary. For this reason, hard macros are used less and less, and are employed mainly when the automated generation approach is far inferior or even impossible. Embedded memories and microprocessors are good examples of hard macros. They typically are provided by the IC manufacturer (who also provides the standard cell library), or the semiconductor vendor who has a particularly desirable function to offer (such as a standard microprocessor or DSP).

In the case of a macro that can be parameterized, a generator called the *module compiler* is used to create the actual physical layout. Regular structures such as PLAs, memories, and multipliers are easily constructed by abutting predesigned leaf cells in a two-dimensional array topology. All interconnections are made by abutment, and no or little extra routing is needed if the cells are designed correctly, which minimizes the parasitic capacitance. The PLA of Figure 8-11 is an example of such a configuration. The whole array can be constructed with a minimal number of cells. The generator itself is a simple software program that determines the relative positioning of the various leaf cells in the array.

---

#### Example 8.4 A Memory Macromodule

Figure 8-13 shows an example of a “hard” memory macrocell. The  $256 \times 32$  SRAM block is generated by a parameterizable module generator. Besides creating the layout, the generator also provides accurate timing and power information. Modern memory generators also include an amount of redundancy to deal with defects.

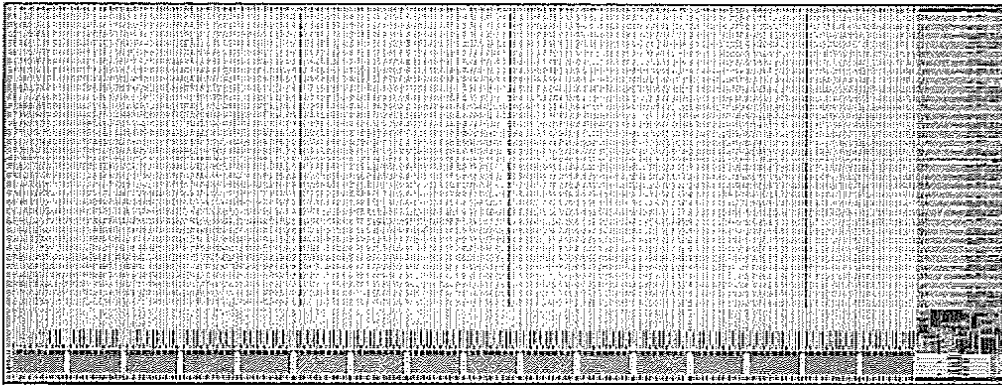


**Figure 8-13** Parameterizable memory “hard” macrocell. This particular instance stores  $256 \times 32$  (or 8192) bits. The decoders are located on the bottom. All eight address bits, as well as the 32 data input and output ports are placed on the right side of the cell. The total area of the memory module, implemented in a  $0.18\text{-}\mu\text{m}$  CMOS technology, equals a mere  $0.094\text{ mm}^2$  (courtesy ST Microelectronics).

**A Soft Macro** represents a module with a given functionality, but without a specific physical implementation. The placement and the wiring of a soft macro may vary from instance to instance. This means that the timing data can only be determined after the final synthesis and placement and routing steps—in other words, the process is unpredictable. Yet, through intrinsic knowledge of the internal structure of the module, and by imposing precise timing and placement constraints on the physical generation process, soft macros most often succeed in offering well-defined timing guarantees. While stepping away from the advantages of the custom design process and relying on the semicustom physical design process, soft macros have the major advantage that they can be ported over a wide range of technologies and processes. This amortizes the design effort and cost over a wide set of designs.

Soft-macrocell generators come in different styles depending on the type of function they target. Virtually all of them can be classified as *structural generators*: Given the desired function and values for the requested parameters, the generator produces a netlist, which is an enumeration of the standard cells used and their interconnections. It also provides a set of timing constraints that the placement and routing tools should meet. The advantage of this approach is that the generator exploits its knowledge of the function under consideration to come up with clever structures that are more efficient than what logic synthesis would produce. For example, the design of fast and area-efficient multipliers has been the topic of decades of research.<sup>1</sup> The multiplier generator just incorporates the best of what the multiplier literature has to offer into an automated generation tool.

<sup>1</sup>Multiplier design is explained more thoroughly in Chapter 11, which discusses the design of arithmetic structures.

### Example 8.5 Multiplier Macromodule

Two instances of an  $8 \times 8$  multiplier module with different aspect ratios are shown in Figure 8-14. The modules are generated using the ModuleCompiler tool from Synopsys [ModuleCompiler01]. As can be observed from the layout, a common standard-cell methodology is used to generate the physical artwork. The contribution of the macrocell generator is to translate the compact input description into an optimized connection of standard cells that meets the timing constraints. This “soft” approach has the advantage that modules with different aspect ratios can easily be generated. Also, porting between different manufacturing technologies is relatively easy.

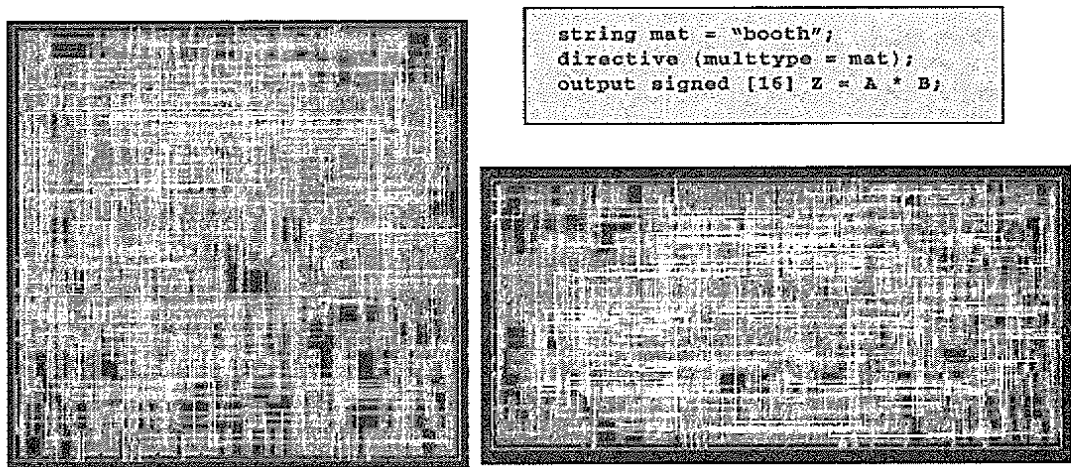


**Figure 8-14** Multiplier “soft” macro modules. Both layouts implement an  $8 \times 8$  booth multiplier, but with different aspect ratios. The compact input description to the compiler is shown in the gray box on top.

The availability of macromodules has substantially changed the semicustom design landscape in the 21<sup>st</sup> century. With the complexity of ICs going up exponentially, the idea of building every new IC from scratch becomes an uneconomic and nonplausible proposition. More and more, circuits are being built from reusable building blocks of increasing complexity and functionality. Typically, these modules are acquired from third-party vendors, who make the functions available through royalty or licensing agreements. Macromodules distributed in this style are called *intellectual property* (or IP) modules. This approach is somewhat comparable to the software world, where a large programming project typically makes intensive use of reusable software libraries. Good examples of commonly available intellectual property modules are embedded microprocessors and microcontrollers, DSP processors, bus interfaces such as PCI, and several special-purpose functional modules such as FFT and filter modules for DSP applications, error-correction coders for wireless communications, and MPEG decoding and encoding for video. Obviously, for an IP module to be useful, it has to not only deliver the hardware, but it also has to come with the appro-

appropriate software tools (such as compilers and debuggers for embedded processors), prediction models, and test benches. The latter are quite important because they represent the only means for the end user to verify that the module delivers the promised functionality and performance.

The design of a system on a chip is rapidly becoming an exercise in reuse at different levels of granularity. At the lowest level, we have the standard cell library; at a level higher, we have the functional modules such as multipliers, datapaths and memories; next, we have the embedded processors; and finally, the application-specific megacells. With more and more of the system functionality migrating onto a single die, it is not surprising to see that a typical ASIC consists of a blend of design styles and modules, embedding a number of hard or soft macrocells within a sea of standard cells.

### Example 8.6 A Processor for Wireless Communications

Figure 8-15 shows an integrated circuit implementing the protocol stack for a wireless indoor communication system [Silva01]. The majority of the area is occupied by the embedded microprocessor (the Tensilica Xtensa processor [Xtensa01]) and its memory system. This processor allows for a flexible implementation of the higher levels of the protocol stack (Application/Network), and enables changes in the functionality of the chip, even after fabrication. The memory modules are generated using module compilers provided by the process vendor. The processor core itself is automatically generated from a higher level description in Verilog, and uses standard cells for its physical implementation. The advantage of using the “soft-core” approach is that the processor instruction set can be

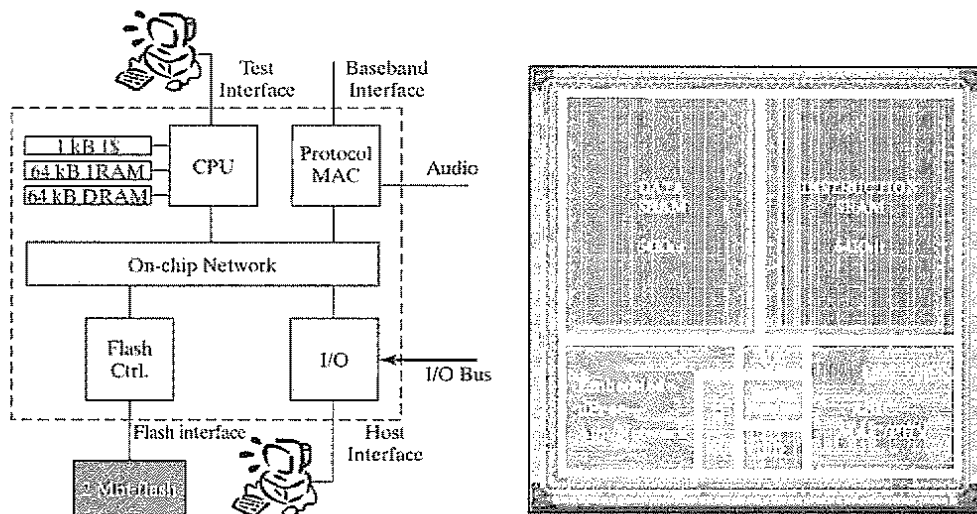


**Figure 8-15** Wireless communications processor—an example of a hybrid ASIC design methodology. The processor combines an embedded microprocessor and its memory system with dedicated hardware accelerators and I/O modules. Observe also the on-chip network module [Silva01].

tailored to the application, and that the processor itself can easily be ported to different technologies and fabrication processes.

Implementing the computation-intensive parts of the protocol (MAC/PHY) on the microprocessor would require very high clock speeds and would unnecessarily increase the power dissipation of the chip. Fortunately, these functions are fixed and typically do not require a flexible implementation. Hence, they are implemented as an accelerator module in standard cells. The hard-wired implementation accomplishes the task of implementing a huge number of computations at a relatively low power level and clock frequency. The designer of a system on a chip is continuously faced with the challenge of deciding what is more desirable—after-the-fabrication flexibility versus higher performance at lower power levels. Fortunately, tools are emerging that help the designer to explore the overall design space and analyze the trade-offs in an informed fashion [Silva01]. Observe also that the chip contains a set of I/O interfaces, as well as an embedded network module, which helps to orchestrate the traffic between processor and the various accelerator and I/O modules.

The generation process of a macro module depends on the hard or soft nature of the block, as well as the level of design entry. In the following sections, we briefly discuss some commonly used approaches.

#### 8.4.4 Semicustom Design Flow

So far, we have defined the components that make up the cell-based design methodology. In this section, we discuss how it all comes together. Figure 8-16 details the traditional sequence of steps to design a semicustom circuit. The steps of what we call the design flow are enumerated in the figure, with a brief description of each:

1. **Design Capture** enters the design into the ASIC design system. A variety of methods can be used to do so, including schematics and block diagrams; hardware description languages (HDLs) such as VHDL, Verilog, and, more recently, C-derivatives such as SystemC; behavioral description languages followed by high-level synthesis; and imported intellectual property modules.
2. **Logic Synthesis** tools translate modules described using an HDL language into a *netlist*. Netlists of reused or generated macros can then be inserted to form the complete netlist of the design.
3. **Prelayout Simulation and Verification**. The design is checked for correctness. Performance analysis is performed based on estimated parasitics and layout parameters. If the design is found to be nonfunctional, extra iterations over the design capture or the logic synthesis are necessary.
4. **Floor Planning**. Based on estimated module sizes, the overall outlay of the chip is created. The global-power and clock-distribution networks also are conceived at that time.

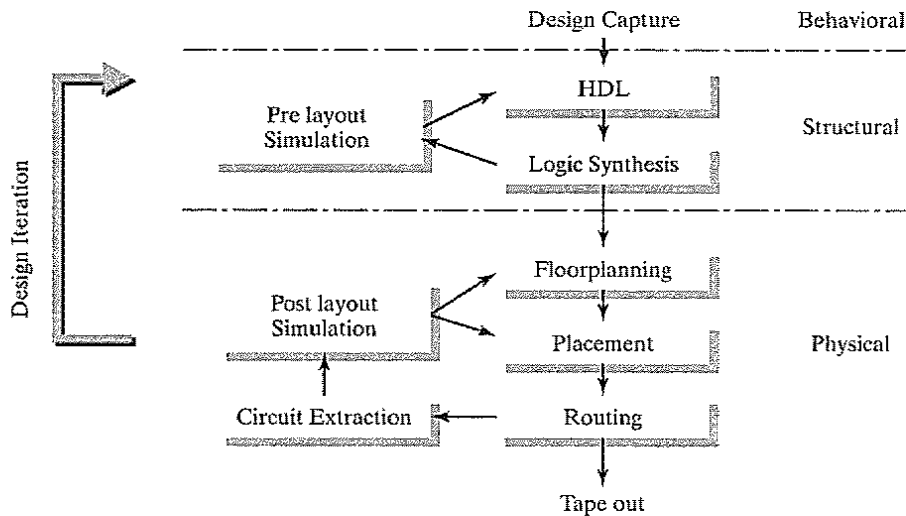
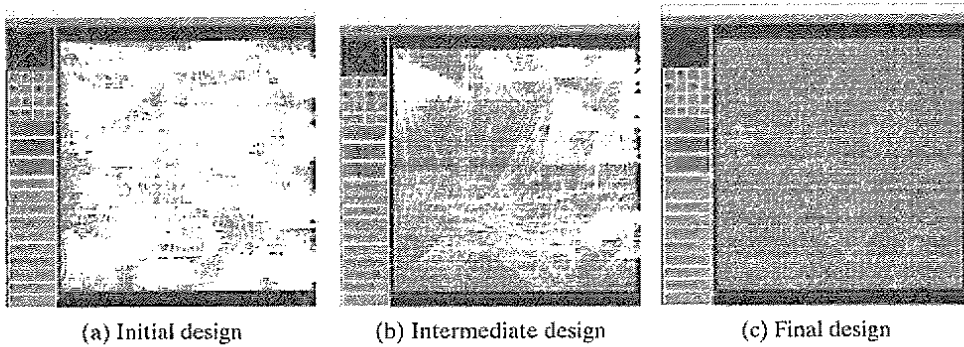


Figure 8-16 The Semicustom (or ASIC) design flow.

5. **Placement.** The precise positioning of the cells is decided.
6. **Routing.** The interconnections between the cells and blocks are wired.
7. **Extraction.** A model of the chip is generated from the actual physical layout, including the precise device sizes, devices parasitics, and the capacitance and resistance of the wires.
8. **Postlayout Simulation and Verification.** The functionality and performance of the chip is verified in the presence of the layout parasitics. If the design is found to be lacking, iterations on the floorplanning, placement, and routing might be necessary. Very often, this might not solve the problem, and another round of the structural design phase might be necessary.
9. **Tape Out.** Once the design is found to be meeting all design goals and functions, a binary file is generated containing all the information needed for mask generation. This file is then sent out to the ASIC vendor or foundry. This important moment in the life of a chip is called *tape out*.

While the design flow just described has served us well for many years, it was found to be severely lacking once technology reached the 0.25- $\mu\text{m}$  CMOS boundary. With design technology proceeding into the deep submicron region, layout parasitics—especially from the interconnect—are playing an increasingly important role. The prediction models used by the logic and structural synthesis tools have a hard time providing accurate estimates for these parasitics. The chances that the generated design meets the timing constraints at the first try are thus very small (Figure 8-17a). The designer (or design team) is then forced to go through a number of costly iterations of synthesis followed by layout generation until an acceptable artwork that meets the timing constraints is obtained (Figure 8-17b and c). Each of these iterations may take several days—just routing a complex chip can take a week on the most advanced computers! The





**Figure 8-17** The timing closure process. The white lines indicate nets with timing violations. In each iteration of the design process, timing errors are removed by optimizing the logic, by insertion of buffers, by constraining the placement, or by streamlining the routing until an error-free design is obtained [Avanti01].

number of needed iterations continues to grow with the scaling of technology. This problem, called *timing closure*, made it obvious that new solutions and a change in design methodology were required.

The common answer is to create a tighter integration between the logical and physical design processes. If the logic synthesis tool, for example, also performs some part of the placement—or directs the placement—more precise estimates of the layout parameters can be obtained. Figure 8-18 shows an example of a design environment that merges RTL synthesis with first-order placement and routing. The resulting netlist is then fed into an optimization tool that performs the detailed placement and routing, while guaranteeing the timing constraints are met. While this approach has shown to be quite successful in reducing the number of design iter-

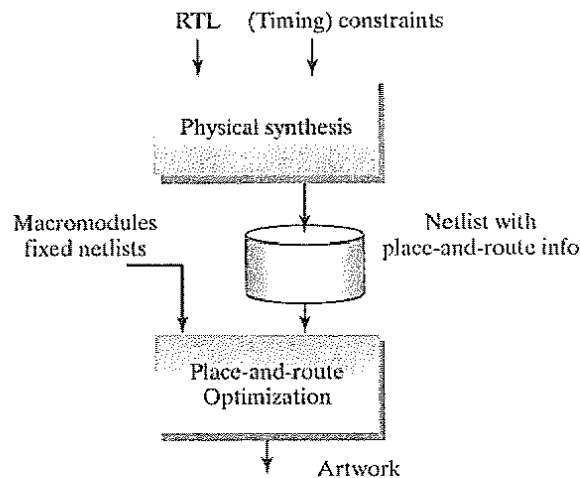


**Figure 8-18** Integrated synthesis place-and-route reduces the number of iterations to reach timing closure in deep submicron.

ations, it throws quite a challenge at the design-tool developers. With the number of parasitic effects increasing with every round of technology scaling, the design optimization process that must take all this into account becomes exponentially complex as well. As a result, other approaches might be required as well. In the coming chapters, we will highlight “design solutions” that can help to alleviate some of these problems. An example is the use of regular and predictable structures, both at the logical and the physical level.

## 8.5 Array-Based Implementation Approaches

While design automation can help reduce the design time, it does not address the time spent in the manufacturing process. All of the design methodologies discussed thus far require a complete run through the fabrication process. This can take from three weeks to several months, and it can substantially delay the introduction of a product. Additionally, with ever-increasing mask costs, a dedicated process run is expensive, and product economics must determine if this is a viable route.

Consequently, a number of alternative implementation approaches have been devised that do not require a complete run through the manufacturing process, or they avoid dedicated processing completely. These approaches have the advantage of having a lower NRE (nonrecurring expense) and are, therefore, more attractive for small series. This comes at the expense of lower performance, lower integration density, or higher power dissipation.

### 8.5.1 Prediffused (or Mask-Programmable) Arrays

In this approach, batches of wafers containing arrays of primitive cells or transistors are manufactured by the vendors and stored. All the fabrication steps needed to make transistors are standardized and executed without regard to the final application.

To transform these uncommitted wafers into an actual design, only the desired interconnections have to be added, determining the overall function of the chip with only a few metallization steps. These layers can be designed and applied to the premanufactured wafers much more rapidly, reducing the turnaround time to a week or less.

This approach is often called the *gate-array* or the *sea-of-gates* approach, depending on the style of the prediffused wafer. To illustrate the concept, consider the gate-array primitive cell shown in Figure 8-19a. It comprises four NMOS and four PMOS transistors, polysilicon gate connections, and a power and ground rail. There are two possible contact points per diffusion area and two potential connection points for the polysilicon strips. We can turn this cell, which does not implement any logic function so far, into a real circuit by adding some extra wires on the metal layer and contact holes. This is illustrated in Figure 8-19b, where the cell is turned into a four-input NOR gate.

The original *gate-array* approach<sup>2</sup> places the cells in rows separated by wiring channels, as shown in Figure 8-20a. The overall look is similar to the traditional standard-cell technique. With the advent of extra metallization layers, the routing channels can be eliminated, and routing can

<sup>2</sup>This approach is often called the *channeled* gate array.

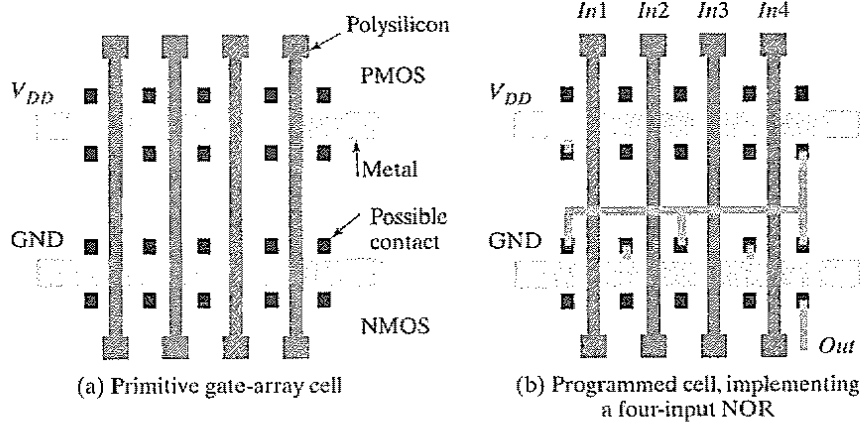


Figure 8-19 An example of the gate-array approach.

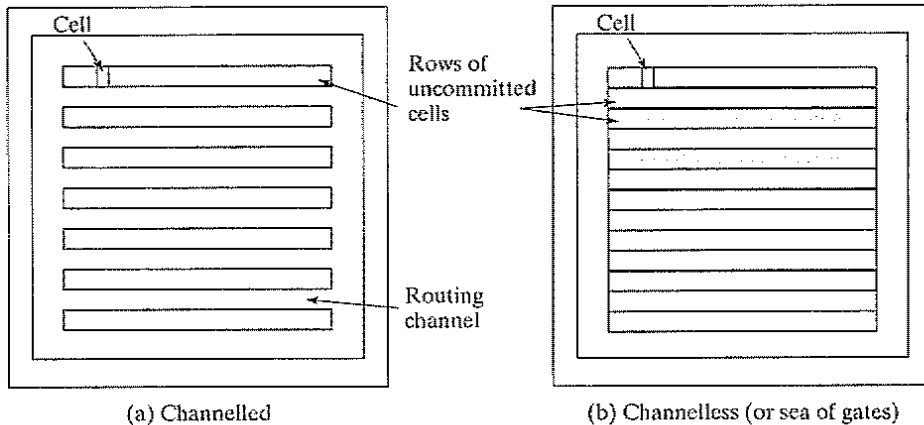
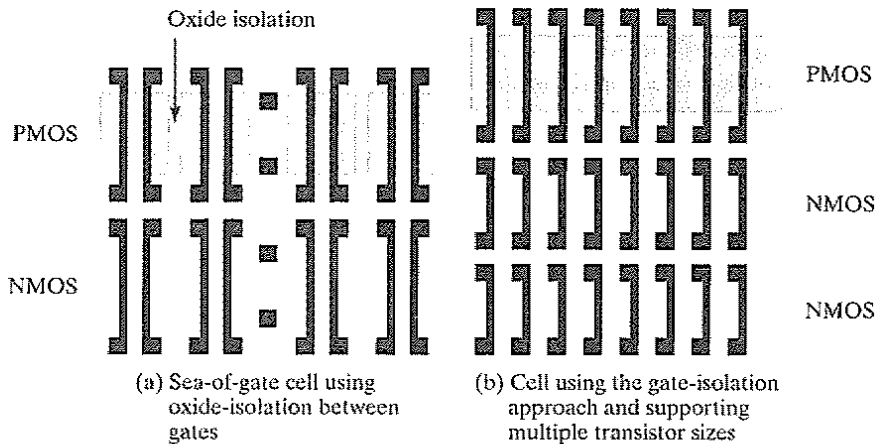


Figure 8-20 Gate-array architectures.

be performed on top of the primitive cells—occasionally leaving a cell unused. This channelless architecture, also called *sea of gates* (Figure 8-20b), yields an increased density, and makes it possible to achieve integration levels of millions of gates on a single die. Another advantage of the sea-of-gates approach is that it customizes the contact layer between metal-1 and diffusion and/or polysilicon, in contrast to the standard gate-array approach where the contacts are predefined (see Figure 8-19a). This extra flexibility leads to a further reduction in cell size.

The primary challenge when designing a gate-array (or sea-of-gates) template is to determine the composition of the primitive cell and the size of the individual transistors. A sufficient number of wiring tracks must be provided to minimize the number of cells wasted to interconnect. The cell should be chosen so that the prefabricated transistors can be utilized to a maximal extent over a wide range of designs. For example, the configuration of Figure 8-19 is well suited for the realization of four-input gates, but wastes devices when implementing two-input gates.



**Figure 8-21** Examples of sea-of-gates primitive cells (from [Veendrick92]).

Multiple cells are needed when implementing a flip-flop. A number of alternative cell structures are pictured in Figure 8-21 in a simplified format. In one approach, each cell contains a limited number of transistors (four to eight). The gates are isolated by means of *oxide isolation* (also called *geometry isolation*). The “dog-bone” terminations on the poly gates allow for denser routing. A second approach provides long rows of transistors, all sharing the same diffusion area. In this architecture, it is necessary to electrically turn off some devices to provide isolation between neighboring gates by tying NMOS and PMOS transistors to  $GND$  and  $V_{DD}$ , respectively. This technique is called *gate isolation*. This approach wastes a number of transistors to provide the isolation, but provides an overall higher transistor density.

Figure 8-22 shows the base cell for a gate-isolated gate array (from [Smith97]). The cell is one routing track wide, and contains one  $p$ -channel and one  $n$ -channel transistor. Also shown is a base cell containing all possible contact positions. There is room for 21 contacts in the vertical direction, which means that the cell has a height of 21 tracks.

It is worth observing that the cell in Figure 8-21b provides two rows of smaller NMOS transistors that can be connected in parallel if needed. Smaller transistors come in handy when implementing pass-transistor logic or memory cells. Sizing the transistors in the cells is a clear challenge. Due to the interconnect-oriented nature of the array-based design methodology, the propagation delay is generally dominated by the interconnect capacitance. This seems to favor larger device sizes that cause a larger area loss when unused. On the other hand, it is possible to construct larger transistors by putting several smaller devices in parallel.

Mapping a logic design onto an array of cells is a largely automated process, involving logic synthesis followed by placement and routing. The quality of these tools has an enormous impact on the final density and performance of a sea-of-gates implementation. Utilization factors in sea-of-gates structures are a strong function of the type of application being implemented. Utilization factors of nearly 100% can be obtained for regular structures such as memories. For

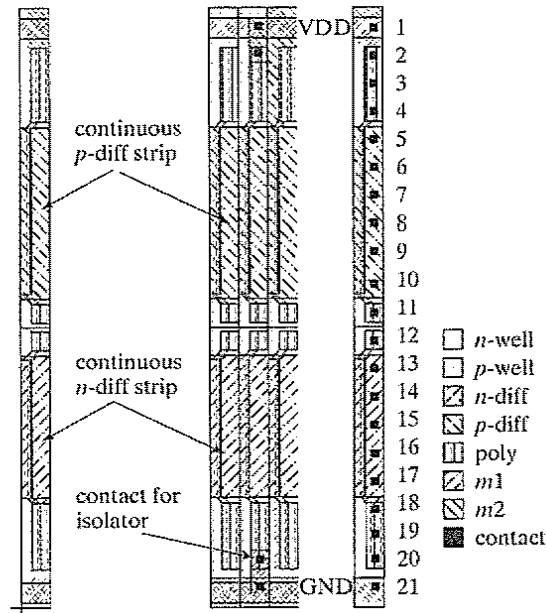


Figure 8-22 Base cell of gate-isolated gate array (from [Smith97]).

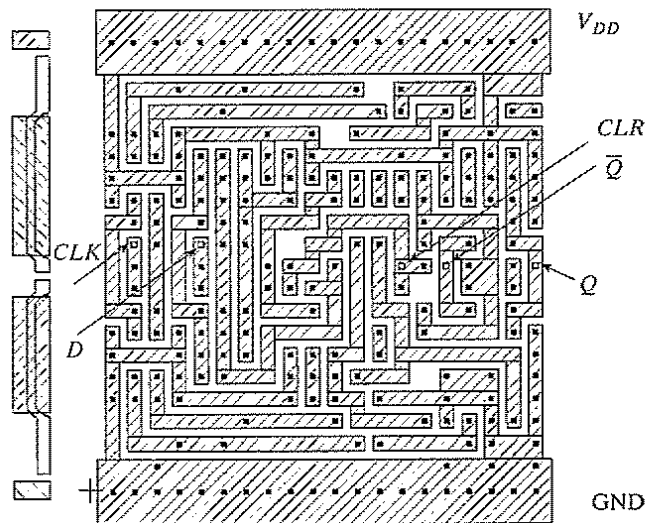


Figure 8-23 Flip-flop implemented in a gate-isolated gate-array library. The base cell is shown on the left (from [Smith97]).

other applications, utilization factors can be substantially lower (< 75%), due largely to wiring restrictions. Figure 8-23 shows an example of a flip-flop macrocell, implemented in a gate-isolated, gate-array library.

Similar to the scenarios unfolding in the standard-cell arena, designers of sea-of-gate arrays discovered that a design with a large number of gates also has large memory needs. Implementing these memory cells on top of the gate-array base-cells is possible, but not very efficient. A more efficient approach is to set aside some area for dedicated memory modules. The mixing of gate arrays with fixed macros is called the *embedded gate-array* approach. Other modules such as microprocessor and microcontrollers are also ideal candidates for embedding.

#### Example 8.7 Sea-of-Gates

An example of a sea-of-gates implementation is shown in Figure 8-24. The array has a maximum capacity of 300 K gates and is implemented in a 0.6- $\mu\text{m}$  CMOS technology. The upper left part of the array implements a memory subsystem, which results in a regular modular layout. The rest of the array implements random logic.

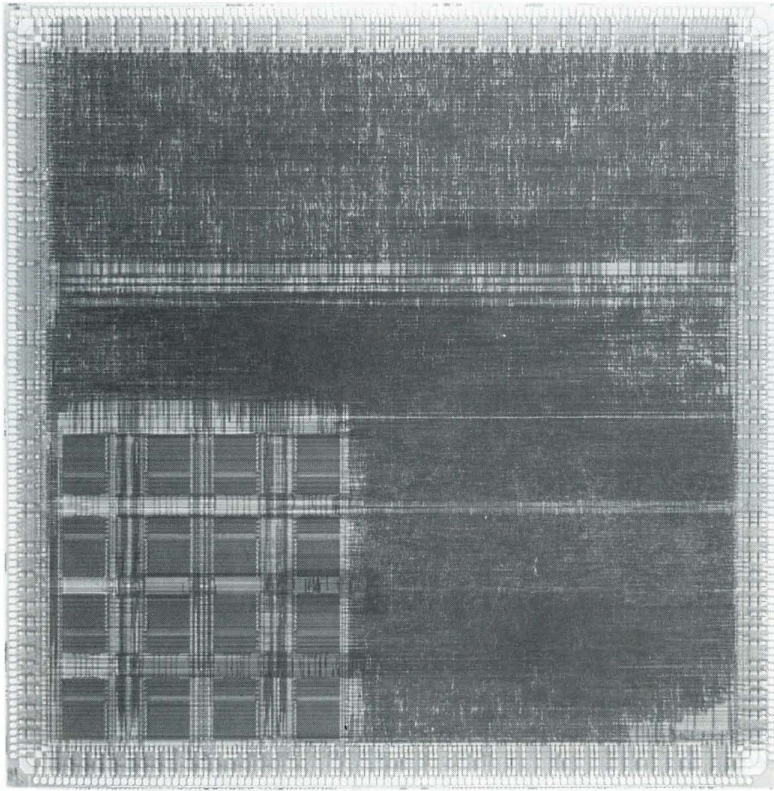


**Figure 8-24** Gate-array die microphotograph (LEA300K) (Courtesy of LSI Logic.)

### Design Consideration—Gate Arrays versus Standard Cells

In the 1980s and 1990s, when the majority of the chips were less than 50,000 gates, design cycles often could be measured in weeks or a few months. The two- or three-week savings in turnaround time for a gate-array design was then a significant portion of the total design cycle, more than enough to offset the additional die size. With today's deep-submicron processes and multimillion-gate complexities come longer design times, and the small reduction in turnaround time is no longer much of an issue. Furthermore, metalization has become the most time-consuming and yield-impacting part of the semiconductor manufacturing process, reducing further the advantage that gate arrays had to offer. Consequently, gate arrays have lost a lot of their luster. Another alternative for rapid prototyping—the prewired arrays discussed in the next section—has arisen, and it has taken a large portion out of the gate-array market.

Still, beware of dismissing the idea of the mask-programmable logic module as a thing of the past. A regular and fixed layout style has the advantage that load factors, wiring parasitics, and cross-coupling noise are easily and accurately estimated. This is in contrast to the standard-cell approach, where these values are ultimately only known after placement, routing, and extraction. One may consider populating sections of a large chip with a regular logic array consisting of uncommitted (prediffused) logic cells superimposed by a wiring grid. The actual programming of the module is performed by placing vias at predefined positions. As shown in Figure 8-25, the use of a via-programmable cross-point switch makes it possible to overlay a wide variety of wiring patterns on a regular repetitive wiring grid. It is the opinion of the authors that prediffused arrays have quite some life left into them.

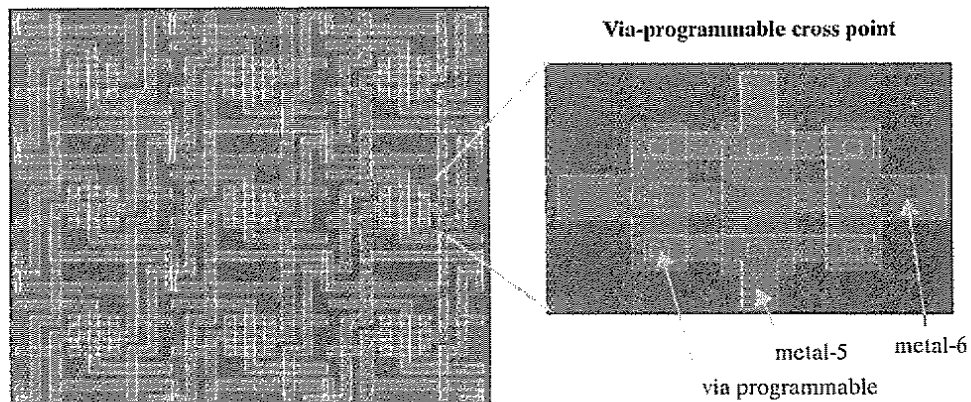


**Figure 8-25** Via-programmable gate array. Vias are used to dedicate a generic wiring grid to a specific wiring pattern, resulting in predictable arrays [Pileggi02].

### 8.5.2 Prewired Arrays

While the prediffused arrays offer a fast road to implementation, it would be even more efficient if dedicated manufacturing steps could be avoided altogether. This leads to the concept of the preprocessed die that can be programmed in the field (i.e., outside the semiconductor foundry) to implement a set of given Boolean functions. Such a programmable, prewired array of cells is called a *field-programmable gate array (FPGA)*. The advantage of this approach is that the manufacturing process is completely separated from the implementation phase and can be amortized over a large number of designs. The implementation itself can be performed at the user site with

negligible turnaround time. The major drawback of this technique is a loss in performance and design density, compared with the more customized approaches.

Two main issues have to be addressed when attempting to implement a set of Boolean functions on top of a regular array of cells without requiring any processing steps:

1. How do we implement “programmable” logic—that is, logic that can be committed to perform any possible Boolean function?
2. How and where do we store the *program*—also called the configuration—that dedicates the programmable array to a certain logic function?

The answer to the second question depends on the memory technology used. Since memory technology is the topic of a later chapter, we limit ourselves here to a high-level overview. In general, three different techniques can be identified:

- **The write-once or fuse-based FPGA.** The logic array is committed to a particular function by blowing “fuses” or by short-circuiting “antifuses.” A fuse is a connection element that is short-circuited by default. A large current causes it to blow, and then it becomes an open circuit. The antifuse has the opposite behavior. An example of an antifuse implementation is shown in Figure 8-26 [El-Ayat89]. The advantage of the write-once approach is that the area overhead of the program memory (i.e., the fuses) is very small. But it has the important disadvantage of being *one-time programmable*. Circuit corrections or extensions are not possible, and new components are required for every design change.
- **The nonvolatile FPGA.** The program is stored in nonvolatile memory, which is memory that retains its value even when the supply voltage is turned off. Examples include EEPROM (*Electrically Erasable Programmable Read-Only Memory*) or Flash memories. Once programmed, the logic remains functional and fixed until a new programming round. The disadvantage of this approach is that nonvolatile memories require special steps in the manufacturing process, such as the deposition of ultrathin oxides. Also, high voltages

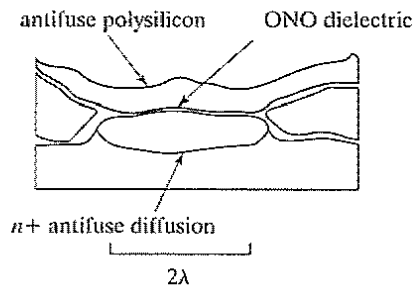


**Figure 8-26** Example of antifuse. A 10-nm-thin layer ( $< 10$  nm) of ONO (oxide–nitride–oxide) dielectric is deposited between conducting polysilicon and diffusion layers. The circuit is open by default, unless a large programming current is forced through it. This causes the dielectric to melt, and a permanent connection with fixed resistance is formed (from [Smith97]).



(> 10 V) are needed for the programming and erasure of the memory cells. Generating these high voltages and distributing them through the logic array adds extra complexity to the design.

- **The Volatile or RAM-Based FPGA.** This popular approach to programming the logic array employs volatile static RAM (random-access memory) cells for the storage of the program. Since these memories lose their stored contents when the FPGA is powered down, a reloading of the configuration from an external permanent memory is necessary every time the part is turned on. To program the component at start-up time, programming data is shifted serially into the part over a single line (or pin). For all practical purposes, one can consider the FPGA RAM cells to be configured as a giant shift register during that period. Once all memories are loaded, normal execution is started. The configuration time is proportional to the number of programmable elements. This can become excessive for today's larger FPGAs, which often feature more than one million gates. Recent parts therefore rely more and more on a parallel programming interface, allowing multiple cells to be programmed at the same time.

In contrast to their nonvolatile counterparts, volatile FPGAs do not have special manufacturing process requirements, and can be implemented in a regular CMOS process. In addition, designers can reuse chips during prototyping. Logic can be modified and upgraded once deployed in the field—a customer can be sent a new configuration file to upgrade the chip, instead of sending a new chip. In addition, logic can be dynamically modified on the fly during execution. The latter approach is called *reconfiguration*, and it became quite popular in the late 1990s. In some sense, this brings a paradigm that was extremely successful in the world of programming (as embodied by the microprocessor) to the domain of logic design.

As for the first question, the answer is somewhat more extensive. Implementing a complex circuit in a programmable fashion requires that both the logic functions as well as the interconnect between them are realized in a configurable fashion. In the coming sections, we first discuss different ways of implementing programmable logic, followed by an overview of programmable interconnection. Finally, we detail a number of specific ways of putting the two together.

### Programmable Logic

Similar to the situation in semicustom design, two fundamentally different approaches towards programmable logic are currently in vogue: array based and cell based.

**Array-Based Programmable Logic** Earlier we discussed how a *programmable logic array* (PLA) implements arbitrary Boolean logic functions in a regular fashion (see page 388). A similar approach can be applied to field-programmable devices as well. Consider, for example, the logic structure of Figure 8-27. A circle (o) at an intersection indicates a programmable connection—that is, an interconnect point that is either enabled or not. An inspection of the diagram reveals that it is equivalent to a PLA, where both the AND and OR planes can be programmed by selectively enabling connections. This approach allows for the implementation of arbitrary

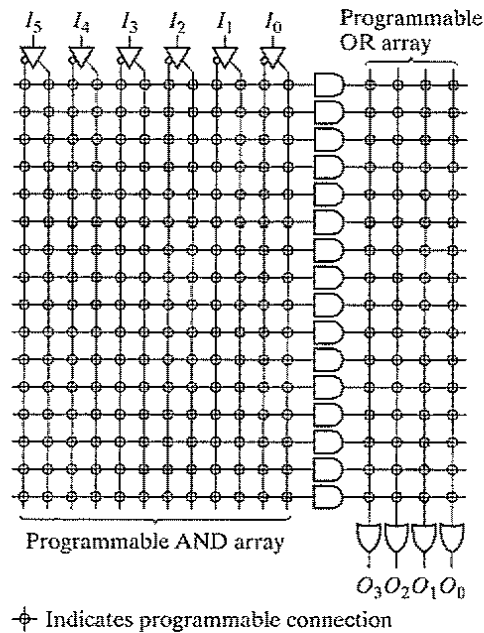
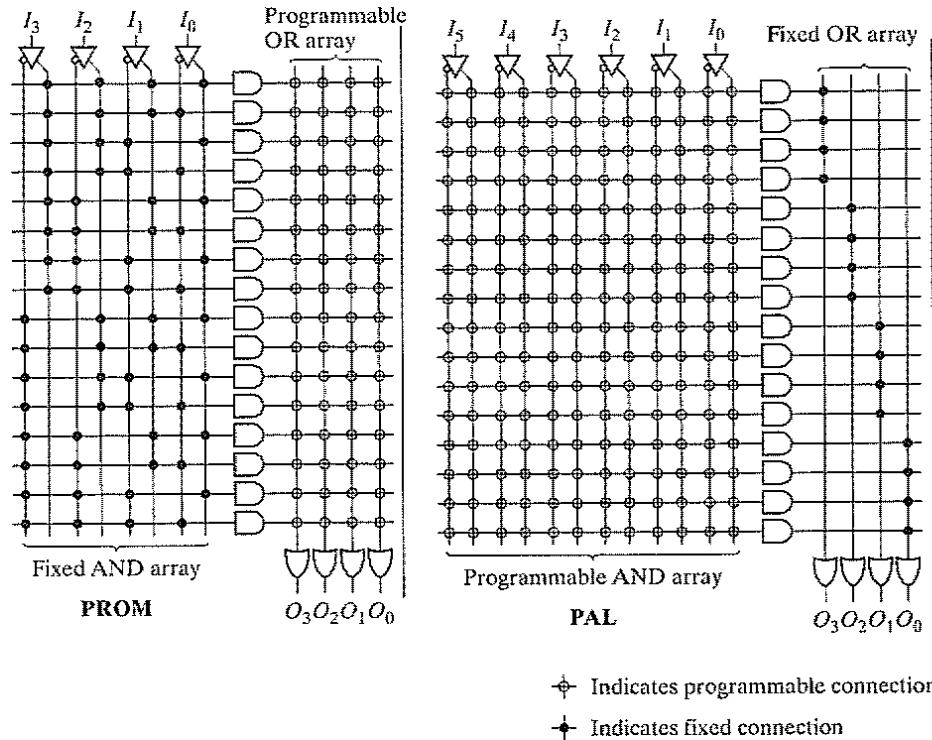


Figure 8-27 Fuse-programmable logic array (PLA).

logic functions in a two-level *sum-of-products* format. The AND plane creates the required minterms, while the OR plane takes the sum of a selected set of products to form the outputs. To include a given input variable (for instance,  $I_1$ ) in a specific minterm, just close the switch at the intersection of the input signal and the minterm. Similarly, a minterm is included into an output by closing the appropriate connection in the OR plane. The functionality of PLA is restricted by the number of inputs, outputs, and minterms.

We can envision variations on this theme, some of which are represented in Figure 8-28. The dot ( $\bullet$ ) at the intersection of two lines represents a nonfusible, hard-wired link. The first structure represents the PROM architecture, in which the AND plane is fixed and enumerates all possible minterms. The second structure, called a *programmable array logic device* (PAL), is located at the other end of the spectrum, where the OR plane is fixed, and the AND plane is programmable. The PLA architecture is the most generic one for the implementation of arbitrary logic functions. The PROM and PAL structures, on the other hand, trade off flexibility for density and performance. Which structure to select depends strongly on the nature of the Boolean functions to be implemented. All these approaches are generally classified under the common term of *programmable logic devices* (or PLDs).

The single-array architecture of the PLA, PROM, and PAL structures in Figure 8-27 and Figure 8-28 becomes less attractive in the era of higher integration density. First of all, implementing very complex logic functions on a single, large array results in a loss of programming density and performance. Secondly, the arrays shown implement only combinational logic. To realize complete, sequential subdesigns, the presence of registers and/or flip-flops is an absolute requirement. These deficiencies can be addressed as follows:



**Figure 8-28** Alternative fuse-based programmable logic devices (or PLDs).

1. Partition the array into a number of smaller sections, often called macrocells.
2. Introduce flip-flops and provide a potential feedback from output signals to the inputs.

One example of how this can be accomplished is shown in Figure 8-29. The PAL consists of  $k$  macrocells, each of which can select from  $i$  inputs and features, at most,  $j$  product terms. Each macrocell contains a single register, which also is programmable—it can be configured as a  $D$ ,  $T$ ,  $J$ - $K$ , or a clocked  $S$ - $R$  flip-flop. The  $k$  output signals are fed back to the input bus, and thus form a subset of the  $i$  input signals.

The PLA approach to configurable logic has two distinct advantages:

- The structure is very regular, which makes the estimation of the parasitics quite easy, and enables accurate predictions of area, speed, and power dissipation.
- It provides an efficient implementation for logic functions that map well into a two-level logic description. Functions with a large fan-in fall into that category. Examples of such are finite-state machines used in controllers and sequencers.

On the other hand, the array structure has the disadvantage of higher overhead. Every intermediate node has a sizable capacitance, which negatively affects performance and power. This is especially true when parts of the array are underutilized—that is, if only some of the minterms are actively used.

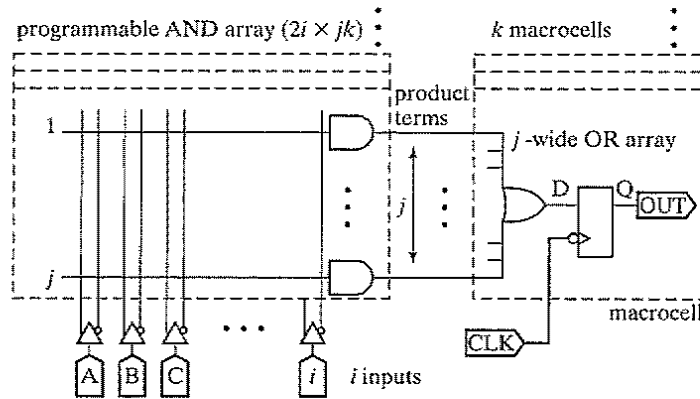


**Figure 8-29** Schematic diagram of a PAL with  $i$  inputs,  $j$  minterms/macrocell and  $k$  macrocells (or outputs) [Smith97].

**Example 8.8 Example of Programmed Macrocell**

Figure 8-30 shows an example of how to program a PROM module. The structure is programmed to realize the logical functions used earlier during the discussion on PLAs (Eq. (8.1)):

$$f_0 = x_0x_1 + \bar{x}_2$$

$$f_1 = x_0x_1x_2 + \bar{x}_2 + \bar{x}_0x_1$$

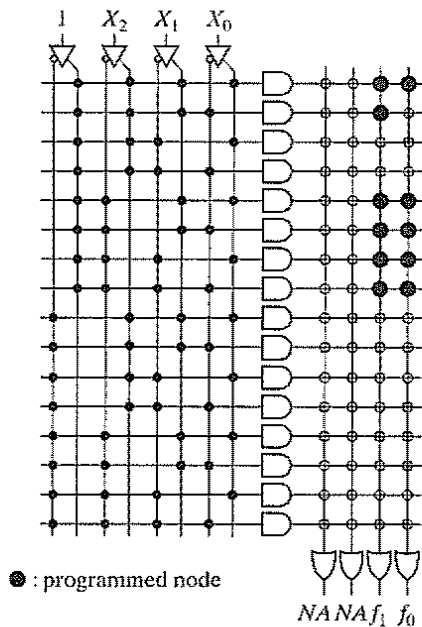


**Figure 8-30** Programming a PROM.

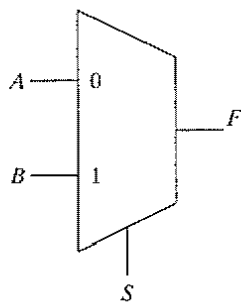
Observe that only a fraction of the array is used as the number of input (3) and output (2) variables are smaller than the dimensions of the  $4 \times 4$  array. Unused input variables are tied either to 0 or 1. The large dots in the output planes represent programmed nodes. The reader is invited to repeat the exercise for the PLA and PAL modules presented in Figure 8-28 and Figure 8-29.

**Cell-Based Programmable Logic** The sum-of-products approach results in regular structures, and is very effective for logic functions that have a large fan-in such as finite-state machines. On the other hand, it performs rather poorly for logic that features a large fan-out, or that benefits from a multilevel logic implementation. (Arithmetic operations such as addition and multiplication are an example of such). Other approaches can be conceived that are more in line with the multilevel approach favored in the standard-cell and sea-of-gate approaches.

There are many ways to design a logic block that can be configured to perform a wide range of logic functions. One approach is to use *multiplexers as function generators*. Consider the two-input multiplexer of Figure 8-31, which implements the logic function  $F$ :

$$F = A \cdot \bar{S} + B \cdot S \quad (8.3)$$

By carefully choosing the connections between the variables  $X$  and  $Y$  and the input ports  $A$ ,  $B$ , and  $S$  of the multiplexer, we can program it to perform ten useful logic operations on one or more of those inputs (see Figure 8-31).



(a)

Configuration			$F =$
$A$	$B$	$S$	
0	0	0	0
0	$X$	1	$X$
0	$Y$	1	$Y$
0	$Y$	$X$	$XY$
$X$	0	$Y$	$X\bar{Y}$
$Y$	0	$X$	$\bar{X}Y$
$Y$	1	$X$	$X + Y$
1	0	$X$	$\bar{X}$
1	0	$Y$	$\bar{Y}$
1	1	1	1

(b)

**Figure 8-31** Using a two-input multiplexer (a) as a configurable logic block. By properly connecting the inputs  $A$ ,  $B$ , and  $S$  to the input variables  $X$  or  $Y$ , or to 0 or 1, 10 different logic functions can be obtained (b).

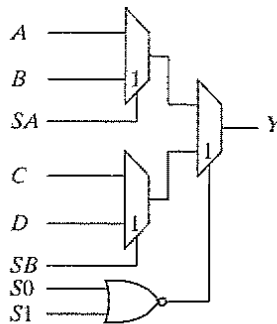


**Figure 8-32** Logic cell as used in the Actel fuse-based FPGA.

A number of multiplexers can be combined to form more complex logic gates. Consider, for example, the logic cell of Figure 8-32, which is used in the Actel ACT family of FPGAs. It consists of three two-input multiplexers and a two-input NOR gate. The cell can be programmed to realize any two- and three-input logic functions, some four-input Boolean functions, and a latch.

### Example 8.9 Programmable Logic Cell

It can be verified that the logic cell of Figure 8-32 acts as a two-input XOR under the programming conditions that follow. Assume the multiplexers select the bottom input signal when the control signal is high. We have the following:

$$A = 1; B = 0; C = 0; D = 1; SA = SB = In1; S0 = S1 = In2$$

As an exercise, determine the programming required for the two-input XNOR function. A three-input AND gate can be realized as follows:

$$A = 0; B = In1; C = 0; D = 0; SA = In2; SB = 0; S0 = S1 = In3$$

Finally, the largest function that can be realized is the four-input multiplexer.  $A$ ,  $B$ ,  $C$ , and  $D$  act as inputs, while  $SA$ ,  $SB$ , and  $(S0 + S1)$  are control signals.

The “multiplexer-as-functional-block” approach provides configurability through programmable interconnections. The *lookup table* (LUT) method employs a vastly different strategy. To configure a fully programmable module with fan-in of  $i$  for a specific function, a two-bit large memory, called the lookup table, is programmed to capture the truth table of that function. The input variables serve as control inputs to a multiplexer, which picks the appropriate value from the memory. The idea is illustrated in Figure 8-33 for a two-input cell. To implement an EXOR function, the lookup table is loaded with the output column of the EXOR truth table, this is “0 1 1 0”. For an input value of “0 0”, the multiplexer selects the first value in the table (“0”), etc. With this approach, any logic function of two inputs can be realized by a simple (re)programming of the memory.

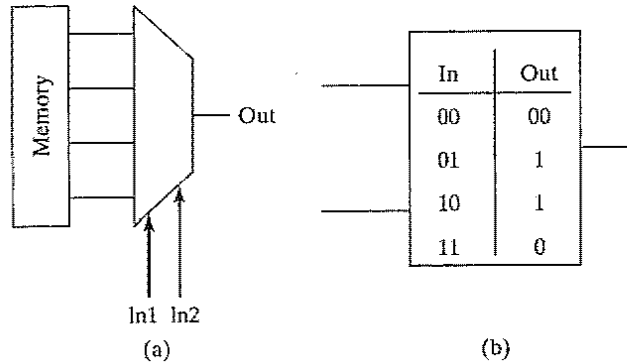


**Figure 8-33** Configurable logic cell based on lookup table. (a) cell schematic; (b) programming the cell to implement an EXOR function.

As in the case of the multiplexer-based approach, more complex gates can be constructed. This is accomplished by either combining a number of LUTs, or by increasing the LUT sizes, or a combination of both. Additional functionality is provided by incorporating flip-flops.

**Example 8.10 LUT-Based Programmable Logic Cell**

Figure 8-34 shows the basic cell, called a *Configurable Logic Block* or CLB, used in the Xilinx 4000 FPGA series [Xilinx4000]. It combines two four-input LUTs feeding a three-

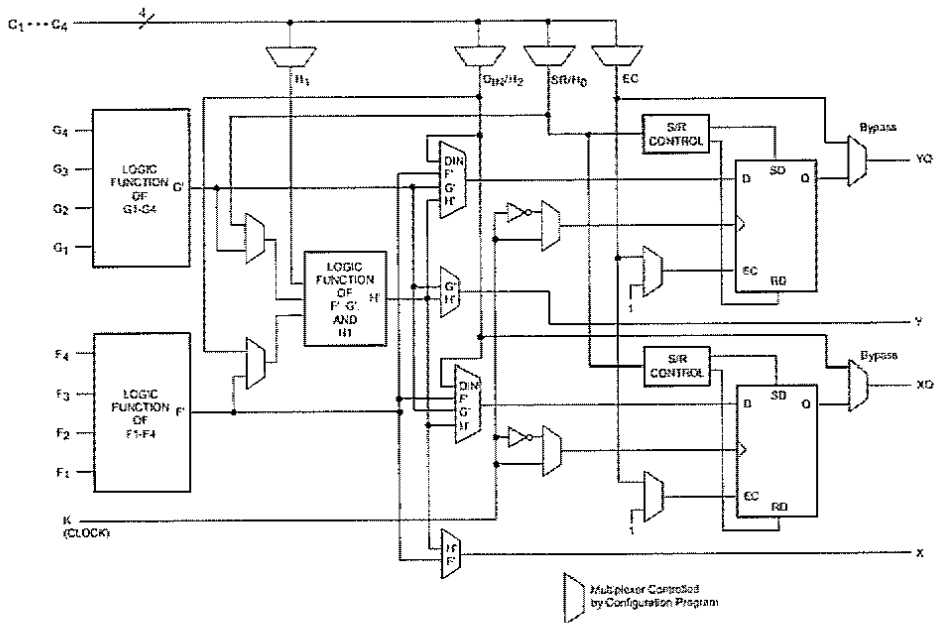


**Figure 8-34** Simplified block diagram of XC4000 Series CLB (RAM and Carry-logic functions not shown) [Xilinx4000].

input LUT. The cell features two flip-flops, whose inputs can be any one of the LUT outputs  $F$ ,  $G$ , or  $H$ , or an extra external input  $D_{in}$ , and whose outputs are available at the  $XQ$  and  $YQ$  output pins. The  $X$  and  $Y$  outputs export the outputs of the LUTs and make it possible to build more complex combinational functions. The cell has four extra inputs ( $C1 \dots C4$ ) that either can be used as inputs or as set/reset and clock-enable signals for the flip-flops.

### Programmable Interconnect

So far, we have discussed in some depth how to make logic programmable. A compelling question is how to make interconnections between those gates changeable or programmable as well. To fully utilize the available logic cells, the interconnect network must be flexible and routing bottlenecks must be avoided. Speed is another prerequisite, since interconnect delay tends to dominate the performance in this style of design. At the same time, the reader should be aware that programmable interconnect comes at a substantial cost in performance in area, performance, and power. In fact, most of the power dissipation in field-programmable architectures is attributable to the interconnect network [George01].

Once again, we can differentiate between mask-programmable, one-time programmable and reprogrammable approaches. It also is worth differentiating between local cell-to-cell interconnections and global signals, such as clocks, that have to be distributed over the complete chip with low delay. In the local-area class, programmable wiring can be classified into two major groupings: array and switchbox routers.

**Array-Based Programmable Wiring** In this approach, wiring is grouped into routing channels, each of which contains a complete grid of horizontal and vertical wires. An interconnect wire can then be programmed into the structure by short-circuiting some of the intersections between horizontal and vertical wires (see Figure 8-35). This can be accomplished by providing a pass transistor at each of the cross points. Closing the interconnection means raising the control signal—by programming a “1” into the connected memory cell  $M$  (see Figure 8-36). This approach is prohibitive and expensive because it requires a large number of transistors and control signals. Also, the large number of transistors connected to each wire leads to a high fan-out, translating into delay and power consumption. A fuse is a more effective programmable connector. In this approach, each routing channel is a fully connected grid of horizontal and vertical interconnect wires, and a fuse is blown whenever a connection is not needed. Unfortunately, interconnect networks tend to be sparsely populated, which requires the interruption of an excessive number of switches and results in prohibitively long programming times.

To circumvent this problem, an *antifuse* can be used (as in Figure 8-26). Antifuses only need to be enabled when a connection is required in the routing channel. This represents a small fraction of the overall grid. Notice in Figure 8-35 how only two antifuses are needed to set up a connection. Be aware that this figure hides the programming circuitry. This operation is a one-time event and cannot be undone. The array-based wiring approach has thus been most successful in the write-once class of FPGAs. Circuit corrections or extensions are not possible, and new



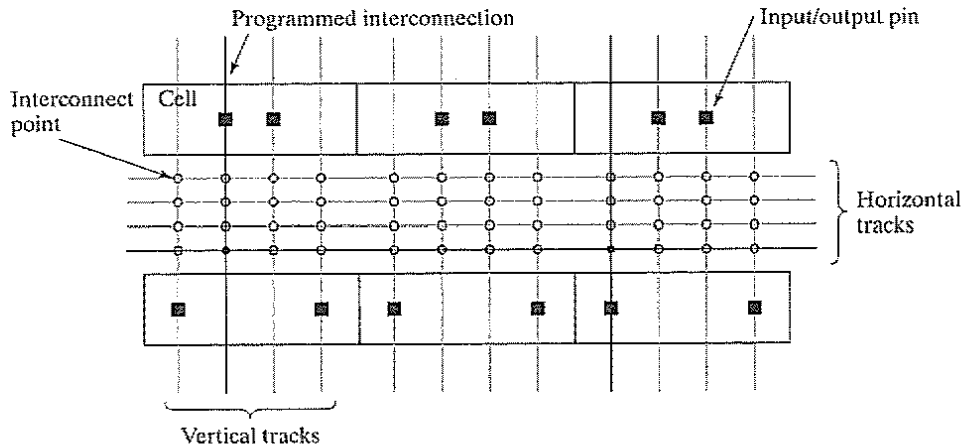


Figure 8-35 Array-based programmable wiring.

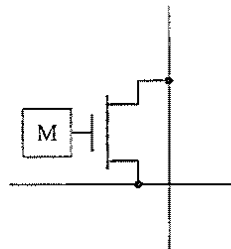
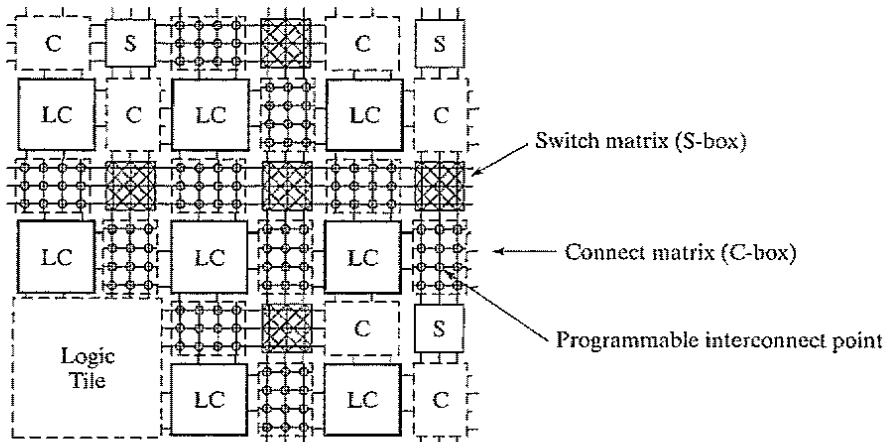


Figure 8-36 Programmable interconnect point. The memory cell controls the interconnection. A stored 0 and 1 mean an open or a closed circuit, respectively. The memory cell can be nonvolatile (EEPROM) or volatile (SRAM).

components are required for every design change. Providing true field (re)programmability requires a more efficient routing strategy.

**Switch-Box-Based Programmable Wiring** It's easy to imagine more efficient programmable-routing approach once we realize that the fully connected wiring grid represents major overkill. By restricting the number of routing resources and interconnect points, we can still manage to wire the desired interconnections, while drastically reducing the overhead. The disadvantage of this approach is that occasionally an interconnection cannot be routed. Most often, this can be addressed by remapping the design—for instance, by choosing another group of logic cells for a given function.

A large number of local interconnections can be accounted for by providing a mesh-like interconnection between neighboring cells. For instance, the outputs of each logic cell (LC) can be distributed to its neighbors to the north, east, south, and west. To account for interconnections between disjoint cells or to provide global interconnections, routing channels are placed between the cells containing a fixed number of uncommitted vertical and horizontal routing wires (Figure 8-37). At the junctions of the horizontal and vertical wires, RAM-programmable switching matrices (S-boxes) are



**Figure 8-37** Programmable mesh-based interconnect network (Courtesy Andre Dehon and John Wawrzyniek.).

provided that direct the routing of the data. Cell inputs and outputs are connected to the global interconnect network by RAM-programmable interconnect points (C-box). Figure 8-38 provides a more detailed view, showing the transistor implementation of the switch and interconnect boxes. Be aware that the single pass-transistor implementation of the switches comes with a threshold-voltage drop. While advantageous from a power perspective, this reduced signal swing has a negative impact on the performance. Special design techniques such as zero-threshold devices, level restorers, or boosted control signals might be required.

The mesh architecture provides a flexible and scalable means for connecting a large number of components. It is quite efficient for local connections, as the number of switches traversed by a single interconnection is small and the fan-out is small. However, the mesh network does not lend itself well to global interconnections. The delay caused by the combination of the many

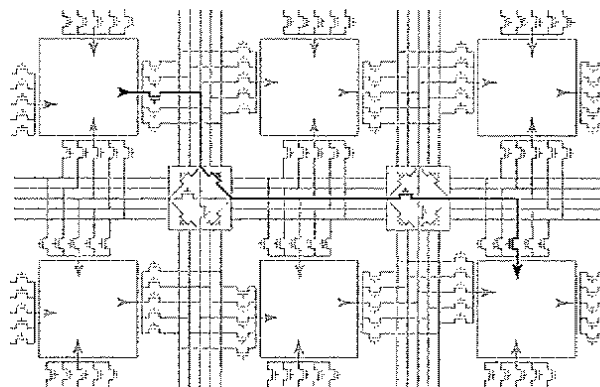


**Figure 8-38** Transistor-level schematic diagram of mesh-based programmable routing network (Courtesy Andre Dehon and John Wawrzyniek.).

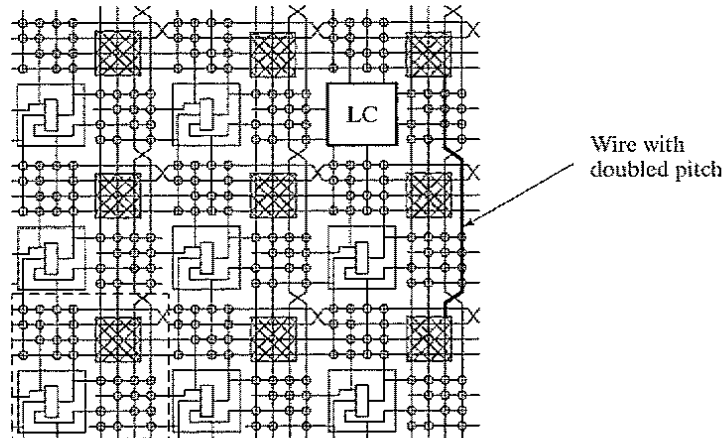


**Figure 8-39** Programmable mesh-based interconnect architecture with overlaid 2 x 2 grid (Courtesy Andre Dehon and John Wawrzyniek.).

switches and the large capacitive load becomes excessive. Most mesh-based FPGA architectures therefore offer alternative wiring resources that allow for effective global wiring. One approach for accomplishing this task is shown in Figure 8-39. In addition to the standard S-box-to-S-box wiring, the network also includes wires connecting S-boxes that are two steps away from each other. Eliminating one S-box from an interconnection decreases the resistance. Similarly, we can include long wires that connect every 4<sup>th</sup>, 8<sup>th</sup>, or 16<sup>th</sup> S-box. What we are creating, in fact, is a number of overlaying meshes with different granularity (single pitch, double pitch, etc.). Long wires are, by preference, mapped on the wiring meshes with the larger pitch.

### Putting It All Together

A complete field-programmable gate array can now be assembled by joining logic-cell and interconnect approaches. Many alternative architectures can be (and have been) conceived. The most important decision to make at the start is the configuration style (write once, nonvolatile, volatile). This puts some constraints on the types of cells and interconnects that can be used. Giving a complete overview is out of the scope of this textbook, so we limit ourselves to two popular architectures, which are illustrative for the field. The interested reader can find more information in [Trimberger94], [Smith97], [Betz99], and [George01].

**The Altera MAX Series [Altera01]** The MAX family of devices (Figure 8-40) belongs to the class of nonvolatile FPGAs (often called EPLDs, or *Electrically Programmable Logic Devices*). It uses a PAL module, (as introduced in Figure 8-29) as the basic logic module. The module (called the *Logic Array Block* or LAB in Altera language) varies little over the members of the family: a wide programmable AND array followed by a narrow fixed OR array and programmable inversion. A LAB typically contains 16 macrocells.

The major differentiation lies in the interconnect architecture between the LABs. The smaller devices (MAX5000, MAX7000) use an array-based routing architecture. The back-

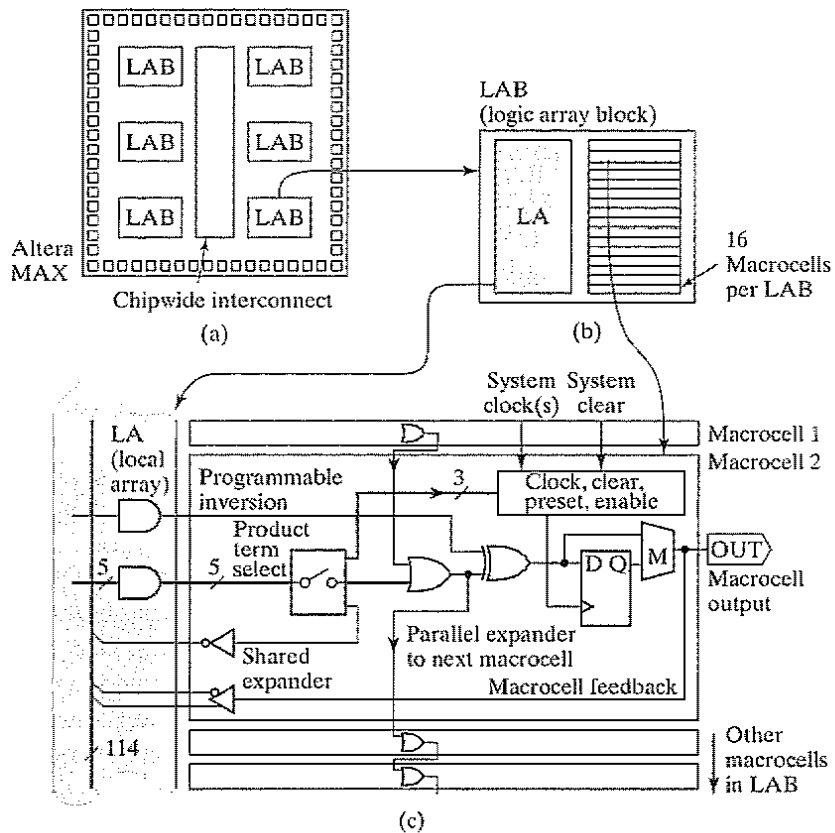


**Figure 8-40** The Altera MAX Architecture. (a) Organization of logic and interconnect; (b) LAB module; (c) a MAX family macrocell. The expanders increase the number of products available by taking another pass through the logic array (from [Smith97]).

bone of the routing channel is formed by the outputs of all the macrocells, complemented with the direct chip inputs. These can be connected to the inputs of the LABs through programmable interconnect points. The advantage of this architecture, called the *Programmable Interconnect Array* or *PIA*, is that it is simple, and the routing delay between the blocks is totally predictable and fixed (see Figure 8-41). The disadvantage is that it does not scale very well. This is why the larger members of the series (MAX9000) have to resort to another scheme. With the number of macrocells reaching up to 560, the single-channel approach runs out of steam, and becomes slow. A mesh-based routing architecture has been opted for instead. Individual macrocells can connect to both row and column channels, which are quite wide (48 to 96 wires).

The EPLD approach delivers up to 15,000 logic gates, and typically is used when high performance is a necessity. Other architectures become desirable when more complex functions have to be implemented.

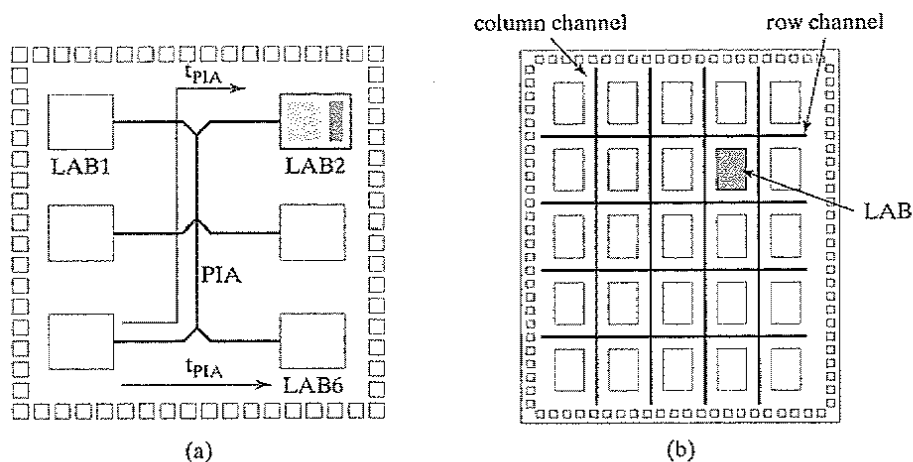


**Figure 8-41** Interconnect architectures used in the Altera MAX series. (a) Array-based architecture used in MAX 3000-7000; (b) Mesh architecture of the MAX9000.

**The Xilinx XC40xx Series** This popular RAM-programmable device family combines the lookup table approach for the implementation of the logic cells, with a mesh-based interconnect network. The largest part in the series (XC4085) supports almost 100,000 gates using a  $56 \times 56$  CLB array. The architecture of the CLB was shown in Figure 8-34. An interesting feature is that the CLB can also be configured as an array of Read/Write memory cells, using the memory lookup tables in the F' and G' blocks. Depending on the selected mode, a single CLB can be configured as either a  $16 \times 2$ ,  $32 \times 1$ , or  $16 \times 1$  bit array. This feature comes in handy, because it is typical for large modules of logic to need comparable amounts of storage.

The interconnect architecture is also quite rich, and combines a wide variety of wiring resources, as shown in Figure 8-42. The overlaid meshes consist of wire segments of lengths 1, 2, and 4. Some components also support direct connections, which link adjacent CLBs without using general wiring resources. Signals routed on the direct interconnect experience minimum wiring delay, as the fan-out is small. These *Directs* are especially effective in the implementation of fast arithmetic modules, which feature many critical local connections. To address global wiring, *long lines* are provided that form a grid of metal interconnect segments that run the entire length or width of the array. These are intended for high fan-out, time-critical signal nets, or nets that are distributed over long distances (such as buses). In addition, special wires are provided for the routing of the clocks.

One topic we have ignored so far in our discussion of configurable array structures is the input/output architecture. For maximum usability, it is crucial that the I/O pins of the component are flexible, and that they provide a wide range of options in terms of direction, logic levels, and drive strengths. One style of input/output block (IOB), used in the XC4000 series, is shown in Figure 8-43. It can be programmed to act as an input, output, or bidirectional port. It includes a flip-flop that can be programmed to be either edge triggered or level sensitive. The slew-rate

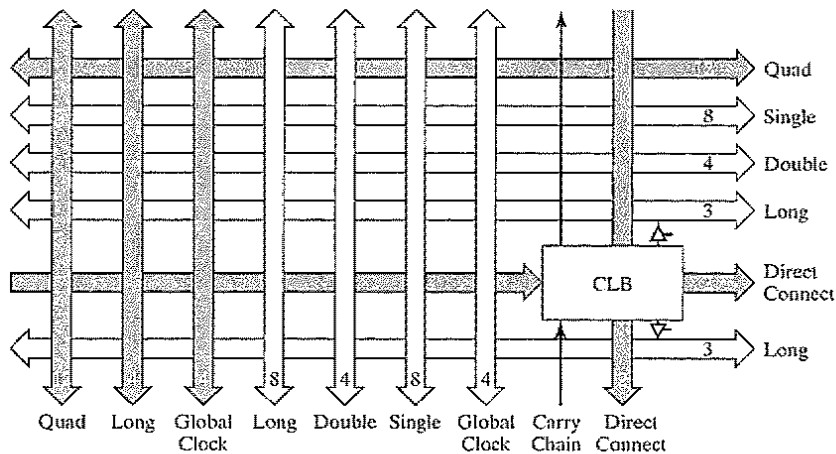


**Figure 8-42** Interconnect architecture of the Xilinx XC4000 series. The numbers annotated on the diagram indicate the amount of each of the resources available.

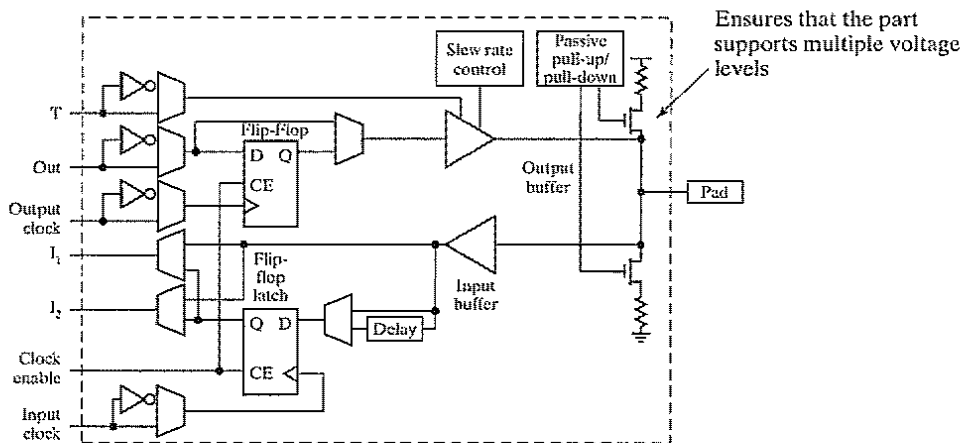


**Figure 8-43** Programmable input/output Block of XC4000 series.

control provides variable drive strengths and allows for a reduction in the rise-fall time for non-critical signals.

### Example 8.11 FPGA Complexity and Performance

To get an impression of what can be achieved with the volatile field-programmable components, consider the Xilinx 4025. It contains approximately 1000 CLBs organized in a  $32 \times 32$  array. This translates into a maximum equivalent gate count of 25,000 gates. The chip contains 422 Kbits of RAM, used mostly for programming. A single CLB is specified to operate at 250 MHz. When taking into account the interconnect network and attempting more complex logic configurations such as adders, clock speeds between 20 and 50 MHz

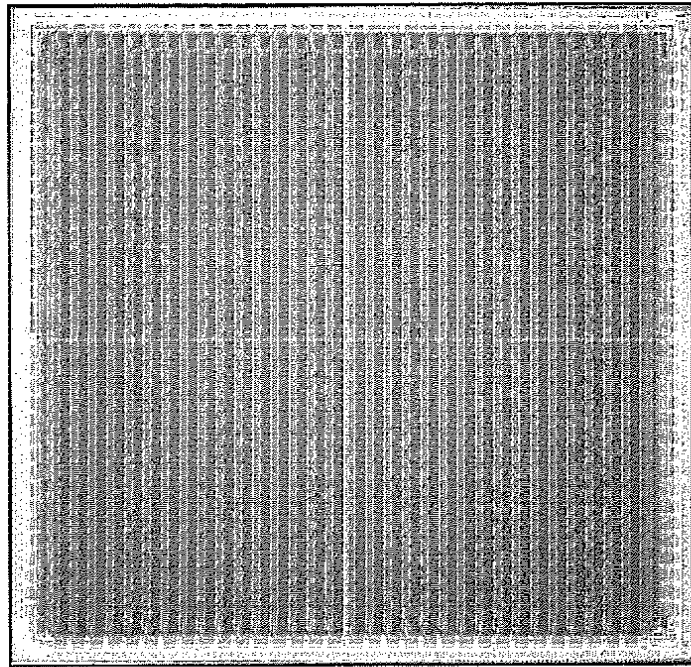


**Figure 8-44** Chip microphotograph of XC4025 volatile FPGA (Courtesy of Xilinx, Inc.).

are attainable. To put the integration complexity in perspective, a 32-bit adder requires approximately 62 CLBs. A chip microphotograph of the XC4025 part is shown in Figure 8-44. The horizontal and vertical routing channels are easily recognizable.

Prewired logic arrays have rapidly claimed a significant part of the logic component market. Their arrival has effectively ended the era of logic design using discrete components represented by the TTL logic family. It is generally believed that the impact of these components is increasing with a further scaling of the technology. To make this approach successful, however, advanced software support in terms of cell placement, signal routing, and synthesis are required. Also, one should not ignore the overhead that flexibility brings with it. Programmable logic is at least 10 times less efficient in terms of energy and performance with respect to ASIC solutions. Hence, its scope has been mostly restricted to prototyping and small-volume applications so far. Yet, flexibility and reuse are alluring. Field-programmable components are bound to see a substantial growth in the years to come.

## 8.6 Perspective—The Implementation Platform of the Future

The designer of today's advanced systems-on-a-chip is offered a broad range of implementation choices. What approach is ultimately chosen is determined by a broad range of factors:

- performance, power and cost constraints
- design complexity
- testability
- time to market, or more precisely, time to revenue
- uncertainty of the market, or late changes in the design
- application range to be covered by the design
- prior experiences of the design team

A number of these factors seem to imply a trend towards more flexible, programmable components that can be reused and that can be modified even after manufacturing. At the same time, solutions that offer the best “bang for the buck” most often end up the winners. Too much flexibility often results in ineffective and expensive solutions, which rapidly end up on the dust heap. Finding the balance between the two extremes is the ultimate challenge of the chip architects of today.

On the basis of these observations, it seems logical to assume that the implementation platform of the future will be a combination of the strategies we have discussed in this chapter, providing implementation efficiency and flexibility when and where needed. The system on a chip is becoming a combination of embedded microprocessors with their memory subsystems, DSPs, fixed ASIC-style hardware accelerators, parameterizable modules, and flexible logic implemented in FPGA style. How these components are balanced is a function of the application requirements and the intended market.

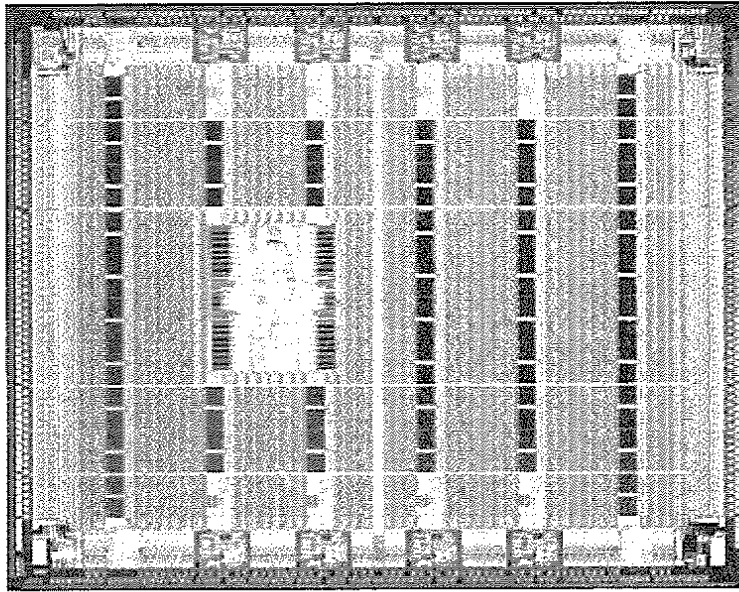
---

### Example 8.12 Examples of Hybrid Implementation Platforms

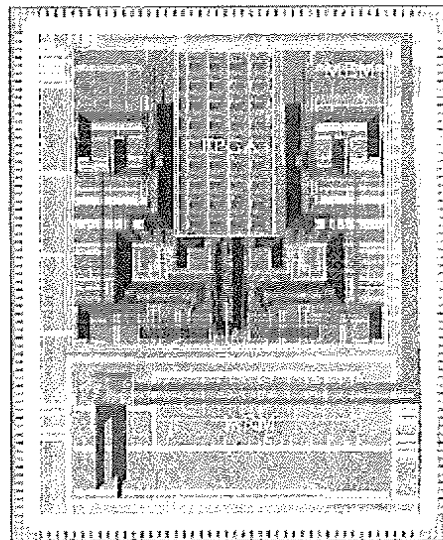
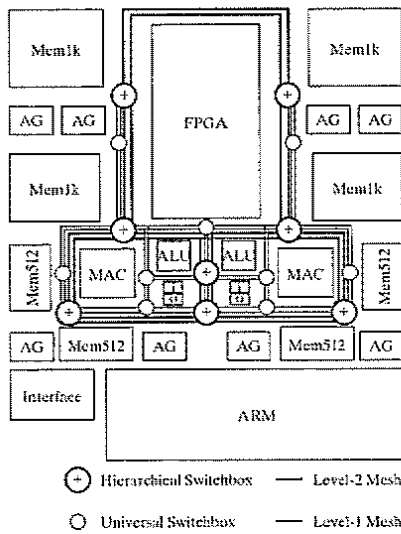
Figure 8-45 shows two contrasting implementation platforms for wireless applications. The first device, the Virtex-II Pro from Xilinx [XilinxVirtex01] is centered around a large FPGA array. A PowerPC microprocessor is embedded in the center of the array. The processor provides an effective implementation approach for application-level functionality and system-level control. To provide higher performance for signal processing applications, an array of embedded  $18 \times 18$  multipliers is added. These dedicated components offer a significant performance, power, and area advantage over a pure FPGA implementation of the same function. Finally, a number of very fast 3.125-Gbps transceivers are provided, allowing for high-speed serial communication off chip.

A somewhat contrasting approach is offered in the design of Figure 8-45b [Zhang00]. The center of this device is an ARM-7 embedded microprocessor, acting as the overall chip manager. Functions that need high performance and energy efficiency are off-loaded to a configurable array of functional units such as multipliers, ALUs, memories, and address generators. These components can be combined dynamically into application-specific processors. The chip also provides an embedded FPGA array for functions that need bit-level granularity.





(a) The Xilinx Virtex-II Pro embeds a PowerPC microprocessor into an FPGA fabric (Courtesy Xilinx, Inc.).



(b) The Maia chip combines embedded microprocessor, configurable accelerators, and FPGA [Zhang00].

**Figure 8-45** Examples of hybrid implementation platforms.

## 8.7 Summary

In this chapter, we have briefly scanned the complex world of design implementation strategies for digital integrated circuits. New implementation styles have rapidly emerged over the last few decades, presenting the designer with a wide variety of options. These design techniques and the accompanying tools are having a major impact on the way design is performed today, and make possible the exciting and impressive processors and application-specific circuits to which we have become so accustomed. We have touched on the following issues in this chapter:

- *Custom design*, where each transistor is individually handcrafted, offers the implementation from an area and performance perspective. This approach has become prohibitively expensive, and should be reserved for the design of the few critical modules in which extreme performance is required, or for often-reused library cells.
- The *semicustom* approach, based on the standard-cell methodology, is the workhorse of today's digital design industry. The advantage is the high degree of automation. The challenge is to deal with the impact of deep-submicron technologies.
- To deal with the increasing complexity of integrated circuits, designers increasingly rely on the availability of large *macrocells* such as memories, multipliers, and microprocessors. These modules are often provided by third-party vendors, and they have spurred a new industry focused on "*intellectual property*."
- Starting a new design for every new emerging application has become prohibitively expensive. The majority of the semiconductor market now focuses on flexible solutions that allow a single component to be used for a variety of applications, either through software programming or reconfiguration. *Configurable hardware* delays the time when the required function is actually committed to the hardware. Different approaches toward late binding also have been discussed. Delaying the binding time comes with an efficiency penalty: The more flexibility that is provided, the larger the impact on performance and power dissipation.

Undoubtedly, new design styles will come on the scene in the near future. Becoming familiar with the available options is an essential part of the learning experience of the beginning digital designer. We hope this chapter, although compressed, entices the reader to further explore the numerous possibilities. One final observation is as follows: Even with the increasing automation of the digital circuit design process, new challenges are continuously emerging—challenges that require the profound insight and intuition offered only by a human designer.

## 8.8 To Probe Further

The literature on design methodologies and automation for digital integrated circuits has exploded in the last few decades. Several reference works are worth mentioning:

- ASIC and FPGA design methodologies: [Smith97]
- FPGA architectures: [Trimberger94], [George01]

- System on a Chip: [Chang99]
- Design methodology and technology: [Bryant01]
- Design synthesis: [DeMicheli94]

State-of-the-art developments in the design automation domain are generally reported in the *IEEE Transactions on CAD*, the *IEEE Transactions on VLSI Systems*, and the *IEEE Design and Test Magazine*. Premier conferences are, among others, the Design Automation Conference (DAC) and the International Conference on CAD (ICCAD). The web sites of the major Electronic Design Automation Companies (Cadence, Synopsys, Mentor, etc.) provide a treasure of information as well.

## References

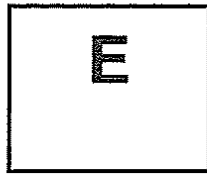
- [Altera01] Altera Device Index, <http://www.altera.com/products/devices/dev-index.html>, 2001.
- [Avanti01] Saturn Efficient and Concurrent Logical and Physical Optimization of SoC Timing, Area and Power, [http://www.synopsys.com/product/avmrgr/saturn\\_ds.html](http://www.synopsys.com/product/avmrgr/saturn_ds.html).
- [Betz99] V. Betz, J. Rose, and A. Marquardt, *Architecture and CAD for Deep-Submicron FPGAs*, Kluwer International Series in Engineering and Computer Science, Kluwer Academic Publishers, 1999.
- [Brayton84] R. Brayton et al., *Logic Minimization Algorithms for VLSI Synthesis*, Kluwer Academic Publishers, 1984.
- [Bryant01] R. Bryant, T. Cheng, A. Kahng, K. Keutzer, W. Maly, R. Newton, L. Pileggi, J. Rabaey, and A. Sangiovanni-Vincentelli, "Limitations and Challenges of Computer-Aided Design Technology for CMOS VLSI," *IEEE Proceedings*, pp. 341–365, March 2001.
- [Cadabra01] AbraCAD Automated Layout Creation, <http://www.cadabratech.com/?id=145products>, Cadabra Design Automation.
- [Chang99] H. Chang et al., "Surviving the SOC Revolution: A Guide to Platform-Based Design," Kluwer Academic Publishers, 1999.
- [DeMicheli94] G. De Micheli, *Synthesis and Optimization of Digital Circuits*, McGraw-Hill, 1994.
- [El-Ayat89] K. El-Ayat, "A CMOS Electrically Configurable Gate Array," *IEEE Journal of Solid State Circuits*, vol. SC-24, no. 3, pp. 752–762, June 1989.
- [George01] V. George and J. Rabaey, *Low-Energy FPGAs*, Kluwer Academic Publishers, 2001.
- [Grundman97] W. Grundmann, D. Dobberpuhl, R. Allmon, and N. Rethman "Designing High-Performance CMOS Processors Using Full Custom Techniques," *Proceedings Design Automation Conference*, pp. 722–727, Anaheim, June 1997.
- [Hill85] D. Hill, "S2C—A Hybrid Automatic Layout System," *Proc. ICCAD-85*, pp. 172–174, November 1985.
- [ModuleCompiler01] Synopsys Module Compiler Datasheet, <http://www.synopsys.com/products/datapath/datapath.html>, Synopsys, Inc.
- [Philips99] The Nexperia System Silicon Implementation Platform, <http://www.semiconductors.philips.com/platforms/nexperia/>, Philips Semiconductors.
- [Pileggi02] Pileggi, Schmit et al., "Via Patterned Gate Array," CMU Center for Silicon System Implementation Technical Report Series, no. CSSI 02-15, April 2002.
- [Prolific01] The ProGenesis Cell Compiler, <http://www.prolificinc.com/progenesis.html>, Prolific, Inc.
- [Rabaey00] J. Rabaey, "Low-Power Silicon Architectures for Wireless Applications," *Proceedings ASPDAC Conference*, Yokohama, January 2000.
- [Silva01] J. L. da Silva Jr., J. Shamberger, M. J. Ammer, C. Guo, S. Li, R. Shah, T. Tuan, M. Sheets, J. M. Rabaey, B. Nikolic, A. Sangiovanni-Vincentelli, P. Wright, "Design Methodology for PicoRadio Networks," *Proc. DATE Conference*, Munich, March 2000.

- [Smith97] M. Smith, *Application-Specific Integrated Circuits*, Addison-Wesley, 1997.
- [Sylvester98] D. Sylvester and K. Keutzer, "Getting to the Bottom of Deep Submicron," *Proc. ICCAD Conference*, pp. 203, San Jose, November 1998.
- [Trimberger94] S. Trimberger, *Field-Programmable Gate Array Technology*, Kluwer Academic Publishers, 1994.
- [Veendrick92] H. Veendrick, *MOS IC's: From Basics to ASICs*, Wiley-VCH, 1992.
- [Xilinx4000] The Xilinx-4000 Product Series, <http://www.xilinx.com/apps/4000.htm>, Xilinx, Inc.
- [XilinxVirtex01] Virtex-II Pro Platform FPGAs,  
[http://www.xilinx.com/xlnx/xil\\_prodcat\\_landing\\_page.jsp?title=Virtex-II+Pro+FPGAs](http://www.xilinx.com/xlnx/xil_prodcat_landing_page.jsp?title=Virtex-II+Pro+FPGAs), Xilinx, Inc.
- [Xtensa01] Xtensa Configurable Embedded Processor Core, <http://www.tensilica.com/technology.html>, Tensilica.
- [Zhang00] H. Zhang, V. Prabhu, V. George, M. Wan, M. Benes, A. Abnous, and J. Rabaey, "A 1 V Heterogeneous Reconfigurable Processor IC for Baseband Wireless Applications," *Proc. ISSCC*, pp. 68-69, February 2000.

### Exercises

For problems and exercises on design methodology, please check <http://bwrc.eecs.berkeley.edu/IcBook>.





## Characterizing Logic and Sequential Cells

*The challenge of library characterization*  
*Characterization methods for logic cells and registers*  
*Cell parameters*

### **The Importance and Challenge of Library Characterization**

The quality of the results produced by a logic synthesis tool is a strong function of the level of detail and accuracy with which the individual cells were characterized. To estimate the delay of a complex module, a logic synthesis program must rely on higher level delay models of the individual cells—falling back to a full circuit- or switch-level timing model for each delay estimation is simply not possible because it takes too much compute time. Hence, an important component in the development process of a standard-cell library is the generation of the delay models. In previous chapters, we learned that the delay of a complex gate is a function of the fan-out (consisting of connected gates and wires), and the rise and fall times of the input signals. Furthermore, the delay of a cell can vary between manufacturing runs as a result of process variations.

In this insert, we first discuss the models and characterization methods that are commonly used for logic cells. Sequential registers require extra timing parameters and thus deserve a separate discussion.

### Characterization of Logic Cells

Unfortunately, no common delay model for standard cells has been adopted. Every vendor has his own favored methods of cell characterization. Even within a single tool, various delay models often can be used, trading off accuracy for performance. The basic concepts are, however, quite similar, and they are closely related to the ones we introduced in Chapters 5 and 6. We therefore opt to concentrate on a single set of models in this section—more precisely, those used in the Synopsys Design Compiler [DesignCompiler01], one of the most popular synthesis tools. Once a model has been adopted, it has to be adopted for all the cells in the block; in other words, it cannot be changed from cell to cell.

The total delay consists of four components, as illustrated in Figure E-1:

$$D_{total} = D_I + D_T + D_S + D_C \quad (E.1)$$

$D_I$  represents the *intrinsic delay*, which is the delay with no output loading.  $D_T$  is the transition component, or the part of the delay caused by the output load.  $D_S$  is the fraction of the delay due to the *input slope*. Finally,  $D_C$  is the *delay of the wire* following the gate. All delays are characterized for both rising and falling transitions.

The simplest model for the transition delay is the linear delay model of Chapter 5. We have

$$D_T = R_{driver}(\Sigma C_{gate} + C_{wire}), \quad (E.2)$$

where  $\Sigma C_{gate}$  is the sum of all input pin capacitances of gates connected to the output of this gate, and  $C_{wire}$  is the estimated wire capacitance. The slope delay  $D_S$  is approximated as a linear function of the transition delay  $D_T$  of the previous gate, written as

$$D_S = S_S D_{Tprev} \quad (E.3)$$

where  $S_S$  is the *slope-sensitivity factor*, and  $D_{Tprev}$  is the transition delay of the previous stage.

The characterization of a library cell must therefore provide the following components, each of them for both rising and falling transitions, and with respect to each of the input pins:

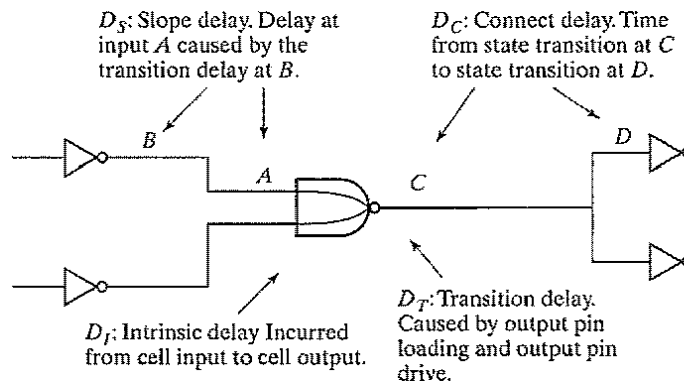


Figure E-1 Delay components of a combinational gate [DesignCompiler01].

- intrinsic delay
- input pin capacitance
- equivalent output driving resistance
- slope sensitivity

In addition to the cell models, the synthesis tools also must have access to a wire model. Since the length of the wires is unknown before the placement of the cells, estimates of  $C_{wire}$  and  $R_{wire}$  are made on the basis of the size of the block and the fan-out of the gate. The length of a wire is most often proportional to the number of destinations it has to connect.

### Example E.1 Three-Input NAND Gate Cell

The characterization of the three-input NAND standard cell gate, presented earlier in Example 8.2, is given in Table E-1. The table characterizes the performance of the cell as a function of the load capacitance and the input-rise (fall) time for two different supply voltages and operating temperatures. The cell is designed in a 0.18- $\mu\text{m}$  CMOS technology.

**Table E-1** Delay characterization of a three-input NAND gate (in ns) as a function of the input node for two operation corners (supply-voltage-temperature pairs of 1.2 V–125°C, and 1.6 V–40°C). The parameters are the load capacitance  $C$  and the input rise (fall) time  $T$ . (Courtesy ST Microelectronics.)

Path	1.2 V–125°C	1.6 V–40°C
$In1-t_{pLH}$	$0.073 + 7.98C + 0.317T$	$0.020 + 2.73C + 0.253T$
$In1-t_{pHL}$	$0.069 + 8.43C + 0.364T$	$0.018 + 2.14C + 0.292T$
$In2-t_{pLH}$	$0.101 + 7.97C + 0.318T$	$0.026 + 2.38C + 0.255T$
$In2-t_{pHL}$	$0.097 + 8.42C + 0.325T$	$0.023 + 2.14C + 0.269T$
$In3-t_{pLH}$	$0.120 + 8.00C + 0.318T$	$0.031 + 2.37C + 0.258T$
$In3-t_{pHL}$	$0.110 + 8.41C + 0.280T$	$0.027 + 2.15C + 0.223T$

While linear delay models offer good first-order estimates, more precise models are often used in synthesis, especially when the real wire lengths are back annotated onto the design. Under those circumstances, nonlinear models have to be adopted. The most common approach is to capture the nonlinear relations as lookup tables for each of these parameters. To increase computational efficiency and minimize storage and characterization requirements, only a limited set of loads and slopes are captured, and linear interpolation is used to determine the missing values.



**Example E.2 Delay Models Using Lookup Tables**

A (partial) characterization of a two-input AND cell (AND2), designed in a 0.25- $\mu\text{m}$  CMOS technology (*Courtesy ST Microelectronics*) follows. The delays are captured for output capacitances of 7 fF, 35 fF, 70 fF, and 140 fF, and input slopes of 40 ps, 200 ps, 800 ps, and 1.6 ns, respectively.

```

cell(AND) {
  area : 36 ;
  pin(Z) {
    direction : output ;
    function : "A*B";
    max_capacitance : 0.14000 ;

    timing() {
      related_pin : "A" ; /* delay between input pin A and output pin Z */
    cell_rise {
      values( "0.10810, 0.17304, 0.24763, 0.39554", \
              "0.14881, 0.21326, 0.28778, 0.43607", \
              "0.25149, 0.31643, 0.39060, 0.53805", \
              "0.35255, 0.42044, 0.49596, 0.64469" ); }
      rise_transition {
      values( "0.08068, 0.23844, 0.43925, 0.84497", \
              "0.08447, 0.24008, 0.43926, 0.84814", \
              "0.10291, 0.25230, 0.44753, 0.85182", \
              "0.12614, 0.27258, 0.46551, 0.86338" );}
      cell_fall(table_1) {
      values( "0.11655, 0.18476, 0.26212, 0.41496", \
              "0.15270, 0.22015, 0.29735, 0.45039", \
              "0.25893, 0.32845, 0.40535, 0.55701", \
              "0.36788, 0.44198, 0.52075, 0.67283" );}
      fall_transition(table_1) {
      values( "0.06850, 0.18148, 0.32692, 0.62442", \
              "0.07183, 0.18247, 0.32693, 0.62443", \
              "0.09608, 0.19935, 0.33744, 0.62677", \
              "0.12424, 0.22408, 0.35705, 0.63818" );}
      intrinsic_rise : 0.13305 ; /* unloaded delays */
      intrinsic_fall : 0.13536 ;
    }
  }
  timing() {
    related_pin : "B" ; /* delay between input pin A and output pin Z */
    ...
  }
}

```

```

intrinsic_rise : 0.12426 ;
  intrinsic_fall : 0.14802 ;
}
}
pin(A) {
  direction : input ;
  capacitance : 0.00485 ; /* gate capacitance */
}
pin(B) {
  direction : input ;
  capacitance : 0.00519 ;
}
}
}

```

**Characterization of Registers**

In Chapter 7, we identified the three important timing parameters of a register. The *setup time* ( $t_{su}$ ) is the time that the data inputs ( $D$  input) must be valid before the clock transition (in other words, the 0 to 1 transition for a *positive edge-triggered* register). The *hold time* ( $t_{hold}$ ) is the time the data input must remain valid after the clock edge. Finally, the propagation delay ( $t_{c-q}$ ) equals the time it takes for the data to be copied to the  $Q$  output after a clock event. The latter parameter is illustrated in Figure E-2a.

Latches have a bit more complex behavior, and thus require an extra timing parameter. While  $t_{c-Q}$  corresponds to the delay of relaunching of data that arrived to a closed latch,  $t_{D-Q}$  equals the delay between  $D$  and  $Q$  terminals when the latch is in transparent mode (Figure E-2b).

The characterization of the  $t_{c-Q}$  ( $t_{D-Q}$ ) delay is fairly straightforward. It consists of a delay measurement between the 50% transitions of  $Clk$  ( $D$ ) and  $Q$ , for different values of the input slopes and the output loads, not unlike the case of combinational logic cells.

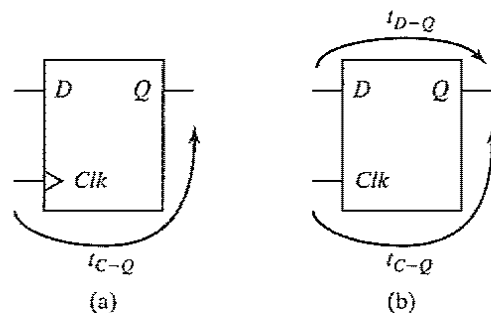


**Figure E-2** Propagation delay definitions for sequential components: (a) register; (b) latch.

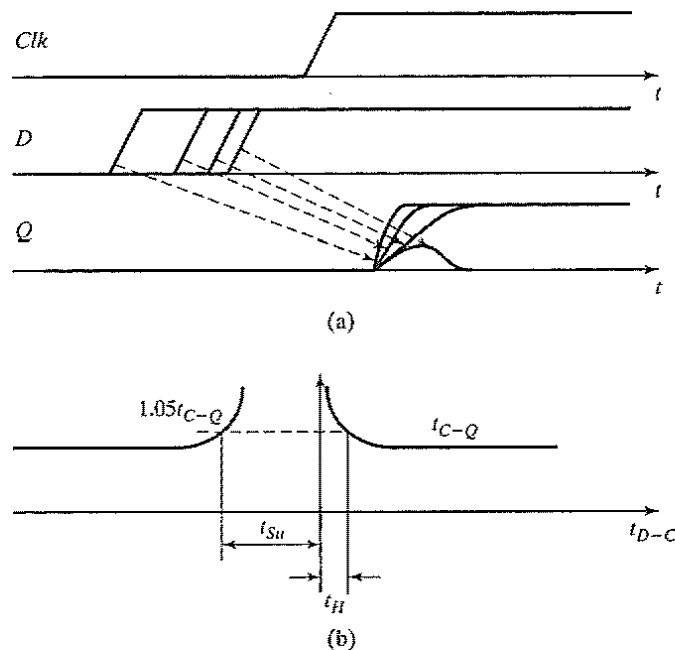


**Figure E-3** Characterization of sequential elements: (a) determining the setup time of a register; (b) definition of setup and hold times.

The characterization of setup and hold times is more elaborate, and depends on what is defined as “valid” in the definitions of both setup and hold times. Consider the case of the setup time. Narrowing the time interval between the arrival of the data at the  $D$  input and the  $Clk$  event does not lead to instantaneous failure (as assumed in the first-order analysis in Chapter 7), but rather to a gradual degradation in the delay of the register. This is documented in Figure E-3a, which illustrates the behavior of a register when the data arrives close to the setup time. If  $D$  changes long before the clock edge, the  $t_{C-Q}$  delay has a constant value. Moving the data transition closer to the clock edge causes  $t_{C-Q}$  to increase. Finally, if the data changes too close to the clock edge, the register fails to register the transition altogether.

Clearly, a more precise definition of the “setup time” concept is necessary. An unambiguous specification can be obtained by plotting the  $t_{C-Q}$  delay against the data-to-clock offset, as shown in Figure E-3b. The degradation of the delay for smaller values of the offset can be observed. The actual definition of the setup time is rather precarious. If it were defined as the minimum  $D$ - $Clk$  offset that causes the flip-flop to fail, the logic following the register would suffer from excessive delay if the offset is close to, but larger than, that point of failure. Another option is to place it at the operation point of the register that minimizes the sum of the data-clock offset and the  $t_{C-Q}$  delay. This point, which minimizes the overall flip-flop overhead, is reached when the slope of the delay curve in Figure E-3b equals 45 degrees [Stojanovic99].

While custom design can take advantage of driving flip-flops close to their point of failure—and take all the risk that comes with it—semicustom design must take a more conservative approach. For the characterization of registers in a standard cell library, both setup and hold times are commonly defined as data-clock offsets that correspond to **some fixed percentage increase in  $t_{C-Q}$** , typically set at 5%, as indicated in Figure E-3b. Note that these curves are different for 0–1 and 1–0 transitions, resulting in different setup (an hold) times for 0 and 1 values. As with clock-to-output delays, setup times also are dependent on clock and data slopes, and they are represented as a two-dimensional table in nonlinear delay models. Identical definitions hold for latches.

**Example E.3 Register Setup and Hold Times**

In this example, we examine setup and hold behavior of the transmission gate master-slave register introduced in Chapter 7. (See Figure 7.18.) The register is loaded with a 100-fF capacitor, and its setup and hold times are examined for clock and data slopes of 100 ps. The simulation results are plotted in Figure E-4. When data settles a “long time” before the clock edge, the clock-to-output delay equals 193 ps. Moving the data transition closer to the clock edge causes the  $t_{C-Q}$  delay to increase. This becomes noticeable at an offset between data and clock of about 150 ps. The register completely fails to latch the data when data precedes the clock by 77 ps. The sum of  $D-Q$  offset and the  $t_{C-Q}$  is minimal at 93 ps. A 5% increase in  $t_{C-Q}$  is observed at 125 ps, and this time is entered in the library as the setup time for this particular slope of data and clock. This characterization of setup time adds a margin to the design of about 30 ps. From these simulations, we also can determine that this register has a hold time of –15 ps.

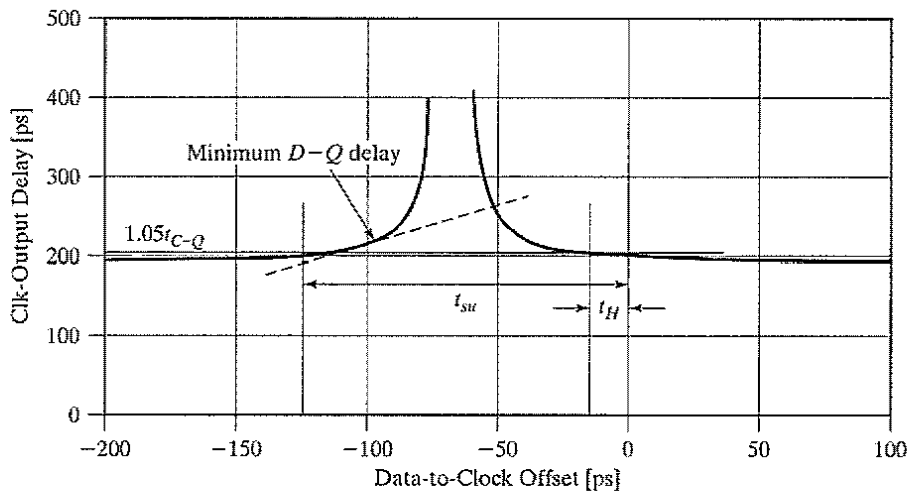
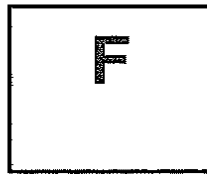


**Figure E-4** Characterization of the clock-to-output delay, setup and hold times of a transmission-gate latch pair.

### References

- [DesignCompiler01] Design Compiler, Product Information, [http://www.synopsys.com/products/logic/design\\_compiler.html](http://www.synopsys.com/products/logic/design_compiler.html), Synopsys, Inc.
- [Stojanovic99] V. Stojanovic, V.G. Oklobdzija, "Comparative analysis of master-slave latches and flip-flops for high-performance and low-power systems," *IEEE Journal of Solid-State Circuits*, vol. 34, no. 4, April 1999.



## Design Synthesis

*Circuit, Logic, and Architectural Synthesis*

One of the most enticing proposals one can make to a designer who has to generate a circuit with tough specifications in a short time is to offer him a tool that automatically translates his specifications into a working circuit that meets all the requirements. One of the main reasons that semiconductor circuits have reached the mind-boggling complexity they have today, is that such synthesis tools actually exist—at least to a certain extent. Synthesis can be defined as the transformation between two different design views. Typically, it represents a translation from a *behavioral* specification of a design entity into a *structural* description. In simple terms, it translates a description of the function a module should perform (the behavior) into a composition—that is, an interconnection of elements (the structure). Synthesis approaches can be defined at each level of abstraction: circuit, logic, and architecture. An overview of the various synthesis levels and their impact is given in Figure F-1. The synthesis procedures may differ depending on the targeted implementation style. For example, logic synthesis translates a logic description given by a set of Boolean equations into an interconnection of gates. The techniques involved in this process strongly depend on the choice of either a two-level (PLA) or a multilevel (standard-cell or gate-array) implementation style. We briefly describe the synthesis tasks at each of the different modeling levels. Refer to [DeMicheli94] for more information and a deeper insight into design synthesis.

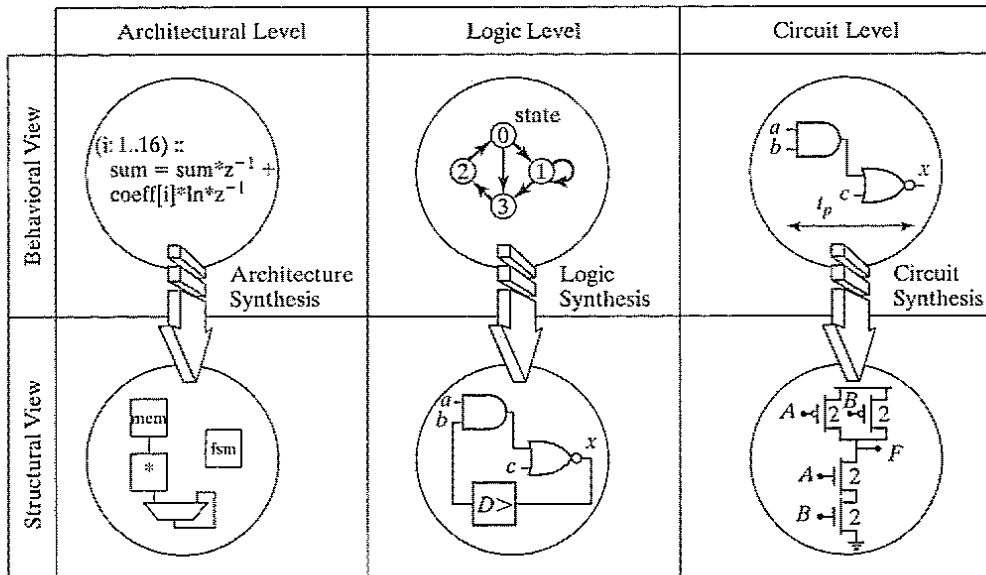


Figure F-1 A taxonomy of synthesis tasks.

### Circuit Synthesis

The task of circuit synthesis is to translate a logic description of a circuit into a network of transistors that meets a set of timing constraints. This process can be divided into two stages:

1. Derivation of *transistor schematics* from the logic equations. This requires the selection of a circuit style (complementary static, pass transistors, dynamic, DCVSL, etc.) and the construction of the logic network. The former task is usually up to the designer, while the latter depends upon the chosen style. For instance, the logic graph technique introduced in Design Methodology Insert D can be used to derive the complementary pull-down and pull-up networks of a static CMOS gate. Similarly, automated techniques have been developed to generate the pull-down trees for the DCVSL logic style so that the number of required transistors is minimized [Chu86].
2. *Transistor sizing* to meet performance constraints. This has been a recurring subject throughout this book. The choice of the transistor dimensions has a major impact on the area, performance, and power dissipation of a circuit. We have also learned that this is a subtle process. For instance, the performance of a gate is sensitive to a number of layout parasitics, such as the size of the diffusion area, fan-out, and wiring capacitances. Notwithstanding these daunting challenges, some powerful transistor-sizing tools have been developed [e.g., Fishburn85, AMPS99, Northrop01]. The key to the success of these tools is the accurate modeling of the performance of the circuit using  $RC$  equivalent circuits and a detailed knowledge of the subsequent layout-generation process. The latter allows for an accurate estimation of the values of the parasitic capacitances.

While circuit synthesis has proven to be a powerful tool, it has not penetrated the design world as much as we might expect. One of the main reasons for this is that the quality of the cell library has a strong influence on the complete design, and designers are reluctant to pass this important task to automatic tools that might produce inferior results. Yet, the need for ever-larger libraries and the impact of transistor-sizing on circuit performance and power dissipation is providing a strong push for a more pervasive introduction of circuit-synthesis tools.

### Logic Synthesis

Logic synthesis is the task of generating a structural view of a logic-level model. This model can be specified in many different ways, such as state-transition diagrams, state charts, schematic diagrams, Boolean equations, truth tables, or HDL (Hardware Description Language) descriptions.

The synthesis techniques differ according to the nature of the circuit (combinational or sequential) or the intended implementation architecture (multilevel logic, PLA, or FPGA). The synthesis process consists of a sequence of optimization steps, the order and nature of which depend on the chosen cost function—area, speed, power, or a combination of these. Typically, logic optimization systems divide the task into two stages:

1. A *technology-independent phase*, where the logic is optimized using a number of Boolean or algebraic manipulation techniques.
2. A *technology-mapping phase*, which takes into account the peculiarities and properties of the intended implementation architecture. The technology-independent description resulting from the first phase is translated into a gate netlist or a PLA description.

The *two-level minimization* tools were the first logic-synthesis techniques to become widely available. The Espresso program developed at the University of California at Berkeley [Brayton84] is an example of a popular two-level minimization program. For some time, the wide availability of these tools made regular, array-based architectures like PLAs and PALs the prime choice for the implementation of random logic functions.

At the same time, the groundwork was laid for sequential or state-machine synthesis. Tasks involved include the *state minimization* that aims at reducing the number of machine states, and the *state encoding* that assigns a binary encoding to the states of a finite state machine [DeMicheli94].

The emergence of *multilevel logic synthesis* environments such as the Berkeley MIS tool [Brayton87] swung the pendulum towards the standard-cell and FPGA implementations that offer higher performance or integration density for a majority of random-logic functions.

The combination of these techniques with sequential synthesis has opened the road to complete register-transfer (RTL) synthesis environments that take as an input an HDL description (in VHDL or Verilog—see Design Methodology Insert C) of a sequential circuit and produce a gate netlist [Carlson91, Kurup97]. Saying the logic synthesis has fundamentally altered the digital circuit design landscape is by no means an understatement. It also is fair to say that the tool set that



made this major paradigm change in design methodology ultimately happen is the *Design Compiler* environment from Synopsys. Even after being in place for almost two decades, Design Compiler continues to dominate the market and represents the synthesis tool of choice for the majority of the digital ASIC designers. Built around a core of Boolean optimization and technology mapping, Design Compiler incorporates advanced techniques such as timing, area and power optimization, cell-based sizing, and test insertion [Kurup97, DesignCompiler].

### Example F.1 Logic Synthesis

To demonstrate the difference between two-level and multilevel logic synthesis, both approaches were applied to the following full-adder equations, which will be treated in substantial detail in Chapter 11.

$$\begin{aligned} S &= (A \oplus B) \oplus C_i \\ C_o &= A \cdot B + A \cdot C_i + B \cdot C_i \end{aligned} \quad (\text{F.1})$$

The MIS-II logic synthesis environment was employed for both the two-level and multilevel synthesis. The minimized truth table representing the PLA implementation is shown in Table F-1. It can be verified that the resulting network corresponds to the preceding full-adder equations. The PLA counts three inputs, seven product terms, and two outputs. Observe that no product terms can be shared between the sum and carry outputs. A NOR-NOR implementation requires 26 transistors in the PLA array (17 and 9 in the OR plane and AND planes, respectively). This count does not include the input and output buffers.

**Table F-1** Minimized PLA truth table for full adder.  
The dashes (–) mean that the corresponding input does not appear in the product term.

A	B	C <sub>i</sub>	S	C <sub>o</sub>
1	1	1	1	–
0	0	1	1	–
0	1	0	1	–
1	0	0	1	–
1	1	–	–	1
1	–	1	–	1
–	1	1	–	1

Figure F-2 shows the multilevel implementation as generated by MIS-II. In the technology-mapping phase, a generic standard-cell library was targeted. Implementation of the adder requires only six standard cells. This corresponds to 34 (!) transistors in a static CMOS implementation.<sup>1</sup> Observe the usage of complex logic gates such as EXOR and OR-AND-INVERT. For this case study, minimization of the area was selected as the prime optimization target. Other implementations can be obtained by targeting performance instead. For instance, the critical timing path from  $C_i$  to  $C_o$  can be reduced by signal reordering. This requires the designer to identify this path as the most critical, a fact that is not obvious from a simple inspection of the full-adder equations.

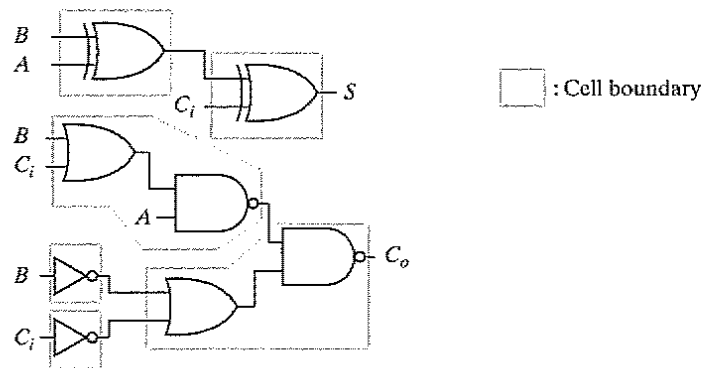


**Figure F-2** Standard-cell implementation of full adder, as generated by multilevel logic synthesis.

### Architecture Synthesis

Architecture synthesis is the latest development in the synthesis area. It is also referred to as *behavioral* or *high-level synthesis*. Its task is to generate a structural view of an architecture design, given a behavioral description of the task to be executed, and a set of performance, area, and/or power constraints. This corresponds to determining what architectural resources are needed to perform the task (execution units, memories, busses, and controllers), binding the behavioral operations to hardware resources, and determining the execution order of the operations on the produced architecture. In synthesis jargon, these functions are called *allocation*, *assignment*, and *scheduling* [Gajski92, DeMicheli94]. While these operations represent the core of architecture synthesis, other steps can have a dramatic impact on the quality of the solution. For example, optimizing transformations manipulate the initial behavioral description so that a superior solution can be obtained in terms of area or speed. *Pipelining* is a typical example of such a transformation. In a sense, this component of the synthesis process is similar to the use of optimizing transformations in software compilers.

<sup>1</sup>How to implement a static complementary CMOS EXOR gate with only nine transistors is left as an exercise for the reader.

**Example F.2 Architecture Synthesis**

To illustrate the concept and capabilities of architecture synthesis, consider the simple computational flowgraph of Figure F-3. It describes a program that inputs three numbers  $a$ ,  $b$ , and  $c$  from off-chip and produces their sum  $x$  at the output.

Two possible implementations, as generated by the HYPER synthesis system ([Rabaey91]), are shown in Figure F-4. The first instance requires four clock cycles and

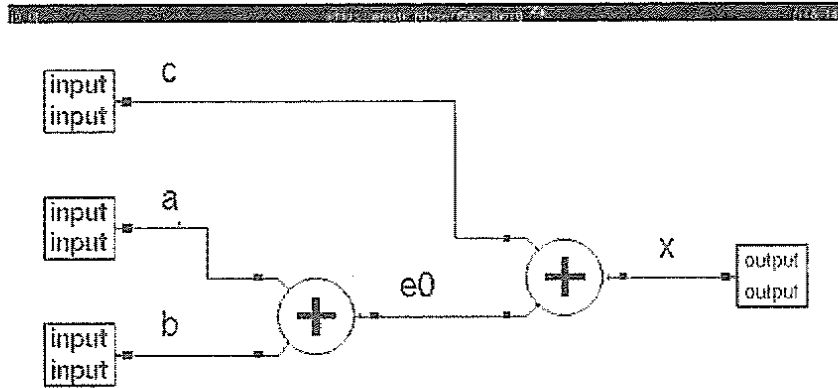


**Figure F-3** Simple program performing the sum of three numbers.

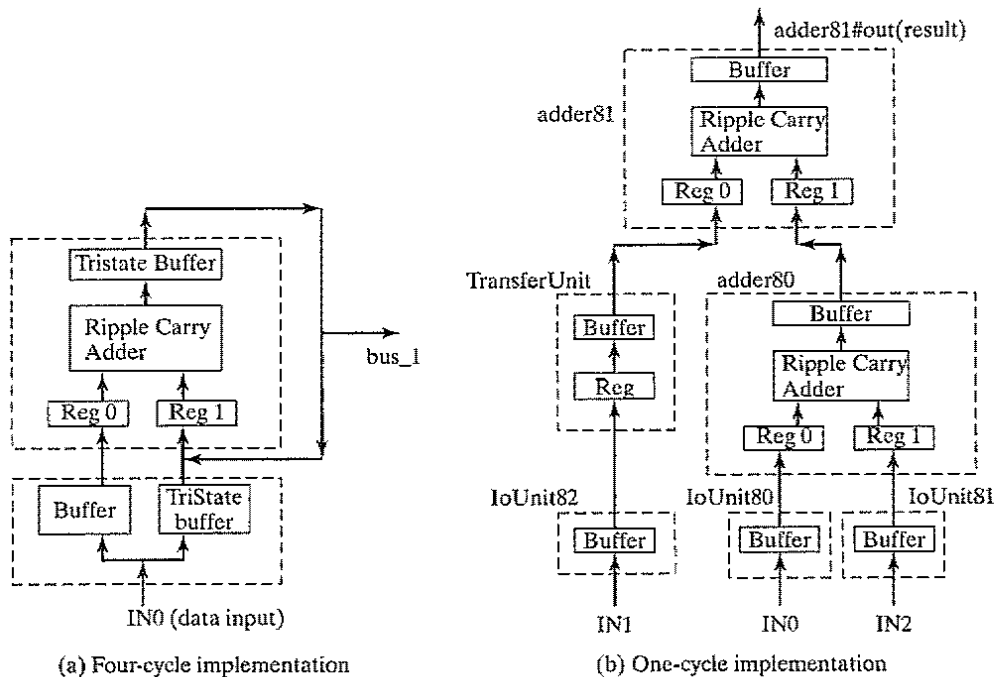


**Figure F-4** Two alternative architectures implementing the sum program.

time-shares the input bus as well as the adder. The second architecture performs the program in a single clock cycle. To achieve this performance, it was necessary to pipeline the algorithm; that is, multiple iterations of the computation overlap. The increased speed translates as expected to a higher hardware cost—one extra adder, extra registers, and a more dedicated bus architecture, including three input ports. Both architectures were produced automatically, given the behavioral description and the clock-cycle constraint. This includes the pipelining transformation.

While architecture compilers have been extensively researched in the academic community (e.g., [DeMan86], [Rabaey91]), their overall impact has remained limited. Commercial introductions have been largely unsuccessful. A number of reasons for this slow penetration can be enumerated:

- Behavioral synthesis assumes the availability of an established synthesis approach at the register-transfer level. This has only recently come to a widespread acceptance. In addition, the discussion about the appropriate input language at the behavioral level has created a lot of confusion. The emergence of widely accepted input languages such as SystemC can change the momentum.
- For a long time, architecture synthesis has concentrated on a limited aspect of the overall design process. The impact of interconnect on the overall design cost, for example, was long ignored. Also, limitations on the architectural scope resulted in inferior solutions apparent to every experienced designer.
- Most importantly, the revolutionary advent of the system-on-a-chip has outstripped the evolutionary progress of the synthesis world. The hybrid nature of embedded system architectures that combine embedded processors with ASIC accelerators ultimately limits the usability of architectural synthesis. Current logic and sequential synthesis tools probably suffice for the accelerators. The challenge has shifted to the synthesis of the software that runs on the embedded processors, chip-level operation systems, driver generators, interconnect network synthesis, and architectural exploration.

Notwithstanding these observations, architectural synthesis has proven to be very successful in a number of application-specific areas. The design of high-performance accelerator units in areas such as wireless communications, storage, imaging, and consumer electronics has benefited greatly from compilers that translate high-level algorithmic functions into hard-wired dedicated solutions.

---

### **Example F.3 Architectural Synthesis of Wireless-Communications Processor [Silva01]**

An advanced baseband processor for a wireless modem is generated automatically from a high-level description in the Simulink environment ([Mathworks01]). Simulink and Matlab are tools used extensively in the world of communications design. Capturing the

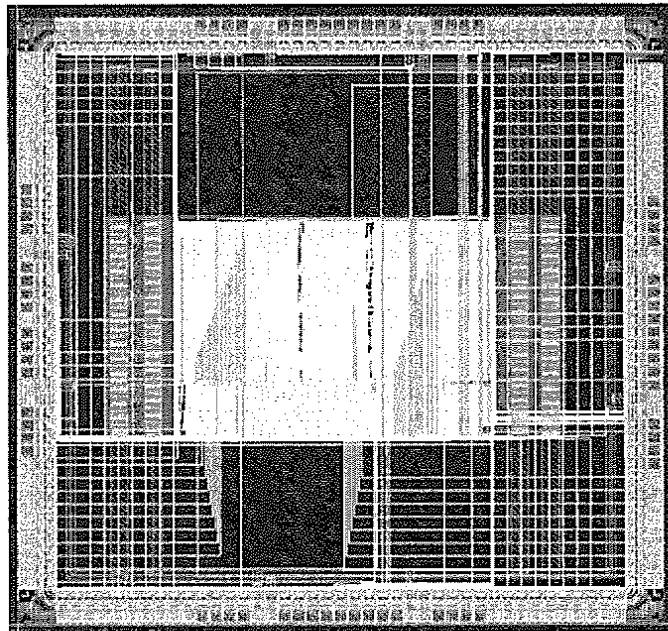
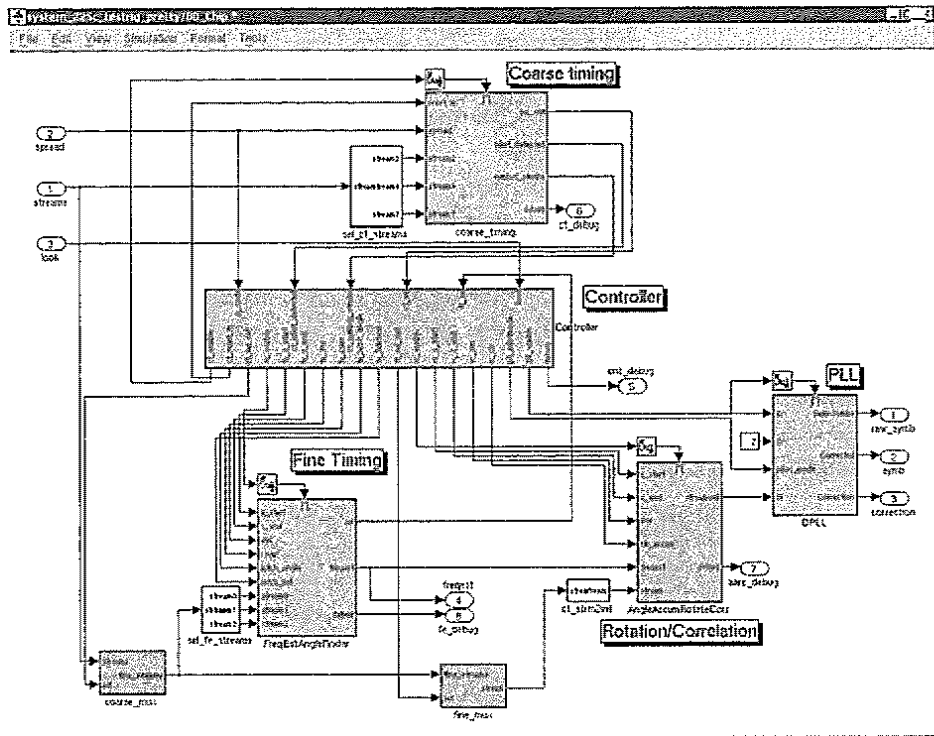


**Figure F-5** Architectural synthesis of wireless baseband processor from Simulink (a) to silicon (b). The core area of the chip, which is pad limited, measures only 2 mm<sup>2</sup> in a 0.18 μm CMOS technology, and counts 600,000 transistors. The high transistor density (0.3 transistor/μm<sup>2</sup>) demonstrates the effectiveness of today's physical design tools.

design specifications in that environment is a major help in bridging the chasm between systems and implementation engineer. The translation process from Simulink to implementation is managed by the “*Chip-in-a-day*” design environment [Davis01]. This tool manages the synthesis of the individual blocks from behavior to gate level, introduces the chip floorplan, performs the clock tree generation, and oversees the execution of the physical synthesis. The overall generation and verification process takes little more than 24 hours. A similar approach has also proven to be very successful in the mapping of high-level signal-processing functions on rapid-prototyping platforms such as FPGAs. The *System Generator* tool from Xilinx, Inc, for instance, maps modules such as filters, modulators, and correlators, described in the Mathworks Simulink environment, directly onto an FPGA module [SystemGenerator].

---

### To Probe Further

For an in-depth overview of design synthesis, please refer to [DeMicheli94].

### References

- [AMPS99] AMPS, Intelligent Design Optimization, [http://www.synopsys.com/products/analysis/amps\\_ds.html](http://www.synopsys.com/products/analysis/amps_ds.html), Synopsys, Inc.
- [Brayton84] R. Brayton et al., *Logic Minimization Algorithms for VLSI Synthesis*, Kluwer Academic Publishers, 1984.
- [Brayton87] R. Brayton, R. Rudell, A. Sangiovanni-Vincentelli, and A. Wang, “MIS: A Multilevel Logic Optimization System.” *IEEE Trans. on CAD*, CAD-6, pp. 1062–81, November 1987.
- [Carlson91] S. Carlson, *Introduction to HDL-Based Design Using VHDL*, Synopsys, Inc. 1991.
- [Chu86] K. Chu and D. Pulfrey, “Design Procedures for Differential Cascode Logic,” *IEEE Journal of Solid State Circuits*, vol. SC-21, no. 6, Dec. 1986, pp. 1082–1087.
- [Davis01] W.R. Davis, N. Zhang, K. Camera, F. Chen, D. Markovic, N. Chan, B. Nikolic, R.W. Brodersen, “A Design Environment for High Throughput, Low Power, Dedicated Signal Processing Systems,” *Proceedings CICC 2001*, San Diego, 2001.
- [DesignCompiler] Design Compiler Technical Datasheet, [http://www.synopsys.com/products/logic/design\\_compiler.html](http://www.synopsys.com/products/logic/design_compiler.html), Synopsys, Inc.
- [DeMan86] H. De Man, J. Rabaey, P. Six, and L. Claesen, “Cathedral-II: A Silicon Compiler for Digital Signal Processing,” *IEEE Design and Test*, vol. 3, no. 6, pp. 13–25, December 1986.
- [DeMicheli94] G. De Micheli, *Synthesis and Optimization of Digital Circuits*, McGraw-Hill, 1994.
- [Fishburn85] J. Fishburn and A. Dunlop, “TILOS: A Polynomial Programming Approach to Transistor Sizing,” *Proceedings ICCAD-85*, pp. 326–328, Santa Clara, 1985.
- [Gajski92] D. Gajski, N. Dutt, A. Wu, and S. Lin, *High-Level Synthesis—Introduction to Chip and System Design*, Kluwer Academic Publishers, 1992.
- [Kurup97] P. Kurub and T. Abassi, *Logic Synthesis using Synopsys*, Kluwer Academic Publishers, 1997.
- [Mathworks01] Matlab and Simulink, <http://www.mathworks.com>, The Mathworks
- [Northrop01] G. Northrop, P. Lu, “A Semicustom Design Flow in High-Performance Microprocessor Design,” *Proceedings 38<sup>th</sup> Design Automation Conference*, Las Vegas, June 2001.
- [Rabaey91] J. Rabaey, C. Chu, P. Hoang and M. Potkonjak, “Fast Prototyping of Datapath-Intensive Architectures,” *IEEE Design and Test*, vol. 8, pp. 40–51, 1991.

[Silva01] J.L. da Silva Jr., J. Shamberger, M.J. Ammer, C. Guo, S. Li, R. Shah, T. Tuan, M. Sheets, J.M. Rabaey, B. Nikolic, A. Sangiovanni-Vincentelli, P. Wright, "Design Methodology for PicoRadio Networks," *Proceedings DATE Conference*, Munich, March 2000.

[SystemGenerator] The Xilinx System Generator for DSP,  
[http://www.xilinx.com/xlnx/xil\\_prodcat\\_product.jsp?title=system\\_generator](http://www.xilinx.com/xlnx/xil_prodcat_product.jsp?title=system_generator), Xilinx, Inc.

## CHAPTER

# 10

## Timing Issues in Digital Circuits

*Impact of clock skew and jitter on performance and functionality*

*Alternative timing methodologies*

*Synchronization issues in digital IC and board design*

*Clock generation*

- 10.1 Introduction
- 10.2 Timing Classification of Digital Systems
  - 10.2.1 Synchronous Interconnect
  - 10.2.2 Mesochronous Interconnect
  - 10.2.3 Plesiochronous Interconnect
  - 10.2.4 Asynchronous Interconnect
- 10.3 Synchronous Design—An In-Depth Perspective
  - 10.3.1 Synchronous Timing Basics
  - 10.3.2 Sources of Skew and Jitter
  - 10.3.3 Clock-Distribution Techniques
  - 10.3.4 Latch-Based Clocking\*
- 10.4 Self-Timed Circuit Design\*
  - 10.4.1 Self-Timed Logic—An Asynchronous Technique
  - 10.4.2 Completion-Signal Generation
  - 10.4.3 Self-Timed Signaling
  - 10.4.4 Practical Examples of Self-Timed Logic
- 10.5 Synchronizers and Arbiters\*
  - 10.5.1 Synchronizers—Concept and Implementation
  - 10.5.2 Arbiters



- 10.6 Clock Synthesis and Synchronization Using a Phase-Locked Loop\*
  - 10.6.1 Basic Concept
  - 10.6.2 Building Blocks of a PLL
- 10.7 Future Directions and Perspectives
  - 10.7.1 Distributed Clocking Using DLLs
  - 10.7.2 Optical Clock Distribution
  - 10.7.3 Synchronous versus Asynchronous Design
- 10.8 Summary
- 10.9 To Probe Further

## 10.1 Introduction

All sequential circuits have one property in common—a well-defined ordering of the switching events must be imposed if the circuit is to operate correctly. If this were not the case, wrong data might be written into the memory elements, resulting in a functional failure. The *synchronous* system approach, in which all memory elements in the system are simultaneously updated using a globally distributed periodic synchronization signal (that is, a global clock signal), represents an effective and popular way to enforce this ordering. Functionality is ensured by imposing some strict constraints on the generation of the clock signals and their distribution to the memory elements distributed over the chip; noncompliance often leads to malfunction.

This chapter starts with an overview of the different timing methodologies. The majority of the text is devoted to the popular *synchronous approach*. We analyze the impact of spatial variations of the clock signal, called *clock skew*, and temporal variations of the clock signal, called *clock jitter*, and introduce techniques to cope with both. These variations fundamentally limit the performance that can be achieved using a conventional design methodology.

At the other end of the spectrum is an approach called *asynchronous design*, which avoids the problem of clock uncertainty altogether by eliminating the need for globally distributed clocks. After discussing the basics of asynchronous design approach, we analyze the associated overhead and identify some practical applications. The important issue of synchronization between different *clock domains* and *interfacing* between asynchronous and synchronous systems also deserve in-depth treatment. Finally, the fundamentals of on-chip clock generation using feedback are introduced, along with trends in timing.

## 10.2 Timing Classification of Digital Systems

In digital systems, signals can be classified depending on how they are related to a local clock [Messerschmitt90][Dally98]. Signals that transition only at predetermined periods in time can be classified as *synchronous*, *mesochronous*, or *plesiochronous* with respect to a system clock. A signal that can transition at arbitrary times, on the other hand, is considered *asynchronous*.

### 10.2.1 Synchronous Interconnect

A synchronous signal is one that has the exact same frequency as the local clock and maintains a known fixed phase offset to that clock. In such a timing framework, the signal is “synchronized” with the clock, and the data can be sampled directly without any uncertainty. In digital logic

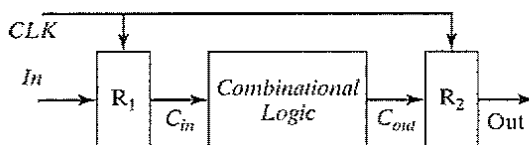


Figure 10-1 Synchronous interconnect methodology.

design, synchronous systems are the most straightforward type of interconnect. The flow of data in such a circuit proceeds in lockstep with the system clock, as illustrated in Figure 10-1.

Here, the input data signal  $In$  is sampled with register  $R_1$  to produce signal  $C_{in}$ , which is synchronous with the system clock, and then it is passed along to the combinational logic block. After a suitable setting period, the output  $C_{out}$  becomes valid. Its value is sampled by  $R_2$  which synchronizes the output with the clock. In a sense, the *certainty period* of signal  $C_{out}$ —the period during which data are valid—is synchronized with the system clock. This allows register  $R_2$  to sample the data with complete confidence. The **length of the uncertainty period**, or the period during which data are not valid, **places an upper bound on how fast a synchronous system can be clocked.**

### 10.2.2 Mesochronous Interconnect

A *mesochronous* signal—*meso* is Greek for “middle”—is a signal that not only has the same frequency as the local clock, but also has an unknown phase offset with respect to that clock. For example, if data are being passed between two different clock domains, the data signal transmitted from the first module can have an unknown phase relationship to the clock of the receiving module. In such a system, it is not possible to directly sample the output at the receiving module because of the uncertainty in the phase offset. A (mesochronous) synchronizer can be used to synchronize the data signal with the receiving clock, as shown in Figure 10.2. The synchronizer serves to adjust the phase of the received signal to ensure proper sampling.

In Figure 10-2, signal  $D_1$  is synchronous with respect to  $Clk_A$ . However,  $D_1$  and  $D_2$  are mesochronous with  $Clk_B$  because of the unknown phase difference between  $Clk_A$  and  $Clk_B$  and the unknown interconnect delay in the path between Block A and Block B. The role of the synchronizer is to adjust the variable delay line such that the data signal  $D_3$  (a delayed version of  $D_2$ ) is aligned properly with the system clock of Block B. In this example, the variable delay element is adjusted by measuring the phase difference between the received signal and the local clock. Register  $R_2$  samples the incoming data during the certainty period, after which the signal  $D_4$  becomes synchronous with  $Clk_B$ .

### 10.2.3 Plesiochronous Interconnect

A *plesiochronous* signal is one that has a frequency that is nominally the same as that of the local clock, yet is slightly different. (In Greek, *plesio* means “near.”) This causes the phase difference to drift in time. This scenario can easily arise when two interacting modules have independent clocks generated from separate crystal oscillators. Since the transmitted signal can arrive at the receiving module at a different rate than the local clock, one needs to utilize a buffering scheme to ensure that all data are received. Typically, plesiochronous interconnect occurs only in distributed

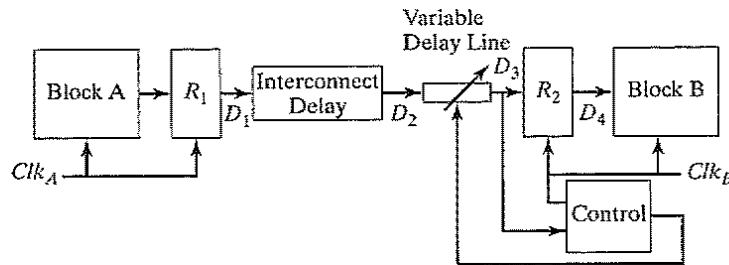


Figure 10-2 Mesochronous communication approach using variable delay line.

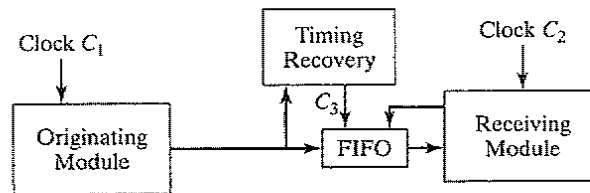


Figure 10-3 Plesiochronous communications by using a FIFO.

systems that contain long-distance communications, since chip- or even board-level circuits typically utilize a common oscillator to derive local clocks. A possible framework for plesiochronous interconnect is shown in Figure 10-3.

In this digital communications framework, the originating module issues data at some unknown rate  $C_1$ , which is plesiochronous with respect to  $C_2$ . The timing recovery unit is responsible for deriving clock  $C_3$  from the data sequence and buffering the data in a FIFO. As a result,  $C_3$  will be synchronous with the data at the input of the FIFO and will be mesochronous with  $C_1$ . Since the clock frequencies from the originating and receiving modules are mismatched, data might have to be dropped if the transmit frequency is faster, or data can be duplicated if the transmit frequency is slower than the receive frequency. However, by making the FIFO large enough, as well as periodically resetting the system whenever an overflow condition occurs, robust communication can be achieved.

### 10.2.4 Asynchronous Interconnect

Asynchronous signals can transition arbitrarily at any time, and they are not slaved to any local clock. As a result, it is not straightforward to map these arbitrary transitions into a synchronized data stream. It is possible to synchronize asynchronous signals by detecting events and by introducing latencies into the data stream synchronized to a local clock. A more natural way to handle asynchronous signals, however, is simply to eliminate the use of local clocks and utilize a self-timed asynchronous design approach. In such an approach, communication between modules is controlled through a handshaking protocol that ensures the proper ordering of operations.

When a logic block completes an operation (Figure 10-4), it will generate a completion signal  $DV$  to indicate that output data are valid. The handshaking signals then initiate a data transfer to the next block, which latches in the new data and begins a new computation by asserting the initialization signal  $I$ . Asynchronous designs are advantageous because computations are

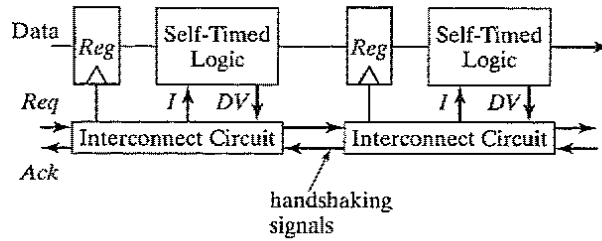


Figure 10-4 Asynchronous design methodology for simple pipeline interconnect.

performed at the native speed of the logic, and block computations occur whenever data become available. There is no need to manage clock *skew*, and the design methodology leads to a very modular approach in which interaction between blocks simply occurs through a handshaking procedure. However, these protocols result in increased complexity and overhead in communication, which impacts performance.

### 10.3 Synchronous Design—An In-Depth Perspective

#### 10.3.1 Synchronous Timing Basics

Virtually all systems designed today use a periodic *synchronization* signal or clock. The generation and distribution of a clock has a significant impact on the performance and power dissipation of the system. For the time being, let us assume a positive *edge-triggered* system, in which the rising edge of the clock denotes the beginning and completion of a clock cycle. In an ideal world, the phase of the clock (i.e., the position of the clock edge relative to the reference) at various points in the system is exactly equal, assuming that the clock paths from the central distribution point to each register are perfectly balanced. Figure 10-5 shows the basic structure of a synchronous pipelined datapath. In the ideal scenario, the clocks at registers 1 and 2 have the same period and transition at the exact same time.

Assume that the following timing parameters of the sequential circuit are available:

- The contamination or minimum delay ( $t_{c-q,cd}$ ) and the maximum propagation delay of the register ( $t_{c-q}$ ).
- The setup ( $t_{su}$ ) and hold times ( $t_{hold}$ ) for the registers.
- The contamination delay ( $t_{logic,cd}$ ) and the maximum delay ( $t_{logic}$ ) of the combinational logic.
- The positions of the rising edges of the clocks  $CLK_1$  and  $CLK_2$  ( $t_{clk1}$  and  $t_{clk2}$ , respectively), relative to a global reference.

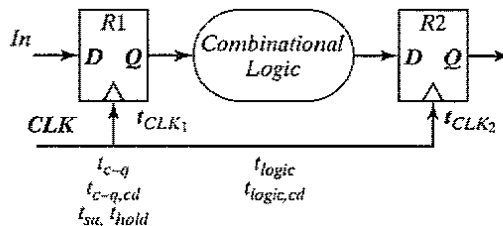


Figure 10-5 Pipelined datapath circuit and timing parameters.

Under the ideal condition that  $t_{clk1} = t_{clk2}$ , the minimum clock period required for this sequential circuit is determined solely by the worst case propagation delays. The period must be long enough for the data to propagate through the registers and logic and to be set up at the destination register before the next rising edge of the clock. As we saw in Chapter 7, this constraint is given by the following expression:

$$T > t_{c-q} + t_{logic} + t_{su} \quad (10.1)$$

At the same time, the hold time of the destination register must be shorter than the minimum propagation delay through the logic network:

$$t_{hold} < t_{c-q, cd} + t_{logic, cd} \quad (10.2)$$

Unfortunately, the preceding analysis is somewhat simplistic, since the clock is never ideal. The different clock events turn out to be neither perfectly periodic nor perfectly simultaneous. As a result of process and environmental variations, the clock signal can have both *spatial* and *temporal* variations, which lead to performance degradation and/or circuit malfunction.

### Clock Skew

The spatial variation in arrival time of a clock transition on an integrated circuit is commonly referred to as *clock skew*. The *clock skew* between two points  $i$  and  $j$  on an IC is given by  $\delta(i, j) = t_i - t_j$ , where  $t_i$  and  $t_j$  are the positions of the rising edge of the clock with respect to the reference. Consider the transfer of data between registers  $R1$  and  $R2$  in Figure 10-5. The clock skew can be positive or negative depending upon the routing direction and position of the clock source. The timing diagram for the case with positive skew is shown in Figure 10-6. As the figure illustrates, the rising clock edge is delayed by a positive  $\delta$  at the second register.

*Clock skew* is caused by static mismatches in the clock paths and differences in the clock load. By definition, skew is constant from cycle to cycle. That is, if in one cycle  $CLK_2$  lagged  $CLK_1$  by  $\delta$ , then on the next cycle, it will lag it by the same amount. It is important to note that clock skew does not result in clock period variation, but only in phase shift.

The clock-skew phenomenon has strong implications for both the performance and the functionality of sequential systems. First, consider the impact of clock skew on performance. We can see from Figure 10-6 that a new input  $In$  sampled by  $R1$  at edge ① will propagate through the com-

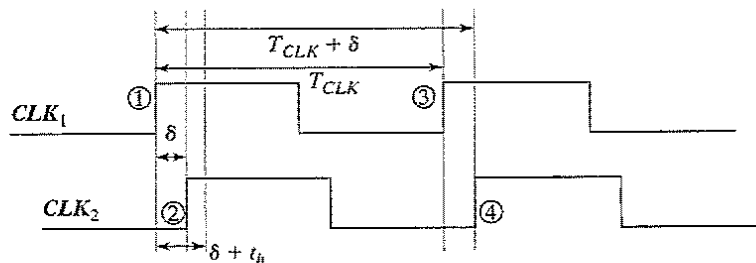


**Figure 10-6** Timing diagram to study the impact of clock skew on performance and functionality. In this sample timing diagram,  $\delta > 0$ .

binational logic and be sampled by  $R2$  on edge ④. If the clock skew is positive, the time available for a signal to propagate from  $R1$  to  $R2$  is increased by the skew  $\delta$ . The output of the combinational logic must be valid one setup time before the rising edge of  $CLK_2$  (point ④). The constraint on the minimum clock period can then be derived as follows:

$$T + \delta \geq t_{c-q} + t_{logic} + t_{su} \quad \text{or} \quad T \geq t_{c-q} + t_{logic} + t_{su} - \delta \quad (10.3)$$

This equation suggests that clock skew actually has the potential to improve the performance of the circuit. That is, the minimum clock period required to operate the circuit reliably reduces with increasing clock skew! This is indeed correct, but unfortunately, increasing skew makes the circuit more susceptible to race conditions, which may harm the correct operation of sequential systems.

This can be illustrated by the following example: Assume again that input  $In$  is sampled on the rising edge of  $CLK_1$  at edge ① into  $R1$ . The new value at the output of  $R1$  propagates through the combinational logic and should be valid before edge ④ at  $CLK_2$ . However, if the minimum delay of the combinational logic block is *small*, the inputs to  $R2$  may change before the clock edge ②, resulting in incorrect evaluation. To avoid races, we must ensure that the minimum propagation delay through the register and logic is long enough that the inputs to  $R2$  are valid for a hold time after edge ②. The constraint can be formally stated as

$$\delta + t_{hold} < t_{(c-q, cd)} + t_{(logic, cd)} \quad (10.4)$$

or

$$\delta < t_{(c-q, cd)} + t_{(logic, cd)} - t_{hold}$$

Figure 10-7 shows the timing diagram for the case in which  $\delta < 0$ . For this case, the rising edge of  $CLK_2$  happens before the rising edge of  $CLK_1$ . On the rising edge of  $CLK_1$ , a new input is sampled by  $R1$ . The new data propagate through the combinational logic, and they are sampled by  $R2$  on the rising edge of  $CLK_2$ , which corresponds to edge ④. As Figure 10-7 and Eq. (10.3) clearly show, a negative skew adversely impacts the performance of a sequential system. However, assuming  $t_{hold} + \delta < t_{(c-q, cd)} + t_{(logic, cd)}$ , a negative skew implies that the system never fails, since edge ② happens before edge ①!

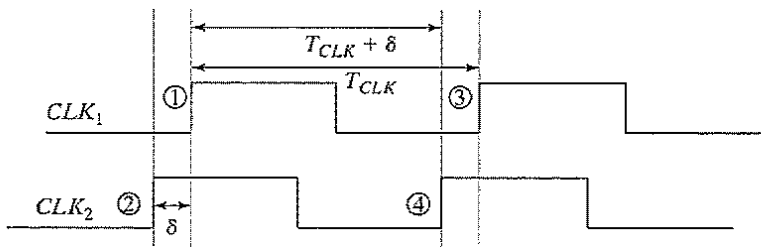


**Figure 10-7** Timing diagram for the case when  $\delta < 0$ . The rising edge of  $CLK_2$  arrives earlier than the edge of  $CLK_1$ .

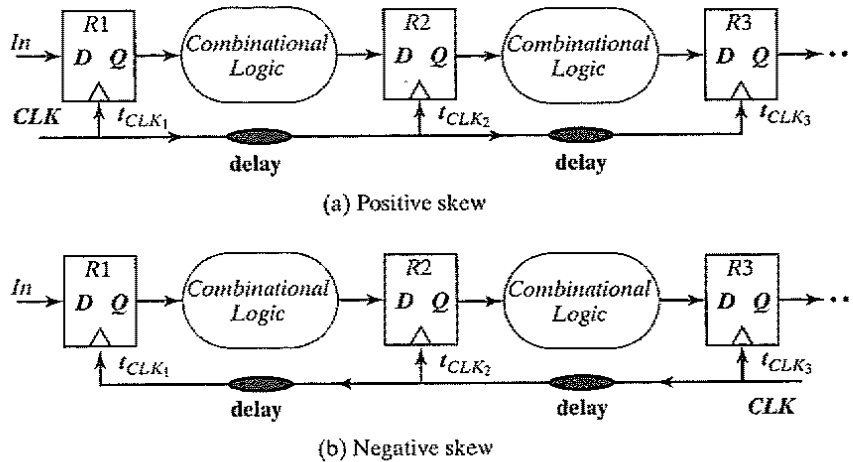


**Figure 10-8** Positive and negative clock skew scenarios.

Example scenarios for positive and negative clock skew are shown in Figure 10-8.

- $\delta > 0$ —This corresponds to a clock routed in the same direction as the flow of the data through the pipeline (Figure 10-8a). In this case, the skew has to be strictly controlled and satisfy Eq. . If the constraint is not met, the circuit malfunctions **independently of the clock period**. Reducing the clock frequency of an edge-triggered circuit does not help getting around skew problems! It is therefore necessary to satisfy the hold-time constraints at design time. On the other hand, positive skew increases the through put of the circuit as expressed by Eq. (10.3). The clock period can be shortened by  $\delta$ . The extent of this improvement is limited, as large values of  $\delta$  soon provoke violations of Eq. .
- $\delta < 0$ —When the clock is routed in the opposite direction of the data (Figure 10-8b), the skew is negative and provides significant immunity to races; if the hold time is zero or negative, races are eliminated because Eq. is unconditionally met! The skew reduces the time available for actual computation so that the clock period has to be increased by  $|\delta|$ . In summary, routing the clock in the opposite direction of the data avoids disasters, but hampers the circuit performance.

Unfortunately, since a general logic circuit can have data flowing in both directions (for example, circuits with feedback), this solution to eliminate races does not always work. Figure 10-9 shows that the skew can assume both positive and negative values, depending on the direction of the data transfer. Under these circumstances, the designer has to account for the worst case skew condition. In general, routing the clock so that only negative skew occurs is not feasible. Therefore, the design of a low-skew clock network is essential.

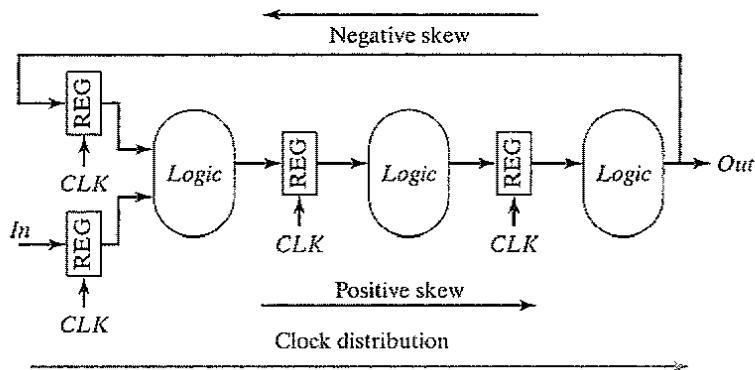


Figure 10-9 Datapath structure with feedback.

**Example 10.1 Propagation and Contamination Delay Estimation**

Consider the logic network shown in Figure 10-10. Determine the contamination and propagation delays of the network, given a worst case gate delay of  $t_{gate}$ . We also assume that the maximum and minimum delays of the gates are identical.

The contamination delay is easily found; it equals  $2t_{gate}$ , and is the delay through  $OR_1$  and  $OR_2$ . On the other hand, computation of the worst case propagation delay is not as simple. At first glance, it would appear that the worst case corresponds to path ①, and its delay is  $5t_{gate}$ . However, when analyzing the data dependencies, it becomes obvious that path ① can never be exercised. Path ① is called a *false path*. If  $A = 1$ , the critical path goes through  $OR_1$  and  $OR_2$ . If  $A = 0$  and  $B = 0$ , the critical path is through  $I_1$ ,  $OR_1$  and  $OR_2$  (corresponding to a delay of  $3t_{gate}$ ). For the case in which  $A = 0$  and  $B = 1$ , the longest path goes through  $I_1$ ,  $OR_1$ ,  $AND_3$  and  $OR_2$ . In other words, for this simple (but contrived) network, the output does not even depend on inputs  $C$  and  $D$  (that is, there is **redundancy**). Therefore, the actual propagation delay is  $4t_{gate}$ . Given the propagation and contamination delay, the minimum and maximum allowable skew can be easily computed.

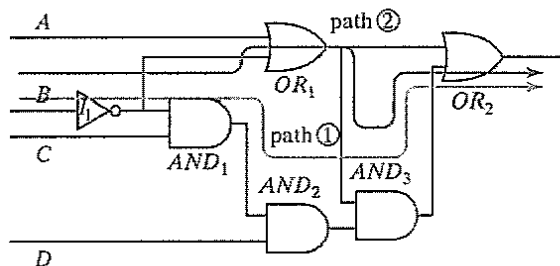


Figure 10-10 Logic network for computation of performance.



**WARNING:** The computation of the worst case propagation delay for combinational logic, due to the existence of *false paths*, cannot be obtained simply by adding the propagation delays of individual logic gates. The critical path is strongly dependent on circuit topology and data dependencies.

### Clock Jitter

*Clock jitter* refers to the temporal variation of the clock period at a given point on the chip—that is, the clock period can reduce or expand on a cycle-by-cycle basis. It is strictly a temporal uncertainty measure, and it is often specified at a given point. **Jitter** can be measured and characterized in a number of ways and is a **zero-mean random variable**. The *absolute jitter* ( $t_{jitter}^i$ ) refers to the worst case variation (absolute value) of a clock edge at a given location with respect to an ideally periodic reference clock edge. The *cycle-to-cycle jitter* ( $T_{jitter}^i$ ) typically refers to the time-varying deviations of a single clock period relative to an ideal reference clock. For a given spatial location  $i$ , it is given as  $T_{jitter}^i(n) = t_{clk,n+1}^i - t_{clk,n}^i - T_{CLK}$ , where  $t_{clk,n+1}^i$  and  $t_{clk,n}^i$  represent the arrival time of the  $n + 1^{\text{th}}$  and the  $n^{\text{th}}$  clock edges at node  $i$ , respectively, and  $T_{CLK}$  is the nominal clock period. Under the worst case conditions, the magnitude of the cycle-to-cycle jitter equals twice the absolute jitter ( $2t_{jitter}^i$ ).

Jitter directly impacts the performance of a sequential system. Figure 10-11 shows the nominal clock period, as well as the variation in period. Ideally, the clock period starts at edge ② and ends at edge ⑤, with a nominal clock period of  $T_{CLK}$ . However, the worst case scenario happens when the leading edge of the current clock period is delayed by jitter (edge ③), while jitter causes the leading edge of the next clock period to occur early (edge ④). As a result, the total time available to complete the operation is reduced by  $2t_{jitter}$  in the worst case and is given by

$$T_{CLK} - 2t_{jitter} \geq t_{c-q} + t_{logic} + t_{su} \quad \text{or} \quad T \geq t_{c-q} + t_{logic} + t_{su} + 2t_{jitter} \quad (10.5)$$

Equation (10.5) illustrates that jitter directly reduces the performance of a sequential circuit. Keeping it within strict bounds is essential if one is concerned about performance.

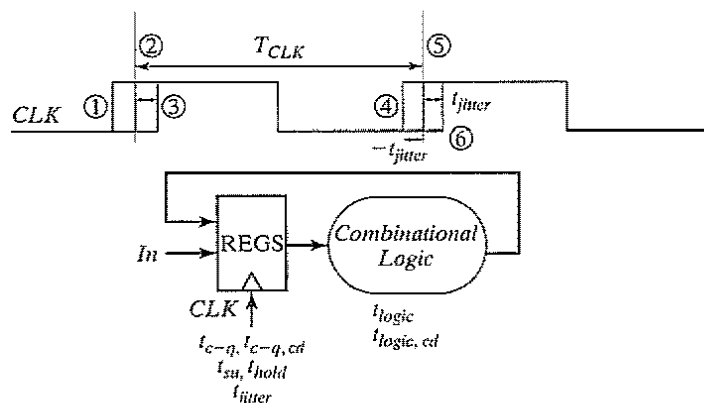


Figure 10-11 Circuit for studying the impact of jitter on performance.

### The Combined Impact of Skew and Jitter

In this section, the combined impact of skew and jitter is studied for conventional edge-triggered clocking. Consider the sequential circuit shown in Figure 10-14.

Assume that as a result of the clock distribution, there is a static skew  $\delta$  between the clock signals at the two registers (assume that  $\delta > 0$ ). Furthermore, the two clocks experience a jitter of  $t_{jitter}$ . To determine the constraint on the minimum clock period, we must look at the minimum available time to perform the required computation. The worst case occurs when the leading edge of the current clock period on  $CLK_1$  happens late (edge ③) and the leading edge of the next cycle of  $CLK_2$  happens early (edge ⑩). This results in the following constraint:

$$T_{CLK} + \delta - 2t_{jitter} \geq t_{c-q} + t_{logic} + t_{su} \quad (10.6)$$

or

$$T \geq t_{c-q} + t_{logic} + t_{su} - \delta + 2t_{jitter}$$

This equation illustrates that positive skew can provide a performance advantage. On the other hand, *jitter* always has a negative impact on the minimum clock period.<sup>1</sup>

To formulate the minimum delay constraint, consider the case in which the leading edge of the  $CLK_1$  cycle arrives early (edge ①), and the leading edges the current cycle of  $CLK_2$  arrives late (edge ⑩). The separation between edges ① and ⑩ should be smaller than the minimum delay through the network. This results in

$$\delta + t_{hold} + 2t_{jitter} < t_{(c-q, cd)} + t_{(logic, cd)} \quad (10.7)$$

or

$$\delta < t_{(c-q, cd)} + t_{(logic, cd)} - t_{hold} - 2t_{jitter}$$

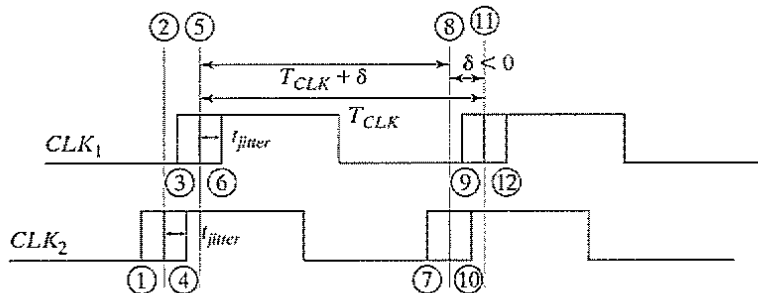


**Figure 10-12** Sequence circuit with a negative clock skew ( $\delta$ ). The skew is assumed to be larger than the *jitter*.

<sup>1</sup>This analysis is definitely for the worst case. It assumes that the jitter values at the source and the destination nodes are independent statistical variables. In reality, the clock edges involved in the hold-time analysis are derived from the same clock edge and are statistically dependent. Taking this dependence into account reduces the timing constraints substantially.

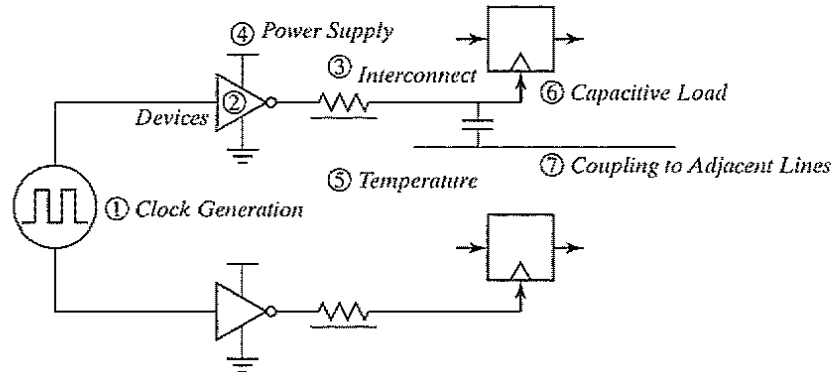


Figure 10-13 Skew and jitter sources in synchronous clock distribution.

This relation indicates that the acceptable skew is reduced by the *jitter* of the two signals.

Now consider the case in which the skew is negative ( $\delta < 0$ ), as shown in Figure 10-12. Assume that  $|\delta| > t_{jitter}$ . It can be verified that the worst case timing is exactly the same as in the previous analysis, with  $\delta$  taking a negative value. That is, negative skew reduces performance.

### 10.3.2 Sources of Skew and Jitter

A perfect *clock* is defined as a periodic signal that simultaneously triggers various memory elements on the chip. However, due to a variety of process and environmental variations, clocks are not ideal. To illustrate the sources of skew and jitter, consider a simplistic view of a typical clock generation and distribution network, as shown in Figure 10-13. A high-frequency clock is either provided from off chip or generated on chip. From a central point, the clock is distributed using multiple *matched* paths to low-level sequential elements. In this picture, two paths are shown. The clock paths include the wiring and the associated distributed buffers required to drive interconnect and loads. A key point to realize in clock distribution is that the **absolute delay through a clock distribution path is not important**; what matters is the relative arrival time at the register points at the end of each path. It is perfectly acceptable for the clock signal to take multiple cycles to get from a central distribution point to a low-level register as long as all clocks arrive at the same time at all the registers on the chip.

There are many reasons why the two parallel paths don't result in exactly the same delay. The sources of clock uncertainty can be classified in several ways. First, errors can be divided into two categories: *systematic* and *random*. *Systematic* errors are nominally identical from chip to chip and are predictable (for instance, variation in total load capacitance of each clock path). In principle, such errors can be modeled and corrected at design time, given sufficiently good models and simulators. Short of that, systematic errors can be deduced from measurements over a set of chips, and the design can be adjusted to compensate. *Random* errors are due to manufacturing variations that are difficult to model and eliminate (for instance, dopant fluctuations that result in threshold variations).

Mismatches may also be characterized as *static* or *time varying*. In practice, a continuum exists between changes that are slower than the time constant of interest and those that are faster. For example, temperature gradients on a chip vary on a millisecond time scale. A clock network

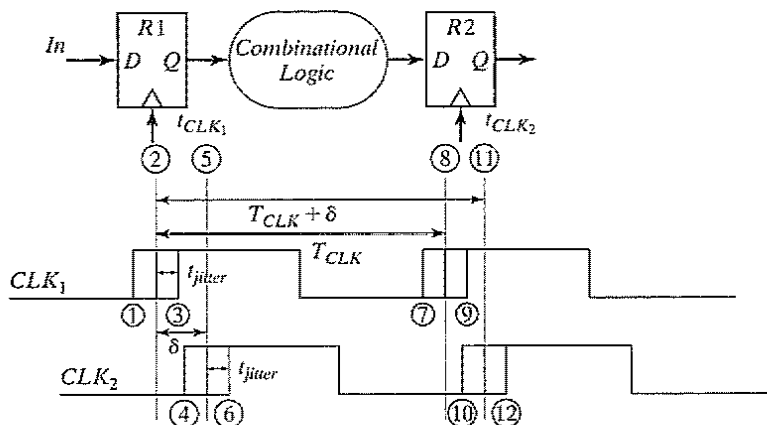


**Figure 10-14** Sequential circuit to study the impact of skew and jitter on *edge-triggered* systems. In this example, a positive skew ( $\delta$ ) is assumed.

tuned by a one-time calibration is vulnerable to the time-varying mismatch caused by the varying thermal gradients. On the other hand, thermal changes appear essentially static to a feedback network with a bandwidth of several megahertz. Another example is fielded by power-supply noise. The clock net is usually by far the largest signal net on the chip, and simultaneous transitions on the clock drivers induce noise in the power supply. This high-speed effect does not create a time-varying mismatch, because it is the same at every clock cycle and affects each rising clock edge the same way. Of course, this power-supply glitch may still cause static mismatch if it is not the same throughout the chip. The various sources of skew and jitter introduced in Figure 10-13 are described and characterized in detail in the sections that follow.

### Clock-Signal Generation (1)

The generation of the clock signal itself causes **jitter**. A typical on-chip clock generator, as described at the end of this chapter, takes a low-frequency reference clock signal and produces a high-frequency global reference for the processor. The core of such a generator is a *voltage-controlled oscillator* (VCO). This is an analog circuit, sensitive to intrinsic device noise and power-supply variations. A major problem is the coupling from the surrounding noisy digital circuitry through the substrate. This is especially a problem in modern fabrication processes that use a lightly doped epitaxy on the heavily doped substrate (to combat latch up). This causes substrate noise to travel over large distances on the chip [Maneatis00]. These noise sources cause temporal variations in the clock signal that propagate unfiltered through the clock drivers to the flip-flops, and result in *cycle-to-cycle* clock-period variations.

### Manufacturing Device Variations (2)

Distributed buffers are integral components of the clock distribution networks. They are required to drive both the register loads and the global and local interconnects. The matching of devices in the buffers along multiple clock paths is critical to minimizing timing uncertainty. Unfortunately, as a result of process variations, device parameters in the buffers vary along different paths, resulting in *static skew*. There are many sources of variations that contribute, such as oxide variations

(which affect the gain and threshold), dopant variations, and lateral dimension (width and length) variations. The doping variations can affect the depth of junction and dopant profiles and cause electrical parameters (such as device threshold and parasitic capacitances) to vary.

The orientation of polysilicon also can have some impact on the device parameters. Keeping the orientation the same across the chip for the clock drivers is therefore critical. Variation in the polysilicon critical dimension is particularly important, because it translates directly into MOS transistor channel length, impacting the drive current and switching characteristics. Spatial variation usually consists of a wafer-level (or within-wafer) variation and a die-level (or within-die) variation. At least part of this variation is systematic and therefore can be modeled and compensated for. The random variations, however, ultimately limit the matching and lower bound of the skew that can be achieved.

### Interconnect Variations (3)

Vertical and lateral dimension variations cause the interconnect capacitance and resistance to vary across a chip. Since this variation is static, it causes **skew** between different paths. One important source of interconnect variation is the *Inter-layer Dielectric (ILD)* thickness variation. In the formation of aluminum interconnect, layers of silicon dioxide are interposed between layers of patterned metallization. Oxide is deposited over a layer of patterned metal features, generally resulting in some remaining step height or surface topography. *Chemical-mechanical polishing (CMP)* is used to “planarize” the surface and remove the topography resulting from deposition and etch (as described in Chapter 3 and shown in Figure 10-15a). While at the feature scale (i.e., over an individual metal line), CMP can achieve excellent planarity, there are limitations on it over a global range. This is due primarily to variations in the polish rate, which is a function of the circuit layout density and pattern effects. Figure 10-15b shows this effect—the polish rate is higher for the lower-spatial-density region, resulting in a smaller dielectric thickness and higher capacitance.

The assessment and control of variation is of critical importance in semiconductor process development and manufacturing. Significant advances have been made to develop analytical

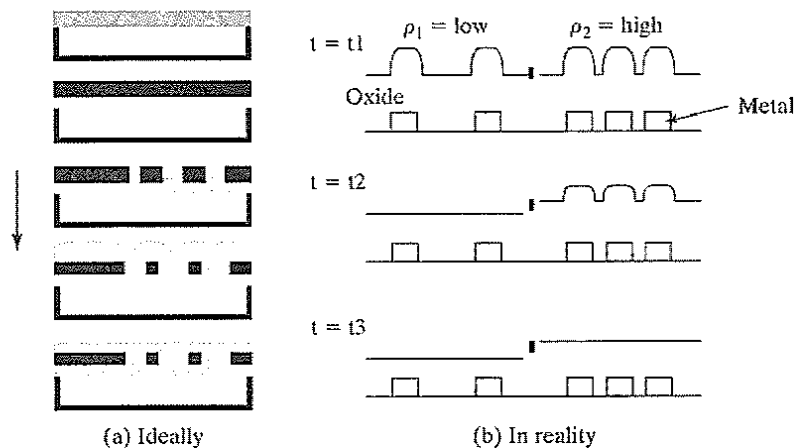


**Figure 10-15** Inter-level Dielectric (ILD) thickness variation due to density (Courtesy of Duane Boning.).

models for estimating the ILD thickness variations, based on spatial density. Since this component is often predictable from the layout, it is possible to actually correct for the systematic component at design time (e.g., by adding appropriate delays or making the density uniform by adding “dummy fills”). Figure 10-16 shows the spatial pattern density and ILD thickness for a

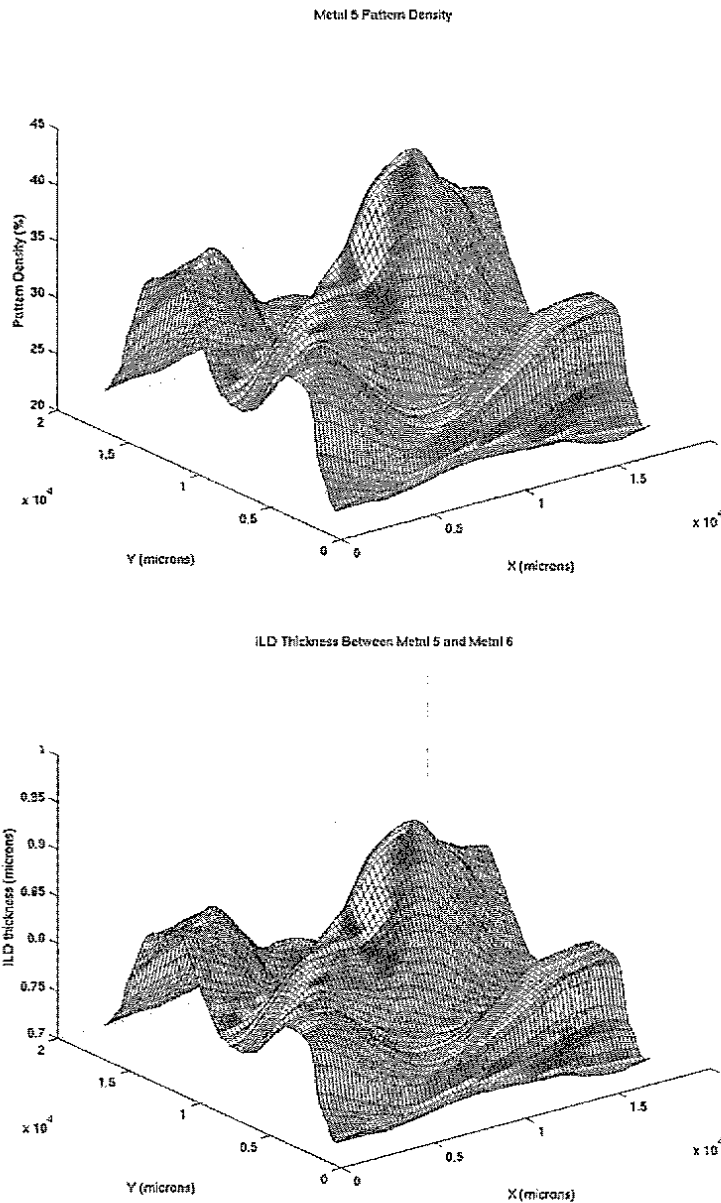


**Figure 10-16** Pattern density and ILD thickness variation for a high-performance microprocessor. (Courtesy of Duane Boning)

high-performance microprocessor. The graphs show a clear correlation between the density and the thickness of the dielectric. Hence, clock distribution networks must exploit such information in order to reduce clock skew.

Other interconnect variations include deviations in the width of the wires and line spacing, which result from photolithography and etch dependencies. At the lower levels of the metallization hierarchy, lithographic effects are more important, while etch effects that depend on width and layout are dominant at the higher levels. The width is a critical parameter because it directly impacts the resistance of the line, and the wire spacing affects the wire-to-wire capacitance. A detailed review of device and interconnect variations is presented in [Boning00]. Recent processors use copper interconnects, in which line thickness variations are also seen to be highly pattern dependent due to CMP dishing and erosion effects [Park00].

#### Environmental Variations (4 and 5)

Environmental variations probably are the most significant contributors to **skew and jitter**. The two major sources of environmental variations are *temperature* and *power supply*. Temperature gradients across the chip result from variations in power dissipation across the die. These gradients can be quite large, as shown in Figure 10-17, which displays a snapshot of the surface temperature of the DEC 21064 microprocessor. Temperature variation has become an important issue with *clock gating*, where some parts of the chip may be idle, while other parts of the chip are fully active. Clock gating has become popular in recent years as a means to minimize power dissipation in idle modules (as described in a later section). Shutting off parts of the chip leads to large temperature variations. Since the device parameters (such as threshold and mobility) depend strongly on temperature, the buffer delay for a clock distribution network can vary drastically from path to path. More importantly, this component is time varying, since the temperature changes as the logic activity of the circuit varies. Hence, it is not sufficient to simulate the clock networks at worst case corners of temperature; instead, the worst case variation in temperature must be simulated. An interesting question is whether temperature variation contributes to skew or to jitter. Clearly, the difference in temperature is time varying, but the changes are rela-

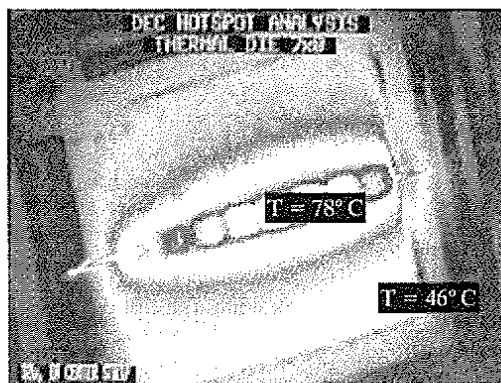


**Figure 10-17** Temperature variation (snapshot) over DEC 21064 microprocessor. The highest temperature occurs at the central clock driver [Herrick00].

tively slow (typical time constants for temperature changes are on the order of milliseconds). Therefore, it is usually considered as a skew component and the worst case conditions are used. Fortunately, by using feedback, it is possible to calibrate the temperature and to compensate for this effect.

Power-supply variations, on the other hand, are the major source of **jitter** in clock distribution networks. The delay through buffers is a very strong function of power supply, as it directly affects the drive of the transistors. As with temperature, the power-supply voltage is a strong function of the switching activity. Therefore, the buffer delay varies strongly from path to path. Power-supply variations can be classified into slow- (or static) and high-frequency variations. Static power-supply variations may result from fixed currents drawn from various modules, while high-frequency variations result from instantaneous  $IR$  drops along the power grid due to fluctuations in switching activity. Inductive effects on the power supply also are a major concern since they cause voltage fluctuations. Again, clock gating has exacerbated this problem, because the logic transitions between the idle and active states can cause major changes in current drawn from the supply. Since the power supply can change rapidly, the period of the clock signal is modulated on a cycle-by-cycle basis, resulting in jitter. The jitter on two different clock points may be correlated or uncorrelated, depending on how the power network is configured and the profile of switching patterns. Unfortunately, high-frequency power-supply changes are difficult to compensate for, even with feedback techniques. Consequently, **power-supply noise fundamentally limits the performance of clock networks**. To minimize power-supply variations, high-performance designs add decoupling capacitance around major clock drivers.

#### Capacitive Coupling (6 and 7)

Changes in capacitive load also contribute to timing uncertainty. There are two major sources of capacitive-load variations: coupling between the clock lines and adjacent signal wires, and variation in gate capacitance. The clock network includes both the interconnect and the gate capacitance of latches and registers. Any coupling between the clock wire and adjacent signal results in timing uncertainty. Since the adjacent signal can transition in arbitrary directions and at arbitrary times, the exact coupling to the clock network is not fixed from cycle to cycle, causing **jitter**. Another major source of clock uncertainty is the variation in the gate capacitance contributed by the connecting sequential elements. The load capacitance is highly nonlinear and depends on the applied voltage. For many latches and registers, the clock load is a function of the current state of the latch/register (i.e., the values stored on the internal nodes of the circuit), as well as the next state. This causes the delay through the clock buffers to vary from cycle to cycle, which causes jitter.

---

#### Example 10.2 Data-Dependent Clock Jitter

Consider the circuit shown in Figure 10-18, where a minimum-sized local clock buffer drives a register. (Actually, each clock buffer drives four registers, though only one is shown here.) The simulation shows  $CKb$ , the output of the first inverter for four possible



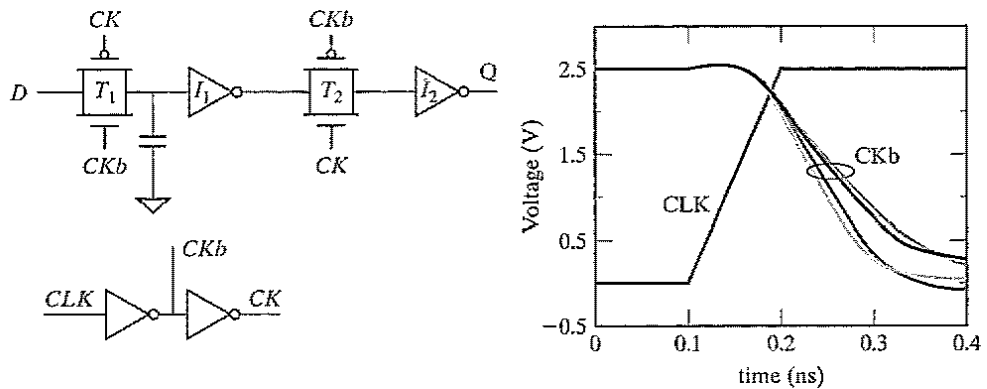


**Figure 10-18** Impact of data-dependent clock load on clock jitter for transmission-gate register.

transitions ( $0 \rightarrow 0$ ,  $0 \rightarrow 1$ ,  $1 \rightarrow 0$  and  $1 \rightarrow 1$ ). The jitter on the clock based on data-dependent capacitance is illustrated. In general, the only way to deal with this problem is to use registers that do not exhibit a large variation in load as a function of data—for example, the differential sense-amplifier register shown in Chapter 7.

### 10.3.3 Clock-Distribution Techniques

It is clear from the previous discussion that clock skew and jitter are major issues in digital circuits, and can fundamentally limit the performance of a digital system. It is therefore necessary to design a clock network that minimizes both. While designing that clock network, a close eye should be kept on the associated power dissipation. In most high-speed digital processors, a majority of the power is dissipated in the clock network. To reduce power dissipation, clock networks must support clock conditioning—that is, the ability to shut down parts of the clock network. Unfortunately, clock gating results in additional clock uncertainty (as described earlier).

In this section, an overview of basic constructs in high-performance clock distribution techniques is presented, along with a case study of clock distribution in the Alpha microprocessors. There are many degrees of freedom in the design of a clock network, including the type of material used for wires, the basic topology and hierarchy, the sizing of wires and buffers, the rise and fall times, and the partitioning of load capacitances.

#### Fabrics for Clocking

Clock networks typically include a network that is used to distribute a **global reference** to various parts of the chip, and a final stage that is responsible for **local distribution** of the clock while considering the local load variations. Most clock distribution schemes exploit the fact that the absolute delay from a central clock source to the clocking elements is irrelevant—only the relative phase between two clocking points is important. Therefore, one common approach to distributing a clock is to use balanced paths (called *trees*).

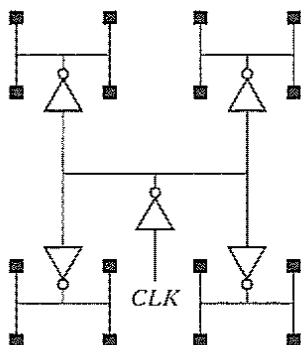


**Figure 10-19** Example of an *H*-tree clock-distribution network for 16 leaf nodes.

The most common type of clock distribution scheme is the *H-tree network*, which is illustrated in Figure 10-19 for a  $4 \times 4$  processor array. The clock is first routed to a central point on the chip. Balanced paths that include both matched interconnect and buffers then distribute the reference to the various leaf nodes. Ideally, if each path is perfectly balanced, the clock skew is zero. Although it might take multiple clock cycles for a signal to propagate from the central point to each leaf node, the arrival times are identical at every leaf node. However, in reality, process and environmental variations cause clock skew and jitter to occur.

The *H-tree* configuration is particularly useful for regular array networks in which all elements are identical and the clock can be distributed as a binary tree (for example, arrays of identical tiled processors). The concept can be generalized to a more generic setting. The more general approach, referred to as *matched RC trees*, represents a floor plan that distributes the clock signal so that the interconnections carrying the clock signals to the functional subblocks are of equal length. That is, the general approach does not rely on a regular physical structure. An example of a matched *RC* is shown in Figure 10-20. The chip is partitioned into 10 balanced load segments (tiles). The global clock driver distributes the clock to the tile drivers located at the dots in the figure. A lower level *RC*-matched tree is used to drive 580 additional drivers inside each tile. A 3D visualization of the clock delay in a tree network is shown in Figure 10-21.

An alternative clock distribution approach is the grid structure of Figure 10-22 [Bailey00]. Grids typically are used in the final stage of a clock network to distribute the clock to the clocking element loads. This approach is fundamentally different from the balanced *RC* approach. The main difference is that the delay from the final driver to each load is not matched. Rather, the absolute delay is minimized, assuming that the grid size is small. A major advantage of such a grid structure is that it allows for late design changes, since the clock is easily accessible at various points on the die. Unfortunately, the penalty is a relatively large power dissipation since the structure has a lot of “excess” interconnect. In addition to the schemes described earlier, other approaches have been devised for clock distribution. The length-matched serpentine approach is just one of them [Young97].

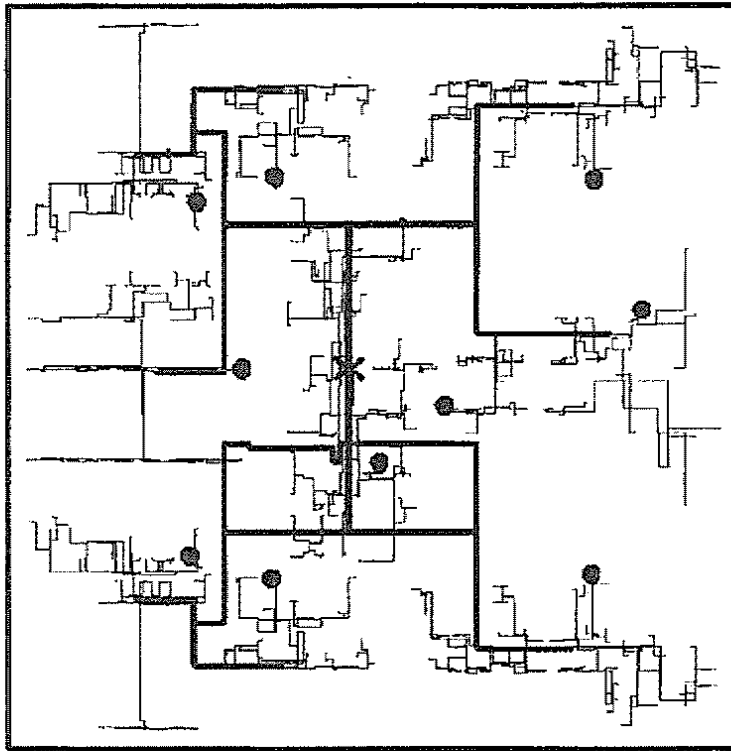


**Figure 10-20** An example RC-matched distribution for an IBM microprocessor [Restle98].

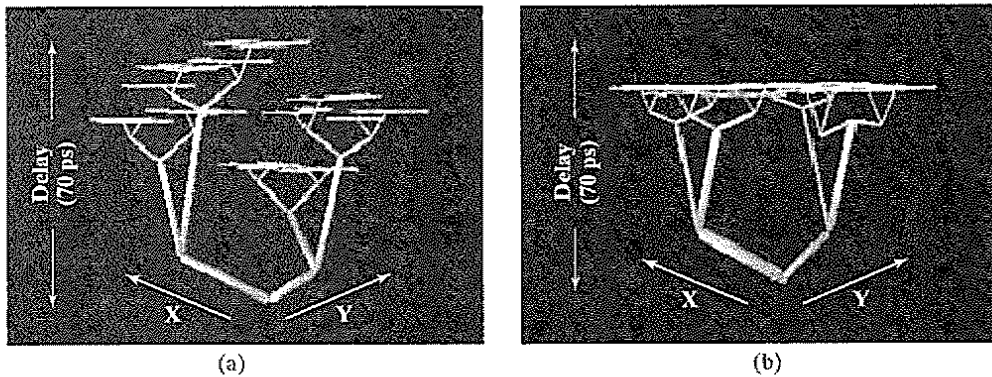


**Figure 10-21** Visualization of clock delay in a tree network driving different loads. The X- and Y-axes represent the die, while the Z-axis represents the clock delay. The width of the lines is proportional to the designed wire width. The unbalanced load creates a large skew, as is clear in (a). By careful tuning of the wire widths, the load is balanced, minimizing the skew, as shown in (b) [Restle01]. See also Colorplate 9.

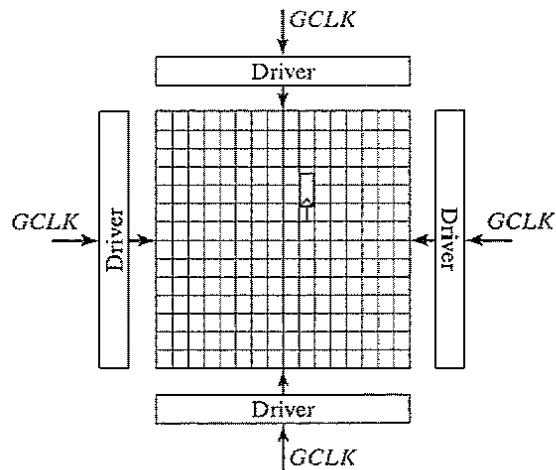


**Figure 10-22** Grid structures allow a low skew distribution and physical design flexibility at the cost of power dissipation [Bailey00].

It is essential to consider clock distribution in the earlier phases of the design of a complex circuit, since it might influence the shape and form of the chip's floor plan. It is tempting for a designer to ignore the clock network in the early phases of a project and consider it only at the end of the design cycle, when most of the chip layout is already frozen. This results in unwieldy clock networks and multiple timing constraints that hamper the performance and operation of the final circuit. With careful planning, a designer can avoid many of these problems, and clock distribution becomes a manageable operation.

#### Clock Distribution Case Study—The Digital Alpha Microprocessors

In this section, the clock distribution strategies for three generations of the Alpha microprocessor are discussed in detail. These processors have always been at the cutting edge of the technology and therefore represent an interesting perspective on the evolution of clock distribution [Herrick00].

**The Alpha 21064 Processor**—The first-generation Alpha microprocessor (21064 or EV4) from Digital Equipment Corporation used a single global clock driver [Dobberpuhl92]. The distribution of clock load capacitance among various functional blocks is shown in Figure 10-23. The total clock load equals 3.25 nF! The processor uses a single-phase clock methodology, and the 200-MHz clock is fed to a binary tree with five levels of buffering. The inputs to the clock drivers are shorted to smooth out the asymmetry in the incoming signals. The final output stage, residing in the middle of the chip, drives the clock net. The clock driver and the associated pre-drivers account for 40% of the effective switched capacitance (12.5 nF), resulting in significant power dissipation. The overall width of the clock driver was on the order of 35 cm in a 0.75- $\mu\text{m}$  technology. A detailed clock skew simulation with process variations indicates that a clock uncertainty of less than 200 ps (< 10%) was achieved.

**The Alpha 21164 Processor**—The second-generation Alpha microprocessor (EV5) operates at a clock frequency of 300 Mhz while using 9.3 million transistors on a 16.5 mm.  $\times$  18.1 mm die in a 0.5- $\mu\text{m}$  CMOS technology [Bowhill95]. A single-phase clocking methodology was selected, and the design made extensive use of dynamic logic, resulting in a substantial clock load of 3.75 nF. The clock distribution system consumes 20 W, which is 40% of the total dissipation of the processor.

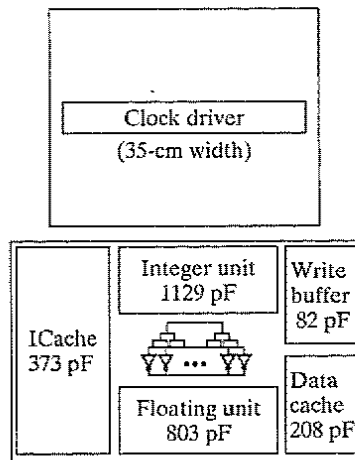
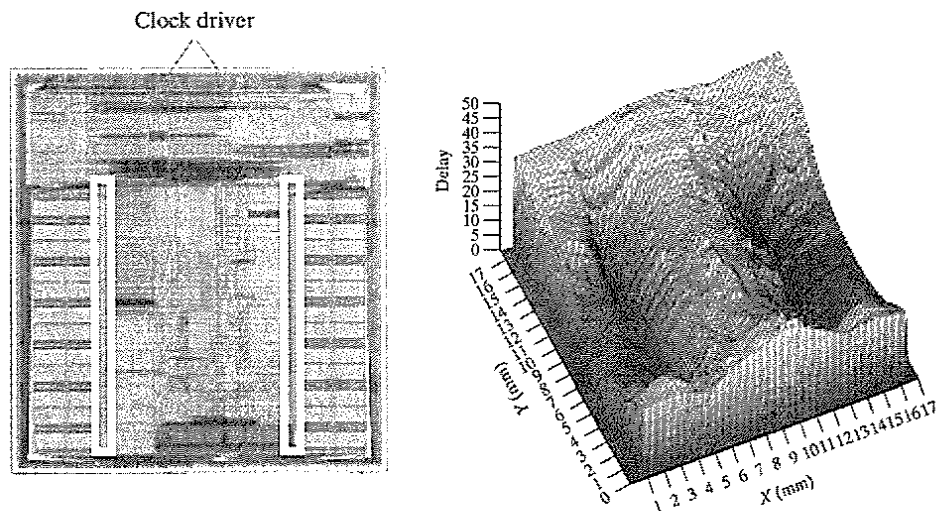


**Figure 10-23** Distribution of clock load capacitance for the 21064 Alpha processor.

The incoming clock signal is first routed through a single six-stage buffer placed at the center of the chip. The resulting signal is distributed in metal-3 to the left and right banks of final clock drivers, positioned between the secondary cache memory and the outside edge of the execution unit (see Figure 10-24a). The produced clock signal is driven onto a grid of metal-3 and metal-4 wires. The equivalent transistor width of the final driver inverter equals 58 cm! To ensure the integrity of the clock grid across the chip, the grid was extracted from the layout, and the resulting  $RC$ -network was simulated. A



(a) Chip microphotograph, showing positioning of clock drivers.

(b) Clock skew simulation.

**Figure 10-24** Clock distribution and skew in a 300-MHz microprocessor. (Courtesy of Digital Equipment Corporation.)

three-dimensional representation of the simulation results is plotted in Figure 10-24b. As evident from the plot, the skew is zero at the output of the left and right drivers. The maximum value of the absolute skew is smaller than 90 ps. The critical instruction and execution units all see the clock within 65 ps.

Clock skew and race problems were addressed using a “mix-and-match” approach. The clock skew problems were eliminated by either routing the clock in the opposite direction of the data (at a small cost in terms of performance) or by ensuring that the data could not overtake the clock. A standardized library of level-sensitive transmission-gate latches was used for the complete chip. To avoid race-through conditions, the following design guidelines were used:

- Careful sizing of the local clock buffers were carefully sized so that their skew was minimal.
- At least one gate had to be inserted between connecting latches. This gate, which can be part of the logic function or just a simple inverter, ensures was a minimum contamination delay. Special design verification tools were developed to guarantee that this rule was obeyed over the complete chip.

To improve the interlayer dielectric uniformity, filler polygons were inserted between widely spaced lines, as shown in Figure 10-25. Though this may increase the capacitance to nearby signal lines, the improved uniformity results in lower variation and clock uncertainty. The dummy fills are automatically inserted, and tied to one of the power rails ( $V_{DD}$  or GND). Dummy insertion is required today to equalize the etch-away of CMP (Chapter 3). This technique is used in many of today’s processes for controlling the clock skew.

This example demonstrates that managing clock skew and clock distribution for large, high-performance synchronous designs is a feasible task. However, making such a circuit work in a reliable way requires careful planning and intensive analysis.

**The Alpha 21264 Processor**—A hierarchical clocking scheme is used in the 600-Mhz Alpha 21264 (EV6) processor (in 0.35- $\mu\text{m}$  CMOS), shown in Figure 10-26 [Bailey98]. The choice of a hierarchical clocking scheme for this processor is a major departure from the preceding processors, which did not have

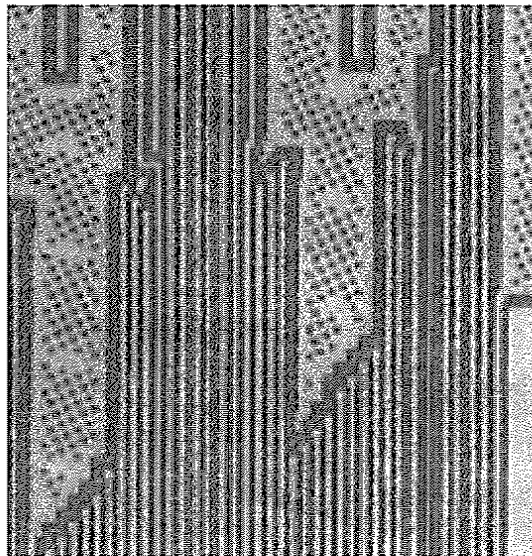


**Figure 10-25** Dummy fills reduce the ILD variation and improve clock skew.

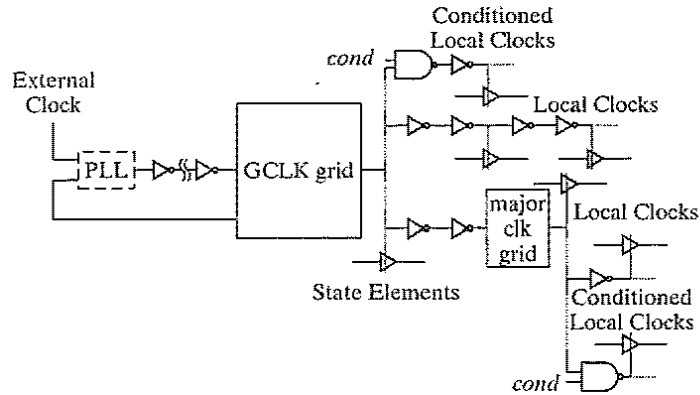


Figure 10-26 Clock hierarchy for the Alpha 21264 Processor.

a hierarchy of clocks beyond the global clock grid. Using a hierarchical clocking approach enables trade-offs between power and skew management. Power is reduced, because the clocking networks for individual blocks can be gated. As seen in previous-generation microprocessors, the clock power contributes to a large fraction of overall power consumption. Also, the flexibility of having local clocks provides the designers with more freedom with respect to circuit styles at the module level. The drawback of using a hierarchical clock network is that skew reduction becomes more difficult. Clocks to various local registers may go through very different paths, which may contribute to the skew. However, by using timing verification tools, the skew can be managed by tweaking of the clock drivers.

The clock hierarchy consists of a *global clock grid*, called *GCLK*, that covers the entire die. State elements and clocking points exist from zero to height levels past *GCLK*. The on-chip generated clock is routed to the center of the die and distributed using tree structures to 16 distributed clock drivers (see Figure 10-27). The global clock distribution network utilizes a windowpane configuration, which achieves low skew by dividing the clock into four regions, which reduces the distance from the drivers to the loads. Each grid pane is driven from four sides, reducing the dependence on process variations. This also helps the power supply and thermal problems, as the drivers are distributed through the chip.

The use of a gridded clock has the advantage of reducing the clock skew, while providing universal availability of the clock signals. The drawback is the increased capacitance of *GCLK*, compared with a tree-distribution approach. In addition to the *GCLK*, at the next level of clock hierarchy, there is a major clock grid. The major clocks were introduced to reduce power: They have localized loads, and they can be sized appropriately to meet the skew and edge requirements for the local loading conditions at timing-critical units.

The lowest level in this hierarchy is formed by the *local clocks*, which are generated as needed from any other clock. Typically, they can be customized to meet local timing constraints. The local clocks provide great flexibility in the design of the logic blocks, but at the same time make it significantly more difficult to manage skew. Furthermore, the local clocks are more susceptible to coupling from data lines, because they are not shielded like the global gridded clocks. As a result, the local clock distribution is highly dependent on its local interconnection and thus has to be designed very carefully.

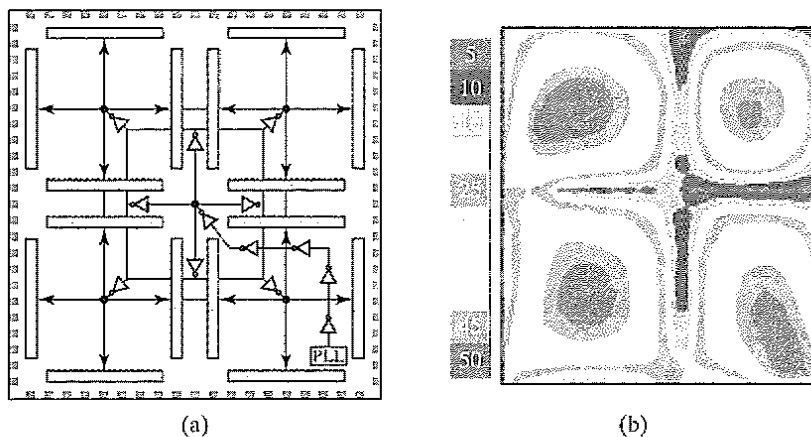


**Figure 10-27** Global clock distribution network in a windowpane structure. Pane structure (a); clock skew distribution over die (b).

#### Design Techniques—Dealing with Clock Skew and Jitter

From the preceding discussions, some useful guidelines for reducing clock skew and jitter can be derived:

1. To minimize skew, *balance clock paths* from a central distribution source to individual clocking elements, using *H-tree* structures or more generally routed matched-tree structures. When using routed clock trees, the effective clock load of each path that includes wiring as well as transistor loads must be equalized.
2. The use of *local clock grids* (instead of routed trees) can reduce skew at the cost of increased capacitive load and power dissipation.
3. If data-dependent clock load variations cause significant jitter, *differential registers* that have a data-independent clock load should be used. The use of gated clocks to save power results in a data-dependent clock load and increased jitter. In clock networks where the fixed load is large (e.g., in clock grids), the data-dependent variation might not be significant.
4. If data flow in one direction, route the *data and the clock in opposite directions*. This eliminates races at the cost of performance.
5. Avoid data-dependent noise by *shielding clock wires* from adjacent signal wires. By placing power lines ( $V_{DD}$  or GND) next to the clock wires, coupling from neighboring signal nets can be minimized or avoided.
6. Variations in interconnect capacitance due to interlayer dielectric thickness variation can be greatly reduced through the use of *dummy fills*. Dummy fills are very common and reduce skew by increasing uniformity. Systematic variations should be modeled and compensated for.
7. Variation in chip temperature across the die causes variations in clock buffer delay. The use of *feedback circuits based on delay-locked loops*, discussed later in this chapter, can compensate for temperature variations.
8. Power-supply variation is a significant component of jitter, as it impacts the cycle-to-cycle delay through clock buffers. High-frequency power-supply variation can be reduced by adding *on-chip decoupling capacitors*. Unfortunately, decoupling capacitors require a significant amount of area, and efficient packaging solutions must be leveraged in order to reduce chip area.



### 10.3.4 Latch-Based Clocking\*

The use of registers in a sequential circuit translates into a robust, reliable design methodology. Yet there are significant performance advantages to be made through the use of a latch-based design style, in which combinational logic is separated by transparent latches. In an edge-triggered system, the worst case logic path between two registers determines the minimum clock period for the entire system. If a logic block finishes before the end of the clock period, it has to sit idle until the next clock edge. The use of a latch-based methodology enables more flexible timing by allowing one stage to pass slack or to borrow time from other stages. The added flexibility also increases overall performance. Note that the latch-based methodology can be thought of as adding logic between latches of master-slave flip-flops.

Consider the latch-based system of Figure 10-28, which uses a two-phase clocking scheme. Assume that the clocks are ideal and that the two clocks are inverted versions of each other (for the sake of simplicity). In this configuration, a stable input is available to the combinational logic block A (*CLB\_A*) on the falling edge of  $CLK_1$  (at edge ②). It has a maximum time equal to the  $T_{CLK}/2$  to evaluate—that is, the entire low phase of  $CLK_1$ . On the falling edge of  $CLK_2$  (at edge ③), the output *CLB\_A* is latched, and the computation of  $CLK_B$  is launched. *CLB\_B* computes on the low phase of  $CLK_2$ , and the output is available on the falling edge of  $CLK_1$  (at edge ④). From a timing perspective, this scenario appears to be equivalent to an edge-triggered system, where *CLB\_A* and *CLB\_B* are cascaded between two edge-triggered registers (see Figure 10-29). In both cases, it appears that the time available to perform the combination of *CLB\_A* and *CLB\_B* is  $T_{CLK}$ .

However, there is an important performance-related difference. In a latch-based system, it is possible for a logic block to utilize time that is left over from the previous logic block. This phenomenon, which results from the transparency of a latch during its on time, is referred to as *slack borrowing* [Bernstein98]. It requires no explicit design changes, as the passing of slack

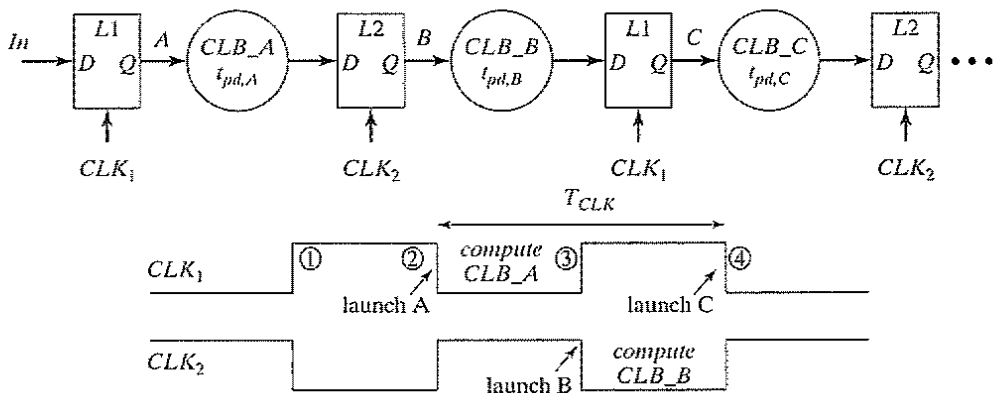


**Figure 10-28** Latch-based design in which transparent latches are separated by combinational logic.

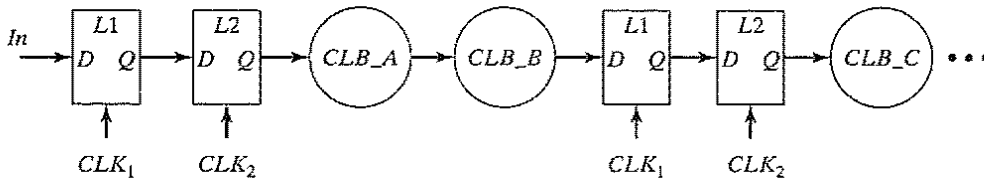


**Figure 10-29** Edge-triggered pipeline (back-to-back latches for edge-triggered registers) of the logic in Figure 10-28.

from one block to the next is automatic. The key advantage of slack borrowing is that it allows logic between cycle boundaries to use more than one clock cycle while satisfying the overall cycle time constraint. Stated in another way, if the sequential system works at a particular clock rate, and the total logic delay for a complete cycle is larger than the clock period, then unused time, or *slack*, has been implicitly borrowed from preceding stages. Formally stated, slack passing has taken place if  $T_{CLK} < t_{pd,A} + t_{pd,B}$ , and the logic functions correctly (for simplicity, the delay associated with latches are ignored). This implies that the clock rate can be higher than the worst case critical path!

As mentioned earlier, slack passing results from the level-sensitive nature of the latches. In Figure 10-28, the input to *CLB\_A* must be valid by the falling edge of  $CLK_1$  (edge ②). What happens if the combinational logic block of the previous stage finishes early and has a valid input data for *CLB\_A* before edge ②? Since the latch is transparent during the entire high phase of the clock, the input data for *CLB\_A* are valid as soon as the previous stage has finished computing. This implies that the maximum time available for *CLB\_A* is its phase time (i.e., the low phase of  $CLK_1$ ) plus any time left from the previous computation.

Consider the latch-based system of Figure 10-30. In this example, signal *a* (input to *CLB\_A*) is valid well before edge ②. This implies that the previous block did not use its entire allotment, producing slack time as denoted by the shaded area. By construction, *CLB\_A* can start computing as soon as signal *a* becomes valid. It uses this slack time to finish well before its allocated time (edge ③). Since  $L_2$  is a transparent latch, valid on the high phase of  $CLK_2$ , *CLB\_B* starts to compute using the slack provided by *CLB\_A*. Again, *CLB\_B* completes before its allocated time (edge ④), and it passes a small amount of slack to the next cycle. As this picture indicates, the total cycle delay—that is, the sum of the delay for *CLB\_A* and *CLB\_B*—is larger than the clock period. Since the pipeline behaves correctly, slack passing has taken place and a higher throughput has been achieved.

An important question related to slack passing involves to the maximum possible slack that can be passed across cycle boundaries. In Figure 10-30, it is easy to see that the earliest time that *CLB\_A* can start computing is ①. This happens if the previous logic block did not use any of its allocated time ( $CLK_1$  high phase) or if it finished by using slack from previous stages. Therefore, the maximum time that can be borrowed from the previous stage is half of a cycle or  $T_{CLK}/2$ . Similarly, *CLB\_B* must finish its operation by edge ④. This implies that

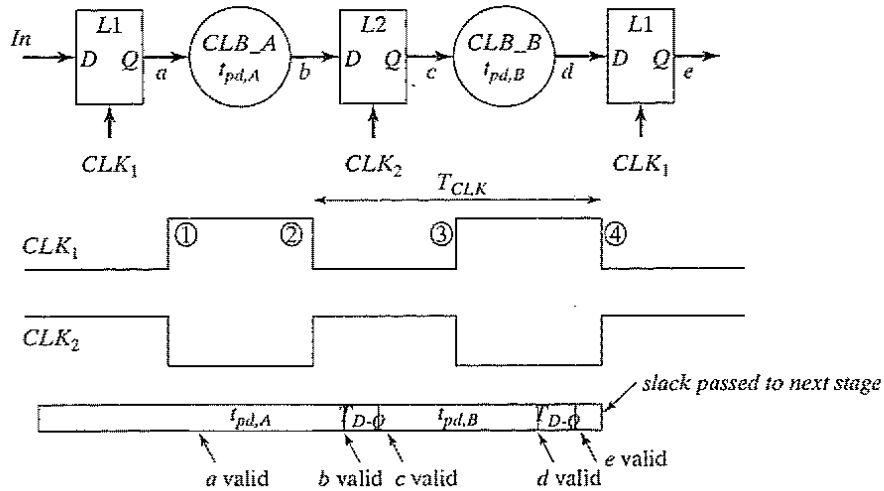


Figure 10-30 Example of slack borrowing.

the maximum logic cycle delay is equal to  $1.5 \times T_{CLK}$ . However, note that for an  $n$ -stage pipeline, the overall logic delay cannot exceed the time available of  $n \times T_{CLK}$ .

### Example 10.3 Slack-Passing Example

First, consider the negative edge-triggered pipeline of Figure 10-31. Assume that the primary input  $In$  is valid slightly after the rising edge of the clock. We can derive that the minimum clock period required is 125 ns. The latency is two clock cycles. (Actually, the output is valid 2.5 cycles after the input settles.) Note that for the first pipeline stage, one-half cycle is wasted, as the input data are available only to  $CL_1$  after the falling edge of the clock. This time can be exploited in a latch-based system.

Figure 10-32 shows a latch-based version of the same circuit. As the timing indicates, exactly the same timing can be achieved with a clock period of 100 ns. This is enabled by slack borrowing between the logical partitions.

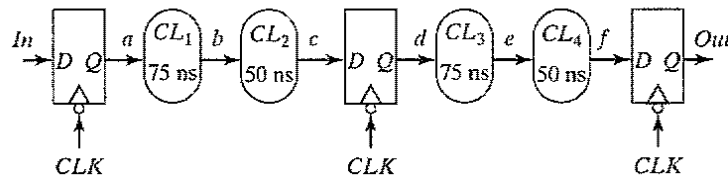


Figure 10-31 Conventional edge-triggered pipeline.

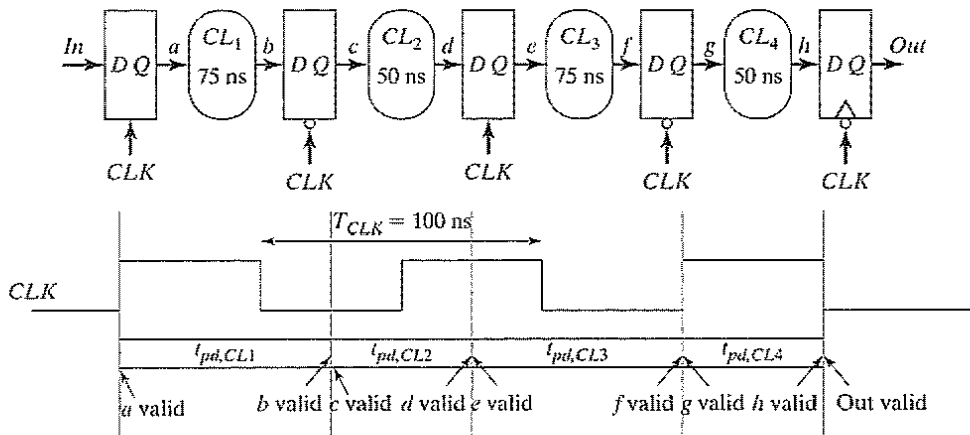


Figure 10-32 Latch-based pipeline.

If slack passing or borrowing intrigues you, we refer you to [Bernstein98], which presents an excellent quantitative analysis of this attractive, yet challenging, approach.

## 10.4 Self-Timed Circuit Design\*

### 10.4.1 Self-Timed Logic—An Asynchronous Technique

The synchronous design approach advocated in the previous sections assumes that all circuit events are orchestrated by a central clock. Those clocks have a dual function:

- They ensure that the *physical timing constraints* are met. The next clock cycle can start only when all logic transitions have settled and the system has come to a steady state. This ensures that only legal logical values are applied in the next round of computation. In short, clocks account for the worst case delays of logic gates, sequential logic elements, and the wiring.
- Clock events serve as a *logical ordering mechanism* for the global system events. A clock provides a time base that determines what will happen and when. On every clock transition, a number of operations are initiated that change the state of the sequential network.

Consider the pipelined datapath of Figure 10-33. In this circuit, the data transitions through logic stages under the command of the clock. The important point is that the clock period is chosen to be larger than the worst case delay of each pipeline stage, or  $T > \max(t_{pd1}, t_{pd2}, t_{pd3}) + t_{pd,reg}$ . This will ensure satisfaction of the physical constraint. At each clock transition, a new set of inputs is sampled, and computation is started again. The throughput of the system—which is equivalent to the number of data samples processed per second—is equivalent to the clock rate. The time at which to sample a new input and the availability of an output depend upon the *logical ordering* of the system events and clearly are orchestrated by the clock in this example.

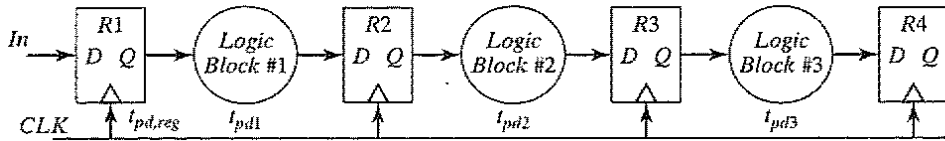


Figure 10-33 Pipelined, synchronous datapath.

The synchronous design methodology has some clear advantages. It presents a structured, deterministic approach to the problem of choreographing the myriad of events that take place in digital designs. The approach taken is to equalize the delays of all operations by making them as bad as the worst of the set. The approach is robust and easy to adhere to, which explains its enormous popularity; however, it does have several pitfalls:

- It assumes that all clock events or timing references happen simultaneously over the complete circuit. This is not the case in reality, because of effects such as clock skew and jitter.
- As all the clocks in a circuit transition at the same time, significant current flows over a very short period of time (due to the large capacitance load). This causes significant noise problems due to package inductance and power-supply grid resistance.
- The linking of physical and logical constraints has some obvious effects on the performance. For instance, the throughput rate of the pipelined system of Figure 10-33 is directly linked to the worst case delay of the slowest element in the pipeline. On average, the delay of each pipeline stage is smaller. The same pipeline could support an average throughput rate that is substantially higher than the synchronous one. For example, the propagation delay of a 16-bit adder is highly data dependent: Adding two 4-bit numbers requires a much shorter time compared with adding two 16-bit numbers.

One way to avoid these problems is to opt for an *asynchronous* design approach and to eliminate all the clocks. Designing a purely asynchronous circuit is a nontrivial and potentially hazardous task. Ensuring a correct circuit operation that avoids all potential race conditions under any operation condition and input sequence requires a careful timing analysis of the network. In fact, the logical ordering of the events is dictated by the structure of the transistor network and the relative delays of the signals. Enforcing timing constraints by manipulating the logic structure and the lengths of the signal paths requires an extensive use of CAD tools and is recommended only when strictly necessary.

A more reliable and robust technique is the self-timed approach, which presents a local solution to the timing problem [Seitz80]. Figure 10-34 uses a pipelined datapath to illustrate how this can be accomplished. It is assumed that each combinational function has a means of indicating that it has completed a computation for a particular piece of data. The computation of a logic block is initiated by asserting a *Start* signal. The combinational logic block computes on the input data, and in a data-dependent fashion (taking the physical constraints into account), generates a *Done* flag once the computation is finished. In addition, the operators must signal each other that either they are ready to receive a next input word or they have a legal data word at

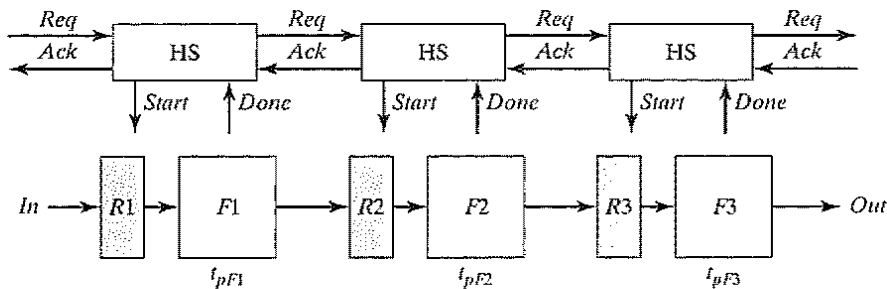


Figure 10-34 Self-timed, pipelined datapath.

their outputs that is ready for consumption. This signaling ensures the logical ordering of the events and can be achieved with the aid of extra *Ack(nowledge)* and *Req(uest)* signals. In the case of the pipelined datapath, the scenario could proceed as follows:

1. An input word arrives, and a *Req(uest)* to the block *F1* is raised. If *F1* is inactive at the time, it transfers the data and acknowledges this fact to the input buffer, which can go ahead and fetch the next word.
2. *F1* is enabled by raising the *Start* signal. After a certain amount of time, which is dependent upon the data values and operating conditions, the *Done* signal goes high, indicating the completion of the computation.
3. A *Req(uest)* is issued to the *F2* module. If this function is free, an *Ack(nowledge)* is raised, the output value is transferred, and *F1* can go ahead with its next computation.

The self-timed approach effectively separates the physical and logical ordering functions implied in circuit timing. The completion signal *Done* ensures that the physical timing constraints are met and that the circuit is in steady state before accepting a new input. The logical ordering of the operations is ensured by the acknowledge–request scheme, often called a *handshaking protocol*. Both interested parties synchronize with each other by mutual agreement (or, if you want, by “shaking hands”). The ordering protocol described previously and implemented in the module HS is only one of many that are possible. The choice of protocol is important, since it has a profound effect on the circuit performance and robustness.

When compared with the synchronous approach, self-timed circuits display some alluring properties:

- In contrast to the global centralized approach of the synchronous methodology, timing signals are generated *locally*, which avoids all problems and overheads associated with distributing high-speed clocks.
- Separating the physical and logical ordering mechanisms results in a potential increase in performance. In synchronous systems, the period of the clock has to be stretched to accommodate the slowest path over all possible input sequences. In self-timed systems, a

completed data word does not have to wait for the arrival of the next clock edge in order to proceed to the subsequent processing stages. Since circuit delays often are dependent on the actual data value, a self-timed circuit proceeds at the *average speed* of the hardware, in contrast to the *worst case* model of synchronous logic. For a ripple-carry adder, the average length of carry propagation is  $O(\log(N))$ . This is a fact that can be exploited in self-timed circuits, while in a synchronous methodology, a worst case performance that varies linearly with the number of bits ( $O(N)$ ) must be assumed.

- The automatic shutdown of blocks that are not in use can result in power savings. In addition, the power consumption overhead of generating and distributing high-speed clocks can be partially avoided. As discussed earlier, this overhead can be substantial. The use of gated clocks in synchronous design yields similar results.
- Self-timed circuits are, by nature, robust regarding variations in manufacturing and operating conditions such as temperature. Synchronous systems are limited by their performance at the extremes of the operating conditions. The performance of a self-timed system is determined by the actual operating conditions.

Unfortunately, these general properties are not without cost—they come at the expense of a substantial circuit-level overhead, which is caused by the need to generate completion signals and the need for handshaking logic that acts as a local traffic agent to order the circuit events (see block HS in Figure 10-34). Both of these topics are treated in more detail in the subsequent sections.

#### 10.4.2 Completion-Signal Generation

A necessary component of self-timed logic is the circuitry to indicate when a particular piece of circuitry has completed its operation for the current piece of data. There are two common and reliable ways to generate the completion signal.

##### Dual-Rail Coding

One common approach to completion-signal generation is the use of *dual-rail coding*. It actually requires the introduction of redundancy in the data representation in order to signal that a particular bit is in either a transition or a steady-state mode. Consider the redundant data model presented in Table 10-1. Two bits ( $B0$  and  $B1$ ) are used to represent a single data bit  $B$ . For the data

**Table 10-1** Redundant signal representation to include transition state.

$B$	$B0$	$B1$
in transition (or reset)	0	0
0	0	1
1	1	0
illegal	1	1

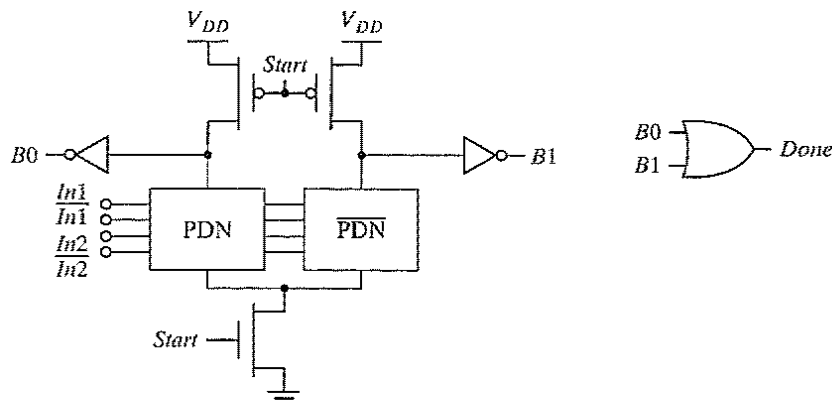


Figure 10-35 Generation of a completion signal in DCVSL.

to be valid or the computation to be completed, the circuit must be in a legal 0 ( $B0 = 0, B1 = 1$ ) or 1 ( $B0 = 1, B1 = 0$ ) state. The ( $B0 = 0, B1 = 0$ ) condition signals that the data are nonvalid and the circuit is in either a reset or a transition mode. The ( $B0 = 1, B1 = 1$ ) state is illegal and should never occur in an actual circuit.

A circuit that actually implements such a redundant representation is shown in Figure 10-35, which is a dynamic version of the DCVSL logic style where the clock is replaced by the *Start* signal [Heller84]. DCVSL uses a redundant data representation by nature of its differential dual-rail structure. When the *Start* signal is low, the circuit is precharged by the PMOS transistors, and the output ( $B0, B1$ ) goes in the *Reset-Transition* state (0, 0). When the *Start* signal goes high, signaling the initiation of a computation, the NMOS pull-down network evaluates, and one of the precharged nodes is lowered. Either  $B0$  or  $B1$ —but never both—goes high, which raises *Done* and signals the completion of the computation.

DCVSL is more expensive in terms of area than a nonredundant circuit due to its differential nature. The completion generation is performed in series with the logic evaluation, and its delay adds directly to the total delay of the logic block. The completion signals of all the individual bits must be combined to generate the completion for an  $N$ -bit data word. Completion generation thus comes at the expense of both area and speed. The benefits of the dynamic timing generation often justify this overhead.

Redundant signal representations other than the one presented in Table 10-1 can also be envisioned. One essential element is the presence of a *transition state* denoting that the circuit is in evaluation mode and the output data are not valid.

#### Example 10.4 Self-Timed Adder Circuit

An efficient implementation of a self-timed adder circuit is shown in Figure 10-36 [Abnous93]. A Manchester-carry scheme is used to boost the circuit performance. The proposed approach is based on the observation that the circuit delay of an adder is dominated by the carry-propagation path. It is therefore sufficient to use the differential



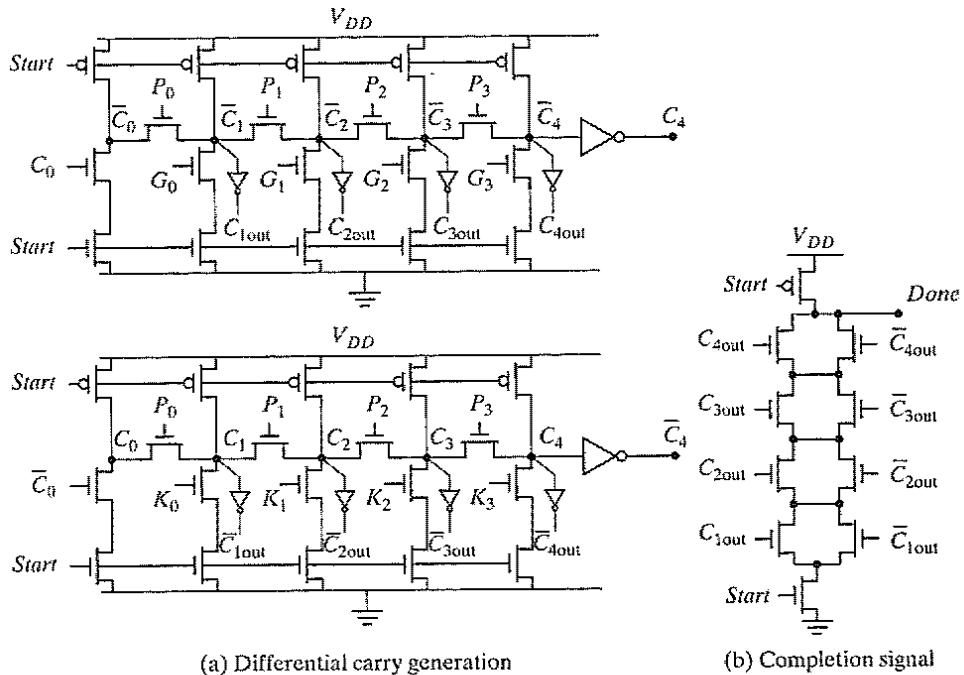


**Figure 10-36** Manchester-carry scheme with differential signal representation.

signaling in the carry path only (Figure 10-36a). The completion signal is efficiently derived by combining the carry signals of the different stages (Figure 10-36b). This safely assumes that the sum generation, which depends upon the arrival of the carry signal, is faster than the completion generation. The benefit of this approach is that the completion generation starts earlier and proceeds in parallel with sum generation, which reduces the critical timing path. All other signals, such as *P*(ropagate), *G*(enerate), *K*(ill), and *S*(um), do not require completion generation and can be implemented in single-ended logic. As shown in the circuit schematics, the differential carry paths are virtually identical. The only difference is that the *G*(enerate) signal is replaced by a *K*(ill). A simple logic analysis demonstrates that this indeed results in an inverted carry signal and, hence, a differential signaling.

### Replica Delay

While the dual-rail coding just described allows tracking of the signal statistics, it comes at the cost of power dissipation. Every single gate must transition for every new input vector, regardless of the value of the data vector. A way to reduce the overhead of completion detection is to use a *critical-path replica* configured as a delay element, as shown in Figure 10-37. To start a computation, the *Start* signal is raised and the computation of the logic network is initiated. At the same time, the start signal is fed into the replica delay line, which tracks the critical path of

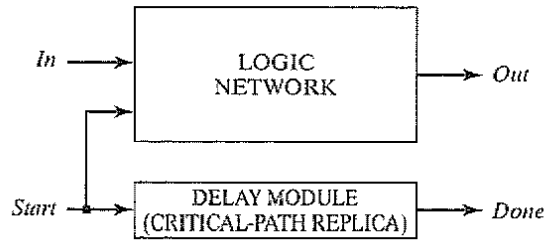


Figure 10-37 Completion-signal generation using delay module.

the logic network. It is important that the replica is structured such that no glitching transitions occur. When the output of the delay line makes a transition, it indicates that the logic is complete as the delay line mimics the critical path. In general, it is important to add extra padding in the delay line in order to compensate for possible random process variations.

The advantage of this approach is that the logic can be implemented using a standard non-redundant circuit style, such as complementary CMOS. Also, if multiple logic units are computing in parallel, it is possible to amortize the overhead of the delay line over multiple blocks. Note that this approach generates the completion signal after a time equal to the worst case delay through the network. As a result, it does not exploit the statistical properties of the incoming data. However, it can track the local effects of process variations and environmental variations (e.g., temperature or power-supply variations). This approach is widely used to generate the internal timing of semiconductor memories where self-timing is a commonly used technique.

### Example 10.5 An Alternate Completion Detection Circuit Using Current Sensing

Ideally, logic should be implemented using nonredundant CMOS (e.g., static CMOS), and the completion signal circuitry should track data dependencies. Figure 10-38 shows an approach that attempts to realize this principle [Dean94]. A current sensor is inserted in series with the combinational logic, and it monitors the current flowing through the logic. The current sensor outputs a low value when no current flows through the logic (i.e., the logic is idle) and a high value when the combinational logic is switching. This signal

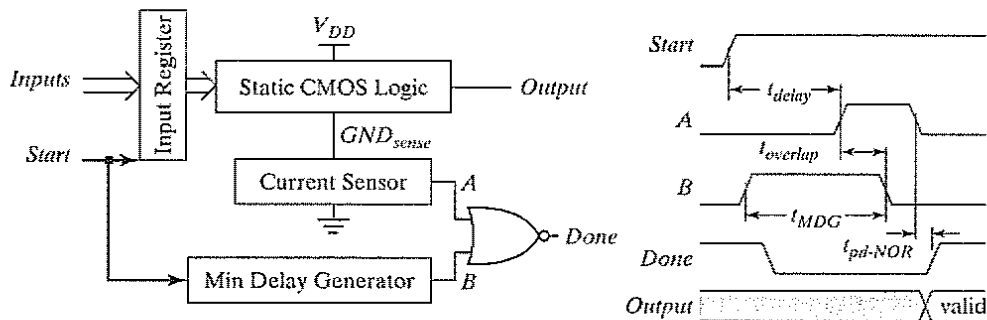


Figure 10-38 Completion-signal generation using current sensing.

effectively determines when the logic has completed its cycle. Note that this approach tracks data-dependent computation times—if only the lower order bits of an adder switch, current will stop flowing once the lower order bits switch to the final value. If the input data vector does not provoke any change in the logic from one cycle to the next, no current is drawn from the supply for static CMOS logic. In this case, a delay element that tracks the minimum delay through the logic and current sensor is used for signal completion. The outputs of the current sensor and minimum delay element are then combined.

This approach is interesting, but requires careful analog design. Ensuring reliability while keeping the overhead circuitry small is the main challenge. These concerns have kept the applicability of the approach very limited, despite its obvious potential.

### 10.4.3 Self-Timed Signaling

Besides the generation of the completion signals, a self-timed approach also requires a handshaking protocol to logically order the circuit events in order to avoid races and hazards. The functionality of the signaling (or handshaking) logic is illustrated by the example of Figure 10-39, which shows a *sender module* transmitting data to a *receiver* [Sutherland89]. The sender places the data value on the data bus ① and produces an event on the *Req* control signal by changing the polarity of the signal ②. In some cases, the request event is a rising transition; at other times, it is a falling one—the protocol described here does not distinguish between them. Upon receiving the request, the receiver accepts the data when possible and produces an event on the *Ack* signal to indicate that the data have been accepted ③. If the receiver is busy or its input buffer is full, no *Ack* event is generated, and the transmitter is stalled until the receiver becomes available by, for instance, freeing space in the input buffer. Once the *Ack* event is produced, the transmitter goes ahead and produces the next data word ④. The four events—*data change*, *request*, *data acceptance*, and *acknowledge*—proceed in a cyclic order. Successive cycles may take different amounts of time, depending on the time it takes to produce or consume the data.

This is called the *two-phase protocol*, since only two phases of operation can be distinguished for each data transmission—the active cycle of the sender and the active cycle of the receiver. Both phases are terminated by certain events. The *Req* event terminates the active cycle of the sender, while the receiver's cycle is completed by the *Ack* event. The sender is free to change the data during its active cycle. Once the *Req* event is generated, it has to keep the data constant as long as the receiver is active. The receiver can only accept data during its active cycle.

The correct operation of the sender–receiver system requires a strict ordering of the signaling events, as indicated by the arrows in Figure 10-39. Imposing this order is the task of the handshaking logic, which, in a sense, performs logic manipulations on events. An essential component of virtually any handshaking module is the *Muller C-element*. This gate, whose schematic symbol and truth table are given in Figure 10-40, performs an AND-operation on events. The output of the *C-element* is a copy of its inputs when both inputs are identical. When the inputs differ, the output retains its previous value. Phrased in a different way, events must occur

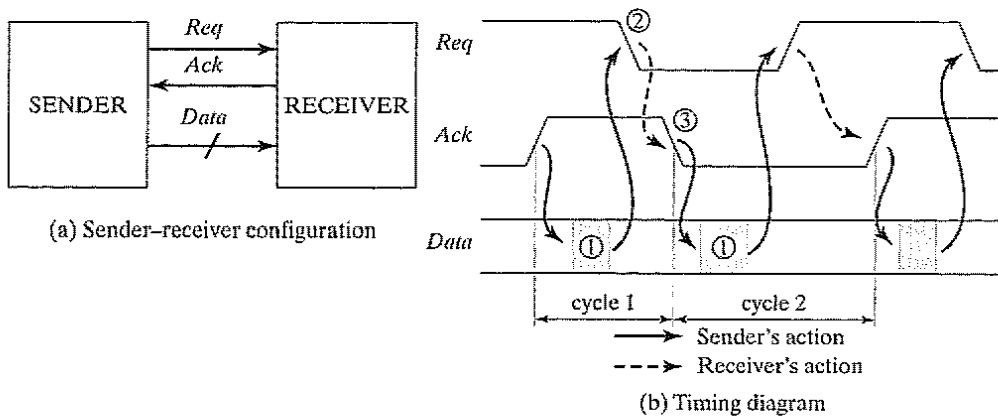


Figure 10-39 Two-phase handshaking protocol.

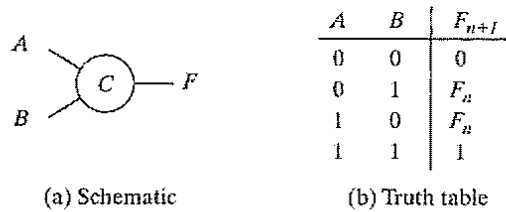


Figure 10-40 Muller C-element.

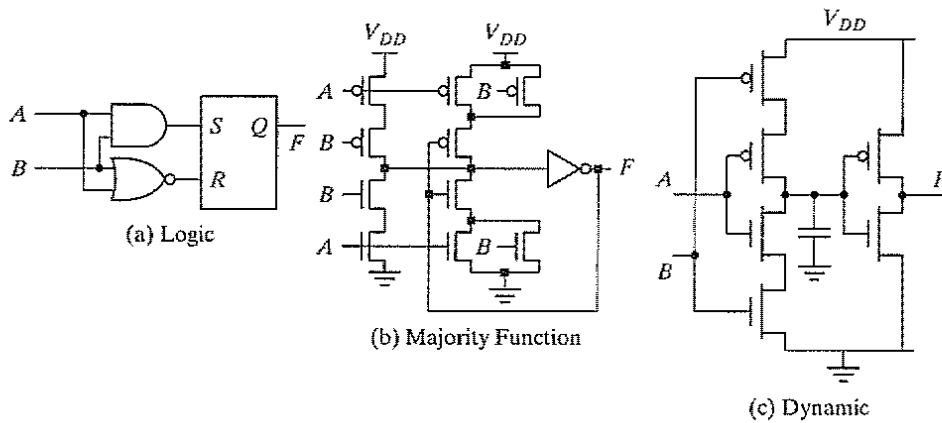
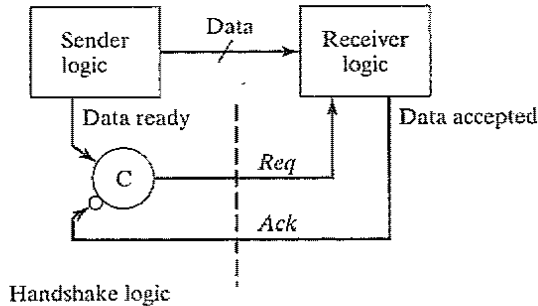


Figure 10-41 Implementations of a Muller C-element.

at both inputs of a Muller C-element for its output to change state and to create an output event. As long as this does not happen, the output remains unchanged and no output event is generated. The implementation of a C-element is centered around a latch, which should not be a surprise, given the similarities in their truth tables. Figure 10-41 presents a static and a dynamic circuit realization of the function.



**Figure 10-42** A Muller C-element implements a two-phase handshake protocol. The circle at the lower input of the Muller C-element stands for inversion.

Figure 10-42 shows how to use this component to enforce the two-phase handshaking protocol for the example of the sender–receiver. Assume that *Req*, *Ack*, and *Data Ready* are initially 0. When the sender wants to transmit the next word, the *Data Ready* signal is set to 1, which triggers the C-element, because both its inputs are at 1. *Req* goes high—this is commonly denoted as  $Req \uparrow$ . The sender now resides in the wait mode, and control is passed to the receiver. The C-element is blocked, and no new data are sent to the data bus (*Req* stays high) as long as the transmitted data are not processed by the receiver. Once this happens, the *Data accepted* signal is raised. This can be the result of many different actions, possibly involving other C-elements communicating with subsequent blocks. An  $Ack \uparrow$  ensues, which unblocks the C-element and passes the control back to the sender. A  $Data ready \downarrow$  event, which might already have happened before  $Ack \uparrow$ , produces a  $Req \downarrow$ , and the cycle is repeated.

### Problem 10.1 Two-Phase Self-Timed FIFO

Figure 10-43 shows a two-phase, self-timed implementation of a FIFO (first-in first-out) buffer with three registers. Assuming that the registers accept a data word on both positive- and negative-going transitions of the *En* signals, and that the *Done* signal is simply a delayed version of *En*, examine the operation of the FIFO by plotting the timing behavior of all signals of interest. How can you observe that the FIFO is completely empty? Full? (Hint: Determine the necessary conditions on the *Ack* and *Req* signals.)

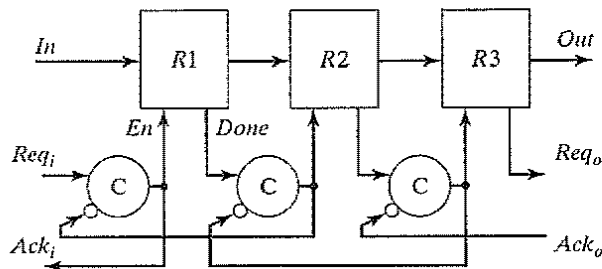


**Figure 10-43** Three-stage, self-timed FIFO, using a two-phase signaling protocol.

The two-phase protocol has the advantage of being simple and fast. However, this protocol requires the detection of transitions that may occur in either direction. Most logic devices in the MOS technology tend to be sensitive to levels or to transitions in one particular direction. Event-triggered logic, as required in the two-phase protocol, requires extra logic as well as state information in the registers and the computational elements. Since the transition direction is important, initializing all the Muller *C*-elements in the appropriate state is essential. If this is not done, the circuit might become deadlocked, which means that all elements are permanently blocked and nothing will ever happen. A detailed study on how to implement event-triggered logic can be found in [Sutherland89], the defining text on micropipelines.

The only alternative is to adopt a different signaling approach, such as *four-phase signaling*, or *return-to-zero (RTZ)*. This class of signaling requires that all controlling signals be brought back to their initial values before the next cycle can be initiated. Once again, this is illustrated with the example of the sender-receiver. The four-phase protocol for this example is shown in Figure 10-44.

The protocol presented is initially the same as the two-phase one. Both the *Req* and the *Ack* are initially in the zero state, however. Once a new data word is put on the bus ①, the *Req* is raised (*Req*↑ or ②), and control is passed to the receiver. When ready, the receiver accepts the data and raises *Ack* (*Ack*↑ or ③). So far, nothing new. The protocol proceeds by bringing both *Req* (*Req*↓ or ④) and *Ack* (*Ack*↓ or ⑤) back to their initial state in sequence. Only when that state is reached is the sender allowed to put new data on the bus ①. This protocol is called *four-phase signalling* because four distinct time zones can be recognized per cycle: two for the sender; two for the receiver. The first two phases are identical to the two-phase protocol, while the last two are devoted to resetting of the state. An implementation of the protocol, based on Muller *C*-elements, is shown in Figure 10-45. It is interesting to note that the four-phase protocol requires two *C*-elements in series (since four states must be represented). The *Data ready* and *Data accepted* signals must be pulses instead of single transitions.

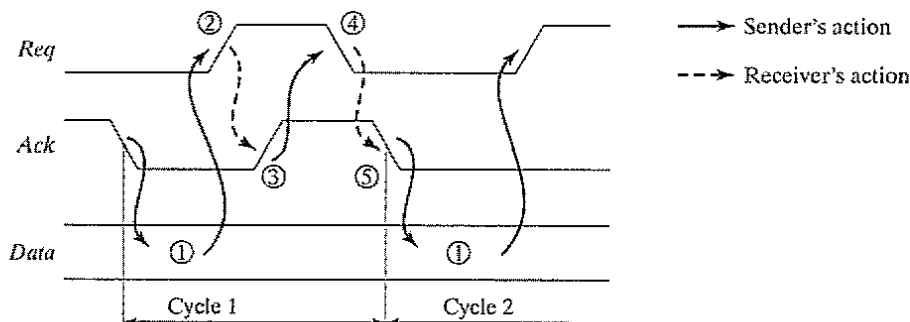


Figure 10-44 Four-phase handshaking protocol.

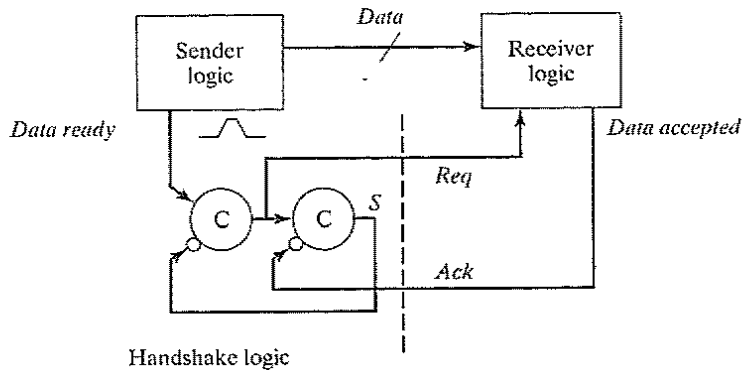


Figure 10-45 Implementation of four-phase handshake protocol using Muller C-elements.

### Problem 10.2 Four-Phase Protocol

Derive the timing diagram for the signals shown in Figure 10-45. Assume that the *Data Ready* signal is a pulse and that the *Data Accepted* signal is a delayed version of *Req*.

The four-phase protocol has the disadvantage of being more complex and slower, since two events on *Req* and *Ack* are needed per transmission. On the other hand, it has the advantage of being robust. The logic in the sender and receiver modules does not have to deal with transitions, which can go either way; it has to consider only rising (or falling) transition events or signal levels. This is readily accomplished with traditional logic circuits. For this reason, four-phase handshakes are the preferred implementation approach for most of the current self-timed circuits. The two-phase protocol is mainly selected when the sender and receiver are far apart and the delays on the control wires (*Ack* and *Req*) are substantial.

### Example 10.6 The Pipelined Datapath—Revisited

We have introduced both the signaling conventions and the concepts of the completion-signal generation. Now it is time to bring them all together. We do this with the example of the pipelined datapath, which was presented earlier. A view of the self-timed datapath, including the timing control, is offered in Figure 10-46. The logic functions *F1* and *F2* are implemented using dual-rail, differential logic.

To understand the operation of this circuit, assume that all *Req* and *Ack* signals, including the internal ones, are set to 0, which means there is no activity in the data path. All *Start* signals are low so that all logic circuits are in precharge condition. An input request ( $Req_i \uparrow$ ) triggers the first C-element. The enable signal *En* of *R1* is raised, effectively latching the input data into the register, assuming a positive edge-triggered or a level-sensitive implementation.  $Ack_i \uparrow$  acknowledges the acceptance of the data. The second C-element is triggered as well, since  $Ack_{int}$  is low. This raises the *Start* signal and starts the evaluation of *F1*. At its completion, the output data are placed on the bus, and a

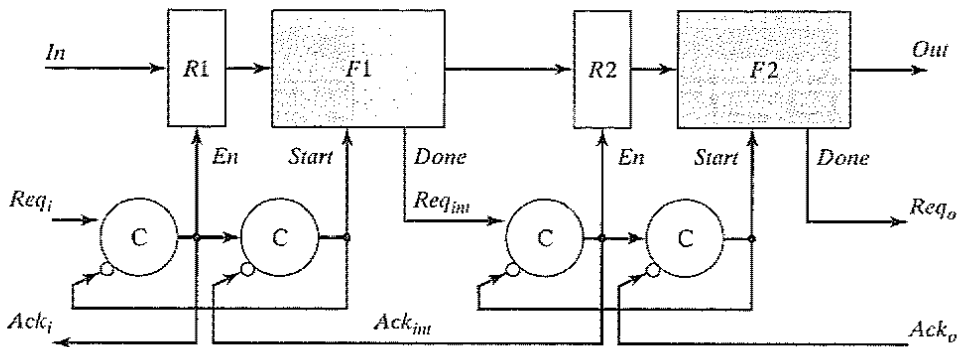


Figure 10-46 Self-timed pipelined datapath—complete composition.

request is initiated to the second stage ( $Req_{in} \uparrow$ ), which acknowledges its acceptance by raising  $Ack_{in}$ .

At this point, stage 1 is still blocked for further computations. However, the input buffer can respond to the  $Ack_i \uparrow$  event by resetting  $Req_i$  to its zero state ( $Req_i \downarrow$ ). In turn, this lowers  $En$  and  $Ack_i$ . Upon receipt of  $Ack_{in} \uparrow$ ,  $Start$  goes low, the precharge phase starts, and  $F1$  is ready for new data. Note that this sequence corresponds to the four-phase handshake mechanism described earlier. The dependencies among the events are presented in a more pictorial fashion in the *state transition diagram (STG)* shown in Figure 10-47. These STGs can become very complex. Computer tools are often used to derive STGs that ensure proper operation and optimize the performance.

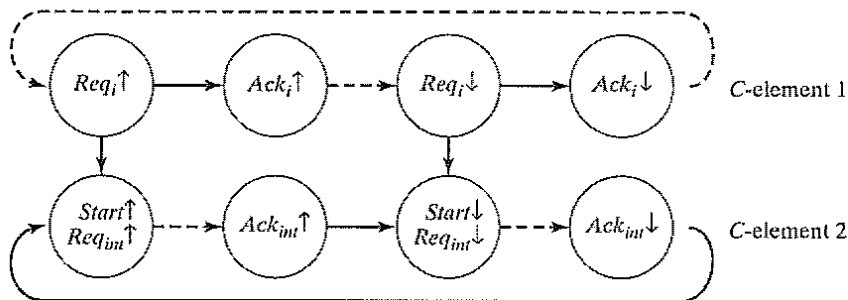
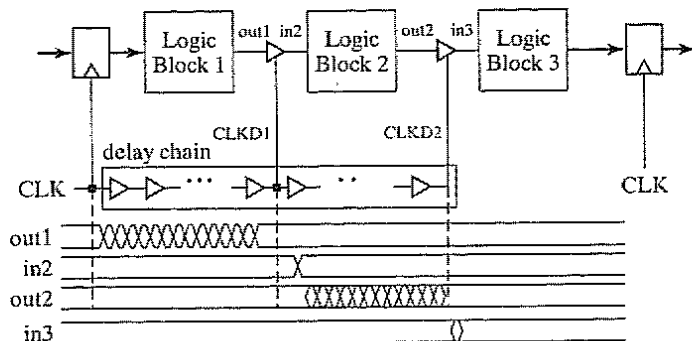


Figure 10-47 State transition diagram for pipeline stage 1. The nodes represent the signaling events, while the arrows express dependencies. Arrows in dashed lines express actions in either the preceding or the following stage.

### 10.4.4 Practical Examples of Self-Timed Logic

Self-timed circuits can provide a significant performance advantage. Unfortunately, the overhead circuitry precludes a widespread application in general-purpose digital computing. Nevertheless, the key concepts of self-timed circuits are being exploited in a number of practical applications. We present a few examples that illustrate the use of self-timed concepts for either power savings or performance enhancement.





**Figure 10-48** Application of self-timing for glitch reduction.

### Glitch Reduction Using Self-Timing

A major source of unnecessary switched capacitance in large datapaths, such as bit-sliced adders and multipliers, is due to spurious transitions caused by *glitch propagation*. Imbalances in a logic network cause inputs of a logic gate or block to arrive at different times, resulting in glitching transitions. In large combinational blocks such as multipliers, transitions happen in waves as the primary input changes ripple through the logic. Enabling a logic block only when all the inputs have settled helps reduce or eliminate the glitching transitions. One approach for doing so is the use of a self-timed gating approach, which partitions each computational logic block into smaller blocks and distinct phases. Tristate buffers are inserted between each of these phases in order to prevent glitches from propagating through the datapath, as shown in Figure 10-48. Assuming an arbitrary logic network, it is fair to assume that the outputs of logic block 1 will not be synchronized. When the tristate buffers at the output of logic block 1 are enabled, the computation of logic block 2 is allowed to proceed. To reduce glitching transitions, the tristate buffer should be enabled only when it is ensured that the outputs of logic block 1 are stable and valid. The control of the tristate buffer can be performed through the use of a self-timed enable signal, generated by passing the system clock through a delay chain that models the critical path of the processor. The delay chain is then tapped at the points corresponding to the locations of the buffers, and the resulting signals are distributed throughout the chip. This technique succeeds in substantially reducing the switching capacitance of combinational logic blocks such as multipliers, even when taking into account the overhead of the delay chain, gating signal distribution, and buffers [Goodman98].

### Post-Charge Logic

An interesting form of self-timed logic is self-resetting CMOS. This structure uses a control structure different from the conventional self-timed pipeline. Instead of waiting for all the logic stages to complete their operation before transitioning to the reset stage, the idea is to precharge a logic block as soon as it completes its operation. Since the precharge happens after the operation instead of before evaluation, it is often termed *postcharge logic*. A block diagram of post-charge logic is shown in Figure 10-49 [Williams00]. As can be seen from this block diagram, the

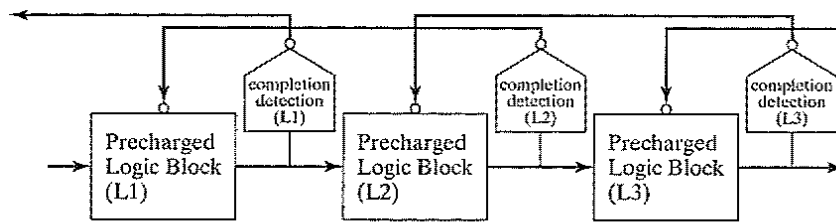


Figure 10-49 Self-resetting logic.

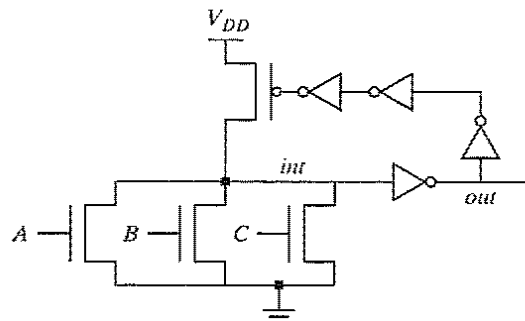


Figure 10-50 Self-resetting three-input OR.

precharging of L1 happens when its successor stage has completed and does not need its input anymore. It is possible to precharge a block based on the completion of its own output, but care must be taken to ensure that the stage that follows has properly evaluated and the input has become obsolete.

It should be noted that, unlike with other logic styles, the signals are represented as pulses and are valid only for a limited duration. The pulse width must be shorter than the reset delay or else there is a contention between the precharge device and the evaluate switches. While this logic style offers potential speed advantages, special care must be taken to ensure correct timing. Also, circuitry that converts level signals to pulses, and vice versa is required. An example of self-resetting logic is shown in Figure 10-50 [Bernstein98]. Assume that all inputs are low and that *int* is initially precharged. If *A* goes high, *int* will fall, causing *out* to go high. This causes the gate to precharge. When the PMOS precharge device is active, the inputs must be in a reset state in order to avoid contention.

### Clock-Delayed Domino

One interesting application of self-timed circuits that uses the delay-matching concept is *clock-delayed (CD) domino* [Yee96][Bernstein00]. This is a style of dynamic logic in which there is no global clock signal. Instead, the clock for one stage is derived from that for the previous stage. A simple example of a CD domino stage is shown in Figure 10-51. The two inverter delays plus the transmission gate along the clock path emulate the worst-case delay through the dynamic logic gate. The transmission gate is always turned on, and the delay of the clock path is adjusted



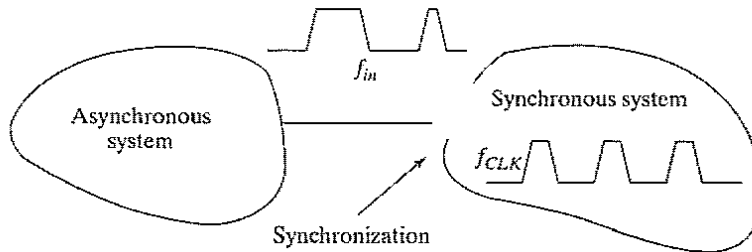


Figure 10-52 Asynchronous-synchronous interface.

potential crash. Therefore, the undefined state must be resolved in one way or another before it is interpreted further. It does not really matter what decision is made, as long as a unique result is available. For instance, it is either decided that the key is not yet pressed, a situation that will be corrected in the next poll of the keyboard, or it is concluded that the key is already pressed.

Thus, an asynchronous signal must be resolved to be either in the high or low state before it is fed into the synchronous environment. A circuit that implements such a decision-making function is called a *synchronizer*. Now comes the bad news: **Building a perfect synchronizer that always delivers a legal answer is impossible** [Chaney73] [Glasser85]! A synchronizer needs some time to come to a decision, and in certain cases this time might be arbitrarily long. An asynchronous-synchronous interface is thus always prone to errors, known as *synchronization failures*. The designer's task is to ensure that the probability of such a failure is small enough that it is not likely to disturb the normal system behavior. Typically, this probability can be reduced in an exponential fashion by waiting longer before making a decision. This is not too troublesome in the keyboard example, but in general, waiting affects system performance and should be avoided as much as possible.

To illustrate why waiting helps reduce the failure rate of a synchronizer, consider a synchronizer as shown in Figure 10-53. This circuit is a latch that is transparent during the low phase of the clock and samples the input on the rising edge of the clock  $CLK$ . However, since the sampled signal is not synchronized to the clock signal, there is a finite probability that the setup time or hold time of the latch is violated. (The probability is a strong function of the transition frequencies of the input and the clock.) As a result, once the clock goes high, there is a chance that the output of the latch resides somewhere in the undefined transition zone. The sampled signal eventually evolves into a legal 0 or 1, even in the latter case, as the latch has only two stable states.

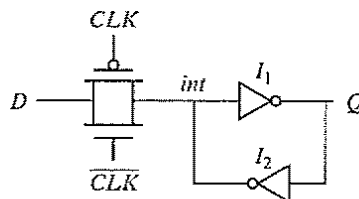
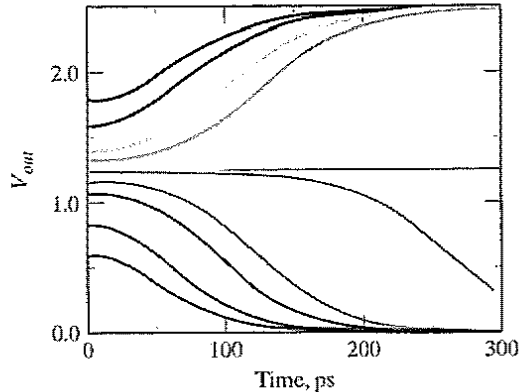


Figure 10-53 A simple synchronizer.

### Example 10.7 Synchronizer Trajectories

Figure 10-54 shows the simulated trajectories of the output nodes of a cross-coupled static CMOS inverter pair for an initial state close to the metastable point. The inverters are composed of minimum-size devices.



**Figure 10-54** Simulated trajectory for a simple synchronizer.

If the input is sampled such that the cross-coupled inverter pair starts at the metastable point, the voltage will remain at the metastable state forever in the absence of noise. If the data are sampled with a small offset (positive or negative), the differential voltage will evolve in an exponential way, with a time constant that is dependent on the strength of the transistors as well as the parasitic capacitances. The time it takes to reach the acceptable signal zones depends upon the initial distance of the sampled signal from the metastable point.

In order to determine the required waiting period, let us build a mathematical model of the behavior of the bistable element and use the results to determine the probability of synchronization failure as a function of the waiting period [Veendrick80].

The transient behavior around the metastable point of the cross-coupled inverter pair is accurately modeled by a system with a single dominant pole. Under this assumption, the transient response of the bistable element after the sampling clock has been turned off can be modeled as

$$v(t) = V_{MS} + (v(0) - V_{MS})e^{-t/\tau} \quad (10.8)$$

where  $V_{MS}$  is the metastable voltage of the latch,  $v(0)$  is the initial voltage after the sampling clock is turned off, and  $\tau$  is the time constant of the system. Simulations indicate that this first-order model is quite precise.

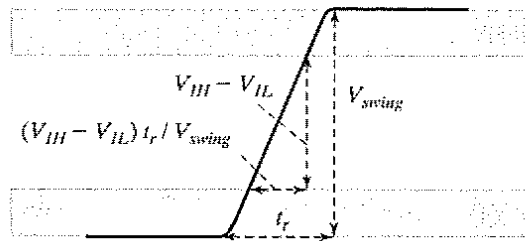


Figure 10-55 Linear approximation of signal slope.

The model can now be used to compute the range of values for  $v(0)$  that causes an error or a voltage in the undefined range, after a waiting period  $T$ . A signal is called **undefined** if its value is situated between  $V_{IH}$  and  $V_{IL}$ :

$$V_{MS} - (V_{MS} - V_{IL})e^{-T/\tau} \leq v(0) \leq V_{MS} + (V_{IH} - V_{MS})e^{-T/\tau} \quad (10.9)$$

Equation (10.9) conveys an important message: **The range of input voltages that cause a synchronization error decreases exponentially with the waiting period  $T$ .** Increasing the waiting period from  $2\tau$  to  $4\tau$  decreases the interval and the chances of an error by a factor of 7.4.

Some information about the asynchronous signal is required in order to compute the probability of an error. Assume that  $V_{in}$  is a periodical waveform with an average period  $T_{signal}$  between transitions and with identical rise and fall times  $t_r$ . Assume also that the slopes of the waveform in the undefined region can be approximated by a linear function, as shown in Figure 10-55. Using this model, we can estimate the probability  $P_{init}$  that  $v(0)$ , the value of  $V_{in}$  at the sampling time, resides in the undefined region:

$$P_{init} = \frac{\left(\frac{V_{IH} - V_{IL}}{V_{swing}}\right)t_r}{T_{signal}} \quad (10.10)$$

The chances for a synchronization error to occur depend upon the frequency of the synchronizing clock,  $\phi$ . The greater the number of sampling events, the higher the chance of running into an error. This means that the average number of synchronization errors per second,  $N_{sync}(0)$ , equals Eq. (10.11) if no synchronizer is used. Therefore, we can write

$$N_{sync}(0) = \frac{P_{init}}{T_\phi} \quad (10.11)$$

where  $T_\phi$  is the sampling period.

From Eq. (10.9), we learned that waiting a period  $T$  before observing the output reduces exponentially the probability that the signal is still undefined:

$$N_{sync}(T) = \frac{P_{init}e^{-T/\tau}}{T_\phi} = \frac{(V_{IH} - V_{IL})e^{-T/\tau}}{V_{swing}} \frac{t_r}{T_{signal}T_\phi} \quad (10.12)$$

The robustness of an asynchronous–synchronous interface is thus determined by the following parameters: signal switching rate and rise time, sampling frequency, and waiting time  $T$ .

### Example 10.8 Synchronizers and Mean Time to Failure

Consider the following design example:  $T_\phi = 5$  ns, which corresponds to a 200-Mhz clock;  $T = T_\phi = 5$  ns;  $T_{signal} = 50$  ns;  $t_r = 0.5$  ns; and  $\tau = 150$  ps. From the VTC of a typical CMOS inverter, it can be derived that  $V_{IH} - V_{IL}$  approximately equals 0.5 V for a voltage swing of 2.5 V. Evaluation of Eq. (10.12) yields an error probability of  $1.38 \times 10^{-9}$  errors/s. The inverse of  $N_{sync}$  is called the *mean time to failure*, or the MTF, and equals  $7 \times 10^8$  s, or 23 years. If no synchronizer were used, the MTF would have been only 2.5  $\mu$ s!

### Design Consideration

When designing a synchronous–asynchronous interface, we must keep in mind the following observations:

- The acceptable failure rate of a system depends upon many economic and social factors and is a strong function of the system's application area.
- The exponential relation in Eq. (10.12) makes the failure rate extremely sensitive to the value of  $\tau$ . Defining a precise value of  $\tau$  is not easy in the first place, because  $\tau$  varies from chip to chip and is a function of temperature as well. The probability of an error occurring can thus fluctuate over large ranges even for the same design. A worst case design scenario is definitely advocated here. If the worst case failure rate exceeds a certain criterion, it can be reduced by increasing the value of  $T$ . A problem occurs when  $T$  exceeds the sampling period  $T_\phi$ . This can be avoided by cascading (or pipelining) a number of synchronizers, as shown in Figure 10-56. Each of those synchronizers has a waiting period equal to  $T_\phi$ . Notice that this arrangement requires the  $\phi$  pulse to be short enough to avoid race conditions. The global waiting period equals the sum of the  $T$ s of all the individual synchronizers. The increase in MTF comes at the expense of an increased latency.

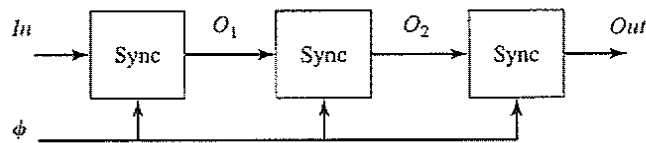


Figure 10-56 Cascading (edge-triggered) synchronizers reduces the main time to failure.

- Synchronization errors are very hard to trace, due to their random nature. Making the mean time to failure very large does not preclude errors. The **number of synchronizers in a system should therefore be severely restricted**. A maximum of one or two per system is advocated. ■

### 10.5.2 Arbiters

Finally, a sibling of the synchronizer called the *arbiter*, interlock element, or mutual-exclusion circuit, should be mentioned. An arbiter is an element that decides which of two events has occurred first. For example, such components allow multiple processors to access a single

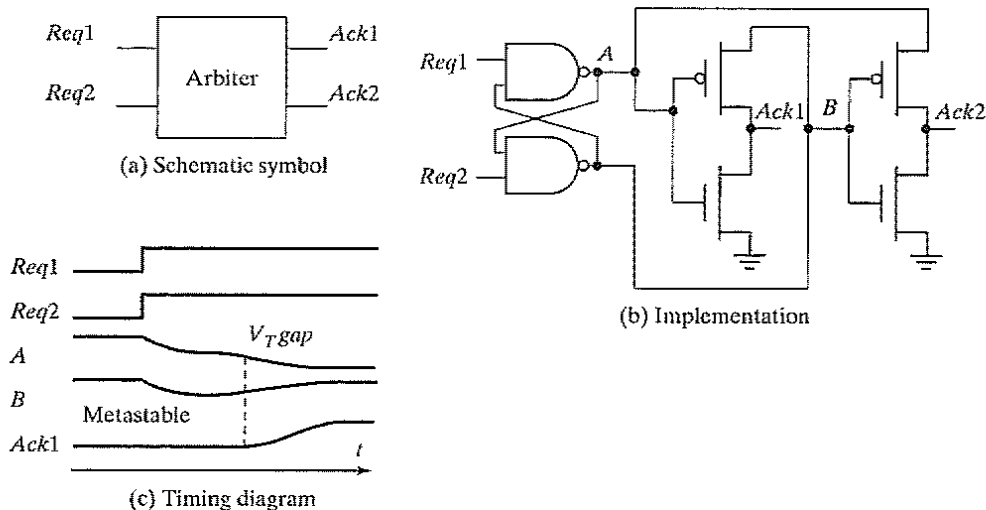


Figure 10-57 Mutual-exclusion element (or arbiter).

resource, such as a large shared memory. A synchronizer is actually a special case of an arbiter, since it determines whether a signal transition happened before or after a clock event. A synchronizer is thus an arbiter with one of its inputs tied to the clock.

An example of a mutual-exclusion circuit is shown in Figure 10-57. It operates on two input-request signals that operate on a four-phase signaling protocol; that is, the *Req(uest)* signal has to go back to the reset state before a new *Req(uest)* can be issued. The output consists of two *Ack(nowledge)* signals that should be mutually exclusive. While *Requests* may occur concurrently, only one of the *Acknowledges* is allowed to go high. The operation is most easily visualized starting with both inputs low—neither device issuing a request—nodes *A* and *B* high, and both *Acknowledges* low. An event on one of the inputs (e.g.,  $Req1 \uparrow$ ) causes the flip-flop to switch, node *A* to go low, and  $Ack1 \uparrow$ . Concurrent events on both inputs force the flip-flop into the metastable state, and the signals *A* and *B* might be undefined for a while. The cross-coupled output structure keeps the output values low until one of the NAND outputs differs from the other by more than a threshold value  $V_T$ . This approach eliminates glitches at the output.

## 10.6 Clock Synthesis and Synchronization Using a Phase-Locked Loop\*

There are numerous digital applications that require the on-chip generation of a periodic signal. Synchronous circuits need a global periodic clock reference to orchestrate the events. Current microprocessors and high-performance digital circuits require clock frequencies in the gigahertz range. Crystal oscillators, by contrast, generate only accurate, low-jitter clocks over a frequency range from 10's of MHz to approximately 200 MHz. To generate the higher frequency required by digital circuits, a *phase-locked loop* (PLL) structure typically is used. A PLL takes an external low-frequency reference crystal frequency signal and multiplies its frequency by a rational number  $N$  (see the left side of Figure 10-58).



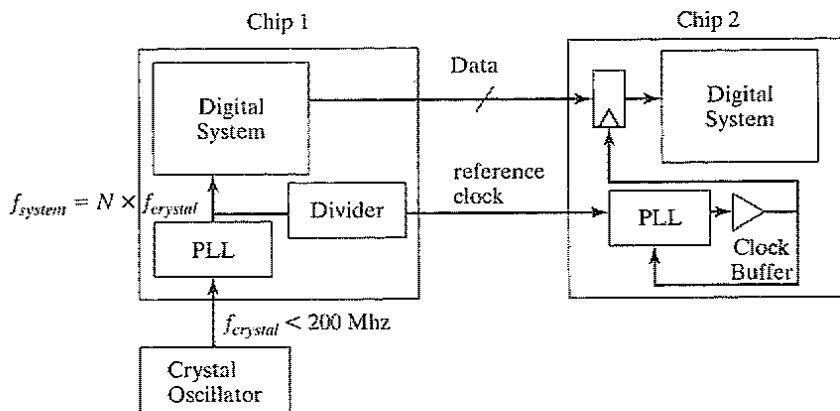


Figure 10-58 Applications of phase locked loops (PLL).

Another and equally important function of a PLL is to synchronize communications between chips. As shown in Figure 10-58, a reference clock is sent along with the parallel data being communicated. (In this example only the transmit path from chip 1 to chip 2 is shown.) Since chip-to-chip communication most often occurs at a lower rate than the on-chip clock rate, the reference clock is divided, but kept in phase with the system clock. In chip 2, the reference clock is used to synchronize all the input flip-flop, which can present a significant clock load in the case of wide data busses. Unfortunately, implementing clock buffers to deal with this problem introduces skew between the data and the sample clock. A PLL aligns (i.e., de-skews) the output of the clock buffer with respect to the data. In addition, the PLL can multiply the frequency of the incoming reference clock, allowing the core of the second chip to operate at a higher frequency than the input reference clock.

### 10.6.1 Basic Concept

A set of two or more periodic signals of the same frequency is well defined if we know one of them and its *phase* with respect to the other signals, as shown in Figure 10-59, where  $\phi_1$  and  $\phi_2$  represent the phases of the two signals. The *relative phase* is the difference between the two.

A PLL is a complex, nonlinear feedback circuit. Its basic operation is best understood with the aid of Figure 10-60 [Jeong87]. The *voltage-controlled oscillator* (VCO) takes an analog control input and generates a clock signal of the desired frequency. In general, there is a nonlinear relationship between the control voltage ( $v_{cont}$ ) and the output frequency. To synthesize a system clock of a particular frequency, it is necessary to set the control voltage to the appropriate value. This is a function of the rest of the blocks and the feedback loop in the PLL. The feedback loop is critical to the tracking process and environmental variations. The feedback also allows for frequency multiplication.

The reference clock is, in general, generated off chip from an accurate crystal reference. It is compared with a divided version of the system clock (i.e., the local clock), using a phase detector, which determines the phase difference between the signals and produces an

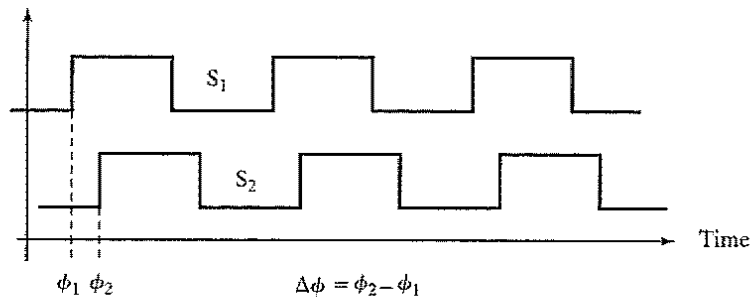


Figure 10-59 Relative and absolute phase of two periodic signals.

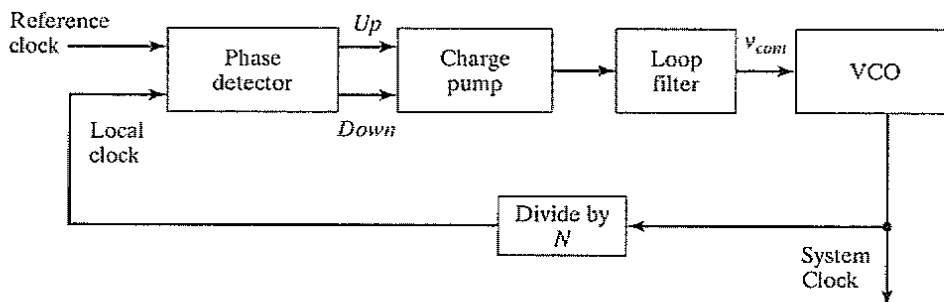


Figure 10-60 Functional composition of a phase-locked loop (PLL).

*Up* or *Down* signal when the local clock lags or leads the reference signal. It detects which of the two input signals arrives earlier and produces the appropriate output signal. The *Up* and *Down* signals are fed into a charge pump, which translates the digital encoded control information into an analog voltage [Gardner80]. An *Up* signal increases the value of the control voltage and speeds up the VCO, which causes the local signal to catch up with the reference clock. A *Down* signal, on the other hand, slows down the oscillator and eliminates the phase lead of the local clock.

Passing the output of the charge pump directly into the VCO creates a jittery clock signal. The edge of the local clock jumps back and forth instantaneously and oscillates around the targeted position. As discussed earlier, clock jitter is highly undesirable, since it reduces the time available for logic computation, and therefore should be kept within a given percentage of the clock period. This is partially accomplished by the introduction of the *loop filter*. This low-pass filter removes the high-frequency components from the VCO control voltage and smooths out its response, which results in a reduction of the jitter. Note that the PLL structure is a feedback structure. The addition of extra phase shifts, as introduced by a high-order filter, may result in instability. Important properties of a PLL are its *lock range*, the range of input frequencies over which the loop can maintain functionality; the *lock time*, the time it takes for the PLL to lock onto a given input signal; and the jitter. When in lock, the system clock is  $N$  times the reference clock frequency.

A PLL is an analog circuit and is inherently sensitive to noise and interference. This is especially true for the loop filter and VCO, for which induced noise has a direct effect on the resulting clock jitter. A major source of interference is the noise coupling through the supply rails and the substrate. This is a particular concern in digital environments, where noise is introduced by a variety of sources. Analog circuits with a high supply rejection, such as differential VCOs, are therefore desirable [Kim90]. In summary, integrating a highly sensitive component into a hostile digital environment is nontrivial and requires expert analog design. More detailed descriptions of various components of a PLL are given in the following subsections.

### 10.6.2 Building Blocks of a PLL

#### Voltage Controlled Oscillator (VCO)

A VCO generates a periodic signal with a frequency that is a linear function of the input control voltage  $v_{cont}$ . In other words, the VCO frequency can be expressed as

$$\omega = \omega_0 + K_{vco} \cdot v_{cont} \quad (10.13)$$

Since the phase is the time integral of the frequency, the output phase of the VCO block is given by

$$\phi_{out} = \omega_0 t + K_{vco} \cdot \int_{-\infty}^t v_{cont} dt \quad (10.14)$$

where  $K_{vco}$  is the gain of the VCO given in rad/s/V,  $\omega_0$  is a fixed frequency offset, and  $v_{cont}$  controls a frequency centered around  $\omega_0$ . The output signal has the form

$$x(t) = A \cdot \cos\left(\omega_0 t + K_{vco} \cdot \int_{-\infty}^t v_{cont} dt\right) \quad (10.15)$$

Various implementation strategies for VCOs were discussed in Chapter 7. Differential ring oscillators are the method of choice at present.

#### Phase Detectors

The phase detector determines the relative phase difference between two incoming signals and outputs a signal that is proportional to this phase difference. One of the inputs to the phase detector is a reference clock that typically is generated off chip, while the other clock input is a divided version of the VCO. Two basic types of phase detectors are commonly used—the *XOR gate* and the *phase frequency detector* (PFD).

**XOR Phase Detector** An XOR gate, the simplest of the two detectors, is useful as a phase detector because of the following observation: the relative phase difference between the inputs is reflected by the time over which the two inputs are different. Figure 10-61 shows the XOR-function of two waveforms. Feeding this output in a low-pass filter results into a dc-signal that is proportional to the phase difference, as shown in Figure 10-61(c).

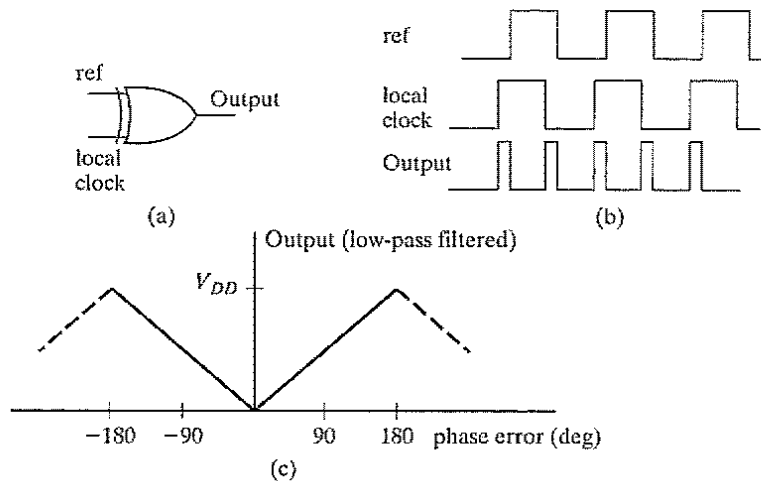


**Figure 10-61** (a) The XOR as a phase detector; (b) its output before low-pass filtering; and (c) transfer characteristics.

For this detector, a deviation in a positive or negative direction from the perfect in-phase condition (i.e., a phase error of zero) produces the same change in duty factor, resulting in the same average voltage. Thus the linear phase range is only 180 degrees. In steady state, a PLL locks into a quadrature phase relationship ( $\frac{1}{2}$  cycle offset) between the two inputs.

**Phase Frequency Detector** The phase frequency detector (PFD) is the most commonly used form of phase detector, and it solves several of the shortcomings of the detector discussed previously [Dally98]. As the name implies, the output of the PFD is dependent on both the phase and frequency difference between the applied signals. Accordingly, it cannot lock to an incorrect multiple of the frequency. The PFD takes two clock inputs and produces two outputs, *UP* and *DN*, as shown in Figure 10-62.

The PFD is a state machine with three states. Assume that both *UP* and *DN* outputs are initially low. When input *A* leads *B*, the *UP* output is asserted on the rising edge of input *A*. The *UP* signal remains in this state until a low-to-high transition occurs on input *B*. At that time, the *DN* output is asserted, causing both flip-flops to reset through the asynchronous reset signal. Notice that there is a small pulse on the *DN* output, whose duration is equal to the delay through the AND gate and register *Reset-to-Q* delay. The pulse width of the *UP* pulse is equal to the phase error between the two signals. The roles are reversed for the case in which input *A* lags *B*. A pulse proportional to the phase error is generated on the *DN* output. If the loop is in lock, short pulses will be generated on the *UP* and *DN* outputs.

The circuit also acts as a frequency detector, providing a measure of the frequency error (see Figure 10-63). For the case in which *A* is at a higher frequency than *B*, the PFD generates a lot more *UP* pulses—with the average pulse proportional to the frequency difference—while the number of *DN* pulses are close to zero, on average. Exactly the opposite is true for the case in

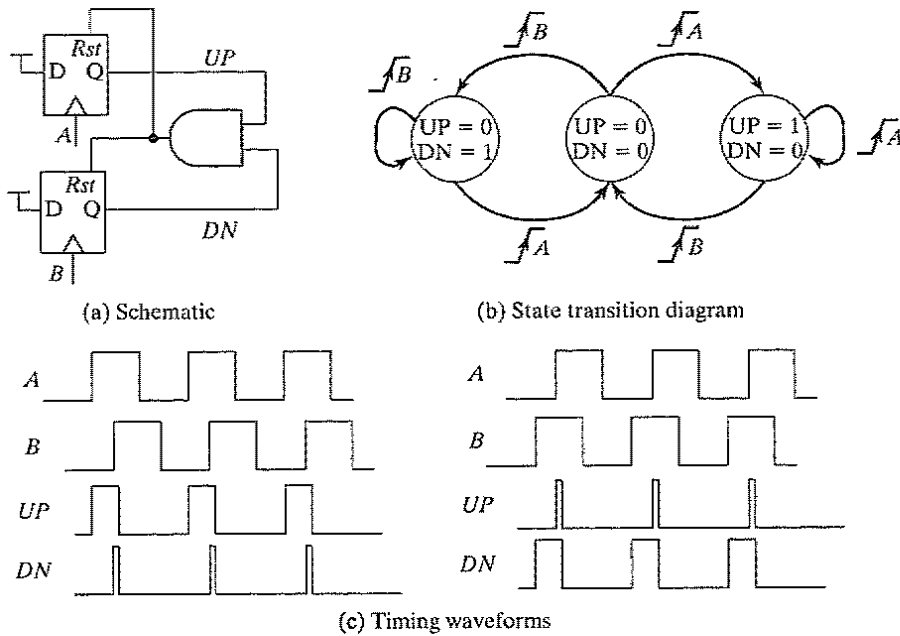


Figure 10-62 Phase frequency detector.

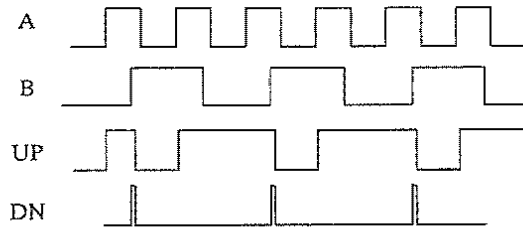


Figure 10-63 Timing of the PFD measuring frequency error.

which *B* has a frequency larger than that of *A*—many more pulses are generated on the *DN* output than on the *UP* output.

The phase characteristics of the phase detector are shown in Figure 10-64. Notice that the linear range has been expanded to  $4\pi$ .

**Charge Pump**

The *UP* and *DN* pulses must be converted into an analog voltage that controls the VCO. One possible implementation is shown in Figure 10-65. A pulse on the *UP* signal adds an amount of charge to the capacitor proportional to the width of the *UP* pulse, while a pulse on the *DN* signal removes charge proportional to the *DN* pulse width. If the width of the *UP* pulse is larger than that of the *DN* pulse, there is a net increase in the control voltage. This effectively increases the frequency of the VCO.

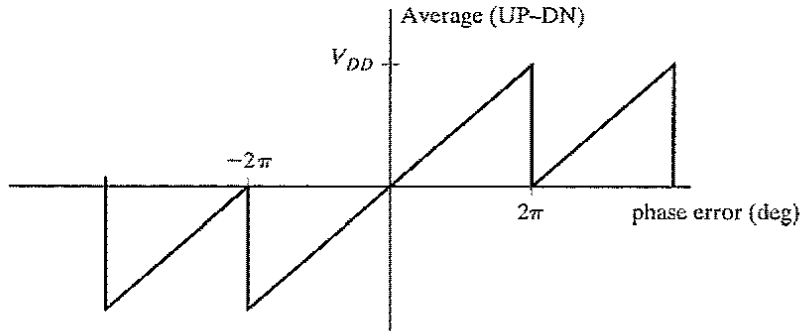


Figure 10-64 PFD phase characteristics.

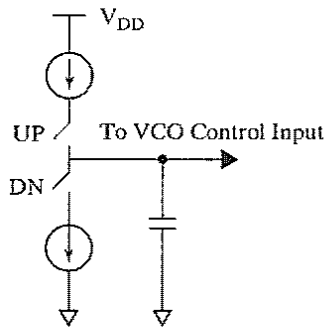
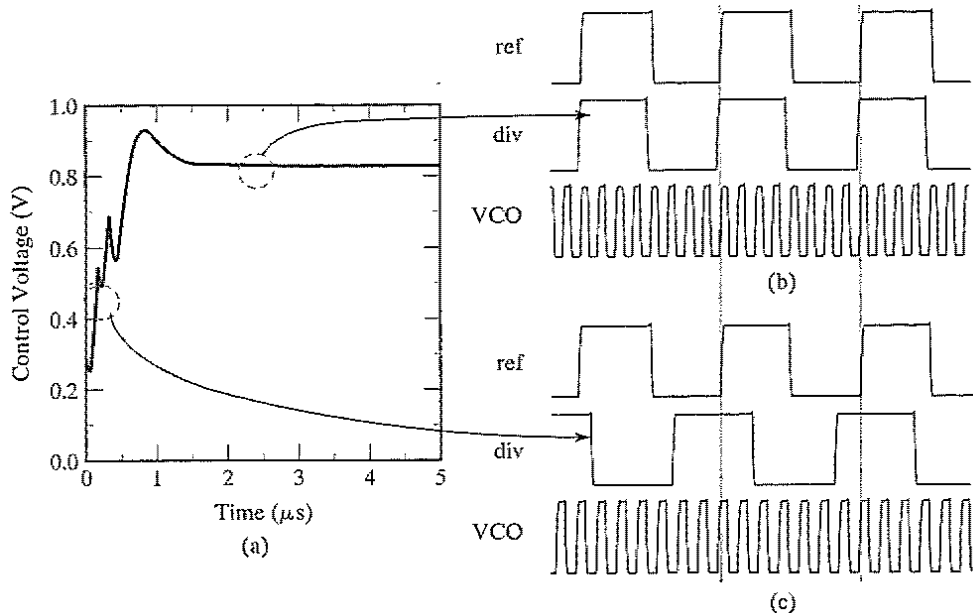


Figure 10-65 Charge pump.

### Example 10.9 Transient Behavior of Phase-Locked Loop

The settling time of a PLL is the time it takes to reach steady-state behavior. The length of the startup transient is strongly dependent on the bandwidth of the loop filter. Figure 10-66 shows a SPICE level simulation of a PLL implemented in a 0.25- $\mu\text{m}$  CMOS. An ideal VCO is used to speed up the simulation. In this example, a reference frequency of 100 MHz is chosen, and the PLL multiplies this frequency by 8 to 800 MHz. The Figure 10-66a illustrates the transient response and the settling process of the control voltage input of the VCO. Once the control voltage reaches its final value, the output frequency (the clock of the digital system) settles to steady state. The simulation on the right shows the reference frequency, the output of the divider, and the output frequency in steady state. Figure 10-66b shows the PLL in lock at  $f_{out} = 8 \times f_{ref}$ , while Figure 10-66c shows the waveforms during the locking process when the output is not in phase with the input, and the frequencies are not related yet by the divide ratio.



**Figure 10-66** SPICE simulation of a PLL. The control voltage of the VCO is shown along with the waveforms before lock and after lock.

### Summary

In a short span of time, phase-locked loops have become an essential component of any high-performance digital design. Their design requires considerable skill, integrating analog circuitry into a hostile digital environment. Yet experience has demonstrated that this combination is perfectly feasible, and it leads to new and better solutions.

## 10.7 Future Directions and Perspectives

This section highlights some of the trends in timing optimization for combining high performance and low power dissipation.

### 10.7.1 Distributed Clocking Using DLLs

A recent trend in high-performance clocking is the use of *delay locked loop* (DLL), a variation of the PLL structure. The schematic of a DLL is shown in Figure 10-67a [Maneatis00]. The key component of a DLL is a *voltage-controlled delay line* (VCDL). It consists of a cascade of adjustable delay elements (for instance, a current-starved inverter). The idea is to **delay the output clock such that it lines up perfectly with the reference**. Unlike the case of a VCO, there is no clock generator. The reference frequency is fed into the input of the VCDL. Similar to the case of a PLL structure, a phase detector compares the reference frequency with the output of the delay line ( $F_O$ ) and generates an *UP-DN* error signal. Note that only a phase and not a phase-frequency detection, is required. When in lock, there is no error between the two clocks. The

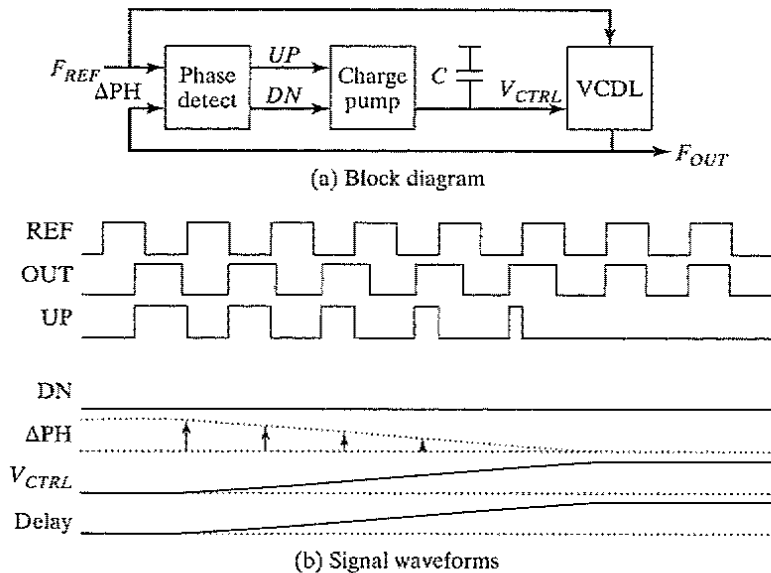


Figure 10-67 Delay-locked loop [Maneatis00].

function of the feedback is to adjust the delay through the VCDL such that the rising edge of the input reference clock ( $f_{REF}$ ) and the output clock ( $f_O$ ) are aligned.

A qualitative sketch of the signals in the DLL is shown in Figure 10-67b and c. Initially, the DLL is out of lock. Since the first edge of the output arrives before the reference edge, an  $UP$  pulse of width equal to the error between the two signals occurs. The role of the charge pump is to generate a charge packet proportional to the error, increasing the VCDL control voltage. This causes the edge of the output signal to be delayed in the next cycle. (This implementation of the VCDL assumes that a larger voltage results in larger delay.) After many cycles, the phase error is corrected, and the two signals are in lock. Note that a DLL does not alter the frequency of the input reference, but rather adjusts its phase.

Figure 10-68 shows the utilization of a DLL structure in a clock distribution network. The chip is partitioned into many small regions (or tiles). A global clock is distributed to each tile in a low-skew manner; this could be done through the package or by using low-skew, on-chip routing schemes. For the purpose of simplicity, the figure shows a two-tile chip, but this is easily extended to many regions. Inside each tile, the global clock is buffered before driving the digital load. In front of each buffer is a VCDL. The goal of the clock network is to deliver a signal to the digital circuit with close-to-zero skew and jitter. As we observed earlier, the static and dynamic variations of the buffers cause the phase error between the buffered clocks to be nonzero and time varying. The feedback inside each tile adjusts the control voltage of VCDL such that the buffered output is locked in phase to the global input clock. The feedback loop compensates for both static process variations and for slow dynamic variations (e.g., temperature). Such configurations have become common in high-performance digital microprocessors, as well as in media



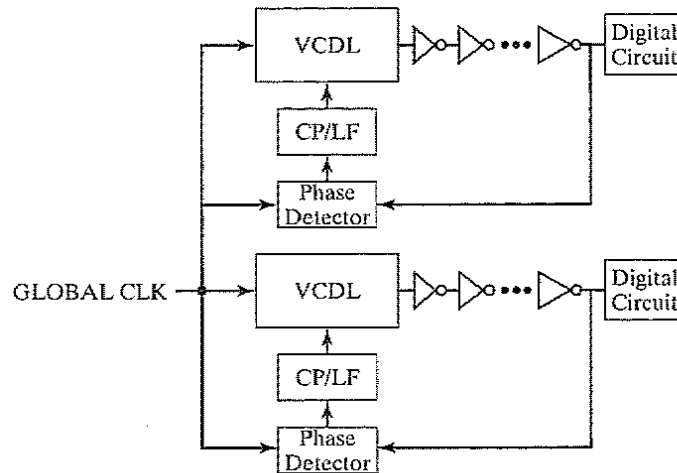


Figure 10-68 DLL approach to clock distribution.

processors. The preceding approach of clock distribution using multiple DLLs can be extended to the use of multiple distributed PLLs on a chip [Gutnik00]. Distributed PLLs offer potential performance advantages, but careful system analysis is required for stable operation.

### 10.7.2 Optical Clock Distribution

By now, the reader should have become aware of the fact that future high-performance multi-GHz systems face some fundamental synchronization problems. The performance of a digital design is fundamentally limited by process and environmental variations. Even with aggressive active clock management schemes, such as the use of DLLs and PLLs, the variations in power supply and clock load result in unacceptable clock uncertainty. Researchers are furiously searching for innovative solutions. An alternative approach that has received a lot of attention is the use of optics for systemwide synchronization. An excellent review of the rationale and trade-offs in optical interconnects versus electrical interconnects is given in [Miller00].

The potential advantages of optical technology for clock distribution are that the delay of optical signals is not sensitive to temperature and that the clock edges do not degrade over long distances (i.e., tens of meters). In fact, it is possible to deliver an optical clock signal with, at most, 10–100 ps of uncertainty over tens of meters. Optical clocks can be distributed on-chip via waveguides or through free space. Figure 10-69 shows the plot of an optical clock architecture, using waveguides. The off-chip optical source is brought to the chip, distributed through waveguides, and converted through receiver circuitry to a local electrical clock distribution network. The chip is divided into small sections (or tiles), and the global clock is distributed from the photon source through waveguides with splitters and bends to each of the sections. Notice that an *H*-tree is used in distributing the optical clock. At the end of the waveguide is a photodetector, which can be implemented using silicon or germanium. Upon reaching the detector in each section, the optical pulses that represent the global clock are converted into current pulses.

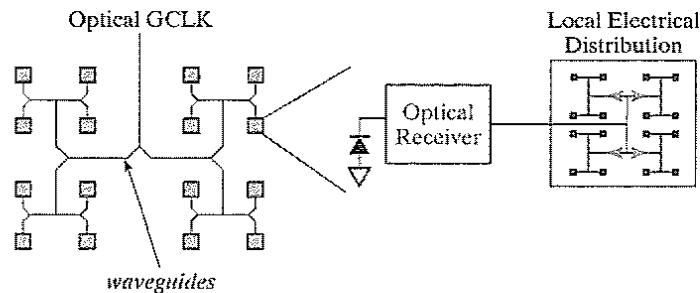


**Figure 10-69** Architecture for optical clock distribution (courtesy of Lionel Kimerling).

These have a very small magnitude (tens of  $\mu\text{A}$ ), and are fed into an amplifier that amplifies the signal into voltage signals appropriate for digital processing. The electrical clock is then distributed to the local load using conventional techniques [Kimerling00].

The optical approach has the advantage that the skew of the global clock to the photodetectors is virtually zero. There are some variations in the arrival time of the optical signal, but they are minimal. For instance, variations at the waveguide bends may cause the energy losses to differ from path to path. Optics has the additional advantage that many of the difficulties associated with electromagnetic wave propagation—such as cross talk and inductive coupling—are avoided.

On the other hand, the challenge lies in the design of the optical receiver. To amplify and transform the small current pulses into reasonable voltage signals requires multiple amplifier stages. These are susceptible to process and environmental variations, and thus also to skew. The problem becomes very similar to the conventional electrical approach. The advantage, however, is that the problem is confined to these receivers, which makes it more tractable.

Optical clocking may have an important future in high-performance systems. The challenges of dealing with process variations in the opto-electronic circuitry must be addressed first for this to become a reality.

### 10.7.3 Synchronous versus Asynchronous Design

The self-timed approach offers a potential solution to the growing clock-distribution problem. It translates the global clock signal into a number of local synchronization problems. Independence from physical timing constraints is achieved with the aid of completion signals. Handshaking logic is needed to ensure the logical ordering of the circuit events and to avoid race conditions. This requires adherence to a certain protocol, which normally consists of either two or four phases.

Despite all its advantages, self-timing has only been used in a number of isolated cases. Examples of self-timed circuits can be found in signal processing [Jacobs90], fast arithmetic units (such as self-timed dividers) [Williams87], simple microprocessors [Martin89] and memory (static RAM, FIFOs). In general, synchronous logic is both faster and simpler, since the overhead of completion-signal generation and handshaking logic is avoided. The design of a

foolproof network of handshaking units that is robust with respect to races, live lock, and dead lock is nontrivial and requires the availability of dedicated design-automation tools.

On the other hand, distributing a clock at high speed becomes exceedingly difficult. Skew management requires extensive modeling and analysis, as well as careful design. It will not be easy to extend this methodology into the next generation of designs. With the increasing timing uncertainty in synchronous circuits, self-timing is bound to become more attractive in the years to come [Sutherland02]. This observation is already reflected in the fact that the routing network for the latest generation of massively parallel supercomputers is completely implemented using self-timing [Seitz92]. For self-timing to become a mainstream design technique, however (if it ever will), further innovations in circuit and signaling techniques and design methodologies are needed.

Other alternative timing approaches might emerge as well. Possible candidates are fully asynchronous designs or islands of synchronous units connected by an asynchronous network. The latter method, called the *globally-asynchronous locally-synchronous approach*, is quite attractive. It avoids the pitfalls of self-timed design at the local circuit level, while eliminating the need for strict phase synchronization between blocks that are quite distant from each other on the die. In fact, the pure phase-synchronicity requirement between large modules in a system-on-a-chip is most often too large a constraint. Mesochronous or plesiochronous communication would work just as well. It is our conjecture that these styles of synchronization will become much more common in the coming decade.

## 10.8 Summary

This chapter has explored the timing of sequential digital circuits:

- An in-depth analysis of the synchronous digital circuits and clocking approaches was presented. Clock *skew* and *jitter* substantially impact the functionality and performance of a system. Important parameters are the clocking scheme used and the nature of the clock generation and distribution network.
- Alternative timing approaches, such as *self-timed design*, are becoming attractive for dealing with clock distribution problems. Self-timed design uses completion signals and handshaking logic to isolate physical timing constraints from event ordering.
- The connection of synchronous and asynchronous components introduces the risk of synchronization failure. The introduction of *synchronizers* helps to reduce that risk, but can never eliminate it.
- *Phase-locked loops* are becoming an important element of the digital designer's toolbox. They are used to generate high-speed clock signals on a chip. The analog nature of the PLL makes its design a real challenge.
- Important trend in clock distribution include the use of *delay-locked loops* to actively adjust delays on a chip.
- The key message of this chapter is that synchronization and timing are among the most intriguing challenges facing the digital designer of the next decade.

## 10.9 To Probe Further

While system timing is an important topic, a comprehensive reference work is not available in this area. One of the best discussions so far is the chapter by Chuck Seitz in [Mead80, Chapter 7]. Other in-depth overviews are given in [Bakoglu90], [Johnson93, Chapter 11], [Bernstein98, Chapter 7], and [Chandrakasan00, Chapters 12 and 13]. A collection of papers on clock distribution networks is presented in [Friedman95]. Numerous other publications are available on this topic in the leading journals, some of which are mentioned in the following list of references.

### References

- [Abnous93] A. Abnous and A. Behzad, "A High-Performance Self-Timed CMOS Adder," in *EE241 Final Class Project Reports*, by J. Rabaey, Univ. of California–Berkeley, May 1993.
- [Bailey98] D. Bailey and B. Benschneider, "Clocking Design and Analysis for a 600-MHz Alpha Microprocessor," *IEEE Journal of Solid-State Circuits*, vol. 33, pp. 1627–1633, November 1998.
- [Bailey00] D. Bailey, "Clock Distribution," in [Chandrakasan00].
- [Bakoglu90] H. Bakoglu, *Circuits, Interconnections and Packaging for VLSI*, Addison-Wesley, pp. 338–393, 1980.
- [Boning00] D. Boning, S. Nassif, "Models of Process Variations in Device and Interconnect," in [Chandrakasan00].
- [Bowhill95] W. Bowhill et al., "A 300 MHz Quad-Issue CMOS RISC Microprocessor," *Technical Digest of the 1995 International Solid State Circuits Conference (ISSCC)*, San Francisco, pp. 182–183, February 1995.
- [Bernstein98] K. Bernstein et al., *High Speed CMOS Design Styles*, Kluwer Academic Publishers, 1998.
- [Bernstein00] K. Bernstein, "Basic Logic Families," in [Chandrakasan00].
- [Chandrakasan00] A. Chandrakasan, W. Bowhill, and F. Fox, *Design of High-Performance Microprocessor Circuits*, IEEE Press, 2000.
- [Chaney73] T. Chaney and F. Rosenberger, "Anomalous Behavior of Synchronizer and Arbiter Circuits," *IEEE Trans. on Computers*, vol. C-22, pp. 421–422, April 1973.
- [Dally98] W. Dally and J. Poulton, *Digital Systems Engineering*, Cambridge University Press, 1998.
- [Dean94] M. Dean, D. Dill, and M. Horowitz, "Self-Timed Logic Using Current-Sensing Completion Detection," *Journal of VLSI Signal Processing*, pp. 7–16, February 1994.
- [Dopperpuhl92] D. Dopperpuhl et al., "A 200 MHz 64-b Dual Issue CMOS Microprocessor," *IEEE Journal on Solid State Circuits*, vol. 27, no. 11, pp. 1555–1567, November 1992.
- [Friedman95] E. Friedman, ed., *Clock Distribution Networks in VLSI Circuits and Systems*, IEEE Press, 1995.
- [Gardner80] F. Gardner, "Charge-Pump Phase-Locked Loops," *IEEE Trans. on Communications*, vol. COM-28, pp. 1849–58, November 1980.
- [Glasser85] L. Glasser and D. Dopperpuhl, *The Design and Analysis of VLSI Circuits*, Addison-Wesley, pp. 360–365, 1985.
- [Goodman98] J. Goodman, A. P. Dancy, A. P. Chandrakasan, "An Energy/Security Scalable Encryption Processor Using an Embedded Variable Voltage DC/DC Converter," *IEEE Journal of Solid State Circuits*, pp. 1799–1809, 1998.
- [Gutnik00] Gutnik, V., A. P. Chandrakasan, "Active GHz Clock Network Using Distributed PLLs," *IEEE Journal of Solid State Circuits*, pp. 1553–1560, November 2000.
- [Heller84] L. Heller et al., "Cascade Voltage Switch Logic: A Differential CMOS Logic Family," *IEEE International Solid State Conference Digest*, San Francisco, pp. 16–17, February 1984.
- [Herrick00] B. Herrick, "Design Challenges in Multi-GHz Microprocessors," *Proceedings ASPDAC 2000*, Yokohama, January 2000.
- [Jacobs90] G. Jacobs and R. Brodersen, "A Fully Asynchronous Digital Signal Processor," *IEEE Journal on Solid State Circuits*, vol. 25, no. 6, pp. 1526–1537, December 1990.
- [Jeong87] D. Jeong et al., "Design of PLL-Based Clock Generation Circuits," *IEEE Journal on Solid State Circuits*, vol. SC-22, no. 2, pp. 255–261, April 1987.

- [Johnson93] H. Johnson and M. Graham, *High-Speed Digital Design—A Handbook of Black Magic*, Prentice Hall, 1993.
- [Kim90] B. Kim, D. Helman, and P. Gray, "A 30 MHz Hybrid Analog/Digital Clock Recovery Circuit in 2  $\mu\text{m}$  CMOS," *IEEE Journal on Solid State Circuits*, vol. SC-25, no. 6, pp. 1385–1394, December 1990.
- [Kimerling00] L. Kimerling, "Photons to the Rescue: Microelectronics becomes Microphotonics," *Interface*, vol. 9, no. 2, 2000.
- [Martin89] A. Martin et al., "The First Asynchronous Microprocessor: Test Results," *Computer Architecture News*, vol. 17, no. 4, pp. 95–110, June 1989.
- [Maneatis00] J. Maneatis, "Design of High-Speed CMOS PLLs and DLLs," in [Chandrakasan00].
- [Mead80] C. Mead and L. Conway, *Introduction to VLSI Design*, Addison-Wesley, 1980.
- [Messerschmitt90] D. Messerschmitt, "Synchronization in Digital Systems," *IEEE Journal on Selected Areas in Communications*, vol. 8, no. 8, pp. 1404–1419, October 1990.
- [Miller00] D. Miller, "Rationale and Challenges for Optical Interconnects to Electronic Chips," *Proceedings of the IEEE*, pp. 728–749, June 2000.
- [Park00] T. Park, T. Tugbawa, and D. Boning, "An Overview of Methods for Characterization of Pattern Dependencies in Copper CMP," *Chemical Mechanical Polish for ULSI Multilevel Interconnection Conference (CMP-MIC 2000)*, pp. 196–205, March 2000.
- [Restle98] P. Restle, K. Jenkins, A. Deutsch, P. Cook, "Measurement and Modeling of On-Chip Transmission Line Effects in a 400 MHz Microprocessor," *IEEE Journal of Solid State Circuits*, pp. 662–665, April 1998.
- [Restle01] P. Restle, "Technical Visualizations in VLSI Design," *Proceedings 38th Design Automation Conference*, Las Vegas, June 2001.
- [Seitz80] C. Seitz, "System Timing," in [Mead80], pp. 218–262, 1980.
- [Seitz92] C. Seitz, "Mosaic C: An Experimental Fine-Grain Multicomputer," in *Future Tendencies in Computer Science, Control and Applied Mathematics*, Proceedings International Conference on the 25th Anniversary of INRIA, Springer-Verlag, pp. 69–85, 1992.
- [Sutherland89] I. Sutherland, "Micropipelines," *Communications of the ACM*, pp. 720–738, June 1989.
- [Sutherland02] I. Sutherland and J. Ebergen, "Computers Without Clocks," *Scientific American*, vol. 287, no. 2, pp. 62–69, August 2002.
- [Veendrick80] H. Veendrick, "The Behavior of Flip Flops Used as Synchronizers and Prediction of Their Failure Rates," *IEEE Journal of Solid State Circuits*, vol. SC-15, no. 2, pp. 169–176, April 1980.
- [Williams87] T. Williams et al., "A Self-Timed Chip for Division," in *Proceedings of Advanced Research in VLSI 1987*, Stanford Conference, pp. 75–96, March 1987.
- [Williams00] T. Williams, "Self-Timed Pipelines," in [Chandrakasan00].
- [Yee96] G. Yee et al., "Clock-Delayed Domino for Adder and Combinational Logic Design," *Proceedings IEEE International Conference on Computer Design (ICCD)*, pp. 332–337, 1996.
- [Young97] I. Young, M. Mar, and B. Brushan, "A 0.35  $\mu\text{m}$  CMOS 3-880 MHz PLL  $N/2$  Clock Multiplier and Distribution Network with Low Jitter for Microprocessors," *IEEE International Solid State Conference Digest*, pp. 330–331, 1997.

## Exercises and Design Problem

Visit the book's web site <http://bwrc.eecs.berkeley.edu/IcBook> for challenging exercises and design problems.



## Design Verification

*Simulation versus Verification*

*Electrical and Timing Verification*

*Formal Verification*

Up to this point, we have relied heavily on simulation as the preferred method for ensuring the correctness of a design and for extracting critical parameters such as speed and power dissipation. Simulation is, however, only one of the techniques the designer has in his toolbox to accomplish those objectives. In general, it is useful to differentiate between *simulation* and *verification*.

In the *simulation* approach, the value of a design parameter such as noise margin, propagation delay, or dissipated energy is determined by applying a set of excitation vectors to the circuit model of choice and extracting parameters from the obtained signal waveforms. While this approach is very flexible, it has the disadvantage that the results depend strongly upon the choice of the excitations. For example, a charge-redistribution condition in a dynamic logic gate is not detected by a simulation if the exact sequence of input patterns that causes the charge sharing is not applied. Similarly, the delay of an adder varies widely depending on the input signal. Identification of the worst-case delay requires a careful choice of the excitation vector so that the complete carry path is exercised. In other words, the designer must have a good understanding of the intrinsics of the circuit module and its operation. Failing to do so produces meaningless results.

*Verification*, on the other hand, attempts to extract the system parameters directly from the circuit description. For instance, the critical path of an adder can be recognized from an inspection of the circuit diagram or a model of it. This approach has the advantage that the result is independent of the choice of excitation vectors and is supposedly foolproof. On the other hand, it relies on a number of implicit assumptions regarding design techniques and methodologies. For the example of the adder, determination of the propagation delay requires an understanding of the logic operation of the composing circuitry—for example, dynamic or static logic—and a definition of the term *propagation delay*. As a second example, it is necessary to identify the register elements first before the maximum clock speed of a synchronous circuit can be determined. The resulting tools are therefore restricted in scope and handle only a limited class of circuit styles, such as single-phase synchronous design. In this insert, we analyze a number of the popular verification techniques.

### Electrical Verification

Given the transistor schematics of a digital design, it is possible to verify whether a number of basic rules are satisfied. Some examples of typical rules help illustrate this concept, and many others can be derived from previous chapters:

- The number of inversions between two C<sup>2</sup>MOS gates should be even.
- In a pseudo-NMOS gate, a well-defined ratio between the PMOS pull-up and NMOS pull-down devices is necessary to guarantee a sufficient noise-margin low  $NM_L$ .
- To ensure that rise and fall times of the signal waveforms stay within limits, minimum bounds can be set on the sizes of the driver transistors as a function of the fan-out.
- The maximum amount of charge sharing in a dynamic design should be such that the noise-margin high is not violated.

Pure common sense can help define a large set of rules to which a design should always adhere. Applying them requires an in-depth understanding of the circuit structure. An electrical verifier, therefore, starts with the identification of well-known substructures in the overall circuit schematic. Typical templates are simple logic gates, pass transistors, and registers. The verifier traverses the resulting network on a rule-per-rule basis. Since electrical rules tend to be specific to a particular design style, they should be able to be easily modified. For example, *rule-based expert systems* allow for an easy updating of the rule base [DeMan85]. The individual rules can be complex and even invoke a circuit simulator for a small subsection of the network to verify whether a given condition is met. In summary, electrical verification is a helpful tool, and it can dramatically reduce the risk of malfunction.

### Timing Verification

As circuits become more complex, it is increasingly difficult to define exactly which paths through the network are critical with respect to timing. One solution is to run extensive SPICE simulations that may take a long time to finish. Even then, this does not guarantee that the iden-

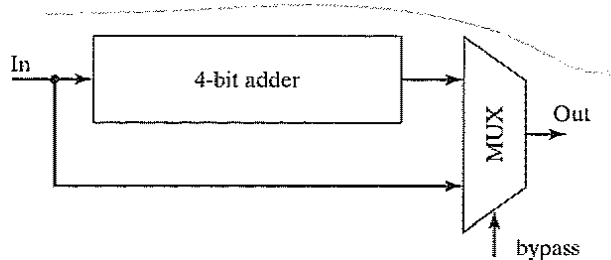


**Figure G-1** Example of false path in timing verification.

tified critical path is the worst case, since the delay path is a function of the applied signal patterns. A timing verifier traverses the electrical network and rank-orders the various paths, based on delay. This delay can be determined in a number of ways. One approach is to build an *RC*-model of the network and compute bounds on the delay of the resulting passive network. To obtain more accurate results, many timing verifiers first extract the details of the longest path(s), based on the *RC*-model, and perform circuit simulation on the reduced circuit in order to obtain a better estimation. Examples of early timing verifiers are the Crystal [Ousterhout83] and TV [Jouppi84] systems.

One problem that hampered many earlier systems is that they identified *false paths*—that is, critical paths that can never be exercised during normal circuit operation. For example, a false path exists in the carry-bypass adder discussed in Chapter 11 (also shown in simplified form in Figure G-1). From a simple analysis of only the circuit topology, one would surmise that the critical path of the circuit passes through the adder and multiplexer modules as illustrated by the arrow. A closer look at the circuit operation reveals that such a path is not feasible. All individual adder bits must be in the propagate mode for *In* to propagate through the complete adder. However, the *bypass* signal is asserted under these conditions, and the bottom path through the multiplexer is selected instead. The actual critical path is thus shorter than what would be predicted from the first-order analysis. Detecting false timing paths is not easy, since it requires an understanding of the logic functionality of the network. Newer timing verifiers are remarkably successful in accomplishing this and have become one of the more important design aids for the high-performance circuit designer [Devadas91].

### Example G.1 Example of Timing Verification

The output of a static timing verifier, the PathMill tool from Synopsys [PathMill], is shown in Figure G-2. The input to the verification process is a transistor netlist, but gate- and block-level models can be included as well. The analysis considers capacitive and resistive parasitics that are obtained from the transistor schematic or layout extraction.

The output of the timing analysis is an ordered list of critical timing paths. For the example of Figure G-2, the longest path extends from node *B* (falling edge) to node *Y* (falling edge) over nodes *S1*, *S2*, and *X3*. The predicted delay is 1.14 ns. Other paths close to



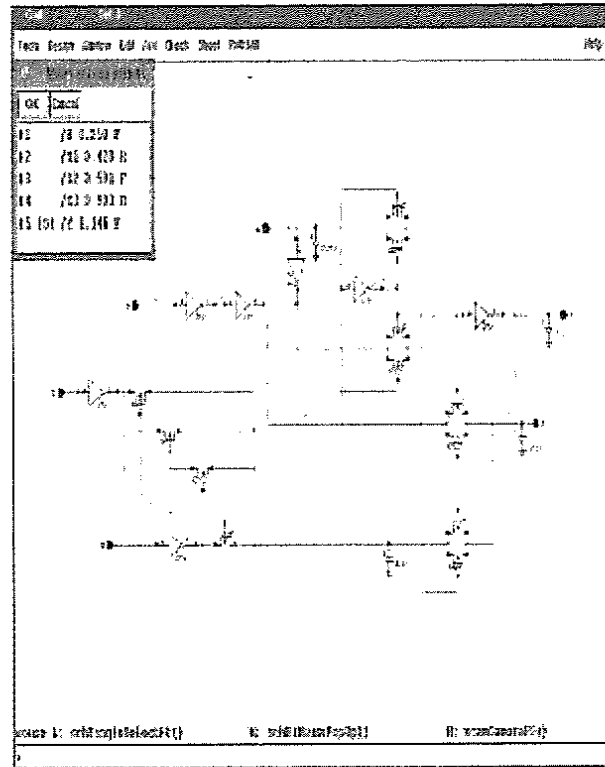


**Figure G-2** Example of static timing verifier response as generated by the PathMill tool (Courtesy of Synopsys, Inc.). The results are displayed using the Cadence DFII tool. The critical timing path runs from node *B* to node *Y* via nodes *S1*, *S2*, and *X3*.

the critical one are in order of decreasing delay:  $B(F) \rightarrow Y(R)$  (1.11 ns),  $B(R) \rightarrow Y(F)$  (1.04 ns),  $C(R) \rightarrow Z(R)$  (1.04 ns), and  $D(R) \rightarrow Y(R)$  (1.00 ns). Observe that the circuit contains multiple chained pass transistors that make the analysis complicated and increase the chances for false paths to occur. An example of the latter is the path  $A(F) \rightarrow X1 \rightarrow X3 \rightarrow Z(R)$  for  $B = 0$ . For a low value on  $B$ , node  $Z$  can only make a falling transition.

### Functional (or Formal) Verification

Each component (transistor, gate, or functional block) of a circuit can be described behaviorally as a function of its inputs and internal state. By combining these component descriptions, an overall circuit model can be generated that symbolically describes the behavior of the complete circuit. Formal verification compares this derived behavior with the designer's initial specification. Although not identical, the two descriptions need to be mathematically equivalent for the circuit to be correct.

Formal verification is the designer's ultimate dream of what design automation should be able to accomplish—*proof that the circuit will work as specified*. Unfortunately, no general and widely accepted verifier has yet been realized. The complexity of the problem is illustrated by the following argument: One way to prove that two circuit descriptions are identical is to compare the outputs while enumerating all possible input patterns and sequences thereof. This is an intractable approach with a computation time exponential in the number of inputs and states.

This does not mean that formal verification is a fantasy, however. Techniques have been proposed and successfully implemented for certain classes of circuits. For instance, assuming that a circuit is synchronous helps minimize the search space. Proving the equivalence between state machines has been one of the main research targets and has led to some remarkable advances (e.g., [Coudert90]). In general, formal verification techniques fall into two major classes:

- *Equivalence Proving*—Design often follows a refinement approach. An initial high-level description is refined into a more detailed one in a step-by-step fashion. Equivalence-proving tools establish that the obtained result is functionally equivalent to the original description. As an example, such a tool could establish that the transistor schematic of an N-input static CMOS NAND gate truly implements the intended NAND function.
- *Property Proving*—A designer often wants to know if her creation possesses some well-defined properties. A possible requirement could be, "My circuit should never experience a race condition." A property-proving tool analyzes whether this goal is met; if it is not met, the tool also analyzes the circumstances.

One of the prime necessities for formal verification to work is that the design is described in a manner that is unambiguous and that has a clearly defined meaning (or semantics). When these conditions are met, formal-verification techniques have yielded some remarkable results and are very effective. For instance, finite-state machines (FSMs) represent an area where formal verification has made some major advances. The secret to the success is a well-defined mathematical description model.

### Summary

Although not yet in the mainstream of the design-automation process, functional verification might become one of the important assets in the designer's toolbox. For this to happen, important progress must be made in the fields of design specification and interpretation.

### References

- [Coudert90] O. Coudert and J. Madre, *Proceedings ICCAD 1990*, pp. 126–129, November 1990.
- [DeMan85] H. De Man, I. Bolsens, E. Vandenmeersch, and J. Van Cleynenbreugel, "DIALOG: An Expert Debugging System for MOS VLSI Design," *IEEE Trans. on CAD*, vol. 4, no. 3, pp. 301–311, July 1985.
- [Devadas91] S. Devadas, K. Keutzer, and S. Malik, "Delay Computations in Combinational Logic Circuits: Theory and Algorithms," *Proc. ICCAD-91*, pp. 176–179, Santa Clara, 1991.

- [Jouppi84] N. Jouppi, *Timing Verification and Performance Improvement of MOS VLSI Designs*, Ph. D. diss., Stanford University, 1984.
- [Ousterhout83] J. Ousterhout, "Crystal: A Timing Analyzer for nMOS VLSI Circuits," *Proc. 3rd Caltech Conf. on VLSI* (Bryant ed.), Computer Science Press, pp. 57-69, March 1983.
- [PathMill] PathMill: Transistor-Level Static Timing Analysis, [http://www.synopsys.com/products/analysis/pathmill\\_ds.html](http://www.synopsys.com/products/analysis/pathmill_ds.html), Synopsys, Inc.

## CHAPTER

# 11

## Designing Arithmetic Building Blocks

*Designing adders, multipliers, and shifters  
for performance, area, or power*

*Logic and system optimizations for datapath modules*

*Power-delay trade-offs in datapaths*

- 11.1 Introduction
- 11.2 Datapaths in Digital Processor Architectures
- 11.3 The Adder
  - 11.3.1 The Binary Adder: Definitions
  - 11.3.2 The Full Adder: Circuit Design Considerations
  - 11.3.3 The Binary Adder: Logic Design Considerations
- 11.4 The Multiplier
  - 11.4.1 The Multiplier: Definitions
  - 11.4.2 Partial-Product Generation
  - 11.4.3 Partial-Product Accumulation
  - 11.4.4 Final Addition
- 11.5 The Shifter
  - 11.5.1 Barrel Shifter
  - 11.5.2 Logarithmic Shifter
- 11.6 Other Arithmetic Operators
- 11.7 Power and Speed Trade-Offs in Datapath Structures\*
  - 11.7.1 Design-Time Power-Reduction Techniques
  - 11.7.2 Run-Time Power Management
  - 11.7.3 Reducing the Power in Standby (or Sleep) Mode

11.8 Perspective: Design as a Trade-off

11.9 Summary

11.10 To Probe Further

## 11.1 Introduction

After the in-depth study of the design and optimization of the basic digital gates, it is time to test our acquired skills on a somewhat larger scale and put them in a more system-oriented perspective.

We will apply the techniques of the previous chapters to design a number of circuits often used in the datapaths of microprocessors and signal processors. More specifically, we discuss the design of a representative set of modules such as adders, multipliers, and shifters. The speed and power of these elements often dominates the overall system performance. Hence, a careful design optimization is required. It rapidly becomes obvious that the design task is not straightforward. For each module, multiple equivalent logic and circuit topologies exist, each of which has its own positives and negatives in terms of area, speed, or power.

Although far from complete, the analysis presented helps focus on the essential trade-offs that must be made in the course of the digital design process. You will see that optimization at only one design level—for instance, through transistor sizing only—leads to inferior designs. A global picture is therefore of crucial importance. Digital designers focus their attention on the gates, circuits, or transistors that have the largest impact on their goal function. The noncritical parts of the circuit can be developed routinely. We also may develop first-order performance models that foster understanding of the fundamental behavior of a module. The discussion also clarifies which computer aids can help to simplify and automate this phase of the design process.

Before analyzing the design of the arithmetic modules, a short discussion of the role of the datapath in the digital-processor picture is appropriate. This not only highlights the specific design requirements for the datapath, but also puts the rest of this book in perspective. Other processor modules—the input/output, controller, and memory modules—have different requirements and were discussed in Chapter 8. After an analysis of the area-power-delay trade-offs in the design of adders, multipliers, and shifters, we will use the same structures to illustrate some of the power-minimization approaches introduced in Chapter 6. The chapter concludes with a short perspective on datapath design and its trade-offs.

## 11.2 Datapaths in Digital Processor Architectures

We introduced the concept of a digital processor in Chapter 8. Its components consist of the datapath, memory, control, and input/output blocks. The datapath is the core of the processor—this is where all computations are performed. The other blocks in the processor are support units that either store the results produced by the datapath or help to determine what will happen in the next cycle. A typical datapath consists of an interconnection of basic combinational functions, such as arithmetic operators (addition, multiplication, comparison, and shift) or logic (AND, OR, and XOR). The design of the arithmetic operators is the topic of this chapter. The

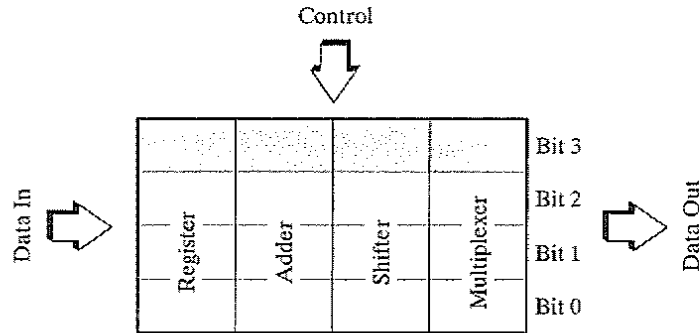


Figure 11-1 Bit-sliced datapath organization.

intended application sets constraints on the datapath design. In some cases, such as in personal computers, processing speed is everything. In most other applications, there is a maximum amount of power that is allowed to be dissipated, or there is maximum energy available for computation while maintaining the desired throughput.

Datapaths often are arranged in a *bit-sliced* organization, as shown in Figure 11-1. Instead of operating on single-bit digital signals, the data in a processor are arranged in a *word*-based fashion. Typical microprocessor datapaths are 32 or 64 bits wide, while the dedicated signal processing datapaths, such as those in DSL modems, magnetic disk drives, or compact-disc players are of arbitrary width, typically 5 to 24 bits. For instance, a 32-bit processor operates on data words that are 32 bits wide. This is reflected in the organization of the datapath. Since the same operation frequently has to be performed on each bit of the data word, the datapath consists of 32 bit slices, each operating on a single bit—hence the term *bit sliced*. Bit slices are either identical or resemble a similar structure for all bits. The datapath designer can concentrate on the design of a single slice that is repeated 32 times.

### 11.3 The Adder

Addition is the most commonly used arithmetic operation. It often is the speed-limiting element as well. Therefore, careful optimization of the adder is of the utmost importance. This optimization can proceed either at the logic or circuit level. Typical logic-level optimizations try to rearrange the Boolean equations so that a faster or smaller circuit is obtained. An example of such a logic optimization is the *carry lookahead adder* discussed later in the chapter. Circuit optimizations, on the other hand, manipulate transistor sizes and circuit topology to optimize the speed. Before considering both optimization processes, we provide a short summary of the basic definitions of an adder circuit (as defined in any book on logic design [e.g., Katz94]).

#### 11.3.1 The Binary Adder: Definitions

Table 11.1 shows the truth table of a binary full adder.  $A$  and  $B$  are the adder inputs,  $C_i$  is the carry input,  $S$  is the sum output, and  $C_o$  is the carry output. The Boolean expressions for  $S$  and  $C_o$  are given in Eq. (11.1).

Table 11-1 Truth table for full adder.

A	B	$C_i$	S	$C_o$	Carry Status
0	0	0	0	0	delete
0	0	1	1	0	delete
0	1	0	1	0	propagate
0	1	1	0	1	propagate
1	0	0	1	0	propagate
1	0	1	0	1	propagate
1	1	0	0	1	generate/propagate
1	1	1	1	1	generate/propagate

$$\begin{aligned}
 S &= A \oplus B \oplus C_i \\
 &= A\bar{B}\bar{C}_i + \bar{A}B\bar{C}_i + \bar{A}\bar{B}C_i + ABC_i \\
 C_o &= AB + BC_i + AC_i
 \end{aligned}
 \tag{11.1}$$

It is often useful from an implementation perspective to define  $S$  and  $C_o$  as functions of some intermediate signals  $G$  (generate),  $D$  (delete), and  $P$  (propagate).<sup>1</sup>  $G = 1$  ( $D = 1$ ) ensures that a carry bit will be *generated* (*deleted*) at  $C_o$  independent of  $C_i$ , while  $P = 1$  guarantees that an incoming carry will propagate to  $C_o$ . Expressions for these signals can be derived from inspection of the truth table:

$$\begin{aligned}
 G &= AB \\
 D &= \bar{A}\bar{B} \\
 P &= A \oplus B
 \end{aligned}
 \tag{11.2}$$

We can rewrite  $S$  and  $C_o$  as functions of  $P$  and  $G$  (or  $D$ ):

$$\begin{aligned}
 C_o(G, P) &= G + PC_i \\
 S(G, P) &= P \oplus C_i
 \end{aligned}
 \tag{11.3}$$

Notice that  $G$  and  $P$  are only functions of  $A$  and  $B$  and are not dependent upon  $C_i$ . In a similar way, we can also derive expressions for  $S(D, P)$  and  $C_o(D, P)$ .

<sup>1</sup>Note that the propagate signal sometimes is also defined as the OR function of the inputs  $A$  and  $B$ —this condition guarantees that the input carry propagates to the output when  $A = B = 1$ , too. We will provide appropriate warning whenever this definition is used.

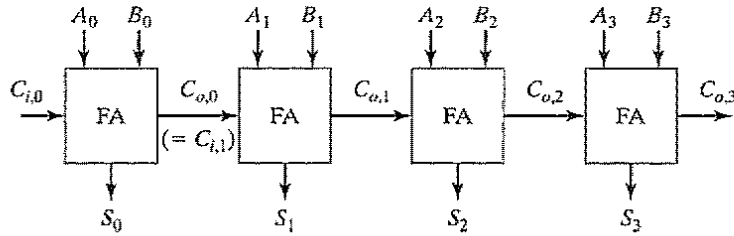


Figure 11-2 Four-bit ripple-carry adder: topology.

An  $N$ -bit adder can be constructed by cascading  $N$  full-adder (FA) circuits in series, connecting  $C_{o,k-1}$  to  $C_{i,k}$  for  $k = 1$  to  $N-1$ , and the first carry-in  $C_{i,0}$  to 0 (Figure 11-2). This configuration is called a *ripple-carry adder*, since the carry bit “ripples” from one stage to the other. The delay through the circuit depends upon the number of logic stages that must be traversed and is a function of the applied input signals. For some input signals, no rippling effect occurs at all, while for others, the carry has to ripple all the way from the *least significant bit (lsb)* to the *most significant bit (msb)*. The propagation delay of such a structure (also called the *critical path*) is defined as the *worst case delay over all possible input patterns*.

In the case of the ripple-carry adder, the worst case delay happens when a carry generated at the least significant bit position propagates all the way to the most significant bit position. This carry is finally consumed in the last stage to produce the sum. The delay is then proportional to the number of bits in the input words  $N$  and is approximated by

$$t_{adder} \approx (N-1)t_{carry} + t_{sum} \quad (11.4)$$

where  $t_{carry}$  and  $t_{sum}$  equal the propagation delays from  $C_i$  to  $C_o$  and  $S$ , respectively.<sup>2</sup>

### Example 11.1 Propagation Delay of Ripple-Carry Adder

Derive the values of  $A_k$  and  $B_k$  ( $k = 0 \dots N-1$ ) so that the worst case delay is obtained for the ripple-carry adder.

The worst case condition requires that a carry be generated at the *lsb* position. Since the input carry of the first full adder  $C_{i,0}$  is always 0, this both  $A_0$  and  $B_0$  must equal 1. All the other stages must be in propagate mode. Hence, either  $A_i$  or  $B_i$  must be high. Finally, we would like to physically measure the delay of a transition on the *msb* sum bit. Assuming an initial value of 0 for  $S_{N-1}$ , we must arrange a  $0 \rightarrow 1$  transition. This is achieved by setting both  $A_{N-1}$  and  $B_{N-1}$  to 0 (or 1), which yields a high sum bit given the incoming carry of 1.

For example, the following values for  $A$  and  $B$  trigger the worst case delay for an 8-bit addition:

$$A: 0000001; B: 01111111$$

<sup>2</sup>Equation (11.4) assumes that both the delay from the input signals  $A_0$  (or  $B_0$ ) to  $C_{o,0}$  for the *lsb*, and the  $C_i$ -to- $C_o$  delay for all other bits equal to  $t_{carry}$ .



To set-up the worst case delay transition, all the inputs can be kept constant with  $A_0$  undergoing a  $0 \rightarrow 1$  transition.

The left-most bit represents the *msb* in this binary representation. Observe that this is only one of the many worst case patterns. This case exercises the  $0 \rightarrow 1$  delay of the final sum. Derive several other cases that exercise the  $0 \rightarrow 1$  and  $1 \rightarrow 0$  transitions.

Two important conclusions can be drawn from Eq. (11.4):

- The propagation delay of the ripple-carry adder is *linearly* proportional to  $N$ . This property becomes increasingly important when designing adders for the wide data paths ( $N = 16 \dots 128$ ) that are desirable in current and future computers.
- When designing the full-adder cell for a fast ripple-carry adder, it is far more important to optimize  $t_{carry}$  than  $t_{sum}$  since the latter has only a minor influence on the total value of  $t_{adder}$ .

Before starting an in-depth discussion on the circuit design of full-adder cells, the following additional logic property of the full adder is worth mentioning:

**Inverting all inputs to a full adder results in inverted values for all outputs.**

This property, also called the *inverting property*, is expressed in the pair of equations

$$\begin{aligned}\bar{S}(A, B, C_i) &= S(\bar{A}, \bar{B}, \bar{C}_i) \\ \bar{C}_o(A, B, C_i) &= C_o(\bar{A}, \bar{B}, \bar{C}_i)\end{aligned}\tag{11.5}$$

and will be extremely useful when optimizing the speed of the ripple-carry adder. It states that the circuits of Figure 11-3 are identical.

### 11.3.2 The Full Adder: Circuit Design Considerations

#### Static Adder Circuit

One way to implement the full-adder circuit is to take the logic equations of Eq. (11.1) and translate them directly into complementary CMOS circuitry. Some logic manipulations can help to reduce the transistor count. For instance, it is advantageous to share some logic between the

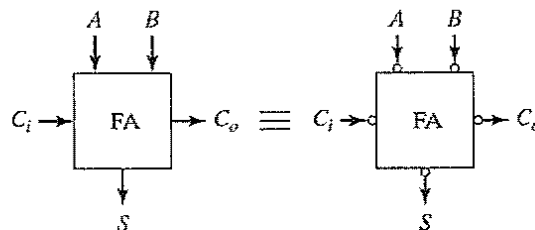


**Figure 11-3** Inverting property of the full adder. The circles in the schematics represent inverters.

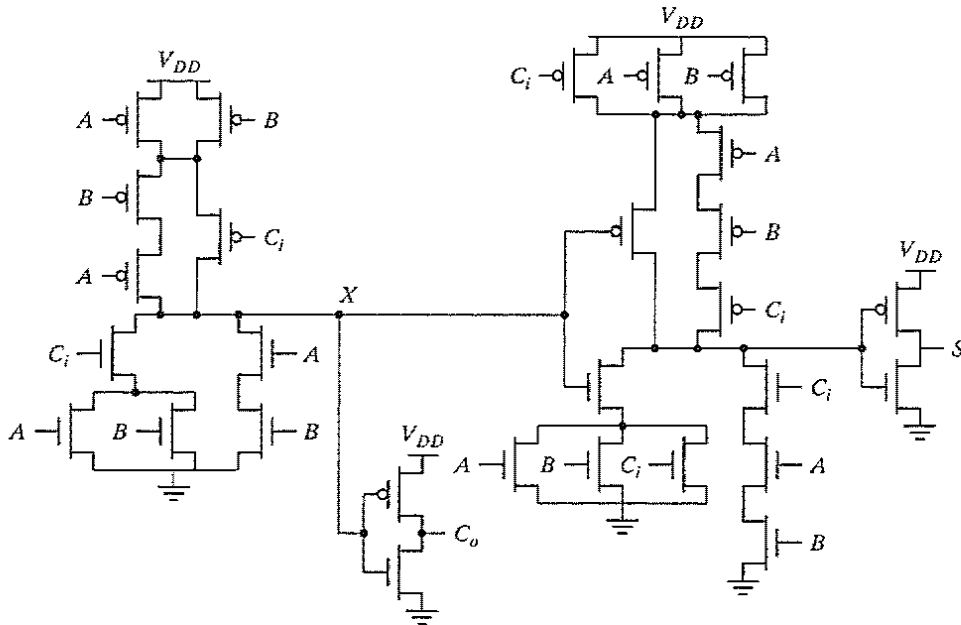


Figure 11-4 Complementary static CMOS implementation of full adder.

sum- and carry-generation subcircuits, as long as this does not slow down the carry generation, which is the most critical part, as stated previously. The following is an example of such a reorganized equation set:

$$C_o = AB + BC_i + AC_i$$

and

$$S = ABC_i + \overline{C_o}(A + B + C_i) \tag{11.6}$$

The equivalence with the original equations is easily verified. The corresponding adder design, using complementary static CMOS, is shown in Figure 11-4 and requires 28 transistors. In addition to consuming a large area, this circuit is slow:

- Tall PMOS transistor stacks are present in both *carry*- and *sum*-generation circuits.
- The intrinsic load capacitance of the  $C_o$  signal is large and consists of two diffusion and six gate capacitances, plus the wiring capacitance.
- The signal propagates through two inverting stages in the carry-generation circuit. As mentioned earlier, minimizing the carry-path delay is the prime goal of the designer of high-speed adder circuits. Given the small load (fan-out) at the output of the carry chain, having two logic stages is too high a number, and leads to extra delay.
- The sum generation requires one extra logic stage, but that is not that important, since a factor appears only once in the propagation delay of the ripple-carry adder of Eq. (11.4).

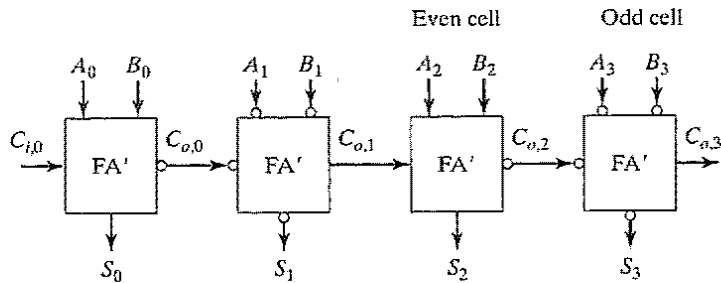


**Figure 11-5** Inverter elimination in carry path. FA' stands for a full adder without the inverter in the carry path.

Although slow, the circuit includes some smart design tricks. Notice that the first gate of the carry-generation circuit is designed with the  $C_i$  signal on the smaller PMOS stack, lowering its logical effort to 2. Also, the NMOS and PMOS transistors connected to  $C_i$  are placed as close as possible to the output of the gate. This is a direct application of a circuit-optimization technique discussed in Section 4.2—transistors on the critical path should be placed as close as possible to the output of the gate. For instance, in stage  $k$  of the adder, signals  $A_k$  and  $B_k$  are available and stable long before  $C_{i,k}$  ( $= C_{o,k-1}$ ) arrives after rippling through the previous stages. In this way, the capacitances of the internal nodes in the transistor chain are precharged or discharged in advance. On arrival of  $C_{i,k}$ , only the capacitance of node  $X$  has to be (dis)charged. Putting the  $C_{i,k}$  transistors closer to  $V_{DD}$  and GND would require not only the (dis)charging of the capacitance of node  $X$ , but also of the internal capacitances.

The speed of this circuit can now be improved gradually by using some of the adder properties discussed in the previous section. First, the number of inverting stages in the carry path can be reduced by exploiting the inverting property—inverting all the inputs of a full-adder cell also inverts all the outputs. This rule allows us to eliminate an inverter in a carry chain, as demonstrated in Figure 11-5.

### Mirror Adder Design

An improved adder circuit, also called the *mirror adder*, is shown in Figure 11-6 [Weste93]. Its operation is based on Eq. (11.3). The carry-generation circuitry is worth analyzing. First, the carry-inverting gate is eliminated, as suggested in the previous section. Secondly, the PDN and PUN networks of the gate are not dual. Instead, they form a clever implementation of the propagate/generate/delete function—when either  $D$  or  $G$  is high,  $\bar{C}_o$  is set to  $V_{DD}$  or GND, respectively. When the conditions for a *Propagate* are valid (or  $P$  is 1),<sup>3</sup> the incoming carry is propagated (in inverted format) to  $\bar{C}_o$ . This results in a considerable reduction in both area and delay. The analysis of the sum circuitry is left to the reader. The following observations are worth considering:

- This full-adder cell requires only 24 transistors.

<sup>3</sup>The  $P = A + B$  definition of the *propagate* signal is used here.

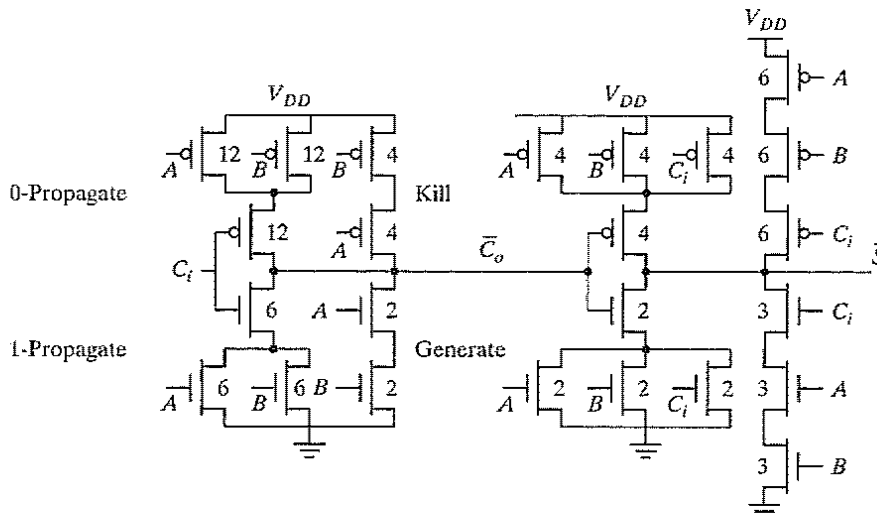
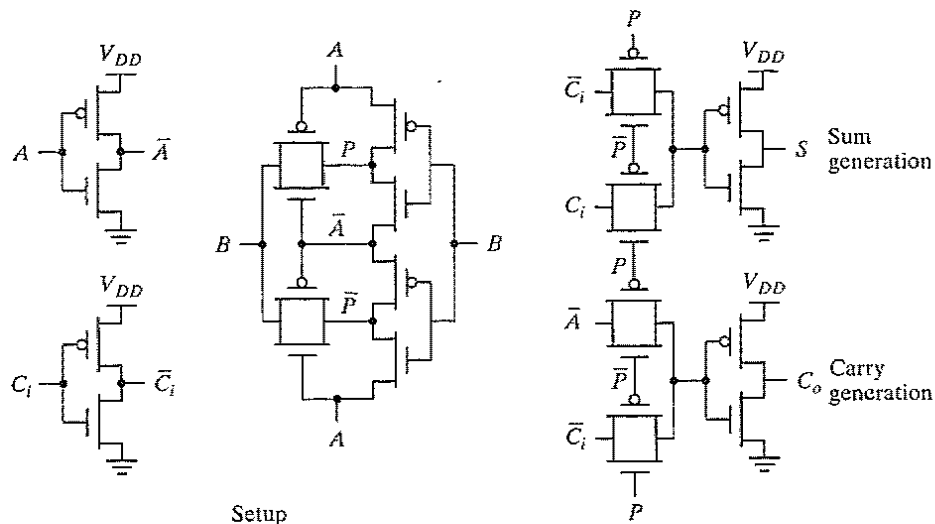


Figure 11-6 Mirror adder—circuit schematics.

- The NMOS and PMOS chains are completely symmetrical, which still yields correct operation due to *self-duality* of both the sum and carry functions. As a result, a maximum of two series transistors can be found in the carry-generation circuitry.
- The transistors connected to  $C_i$  are placed closest to the output of the gate.
- Only the transistors in the carry stage have to be optimized for speed. All transistors in the sum stage can be of minimum size. When laying out the cell, the most critical issue is the minimization of the capacitance at node  $\bar{C}_o$ . Shared diffusions reduce the stack node capacitances.
- In the adder cell of Figure 11-4, the inverter can be sized independently to drive the  $C_i$  input of the adder stage that follows. If the carry circuit in Figure 11-6 is symmetrically sized, each of its inputs has a logical effort of 2. This means that the optimal fan-out, sized for minimum delay, should be  $(4/2) = 2$ . However, the output of this stage drives two internal gate capacitances and six gate capacitances in the connecting adder cell. A clever solution to keep the transistor sizes the same in each stage is to increase the size of the carry stage to about three to four times the size of the sum stage. This maintains the optimal fan-out of 2. The resulting transistor sizes are annotated on Figure 11-6, where a PMOS/NMOS ratio of 2 is assumed.

### Transmission-Gate-Based Adder

A full adder can be designed to use multiplexers and XORs. While this is impractical in a complementary CMOS implementation, it becomes attractive when the multiplexers and XORs are implemented as transmission gates. A full-adder implementation based on this approach is shown in Figure 11-7 and uses 24 transistors. It is based on the *propagate-generate* model, introduced in Eq. (11.3). The propagate signal, which is the XOR of inputs  $A$  and  $B$ , is used to



**Figure 11-7** Transmission-gate-based full-adder cell with sum and carry delays of similar value (after [Weste93]).

select the true or complementary value of the input carry as the new sum output. Based on the propagate signal, the output carry is either set to the input carry, or either one of inputs  $A$  or  $B$ . One of interesting features of such an adder is that it has similar delays for both sum and carry outputs.

### Manchester Carry-Chain Adder

The carry-propagation circuitry in Figure 11-7 can be simplified by adding generate and delete signals, as shown in Figure 11-8a. The propagate path is unchanged, and it passes  $C_i$  to the  $C_o$  output if the propagate signal ( $A_i \oplus B_i$ ) is true. If the propagate condition is not satisfied, the output is either pulled low by the  $D_i$  signal or pulled up by  $\bar{G}_i$ . The dynamic implementation (Figure 11-8b), makes even further simplification possible. Since the transitions in a dynamic circuit are monotonic, the transmission gates can be replaced by NMOS-only pass transistors. Precharging the output eliminates the need for the kill signal (for the case in which the carry chain propagates the complementary values of the carry signals).

A *Manchester carry-chain adder* uses a cascade of pass transistors to implement the carry chain [Kilburn60]. An example, based on the dynamic circuit version introduced in Figure 11-8, is shown in Figure 11-9. During the precharge phase ( $\phi = 0$ ), all intermediate nodes of the pass-transistor carry chain are precharged to  $V_{DD}$ . During evaluation, the  $A_k$  node is discharged when there is an incoming carry and the propagate signal  $P_k$  is high, or when the generate signal for stage  $k$  ( $G_k$ ) is high.

Figure 11-10 shows an example layout of the Manchester carry chain in stick-diagram format. The datapath layout consists of three rows of cells organized in bit-sliced style: The top row

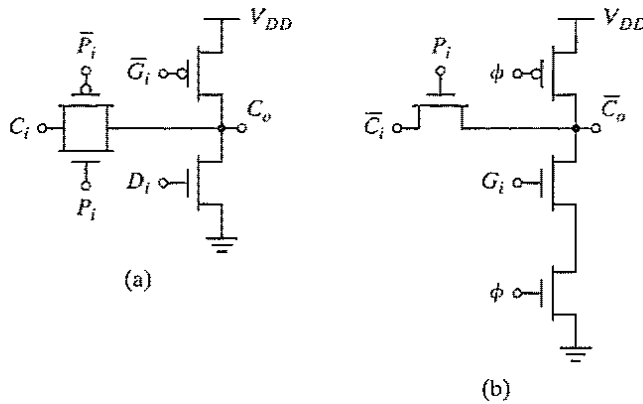


**Figure 11-8** Manchester carry gates. (a) Static, using propagate, generate, and kill, (b) dynamic implementation, using only propagate and generate signals.

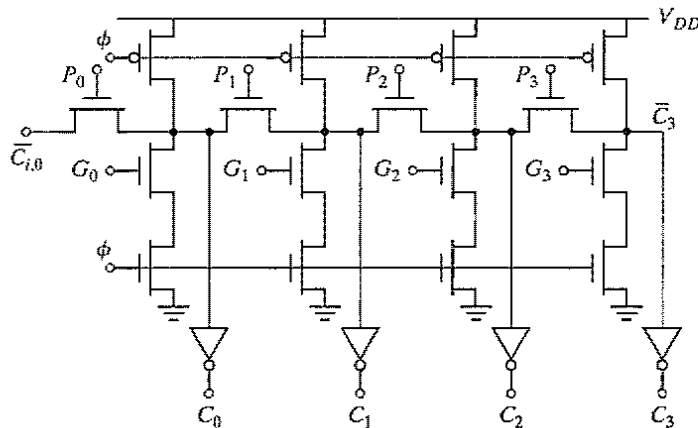


**Figure 11-9** Manchester carry-chain adder in dynamic logic (four-bit section).

of cells computes the propagate and generate signals, the middle row propagates the carry from left to right, and the bottom row generates the final sums.

The worst case delay of the carry chain of the adder in Figure 11-9 is modeled by the linearized RC network of Figure 11-11. As derived in Chapter 4, the propagation delay of such a network equals

$$t_p = 0.69 \sum_{i=1}^N C_i \left( \sum_{j=1}^i R_j \right) = 0.69 \frac{N(N+1)}{2} RC \quad (11.7)$$

when all  $C_i = C$  and  $R_j = R$ .

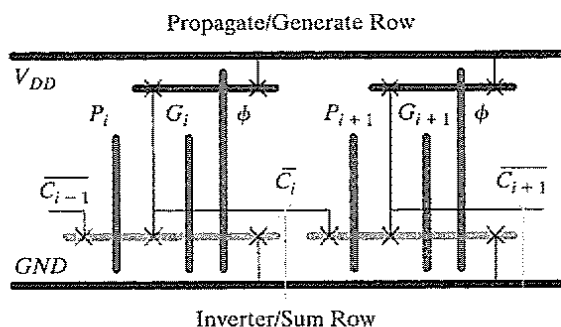


Figure 11-10 Stick diagram of two bits of a Manchester carry chain.

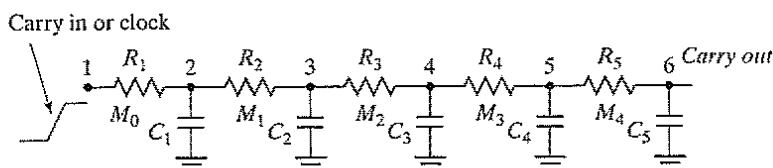


Figure 11-11 Equivalent network to determine propagation delay of a carry chain.

### Example 11.2 Sizing of Manchester Carry Chain

The capacitance per node on the carry chain equals four diffusion capacitances, one inverter input capacitance, and the wiring capacitance proportional to the size of the cell. The inverter and the PMOS precharging transistor can be kept at unit size. Together with the wire capacitance, the fixed capacitance can be estimated as 15 fF (for our technology). If a unit-sized transistor with width  $W_0$  has a resistance of 10 k $\Omega$  and a diffusion capacitance of 2 fF, then the RC time constant for a chain of transistors of width  $W$  is

$$RC = \left( 6 \text{ fF} \cdot \frac{W}{W_0} + 15 \text{ fF} \right) \cdot 10 \text{ k}\Omega \cdot \frac{W_0}{W}$$

Increasing the transistor width reduces this time constant, but it also loads the gates in the previous stage. Therefore, the transistor size is limited by the input loading capacitance.

Unfortunately, the distributed RC-nature of the carry chain results in a propagation delay that is quadratic in the number of bits  $N$ . To avoid this, it is necessary to insert signal-buffering inverters. The optimum number of stages per buffer depends on the equivalent resistance of the inverter and the resistance and capacitance of the pass transistors, as was discussed in Chapter 9. In our technology, and in most other practical cases, this number is between 3 and 4. Adding the inverter makes the overall propagation delay a linear function of  $N$ , as is the case with ripple-carry adders.

### 11.3.3 The Binary Adder: Logic Design Considerations

The ripple-carry adder is only practical for the implementation of additions with a relatively small word length. Most desktop computers use word lengths of 32 bits, while servers require 64; very fast computers, such as mainframes, supercomputers, or multimedia processors (e.g., the Sony PlayStation2) [Suzuoki99], require word lengths of up to 128 bits. The linear dependence of the adder speed on the number of bits makes the usage of ripple adders rather impractical. Logic optimizations are therefore necessary, resulting in adders with  $t_p < O(N)$ . We briefly discuss a number of those in the sections that follow. We concentrate on the circuit design implications, since most of the presented structures are well known from the traditional logic design literature.

#### The Carry-Bypass Adder

Consider the four-bit adder block of Figure 11-12a. Suppose that the values of  $A_k$  and  $B_k$  ( $k = 0 \dots 3$ ) are such that all propagate signals  $P_k$  ( $k = 0 \dots 3$ ) are high. An incoming carry  $C_{i,0} = 1$  propagates under those conditions through the complete adder chain and causes an outgoing carry  $C_{o,3} = 1$ . In other words,

$$\begin{aligned} \text{if } (P_0 P_1 P_2 P_3 = 1) \text{ then } C_{o,3} &= C_{i,0} \\ \text{else either DELETE or GENERATE occurred} \end{aligned} \quad (11.8)$$

This information can be used to speed up the operation of the adder, as shown in Figure 11-12b. When  $BP = P_0 P_1 P_2 P_3 = 1$ , the incoming carry is forwarded immediately to the next block through the bypass transistor  $M_b$ —hence the name *carry-bypass adder* or *carry-skip adder* [Lehman62]. If this is not the case, the carry is obtained by way of the normal route.

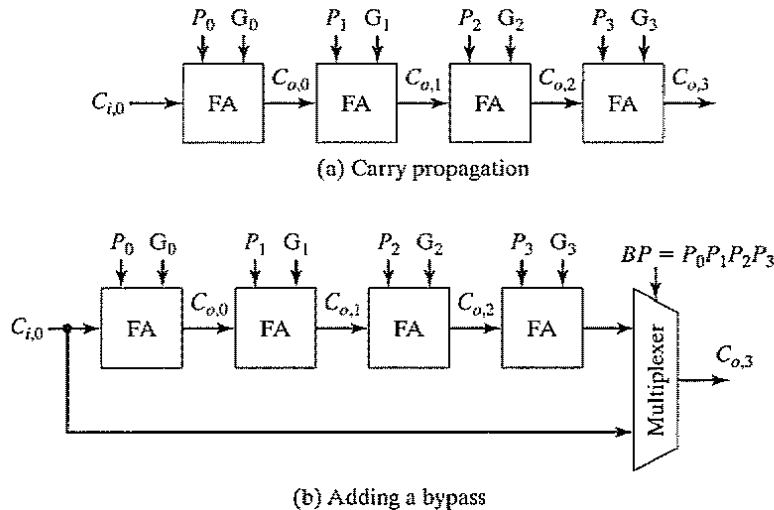
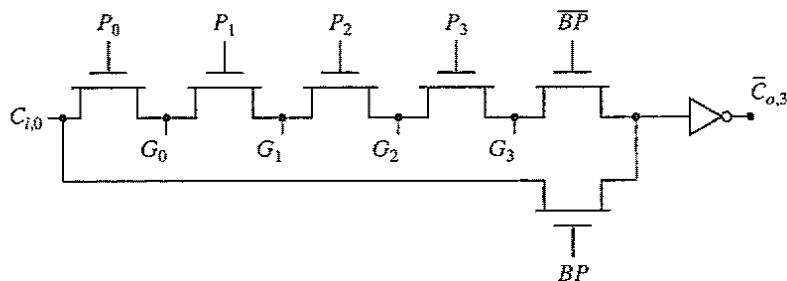


Figure 11-12 Carry-bypass structure—basic concept.



**Example 11.3 Carry Bypass in Manchester Carry-Chain Adder**

Figure 11-13 shows the possible carry-propagation paths when the full-adder circuit is implemented in Manchester-carry style. This picture demonstrates how the bypass speeds up the addition: The carry propagates either through the bypass path, or a carry is generated somewhere in the chain. In both cases, the delay is smaller than the normal ripple configuration. The area overhead incurred by adding the bypass path is small and typically ranges between 10 and 20%. However, adding the bypass path breaks the regular bit-slice structure (as was present in Figure 11-10).



**Figure 11-13** Manchester carry-chain implementation of bypass adder.

Let us now compute the delay of an  $N$ -bit adder. At first, we assume that the total adder is divided in  $(N/M)$  equal-length bypass stages, each of which contains  $M$  bits. An approximating expression for the total propagation time can be derived from Figure 11-14a and is given in Eq. (11.9). Namely,

$$t_p = t_{setup} + M t_{carry} + \left(\frac{N}{M} - 1\right) t_{bypass} + (M - 1) t_{carry} + t_{sum} \tag{11.9}$$

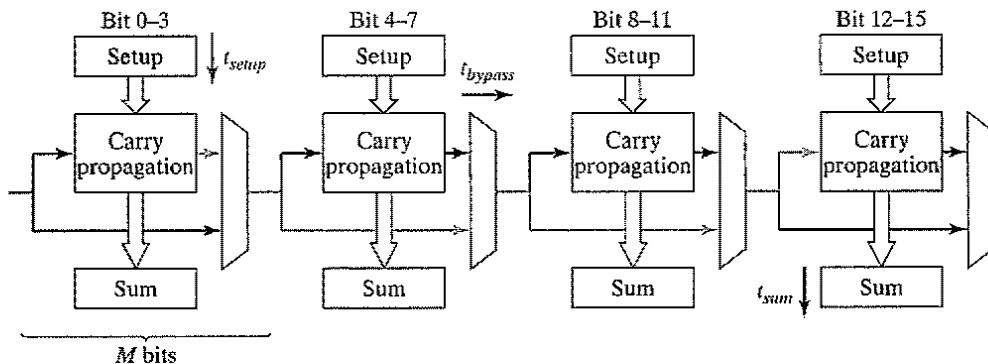


**Figure 11-14** ( $N = 16$ ) carry-bypass adder: composition. The worst case delay path is shaded in gray.

with the composing parameters defined as follows:

- $t_{setup}$ : the fixed overhead time to create the generate and propagate signals.
- $t_{carry}$ : the propagation delay through a single bit. The worst case carry-propagation delay through a single stage of  $M$  bits is approximately  $M$  times larger.
- $t_{bypass}$ : the propagation delay through the bypass multiplexer of a single stage.
- $t_{sum}$ : the time to generate the sum of the final stage.

The critical path is shaded in gray on the block diagram of Figure 11-14. From Eq. (11.9), it follows that  $t_p$  is still linear in the number of bits  $N$ , since in the worst case, the carry is generated at the first bit position, ripples through the first block, skips around  $(N/M - 2)$  bypass stages, and is consumed at the last bit position without generating an output carry. The optimal number of bits per skip block is determined by technological parameters such as the extra delay of the bypass-selecting multiplexer, the buffering requirements in the carry chain, and the ratio of the delay through the ripple and the bypass paths.

Although still linear, the slope of the delay function increases in a more gradual fashion than for the ripple-carry adder, as pictured in Figure 11-15. This difference is substantial for larger adders. Notice that the ripple adder is actually faster for small values of  $N$ , for which the overhead of the extra bypass multiplexer makes the bypass structure not interesting. The cross-over point depends upon technology considerations and is normally situated between four and eight bits.

---

#### Problem 11.1 Delay of Carry-Skip Adder

Determine an input pattern that triggers the worst case delay in a 16-bit ( $4 \times 4$ ) carry-bypass adder. Assuming that  $t_{carry} = t_{setup} = t_{skip} = t_{sum} = 1$ , determine the delay and compare it with that of a normal ripple adder.

---

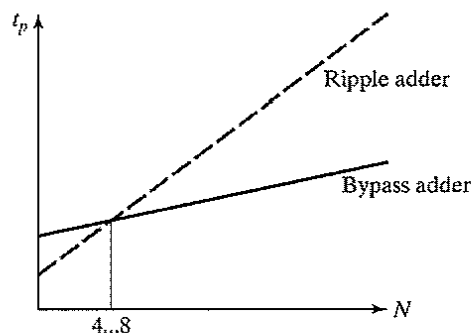


**Figure 11-15** Propagation delay of ripple-carry versus carry-bypass adder.

### The Linear Carry-Select Adder

In a ripple-carry adder, every full-adder cell has to wait for the incoming carry before an outgoing carry can be generated. One way to get around this linear dependency is to anticipate both possible values of the carry input and evaluate the result for both possibilities in advance. Once the real value of the incoming carry is known, the correct result is easily selected with a simple multiplexer stage. An implementation of this idea, appropriately called the *carry-select adder* [Bedrij62], is demonstrated in Figure 11-16. Consider the block of adders, which is adding bits  $k$  to  $k + 3$ . Instead of waiting on the arrival of the output carry of bit  $k - 1$ , both the 0 and 1 possibilities are analyzed. From a circuit point of view, this means that two carry paths are implemented. When  $C_{o,k-1}$  finally settles, either the result of the 0 or the 1 path is selected by the multiplexer, which can be performed with a minimal delay. As is evident from Figure 11-16, the hardware overhead of the carry-select adder is restricted to an additional carry path and a multiplexer, and equals about 30% with respect to a ripple-carry structure.

A full carry-select adder is now constructed by chaining a number of equal-length adder stages, as in the carry-bypass approach (see Figure 11-17). The critical path is shaded in gray. From inspection of the circuit, we can derive a first-order model of the worst case propagation delay of the module, written as

$$t_{add} = t_{setup} + Mt_{carry} + \left(\frac{N}{M}\right)t_{mux} + t_{sum} \quad (11.10)$$

where  $t_{setup}$ ,  $t_{sum}$ , and  $t_{mux}$  are fixed delays and  $N$  and  $M$  represent the total number of bits, and the number of bits per stage, respectively.  $t_{carry}$  is the delay of the carry through a single full-adder cell. The carry delay through a single block is proportional to the length of that stage or equals  $Mt_{carry}$ .

The propagation delay of the adder is, again, linearly proportional to  $N$  (Eq. (11.10)). The reason for this linear behavior is that the *block-select* signal that selects between the 0 and 1 solutions still has to ripple through all stages in the worst case.

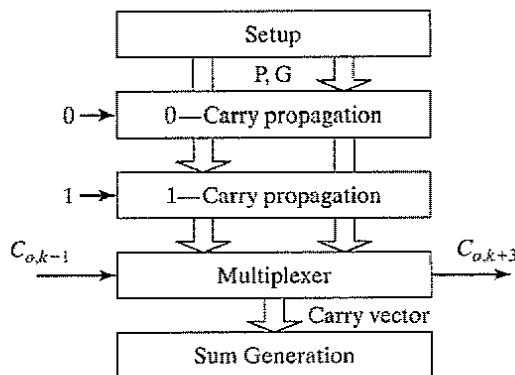


Figure 11-16 Four-bit carry-select module—topology.

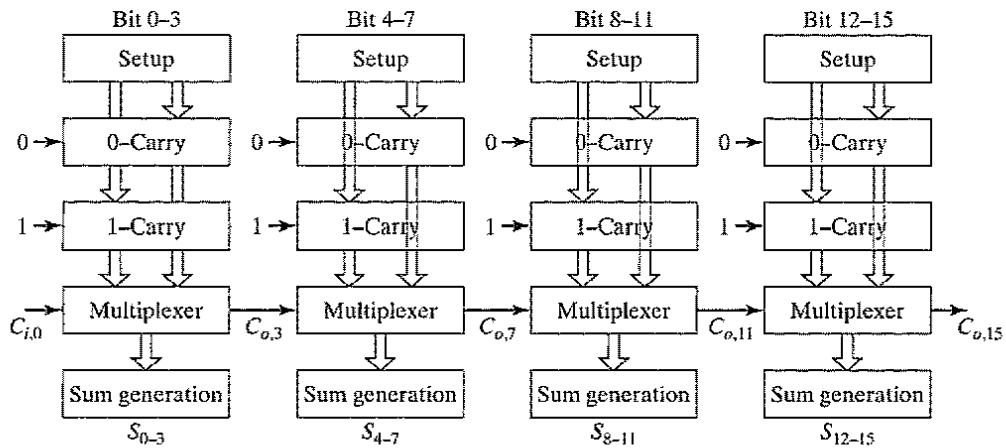


Figure 11-17 Sixteen-bit, linear carry-select adder. The critical path is shaded in gray.

### Problem 11.2 Linear Carry-Select Delay

Determine the delay of a 16-bit linear carry-select adder by using unit delays for all cells. Compare the result with that of Problem 11.1. Compare various block configurations as well.

### The Square-Root Carry-Select Adder

The next structure illustrates how an alert designer can make a major impact. To optimize a design, it is essential to locate the critical timing path first. Consider the case of a 16-bit linear carry-select adder. To simplify the discussion, assume that the full-adder and multiplexer cells have identical propagation delays equal to a normalized value of 1. The worst case arrival times of the signals at the different network nodes with respect to the time the input is applied are marked and annotated on Figure 11-18a. This analysis demonstrates that the critical path of the adder ripples through the multiplexer networks of the subsequent stages.

One striking opportunity is readily apparent. Consider the multiplexer gate in the last adder stage. The inputs to this multiplexer are the two carry chains of the block and the block-multiplexer signal from the previous stage. A major mismatch between the arrival times of the signals can be observed. The results of the carry chains are stable long before the multiplexer signal arrives. It makes sense to equalize the delay through both paths. This can be achieved by progressively adding more bits to the subsequent stages in the adder, requiring more time for the generation of the carry signals. For example, the first stage can add 2 bits, the second contains 3, the third has 4, and so forth, as demonstrated in Figure 11-18b. The annotated arrival times show that this adder topology is faster than the linear organization, even though an extra stage is needed. In fact, the same propagation delay is also valid for a 20-bit adder. Observe that the discrepancy in arrival times at the multiplexer nodes has been eliminated.

In effect, the simple trick of making the adder stages progressively longer results in an adder structure with sublinear delay characteristics. This is illustrated by the following analysis:

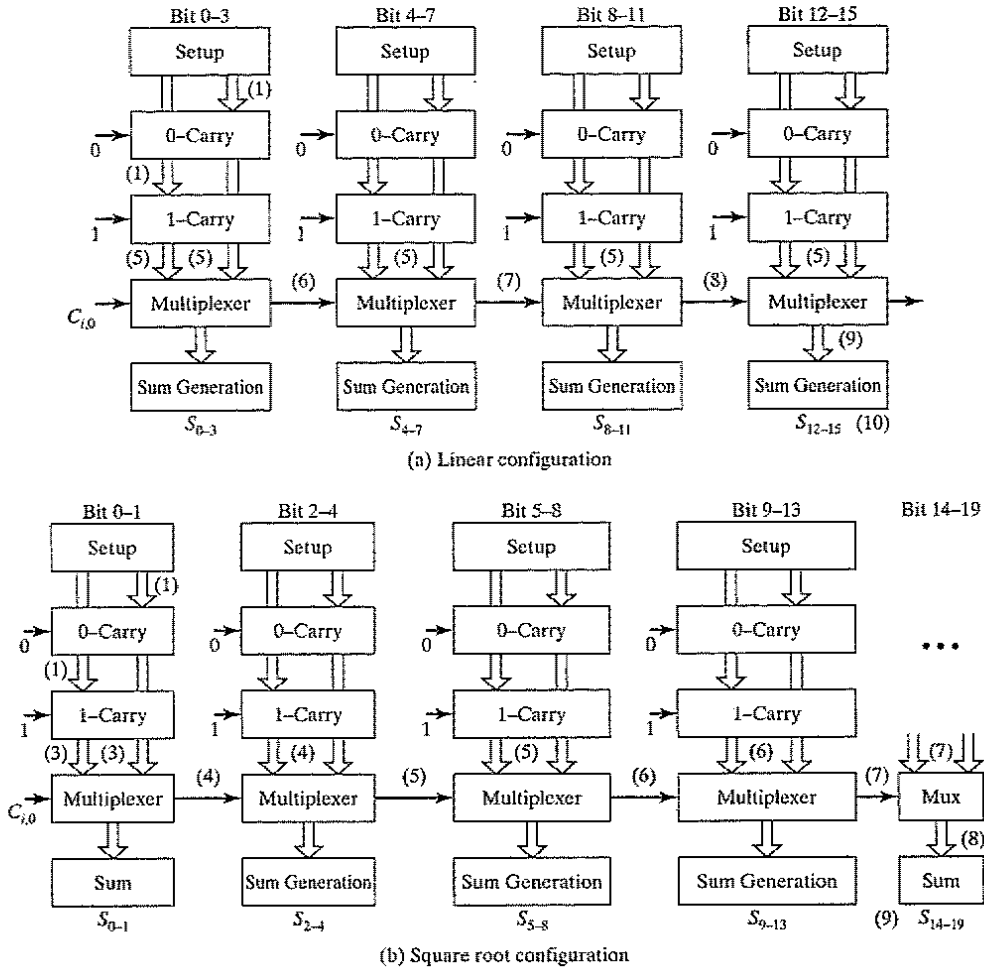


**Figure 11-18** Worst case signal arrival times in carry-select adders. The signal arrival times are marked in parentheses.

Assume that an  $N$ -bit adder contains  $P$  stages, and the first stage adds  $M$  bits. An additional bit is added to each subsequent stage. The following relation then holds:

$$\begin{aligned}
 N &= M + (M + 1) + (M + 2) + (M + 3) + \dots + (M + P - 1) \\
 &= MP + \frac{P(P - 1)}{2} = \frac{P^2}{2} + P\left(M - \frac{1}{2}\right)
 \end{aligned}
 \tag{11.11}$$

If  $M \ll N$  (e.g.,  $M = 2$ , and  $N = 64$ ), the first term dominates, and Eq. (11.11) can be simplified to

$$N \approx \frac{P^2}{2}
 \tag{11.12}$$

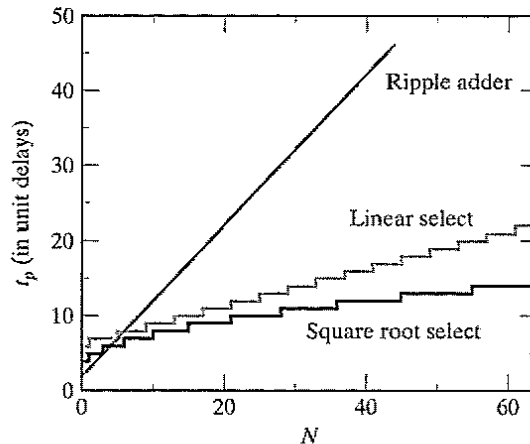


**Figure 11-19** Propagation delay of square-root carry-select adder versus linear ripple and select adders. The unit delay model is used to model the cell delays.

or

$$P \approx \sqrt{2N} \quad (11.13)$$

Equation (11.13) can be used to express  $t_{add}$  as a function of  $N$  by rewriting Eq. (11.10):

$$t_{add} = t_{setup} + Mt_{carry} + (\sqrt{2N})t_{mux} + t_{sum}. \quad (11.14)$$

The delay is proportional to  $\sqrt{N}$  for large adders ( $N \gg M$ ), or  $t_{add} = O(\sqrt{N})$ . This square-root relation has a major impact, which is illustrated in Figure 11-19, where the delays of both the linear and square-root select adders are plotted as a function of  $N$ . It can be observed that for large values of  $N$ ,  $t_{add}$  becomes almost a constant.

### Problem 11.3 Unequal Bypass Groups in Carry-Bypass Adder

A careful reader might be interested in applying the previous technique to carry-bypass adders. We saw earlier that their delay is a linear function of a number of bits. Can they be modified to achieve better than linear delay by using variable group sizes?

It does make sense to make the consecutive groups gradually larger. However, the technique used in carry-select adders does not directly apply to this case, and a progressive increase in stage sizes eventually increases the delay. Consider a carry-bypass adder in which the last stage is the largest: The carry signal that propagates through that stage and gets consumed at the *msb* position (with no chance of bypassing it) is on the critical path for the sum generation. Increasing the size of the last group does not help the problem.

Based on this discussion and assuming constant delays for carry and bypass gates, sketch the profile of the carry bypass network that achieves a delay that is better than linear.

### The Carry-Lookahead Adder\*

**The Monolithic Lookahead Adder** When designing even faster adders, it is essential to get around the rippling effect of the carry that is still present in one form or another in both the carry-bypass and carry-select adders. The *carry-lookahead* principle offers a possible way to do so [Weinberger56, MacSorley61]. As stated before, the following relation holds for each bit position in an  $N$ -bit adder:

$$C_{o,k} = f(A_k, B_k, C_{o,k-1}) = G_k + P_k C_{o,k-1} \quad (11.15)$$

The dependency between  $C_{o,k}$  and  $C_{o,k-1}$  can be eliminated by expanding  $C_{o,k-1}$ :

$$C_{o,k} = G_k + P_k(G_{k-1} + P_{k-1}C_{o,k-2}) \quad (11.16)$$

In a fully expanded form,

$$C_{o,k} = G_k + P_k(G_{k-1} + P_{k-1}(\dots + P_1(G_0 + P_0 C_{i,0}))) \quad (11.17)$$

with  $C_{i,0}$  typically equal to 0.

This expanded relationship can be used to implement an  $N$ -bit adder. For every bit, the carry and sum outputs are independent of the previous bits. The ripple effect has thus been effectively eliminated, and the addition time should be independent of the number of bits. A block diagram of the overall composition of a carry-lookahead adder is shown in Figure 11-20.

Such a high-level model contains some hidden dependencies. When we study the detailed schematics of the adder, it becomes obvious that the constant addition time is wishful thinking and that the real delay is at least increasing linearly with the number of bits. This is illustrated in Figure 11-21, where a possible circuit implementation of Eq. (11.17) is shown for  $N = 4$ . Note that the circuit exploits the self-duality and the recursivity of the carry-lookahead equation to build a mirror structure, similar in style to the single-bit full adder of Figure 11-6.<sup>4</sup> The large fan-in of the circuit makes it prohibitively slow for larger values of  $N$ . Implementing it with simpler gates requires multiple logic levels. In both cases, the propagation delay increases. Further-

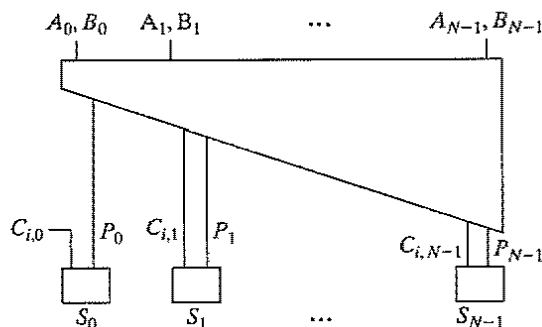
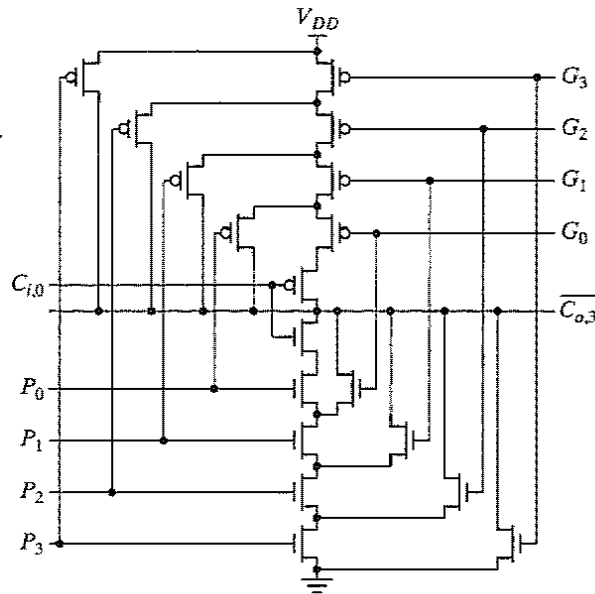


Figure 11-20 Conceptual diagram of a carry-lookahead adder.

<sup>4</sup>Similar to the mirror adder, this circuit requires that the *Propagate* signal be defined as  $P = A + B$ .



**Figure 11-21** Schematic diagram of mirror implementation of four-bit lookahead adder (from [Weste85]).

more, the fan-out on some of the signals tends to grow excessively, slowing down the adder even more. For instance, the signals  $G_0$  and  $P_0$  appear in the expression for every one of the subsequent bits. Hence, the capacitance on these lines is substantial. Finally, the area of the implementation grows progressively with  $N$ . Therefore, the lookahead structure suggested by Eq. (11.16) is only useful for small values of  $N$  ( $\leq 4$ ).

**The Logarithmic Lookahead Adder—Concept** For a carry-lookahead group of  $N$  bits, the transistor implementation has  $N + 1$  parallel branches with up to  $N + 1$  transistors in the stack. Since wide gates and large stacks display poor performance, the carry-lookahead computation has to be limited to up to two or four bits in practice. In order to build very fast adders, it is necessary to organize carry propagation and generation into recursive trees. A more effective implementation is obtained by hierarchically decomposing the carry propagation into subgroups of  $N$  bits:

$$\begin{aligned}
 C_{o,0} &= G_0 + P_0 C_{i,0} \\
 C_{o,1} &= G_1 + P_1 G_0 + P_1 P_0 C_{i,0} = (G_1 + P_1 G_0) + (P_1 P_0) C_{i,0} = G_{1:0} + P_{1:0} C_{i,0} \\
 C_{o,2} &= G_2 + P_2 G_1 + P_2 P_1 G_0 + P_2 P_1 P_0 C_{i,0} = G_2 + P_2 C_{o,1} \\
 C_{o,3} &= G_3 + P_3 G_2 + P_3 P_2 G_1 + P_3 P_2 P_1 G_0 + P_3 P_2 P_1 P_0 C_{i,0} \\
 &= (G_3 + P_3 G_2) + (P_3 P_2) C_{o,1} = G_{3:2} + P_{3:2} C_{o,1}
 \end{aligned} \tag{11.18}$$



In Eq. (11.18), the carry-propagation process is decomposed into subgroups of two bits.  $G_{i:j}$  and  $P_{i:j}$  denote the generate and propagate functions, respectively, for a group of bits (from bit positions  $i$  to  $j$ ). Therefore, we call them *block generate* and *propagate* signals.  $G_{i:j}$  equals 1 if the group generates a carry, independent of the incoming carry. The block propagate  $P_{i:j}$  is true if an incoming carry propagates through the complete group. This condition is equivalent to the carry bypass, discussed earlier. For example,  $G_{3:2}$  is equal to 1 when a carry either is generated at bit position 3 or is generated at position 2 and propagated through position 3, or  $G_{3:2} = G_3 + P_3G_2$ .  $P_{3:2}$  is true when an incoming carry propagates through both bit positions, or  $P_{3:2} = P_3P_2$ .

Note that the format of the new expression for the carry is equivalent to the original one, except that the generate and propagate signals are replaced with block generate and propagate signals. The notation  $G_{i:j}$  and  $P_{i:j}$  generalizes the original carry equations, since  $G_i = G_{i:i}$  and  $P_i = P_{i:i}$ . Another generalization is possible by treating the generate and propagate functions as a pair  $(G_{i:j}, P_{i:j})$ , rather than considering them as separate functions. A new Boolean operator, called the *dot* operator ( $\cdot$ ), can be introduced. This operator on the pairs and allows for the combination and manipulation of blocks of bits:

$$(G, P) \cdot (G', P') = (G + PG', PP') \quad (11.19)$$

Using this operator we can now decompose  $(G_{3:2}, P_{3:2}) = (G_3, P_3) \cdot (G_2, P_2)$ . The dot operator obeys the associative property, but it is not commutative.

---

#### Example 11.4 Ripple-Carry Adder Expressed by Using the Dot Operator

With the dot operator, a four-bit ripple carry adder can be re-written as

$$(C_{a,3}, 0) = [(G_3, P_3) \cdot (G_2, P_2) \cdot (G_1, P_1) \cdot (G_0, P_0)] \cdot (C_{i,0}, 0)$$

The associative property allows us to rewrite this function and express  $C_{a,3}$  as a function of 2 group carries:

$$\begin{aligned} (G_{3:0}, P_{3:0}) &= [(G_3, P_3) \cdot (G_2, P_2)] \cdot [(G_1, P_1) \cdot (G_0, P_0)] \\ &= (G_{3:2}, P_{3:2}) \cdot (G_{1:0}, P_{1:0}) \end{aligned}$$


---

By exploiting the associative property of the dot operator, a tree can be constructed that effectively computes the carries at all  $2^i - 1$  positions (that is, 1, 3, 7, 15, etc.) for  $i = 1 \dots \log_2(N)$ . The crucial advantage is that the computation of the carry at position  $2^i - 1$  takes only  $\log_2(N)$  steps. In other words, the output carry of an  $N$ -bit adder can be computed in  $\log_2(N)$  time. This is a major improvement over the previously described adders. For example, for an adder of 64 bits, the propagation delay of a linear adder is proportional to 64. For a square-root select adder, it is reduced to 8, while, for a logarithmic adder, the proportionality constant is 6. This is illustrated in Figure 11-22, which shows the block diagram of a 16-bit logarithmic adder. The carry at position 15 is computed by combining the results of blocks (0:7) and (8:15). Each of these, in turn, is

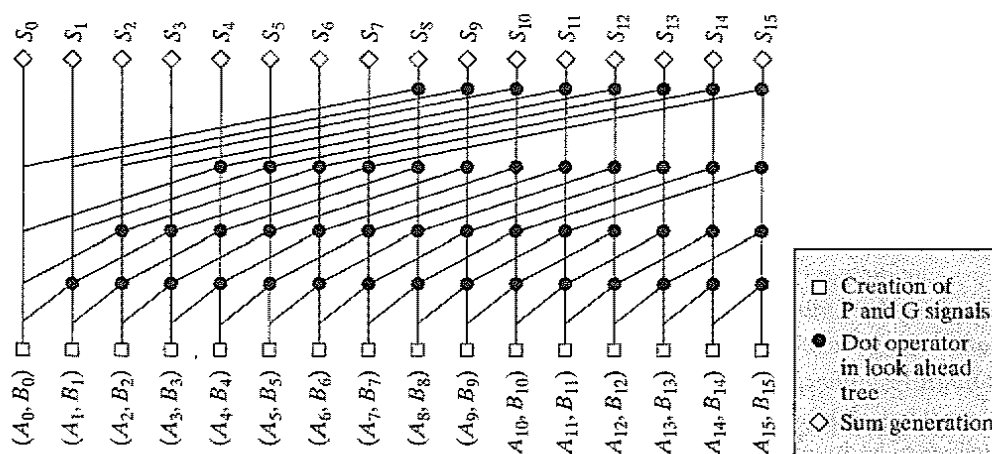


Figure 11-22: Schematic diagram for Kogge–Stone 16-bit lookahead logarithmic adder.

composed hierarchically. For instance, (0:7) is the composition of (0:3) and (4:7), while (0:3) consists of (0:1) and (2:3), etc.

Computing the carries at just the  $2^i - 1$  positions is obviously not sufficient. It is necessary to derive the carry signals at the intermediate positions as well. One way to accomplish this is by replicating the tree at every bit position, as illustrated in Figure 11-22 for  $N = 16$ . For instance, the carry at position 6 is computed by combining the results of blocks (6:3) and (2:0). This complete structure, which frequently is referred to as a *Kogge–Stone tree* [Kogge73], is a member of the *radix-2* class of trees. Radix-2 means that the tree is binary: It combines two carry words at a time at each level of hierarchy. The total adder requires 49 complex logic gates each to implement the dot operator. In addition, 16 logic modules are needed for the generation of the propagate and generate signals at the first level ( $P_i$  and  $G_i$ ), as well as 16 sum-generation gates.

#### Design Example—Implementing a Lookahead Adder in Dynamic Logic

The combination of carry-lookahead (CLA) techniques and dynamic logic seems to be ideal when very high performance is the ultimate goal. It is therefore useful to walk through the complete design of a dynamic CLA.

The first module generates the propagate and generate signal, as shown in Figure 11-23. The addition of a separate inverter to drive the keeper represents a small twist. This approach is beneficial in gates that drive a sizable fan-out. By decoupling its driver from the fan-out it allows for a quick disengagement of the keeper after the transition starts. The inverter that is driving successive logic gates, on the other hand, is optimized to drive a fan-out of two (for  $G$  outputs) or three (for  $P$  outputs) NMOS pull-down networks.

Each of the black dots in Figure 11-22 represents two gates that compute the block-level propagate and generate signals, as shown in Figure 11-24. Since these gates are not located at the beginning of the pipeline, the evaluation transistor (also called the *foot switch*) is optional, as discussed in Chapter 6. This approach is commonly used in dynamic datapaths. During the precharge phase, all the outputs of the domino gates are guaranteed to be low, turning off any discharge path in the succeeding domino stages. Elimination of the foot switch in any stage other than the first lowers the logical effort of the gates and speeds up

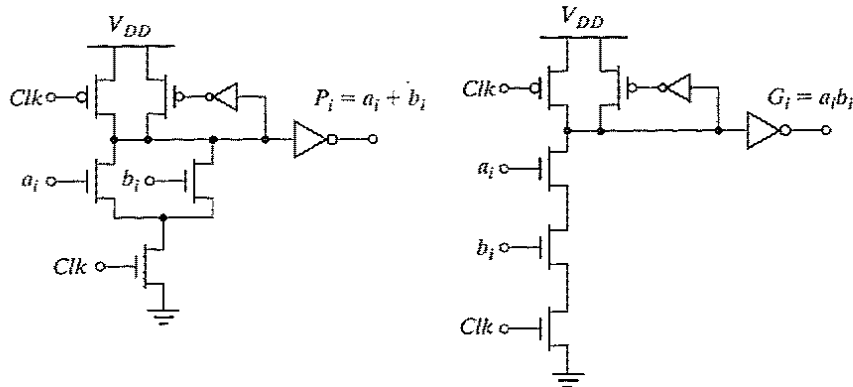


**Figure 11-23** Dynamic Implementation of propagate and generate signals.

the evaluation. For example, the propagate gate in Figure 11-24 has a logical effort of two-thirds instead of unity (assuming that the inverter is symmetrical). However, there is a drawback to this method. During the precharge phase, a short-circuit current exists in all gates without a foot switch until their inputs get precharged. To avoid the short-circuit current, the clock at each stage  $Clk_k$  is delayed from the previous stage. This approach is called *clock-delayed domino* as was introduced in Chapter 10. Note that the clock is delayed by the same amount for all bit-slices per stage, thus simplifying the implementation.

By putting together seven stages of logic in a bit-sliced fashion— $P$ - $G$  generation, followed by six dot operators—a 64-bit adder can be constructed. The only logic stage that is missing to complete the dynamic adder design is the final sum generation. The sum generation requires an XOR function, which is not easily built in domino logic. Static XOR gates could be used, but these produce nonmonotonic transitions and thus cannot be used to drive other domino gates. This might not be a problem per se, since the sum generation typically is the final stage of the addition operation. However, the latch that follows the sum generation cannot be transparent, because this could cause a violation of the transition rule for the succeeding domino gates.

One way of implementing the sum in domino logic is through *sum selection*, in which both care for the sum are computed as  $S_i^0 = a_i \oplus b_i$  and  $S_i^1 = a_i \oplus b_i$ . The dynamic gate of Figure 11-25 is then used to select one of these possibilities, based on the incoming carry.

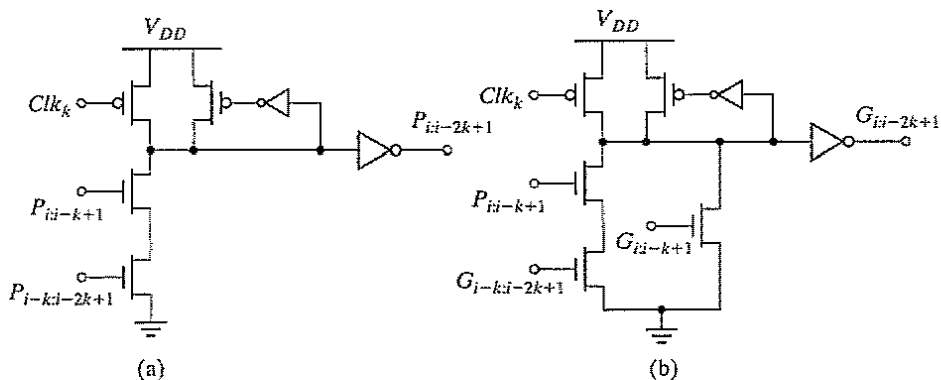


**Figure 11-24** Implementation of the dot operator in dynamic logic: (a) propagate and (b) generate logic at stage  $k$  and bit position  $i$  (see Figure 11-22).

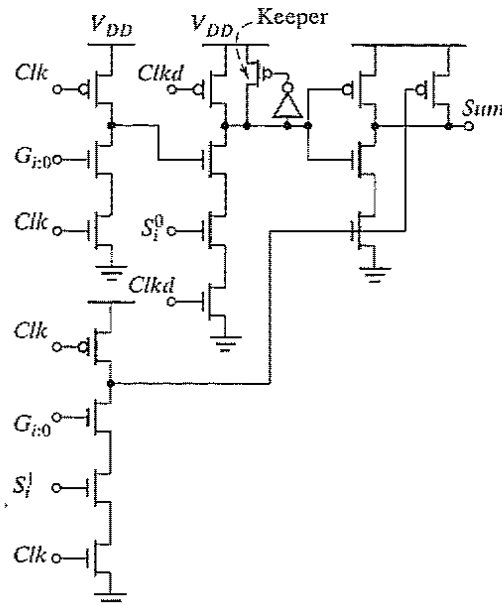


Figure 11-25 Sum select in dynamic logic.

The implementation of the multiplexer gate requires three logic levels, because no complementary carry is available in domino logic. As usual, keepers should be placed at all dynamic nodes, but the one shown in the figure is absolutely critical. The first two dynamic stages (on top) violate the dynamic logic design rules: two dynamic gates are cascaded without introducing an inverter. A glitch might happen at the output of the second gate if both gates are evaluated with the same clock. Delaying the clock of the second gate (*Clkd*) helps to address this issue, although the delayed clock presents a *hard-timing edge*—all the inputs to the second gate must have finished their transition before the clock raises.

It should be emphasized that when a designer chooses to use these design techniques, circuit robustness cannot be compromised. All clocks are subject to random skew, and the delayed clock must have enough margin to absorb the worst case skew. If *Clkd* arrives early, the adder will malfunction. However, proper sizing of the keeper may add a kind of safety net to the design. It can suppress the glitch at the output of the second stage, in case the clock arrives early. The keeper must be sized large enough to minimize this glitch, but not so large that it would compromise performance.

Another option is to implement the adder in differential domino logic, where both signal polarities are available, and the inversion problem is avoided. However, the overall design would be quite power hungry. ■

#### Problem 11.4 Static Adder Tree Design

Design a 16-bit carry-lookahead adder tree in static complementary CMOS. Design the lookahead tree by using inverted logic gates, avoiding the addition of inverters. Highlight the critical path of this adder. What are the logical efforts of gates along the critical path? How would you size it for minimal delay?

**Logarithmic Lookahead Adder—Alternatives** Designers of fast adders sometimes revert to other styles of tree structures as they trade off for area, power, or performance. We briefly discuss the Brent–Kung adder and the radix-4 adder, two of the more common alternative structures.

The Kogge–Stone tree of Figure 11-22 has some interesting properties. First, its interconnect structure is regular, which makes implementation quite easy. Furthermore, the fan-out throughout the tree is fairly constant, especially on the critical paths. The task of sizing the transistors for optimal performance is therefore simplified. At the same time, however, the replication of the carry trees to generate the intermediate carries comes at a large cost in terms of both area and power. Designers sometimes trade off some delay for area and power by choosing less complex trees. A simpler tree structure computes only the carries to the powers-of-two bit positions [Brent82], as illustrated in Figure 11-26 for  $N = 16$ .

The forward binary tree realizes the carry signals only at positions  $2^N - 1$ :

$$\begin{aligned}
 (C_{0,0}, 0) &= (G_0, P_0) \cdot (C_{i,0}, 0) \\
 (C_{0,1}, 0) &= [(G_1, P_1) \cdot (G_0, P_0)] \cdot (C_{i,0}, 0) = (G_{1:0}, P_{1:0}) \cdot (C_{i,0}, 0) \\
 (C_{0,3}, 0) &= [(G_{3:2}, P_{3:2}) \cdot (G_{1:0}, P_{1:0})] \cdot (C_{i,0}, 0) = (G_{3:0}, P_{3:0}) \cdot (C_{i,0}, 0) \\
 (C_{0,7}, 0) &= [(G_{7:4}, P_{7:4}) \cdot (G_{3:0}, P_{3:0})] \cdot (C_{i,0}, 0) = (G_{7:0}, P_{7:0}) \cdot (C_{i,0}, 0) \\
 &\dots
 \end{aligned}
 \tag{11.20}$$

The forward binary-tree structure is not sufficient to generate the complete set of carry bits. An *inverse binary tree* is needed to realize the other carry bits (shown in gray lines in Figure 11-26). This structure combines intermediate results to produce the remaining carry bits. It is left for the reader to verify that this structure produces the correct expressions for all carry

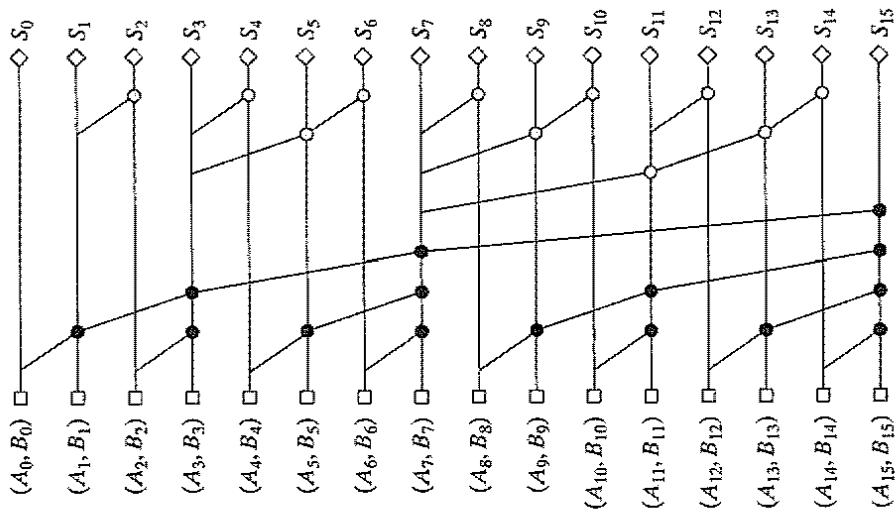


Figure 11-26 A 16-bit Brent–Kung tree. The reverse binary tree is colored gray.

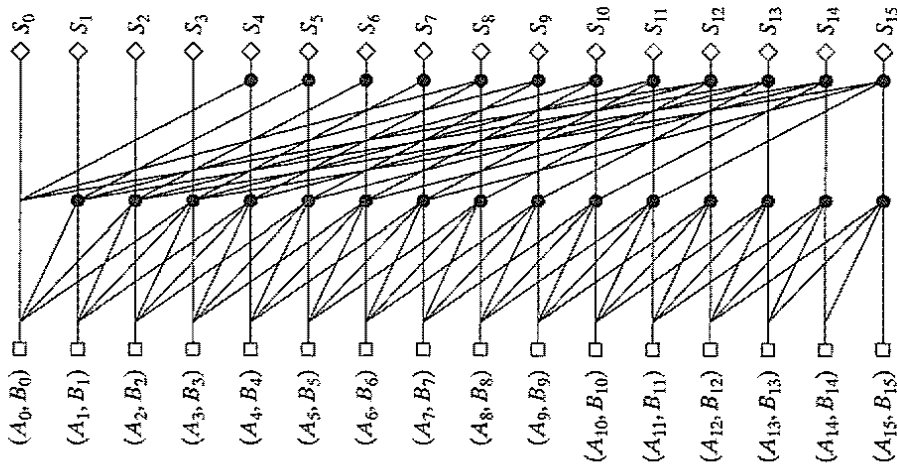


Figure 11-27 Radix-4 Kogge–Stone tree for 16-bit operands.

bits. The resulting structure, commonly called the *Brent–Kung adder*, uses 27 dot gates, or almost half of the 49 needed for a full radix-2 tree, and it needs fewer wires as well. The wiring structure is less regular, however, and fan-out varies from gate to gate, making performance optimization more difficult. Especially the fan-out of the middle node ( $C_{0,7}$ ), which equals one sum and five dot operations for this example, is of major concern. This observation makes the Brent–Kung adder rather unsuited for very large adders ( $> 32$  bits).

An option to reduce the depth of the tree is to combine four signals at a time at each level of the hierarchy. The resulting tree is now of class *radix-4*, because it uses building blocks of order 4 as shown in Figure 11-27. A 16-bit addition needs only two stages of carry logic. Be aware that each gate is more complex and that having less logic stages may not always result in faster operation (as we saw in Chapter 5).

---

#### Problem 11.5 Radix-4 Dot Operator in Dynamic Logic

Design the radix-4 dot operators in dynamic logic. Use the radix-2 circuits as reference. How is the sum select implemented for radix-4? Using the method of logical effort, compare the delays of radix-2 and radix-4 designs for 16-bit adders. Which one is faster?

---

On average, a lookahead adder is several times larger than a ripple adder, but has dramatic speed advantages for larger operands. The logarithmic behavior makes it preferable over bypass or select adders for larger values of  $N$ . The exact value of the cross point depends heavily on technology and circuit design factors.

The discussion of adders is by no means complete. Due to its impact on the performance of computational structures, the design of fast adder circuits has been the subject of many publications. It is even possible to construct adder structures with a propagation delay that is *independent of the number of bits*. Examples of those are the carry-save structures and the redundant

binary arithmetic structures [Swartzlander90]. These adders require number-encoding and -decoding steps, whose delay is a function of  $N$ . Therefore, they are only interesting when embedded in larger structures such as multipliers or high-speed signal processors.

## 11.4 The Multiplier

Multiplications are expensive and slow operations. The performance of many computational problems often is dominated by the speed at which a multiplication operation can be executed. This observation has, for instance, prompted the integration of complete multiplication units in state-of-the-art digital signal processors and microprocessors.

Multipliers are, in effect, complex adder arrays. Therefore, the majority of the topics discussed in the preceding section are of value in this context as well. The analysis of the multiplier gives us some further insight into how to optimize the performance (or the area) of complex circuit topologies. After a short discussion of the multiply operation, we discuss the basic array multiplier. We also discuss different approaches to partial product generation, accumulation and their final summation.

### 11.4.1 The Multiplier: Definitions

Consider two *unsigned* binary numbers  $X$  and  $Y$  that are  $M$  and  $N$  bits wide, respectively. To introduce the multiplication operation, it is useful to express  $X$  and  $Y$  in the binary representation

$$X = \sum_{i=0}^{M-1} X_i 2^i \quad Y = \sum_{j=0}^{N-1} Y_j 2^j \quad (11.21)$$

with  $X_i, Y_j \in \{0, 1\}$ . The multiplication operation is then defined as follows:

$$\begin{aligned} Z = X \times Y &= \sum_{k=0}^{M+N-1} Z_k 2^k \\ &= \left( \sum_{i=0}^{M-1} X_i 2^i \right) \left( \sum_{j=0}^{N-1} Y_j 2^j \right) = \sum_{i=0}^{M-1} \left( \sum_{j=0}^{N-1} X_i Y_j 2^{i+j} \right) \end{aligned} \quad (11.22)$$

The simplest way to perform a multiplication is to use a single two-input adder. For inputs that are  $M$  and  $N$  bits wide, the multiplication takes  $M$  cycles, using an  $N$ -bit adder. This *shift-and-add* algorithm for multiplication adds together  $M$  *partial products*. Each partial product is generated by multiplying the multiplicand with a bit of the multiplier—which, essentially, is an AND operation—and by shifting the result on the basis of the multiplier bit's position.

A faster way to implement multiplication is to resort to an approach similar to manually computing a multiplication. All the partial products are generated at the same time and organized in an array. A multioperand addition is applied to compute the final product. The approach is illustrated in Figure 11-28. This set of operations can be mapped directly into hardware. The

	1 0 1 0 1 0	Multiplicand
×	1 0 1 1	Multiplier
	1 0 1 0 1 0	} Partial products
	1 0 1 0 1 0	
	0 0 0 0 0 0	
	+ 1 0 1 0 1 0	
	1 1 1 0 0 1 1 1 0	Result

**Figure 11-28** Binary multiplication—an example.

resulting structure is called an *array multiplier* and combines the following three functions: *partial-product generation*, *partial-product accumulation*, and *final addition*.

#### Problem 11.6 Multiplication by a Constant

It is often necessary to implement multiplication of an operand by a constant. Describe how you would proceed with this task.

#### 11.4.2 Partial-Product Generation

Partial products result from the logical AND of multiplicand  $X$  with a multiplier bit  $Y_i$  (see Figure 11-29). Each row in the partial-product array is either a copy of the multiplicand or a row of zeroes. Careful optimization of the partial-product generation can lead to some substantial delay and area reductions. Note that in most cases the partial-product array has many zero rows that have no impact on the result and thus represent a waste of effort when added. In the case of a multiplier consisting of all ones, all the partial products exist, while in the case of all zeros, there is none. This observation allows us to reduce the number of generated partial products by half.

Assume, for example, an eight-bit multiplier of the form 01111110, which produces six nonzero partial-product rows. One can substantially reduce the number of nonzero rows by recoding this number ( $2^7 + 2^6 + 2^5 + 2^4 + 2^3 + 2^2$ ) into a different format. The reader can verify that the form  $100000\bar{1}0$ , with  $\bar{1}$  a shorthand notation for  $-1$ , represents the same number. Using

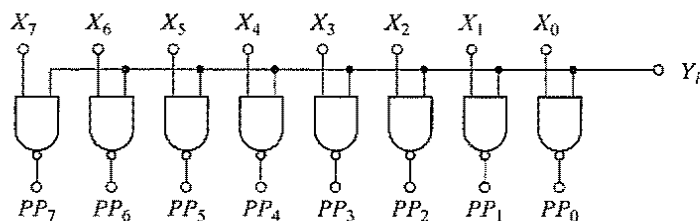


**Figure 11-29** Partial-product generation logic.



this format, we have to add only two partial products, but the final adder has to be able to perform subtraction as well. This type of transformation is called *Booth's recoding* [Booth51], and it reduces the number of partial products to, at most, one half. It ensures that for every two consecutive bits, at most one bit will be 1 or -1. Reducing the number of partial products is equivalent to reducing the number of additions, which leads to a speedup as well as an area reduction. Formally, this transformation is equivalent to formatting the multiplier word into a base-4 scheme, instead of the usual binary format:

$$Y = \sum_{j=0}^{(N-1)/2} Y_j 4^j \text{ with } (Y_j \in \{-2, -1, 0, 1, 2\}) \quad (11.23)$$

Note that 1010...10 represents the worst case multiplier input because it generates the most partial products (one half). While the multiplication with {0, 1} is equivalent to an AND operation, multiplying with {-2, -1, 0, 1, 2} requires a combination of inversion and shift logic. The encoding can be performed on the fly and requires some simple logic gates.

Having a variable-size partial-product array is not practical for multiplier design, and a *modified Booth's recoding* is most often used instead [MacSorley61]. The multiplier is partitioned into three-bit groups that overlap by one bit. Each group of three is recoded, as shown in Table 11-2, and forms one partial product. The resulting number of partial products equals half of the multiplier width. The input bits to the recoding process are the two current bits, combined with the upper bit from the next group, moving from *msb* to *lsb*.

**Table 11-2** Modified Booth's recoding.

Partial Product Selection Table	
Multiplier Bits	Recoded Bits
000	0
001	+ Multiplicand
010	+ Multiplicand
011	+ 2 × Multiplicand
100	- 2 × Multiplicand
101	- Multiplicand
110	- Multiplicand
111	0

In simple terms, the modified Booth's recoding essentially examines the multiplier for strings of ones from *msb* to *lsb* and replaces them with a leading 1, and a  $-1$  at the end of the string. For example, 011 is understood as the beginning of a string of ones and is therefore replaced by a leading 1 (or 100), while 110 is seen as the end of a string and is replaced by a  $-1$  at the least significant position (or  $0\bar{1}0$ ).

---

**Example 11.5 Modified Booth's Recoding**

Consider the eight-bit binary number 01111110 shown earlier. This can be divided into four overlapping groups of three bits, going from *msb* to *lsb*: 00 (1), 11 (1), 11 (1), 10 (0). Recoding by using Table 11-2 yields: 10 ( $2 \times$ ), 00 ( $0 \times$ ), 00 ( $0 \times$ ),  $\bar{1}0$  ( $-2 \times$ ), or, in combined format, 100000 $\bar{1}0$ . This is equivalent to the result we obtained before.

---

**Problem 11.7 Booth's Recoder**

Design the combinational logic that implements a modified Booth's recoding for a parallel multiplier, using Table 11-2. Compare its implementation in complementary and pass-transistor CMOS.

---

**11.4.3 Partial-Product Accumulation**

After the partial products are generated, they must be summed. This accumulation is essentially a multioperand addition. A straightforward way to accumulate partial products is by using a number of adders that will form an array—hence, the name, *array multiplier*. A more sophisticated procedure performs the addition in a tree format.

**The Array Multiplier**

The composition of an array multiplier is shown in Figure 11-30. There is a one-to-one topological correspondence between this hardware structure and the manual multiplication shown in Figure 11-28. The generation of  $N$  partial products requires  $N \times M$  two-bit AND gates (in the style of Figure 11-29).<sup>5</sup> Most of the area of the multiplier is devoted to the adding of the  $N$  partial products, which requires  $N - 1$   $M$ -bit adders. The shifting of the partial products for their proper alignment is performed by simple routing and does not require any logic. The overall structure can easily be compacted into a rectangle, resulting in a very efficient layout.

Due to the array organization, determining the propagation delay of this circuit is not straightforward. Consider the implementation of Figure 11-30. The partial sum adders are implemented as ripple-carry structures. Performance optimization requires that the critical timing path be identified first. This turns out to be nontrivial. In fact, a large number of paths of almost identical length can be identified. Two of those are highlighted in Figure 11-31. A closer

---

<sup>5</sup>This particular implementation does not employ Booth's recoding. Adding recoding does not substantially change the implementation. The number of adders is reduced by half, and the partial-product generation is slightly more complex.

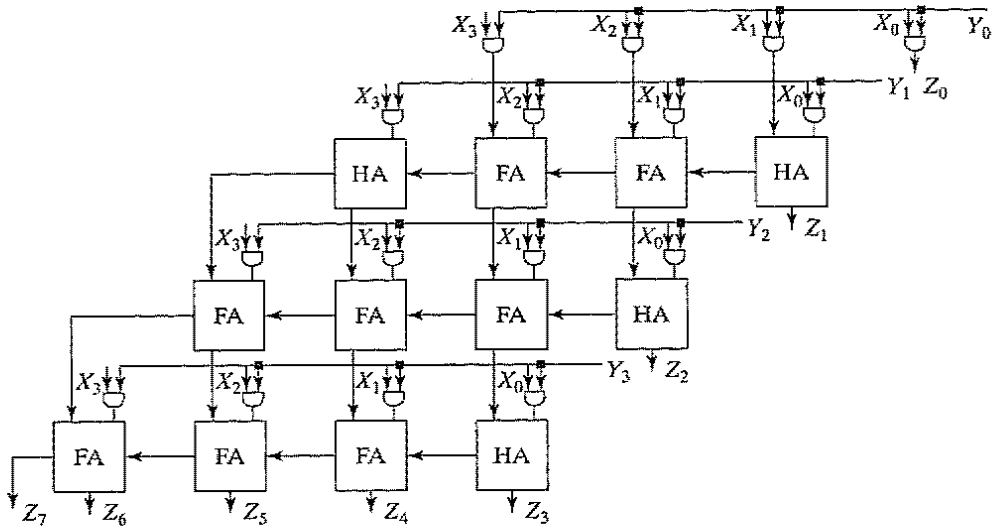


**Figure 11-30** A 4 × 4 bit-array multiplier for unsigned numbers—composition. HA stands for a half adder, or an adder cell with only two inputs. The hardware for the generation and addition of one partial product is shaded in gray.

look at those critical paths yields an approximate expression for the propagation delay (derived here for critical path 2). We write this as

$$t_{mult} \approx [(M - 1) + (N - 2)]t_{carry} + (N - 1)t_{sum} + t_{and} \tag{11.24}$$

where  $t_{carry}$  is the propagation delay between input and output carry,  $t_{sum}$  is the delay between the input carry and sum bit of the full adder, and  $t_{and}$  is the delay of the AND gate.

Since all critical paths have the same length, speeding up just one of them—for instance, by replacing one adder by a faster one such as a carry-select adder—does not make much sense from a design standpoint. All critical paths have to be attacked at the same time. From Eq. (11.24), it can be deduced that the minimization of  $t_{mult}$  requires the minimization of both  $t_{carry}$

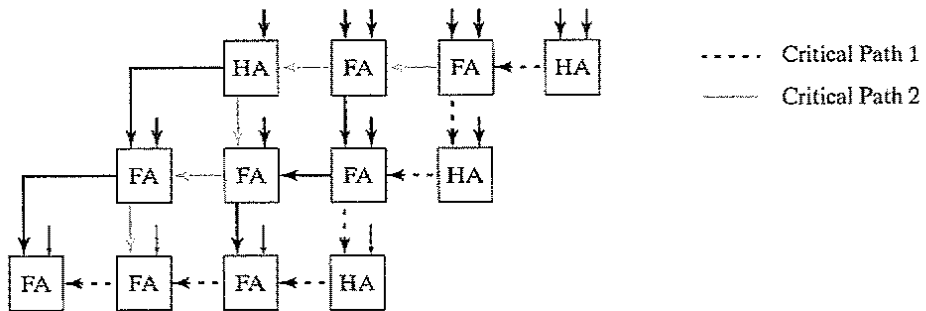


**Figure 11-31** Ripple-carry based 4 × 4 multiplier (simplified diagram). Two of the possible critical paths are highlighted.

and  $t_{sum}$ . In this case, it could be beneficial for  $t_{carry}$  to equal  $t_{sum}$ . This contrasts with the requirements for adder cells discussed before, where a minimal  $t_{carry}$  was of prime importance. An example of a full-adder circuit with comparable  $t_{sum}$  and  $t_{carry}$  delays was shown in Figure 11-7.

**Problem 11.8 Signed-Binary Multiplier**

The multiplier presented in Figure 11-30 only handles unsigned numbers. Adjust the structure so that two's-complement numbers are also accepted.

**Carry-Save Multiplier**

Due to the large number of almost identical critical paths, increasing the performance of the structure of Figure 11-31 through transistor sizing yields marginal benefits. A more efficient realization can be obtained by noticing that the multiplication result does not change when the output carry bits are passed diagonally downwards instead of only to the right, as shown in Figure 11-32. We include an extra adder called a *vector-merging* adder to generate the final result. The resulting multiplier is called a *carry-save multiplier* [Wallace64], because the carry bits are not immediately added, but rather are “saved” for the next adder stage. In the final stage, carries and sums are merged in a fast carry-propagate (e.g., carry-lookahead) adder stage. While this structure has a slightly increased area cost (one extra adder), it has the advantage that its worst case critical path is shorter and uniquely defined, as highlighted in Figure 11-32 and is expressed as

$$t_{mult} = t_{and} + (N - 1)t_{carry} + t_{merge} \tag{11.25}$$

still assuming that  $t_{add} = t_{carry}$ .

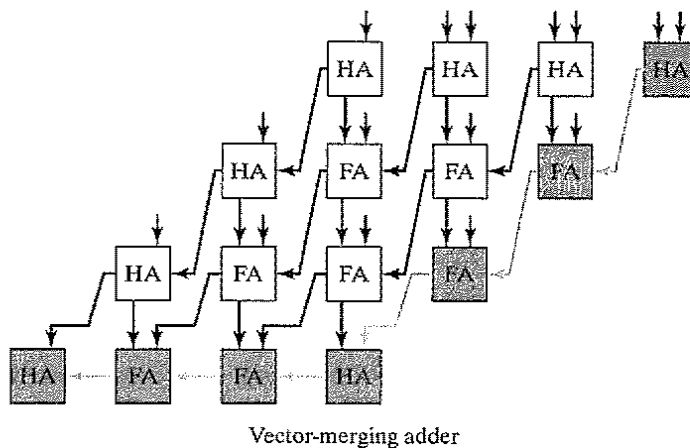


**Figure 11-32** A 4 × 4 carry-save multiplier. The critical path is highlighted in gray.

### Example 11.6 Carry-Save Multiplier

When mapping the carry-save multiplier of Figure 11-32 onto silicon, one has to take into account some other topological considerations. To ease the integration of the multiplier into the rest of the chip, it is advisable to make the outline of the module approximately rectangular. A floor plan for the carry-save multiplier that achieves this goal is shown in Figure 11-33. Observe the regularity of the topology. This makes the generation of the structure amenable to automation.

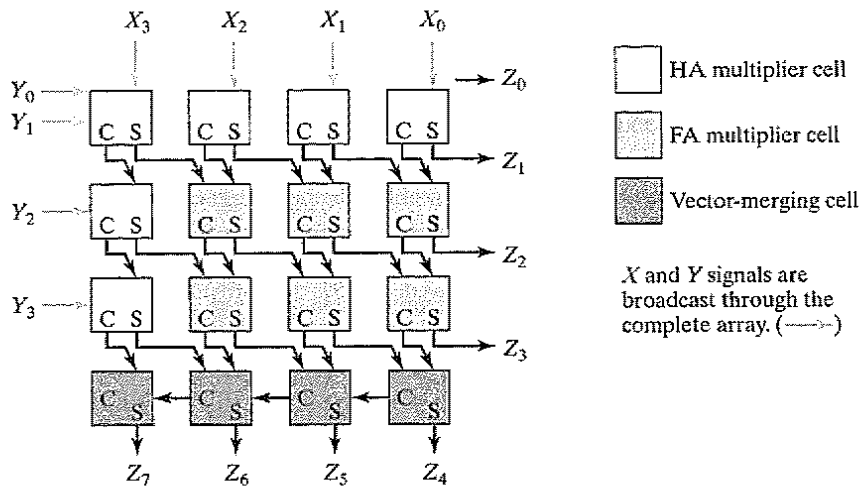


**Figure 11-33** Rectangular floorplan of carry-save multiplier. Different cells are differentiated by shades of gray.  $X$  and  $Y$  signals are AND'ed before being added. The leftmost column of cells is redundant and can be eliminated.

### The Tree Multiplier

The partial-sum adders can also be rearranged in a treelike fashion, reducing both the critical path and the number of adder cells needed. Consider the simple example of four partial products each of which is four bits wide, as shown in Figure 11-34a. The number of full adders needed for this operation can be reduced by observing that only column 3 in the array has to add four bits. All other columns are somewhat less complex. This is illustrated in Figure 11-34b, where the original matrix of partial products is reorganized into a tree shape to visually illustrate its varying depth. The challenge is to realize the complete matrix with a minimum depth and a minimum number of adder elements. The first type of operator that can be used to cover the array is a full adder, which takes three inputs and produces two outputs: the sum, located in the same column and the carry, located in the next one. For this reason, the FA is called a *3-2 compressor*. It is denoted by a circle covering three bits. The other operator is the half-adder, which takes two input bits in a column and produces two outputs. The HA is denoted by a circle covering two bits.



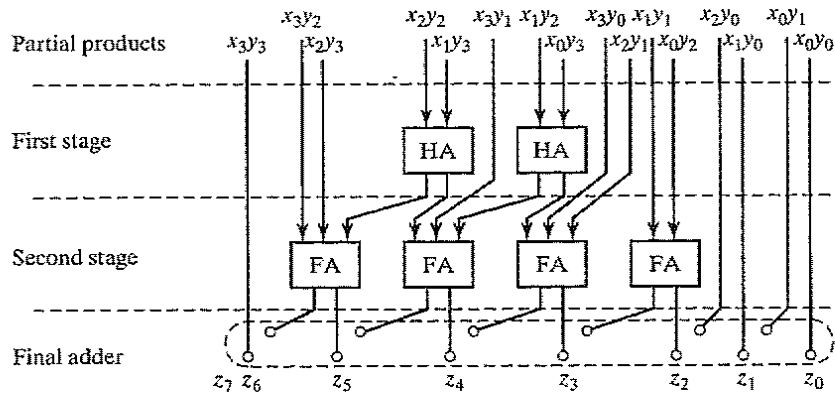


**Figure 11-35** Wallace tree for four-bit multiplier.

option if all input bits to the adder arrive at the same time, as it yields the smallest possible delay. This is the case if a pipeline stage is placed right before the final addition. Pipelining is a technique frequently used in high-performance multipliers. In nonpipelined multipliers, the arrival-time profile of the inputs to the final adder is quite uneven due to the varying logic depths of the multiplier tree. Under these circumstances, other adder topologies, such as carry select, often yield performance numbers similar to lookahead at a substantially reduced hardware cost [Oklobdzija01].

#### 11.4.5 Multiplier Summary

All the presented techniques can be combined to yield multipliers with extremely high performance. For instance, a  $54 \times 54$  multiplier can achieve a propagation delay of only 4.4 ns in a 0.25- $\mu\text{m}$  CMOS technology by combining Booth encoding with a Wallace tree by using 4–2 compression in pass-transistor implementation and by using a mixed carry-select, carry-lookahead topology for the final adder [Ohkubo95]. More information on these multipliers (and others) can be found in the references [e.g., Swartzlander90, Oklobdzija01].

### 11.5 The Shifter

The shift operation is another essential arithmetic operation that requires adequate hardware support. It is used extensively in floating-point units, scalars, and multiplications by constant numbers. The latter can be implemented as a combination of add and shift operations. Shifting a data word left or right over a constant amount is a trivial hardware operation and is implemented by the appropriate signal wiring. A programmable shifter, on the other hand, is more complex and requires active circuitry. In essence, such a shifter is nothing less than an intricate multiplexer circuit. A simple one-bit left–right shifter is shown in Figure 11-36. Depending on the control signals, the input word is either shifted left or right, or else it remains unchanged. Multi-bit shifters can be built by cascading a number of these units. This approach rapidly becomes complex, unwieldy, and ultimately too slow for larger shift values. Therefore, a more structured

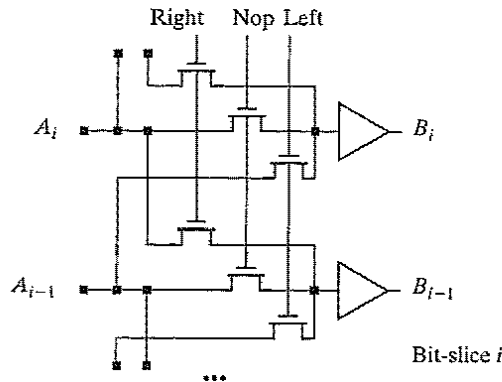


**Figure 11-36** One-bit (left-right) programmable shifter. The data passes undisturbed under the nop condition.

approach is advisable. Next, we discuss two commonly used shift structures, the *barrel shifter* and the *logarithmic shifter*.

### 11.5.1 Barrel Shifter

The structure of a barrel shifter is shown in Figure 11-37. It consists of an array of transistors, in which the number of rows equals the word length of the data, and the number of columns equals the maximum shift width. In this case, both are set equal to four. The control wires are routed diagonally through the array. A major advantage of this shifter is that the signal has to pass through at most one transmission gate. In other words, the propagation delay is theoretically constant and independent of the shift value or shifter size. This is not true in reality, however, because the capacitance at the input of the buffers rises linearly with the maximum shift width.

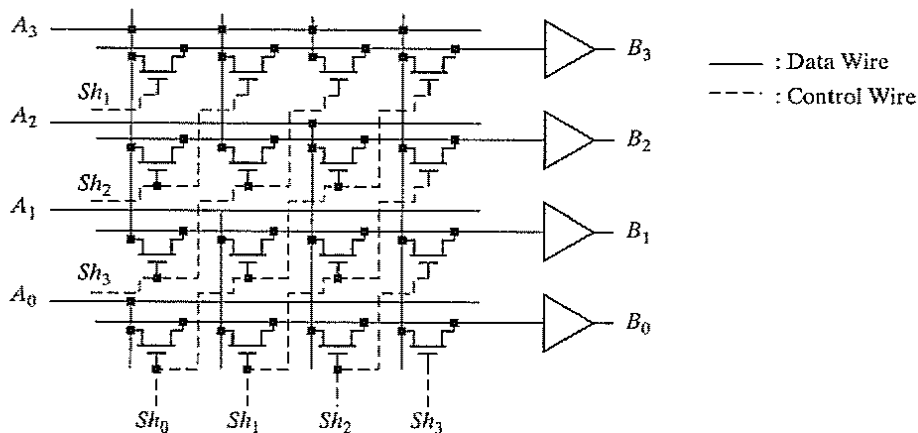


**Figure 11-37** Barrel shifter with a programmable shift width from zero to three bits to the right. The structure supports automatic repetition of the sign bit ( $A_3$ ), also called *sign-bit extension*.



An important property of this circuit is that the layout size is not dominated by the active transistors as in the case of all other arithmetic circuits, but by the number of wires running through the cell. More specifically, the size of the cell is bounded by the pitch of the metal wires!

Another important consideration when selecting a shifter is the format in which the shift value must be presented. From the schematic diagram of Figure 11-37, we see that the barrel shifter needs a control wire for every shift bit. For example, a four-bit shifter needs four control signals. To shift over three bits, the signals  $Sh_3:Sh_0$  take on the value 1000. Only one of the signals is high. In a processor, the required shift value normally comes in an encoded binary format, which is substantially more compact. For instance, the encoded control word needs only two control signals and is represented as 11 for a shift over three bits. To translate the latter representation into the former (with only one bit high), an extra module called a *decoder* is required. (Decoders are treated in detail in Chapter 12.)

---

**Problem 11.9 Two's Complement Shifter**

Explain why the shifter shown in Figure 11-37 implements a two's complement shift.

---

### 11.5.2 Logarithmic Shifter

While the barrel shifter implements the whole shifter as a single array of pass transistors, the logarithmic shifter uses a staged approach. The total shift value is decomposed into shifts over powers of two. A shifter with a maximum shift width of  $M$  consists of a  $\log_2 M$  stages, where the  $i$ th stage either shifts over  $2^i$  or passes the data unchanged. An example of a shifter with a maximum shift value of seven bits is shown in Figure 11-38. For instance, to shift over five bits, the first stage is set to shift mode, the second to pass mode, and the last stage again to shift. Notice that the control word for this shifter is already encoded, and no separate decoder is required.

The speed of the logarithmic shifter depends on the shift width in a logarithmic way, since an  $M$ -bit shifter requires  $\log_2 M$  stages. Furthermore, the series connection of pass transistors slows the shifter down for larger shift values. A careful introduction of intermediate buffers is therefore necessary, as discussed in Chapter 6.

In general, we conclude that a barrel shifter is appropriate for smaller shifters. For larger shift values, the logarithmic shifter becomes more effective, in terms of both area and speed. Furthermore, the logarithmic shifter is easily parameterized, allowing for automatic generation. The most important concept of this section is that the exploitation of regularity in an arithmetic operator can lead to dense and high-speed circuit implementations.

## 11.6 Other Arithmetic Operators

In the previous sections, we only discussed a subset of the large number of arithmetic circuits required in the design of microprocessors and signal processors. Besides adders, multipliers, and shifters, other operators such as comparators, dividers, counters, and goniometric operators (sine, cosine, tangent) are often needed. A full analysis of these circuits is beyond the scope of

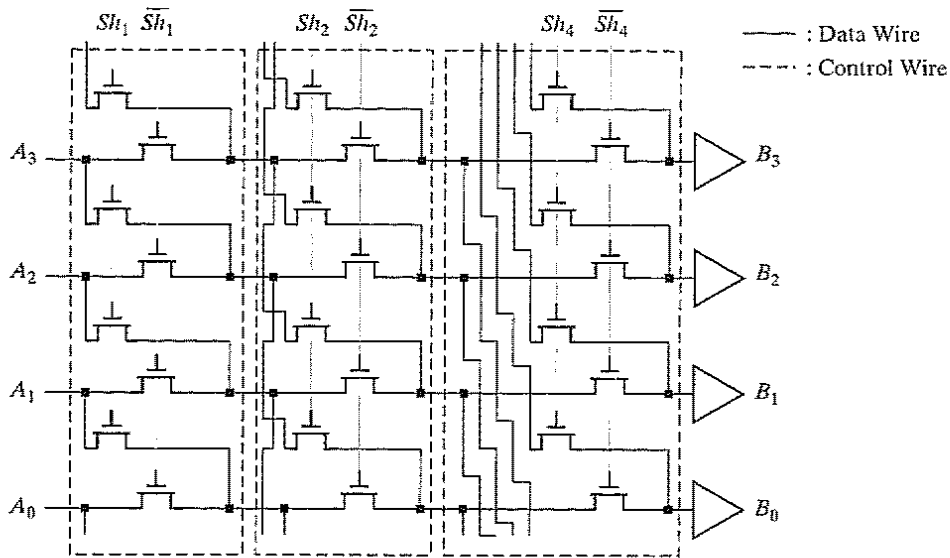


**Figure 11-38** Logarithmic shifter with maximal shift width of seven bits to the right. (Only the four least significant bits are shown.)

this book. We refer the interested reader to some of the excellent references available on the topic (e.g., [Swartzlander90], [Oklobdzija01]).

The reader should be aware that most of the design ideas introduced in this chapter apply to these other operators as well. For instance, comparators can be devised with a linear, square root, and logarithmic dependence on the number of bits. In fact, some operators are simple derivatives of the adder or multiplier structures presented earlier. For example, Figure 11-39 shows how a two's complement subtractor can be realized by combining a two's complement adder with an extra inversion stage, or how a subtractor can be used to implement  $A \geq B$ .

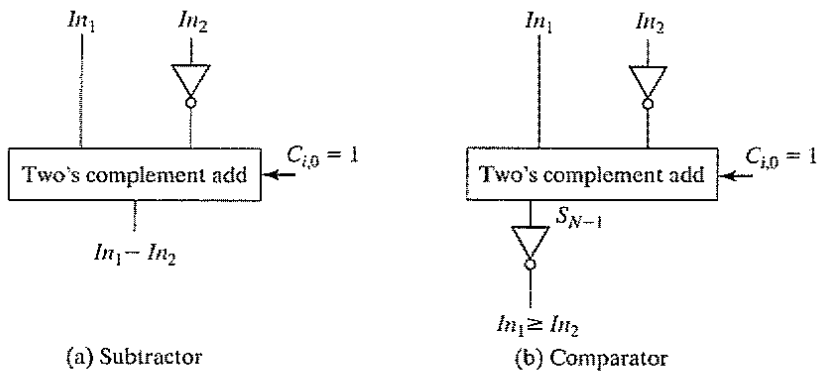


**Figure 11-39** Arithmetic structures derived from a full adder.

**Problem 11.10** Comparator

Derive a logic diagram for a comparator that implements the following logic functions:  $\geq$ ,  $=$ , and  $\leq$ .

**Case Study—Design of an Arithmetic-Logic Unit (ALU)**

The core of any microprocessor or microcontroller is the arithmetic-logic unit (or ALU). The ALU combines addition and subtraction with other operations, such as shifting and bitwise logic operations (AND, OR, and XOR).

An ALU taken from a 64-bit high-end microprocessor is shown in Figure 11-40 [Mathew01.] It consists of two levels of wide multiplexers, a 64-bit adder, a logic unit, an operator-merging multiplexer and the write-back bus driver. The first pair of 9:1 multiplexers selects the from nine different input sources, three of which are from register files and caches. The other six are bypass paths that come directly from the six ALUs—the microprocessor in question can issue six integer instructions in one cycle. One of the bypass loops actually feeds the output of the ALU back to its own input, creating a single cycle loop that defines the critical path. The second 5:1 multiplexer on the  $A$  input performs a partial shifting of the operand, while the 2:1 multiplexer on the  $B$  input simply inverts the operand to implement subtraction. The adder executes two's complement addition or subtraction on the operands  $A$  and  $B$ . Two's complement subtraction is performed by inverting all the bits of the operand  $B$  (using the 2:1 MUX) and by setting the carry-in to one. The sum-selection block not only implements the sum selection, but also merges the outputs of arithmetic and logic units. Finally, a strong buffer drives the loop-back bus, which presents a large load to the ALU. For example, for a six-issue Intel/HP Itanium processor [Fetzer02], the bus has to connect to all six units, translating into more than 2 mm of wire length in a 0.18- $\mu\text{m}$  technology. When added to the load from the register file, it presents over 0.5 pF of capacitive load.

An ALU represents a typical example of a bit-sliced design. Each slice in each block is pitch matched, which minimizes the vertical routing. A floor plan of the 64-bit ALU is shown in Figure 11-41. Intercell routing is done horizontally in metal-3, except for the long horizontal wires between adder stages 1 and 2 and 2 and 3, which are laid out in a combination of metal-3 and metal-4. For example, if the adder is implemented as a radix-4 CLA, the longest wire after the second PG stage crosses 48 cells.

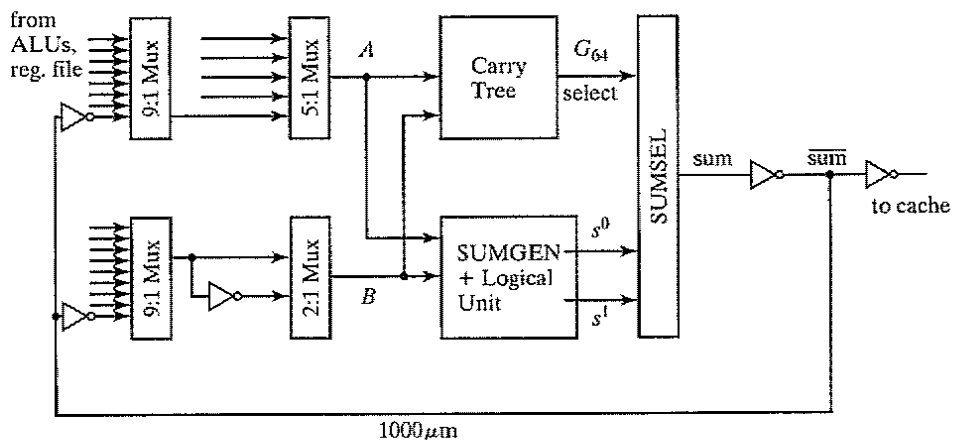


**Figure 11-40** A 64-bit arithmetic-logic unit.

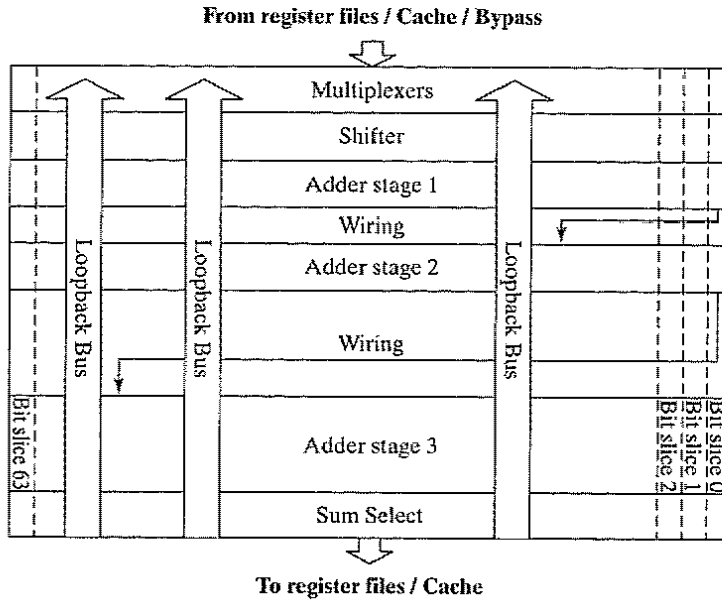


Figure 11-41 Floor plan of a 64-bit ALU.

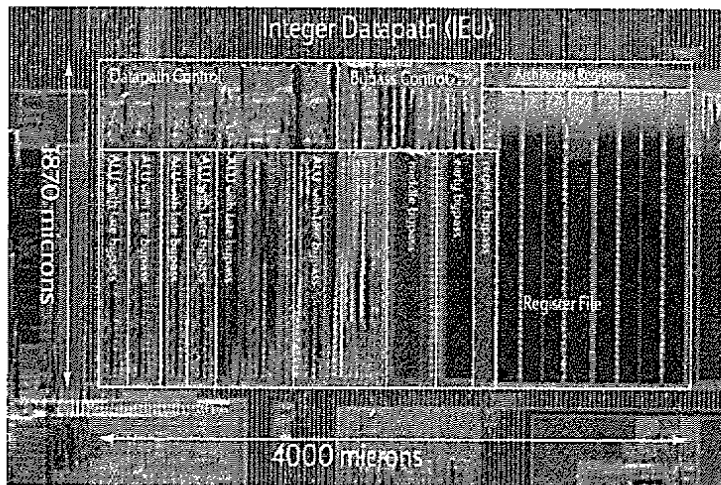


Figure 11-42 Microphotograph of the Itanium processor, showing bit-sliced design of six ALUs together with bypasses, register file, and control logic. (Courtesy of Intel.)

The loop-back wiring is routed in the top-level metal (e.g., metal-5). In case of a multiple-issue microprocessor, these busses span across all ALUs, as can be seen in Figure 11-42. The number of loop-back busses frequently determines the bit-pitch in multiissue ALUs. In our example, nine 64-bit-wide busses have to cross back over the ALU. To avoid needing to add extra wiring space, the bit width is set to nine

bus-wire pitches. Since these wires are long, they are designed with double width and at least double spacing to reduce their resistance and capacitance. ■

### 11.7 Power and Speed Trade-Offs in Datapath Structures\*

In the preceding discussion on adders, multipliers, and shifters, we mainly explored the trade-off between speed and area and ignored power considerations. In this section, we briefly analyze the third dimension of the design exploration space. Since most of the approaches to minimize power were already introduced in Chapter 6, the discussion that follows serves mostly as an illustration of the concepts advanced there.

Typical digital designs are either *latency* or *throughput* constrained. A latency-constrained design has to finish computation by a given deadline. Interactive communication and gaming are examples of such. Throughput-constrained designs, on the other hand, must maintain a required data throughput. A 1000BaseT Gigabit Ethernet connection has to maintain a constant throughput of 1 Gigabit/s. The architectural optimization techniques that are available to the designer differ based on the design constraints. Pipelining or parallelization, for instance, works effectively for the throughput-constrained scenario, but it may not be applicable to the latency-constrained case. For example, a throughput of 1 Gb/s over copper wires is achieved in Gigabit Ethernet by processing four 250 Mb/s streams of data in parallel.

With a fixed architecture of the datapath, speed, area, and power can be traded off through the choice of the supply voltage(s), transistor thresholds, and device sizes. This opens the door for a large variety of power minimization techniques, which are summarized in Table 11-3. They are classified as follows:

- **Enable Time**—Some design techniques are implemented (or enabled) at *design time*. Transistor widths and lengths, for instance, are fixed at the time of design. Supply voltage and transistor thresholds, on the other hand, can be either assigned statically during the design phase, or changed dynamically at *run time*. Other techniques primarily address the time that a function or module in a digital design is in idle mode (or standby). It is only logical to require that the power dissipation of a module in *sleep mode* should be absolutely minimal.

**Table 11-3** Power minimization techniques.

	Constant Throughput/Latency		Variable Throughput/Latency
	Design Time	Sleep Mode	Run Time
Active	Lower $V_{DD}$ , Multi- $V_{DD}$ , Transistor Sizing Logic Optimizations	Clock gating	Dynamic voltage scaling
Leakage	Multi- $V_{th}$ + Active Techniques	Sleep transistors, Variable $V_{th}$	Variable $V_{th}$ + Active Techniques

- **Targeted Dissipation Source**—Another classification of the power-management techniques concerns the source of power dissipation they address: active (dynamic) power or leakage (static) power. Lowering the supply voltage, for example, is a very attractive technique: It not only reduces the energy consumed per transition in a quadratic way—albeit at the expense of performance—but also reduces the leakage current. On the other hand, increasing the threshold voltage mainly impacts the leakage component.

The sleep mode of operation deserves some special attention. If a digital block still receives a clock while in idle mode, its clock distribution network, together with the attached flip-flops, continues to consume energy, even while no computation is performed. Recall that, typically, one third of total energy of a digital system is consumed in clock distribution network. A common method to reduce power in idle mode is the *clock gating* technique introduced in Chapter 10. In this approach, the main clock connection to a module is turned off (or *gated*) whenever the block is idle. However, clock gating does not reduce the leakage power of the idle block. More complicated schemes to lower the standby power have to be used, such as increasing the transistor thresholds or switching off the power rails.

In the following sections, we discuss each of these design-time and run-time techniques in detail.

### 11.7.1 Design-Time Power-Reduction Techniques

#### Reducing the Supply Voltage

A reduction in supply voltage results in quadratic power savings and thus is the most attractive approach. On the negative side, the delay of CMOS gates increases inversely with supply voltage. At the datapath level, this loss of performance can be compensated for by other means, such as logical and architectural optimizations. For example, a ripple-carry adder can be replaced by a faster structure, such as a lookahead adder. The latter implementation is larger and more complex, which translates into a larger physical and switching capacitance. This is more than offset by the fact that the faster adder can run at a lower supply voltage for the same performance.

The trade-off between ripple and lookahead operates at the logical level. Similarly, and even more effectively, architectural optimizations can be employed to compensate for the effect of a reduced  $V_{DD}$ , as illustrated in Example 11.7.

---

#### Example 11.7 Minimizing the Power Consumption by Using Parallelism

To illustrate how architectural techniques can be used to compensate for reduced speed, a simple eight-bit datapath consisting of an adder and a comparator is analyzed, assuming a 2- $\mu\text{m}$  CMOS technology [Chandrakasan92]. As shown in Figure 11-43, inputs  $A$  and  $B$  are added, and the result is compared with input  $C$ . Assume that the worst case delay through the adder, comparator, and latch is approximately 25 ns at a supply voltage of 5 V. At best, the system can be clocked with a clock period of  $T = 25$  ns. When required to run at this maximum possible throughput, it is clear that the operating

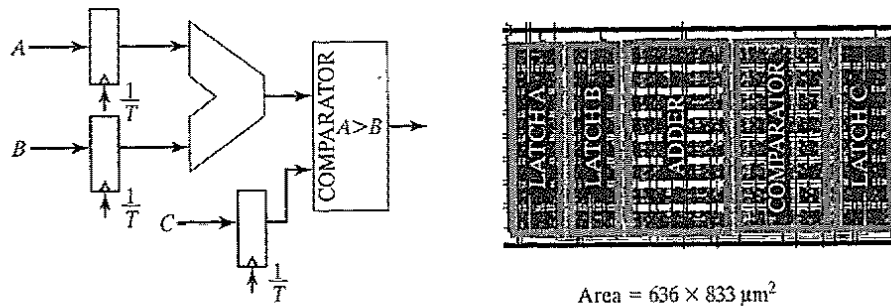


Figure 11-43 A simple datapath with corresponding layout.

voltage cannot be reduced any further because no extra delay can be tolerated. We use this topology as the reference datapath for our study and present power improvement numbers with respect to this reference. The average power consumed by the reference datapath is given by

$$P_{ref} = C_{ref} V_{ref}^2 f_{ref} \quad (11.26)$$

where  $C_{ref}$  is the total effective capacitance being switched per clock cycle. The effective capacitance can be determined by averaging the energy over a sequence of random input patterns with a uniform distribution.

One way to maintain throughput while reducing the supply voltage is to utilize a parallel architecture. As shown in Figure 11-44, two identical adder-comparator datapaths connect in parallel, allowing each unit to work at half the original rate while maintaining the original throughput. Since the speed requirements for the adder, comparator, and latch have decreased from 25 ns to 50 ns, the voltage can be dropped from 5 V to 2.9 V—the voltage that doubles the delay. While the datapath capacitance has increased by a factor of two, the operating frequency has correspondingly decreased by a factor of two. Unfortunately, there also is a slight increase in the total effective capacitance due to the extra routing and data multiplexing. This results in an increased capacitance by a factor of 2.15. The power for the parallel datapath is thus given by

$$P_{par} = C_{par} V_{par}^2 f_{par} = (2.15 C_{ref}) (0.58 V_{ref})^2 \left( \frac{f_{ref}}{2} \right) \approx 0.36 P_{ref} \quad (11.27)$$

The approach presented *trades off area for power*, as the resulting area is approximately 3.4 times larger than the original design. This technique is only applicable when the design is not area constrained. Furthermore, parallelism introduces extra routing overhead, which might cause additional dissipation. Careful optimization is needed to minimize this overhead.

Parallelism is not the only way to compensate for the loss in performance. Other architectural approaches, such as the use of pipelining, can accomplish the same goal. The most impor-

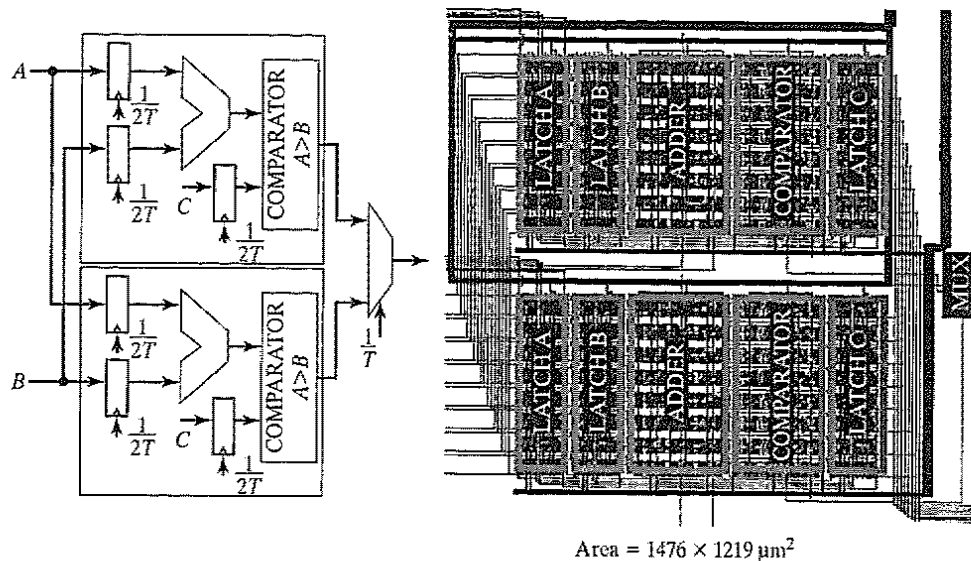


Figure 11-44 Parallel implementation of the simple datapath.

tant message in the preceding analysis is that if power dissipation is the prime concern, dropping the supply voltage is the most effective means to achieve that goal. The subsequent loss in performance can be compensated for, if necessary, by an increase in area. Within certain bounds, this is acceptable, since area is no longer the compelling issue it used to be due to the dramatic increase in integration levels of the last decade.

#### Problem 11.11 Reducing the Supply Voltage, Using Pipelining

A pipeline stage is introduced between the adder and the comparator of the reference datapath of Figure 11-44. You may assume that this roughly halves the propagation delay of the logic, while it increases the capacitance by 15%. Obviously, an extra pipeline register is needed on input *C* as well. Determine how much power can be saved by this approach, given that the throughput has to remain constant compared with the reference datapath. Comment on the area overhead.

#### Using Multiple Supply Voltages

Reducing the supply voltage is fairly straightforward, but it may not be optimal. Reduced supply evenly lowers the power dissipation of all logic gates, while evenly increasing their delay. A better approach is to selectively decrease the supply voltage on some of the gates:

- those which correspond to fast paths and finish the computation early, and
- those with gates that drive large capacitances, have the largest benefit for the same delay increment.



This approach, however requires the use of more than one supply voltage. Multiple supply voltages are already employed frequently in today's ICs. A separate supply voltage is provided for the I/O for compatibility reasons, where the I/O ring is designed with transistors with thicker gate oxides to sustain higher voltages. The logic core is powered from lower voltage supplies and uses transistors with thinner oxides. This approach can be extended to lower the power dissipation of a circuit. For instance, every module could select the most appropriate voltage from two (or more) supply options. Even more extreme, multiple voltages can be assigned on a gate-by-gate basis.

**Module-Level Voltage Selection** Consider, for instance, the digital system shown in Figure 11-45, which consists of a datapath block with a critical path of 10 ns and a control block with a much shorter critical path of 4 ns, operating from the same supply voltage of 2.5 V. Also, assume that the datapath block has a fixed latency and throughput and that no architectural transformation can be applied to lower its supply. Since the control block finishes early (in other words, it has *timing slack*), its supply voltage can be lowered. A reduction to  $V_{DDL} = 1$  V increases its critical path delay to 10 ns, and lowers its power dissipation by more than five times.<sup>6</sup> We effectively exploit the discrepancy in the critical-path length of the various modules (called the *slack*) to selectively lower the power consumption of the modules with the larger slack.

When combining multiple supply voltages on a die, *level converters* are required whenever a module at the lower supply has to drive a gate at the higher voltage. If a gate supplied by  $V_{DDL}$  drives a gate at  $V_{DDH}$ , the PMOS transistor never turns off, resulting in static current and reduced output swing as illustrates in Figure 11-46. A level conversion performed at the boundaries of supply voltage domains prevents these problems. An asynchronous level converter, based on the DVSL template (Chapter 6) and similar to the low-swing signalling gate of Figure 9-32, is shown in Figure 11-46. The cross-coupled PMOS transistors perform the level conversion by using positive feedback. The delay of this level converter is quite sensitive to transistor-sizing and supply-voltage issues. The NMOS transistors operate with a reduced overdrive,  $V_{DDL} - V_{Th}$ , compared with the PMOS devices. They have to be made large to be able to overpower the positive feedback. For a low value of  $V_{DDL}$ , the delay can become very long. Due to

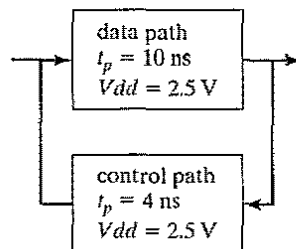


Figure 11-45 Design with diverging critical-path lengths.

<sup>6</sup>This uses the simplifying assumption that the propagation delay is inversely proportional to the supply voltage.

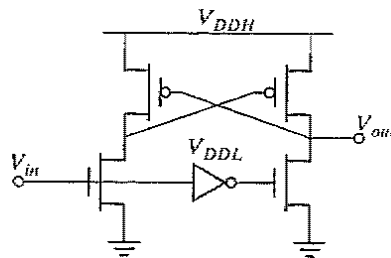
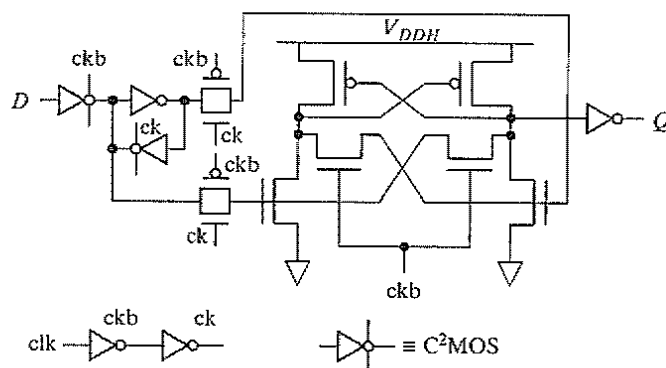


Figure 11-46 Level converter.

the reduced overdrive, the circuit is also very sensitive to variations in the supply voltage. Note that level converters are not needed for a step-down change in voltage.

The overhead of the level conversion can be somewhat mitigated by observing that most conversions are performed at a register boundary. For instance, the control inputs to the datapath block of Figure 11-45 are commonly sampled in a register. A practical way to perform the level conversion is, then, to embed it inside the register. A level-converting register is shown in Figure 11-47. It is a conventional transmission gate implementation of a master-slave latch pair, where a cross-coupled PMOS pair is embedded in the slave latch to perform level conversion.

**Multiple Supplies Inside a Block** The same approach can be applied at much smaller granularity by individually setting the supply voltage for each cell inside a block [Usami95, Hamada01]. Examining the histogram of the critical-path delays for a typical digital block reveals that only a few paths are critical or near critical and that many paths have much shorter delays. The shorter paths essentially waste energy, as there is no reward for finishing early. For each of these paths, the supply voltage could be lowered to the optimum level. Minimum energy consumption would be achieved if all paths become critical. However, this is not easily achievable, as many logic gates are shared between different paths, and it is impractical to generate and

Figure 11-47 Level-converting register. Shaded gates are supplied from  $V_{DDL}$  [Usami95].

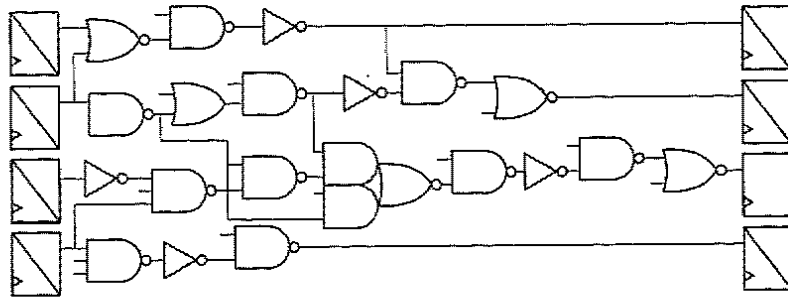


**Figure 11-48** Dual-supply design using clustered voltage scaling. Each path starts with a high supply and switches to a low supply (gray logic gates) if there is a delay slack. Level conversion is performed in the registers.

distribute a wide range of supply voltages. A more practical implementation, employing only two supplies, is shown in Figure 11-48. Using a *clustered voltage-scaling* technique, each path starts with the high supply voltage and switches to the low supply when delay slack is available. Level conversion is performed in the registers at the end of the paths, using circuits such as the one introduced in Figure 11-47. Note that the level conversion is necessary only if the logic section that follows cannot run entirely off the low supply.

The impact of this approach is illustrated in Figure 11-49, which plots the path-length distribution of a typical logic block for single and dual supplies. When a single supply is used, a large fraction of the paths is substantially shorter than critical. Adding the second supply shifts the delay distribution closer to the target delay, making many more paths critical. If the design has very few critical paths and most of paths finish early, energy savings would be large. On the other hand, if most of the paths inside a block are critical, introducing the second supply does not yield any energy savings. You may wonder if adding a third or even a fourth supply voltage may yield even greater benefits to equalize the larger delay spreads. Unfortunately, a number of studies have shown that for typical path-delay distributions, adding more supplies only yields marginal savings [Hamada01, Augsburg02].

Similarly, one may ask whether this dual-supply technique yields a larger benefit, compared with a uniform reduction the supply. In using clustered voltage scaling, the dual-supply approach is **more effective when large switched capacitances are concentrated toward the**

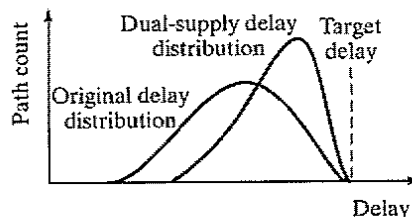


**Figure 11-49** Typical path-delay distribution before and after applying the second supply.

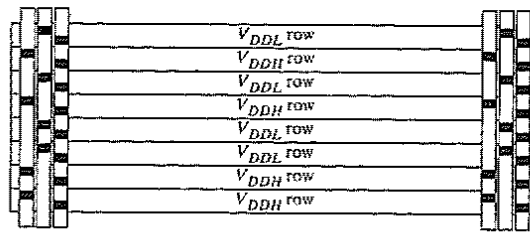


**Figure 11-50** Layout of a dual-supply logic block where all cells at different supplies are placed in different rows.

**end of the block**, such as in buffer chains [Stojanovic02]. This observation is in accordance with the concept of low-swing busses, introduced in Chapter 9. A bus typically presents the largest capacitance, and it is more advantageous to lower the supply voltage on its driver than that on any other logic gate. Since it has the largest capacitance, the payoff in power savings is the largest for the same increase in delay.

Distributing multiple supply voltages on a die complicates the design of the power-distribution network and tends to tax the traditional place-and-route tools. As we saw many times before, a structured approach can help to minimize the impact. One simple option is to place cells with different supplies into different rows of a standard cell layout, as shown in Figure 11-50. The second supply can be brought in from outside the chip, or it can be generated on the die, using an internal DC–DC converter. Step-down switching DC–DC converters have a conversion efficiency of well over 90% and yield only a minimal overhead. Still the  $V_{DDL}$  distribution network has to meet all necessary design requirements, such as decoupling to minimize the voltage variations and immunity to electromigration.

### Using Multiple Device Thresholds

The use of devices with multiple thresholds offers another way of trading off speed for power. Most sub-0.25- $\mu\text{m}$  CMOS technologies offer two types of  $n$ - and  $p$ -type transistors, with thresholds differing by about 100 mV. This higher threshold device features a leakage current that is about one order of magnitude lower than that of the lower threshold transistor, at the expense of a ~30% reduction in active current. Therefore, the low-threshold devices are preferably used in timing-critical paths, while the high thresholds are used anywhere else. The assignment can be done on a per-cell basis, rather than per individual transistor [Wei99, Kato00]. Note that the use of multiple thresholds does not require level converters or any other special circuits, as shown Figure 11-51. Clustering of the logic is not required either; as many gates as possible should be converted to high threshold until the timing slack is completely consumed. A careful assignment of the thresholds can reduce the leakage power by as much as 80%–90%.

While the multiple-threshold approach primarily addresses the leakage current, it yields a small reduction in active power as an additional benefit. This is primarily due to a reduced gate-channel capacitance in the off state and a small reduction in signal swing on the internal nodes of a gate ( $V_{DD} - V_{ThH}$ ). Such a reduction is partially offset by increased source and drain junction sidewall capacitances. The overall active power reduction turns out to be only about 4%.

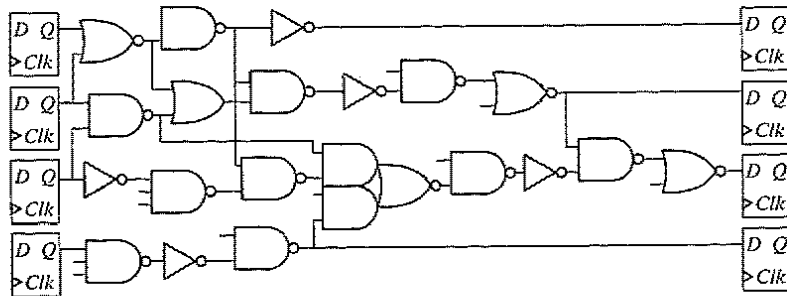


**Figure 11-51** Use of dual-threshold gates. Gray-shaded gates use low thresholds and are employed only in critical paths.

### Reducing Switching Capacitance through Transistor Sizing

The input capacitance of a complementary CMOS gate is directly proportional to its size and, therefore, also to its speed. In Chapter 6, we examined the optimal sizing of gates and found that each gate in a logic path should be sized to have an effective fan-out of approximately 4 to achieve the minimum delay for that path. An interesting question is how to size a circuit for minimum energy when the allowable delay is longer than minimal?

We know that for an inverter chain with a given load and number of stages, the minimum delay is achieved when the size of each inverter in the chain is the geometric mean of its neighbors:

$$s_i^2 = s_{i+1}s_{i-1} \quad (11.28)$$

When the minimum delay that is achieved by this sizing is below the desired delay, an optimization problem can be formulated that minimizes the switching capacitance under delay constraints. One option is to reduce the number of stages and increase the tapering factor, as suggested in Chapter 9. Even better, an analytical solution exists for this problem [Ma94], which establishes that the optimal approach is to adjust the tapering factor at each stage according to the following equation:

$$s_i^2 = \frac{s_{i+1}s_{i-1}}{1 + \mu s_{i-1}} \quad (11.29)$$

The parameter  $\mu$  is a nonnegative number that depends on the amount of timing slack available (with respect to the chain sized for the minimum delay). This solution is intuitively clear—the last stages in the inverter chain are the largest; hence, they are the prime candidates for downsizing. Since downsizing any of the inverters in the chain by a given percentage causes the same delay increment. Hence, we rather do it at the stage where we get the largest impact, which is the largest one.

The same principle applies to a logic path. When it is optimized for minimum delay, the delay of each stage is the same (while the intrinsic delays of gates may differ). Therefore,

the delay of the largest energy consuming gates should be increased first. This idea can be extrapolated to the energy–delay optimization of a general combinational logic block. However, applying it in practice is not trivial. Downsizing one path affects the delay of all paths that share logic gates with it, making it difficult to isolate and optimize one particular path. In addition, many paths in a general combinational block are reconvergent.

### Example 11.8 Energy-Delay Trade-Offs in Adder Design

Let us examine the energy-delay optimization of the 64-bit Kogge–Stone tree adder. There are many paths through an adder, and not all of these paths are balanced. A crucial question is how to identify the paths for resizing or initial sizing. One option is to select all the paths in the adder equal to the critical path. Since the paths through an adder roughly correspond to different bit slices, we allocate each gate in the adder to a bit slice. There are 64 bit slices, and a total of nine stages of logic. This partition works well for Figure 11-52a shows the resulting energy map for the minimum delay. It can be seen that the adder consumes the largest energy along the longest carry paths. Figure 11-52b shows the energy profile of the same adder, this time resized, allowing for a 10% delay increase. The energy dissipation is reduced by 54%. In contrast, a dual-supply solution saves only 27%, while a single reduced supply yields 22% savings [Stojanovic02]. In summary, **sizing is an effective power-reduction method for datapaths, where the majority of energy is consumed inside the block, rather than in driving the external load.**

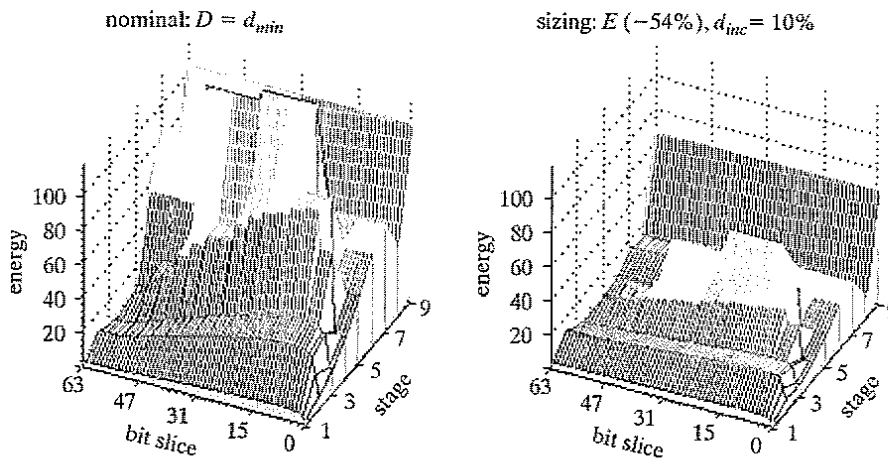
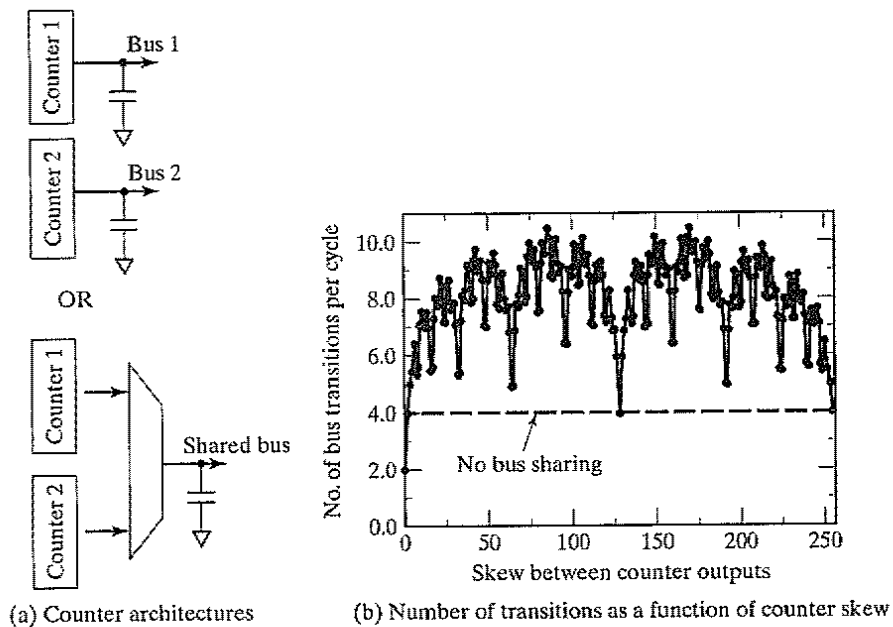


**Figure 11-52** Energy profiles of a 64-bit adder: (a) sized for minimum delay, (b) sized for 10% delay increment and minimized energy.

### Reducing Switching Capacitance through Logic and Architecture Optimizations

As the effective capacitance is the product of the physical capacitance and the switching activity, minimization of both factors is recommended. A wide variety of logic and architectural optimizations exist that reduce the activity at no expense in performance. Some of those were already introduced in Chapter 6. For the sake of brevity, we only show a small number of representative optimizations. (Refer to [Rabaey96] and [Chandrakasan98] for an in-depth overview.)

**Reducing Switching Activity by Resource Allocation** Multiplexing multiple operations on a single hardware unit has a detrimental effect on the power consumption. Besides increasing the physical capacitance, it can also increase the switching activity. This is illustrated with a simple experiment in Figure 11-53, which compares the power consumption of two counters running simultaneously. In the first case, both counters run on separate hardware, while in the second case, they are multiplexed on the same unit. Figure 11-53b plots the number of switching events as a function of the skew between the two counters. The nonmultiplexed case is always superior, except when both counters run in a completely synchronous fashion. The multiplexing tends to randomize the data signals presented to the operational unit, which results in increased switching activity. When power consumption is a concern, it is often beneficial to avoid the excessive reuse of resources. Observe that CMOS hardware units consume only negligible amounts of power when idle. Providing dedicated, specialized operators only presents an extra cost in area, while being generally beneficial in terms of speed and power.



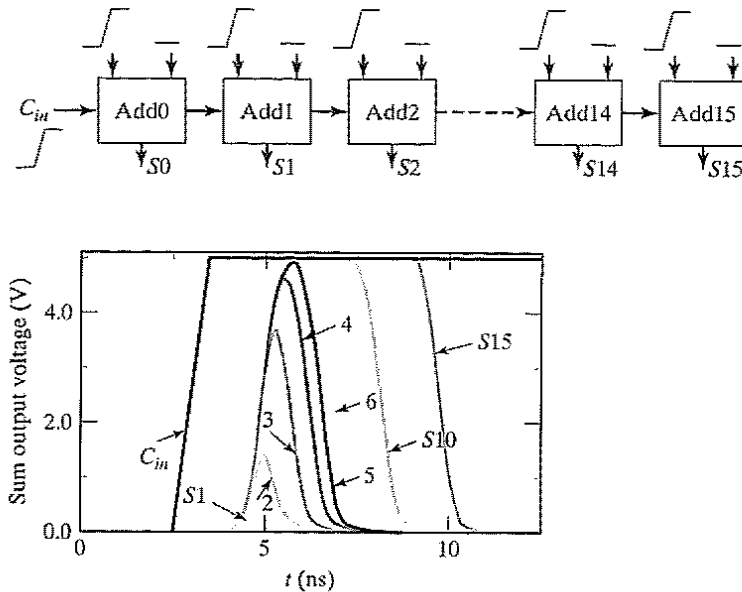


Figure 11-54 Glitching in the sum bits of a 16-bit ripple-carry adder.

**Reducing Glitching through Path Balancing** Dynamic hazards, or *glitching*, are a major contribution to the dissipation in complex structures such as adders and multipliers. The wide discrepancy in the lengths of the signal paths in some of those structures can be the cause of spurious transients. This is demonstrated in Figure 11-54, which displays the simulated response of a 16-bit ripple adder for all inputs going simultaneously from 0 to 1. A number of the sum bits are shown as a function of time. The sum signals should be zero for all bits. Unfortunately, a 1 appears briefly at all of the outputs, since the carry takes a significant amount of time to propagate from the first bit to the last. Notice how the glitch becomes more pronounced as it travels down the chain.

A dramatic reduction in glitching activity can be obtained by selecting structures with balanced signal paths. The tree lookahead adder structures (such as Kogge–Stone) and the tree multipliers have this property; therefore, they should be more attractive from a power point of view, even in the presence of a larger physical capacitance. An inspection of the lookahead structure of Figure 11-22 reveals that the timing paths to the inputs of dot operators are of a similar length, although some deviations may occur due to differences in loading and fan-out.

### 11.7.2 Run-Time Power Management

#### Dynamic Supply Voltage Scaling (DVS)

A static reduction of the supply voltage, as discussed in the preceding paragraphs, lowers the energy per operation and extends the battery life at the expense of performance. This performance penalty is often not acceptable, especially in applications that are latency constrained.



Substantial power reductions are still obtainable, based on the realization that the peak performance is not continuously required. Consider, for instance, a general-purpose processor to be used in portable applications, such as notebooks, electronic organizers, and cellular phones. The computational functions to be executed on such a processor fall into three major categories: compute-intensive tasks, low-speed functions, and idle-mode operation. Compute-intensive and short-latency tasks need the full computational throughput of the processor to achieve real-time constraints. MPEG video and audio decompression are examples of such. Low-throughput and long-latency tasks, such as text processing, data entry, and memory backups, operate under far more relaxed completion deadlines and require only a fraction of the maximum throughput of the microprocessor. There is no reward for finishing the computation early, and if a task is completed early, it can be considered a waste of energy. Finally, portable processors spend a large fraction of their time on idle, waiting for a user action or an external wake-up event. In sum, the computational throughput and latency expected from a mobile processor vary drastically over time.

Even compute-intensive operations, such as MPEG decoding, show variable computational requirements while processing a typical stream of data. For example, the number of times an MPEG decoder computes an inverse discrete cosine transform (IDCT) per video frame varies widely, depending upon the amount of motion in the video scenes. This is illustrated in Figure 11-55, which plots the distribution of the number of IDCTs/frame for a typical video sequence. The processor that is executing this algorithm experiences a different computational workload from frame to frame.

Lowering the clock frequency when executing the reduced workloads reduces the power, but does not save on energy—every operation is still executed at the high voltage level. However, if both supply voltage and frequency are lowered simultaneously, the energy is reduced. In order to maintain the required throughput for high workloads and minimize energy for low workloads, both supply and frequency must be dynamically varied according to the requirements application that is currently being executed. This technique is called *dynamic voltage scaling* (DVS). The concept is illustrated in Figure 11-56 [Burd00, Gutnik97]. It operates under

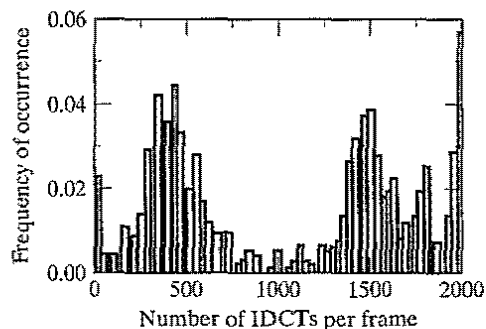
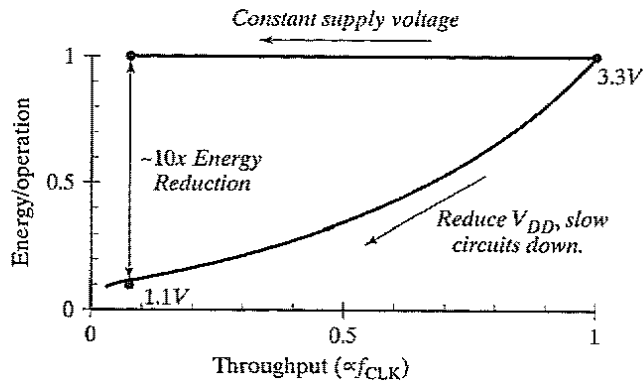


Figure 11-55 Typical IDCT histogram for MPEG decoding.



**Figure 11-56** Energy/operation versus throughput ( $1/T$ ) for constant and variable supply voltage operation.

the guideline that a function should always be operated at the lowest supply voltage that meets the timing constraints.

The DVS concept is enabled by the observation that the delay of most CMOS circuits and functions track each other well over a range of supply voltages, which is a necessity for system operation under varying supply conditions. Figure 11-57 shows the delays of a number of representative CMOS blocks (such as NAND gates, ring oscillators, register files, and SRAM), over a supply voltage range from 1 V to 4 V [Burd00]. Excellent performance tracking can be observed. Note that some circuit families, such as NMOS-only pass-transistor logic do not follow this behavior over the complete range of supplies.

A practical implementation of a dynamic-voltage scaling system now consists of the following components:

- a processor that can operate under a wide variety of supply voltages,

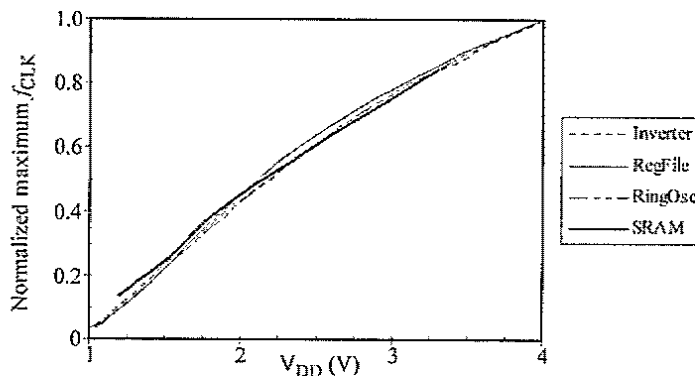


**Figure 11-57** Delay of representative CMOS functions as a function of supply voltage for a 0.6- $\mu\text{m}$  CMOS technology.

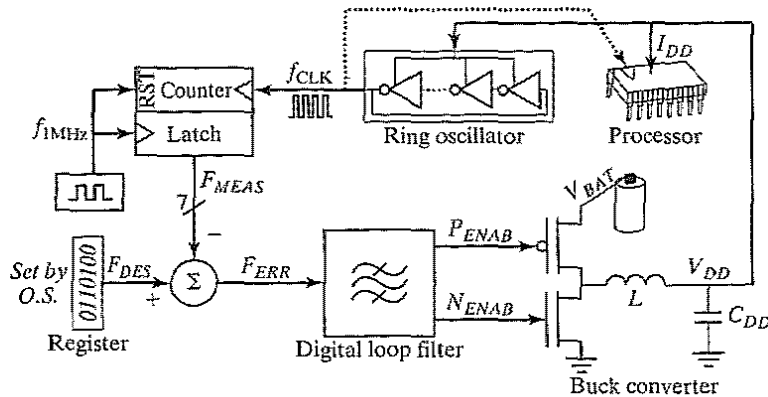


Figure 11-58 Block diagram of a dynamic voltage-scaled system.

- a supply-regulation loop that sets the minimum voltage necessary for operation at a desired frequency, and
- an operating system that calculates the required frequencies to meet requested throughputs and task completion deadlines.

One possible implementation is shown in Figure 11-58. The core of the DVS system is a ring oscillator, whose oscillating frequency matches the microprocessor critical path. When included inside the power-supply control loop, this ring oscillator provides the translation between the supply voltage and the clock frequency. The operating system digitally sets the desired frequency ( $F_{DES}$ ). The current value of ring oscillator frequency is measured and compared with the desired frequency. The difference is used as a feedback error. By adjusting the supply voltage, the supply-voltage loop changes the ring oscillator frequency to set this error value to 0.

The task of the scheduler (or real-time operating system) is to determine dynamically the optimal frequency (or voltage) as a function of the combined computational requirements of all active tasks in the system. In the more complex case of a general-purpose processor, each task should supply a completion deadline (e.g., video frame rate) or a desired execution frequency. The voltage scheduler then estimates the number of processor cycles necessary for completing each of the tasks and computes the optimal processor frequency [Pering99]. In the case of a single task with varying performance requirements, a queue can be used to determine the computational load and to adjust the voltage accordingly. This is illustrated in Figure 11-59, where the depth of the input queue is used to set the supply voltage (and frequency) of a stream-based signal processor [Gutnik97].

### Dynamic Threshold Scaling (DTS)

In analogy to the dynamic variation of the supply voltage, it is attractive to adjust the threshold voltage of the transistors dynamically. For low-latency computation, the threshold should be lowered to its minimal value; for low speed computation, it can be increased; and in the standby

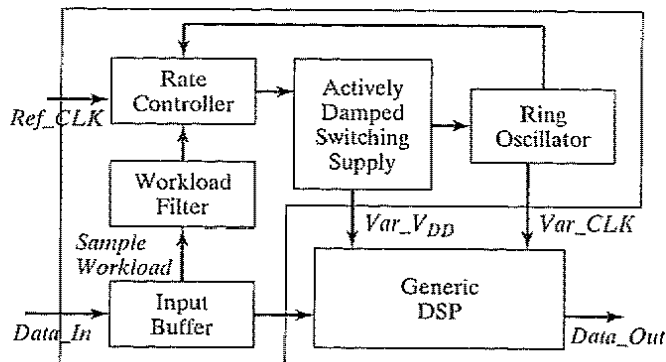


**Figure 11-59** Using a queue to determine the workload in a signal processor [Gutnik97].

mode, it should be set to the highest possible value to minimize the leakage current. Substrate bias is the control knob that allows us to vary the threshold voltages dynamically. In order to do so, we have to operate the transistors as four-terminal devices. This is only possible in a triple-well process, as independent control of all four terminals of both  $n$ - and  $p$ -type devices is required, as shown in Figure 11-60. Substrate biasing can be implemented for a complete chip, on a block-by-block or a cell-by-cell basis. Per cell granularity of substrate biasing, however, has a large layout cost.

Similar to dynamic supply-voltage scaling scheme, the variable threshold voltage scheme is based on a feedback loop, which can be set to accomplish a variety of goals:

- It can lower the leakage in the standby mode
- It can compensate for threshold variations across the chip during normal operation of the circuit
- It can throttle the throughput of the circuit to lower both the active and leakage power based on performance requirements.

Since the current flow into the substrate is much smaller than into the supply lines, DTS has a smaller circuit overhead than DVS. A feedback system, designed to control the leakage in

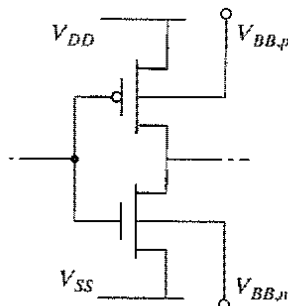


**Figure 11-60** An inverter with body terminals used for threshold control.

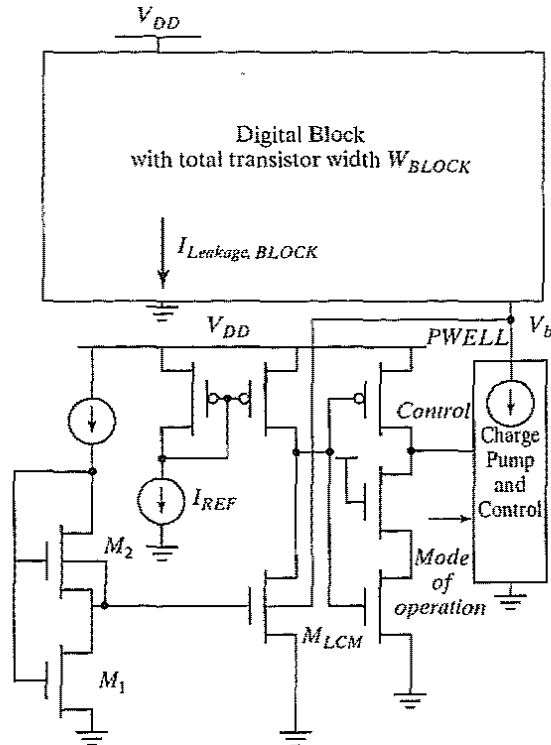


Figure 11-61 Variable threshold control scheme implemented with a leakage current monitor [Kuroda96].

a digital module, is shown in Figure 11-61 [Kuroda96 and Kuroda01]. It consists of a leakage control monitor and a substrate bias charge pump, added to the digital block of interest.

The leakage current monitor is crucial for implementing this scheme. Transistors  $M_1$  and  $M_2$  are biased to operate in the subthreshold region. When an NMOS transistor is in the subthreshold, its current is given by

$$I_D = I_S/W_0 \cdot W \cdot 10^{V_{GS}/S} \quad (11.30)$$

where  $S$  is the subthreshold slope. The output of the bias generator  $V_b$  equals

$$V_b = S \cdot \log(W_2/W_1) \quad (11.31)$$

From the total transistor width of all transistors in the block that is to be monitored,  $W_{BLOCK}$ , the total current scaling factor can be found:

$$\frac{I_{LCM}}{I_{BLOCK}} = \frac{W_{LCM}}{W_{BLOCK}} \cdot 10^{\frac{V_b}{S}} = \frac{W_{LCM}}{W_{BLOCK}} \cdot \frac{W_2}{W_1} \quad (11.32)$$

To minimize the power penalty of the monitoring, the leakage monitor should be made as small as possible. However, if it is too small, the overall leakage monitoring response gets slower and the substrate biasing does not track variations closely. The optimal value can be set very low, with the monitor transistor being as small as 0.001% of the total transistor width on the chip.

A conventional charge pump siphons current in and out of the substrate. The control circuit monitors the leakage current. If it is above the preset value—corresponding to the mode of operation, set externally by the user or the operating system—the charge pump increases the negative back bias by pumping current out of the substrate. The charge pump shuts off when the leakage current reaches the target value. Junction leakages and impact ionization in the circuit will eventually raise the substrate bias voltage again, which activates the feedback loop new. Since it does not have to provide large supply currents on a continuous basis, this scheme is simpler to implement than dynamic voltage scaling.

Unfortunately, the effectiveness of adaptive body biasing is decreasing with further technology scaling. This is due to inherently lower body-effect factors and increased junction leakage attributable to band-to-band tunneling.

### 11.7.3 Reducing the Power in Standby (or Sleep) Mode

The idle mode represents an extreme corner of the dynamic power-management space. As no active switching occurs, all power dissipation is due to leakage—assuming that appropriate clock and input gating is in place. One option to reduce the leakage during standby is the DTS technique presented in the previous section. A simpler power-down scheme utilizes large sleep transistors to switch off the power supply rails when the circuit is in the sleep mode. This straightforward approach significantly reduces the leakage current, but increases the design complexity. It can be implemented by using a power switch on the supply rail only, or, even better, on both supply and ground rails, as shown Figure 11-62.

In normal operation mode, the *SLEEP* signal is high, and the sleep transistors must present as small a resistance as possible. The finite resistance of these transistors results in noise on supply rails, attributable to changes in supply current drawn by the logic. The sizing and the selection of the thresholds of the sleep transistors is subject to a trade-off process. To minimize fluctuations in the supply voltage, the sleep transistors should have a very low on-resistance, and therefore be very wide. However, increasing their size brings with it a major layout penalty. When transistors with a higher threshold are available, a better leakage suppression can be achieved. However, high-threshold devices must be even larger to yield the same resistance as low-threshold devices. The principles of leakage reduction are a direct extension of principles introduced in Section 6.4.2. Adding the sleep transistor effectively increases the transistor stack height, resulting in leakage reductions of the order of tens (for low threshold switches) to a thousand (for high threshold switches) times.

As opposed to simple clock gating, switching off the power supplies erases the state of the registers inside the block. In some applications, this is acceptable, such as when a completely

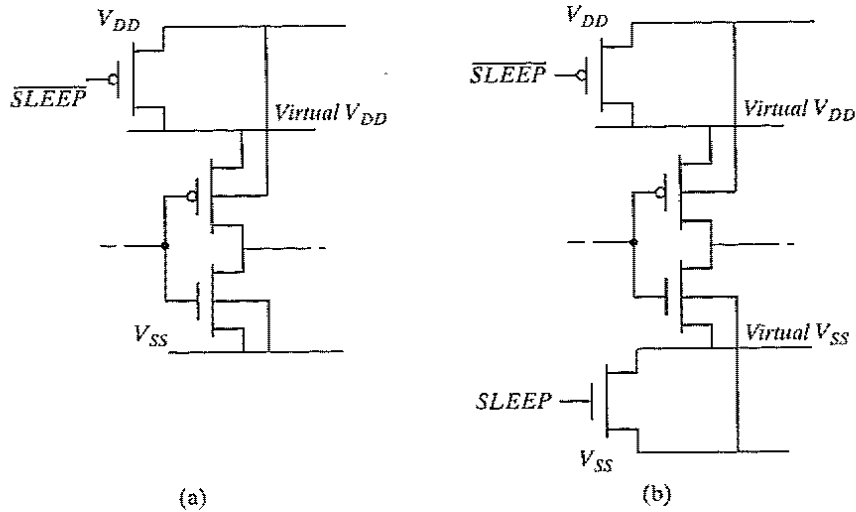


**Figure 11-62** Sleep transistors used (a) only on the supply rail, (b) on both supply and ground.

new task is executed after the block wakes up again. However, additional effort is required when the state needs to be preserved. One option is to connect all the registers to the nongated supply rails,  $V_{DD}$  and  $V_{SS}$ , as discussed in Chapter 7 and shown in Figure 7-18. An alternative is to use the operating system to save the state of all registers to a nonvolatile memory.

### 11.8 Perspective: Design as a Trade-off

The analysis of the adder and multiplier circuits makes it clear again that digital circuit design is a trade-off between area, speed, and power requirements. This is demonstrated in Figure 11-63, which plots the normalized area and speed for some of the adders discussed earlier as a function of the number of bits.<sup>7</sup> The overall project goals and constraints determine which factor is dominant.

The die area has a strong impact on the cost of an integrated circuit. A larger chip size means that fewer parts fit on a single wafer as discussed in Chapter 1. Reducing the area can help the viability of a product. Ultimate performance is what makes the newest microprocessor sell, and the lowest possible power consumption is a great marketing argument for a cellular phone. Understanding the market of a product is therefore essential when deciding on how to play the trade-off game. One should be aware that all design constraints—speed, power, and area—contribute to the feasibility or market success of a design.

In this context, it is worth summarizing some of the important design concepts that have been introduced in the course of this chapter:

<sup>7</sup>Be aware that these results are for a particular implementation in a particular technology. Extrapolation to other technologies should be done with care.

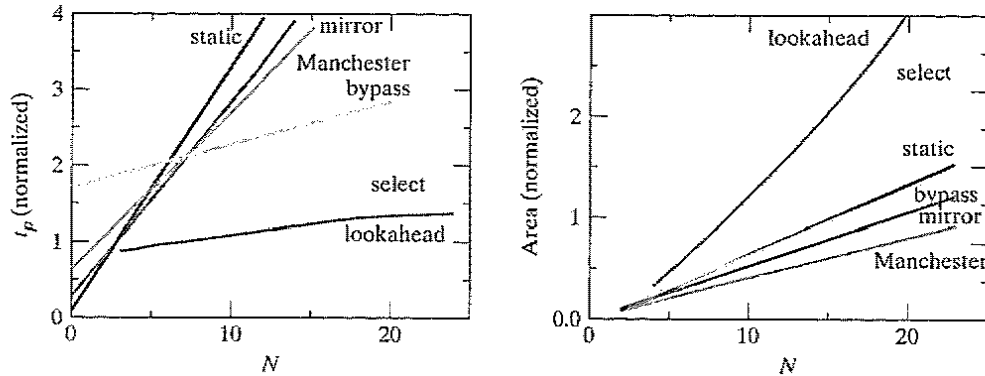


**Figure 11-63** Area and propagation delay of various adder structures as a function of the number of bits  $N$ . Based on results from [Vermassen86].

1. The most important rule is to select the *right structure* before starting an elaborate circuit optimization. Going for the optimal performance of a complex structure by rigorously optimizing transistor sizes and topologies probably will not give you the best result. Optimizations at higher levels of abstraction, such as the logic or architectural level, can often generate more dramatic results. Simple first-order calculations can help give a global picture on the pros and cons of a proposed structure.
2. Determine the *critical timing path* through the circuit, and focus most of your optimization efforts on that part of the circuit. In addition to hand analysis, computer-aided design tools are available to help determine the critical paths and size the transistors appropriately. Be aware that some noncritical paths can be downsized to reduce power consumption.
3. Circuit size is not only determined by the number and size of transistors, but also by other factors such as *wiring and the number of vias and contacts*. These factors are becoming even more important with shrinking dimensions or when extreme performance is a goal.
4. Although an obscure optimization can sometimes help to get a better result, be wary if this results in an irregular and convoluted topology. *Regularity and modularity* are a designer's best friend.
5. Power and speed can be traded off through a choice of circuit sizing, supply voltages, and transistor thresholds.

## 11.9 Summary

In this chapter, we have studied the implementation of arithmetic datapath operators from a performance, area, and power perspective. Special attention was devoted to the development of *first-order performance models* that allow for a fast analysis and comparison of various logic structures before diving into the tedious transistor-level optimizations.



- A datapath is best implemented in a *bit-sliced* fashion. A single layout slice is used repetitively for every bit in the data word. This regular approach eases the design effort and results in fast and dense layouts.
- A *ripple-carry* adder has a performance that is linearly proportional to the number of bits. Circuit optimizations concentrate on reducing the delay of the carry path. A number of circuit topologies were examined, showing how careful optimization of the circuit topology and the transistor sizes helps to reduce the capacitance on the carry bit.
- Other adder structures use logic optimizations to increase the performance. The performance of *carry-bypass*, *carry-select* and *carry-lookahead* adders depends on the number of bits in square root and logarithmic fashion, respectively. This increase in performance comes at a cost in area, however.
- A *multiplier* is nothing more than a collection of cascaded adders. Its critical path is far more complex, and performance optimizations proceed along vastly different routes. The carry-save technique relies on a logic manipulation to turn the adder array into a regular structure with a well-defined critical timing path that can easily be optimized. Booth recoding and partial product accumulation in a tree reduces the complexity and delay of larger multipliers.
- The performance and area of a programmable shifter are dominated by the *wiring*. The exploitation of regularity can help to minimize the impact of the interconnect wires. This is exemplified in the barrel and the logarithmic shifter structures.
- *Power consumption* can be reduced substantially by the proper choice of circuit, logical, or architectural structure. This might come at the expense of area, but area might not be that critical in the age of submicron devices.
- A wide range of design-time and run-time techniques are at the disposition of a designer to minimize the power consumption. At *design time*, power and delay can be traded off through the choice of supply voltages and thresholds in addition to transistor sizing and logic optimization. The use of parallelism and pipelining can help to *reduce the supply voltage*, while maintaining the same throughput. The *effective capacitance* can be reduced by avoiding waste, as introduced by excessive multiplexing, for example.
- Some applications operate under variable throughput or latency conditions. Using *variable supplies and transistor thresholds* can lower the active or leakage power in such systems. Minimization of the standby energy consumption is essential for portable battery-operated devices.

### 11.10 To Probe Further

The literature on arithmetic and computer elements is vast. Important sources for newer developments are the *Proceedings of the IEEE Symposium on Computer Arithmetic*, the *IEEE Transactions on Computers* and the *IEEE Journal of Solid-State Circuits* (for integrated circuit implementation). An excellent collection of the most significant papers in the area can be found in some IEEE Press reprint volumes [Swartzlander90]. A number of other references, such as [Omondi94], [Koren98], and [Oklobdzija01], are provided for further reading.

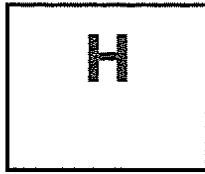
## References

- [Augsburger02] S. Augsburger, "Using Dual-Supply, Dual-Threshold and Transistor Sizing to Reduce Power in Digital Integrated Circuits," M.S. Project Report, University of California, Berkeley, April 2002.
- [Bedrij62] O. Bedrij, "Carry Select Adder," *IRE Trans. on Electronic Computers*, vol. EC-11, pp. 340-346, 1962.
- [Booth51] A. Booth, "A Signed Binary Multiplication Technique," *Quart. J. Mech. Appl. Math.*, vol. 4., part 2, 1951.
- [Brent82] R. Brent and H.T. Kung, "A Regular Layout for Parallel Adders," *IEEE Trans. on Computers*, vol. C-31, no. 3, pp. 260-264, March 1982.
- [Burd00] T.D. Burd, T.A. Pering, A.J. Stratakos, R.W. Brodersen, "A Dynamic Voltage Scaled Microprocessor System," *IEEE Journal of Solid-State Circuits*, vol. 35, no. 11, November 2000.
- [Chandrakasan92] A. Chandrakasan, S. Sheng, and R. Brodersen, "Low Power CMOS Digital Design," *IEEE Journal of Solid State Circuits*, vol. SC-27, no. 4, pp. 1082-1087, April 1992.
- [Chandrakasan98] A. Chandrakasan and R. Brodersen, Ed., *Low-Power CMOS Design*, IEEE Press, 1998.
- [Fetzer02] E.S. Fetzer, J.T. Orton, "A Fully-Bypassed 6-Issue Integer Datapath and Register File on an Itanium Microprocessor," 2002 *IEEE International Solid-State Circuits Conference, Digest of Technical Papers*, San Francisco, CA, pp. 420-421, February 2002.
- [Gutnik97] V. Gutnik, and A. P. Chandrakasan, "Embedded Power Supply for Low-Power DSP," *IEEE Transactions on Very Large Integration (VLSI) Systems*, vol. 5, no. 4, pp. 425-435, December 1997.
- [Hamada01] M. Hamada, Y. Ootaguro, and T. Kuroda, "Utilizing Surplus Timing for Power Reduction," *Proceedings of the IEEE 2001 Custom Integrated Circuits Conference*, San Diego, CA, pp. 89-92, May 2001.
- [Kato00] N. Kato *et al.*, "Random Modulation: Multi-Threshold-Voltage Design Methodology in Sub-2-V Power Supply CMOS," *IEICE Transactions on Electronics*, vol. E83-C, no. 11, p. 1747-1754, November 2000.
- [Katz94] R.H. Katz, *Contemporary Logic Design*, Benjamin Cummings, 1994.
- [Kilburn60] T. Kilburn, D.B.G. Edwards and D. Aspinall, "A Parallel Arithmetic Unit Using a Saturated-Transistor Fast-Carry Circuit," *Proceedings of the IEE*, Pt. B, vol. 107, pp. 573-584, November 1960.
- [Kogge73] P.M. Kogge and H.S. Stone, "A Parallel Algorithm for the Efficient Solution of a General Class of Recurrence Equations," *IEEE Transactions on Computers*, vol. C-22, pp. 786-793, August 1973.
- [Koren98] I. Koren, *Computer Arithmetic Algorithms*, Brookside Court Publishers, 1998.
- [Kuroda96] T. Kuroda and T. Sakurai, "Threshold Voltage Control Schemes Through Substrate Bias for Low-Power High-Speed CMOS LSI Design," *Journal on VLSI Signal Processing*, vol. 13, no. 2/3, pp. 191-201, 1996.
- [Kuroda01] T. Kuroda, and T. Sakurai, "Low-Voltage Technologies," in *Design of High-Performance Microprocessor Circuits*, Chandrakasan, Bowhil, Fox (eds.), IEEE Press, 2001.
- [Lehman62] M. Lehman and N. Burla, "Skip Techniques for High-Speed Carry Propagation in Binary Arithmetic Units," *IRE Transactions on Electronic Computers*, vol. EC-10, pp. 691-698, December 1962.
- [Ma94] S. Ma, P. Franzon, "Energy Control and Accurate Delay Estimation in the Design of CMOS Buffers," *IEEE Journal of Solid-State Circuits*, vol. 29, no. 9, pp. 1150-1153, September 1994.
- [MacSorley61] O. MacSorley, "High Speed Arithmetic in Binary Computers," *IRE Proceedings*, vol. 49, pp. 67-91, 1961.
- [Mathew01] S. K. Mathew *et al.*, "Sub-500-ps 64-b ALUs in 0.18- $\mu$ m SOI/Bulk CMOS: Design and Scaling Trends," *IEEE Journal of Solid-State Circuits*, vol. 36, no. 11, pp. 1636-1646, November 2001.
- [Ohkubo95] N. Ohkubo *et al.*, "A 4.4 ns CMOS 54\*54-b Multiplier Using Pass-Transistor Multiplexer," *IEEE Journal of Solid-State Circuits*, vol. 30, no. 3, pp. 251-257, March 1995.
- [Oklobdzija01] V. G. Oklobdzija, "High-Speed VLSI Arithmetic Units: Adders and Multipliers," in *Design of High-Performance Microprocessor Circuits*, Chandrakasan, Bowhil, Fox (eds.), IEEE Press, 2001.
- [Omondi94] A. Omondi, *Computer Arithmetic Systems*, Prentice Hall, 1994.
- [Pering00] T. A. Pering, *Energy-Efficient Operating System Techniques*, Ph.D. Dissertation, University of California, Berkeley, 2000.

- [Rabaey96] J. Rabaey, and M. Pedram, Eds., "Low-Power Design Methodologies," Kluwer Academic Publishers, 1996.
- [Stojanovic02] V. Stojanovic, D. Markovic, B. Nikolic, M. A. Horowitz, and R. W. Brodersen, "Energy-Delay Tradeoffs in Combinational Logic using Gate Sizing and Supply Voltage Optimization," *European Solid-State Circuits Conference, ESSCIRC'2002*, Florence, Italy, September 24–26, 2002.
- [Suzuoki99] M. Suzuoki *et al.*, "A Microprocessor with a 128-bit CPU, Ten Floating-Point MAC's, Four Floating-Point Dividers, and an MPEG-2 Decoder," *IEEE Journal of Solid-State Circuits*, vol. 34, no. 11, pp. 1608–1618, November 1999.
- [Swartzlander90] E. Swartzlander, ed., *Computer Arithmetic—Part I and II*, IEEE Computer Society Press, 1990.
- [Usami95] K. Usami, and M. Horowitz, "Clustered Voltage Scaling Technique for Low-Power Design," *Proceedings, 1995 International Symposium on Low Power Design*, Dana Point, CA, pp. 3–8, April 1995.
- [Vermassen86] H. Vermassen, "Mathematical Models for the Complexity of VLSI," (in dutch), Master's Thesis, Katholieke Universiteit, Leuven, Belgium, 1986.
- [Wallace64] C. Wallace, "A Suggestion for a Fast Multiplier," *IEEE Trans. on Electronic Computers*, EC-13, pp. 14–17, 1964.
- [Weinberger56] A. Weinberger and J. L. Smith, "A One-Microsecond Adder Using One-Megacycle Circuitry," *IRE Transactions on Electronic Computers*, vol. 5, pp. 65–73, 1956.
- [Wei99] L. Wei, Z. Chen, K. Roy, M.C. Johnson, Y. Ye, and V. K. De, "Design and Optimization of Dual-Threshold Circuits for Low-Power Applications," *IEEE Transactions on Very Large Scale Integration (VLSI) Systems*, vol. 7, no. 1, pp. 16–24, March 1999.
- [Weinberger81] A. Weinberger, "A 4:2 Carry-Save Adder Module," *IBM Technical Disclosure Bulletin*, vol. 23, January 1981.
- [Weste85&93] N. Weste and K. Esbragian, *Principles of CMOS VLSI Design: A Systems Perspective*, 2d ed., Addison-Wesley, 1985 and 1993.

## Exercises

For the latest problem sets, design challenges and design projects related to arithmetic modules, log in to <http://bwrc.eecs.berkeley.edu/IcBook>.



## Validation and Test of Manufactured Circuits

*Manufacturing test*

*Design for testability*

*Test pattern generation*

### H.1 Introduction

While designers tend to spend numerous hours on the analysis, optimization, and layout of their circuits, one issue is often overlooked: When a component returns from the manufacturing plant, how does one know if it actually works? Does it meet the functionality and performance specifications? The customer expects a delivered component to perform as described in the specification sheets. Once a part is shipped or deployed in a system, it is expensive to discover that it does not work. The later a fault is detected, the higher the cost of correction. For instance, replacing a component in a sold television set means replacement of a complete board as well as the cost of labor. Shipping a nonworking or partially functional device should be avoided if at all possible.

A correct design does not guarantee that the manufactured component will be operational. A number of manufacturing defects can occur during fabrication, either due to faults in the base material (for instance, impurities in the silicon crystal), or as a result of variations in the process, such as misalignment. Other faults might be introduced during the stress tests that are performed after the manufacturing. These tests expose a part to cycles of temperature and mechanical stress to ensure its operation over a wide range of working conditions. Typical faults include short circuits between wires or layers and broken interconnections. This translates into network nodes that are either shorted to each other or to the supply rails, or that may be floating.

Making sure a delivered part is operating correctly under all possible input conditions is not as simple as it would seem at a first glance. When analyzing the circuit behavior during the design phase, the designer has unlimited access to all the nodes in the network. He is free to apply input patterns and observe the resulting response at any node he desires. This is not the case once the part is manufactured. The only access one has to the circuit is through the input-output pins. A complex component such as a microprocessor is composed of tens to hundreds of millions of transistors and contains an uncountable number of possible states. It is a very lengthy process—if it is possible at all—to bring such a component into a particular state and to observe the resulting circuit response through the limited bandwidth offered by the input-output pads. Hardware testing equipment tends to be very expensive and every second a part spends in the tester adds to its price.

It is therefore advisable to consider the testing early in the design process. Some small modifications in a circuit can help make it easier to validate the absence of faults. This approach to design has been dubbed *design for testability (DFT)*. While often despised by circuit designers who prefer to concentrate on the exciting aspects of design, such as transistor optimization, DFT is an integral and important part of the design process and should be considered as early as possible in the design flow. “*If you don’t test it, it won’t work! (Guaranteed)*” [Weste93]. A DFT strategy contains two components:

1. Provide the necessary *circuitry* so that the test procedure can be swift and comprehensive.
2. Provide the necessary *test patterns* (excitation vectors) to be employed during the test procedure. For reasons of cost, it is desirable that the test sequence be as short as possible while covering the majority of possible faults.

In the subsequent sections, we briefly cover some of the most important issues in each of these domains. Before doing so, a short description of a typical test procedure helps to put things in perspective.

## H.2 Test Procedure

Manufacturing tests fall into a number of categories depending upon the intended goal:

- **The diagnostic test** is used during the debugging of a chip or board and tries to accomplish the following: Given a failing part, identify and locate the offending fault.
- **The functional test** (also called *go/no go* test) determines whether or not a manufactured component is functional. This problem is simpler than the diagnostic test since the only answer expected is yes or no. As this test must be executed on every manufactured die and has a direct impact on the cost, it should be as simple and swift as possible.
- **The parametric test** checks on a number of nondiscrete parameters, such as noise margins, propagation delays, and maximum clock frequencies, under a variety of working conditions, such as temperature and supply voltage. This requires a different set-up from

the functional tests that only deal with 0 and 1 signals. Parametric tests generally are subdivided into static (dc) and dynamic (ac) tests.

A typical manufacturing test proceeds as follows. The predefined test patterns are loaded into the tester that provides excitations to the *device under test* (DUT) and collects the corresponding responses. The test patterns are defined in a *test program* that describes the waveforms to be applied, voltage levels, clock frequency, and expected response. A probe card, or DUT board, is needed to connect the outputs and inputs of the tester to the corresponding pins on the die or package.

A new part is automatically fed into the tester. The tester executes the test program, applies the sequence of input patterns to the DUT, and compares the obtained response with the expected one. If differences are observed, the part is marked as faulty (e.g., with an ink spot), and the probes are automatically moved to the next die on the wafer. During the scribing process that divides the wafer into the individual dies, spotted parts will be automatically discarded. For a packaged part, the tested component is removed from the test board and placed in a good or faulty bin, depending upon the outcome of the test. The whole procedure takes in the range of a few seconds per part, making it possible for a single tester to handle thousands of parts in an hour.

Figure H-1 shows a picture of a high-end tester for logic circuits. Automatic testers are very expensive pieces of equipment. The increasing performance requirements, imposed by the high-speed ICs of today, have aggravated the situation, causing the cost of the test equipment to skyrocket. Reducing the time that a die spends on the tester is the most effective way to reduce the test cost. Unfortunately, with the increasing complexity of ICs, an opposite trend can be observed. Design approaches to reduce the test burden are thus very desirable.

### H.3 Design for Testability

#### H.3.1 Issues in Design for Testability

As mentioned, a high-speed tester that can adequately handle state-of-the-art components comes at an astronomical cost. Reducing the test time for a single component can help increase the

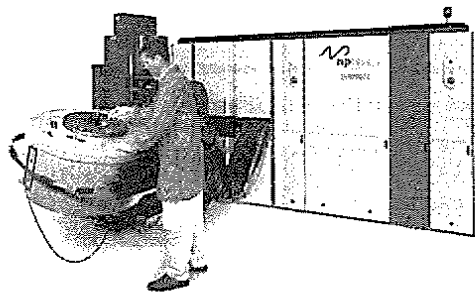
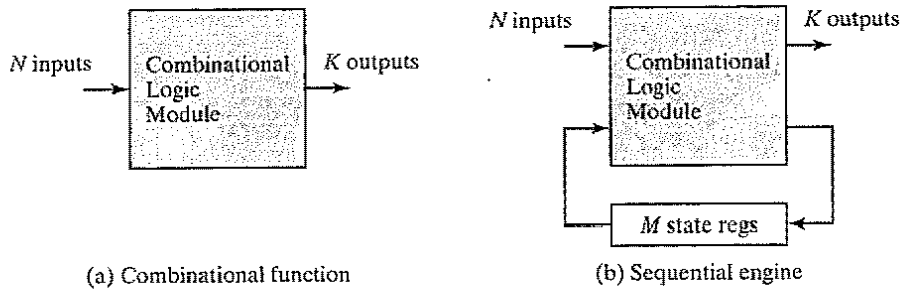


Figure H-1 Automatic tester (Courtesy Shlumberger).



**Figure H-2** Combinational and sequential devices under test.

throughput of the tester, and has an important impact on the testing cost. By considering testing from the early phases of the design process, it is possible to simplify the whole validation process. In this section, we describe some approaches that achieve that goal. Before detailing these techniques, we should first understand some of the intricacies of the test problem.

Consider the combinational circuit block of Figure H-2a. The correctness of the circuit can be validated by exhaustively applying all possible input patterns and observing the responses. For an  $N$ -input circuit, this requires the application of  $2^N$  patterns. For  $N = 20$ , more than 1 million patterns are needed. If the application and observation of a single pattern takes  $1 \mu\text{sec}$ , the total test of the module requires 1 sec. The situation gets more dramatic when considering the sequential module of Figure H-2b. The output of the circuit depends not only upon the inputs applied, but also upon the value of the state. To exhaustively test this finite state machine (FSM) requires the application of  $2^{N+M}$  input patterns, where  $M$  is the number of state registers [Williams83, Weste93]. For a state machine of moderate size (e.g.,  $M = 10$ ), this means that 1 billion patterns must be evaluated, which takes 16 minutes on our  $1 \mu\text{sec}/\text{pattern}$  testing equipment. Modeling a modern microprocessor as a state machine translates into an equivalent model with over 50 state registers. Exhaustive testing of such an engine would require over a billion years!

Obviously, an alternative approach is required. A more feasible testing approach is based on the following premises.

- An exhaustive enumeration of all possible input patterns contains a substantial amount of *redundancy*; that is, a single fault in the circuit is covered by a number of input patterns. Detection of that fault requires only one of those patterns, while the other patterns are superfluous.
- A substantial reduction in the number of patterns can be obtained by relaxing the condition that all faults must be detected. For instance, detecting the last single percentage of possible faults might require an exorbitant number of extra patterns, and the cost of detecting them might be larger than the eventual replacement cost. Typical test procedures only attempt a 95–99% fault coverage.

By eliminating redundancy and providing a reduced fault coverage, it is possible to test most combinational logic blocks with a limited set of input vectors. This does not solve the sequential problem, however. To test a given fault in a state machine, it is not sufficient to apply the correct input excitation; the engine must be brought to the desired state first. This requires that a sequence of inputs be applied. Propagating the circuit response to one of the output pins might require another sequence of patterns. In other words, testing for a single fault in an FSM requires a sequence of vectors. Once again, this might make the process prohibitively expensive.

One way to address the problem is to turn the sequential network into a combinational one by breaking the feedback loop in the course of the test. This is one of the key concepts behind the *scan-test* methodology described later. Another approach is to let the circuit test itself. Such a test does not require external vectors and can proceed at a higher speed. The concept of *self-test* will be discussed in more detail later. When considering the testability of designs, two properties are of foremost importance:

1. **Controllability**, which measures the ease of bringing a circuit node to a given condition using only the input pins. A node is easily controllable if it can be brought to any condition with only a single input vector. A node (or circuit) with low controllability needs a long sequence of vectors to be brought to a desired state. It should be clear that a high degree of controllability is desirable in testable designs.
2. **Observability**, which measures the ease of observing the value of a node at the output pins. A node with a high observability can be monitored directly on the output pins. A node with a low observability needs a number of cycles before its state appears on the outputs. Given the complexity of a circuit and the limited number of output pins, a testable circuit should have a high observability. This is exactly the purpose of the test techniques discussed in the sections that follow.

Combinational circuits fall under the class of easily observable and controllable circuits, since any node can be controlled and observed in a single cycle.

*Design-for-test* approaches for the sequential modules can be classified in three categories: ad hoc test, scan-based test, and self-test.

### H.3.2 Ad Hoc Testing

As suggested by the title, ad hoc testing combines a collection of tricks and techniques that can be used to increase the observability and controllability of a design and that are generally applied in an application-dependent fashion.

An example of such a technique is illustrated in Figure H-3a, which shows a simple processor with its data memory. Under normal configuration, the memory is only accessible through the processor. Writing and reading a data value into and out of a single memory position requires a number of clock cycles. The controllability and observability of the memory can be dramatically improved by adding multiplexers on the data and address busses (Figure H-3b).



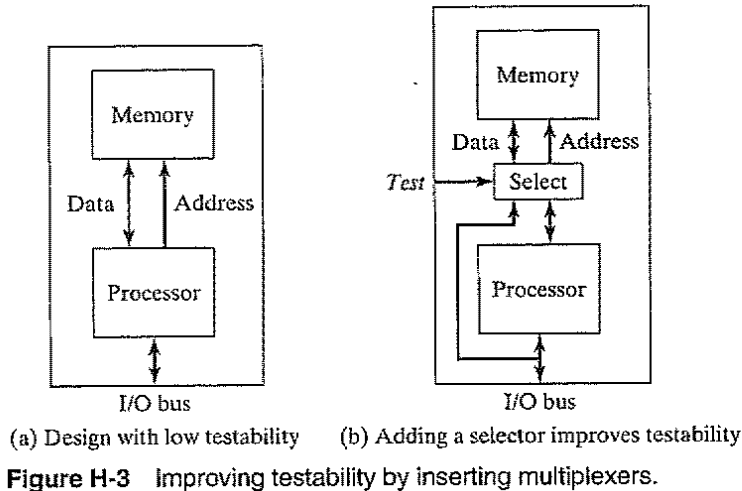


**Figure H-3** Improving testability by inserting multiplexers.

During normal operation mode, these selectors direct the memory ports to the processor. During test, the data and address ports are connected directly to the I/O pins, and testing the memory can proceed more efficiently. The example illustrates some important design-for-testability concepts.

- It is often worthwhile to introduce *extra hardware* that has no functionality except improving the testability. Designers are often willing to incur a small penalty in area and performance if it makes the design substantially more observable or controllable.
- Design-for-testability often means that extra I/O pins must be provided besides the normal functional I/O pins. The *test* port in Figure H-3b is such an extra pin. To reduce the number of extra pads that would be required, one can multiplex test signals and functional signals on the same pads. For example, the I/O bus in Figure H-3b serves as a data bus during normal operation and provides and collects the test patterns during testing.

An extensive collection of ad hoc test approaches has been devised. Examples include the partitioning of large state machines, addition of extra test points, provision of reset states, and introduction of test busses. While very effective, the applicability of most of these techniques depends upon the application and architecture at hand. Their insertion into a given design requires expert knowledge and is difficult to automate. Structured and automatable approaches are more desirable.

### H.3.3 Scan-Based Test

One way to avoid the sequential-test problem is to turn all registers into externally loadable and readable elements. This turns the circuit-under-test into a combinational entity. To control a node, an appropriate vector is constructed, loaded into the registers and propagated through the logic. The result of the excitation propagates to the registers and is latched, after which the con-

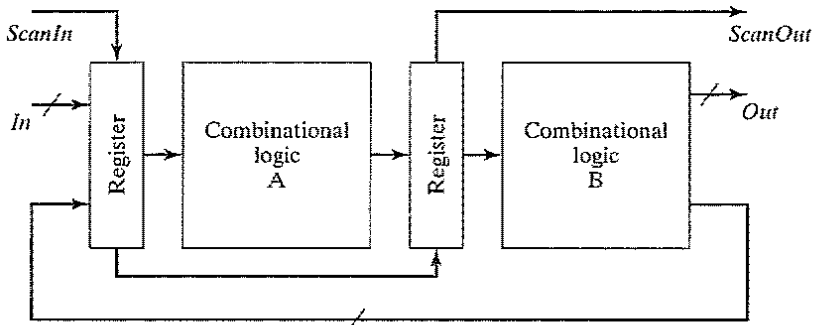


Figure H-4 Serial-scan test.

tents are transferred to the external world. Connecting all the registers in a design to a test bus regrettably introduces an unacceptable amount of overhead. A more elegant approach is offered by the serial-scan approach illustrated in Figure H-4.

The registers have been modified to support two operation modes. In the normal mode, they act as *N*-bit-wide clocked registers. During the test mode, the registers are chained together as a single serial shift register. A test procedure now proceeds as follows.

1. An excitation vector for logic module A (and/or B) is entered through pin *ScanIn* and shifted into the registers under control of a test clock.
2. The excitation is applied to the logic and propagates to the output of the logic module. The result is latched into the registers by issuing a single system-clock event.
3. The result is shifted out of the circuit through pin *ScanOut* and compared with the expected data. A new excitation vector can be entered simultaneously.

This approach incurs only a minimal overhead. The serial nature of the scan chain reduces the routing overhead. Traditional registers are easily modified to support the scan technique, as demonstrated in Figure H-5, which shows a 4-bit register extended with a scan chain. The only addition is an extra multiplexer at the input. When *Test* is low, the circuit is in normal operation

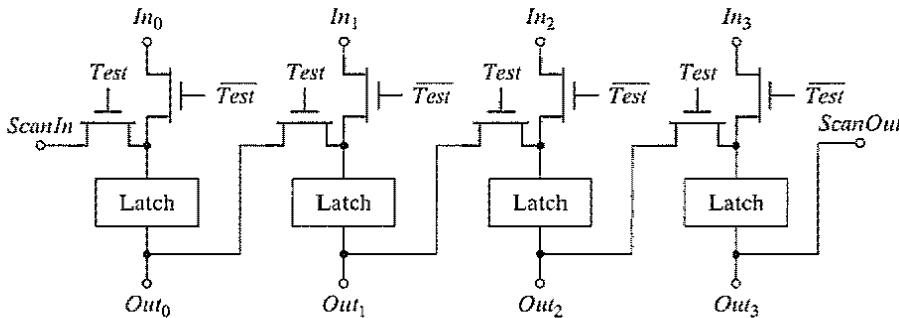


Figure H-5 Register extended with serial-scan chain.

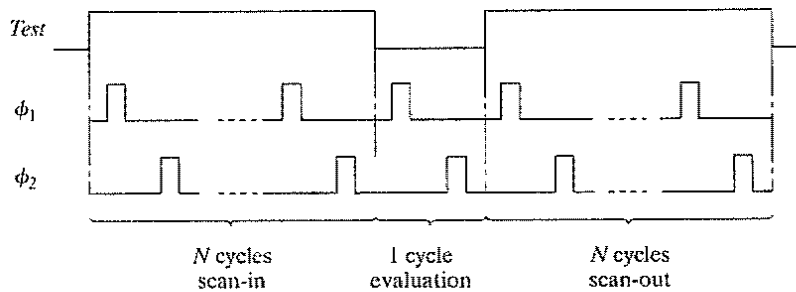
mode. Setting *Test* high selects the *ScanIn* input and connects the registers into the scan chain. The output of the register *Out* connects to the fan-out logic, but also doubles as the *ScanOut* pin that connects to the *ScanIn* of the neighboring register. The overhead in both area and performance is small and can be limited to less than 5%.

### Problem H.1 Scan-Register Design

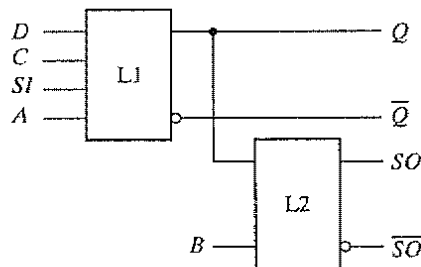
Modify the static, two-phase master-slave register of Figure 7-10 to support serial scan.

Figure H-6 depicts the timing sequence that would be employed for the circuit in Figure H-4 under the assumption of a two-phase clocking approach. For a scan chain  $N$  registers deep, the *Test* signal is raised, and  $N$  clock pulses are issued, loading the registers. *Test* is lowered, and a single clock sequence is issued, latching the results from the combinational logic into the registers under normal circuit-operation conditions. Finally,  $N$  extra pulses (with  $Test = 1$ ) transfer the obtained result to the output. Note again that the scan-out can overlap with the entering of the next vector.

Many variants of the serial-scan approach can be envisioned. A very popular one, which was actually the pioneering approach, was introduced by IBM and is called *level-sensitive scan design* (LSSD) [Eichelberger78]. The basic building block of the LSSD approach is the *shift-register latch* (SRL) shown in Figure H-7. It consists of two latches  $L1$  and  $L2$ , the latter being



**Figure H-6** Timing diagram of test-sequence.  $N$  represents the number of registers in the test chain.



**Figure H-7** Shift-register latch.

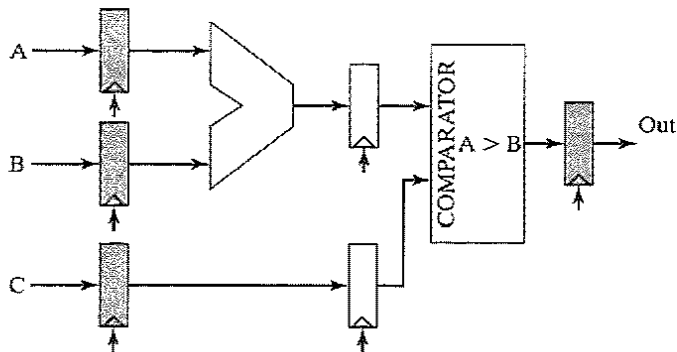


**Figure H-8** Pipelined datapath using partial scan. Only the shaded registers are included in the chain.

present only for testing purposes. In normal circuit operation, signals  $D$ ,  $Q$  ( $Q$ ), and  $C$  serve as latch input, output, and clock. The test clocks  $A$  and  $B$  are low in this mode. In scan mode,  $SI$  and  $SO$  serve as scan input and scan output. Clock  $C$  is low, and clocks  $A$  and  $B$  act as nonoverlapping, two-phase test clocks.

The LSSD approach represents not only a test strategy, but also a complete clocking philosophy. By strictly adhering to the rules implied by this methodology, it is possible to automate to a large extent the test generation and the timing verification. This is why the use of LSSD was obligatory within IBM for a long time. The prime disadvantage of the approach is the complexity of the SRL latch.

It is not always necessary to make all the registers in the design scannable. Consider the pipelined datapath of Figure H-8. The pipeline registers in this design are only present for performance reasons and do not strictly add to the state of the circuit. It is, therefore, meaningful to make only the input and output registers scannable. During test generation, the adder and comparator can be considered together as a single combinational block. The only difference is that during the test execution, two cycles of the clocks are needed to propagate the effects of an excitation vector to the output register. This approach is called *partial scan* and is often employed when performance is of prime interest. The disadvantage is that deciding which registers to make scannable is not always obvious and may require interaction with the designer.

### H.3.4 Boundary-Scan Design

Until recently, the test problem was most compelling at the integrated circuit level. Testing circuit boards was facilitated by the abundant availability of test points. The through-hole mounting approach made every pin of a package observable at the back side of the board. For test, it was sufficient to lower the board onto a set of test probes (called “bed-of-nails”) and apply and observe the signals of interest. The picture changed with the introduction of advanced packaging techniques such as surface-mount or multichip modules (Chapter 2). Controllability and observability are not as readily available anymore, because the number of probe points is dramatically

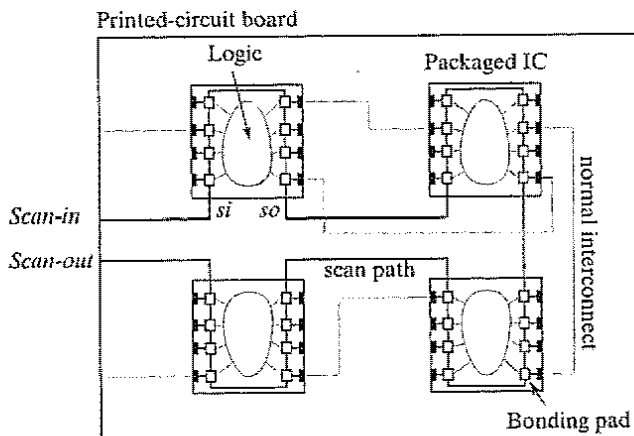


Figure H-9 The boundary-scan approach to board testing.

reduced. This problem can be addressed by extending the scan-based test approach to the component and board levels.

The resulting approach is called *boundary scan* and has been standardized to ensure compatibility between different vendors ([IEEE1149]). In essence, it connects the input-output pins of the components on a board into a serial scan chain, as shown in Figure H-9. During normal operation, the boundary-scan pads act as normal input-output devices. In test mode, vectors can be scanned in and out of the pads, providing controllability and observability at the boundary of the components (hence, the name). The test operation proceeds along similar lines as described in the previous paragraph. Various control modes allow for testing the individual components as well as the board interconnect. The overhead incurred includes slightly more complex input-output pads and an extra on-chip test controller (an FSM with 16 states). Boundary scan is now provided in most commodity components.

### H.3.5 Built-in Self-Test (BIST)

An alternative and attractive approach to testability is having the circuit itself generate the test patterns instead of requiring the application of external patterns [Wang86]. Even more appealing is a technique where the circuit itself decides if the obtained results are correct. Depending upon the nature of the circuit, this might require the addition of extra circuitry for the generation and analysis of the patterns. Some of this hardware might already be available as part of the normal operation, and the size overhead of the self-test can be small.

The general format of a built-in self-test design is illustrated in Figure H-10 ([Kornegay92]). It contains a means for supplying test patterns to the device under test and a means of comparing the device's response to a known correct sequence.

There are many ways to generate stimuli. Most widely used are the *exhaustive* and the *random* approaches. In the exhaustive approach, the test length is  $2^N$ , where  $N$  is the number of inputs to the circuit. The exhaustive nature of the test means that all detectable faults will be

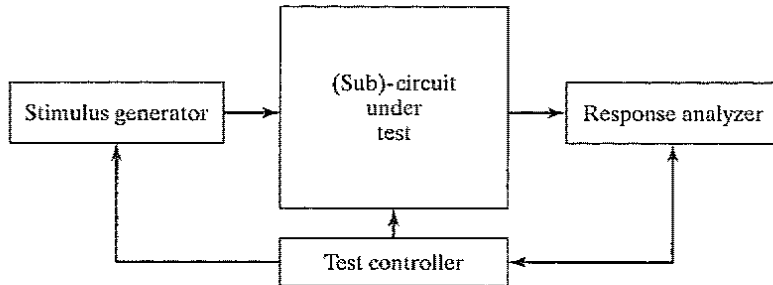


**Figure H-10** General format of built-in self-test structure.

detected, given the space of the available input signals. An  $N$ -bit counter is a good example of an exhaustive pattern generator. For circuits with large values of  $N$ , the time to cycle through the complete input space might be prohibitive. An alternative approach is to use random testing that implies the application of a randomly chosen sub-set of  $2^N$  possible input patterns. This subset should be selected so that a reasonable fault coverage is obtained. An example of a pseudorandom pattern generator is the *linear-feedback shift register* (or LFSR), which is shown in Figure H-11. It consists of a serial connection of 1-bit registers. Some of the outputs are XOR'd and fed back to the input of the shift register. An  $N$ -bit LFSR cycles through  $2^N - 1$  states before repeating the sequence, which produces a seemingly random pattern. Initialization of the registers to a given seed value (different from 0 for our example circuit) determines what will be generated, subsequently.

The response analyzer could be implemented as a comparison between the generated response and the expected response stored in an on-chip memory, but this approach represents too much area overhead to be practical. A cheaper technique is to compress the responses before comparing them. Storing the compressed response of the correct circuit requires only a minimal amount of memory, especially when the compression ratio is high. The response analyzer then

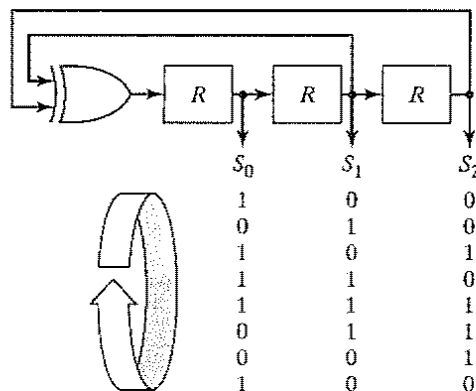


**Figure H-11** Three-bit linear-feedback shift register and its generated sequence.

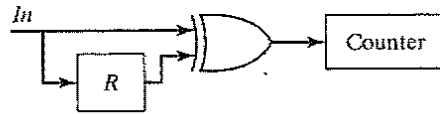
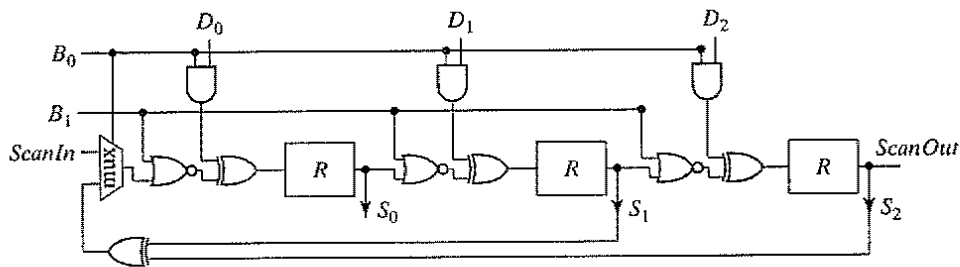


Figure H-12 Single bit-stream signature analysis.

consists of circuitry that dynamically compresses the output of the circuit under test and a comparator. The compressed output is often called the *signature* of the circuit, and the overall approach is dubbed *signature analysis*.

An example of a signature analyzer that compresses a single bit stream is shown in Figure H-12. Inspection reveals that this circuit simply counts the number of 0 → 1 and 1 → 0 transitions in the input stream. This compression does not guarantee that the received sequence is the correct one; that is, there are many different sequences with the same number of transitions. Since the chances of this happening are slim, it may be a risk worth taking if kept within bounds.

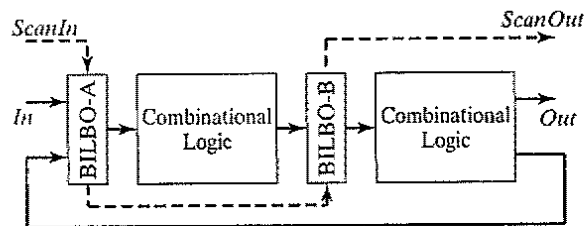
Another technique is illustrated in Figure H-13a. It represents a modification of the linear-feedback shift register and has the advantage that the same hardware can be used for both pattern generation and signature analysis. Each incoming data word is successively XOR'd with the contents of the LFSR. At the end of the test sequence, the LFSR contains the signature, or *syndrome*, of the data sequence, which can be compared with the syndrome of the correct circuit. The circuit not only implements a random-pattern generator and signature analyzer, but also can



(a) A 3-bit BILBO register

$B_0 B_1$	Operation mode
1 1	Normal
0 0	Scan
1 0	Pattern generation or signature analysis
0 1	Reset

(b) BILBO modes



(c) BILBO application

Figure H-13 Built-in logic block observation, or BILBO.

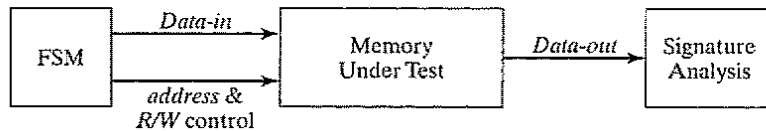


Figure H-14 Memory self-test.

be used as a normal register and scan register, depending on the values of the control signals  $B_0$  and  $B_1$  (Figure H-13b). This test approach, which combines all the different techniques, is known as *built-in logic block observation*, or *BILBO* [Koeneman79]. Figure H-13c illustrates the typical use of BILBO. Using the scan option, the seed is shifted into the BILBO register A while BILBO register B is initialized. Next, registers A and B are operated in the random pattern-generation and signature-analysis modes, respectively. At the end of the test sequence, the signature is read from B using the scan mode.

Finally, it is worth mentioning that self-test is extremely beneficial when testing regular structures such as memories. It is not easy to ensure that a memory, which is a sequential circuit, is fault free. The task is complicated by the fact that the data value read from or written into a cell can be influenced by the values stored in the neighboring cells because of cross coupling and other parasitic effects. Memory tests, therefore, include the reading and writing of a number of different patterns into and from the memory using alternating addressing sequences. Typical patterns can be all zeros or ones, or checkerboards of zeros and ones. Addressing schemes can include the writing of the complete memory, followed by a complete read-out or various alternating read-write sequences. With a minimal overhead compared with the size of a memory, this test approach can be built into the integrated circuit itself, as illustrated in Figure H-14. This approach significantly improves the testing time and minimizes the external control. Applying self-test is bound to become more important with the increasing complexity of integrated components and the growing popularity of embedded memories.

The advent of the systems-on-a-chip era does not make the test job any easier. A single IC may contain micro- and signal processors, multiple embedded memories, ASIC modules, FPGAs and on-chip busses and networks. Each of these modules has its own preferred way of being tested, and combining those into a coherent strategy is quite a challenge. Built-in self-test is really the only way out. A structured test-methodology for systems-on-a-chip, based on BIST is shown in Figure H-15. Each of the modules composing the system connects to the on-chip network through a "wrapper." This is a customized interface between the block and the network, supporting functions such as synchronization and communication. This wrapper can be extended to include a test support module. For instance, for an ASIC module that includes a scan chain, the test support module provides the interface to the scan chain and a buffer for the test patterns. This buffer can be directly written and read through the system bus. Similarly, a memory module can be equipped with a pattern generator and signature analysis. All of this would still not suffice if there were no general test orchestrator. Fortunately, most of these SOC's include a programmable processor which can be used at start-up time to direct the test and the verification of the other modules. Test patterns and signatures can be stored



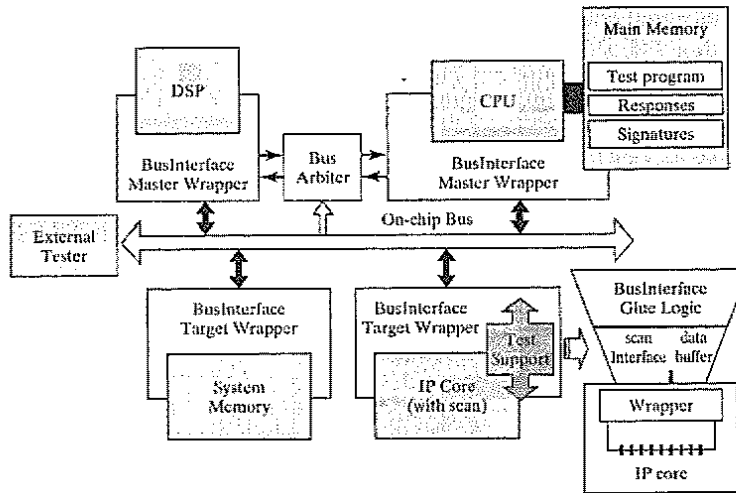


Figure H-15 System-on-a-chip test methodology.

in the main memory of the processor, and supplied to the module under test at test time. This approach has the advantage that it uses the resources that are already available on the die. Furthermore, the BIST self-test approach allows for the tests to be performed under actual clock speeds, decreasing the test time. The requirements for the external tester are minimized, reducing the tester cost. The development of a structured approach to self-test, as pictured in Figure H-15, is a topic of active research [Krstic01]. ■

## H.4 Test-Pattern Generation

In the preceding sections, we have discussed how to modify a design so that test patterns can be effectively applied. What we have ignored so far is the complex task of determining what patterns should be applied so that a good fault coverage is obtained. This process was extremely problematic in the past, when the test engineer—a different person than the designer—had to construct the test vectors after the design was completed. This invariably required a substantial amount of wasteful reverse engineering that could have been avoided if testing had been considered early in the design flow. An increased sensitivity to design for testability and the emergence of automatic test-pattern generation (ATPG) has substantially changed this picture.

In this section, we delve somewhat deeper into the ATPG issue and present techniques to evaluate the quality of a test sequence. Before doing so, we must analyze the fault concept in more detail.

### H.4.1 Fault Models

Manufacturing faults can be of a wide variety and manifest themselves as short circuits between signals, short circuits to the supply rails, and floating nodes. In order to evaluate the effectiveness of a test approach and the concept of a good or bad circuit, we must relate these faults to the circuit model, or, in other words, derive a *fault model*. The most popular approach is called the *stuck-at* model. Most testing tools consider only the short circuits to the supplies. These are

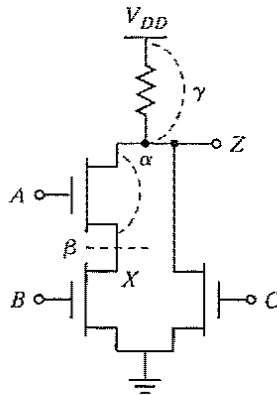


**Figure H-16** Resistive-load gate, annotated with a number of stuck-at-open ( $\beta$ ) and stuck-at-short ( $\alpha$ ,  $\gamma$ ) faults.

called the *stuck-at-zero* (sa0) and *stuck-at-one* (sa1) faults for short circuits to *GND* and *V<sub>DD</sub>*, respectively.

It can be argued that the sa0-sa1 model does not cover the complete range of faults that can occur in a state-of-the-art integrated circuit, and that *stuck-at-open* and *stuck-at-short* faults should also be introduced. However, adding these faults complicates the test pattern generation process. Moreover, a large number of these faults are covered by the sa0-sa1 model. To illustrate this observation, consider the resistive-load MOS gate of Figure H-16. All shorts to the supplies are modeled by the introduction of sa0 and sa1 faults at nodes *A*, *B*, *C*, *Z*, and *X*. The figure has been annotated with some stuck-at-open ( $\beta$ ) and stuck-at-short faults ( $\alpha$ ,  $\gamma$ ). It can be observed that these faults are already covered by the sa0 and sa1 faults on the various nodes. For example, fault  $\alpha$  is covered by  $A_{sa1}$ ,  $\beta$  is covered by  $A_{sa0}$  or  $B_{sa0}$ , while  $\gamma$  is equivalent to  $Z_{sa1}$ .

Even so, shorts and open-circuit faults can cause some interesting artifacts to occur in CMOS circuits that are not covered by the sa0-sa1 model and are worth mentioning. Consider the two-input NAND gate of Figure H-17, where a stuck-at-open fault  $\alpha$  has occurred. The truth table of the faulty circuit is shown in the figure as well. For the combination ( $A = 1$ ,  $B = 0$ ), the output node is floating and retains its previous value, while the correct value should be a 1. Depending upon the previous excitation vector, this fault may or may not be detected. In fact, the circuit behaves as a sequential network. To detect this fault, two vectors must be applied in sequence. The first one forces the output to 0 (or  $A = 1$  and  $B = 1$ ), while the second applies the  $A = 1$ ,  $B = 0$  pattern. Also stuck-at-short faults are troublesome in CMOS circuits since they can cause dc currents to flow between the supply rails for certain input values, which produces undefined output voltages.

Even though the sa0-sa1 fault model is not perfect, its ease of use and relatively large coverage of the fault space have made it the de facto standard model. It is often supplemented with other techniques, such as functional test, *IDDQ test*—which measures the change in quiescent current of a CMOS circuit due to short circuits—and delay test. No single test model is completely foolproof, and a combination of several testing methods is often required [Bhavsar01].

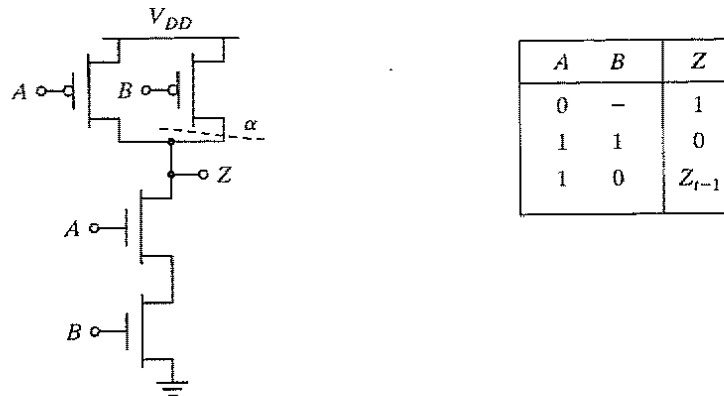


Figure H-17 Two-input complementary CMOS NAND gate and its truth table in the presence of a stuck-at-open fault.

#### H.4.2 Automatic Test-Pattern Generation (ATPG)

The task of the automatic test-pattern generation (ATPG) process is to determine a minimum set of excitation vectors that cover a sufficient portion of the fault set as defined by the adopted fault model. One possible approach is to start from a random set of test patterns. Fault simulation then determines how many of the potential faults are detected. With the obtained results as guidance, extra vectors can be added or removed iteratively. An alternative and potentially more attractive approach relies on the knowledge of the functionality of a Boolean network to derive a suitable test vector for a given fault. To illustrate the concept, consider the example of Figure H-18. The goal is to determine the input excitation that exposes an sa0 fault occurring at node  $U$  at the output of the network  $Z$ . The first requirement of such an excitation is that it should force the fault to occur (*controllability*, again). In this case, we look for a pattern that would set  $U$  to 1 under normal circumstances. The only option here is  $A = 1$  and  $B = 1$ . Next, the faulty signal has to propagate to output node  $Z$ , so that it can be *observed*. This phase is called *path sensitizing*. For any change in node  $U$  to propagate, it is necessary for node  $X$  to be set to 1 and node  $E$  to 0. The (unique) test vector for  $U_{sa0}$  can now be assembled:  $A = B = C = D = 1, E = 0$ .

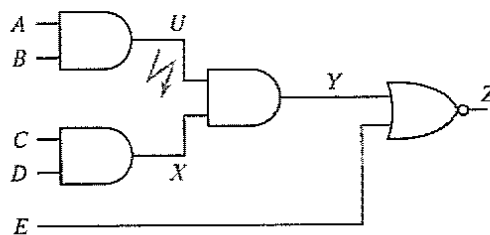


Figure H-18 Simple logic network, with sa0 fault at node  $U$ .

This example is extremely simple, and the derivation of a minimum test-vector set for more complex circuits is substantially more complex. A number of excellent approaches to address this problem have been developed. Landmark efforts in this domain are the *D* [Roth66] and PODEM algorithms [Goel81], which underlie many current ATPG tools. It suffices to say that ATPG is currently in the mainstream of design automation, and powerful tools are available from many vendors.

### H.4.3 Fault Simulation

A fault simulator measures the quality of a test program. It determines the *fault coverage*, which is defined as the total number of faults detected by the test sequence divided by two times the number of nodes in the network—each node can give rise to an sa0 and sa1 fault. Naturally, the obtained coverage number is only as good as the fault model employed. In an sa0-sa1 model, some of the bridge and short faults are not covered and will not appear in the coverage statistics.

The most common approach to fault simulation is the parallel fault-simulation technique, in which the correct circuit is simulated concurrently with a number of faulty ones, each of which has a single fault injected. The results are compared, and a fault is labeled as detected for a given test vector set if the outputs diverge. This description is overly simplistic, and most simulators employ a number of techniques, such as selecting the faults with a higher chance of detection first, to expedite the simulation process. Hardware fault-simulation accelerators, based on parallel processing and providing a substantial speedup over pure software-based simulators, are available as well [Agrawal88, pp. 159–240].

## H.5 To Probe Further

For an in-depth treatment of the Design-for-Testability topic, please refer to [Agrawal88] and [Abramovic91]. A great overview of the testing challenges and solutions for high-performance microprocessors can be found in [Bhavsar01].

## References

- [Abramovic91] M. Abramovic, M. Breuer, and A. Friedman, *Digital Systems Testing and Testable Design*, IEEE Press, Piscataway, NJ, 1991.
- [Agrawal88] V. Agrawal and S. Seth, Eds. *Test Generation for VLSI Chips*, IEEE Computer Society Press, 1988.
- [Bhavsar01] D. Bhavsar, "Testing of High-Performance Microprocessors," in *Design of High-Performance Microprocessor Circuits*, A. Chandrakasan et al., Ed., pp. 523–44, IEEE Press, 2001.
- [Eichelberger78] E. Eichelberger and T. Williams, "A Logic Design Structure for VLSI Testability," *Journal on Design Automation of Fault-Tolerant Computing*, vol. 2, pp. 165–78, May 1978.
- [Goel81] P. Goel, "An Implicit Enumeration Algorithm to Generate Tests for Combinational Logic Circuits," *IEEE Trans. on Computers*, vol. C-30, no. 3, pp. 26–268, June 1981.
- [IEEE1149] IEEE Standard 1149.1, "IEEE Standard Test Access Port and Boundary-Scan Architecture," IEEE Standards Board, New York.
- [Koeneman79] B. Koeneman, J. Mucha, and O. Zwihehoff, "Built-in Logic-Block Observation Techniques," in *Digest 1979 Test Conference*, pp. 37–41, October 1979.

- [Kornegay92] K. Kornegay, *Automated Testing in an Integrated System Design Environment*, Ph. D dissertation., Mem. No. UCB/ERL M92/104, Sept. 1992.
- [Krstic01] A. Krstic, W. Lai, L. Chen, K. Cheng, and S. Dey, "Embedded Software-Based Self-Testing for SOC Design," <http://www.gigascate.org/pubs/139.html>, December 2001.
- [Roth66] J. Roth, "Diagnosis of Automata Failures: A Calculus and a Method," *IBM Journal of Research and Development*, vol. 10, pp. 278–291, 1966.
- [Wang86] L. Wang and E. McCluskey, "Complete Feedback Shift-Register Design for Built-in Self Test," *Proc. ICCAD 1986*, pp. 56–59, November, 1986.
- [Weste93] N. Weste and K. Eshraghian, *Principles of CMOS VLSI Design—A Systems Perspective*, Addison-Wesley, 1993.
- [Williams83] T. Williams and K. Parker, "Design for Testability—A Survey," *Proceedings IEEE*, vol. 71, pp. 98–112, Jan. 1983.